

UNIVERSIDADE DE LISBOA, FACULDADE DE FARMÁCIA

DEPARTAMENTO DE QUÍMICA FARMACÊUTICA E TERAPÊUTICA



**SYNTHESIS AND COMPUTER-ASSISTED DESIGN OF
MITOCHONDRIAL ELECTRON TRANSPORT-CHAIN INHIBITORS
AS ANTIMALARIAL AGENTS**

MARTA ANDREIA PAIS CARRASCO

DOUTORAMENTO EM FARMÁCIA

(ESPECIALIDADE DE QUÍMICA FARMACÊUTICA E TERAPÊUTICA)

2014

UNIVERSIDADE DE LISBOA, FACULDADE DE FARMÁCIA

DEPARTAMENTO DE QUÍMICA FARMACÊUTICA E TERAPÊUTICA



**SYNTHESIS AND COMPUTER-ASSISTED DESIGN OF
MITOCHONDRIAL ELECTRON TRANSPORT-CHAIN INHIBITORS
AS ANTIMALARIAL AGENTS**

MARTA ANDREIA PAIS CARRASCO

Tese orientada pelo Doutor Daniel dos Santos e pelo Prof. Doutor Rui Moreira,
especialmente elaborada para a obtenção do grau de doutor no ramo de Farmácia,
especialidade de Química Farmacêutica e Terapêutica.

2014

O presente trabalho foi desenvolvido sob orientação do Doutor Daniel dos Santos e co-orientação do Professor Doutor Rui Moreira, no iMed.Ulisboa (Instituto de Investigação do Medicamento) da Faculdade de Farmácia da Universidade de Lisboa. Este trabalho foi financiado pela Fundação para a Ciência e Tecnologia através da bolsa de doutoramento SFRH/BD/61611/2009 e dos projectos PTDC/SAU-FCT/098734/2008, PTDC/SAU-FAR/118459/2010 e Pest-OE/SAL/UI4013/2011.

This work was developed under scientific supervision of Dr. Daniel dos Santos and co-supervision of Dr. Rui Moreira, at iMed.Ulisboa (Instituto de Investigação do Medicamento), Faculty of Pharmacy, University of Lisbon. The work was financially supported by Fundação para a Ciência e Tecnologia, through the doctoral grant SFRH/BD/61611/2009, and projects PTDC/SAU-FCT/098734/2008, PTDC/SAU-FAR/118459/2010 and Pest-OE/SAL/UI4013/2011.

List of publications

Papers in international scientific periodicals with referees

1. Marta P. Carrasco, Jiri Gut, Philip J. Rosenthal, Rui Moreira, Daniel J. V. A. dos Santos. Modelling the Oxidation Site of *Plasmodium falciparum* bc₁ Complex: Homology Modeling, Docking Studies and Virtual Screening. *In preparation*.
2. Marta P. Carrasco, Lídia Gonçalves, Marta Machado, Jiri Gut, Fátima Nogueira, Daniel J. V. A. dos Santos, Philip J. Rosenthal, Rui Moreira. Azaaurones as a Privileged Platform for Designing Potent Antimalarial Drugs: Synthesis, Antimalarial Activity and, Mechanistic Studies. *In preparation*.
3. Marta P. Carrasco, Ana S. Newton, Lídia Gonçalves, Ana Góis, Marta Machado, Jiri Gut, Fátima Nogueira, Thomas Hänscheid, Rita C Guedes, Daniel J. V. A. dos Santos, Philip J. Rosenthal, Rui Moreira. Probing the Aurone Scaffold Against *Plasmodium falciparum*: Design, Synthesis and Antimalarial Activity. *European Journal of Medicinal Chemistry*, *accepted*.
4. Tiago Rodrigues, Ana S. Ressurreição, Filipa P. da Cruz, Inês S. Albuquerque, Jiri Gut, Marta P. Carrasco, Daniel Gonçalves, Rita C. Guedes, Daniel J. V. A. dos Santos, Maria M. Mota, Philip J. Rosenthal, Rui Moreira, Miguel Prudêncio, Francisca Lopes. Flavones as Isosteres of 4(1*H*)-Quinolones: Discovery of Ligand Efficient and Dual Stage Antimalarial Lead Compounds. *European Journal of Medicinal Chemistry*, **2013**, 69, 872-880.
5. Marta P. Carrasco, Jiri Gut, Tiago Rodrigues, Maria H. L. Ribeiro, Francisca Lopes, Philip J. Rosenthal, Rui Moreira, Daniel J. V. A. dos Santos. Exploring the Molecular Basis of Q_o bc₁ Complex Inhibitors Activity to Find Novel Antimalarial Hits. *Molecular Informatics*, **2013**, 32, 659-670
6. Tiago Rodrigues, Rita C. Guedes, Daniel J. V. A. dos Santos, Marta Carrasco, Jiri Gut, Philip J. Rosenthal, Rui Moreira, Francisca Lopes. Design, Synthesis and Structure-activity Relationships of (1*H*-pyridin-4-ylidene)amines as Potential Antimalarials. *Bioorganic & Medicinal Chemistry Letters*, **2009**, 19, 3476-3480.

Oral communications in conferences

1. Marta P. Carrasco, João Lavrado, Rui Moreira, Alexandra Paulo, DANIEL J. V. A. DOS SANTOS, Fighting cancer and malaria – computational strategies, *6th Theoretical Biophysics Symposium*, **2013**, Gothenburg, Sweden.
2. MARTA CARRASCO, Rui Moreira, Daniel J. V. A. dos Santos; Using Computational Chemistry to Find New and More Potent Antimalarial Drugs; *2nd Post-Graduate iMed.UL Students Meeting*, **2010**, Lisboa, Portugal.
3. Marta Carrasco, Tiago Rodrigues, Rui Moreira, DANIEL J. V. A. DOS SANTOS; Computational Screening Over the Yeast bc_1 Complex; *2nd National Meeting on Medicinal Chemistry*, **2010**, Coimbra, Portugal.

Posters in conferences

1. Marta P. Carrasco, Jiri Gut, Lídia M. Gonçalves, Daniel J. V. A. dos Santos, Philip J. Rosenthal, Rui Moreira. Probing the Chemical Space Around Aurone Scaffold – Improving Antimalarial Activity; *10th National Meeting on Organic Chemistry*, **2013**, Lisboa, Portugal.
2. Marta P. Carrasco, Daniel J. V. A. dos Santos. Modelling the Oxidation Site of *Plasmodium Falciparum* bc_1 complex; *3rd SEQT Summer School “Medicinal Chemistry Drug Discovery: The Pharma Perspective”*, 2013, Tres Cantos, Madrid, Spain.
3. Marta P. Carrasco, Daniel J. V. A. dos Santos, Jiri Gut, Philip J. Rosenthal, Rui Moreira. Synthesis and Biological Evaluation of Novel Aurone Derivatives as Potential Antimalarial Agents; *2nd Meeting of the Paul Ehrlich MedChem Euro-PhD Network*, **2012**, Ljubljana, Slovenia.
4. Marta P. Carrasco, Daniel J. V. A. dos Santos, Rui Moreira. Development of Novel Aurone Derivatives as Potential Antimalarial Agents; *22nd International Symposium on Medicinal Chemistry*, **2012**, Berlin, Germany.

5. Marta P. Carrasco, Jiri Gut, Philip Rosenthal, Rui Moreira, Daniel J. V. A. dos Santos; Towards New bc_1 Complex Inhibitors as Antimalarial Drugs: a Virtual Screening Approach; *São Paulo Advanced School on Chemistry (ESPCA)*, **2011**, Campinas (SP), Brasil.
6. Marta P. Carrasco, Jiri Gut, Philip Rosenthal, Rui Moreira, Daniel J. V. A. dos Santos; Searching for New bc_1 Complex Inhibitors as Antimalarial Drugs Using Virtual Screening; *5th Symposium on Theoretical Biophysics*, **2011**, Madeira, Portugal
7. Marta Carrasco, Tiago Rodrigues, Rui Moreira, Daniel J. V. A. dos Santos; Using Computational Chemistry to Find New and More Potent Antimalarial Drugs; *2nd National Meeting on Medicinal Chemistry*, **2010**, Coimbra, Portugal.
8. Marta Carrasco, Tiago Rodrigues, Rui Moreira, Daniel J. V. A. dos Santos; Using Computational Chemistry to Find New and More Potent Antimalarial Drugs; *Celebrating Computational Chemistry*, **2010**, Oxford, UK.
9. Tiago Rodrigues, Rita C. Guedes, Daniel J. V. A. dos Santos, Marta Carrasco, Jiri Gut, Philip Rosenthal, Rui Moreira, Francisca Lopes; (1*H*-pyridin-4-ylidene)amines: a New Scaffold for Antimalarial Drug Candidates; *2nd PYChem*, **2010**, Aveiro, Portugal.
10. Marta Carrasco, Rui Moreira, Daniel J. V. A. dos Santos; Fighting Malaria: a Computational Approach; *2nd PYChem*, **2010**, Aveiro, Portugal.

To my father

Acknowledgments

First of all, I would like to express my gratitude to my supervisors Professor Rui Moreira and Dr. Daniel dos Santos for their contribution on my scientific and personal growth with all the advices and the dedication expressed during these years I was working in their group.

Additionally, I would like to thank to Professor Philip Rosenthal, Jiri Gut, Dr. Lídia Gonçalves, Dr. Fátima Nogueira, Dr. Thomas Hänscheid, Dr. Maria Ribeiro, Dr. Maria Jose Lafuente, Vânia André, João Ferreira, Dr. Francisca Lopes and Dr. Rita Guedes for their extremely important collaboration throughout these years. Their work was indispensable to achieve the successful completion of this project. I also want to thank Francisco Carvalho for his friendship and support.

I also would like to express my deep gratitude to my colleagues for all the funny moments, discussions, and, more important, their friendship: Ana Ressureição, Ana Rita Duarte, André Dias, Ângelo Monteiro, Carlos Ribeiro, Catarina Charneira, Daniela Miranda, Eduardo Ruivo, João Lavrado, Mariana Reis, Marta Figueiras, Paulo Madeira, Teresa Almeida, Teresa Cardote, Rudi Oliveira and Susana Lucas. You are very important to me and played a very special role in this journey.

I also would like to thank Professor Carlos Afonso for accepting me in his lab in the last months. I had the opportunity not only to finish my work but also to meet new incredible colleagues. I also want to thank all of them for their friendship and support.

I also express my gratitude to my family and friends for their unconditional support, patience and continuous motivation.

Finally, I would like to thank Fundação para a Ciência e Tecnologia for the financial support to this PhD program (PhD grant SFRH/BD/61611/2009).

Table of contents

Table of contents	i
List of figures	vii
List of schemes	xi
List of tables	xiii
List of abbreviations and symbology	xv
Abstract	xix
Resumo	xxi
Preamble	xxv
CHAPTER 1 – INTRODUCTION	
1.1. Malaria – An overview	1
1.2. Life cycle of malaria parasite	3
1.3. Antimalarial chemotherapy during erythrocytic stage	5
1.3.1. Targeting parasite membrane biosynthesis	6
1.3.2. Targeting parasite transporters	7
1.3.3. Targeting digestive vacuole	8
1.3.4. Targeting the mitochondria	15
1.3.5. Targeting the apicoplast	36
1.3.6. Targeting the cytosol	40
1.4. Antimalarial chemotherapy during liver stage	44
1.5. Antimalarial drug resistance and artemisinin-based combination therapies	45
1.6. Computational approaches in antimalarial drug discovery	47
1.7. Concluding remarks	50
CHAPTER 2 – <i>S. CEREVISIAE</i> BC₁ COMPLEX AS A MODEL FOR <i>P. FALCIPARUM</i> BC₁ COMPLEX	
2.1. Background	57

2.2. Validation of <i>P. falciparum</i> bc ₁ complex model and binding mode of stigmatellin	59
2.3. Binding mode of atovaquone	67
2.4. Binding mode of floxacrine and WR249685	69
2.5. Binding mode of GW844520	73
2.6. Concluding remarks	76
CHAPTER 3 – VIRTUAL SCREENING STUDIES OVER <i>S. CEREVISIAE</i> BC₁ COMPLEX	
3.1. Background	81
3.2. Virtual screening of TCAMS	81
3.2.1. Comparison between AutoDock and AutoDock Vina	82
3.2.2. Structure-based virtual screening	83
3.3. Virtual screening of MOE Database	87
3.3.1. Biological activity	91
3.3.2. Synthetic approaches to obtain compound 3.17	94
3.3.3. Synthesis of quinoline 3.35 – A simpler model of compound 3.17	100
3.4. Concluding remarks	104
CHAPTER 4 – HOMOLGY MODEL OF <i>P. FALCIPARUM</i> Q₀ SITE OF BC₁ COMPLEX AND VIRTUAL SCREENING STUDY	
4.1. Background	109
4.2. Identity between species in bc ₁ complex Q ₀ binding site and definition of the pocket	111
4.3. Homology model building and docking studies	118
4.4. Virtual screening studies over the homology model of <i>P. falciparum</i> bc ₁ complex	128
4.5. Concluding remarks	132
CHAPTER 5 – SYNTHESIS OF AURONE DERIVATIVES AS POTENTIAL ANTIMALARIALS	
5.1. Background	137
5.2. Synthetic approaches	140

5.3. Biological evaluation	147
5.3.1. Activity against <i>P. falciparum</i> W2 strain	147
5.3.2. Heme polymerization inhibition assay	152
5.3.3. <i>In vitro</i> drug combination assay	155
5.4. Concluding remarks	157
CHAPTER 6 – SYNTHESIS OF AZAAURONE DERIVATIVES AS POTENTIAL <i>bc</i>₁ COMPLEX INHIBITORS	
6.1. Background	161
6.2. Synthetic approaches	163
6.3. Biological evaluation	179
6.3.1. Activity against <i>P. falciparum</i> W2 strain	179
6.3.2. Activity against falcipain-2	184
6.3.3. <i>In vitro</i> drug combination assay	185
6.4. Docking studies over <i>P. falciparum</i> <i>bc</i> ₁ complex	187
6.5. Concluding remarks	189
CHAPTER 7 – CONCLUSIONS	193
CHAPTER 8 – EXPERIMENTAL PART	
8.1. Molecular docking over <i>S. cerevisiae</i> <i>bc</i> ₁ complex	197
8.1.1. Structure preparation	197
8.1.2. Docking of the inhibitors	198
8.2. Virtual screening studies over <i>S. cerevisiae</i> <i>bc</i> ₁ complex	198
8.2.1. Structure preparation and docking	198
8.2.2. Tested compounds	199
8.3. Homology model of <i>P. falciparum</i> <i>bc</i> ₁ complex Q _o binding site	199
8.3.1. Template structures	199
8.3.2. Definition of Q _o binding site	199

8.3.3. Sequence alignment	199
8.3.4. Model building	200
8.4. Chemistry	200
8.5. Synthesis of quinolone derivatives	201
8.5.1. Synthesis of compounds 3.26 and 3.35	201
8.5.2. Synthesis of compounds 3.27 and 3.36	202
8.5.3. Synthesis of 3-(hydroxymethyl)-6,7-dihydroquinolin-4-ol (3.37)	202
8.5.4. Synthesis of 3-(4-hydroxybenzyl)quinolin-4(1H)-one (3.38)	203
8.5.5. Synthesis of 3-(4-hydroxy-3-((4-methylpiperazin-1-yl)methyl)benzyl)-6,7-dihydroquinolin-4-ol (3.34)	203
8.6. Synthesis of aurone derivatives	204
8.6.1. General procedure for the synthesis of aurones 5.24 to 5.29	204
8.6.2. General procedure for the synthesis of aurones 5.30 and 5.31	207
8.6.3. General procedure for the synthesis of aurones derivatives 5.32-5.38 and 5.45-5.54 via Suzuki Coupling	208
8.6.4. General procedure for the synthesis of aurones derivatives 5.39 and 5.40 via Buchwald Coupling	215
8.6.5. Synthesis of (Z)-2-benzylidene-3-oxo-2,3-dihydrobenzofuran-6-yl trifluoromethanesulfonate (5.70)	217
8.6.6. General procedure for the synthesis of ethers derivatives 5.41 and 5.42	217
8.6.7. General procedure for the synthesis of ethers derivatives 5.43 and 5.44	218
8.6.8. General procedure for the synthesis of Mannich Bases derivatives 5.55 to 5.58	219
8.6.9. General procedure for the synthesis of benzonitrile derivatives 5.62 and 5.63	221
8.6.10. General procedure for the synthesis of carboxylic acid derivatives 5.64 and 5.65	222
8.6.11. General procedure for the synthesis of hydroxamate derivatives 5.66 and 5.67	223

8.6.12. General procedure for the synthesis of benzaldehyde derivatives 5.68 and 5.69	224
8.7. Synthesis of azaaurone derivatives	224
8.7.1. General procedure for the synthesis of compounds 6.87 to 6.91	224
8.7.2. General procedure for the synthesis of compounds 6.92 to 6.96	226
8.7.3. General procedure for the synthesis of compounds 6.97 to 6.101	228
8.7.4. General procedure for the synthesis of benzonitrile derivatives 6.102 and 6.104	229
8.7.5. General procedure for the synthesis of carboxylic acid derivatives 6.105 and 6.107	230
8.7.6. General procedure for the synthesis of hydroxamate derivatives 6.108 and 6.110	231
8.7.7. General procedure for the synthesis of benzaldehyde derivatives 6.111 and 6.113	232
8.7.8. General procedure for the synthesis of benzaldehydes derivatives 6.114 to 6.133 via Suzuki Coupling	233
8.7.9. General procedure for the synthesis of azaaurone derivatives 6.25 to 6.55	239
8.7.10. General procedure for the synthesis of azaaurone derivatives 6.56 to 6.86	253
8.8. Biological assays	266
8.8.1. Biological activity against <i>P. falciparum</i> W2 and FCR3 strains	266
8.8.2. Biological activity against <i>P. falciparum</i> Dd2 strain	266
8.8.3. Biological activity against <i>S. cerevisiae</i>	267
8.8.4. Hemozoin-like crystals growth inhibition	267
8.8.5. <i>In vitro</i> drug combination assay	268
8.8.6. Cytochrome <i>bc</i> ₁ complex activity	268
8.8.7. Growth inhibition assays	268
8.8.8. <i>In vitro</i> cytotoxicity	269

APPENDICES

Appendix A – Protein sequences 273

Appendix B – Identity in Q_o binding site 275

REFERENCES 279

List of figures

Figure 1.1. Number of malaria confirmed cases in 2010 ¹ .	2
Figure 1.2. The life cycle of malaria parasites. Adapted from Mueller <i>et al</i> ¹³ .	4
Figure 1.3. Potential drug targets of asexual erythrocytic stage. Adapted from Kappe <i>et al</i> ²⁶ .	6
Figure 1.4. Chemical structure of two inhibitors of phospholipid biosynthesis.	7
Figure 1.5. Chemical structure of furosemide (1.3), an inhibitor of new permeability pathways.	8
Figure 1.6. Examples of inhibitors acting in different proteases.	10
Figure 1.7. Examples of inhibitors of hemozoin formation.	11
Figure 1.8. Main features that contribute for the antimalarial activity of CQ. Adapted from Egan <i>et al</i> ⁵⁸ .	12
Figure 1.9. Chemical structures of artemisinin and some derivatives.	13
Figure 1.10. Examples of fully synthetic endoperoxides.	15
Figure 1.11. Parasite's mitochondrial electron transport chain. From Stocks <i>et al</i> ⁶⁷ .	16
Figure 1.12. Examples of human dihydroorotate dehydrogenase inhibitors.	19
Figure 1.13. Examples of <i>P. falciparum</i> dihydroorotate dehydrogenase inhibitors.	20
Figure 1.14. Structure of the dimeric bc_1 complex.	22
Figure 1.15. Q-cycle mechanism of the bc_1 complex catalytic core. The main components of cytochrome bc_1 are represented in the scheme: cytochrome c_1 – in checker board, Q_o binding site (including ISP) – in grid and, Q_i binding site – in diagonal lines. Abbreviations: Q – ubiquinone; QH_2 – ubiquinol; SQ – stable semi-ubiquinone intermediate; ISP – iron-sulfur protein; IMS – mitochondrial inter-membrane space; IMM – inner mitochondrial membrane.	23
Figure 1.16. Chemical structures of atovaquone (1.52) and proguanil (1.53) that are the active molecules in Malarone.	26
Figure 1.17. Binding mode of atovaquone into bc_1 complex Q_o site.	26
Figure 1.18. Examples of some atovaquone analogs.	27
Figure 1.19. Examples of 4(1 <i>H</i>)-quinolones with potent antimalarial activity.	29
Figure 1.20. Examples of pyridones and analogs acting on <i>Pf</i> bc_1 complex.	30

Figure 1.21. Examples of acridones and acridinediones derivatives.	32
Figure 1.22. Examples of several compounds acting on <i>Pf bc₁</i> complex.	34
Figure 1.23. Examples of inhibitors of <i>bc₁</i> complex Q _i binding site.	35
Figure 1.24. Examples of inhibitors of SDH and ATP synthase.	36
Figure 1.25. Examples of inhibitors of fatty acid biosynthesis.	37
Figure 1.26. Examples of compounds inhibiting isoprenoids and heme biosynthesis.	38
Figure 1.27. Examples of antibiotics acting against <i>P. falciparum</i> .	40
Figure 1.28. Examples of antifolates acting as antimalarial drugs.	42
Figure 1.29. Inhibitors of glycolysis and purine salvage pathway.	44
Figure 1.30. Compounds acting against <i>P. falciparum</i> liver stage.	45
Figure 1.31. Examples of antimalarial compounds discovered by virtual screening.	50
Figure 2.1. The Q _o <i>bc₁</i> complex inhibitors studied.	58
Figure 2.2. Comparison of the poses of crystallographic stigmatellin (carbon atoms in yellow) and the best ranked pose of this inhibitor (carbon atoms in blue). Hydrogen bonds are represented by grey lines.	61
Figure 2.3. Correlation obtained between the experimental log IC ₅₀ and calculated ΔG_{bind} obtained using the 3CX5 coordinates with neutral His181 ($r^2=0.87$). The square represents the binding free energy obtained for atovaquone in the presence of the minimized water molecule in the vicinity of Glu272 ($r^2=0.92$; linear fit not presented).	64
Figure 2.4. Predicted binding poses for atovaquone without the crystallographic water (carbon atoms in yellow) and in the presence of a minimized water molecule near Glu272 (carbon atoms in blue). Hydrogen bonds are represented by grey lines.	68
Figure 2.5. Predicted binding pose for WR249685 on the left, and a comparison of the poses of crystallographic stigmatellin (green), atovaquone (grey) and WR249685 (orange), on the right.	70
Figure 2.6. Predicted binding pose for enantiomers <i>R</i> (carbon atoms in yellow) and <i>S</i> (carbon atoms in purple) of floxacrine. Hydrogen bonds are represented by grey lines.	71
Figure 2.7. Chemical structure of the tested molecule on the left, and comparison between the predicted binding poses of WR249685 (carbon atoms in yellow) and of the new tested molecule (carbon atoms in purple) on the right.	73

Figure 2.8. Predicted binding pose of GW844520. Hydrogen bonds are represented by grey lines.	74
Figure 3.1. Predicted binding mode of TCMDC-134570 obtained with AD. Hydrogen bonds are represented by grey lines.	85
Figure 3.2. Binding free energy correlation between AD and AD Vina.	85
Figure 3.3. Overall score values obtained for TCAMS virtual screening using PDB 3CX5 and AD.	86
Figure 3.4. Predicted binding pose of TCMDC-140353 obtained with AD.	87
Figure 3.5. Chemical structures of the purchased compounds.	88
Figure 3.6. Predicted binding pose of compound 3.19 . Hydrogen bonds are represented by grey lines.	94
Figure 3.7. Expansion of the ¹ H NMR spectra of isomer B of compound 3.27 .	97
Figure 4.1. Sequence of <i>P. falciparum</i> Rieske Iron-Sulfur Protein (UniProt code Q8IL75).	111
Figure 4.2. Sequence of <i>P. falciparum</i> cytochrome <i>b</i> (UniProt code Q7HP03).	112
Figure 4.3. Superposition of Rieske ISP and cytochrome <i>b</i> of <i>S. cerevisiae</i> (in pink), <i>B. Taurus</i> (in purple), <i>G. gallus</i> (in yellow) and <i>R. shaeroides</i> (in green) on the left, and superposition of the bound stigmatellin in the active site of the respective species (the same color pattern was used for stigmatellin).	113
Figure 4.4. Interactions between stigmatellin and Q _o binding site residues in <i>S. cerevisiae</i> X-ray structure (PDB code 3CX5).	115
Figure 4.5. Cytochrome <i>b</i> and Rieske ISP on the left and Q _o binding site of yeast <i>bc</i> ₁ complex on the right with bound stigmatellin highlighting in yellow the amino acid residues that are mutated in <i>P. falciparum</i> .	117
Figure 4.6. Comparison between the position of Pro260 in the several species: <i>S. cerevisiae</i> (in pink), <i>B. Taurus</i> (in purple), <i>G. gallus</i> (in yellow) and <i>R. shaeroides</i> (in green), and the one obtained by homology modeling before and after energy minimization (in orange and grey, respectively).	119
Figure 4.7. Comparison between the position of Phe264 in the several species: <i>S. cerevisiae</i> (in pink), <i>B. Taurus</i> (in purple), <i>G. gallus</i> (in yellow) and <i>R. shaeroides</i> (in green), and the one obtained by homology modeling before and after energy minimization (in orange and grey, respectively).	120

Figure 4.8. Ramachandran plot of the modeled 3D structure of <i>P. falciparum</i> bc_1 complex Q_0 binding site obtained with PROCHECK ²⁸⁵ . The different colorated areas specify: most favored regions (in red), additional allowed regions (in yellow), generously allowed regions (in beige), and disallowed regions (in white).	121
Figure 4.9. The Q_0 bc_1 complex inhibitors used to validate the homology model.	123
Figure 4.10. Predicted binding pose for stigmatellin on the left. Hydrogen bonds are represented by grey lines. Superposition of the bound stigmatellin in the crystallographic structures of several species: <i>S. cerevisiae</i> (in pink), <i>B. Taurus</i> (in purple), <i>G. gallus</i> (in yellow) and <i>R. shaeroides</i> (in green), and the one predicted by docking calculations (in grey) on the right.	125
Figure 4.11. Predicted binding poses for WR 249685.	126
Figure 4.12. Predicted binding pose for Quinolone 1. Hydrogen bonds are represented by grey lines.	127
Figure 4.13. Chemical structures of the selected potential bc_1 complex inhibitors.	130
Figure 4.14. Predicted binding poses of compounds 4.4 (A), 4.6 (B), 4.7 (C), 4.9 (D), 4.11 (E) and 4.12 (F). Hydrogen bonds are represented by grey lines.	131
Figure 5.1. General structure of aurones.	137
Figure 5.2. Isobologram showing the relationship between the FIC_{50} s of CQ and compound 5.57 against <i>Plasmodium falciparum</i> Dd2 strain. Numbers on each plotted point correspond to the calculated CI value for the utilized combination ratio.	156
Figure 6.1. ¹ H NMR of compound 6.27 .	175
Figure 6.2. ¹ H NMR of compound 6.58 .	175
Figure 6.3. Superposition of the ¹ H NMR spectra of compound 6.30 at 25 °C (in purple), 30 °C (in blue), 50 °C (in green) and 70 °C (in red).	177
Figure 6.4. X-ray crystallographic structure of compound 6.64 .	178
Figure 6.5. Isobologram showing the relationship between the FIC_{50} s of the quinolines CQ and mefloquine and compound 6.60 against <i>Plasmodium falciparum</i> Dd2 and 3D7 strains. Numbers on each plotted point correspond to the calculated CI value for the utilized combination ratio.	186
Figure 6.6. Predicted binding poses of compounds 6.66 (A), 6.60 (B), 6.75 (C), and 6.77 (D). Hydrogen bonds are represented by grey lines.	188

List of schemes

Scheme 1.1. Mechanism of formation of hemozoin crystal as possible drug target in <i>P. falciparum</i> digestive vacuole. Adapted from Ettari <i>et al</i> ⁴⁸ .	9
Scheme 1.2. Fe(II)-mediated formation of primary or secondary carbon radicals from artemisinin. From Schlitzer <i>et al</i> ⁷ .	14
Scheme 1.3. Hydroxy-2-dodecyl-4-(1 <i>H</i>)-quinolone (HDQ) and the rational design of novel quinolones as <i>Pf</i> DHD2 inhibitors.	18
Scheme 1.4. Reaction catalysed by DHODH. Abbreviations: FMN – flavin mononucleotide; FMNH ₂ – reduced flavin mononucleotide; Q – ubiquinone; QH ₂ – ubiquinol. Adapted from Stocks <i>et al</i> ⁶⁷ .	19
Scheme 1.5. Two oxidation states of coenzyme Q: the fully reduced ubiquinol form (1.49) and the fully oxidized ubiquinone form (1.51), and the stable semi-ubiquinone intermediate (1.50).	24
Scheme 1.6. Design of ELQ-300 (1.63) based on the structure of endochin (1.57) and GW844520 (1.64).	30
Scheme 1.7. Simplified folate pathway. Adapted from Schlitzer <i>et al</i> ⁷ .	41
Scheme 3.1. Representation of the overall screening process.	88
Scheme 3.2. Retrosynthetic approach for the synthesis of compound 3.17 .	95
Scheme 3.3. Reaction conditions: (a) Diethyl ethoxymethylenemalonate, reflux; (b) Diphenyl ether, reflux.	95
Scheme 3.4. Mechanism of formation of both benzoquinolone isomers of compound 3.27 .	96
Scheme 3.5. Comparison between the resonance structures obtained for both isomers A and B of compound 3.27 .	98
Scheme 3.6. Alternative approach to obtain intermediate 3.27 .	99
Scheme 3.7. Alternative approach to obtain intermediate 3.29 .	100
Scheme 3.8. Achievement of the model compound 3.34 from the tested compound 3.17 .	100
Scheme 3.9. Synthetic procedure to obtain compound 3.34 .	101
Scheme 3.10. Alternative synthetic procedure to obtain compound 3.34 using an unsubstituted quinolone as starting material.	102
Scheme 3.11. Proposed mechanism for the synthesis of compound 3.38 .	103

Scheme 3.12. Chemical structure of the two tested quinolone derivatives and their antimalarial activity against <i>P. falciparum</i> W2 strain.	104
Scheme 4.1. Representation of the overall screening process.	128
Scheme 5.1. Reagents and conditions: (a) 5.59 or 5.60 , Al ₂ O ₃ , MeOH, reflux under N ₂ , 24 hours. (b) 5.61 , glacial AcOH, HCl (cat), RT, 4 hours. R substituents are according to Table 5.3.	144
Scheme 5.2. Reactions and conditions: (a) substituted phenol, Na ₂ CO ₃ , dry DMF, reflux, 24 hours; (b) H ₂ O ₂ (30%), KOH, MeOH, EtOH, reflux, 5 hours; (c) <i>N,O</i> -dimethylhydroxylamine, TEA, TBTU, dry DMF, RT, overnight; (d) LiAlH ₄ , dry THF, -5 °C.	145
Scheme 5.3. Reactions and conditions: (a) Pd(PPh ₃) ₂ Cl ₂ , Na ₂ CO ₃ (1M), 1,4-dioxane, 100 °C, 3 hours; (b) Pd ₂ (dba) ₃ , (<i>R</i>)-BINAP, NaO ^t Bu, dry toluene, 110 °C, 15 min, MW.	145
Scheme 5.4. Reactions and conditions: (a) aliphatic amine, formaldehyde solution, EtOH, reflux, 5 hours.	146
Scheme 6.1. General structure of aurones (left) and azaaurones.	161
Scheme 6.2. Schematic contraction of the quinolone ring to obtain 3-indolinone.	163
Scheme 6.3. Reagents and conditions: (a) BCl ₃ 1M in DCM, chloroacetonitrile, ZnCl ₂ , dry 1,2-DCE, reflux. (b) HCl 1M, reflux. (c) AcOH, Ac ₂ O. (c) NaH, dry DMF.	164
Scheme 6.4. Sugasawa reaction mechanism.	165
Scheme 6.5. Proposed reaction procedure for the synthesis of the azaaurone derivatives.	166
Scheme 6.6. Alternative reaction procedure for the synthesis of the azaaurone derivatives.	171
Scheme 6.7. Reagents and conditions: KOH (50% in H ₂ O), MeOH, RT.	171
Scheme 6.8. Proposed reaction procedure for the reduction of azaaurone derivatives.	178
Scheme 6.9. Structure-activity relationships for azaaurone derivatives.	189

List of tables

Table 2.1. Root mean square deviation (RMSD) and binding free energy (ΔG) obtained for stigmatellin in different docking experiments with neutral His181 (His181), with His181 protonated (His181 H ⁺) and with the crystallographic water near Glu272 (His181 + water).	60
Table 2.2. Docking results of the available inhibitors at different experimental conditions: with neutral His181 (His), with His181 protonated (His H ⁺) and with a crystallographic water near Glu272 (+ water). Free energies in kcal.mol ⁻¹ , K_i and IC ₅₀ in nM. Experimental values obtained by Biagini <i>et al</i> ¹³³ .	66
Table 3.1. Summary of the results obtained for 4(1 <i>H</i>)-pyridones and 4(1 <i>H</i>)-quinolones during the screening of TCAMS.	84
Table 3.2. Some physical properties and antiplasmodial activity of the purchased compounds.	90
Table 3.3. Sensitivity of cytochrome <i>bc</i> ₁ complex activity on isolated mitochondria to compounds 3.17 and 3.19 .	92
Table 3.4. Growth inhibition of wild type (Dd2) and transgenic (Dd2- γ DHODH) <i>P. falciparum</i> strains in the absence and presence of 1 μ M proguanil with different compounds.	93
Table 3.5. Activity against CQ-resistant strain W2 and atovaquone-resistant strain FCR3 of <i>P. falciparum</i> , and <i>S. cerevisiae</i> .	93
Table 4.1. Protein sequences of Rieske ISP and cytochrome <i>b</i> for the several species and summary of the crystal structures used as templates.	112
Table 4.2. Identity between species in Rieske ISP (complete protein sequence) for <i>Pf</i> (<i>P. falciparum</i>), <i>Sc</i> (<i>S. cerevisiae</i>), <i>Bt</i> (<i>B. Taurus</i>), <i>Gg</i> (<i>G. gallus</i>), <i>Rs</i> (<i>R. sphaeroides</i>) and <i>Hs</i> (<i>H. sapiens</i>). Values obtained from Uniprot ²⁴⁹ .	114
Table 4.3. Identity between species in cytochrome <i>b</i> (complete protein sequence) for <i>Pf</i> (<i>P. falciparum</i>), <i>Sc</i> (<i>S. cerevisiae</i>), <i>Bt</i> (<i>B. Taurus</i>), <i>Gg</i> (<i>G. gallus</i>), <i>Rs</i> (<i>R. sphaeroides</i>) and <i>Hs</i> (<i>H. sapiens</i>). Values obtained from Uniprot ²⁴⁹ .	114
Table 4.4. Identity between species in Q _o binding site.	116
Table 4.5. Docking results for the tested inhibitors. Free energies in kcal/mol, K_i and IC ₅₀ in units of nM. Experimental values obtained from Cowley <i>et al</i> ¹⁰⁵ (for Quinolone 1) and Biagini <i>et al</i> ¹³³ (for the other compounds). Docking calculations performed with His181 in its neutral state.	124
Table 4.6. Some physical properties and score of the selected compounds. cLogP values obtained from ALOGPS 2.1 ²⁶³ .	129

Table 5.1. Structure and <i>in vitro</i> antimalarial activity of selected naturally occurring aurones ²⁹⁶ .	138
Table 5.2. Structure and <i>in vitro</i> antimalarial activity of synthetic aurone derivatives ²⁹⁸ .	139
Table 5.3. Structure, clog <i>P</i> values, Lipinski rule of 5 violations, and yields for the synthesis (final step) of aurones 5.24-5.58 .	141
Table 5.4. Antiplasmodial activity (IC ₅₀) against the CQ-resistant <i>Plasmodium falciparum</i> W2 strain, cytotoxicity (EC ₅₀) against Human Embryonic Kidney 293T cells and selectivity index (SI = EC ₅₀ /IC ₅₀) for aurones 5.24-5.58 .	149
Table 5.5. Physicochemical parameters for chosen compounds. cLog <i>P</i> values were calculated using AlogPS 2.1 software from Virtual Computational Chemistry Laboratory ²⁶³ . pKa values were obtained from SPARC software ³²⁰ , except when indicated. Values of log <i>D</i> , VAR and LAR were calculated using the equations available in ref 319.	153
Table 5.6. Antiplasmodial activity (IC ₅₀) against the CQ-resistant (W2) and mefloquine and CQ resistant (Dd2) <i>P. falciparum</i> strains.	155
Table 6.1. Structure and <i>in vitro</i> antimalarial activity of published azaaurone derivatives ²⁹⁸ .	162
Table 6.2. Structure, clog <i>P</i> values, Lipinski rule of 5 violations, and yields for the synthesis (final step) of acetylated azaaurones 6.25-6.55 .	167
Table 6.3. Reactions conditions for aldol condensation to obtain azaaurone derivatives.	169
Table 6.4. Structure, clog <i>P</i> values, Lipinski rule of 5 violations, and yields for the synthesis (final step) of azaaurones 6.56-6.86 .	172
Table 6.5. Reactions conditions for the reduction of azaaurone derivatives.	179
Table 6.6. Antiplasmodial activity (IC ₅₀) against the CQ-resistant <i>Plasmodium falciparum</i> W2 strain, cytotoxicity (EC ₅₀) against Human Embryonic Kidney 293T cells and selectivity index (SI = EC ₅₀ /IC ₅₀) for azaaurones 6.25-6.55 (Series A-E).	181
Table 6.7. Antiplasmodial activity (IC ₅₀) against the CQ-resistant <i>Plasmodium falciparum</i> W2 strain, cytotoxicity (EC ₅₀) against Human Embryonic Kidney 293T cells and selectivity index (SI = EC ₅₀ /IC ₅₀) for azaaurones 6.56-6.86 (Series F-J).	182
Table 6.8. Antiplasmodial activity (IC ₅₀) against the CQ-resistant (W2), mefloquine (MEF) and CQ resistant (Dd2) and sensitive (3D7) <i>P. falciparum</i> strains.	185

List of abbreviations and symbology

ABC	ATP-binding Cassette
ACT	Artemisinin-based Combination Therapy
AD	AutoDock 4.0
ADME	Absorption, Distribution, Metabolism and Excretion
AD Vina	AutoDock Vina
ATP	Adenosine Triphosphate
br	Broad
(<i>R</i>)-BINAP	(<i>R</i>)-(+)-(1,1'-Binaphthalene-2,2'-diyl)bis(diphenylphosphine)
<i>Bt</i>	<i>Bos taurus</i>
CI	Combination Index
CoMFA	Comparative Molecular Field Analysis
CoMSIA	Comparative Molecular Similarity Indices Analysis
CQ	Chloroquine
d	Doublet
DCE	Dichloroethane
dd	Doublet of Doublets
ddd	Doublet of Doublet of Doublets
DFT	Density Functional Theory
DHFR	Dihydrofolate Reductase
DHODH	Dihydroorotate Dehydrogenase
DHPS	Dihydropteroate Synthase
DMAPP	Dimethylallylpyrophosphate
DMF	<i>N,N</i> -Dimethylformamide
DNA	Deoxyribonucleic Acid
DPAP1	Dipeptidyl Amino Peptidase 1
dTMP	Deoxythymidinemonophosphate
DV	Digestive Vacuole
EtOAc	Ethyl Acetate
EtOH	Ethanol
FabG	β -ketoacyl-ACP-reductase
FabI or ENR	enoyl-ACP-reductase
FabZ	β -hydroxyacyl-ACP-dehydratase

<i>Gg</i>	<i>Gallus gallus</i>
GSK	GlaxoSmithKline
HDQ	Hydroxy-2-dodecyl-4-(1 <i>H</i>)-quinolone
HTS	High-Throughput Screening
<i>Hs</i>	<i>Homo sapiens</i>
IPP	Isopentenyl Pyrophosphate
ISP	Iron-Sulfur Protein
<i>J</i>	Coupling Constant
LAR	Lipid Accumulation Ratio
<i>m</i>	Multiplet
MAO	Monoamine Oxidase
MeOH	Methanol
mETC	Mitochondrial Electron Transport Chain
MDR	Multidrug Resistance
MEF	Mefloquine
<i>mp</i>	Melting Point
MOE	Molecular Operating Environment
MQO	Malate Quinone Oxidoreductase
MW	Microwaves
NADH	Nicotinamide Adenine Dinucleotide
NDH2	NADH:ubiquinone Oxidoreductase
NMR	Nuclear Magnetic Resonance
NPP	New Permeability Pathways
<i>Pb</i>	<i>Plasmodium berghei</i>
PDB	Protein Data Bank
<i>Pf</i>	<i>Plasmodium falciparum</i>
Q _i	Quinone Reduction Site
Q _o	Quinol Oxidation Site
QSAR	Quantitative Structure-Activity Relationship
RMSD	Root Mean Square Deviation
RNA	Ribonucleic Acid
<i>Rs</i>	<i>Rhodobacter sphaeroides</i>
RT	Room Temperature
<i>s</i>	Singlet

SAR	Structure-Activity Relationship
SDH	Succinate:ubiquinone Oxidoreductase
<i>Sc</i>	<i>Saccharomyces cerevisiae</i>
SI	Selectivity Index
t	Triplet
TBTU	<i>N,N,N',N'</i> -Tetramethyl- <i>O</i> -(benzotriazol-1-yl)uronium tetrafluoroborate
TCAMS	Tres Cantos Antimalarial Set
TEA	Triethylamine
TES	Triethylsilane
TFA	Trifluoroacetic Acid
THF	Tetrahydrofuran
TLC	Thin Layer Chromatography
VAR	Vacuolar Accumulation Ratio
VS	Virtual Screening
WHO	World Health Organization

Malaria remains a critical global health problem, with terrible social and economic consequences in countries where this disease is endemic. The problem is exacerbated by the emergence and spread of parasites that are resistant to well-established antimalarial drugs. As a result, there is an urgent need for novel drugs, preferably acting on under exploited parasite targets in order to overcome clinical resistance.

Cytochrome bc_1 complex is a crucial element in the mitochondrial respiratory chain, being indispensable for the survival of several species of *Plasmodia* that cause malaria and, therefore, it is a promising target for antimalarial drug development. Moreover, in the absence of a crystal structure for the *P. falciparum* bc_1 complex, key structural and mechanistic information has been inferred from analogous mammalian, bacterial and yeast bc_1 systems.

In the present work, a molecular docking study based on the most recently obtained X-ray structure of the *Saccharomyces cerevisiae* bc_1 complex (PDB code: 3CX5) and using several reported inhibitors with experimentally determined IC_{50} values against the *Plasmodium falciparum* bc_1 complex is presented. This Q_o model was also used to search the drug-like database included in the MOE package for novel potential bc_1 complex inhibitors allowing to obtain five compounds with demonstrated activity against the chloroquine-resistant W2 strain of *P. falciparum*. Moreover, the most active compounds were also active against the atovaquone-resistant *P. falciparum* FCR3 strain and *S.cerevisiae*.

Furthermore, considering that a reliable three-dimensional structure of this *Pf* enzymatic complex is essential for successful drug design and having in mind the increasing interest in obtaining potential antimalarial drugs that can act in this target, a homology model of cytochrome bc_1 Q_o binding site was further developed based on yeast crystallographic structure.

Additionally, a library containing several structurally diverse aurone and azaaurone derivatives were also synthesized and tested for their antimalarial activity. The aurone derivatives synthesized showed to be moderate active with IC_{50} values in the low

micromolar range while the azaaurone analogues presented much higher potency with some compounds being active in the nanomolar range. Despite the mechanism of action of these two classes of compounds is still not very clear, this study highlights the usefulness of aurones and azaaurones to be derivatized in order to rapidly deliver lead compounds for further optimization and also the potential of these two scaffolds as promising antimalarial compounds.

Keywords: Malaria, *Plasmodium falciparum*, bc_1 complex, molecular docking, virtual screening, aurones, azaaurones.

A malária continua a ser um grave problema de saúde, com enormes consequências sociais e económicas que afectam os países onde esta doença é endémica. Este problema tem vindo a crescer devido ao agravamento do aparecimento de parasitas resistentes aos fármacos antimaláricos disponíveis. Apesar da importância geral desta doença, o desenvolvimento de novos fármacos tem sido negligenciado pela indústria farmacêutica nos países industrializados. Deste modo, existe uma necessidade urgente de obter novos fármacos, de preferência que actuem em alvos menos explorados, de modo a se poder superar todos os problemas relacionados com a resistência.

Nos últimos anos o esforço para desenvolver novos fármacos tem vindo a aumentar sendo que várias parcerias entre a indústria e a academia têm mesmo sido formadas. Esta união de esforços permite não só expandir o conhecimento existente acerca de fármacos antimaláricos mas também potenciar o progresso na obtenção de novos fármacos.

Devido à complexidade do ciclo de vida do parasita, vários alvos têm sido utilizados nos últimos tempos de modo a permitir desenvolver um fármaco que seja eficiente e selectivo para o parasita. Um desses alvos é a cadeia de transporte electrónico que inclui o citocromo bc_1 . O citocromo bc_1 é um elemento crucial para o correcto funcionamento da cadeia de transporte electrónico do parasita. Sendo essencial para a sobrevivência do parasita responsável pela malária, este pode ser considerado um alvo promissor para o desenvolvimento de fármacos antimaláricos. Na ausência de uma estrutura cristalográfica do citocromo bc_1 do *P. falciparum*, toda a informação acerca da sua estrutura e do seu mecanismo tem sido obtida através de estudos desenvolvidos nos seus análogos provenientes de mamíferos, bactérias e leveduras.

Neste projecto desenvolveu-se inicialmente um estudo de *docking* molecular com base na estrutura cristalográfica do citocromo bc_1 da levedura *Saccharomyces cerevisiae* (PDB 3CX5) e utilizando vários inibidores conhecidos com valores de IC_{50} determinados experimentalmente. Tal permitiu analisar a possibilidade de a estrutura cristalográfica da levedura poder ser utilizada como um bom modelo para o *P. falciparum*. Mais

importante, permitiu também compreender o modo de interacção dos inibidores seleccionados com o centro activo Q_o e prever o potencial inibitório destas moléculas.

Este modelo foi posteriormente utilizado para se proceder a um estudo de *screening* virtual utilizando a biblioteca de compostos incluída no programa MOE. Este estudo permitiu obter cinco compostos com actividade antimalárica contra a estirpe W2 resistente à cloroquina. Os compostos mais activos demonstraram também actividade contra a estirpe resistente à atovaquona e contra a levedura. Infelizmente, os estudos biológicos feitos especificamente na cadeia de transporte electrónico não permitiram comprovar que estes compostos actuam definitivamente neste alvo.

Tendo em conta a importância de se ter uma estrutura tridimensional adequada para se poder desenhar novos inibidores e considerando o crescente interesse neste alvo, procedeu-se ao desenvolvimento de um modelo por homologia do sítio activo Q_o do citocromo bc_1 do *P. falciparum* com base numa estrutura cristalográfica conhecida. Para tal, procedeu-se a um estudo inicial das estruturas cristalográficas deste alvo disponíveis de várias espécies e fez-se a uma comparação exaustiva de modo a seleccionar o melhor modelo. A *S. cerevisiae* foi a espécie escolhida devido ao grau de homologia entre as duas estruturas homólogas e a resolução da sua estrutura cristalográfica. O modelo por homologia foi desenvolvido utilizando as ferramentas disponíveis no MOE e foi validado utilizando técnicas de *docking* e *screening* virtual. Este estudo de *screening* foi efectuado com base na mesma biblioteca de compostos utilizada anteriormente e permitiu identificar novas moléculas com estruturas químicas bastante interessantes e com potencial para actuar neste alvo. Os dados biológicos destas moléculas não estão ainda disponíveis não permitindo definitivamente validar este modelo por homologia como o modelo mais correcto da estrutura cristalográfica do sítio activo Q_o do citocromo bc_1 do *P. falciparum*. Apesar disso, foi feito um enorme avanço em termos de obter uma estrutura tridimensional mais fidedigna deste alvo o que será útil para desenvolver novos inibidores selectivos para o citocromo bc_1 .

Na segunda parte deste trabalho, uma biblioteca de compostos contendo diversos derivados de auronas e azaauronas foi também sintetizada e testada para avaliar a sua actividade antimalárica. As auronas são produtos naturais com actividade antiparasitária já reconhecida. Estes compostos foram primeiramente sintetizados com o objectivo inicial

de obter estruturas quimicamente diversas e mais complexas de modo a permitir reconhecer que tipo de alterações permite aumentar o seu potencial antimalárico. Deste modo foram sintetizados vários compostos recorrendo a reacções de acoplamento catalisadas por paládio, como as reacções de Suzuki e Buchwald, devido à facilidade de aumentar rapidamente uma biblioteca de compostos utilizando estes procedimentos. Foram também sintetizados alguns derivados por introdução de uma amina alifática no anel A da aurona de modo a obter bases de Mannich. As moléculas sintetizadas mostraram actividade moderada contra o *P. falciparum* com valores de IC₅₀ na ordem dos micromolar. Foram feitos ainda vários estudos biológicos com o objectivo de se identificar o modo de acção desta classe de compostos mas tal não foi possível. Novos estudos terão ainda que ser feitos.

Os derivados de azaauronas foram obtidos de um modo semelhante ao utilizado para os derivados de auronas. Contudo, neste caso, foi necessário utilizar um método de síntese convergente de modo a se obter os compostos mais eficientemente. Tal deveu-se a problemas associados ao facto de a síntese destes compostos ser mais complexa e menos eficiente que a síntese dos derivados de auronas o que levou não só a uma diminuição do rendimento das reacções mas também a um aumento considerável de produtos secundários e, conseqüentemente, a um acréscimo na dificuldade em isolar os produtos. Ao contrário dos derivados de auronas, estes novos compostos demonstraram ser bastante mais activos que os seus análogos com valores de IC₅₀ na ordem dos nanomolar. Mais ainda, estes compostos apresentam também citotoxicidade negligenciável. Dado que estes compostos contêm um aceitador de Michael na sua estrutura, foram testados contra a falcipaina-2, uma protease muito importante para a degradação de hemoglobina no vacúolo digestivo do parasita e essencial para a sua sobrevivência. Infelizmente os resultados obtidos indicam que este não é o alvo desta classe de compostos dado que apenas três apresentaram baixo poder inibitório na ordem dos 10 µM. Foi feito ainda um estudo de sinergismo na presença de cloroquina e mefloquina que permitiu demonstrar o potencial sinérgico desta classe de potenciais antimaláricos. Mais ainda, a semelhança estrutural destes compostos com as quinolonas, reconhecidos inibidores do citocromo *bc₁*, e os estudos de *docking* efectuados com base no modelo por homologia desenvolvido anteriormente permite sugerir que seja este o

alvo desta classe de compostos. Contudo, estudos biológicos adicionais serão necessários para identificar o modo de acção dos derivados de azaauronas.

Finalmente, apesar de o modo de acção destas duas classes de compostos não estar ainda completamente identificado, o estudo desenvolvido demonstra que tanto as auronas como as azaauronas podem ser derivatizadas de modo a se obter novos compostos mais activos. Mais ainda, estas duas classes de compostos podem ser consideradas promissoras no desenvolvimento de fármacos antimaláricos.

O estudo desenvolvido pode ser então considerado um passo importante não só na caracterização de um importante alvo terapêutico para a malária mas também na identificação de novas classes de compostos com potencial para ser posteriormente optimizadas de modo a obter novos fármacos antimaláricos com actividade relevante.

Palavras-chave: Malária, *Plasmodium falciparum*, citocromo *bc*₁, *docking* molecular, *screening* virtual, auronas, azaauronas.

Malaria is responsible for causing an estimated 200 million clinical cases and more than 500 000 deaths annually¹ being drug resistance to currently established antimalarial drugs such as chloroquine (CQ) a major problem of concern. Therefore, novel and innovative inhibitors active against *Plasmodium falciparum*, which produces the most aggressive form of malaria, are urgently required to develop new treatments able to fight malaria².

Nowadays, there is an increased concern related with this infection since no new drugs have been approved in the last 15 years and an efficient vaccine is still not available. Fortunately, this situation led to an encouragement of both academia and pharmaceutical companies to actively take an effort in order to develop new antimalarial drugs that are able to hinder this disease³.

However, in spite of all efforts, all the numbers related with this disease are still high and surely not acceptable when considering the target expected for 2015 (Figure 1).

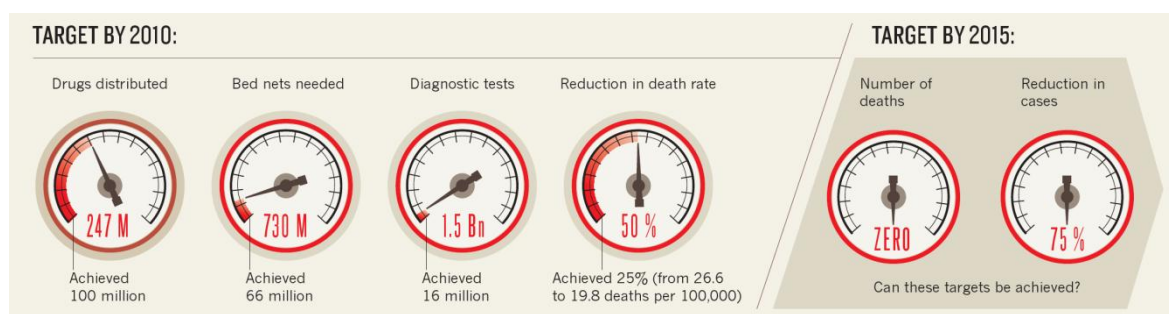


Figure 1. Malaria numbers: targets achieved by 2010 and targets aspired to achieve by 2015. From Shetty *et al.*⁴.

Several factors can be responsible for contributing for malaria burden including political, social and economic aspects. Moreover, all issues related with the vector control, and consequently transmission, the widespread of parasite resistance to existent antimalarial drugs and the lack of an efficient vaccine to prevent infection are surely some of the main reasons responsible for the failing in achieving these goals.

This project focused mainly in obtaining new potential antimalarial drugs using straightforward chemical procedures that could conduct to the development of economically affordable antimalarial drugs acting in the mitochondrial electron transport chain (mETC), particularly in the bc_1 complex. The electron transport chain in malaria parasites was first recognized as an attractive drug target since the development and clinical use of atovaquone in 1992⁵. To achieve this goal, the work was developed using two diverse but complementary approaches in medicinal chemistry: the synthesis of novel compounds in parallel with the application of computed-aided drug design tools. In this way, new compounds could be synthesized in order to be tested for their antimalarial potential and, in the same time, new scaffolds could be developed using, for instance, virtual screening and docking procedures. The junction of these two techniques can be considered extremely significant to successfully achieve the goals proposed for this project.

CHAPTER ONE

List of contents

1.1. Malaria – An overview	1
1.2. Lyfe cycle of malaria parasite	3
1.3. Antimalarial chemotherapy during erythrocytic stage	5
1.4. Antimalarial chemotherapy during liver stage	44
1.5. Antimalarial drug resistance and artemisinin-based combination therapies	45
1.6. Computational approaches in antimalarial drug discovery	47
1.7. Concluding remarks	50

1. Introduction

1.1. Malaria – An overview

Malaria has always been one of the most important causes of death of populations throughout the tropics for thousands of years. Besides the important advances in order to understand this disease and develop new drugs in the past years, it continues to be one of the greatest causes of serious sickness and death in the world. More specifically, this disease is responsible for infecting around 200 million people each year resulting in an estimated 500 000 – 900 000 deaths^{1, 6} (Figure 1.1). In accordance with the latest WHO data from 2010, about 90% of all malaria deaths occur in Africa being predominant in young children and pregnant women¹. This disease has a broad distribution in both the subtropics and tropics. More specifically, the countries of sub-Saharan Africa comprise the majority of all malaria cases while the remnant is mostly concentrated in India, Brazil, Afghanistan, Sri Lanka, Thailand, Indonesia, Vietnam, Cambodia, and China¹.

Malaria infection is caused by protozoal parasites of the genus *Plasmodium*. From more than 100 *Plasmodium* species that are identified, five are the most virulent in humans and can cause different disease patterns. Included in those species are *P. vivax*, *P. ovale*, *P. falciparum*, *P. malariae*⁷, and, more recently discovered, *P. knowlesi*⁸.

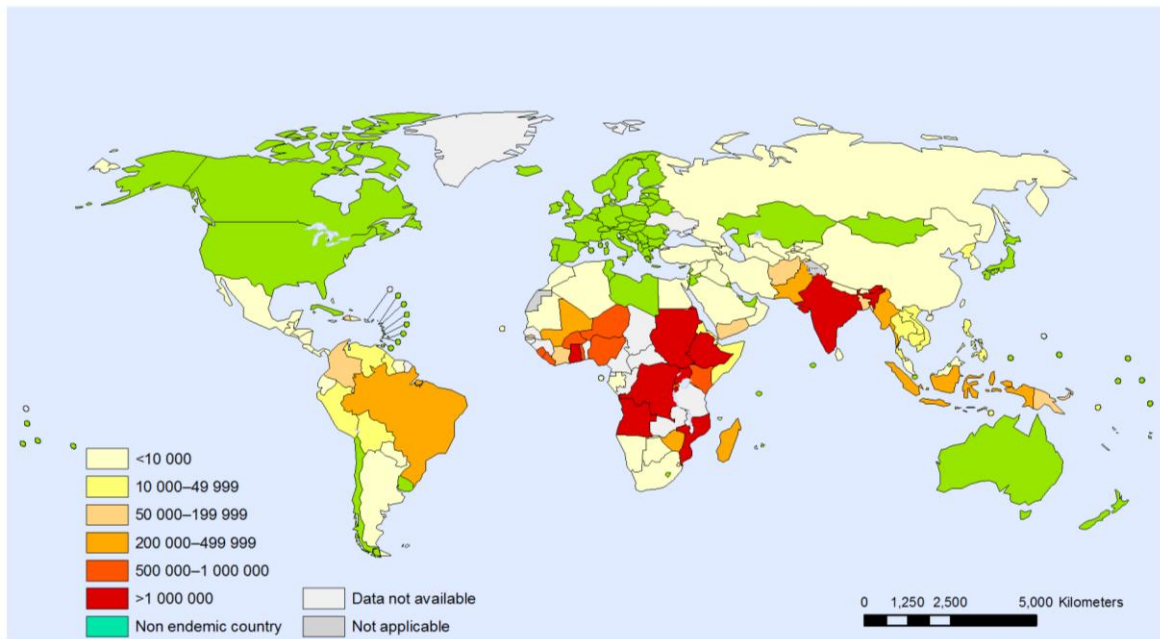


Figure 1.1. Number of malaria confirmed cases in 2010¹.

These *Plasmodia* species differ essentially in their morphology and immunology, their geographical distribution and, more important, in their relapse patterns and drug responses⁹. In spite of the infections caused by *P. falciparum* are the most severe form of the disease being responsible for almost all the fatal cases, particularly in young children and pregnant women¹⁰⁻¹¹, *P. vivax* also contributes significantly to the overall morbidity¹²⁻¹³. *P. falciparum* specie is also crucial in the alarming development of resistance to antimalarial drugs¹⁴. The emergence and spread of drug resistance in this specie is one of the most important factors demoralizing malaria control programs in most of the malaria endemic areas. Considering the present situation where not only the drug resistance is widely spread but also the mosquito vectors are insecticide-resistant¹⁵ and an effective vaccine is still not available¹⁶⁻¹⁷, chemotherapy and chemoprophylaxis remains the main approach to fight malaria infections. In this way, there is an urgent need for novel drugs, preferably acting on underexploited parasite targets in order to overcome clinical resistance and help to solve such public health problem^{14, 18}.

1.2. Life cycle of malaria parasite

Malaria infections is primarily transmitted through the salivary glands of infected female *Anopheles* mosquitoes that bite humans. The life cycle of malaria parasites is particularly complex and starts when sporozoites enter into the bloodstream (Figure 1.2). It can be divided in several stages that include, specifically, the tissue and the erythrocytic or blood schizony, both in the human host, and the sexual phase in the mosquito. Additionally, it is during the blood-stage that the symptoms of the disease appear due to repeated lysis and invasion of the erythrocytes. More specifically, in the first step of the life cycle of parasites, during the blood extraction, the mosquito injects saliva into the skin lesion transferring about 15-20 sporozoites into the blood human stream ①. In minutes, the sporozoites that are circulating in the blood stream, invade liver cells where they are able to hide themselves from the host's immune system ②. Once in the liver, they develop into exoerythrocytic schizonts, containing 10 000 - 30 000 merozoites ③¹⁹. After one or two weeks, the schizont membrane suffers rupture and the merozoites are released into the blood stream ④. Afterward, the erythrocytic phase of the parasite's life cycle takes place ⑤.

P. vivax and *P. ovale* have a dormant stage where the sporozoites may turn into hypnozoites ⑥, remaining in the liver for long time before the development of exoerythrocytic schizogony. Parasites of these two species can re-emerge later beginning a blood-infection and, consequently, causing relapses months or even years after the initial infection. In the life cycle of *P. falciparum* and *P. malariae* there is an absence of this liver persistent phase^{7, 19}.

After their release into the blood stream, merozoites are once more able to hide from the host's immune system by invading erythrocytes. Here, the parasite develops from a ring stage into a blood schizont via a trophozoite stage ⑦. After some time, dependent of each *Plasmodium* species, the erythrocyte ruptures and 16 to 32 new merozoites are released. These new merozoites, in turn, invade more erythrocytes and a new erythrocytic cycle begins. The release of merozoites is responsible for increasing infection and, consequently, causing the clinical manifestation of the disease. This asexual

cycle can persevere for an indefinite period if the treatment is not adequate¹⁷. After a certain number of asexual life cycles, some merozoites undergo transformation into sexual forms, the gametocytes ③, which can be transferred to another mosquito during its blood meal. This process is still not well understood²⁰, however, it is suggested that secreted parasite factors induce this differentiation²¹⁻²². After the ingestion of gametocytes by the mosquito during the blood meal, they suffer sexual reproduction within the midgut and thousands of infective sporozoites are produced ⑨. The sporozoites are now able to migrate to the salivary gland where they are ready to infect the next host^{7, 23}. Therefore, when an infected *Anopheles* mosquito bites another human during its blood meal, this life cycle is able to start once again.

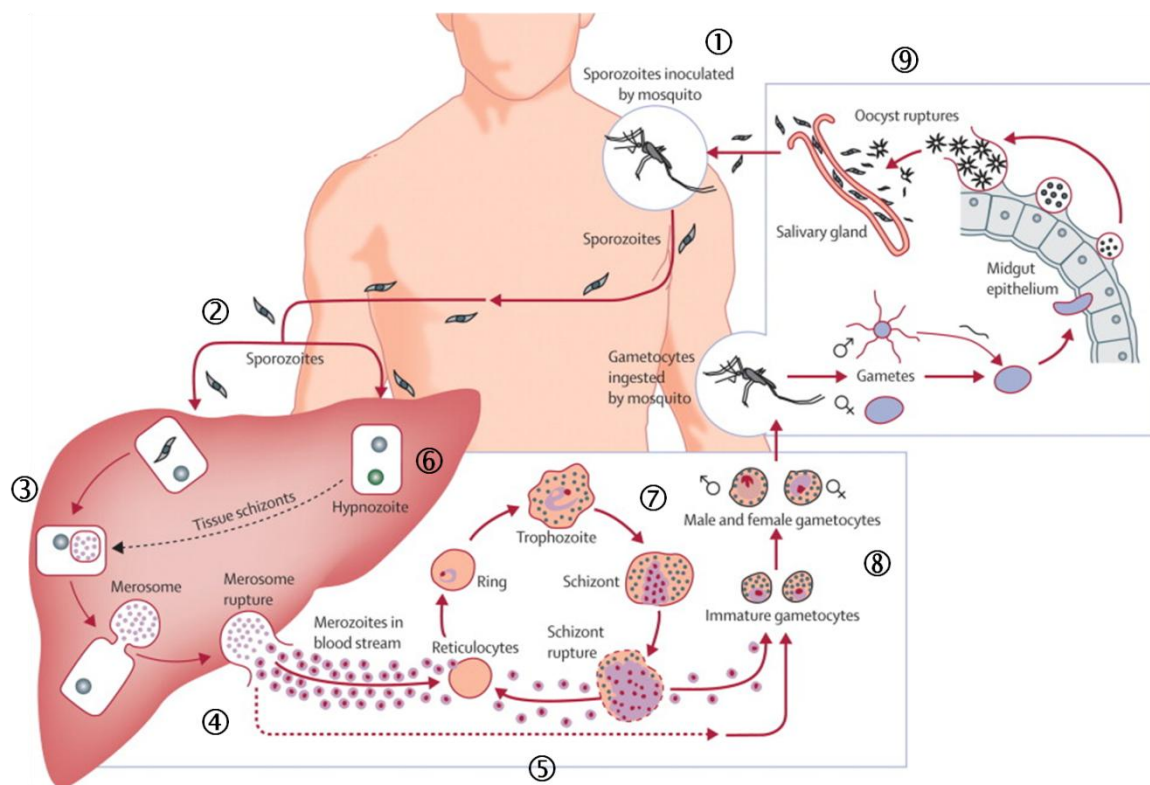


Figure 1.2. The life cycle of malaria parasites. Adapted from Mueller *et al*¹³.

Due to the different stages of the parasite life cycle (Figure 1.2), specific drugs targeting those stages, can be developed. Therefore, blood schizontocides act during the

asexual intraerythrocytic stages whilst tissue schizonticides kill parasites in the liver stage preventing the invasion of erythrocytes. As a result, it can be considered that tissue schizonticides act as a prophylactic drug. Hypnozoiticides can be used in the case of *P. vivax* and *P. ovale* since both species undergo persistent intrahepatic stages. For the sexual forms of the parasites, gametocytocides can be used. This kind of drug is able not only to destroy intraerythrocytic sexual forms but also to prevent transmission from human to mosquito. Moreover, since *P. falciparum* does not have a dormant liver stage, blood schizonticidal drugs are adequate to cure the infection caused by this species. In another way, for infections due to *P. vivax* and *P. ovale*, a combination between blood and tissue schizonticidal drugs is essential^{7, 24}.

1.3. Antimalarial chemotherapy during erythrocytic stage

The erythrocytic stage of *P. falciparum*'s life cycle involves a huge amplification of the parasite population through periodic cycles of invasion, growth, division, and egress from erythrocytes, *i.e.*, escape of mature malaria parasites from host red blood cells (Figure 1.2). In this way, the comprehension of all the biological mechanisms involved in this stage is essential to successfully develop new compounds. To achieve this goal, the sequencing of the *P. falciparum* genome was crucial²⁵. The malaria parasite is able to offer several possible drug targets associated with its variety of organelles. More specifically, during the erythrocytic stage, targets like cytosol, apicoplast, mitochondrion, membrane and the digestive vacuole (DV) can be considered (Figure 1.3).

Usually, essential surviving processes to the parasite can be regarded as valuable targets. Some examples of antimalarial drugs targeting specific parasite's organelles will be described.

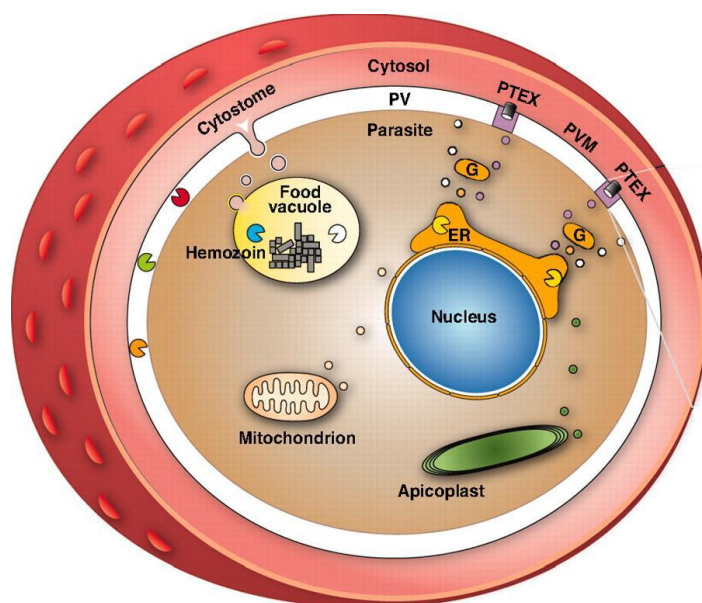


Figure 1.3. Potential drug targets of asexual erythrocytic stage. Adapted from Kappe *et al*²⁶.

1.3.1. Targeting parasite membrane biosynthesis

The amount of lipid in infected erythrocytes is considerably higher than in healthy cells since the intraerythrocytic parasite contains different type of membranes. Moreover, growing and dividing parasites need a large amount of phospholipids. In this way, the phospholipid metabolism can be considered an effective target for antimalarial drugs not only due to its specificity but also because of its importance for parasite growth²⁷⁻²⁹. Phosphatidylcholine is the major parasite phospholipid, constituting around 50% of the total phospholipids of infected erythrocyte, and is obtained by *de novo* synthesis from choline²⁸. Therefore, molecules targeting the parasite's supply of choline can be considered potential antimalarial drugs. Usually, quaternary ammonium and bis-ammonium quaternary salts containing one long lipophilic alkyl chain demonstrated high *in vitro* parasite inhibitory activity and significant *in vivo* effectiveness^{27, 29}. G25 (**1.1**, Figure 1.4) is an important member of this group showing an IC₅₀ value against *P. falciparum* of 0.64 nM and low toxicity²⁷. Moreover, a low dose of this antimalarial drug could also cure infected monkeys³⁰. Albitiazolium (**1.2**, Figure 1.4) is another example of a compound that inhibits the transport of choline into the parasite blocking the synthesis of phosphatidylcholine. This compound reached Phase II clinical trials³¹ but it lacked in its

oral bioavailability³² leading to its removal from trials. Due to the importance of having an oral antimalarial drug, attempts were made not only to obtain an orally bioavailable pro-drug of albitiazolium (**1.2**)³³⁻³⁴ but also to increase the wide-ranging bioavailability of this class of drugs³⁵⁻³⁷.

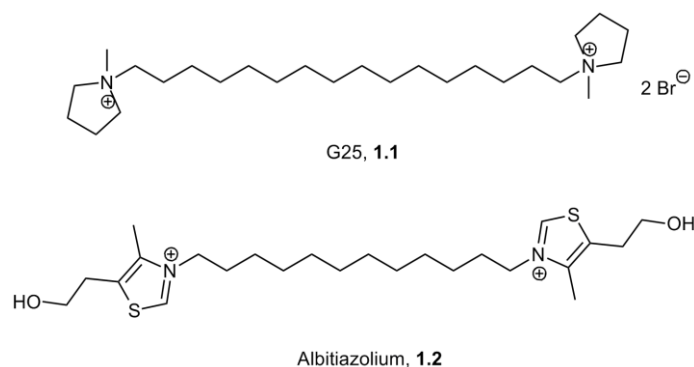
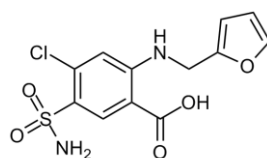


Figure 1.4. Chemical structure of two inhibitors of phospholipid biosynthesis.

1.3.2. Targeting parasite transporters

The transport pathways along the parasite membrane are other important target for antimalarial drugs³⁸. This type of targets is of extreme importance since they are unique for malaria parasite showing significantly differences from other transporters in host cells. More specifically, during the asexual reproductive phase, the permeability of the host erythrocytes' plasma membrane increases in order to permit the movement of different solutes including sugars, amino acids, nucleosides and inorganic ions that are essential for parasite's survival³⁹. The induction of new permeability pathways (NPP) by the internal parasite is responsible for this occurrence. Moreover, several of these transporters are also related with the resistance to established antimalarial drugs like chloroquine (CQ)⁴⁰⁻⁴¹. In this way, the antimalarial potential of these drug targets can be exploited not only by inhibiting the transport of essential nutrients but also by designing cytotoxic drugs that selectively enter the parasite through these transporters³⁸. A number of inhibitors of the NPP have already been identified. Furosemide (Figure 1.5, **1.3**) and their analogues are examples of compounds inhibiting the activity of these targets in the submicromolar

range. Unfortunately, although there is a significant interest in NPP as a potential antimalarial target, the majority of the compounds tested lack potency and/or specificity³⁸⁻³⁹.



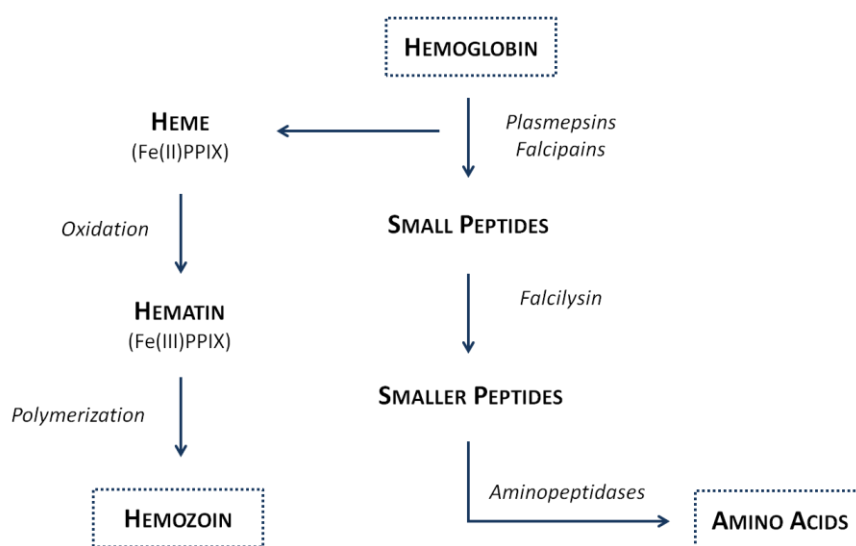
Furosemide, 1.3

Figure 1.5. Chemical structure of furosemide (1.3), an inhibitor of new permeability pathways.

1.3.3. Targeting digestive vacuole

One of the most important targets for antimalarial drugs is the acidic parasite digestive vacuole (DV). The major function of this organelle is to degrade the host red cell hemoglobin providing amino acids to the parasite⁴²⁻⁴³. All this process is attributable to a complex machinery that includes a variety of proteases that degrade the host hemoglobin in order to obtain free amino acids that can be further incorporated into newly synthesized proteins. More specifically, several aspartic endopeptidases (plasmepsins), three different cysteine endopeptidases (falcipains), the metalloprotease falcilysin, and aminopeptidases are essential for this process (Scheme 1.1)⁴⁴. However, the considerable degradation of hemoglobin also induces the formation of large quantity of heme which is toxic to the parasite due to induced oxidative stress. Therefore, the high accumulation of heme within the DV is responsible for causing the parasite death⁴⁵⁻⁴⁶. To overcome these possible toxic effects, heme is polymerized into insoluble hemozoin pigment by a biomineralization process (Scheme 1.1)⁴⁷.

As a result, antimalarial drugs can act in DV either by inhibiting the proteases function, preventing hemoglobin hydrolyses, or by blocking hemozoin formation, leading to the accumulation of toxic heme.



Scheme 1.1. Mechanism of formation of hemozoin crystal as possible drug target in *P. falciparum* digestive vacuole. Adapted from Ettari *et al*⁴⁸.

- Inhibition of parasite proteases

Several studies suggest that proteases involved in hemoglobin degradation within the DV are crucial for the parasite growth and, therefore, for its survival. The importance of these enzymes relies in the fact that the malaria parasite has a restricted ability for *de novo* biosynthesis of the amino acids that are required to synthesize its own proteins⁴³. In this way, host amino acids are essential for parasite survival. The protease cascade is described in Scheme 1.1. These enzymes work in a semi-ordered pathway⁴⁹, with aspartyl proteases (plasmepsins) being the first to be involved in this pathway by contributing for the initial cleavage of the hemoglobin. Then, successive degradation to obtain small peptides is obtained first by cysteine proteases, namely falcipains, and after both by the metalloprotease falcilysin and dipeptidyl amino peptidase 1 (DPAP1). The small peptides are then transported from the DV to the cytoplasm of the intraerythrocytic parasite where are finally degraded into amino acids by aminopeptidases⁴⁴. In this way, it is expected that this cluster of enzymes can be considered of extreme interest for the design and development of antimalarial drugs. Figure 1.6 summarizes some examples of peptidic- and non-peptidic based inhibitors of these proteases⁵⁰⁻⁵⁶.

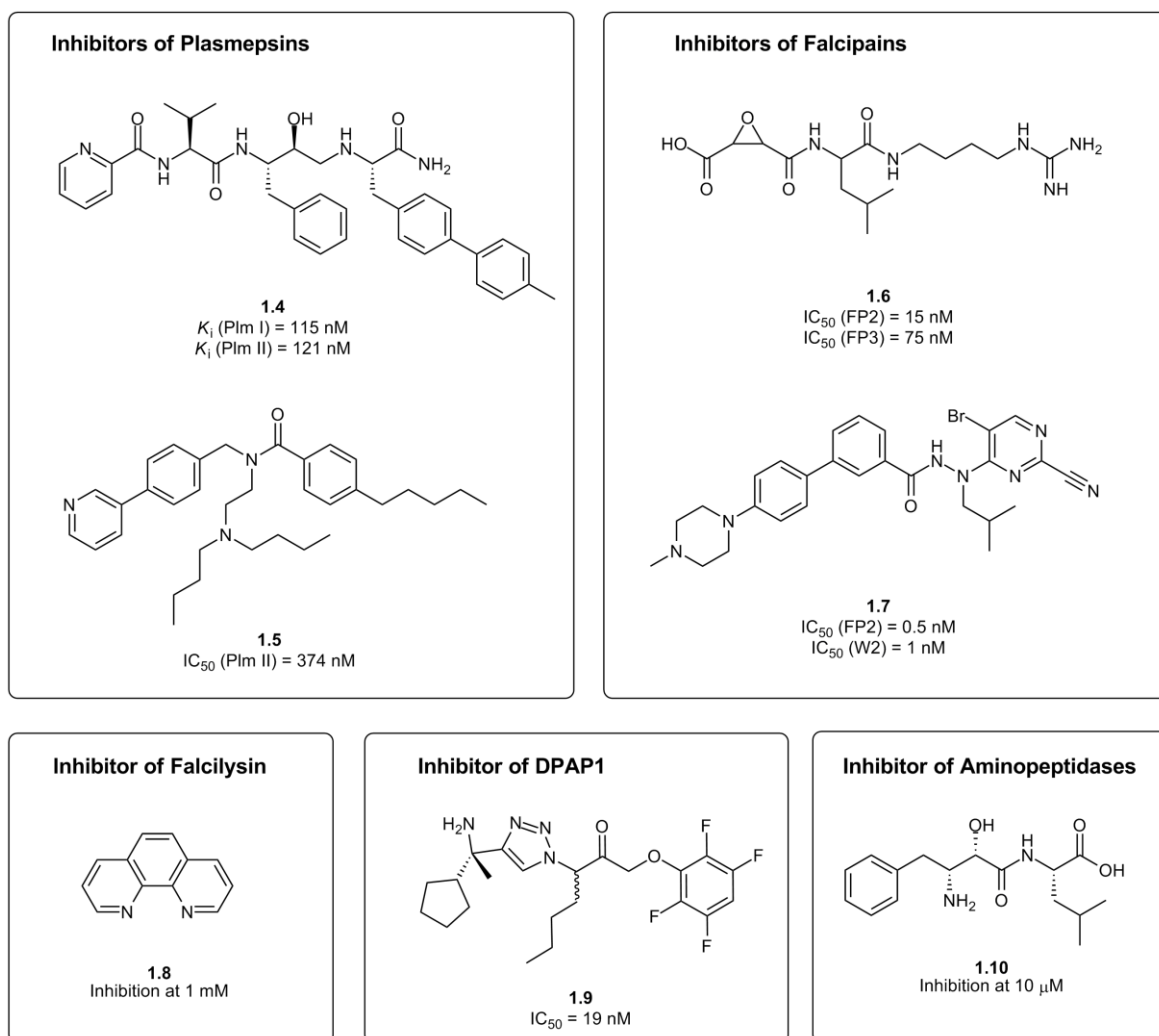


Figure 1.6. Examples of inhibitors acting in different proteases.

- Inhibition of hemozoin formation

The inhibition of hemozoin formation is already a validated drug target and is considered a valuable target for the design of novel antimalarial drugs⁴⁶. Several classes of compounds were already shown to interact with heme by preventing its polymerization, namely, 4-aminoquinolines, azoles, isonitriles, xanthenes, methylene blue, and others (Figure 1.7)⁴⁷.

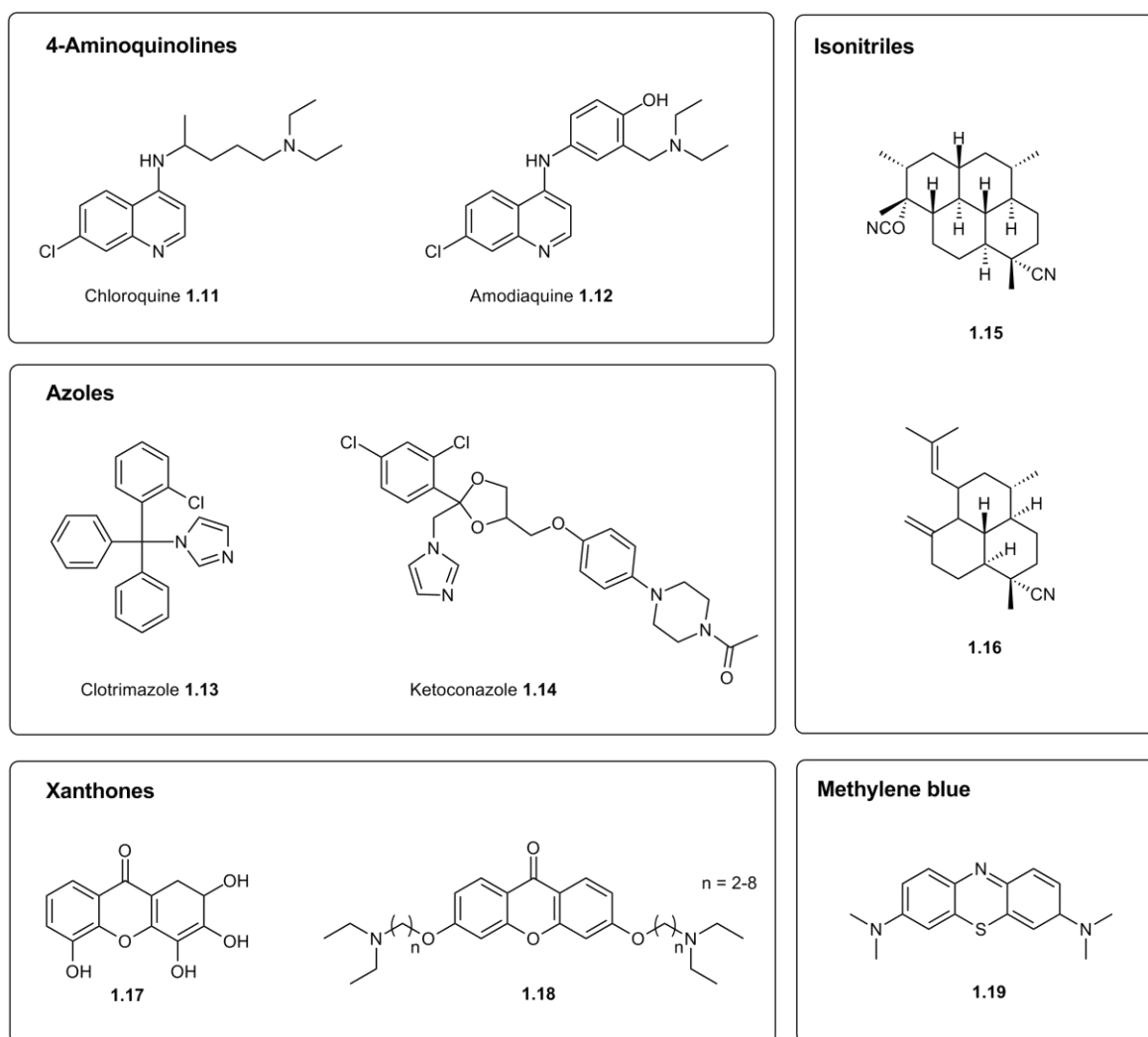


Figure 1.7. Examples of inhibitors of hemozoin formation.

Chloroquine (CQ, **1.11**, Figure 1.7) is probably the most important antimalarial drug displaying this type of mode of action. This molecule was first obtained in 1934 and quickly became the most generally used antimalarial drug⁵⁷. Studies performed on this class of antimalarials and, more specifically, on CQ, permitted to conclude about the most important features that contribute for its antimalarial potential (Figure 1.8). Accordingly, the 4-aminoquinoline nucleus provides a heme complexing template. The π - π interaction between this nucleus and the electronic system of heme are essential to block the hemozoin formation. Also, the introduction of the 7-chloro group is important for inhibition of hemozoin formation. Furthermore, 4-aminoquinolines lacking 7-chloro group do not inhibit hemozoin formation in spite of the complexes with heme are still formed⁵⁸.

Studies performed with several substituents in position 7 also showed that the chloro group displays better antimalarial activity. The aminoalkyl side chain is also a requirement for strong antiplasmodial activity since it probably facilitates drug accumulation in the DV. Moreover, it appears to enhance the strength of interaction with heme in some cases, but this effect does not emerge as crucial for its biological activity. The presence of basic side chain, which can assist accumulation in the DV by pH trapping, is an indispensable requirement. More specifically, to be effective, this kind of drugs needs to be accumulated in the acidic DV. Consequently, potent 4-aminoquinolines are generally diprotic weak bases. Although the protonated specie is always in equilibrium with the neutral one, the lower pH of the DV leads to an equilibrium shift toward the protonated CQ and, therefore, this is the more abundant specie within the DV. In its unprotonated form, the drug is able to cross the membrane of the parasitized erythrocyte. Nevertheless, once protonated due to the acidic pH of the DV, the drug become impermeable and is trapped in the compartment of the parasite since membranes are not permeable to charged species⁵⁷⁻⁵⁸.

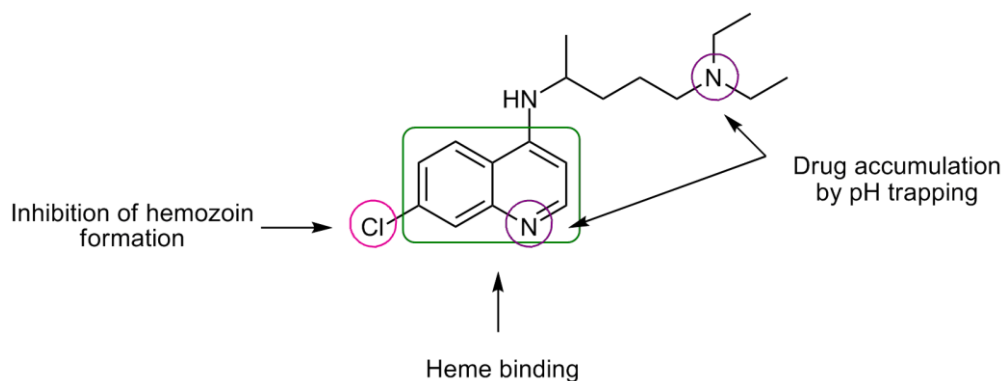


Figure 1.8. Main features that contribute for the antimalarial activity of CQ. Adapted from Egan *et al*⁵⁸.

This 4-aminoquinoline has been the most successful drug for the treatment and prophylaxis of malaria and was very effective until resistant strains began to emerge. Due to the rapid spread of resistance against CQ, the search of novel quinoline-based antimalarials, with the desired pharmacological benefits, is imperative⁵⁷.

- Artemisinin and other endoperoxides as potent antimalarial drugs

The DV also seems to be the target of artemisinin (**1.20**, Figure 1.9) and its related endoperoxides as potent antimalarial drugs. This class of compounds is of extreme importance since, until now, only diminutive drug resistance has been demonstrated⁵⁹.

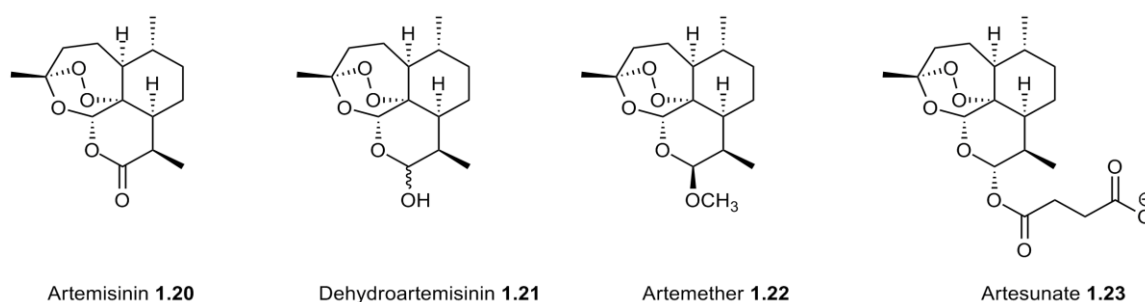
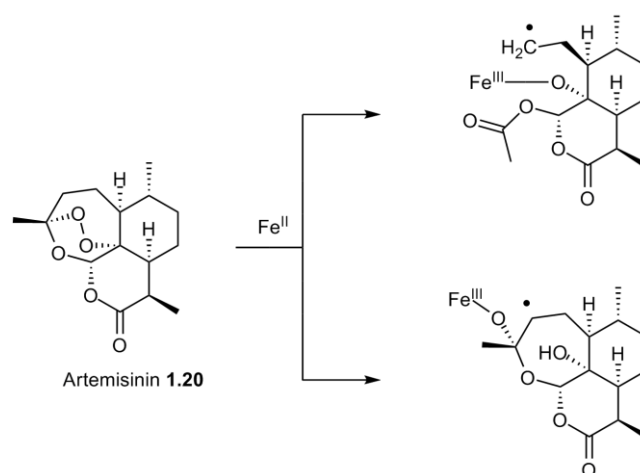


Figure 1.9. Chemical structures of artemisinin and some derivatives.

Being a sesquiterpene lactone endoperoxide, artemisinin drugs belong to a distinctive class of highly active antimalarial agents. The reduction of artemisinin's lactone substructure to a hemiacetal originates dihydroartemisinin (**1.21**), which can be transformed in order to permit the preparation of a set of semisynthetic analogues, including artemether (**1.22**). Although this derivative is more potent, it presents short plasma half-life and produces severe side-effects *in vivo*. To overcome the problem of the low water-solubility of these compounds, a water soluble derivative of artemisinin, artesunate (**1.23**), was developed. In the case of the treatment of advanced cases of *P. falciparum* this kind of drug is of extreme importance since it can be injected intravenously and, consequently, the drug can be delivered quickly contributing to a rapid diminishing of the parasitemia⁵⁷.

The main important feature of all artemisinins is the 1,2,4-trioxene moiety or, more precisely, the endoperoxide. This substructure is considered of extreme importance for the antimalarial activity. In spite of the increasing significance of artemisinins in the antimalarial chemotherapy, the mechanism of action of these drugs is still not completely elucidated. However, there are strong evidences suggesting that the heme iron play

critical roles in the mechanism of action, which is comprised of two main distinct steps (Scheme 1.2)⁶⁰⁻⁶¹. In the first step, the heme iron attacks and breaks the endoperoxide linkage of artemisinin to produce an oxygen free radical, which is then rearranged to obtain a more stable carbon free radical. During the second step, the carbon free radical will subsequently react leading to the alkylation of specific malarial proteins and causing lethal damage to malarial parasites.



Scheme 1.2. Fe(II)-mediated formation of primary or secondary carbon radicals from artemisinin. From Schlitzer *et al*⁷.

Once it became perceptible that the antimalarial activity of artemisinin derivatives was due to the endoperoxide substructure, several fully synthetic endoperoxides were synthesized. This was a huge advantage for the development of new potent antimalarial drugs since it was very difficult to obtain the starting artemisinin to synthesize its derivatives. Some examples of fully synthetic endoperoxides are highlighted in Figure 1.10.

Compound **1.25**, known as OZ439, presents an EC₅₀ value of 4 nM and is now in Phase IIa clinical studies⁶². This compound exhibits a huge increase in the pharmacokinetic half-life and blood concentration versus time profile in preclinical species. The stabilization of the intrinsically unstable pharmacophoric endoperoxide bond

was probably responsible for the improved antimalarial potential of compound **1.25** when compared with the first generation 1,2,4-trioxolane **1.24**.

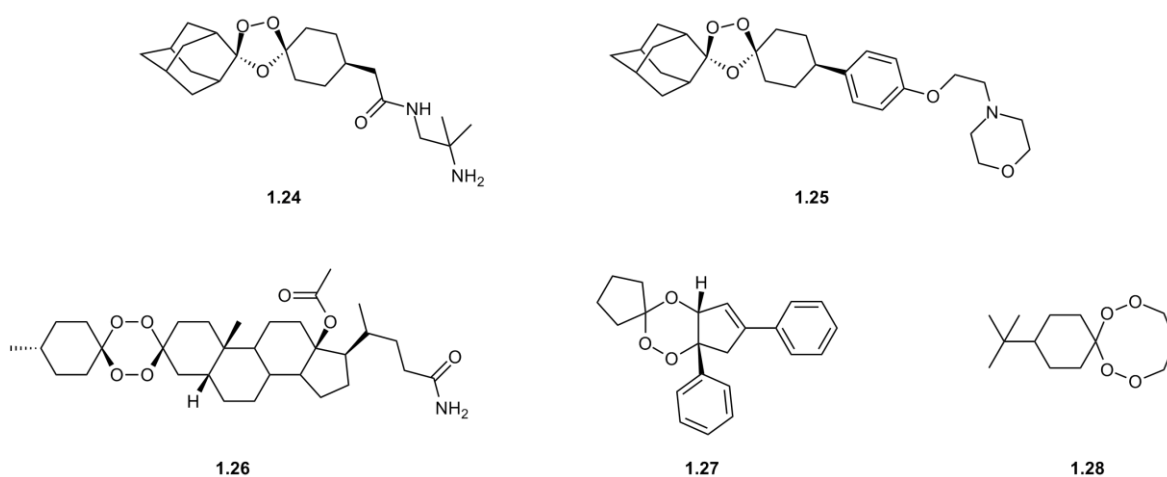


Figure 1.10. Examples of fully synthetic endoperoxides.

1.3.4. Targeting the mitochondria

In contrast to the majority of the eukaryotic organisms in which the mitochondrial electron transport chain (mETC) plays a central role in the oxidative energy metabolism, for *P. falciparum*, this pathway is not associated with the synthesis of ATP. In fact, the anaerobic glycolysis is the main source of this high-energy compound. The main role of the mETC is to keep an electrochemical gradient across the mitochondrial membrane and also to keep a constant pool of ubiquinone to be used in other critical processes such as the *de novo* pyrimidine biosynthesis. Malaria parasites lack completely the ability to salvage pyrimidines that are essential for the synthesis of nucleic acids, glycoproteins and phospholipids thus requiring other metabolic pathways to obtain these biological building blocks. In this way, it is well recognized that the mitochondria of *Plasmodia* play a critical and indispensable part in the life cycle of this parasite. Moreover, there are significant molecular and functional differences between the parasite's mitochondria and the mitochondria of human host cells that enable the exploitation of this organelle as safe and valuable target for antimalarial chemotherapy⁶³⁻⁶⁴.

The mETC of malaria parasites (Figure 1.11) comprises five dehydrogenases, specifically NADH:ubiquinone oxidoreductase (*Pf*NDH2), succinate:ubiquinone oxidoreductase (Complex II or SDH), glycerol-3-phosphate dehydrogenase, malate quinone oxidoreductase (MQO) and dihydroorotate dehydrogenase (DHODH). Additionally, considering this group of enzymes, some differences can be found between the mitochondrial parasite and the human host since *Pf*NDH2 and MQO are not present in human mitochondria whilst DHODH displays distinct biological differences when compared with the homolog host.

Other important elements of the mETC are ubiquinol:cytochrome *c* oxidoreductase (Complex III or cytochrome *bc*₁) and cytochrome *c* oxidase (Complex IV). Probably, one of the most important functions of the dehydrogenases enzymes is to provide an electron pool for these last two components of the mETC. In addition, both ubiquinone (coenzyme Q) and cytochrome *c* act as electron carriers between these two complexes⁶⁵⁻⁶⁶.

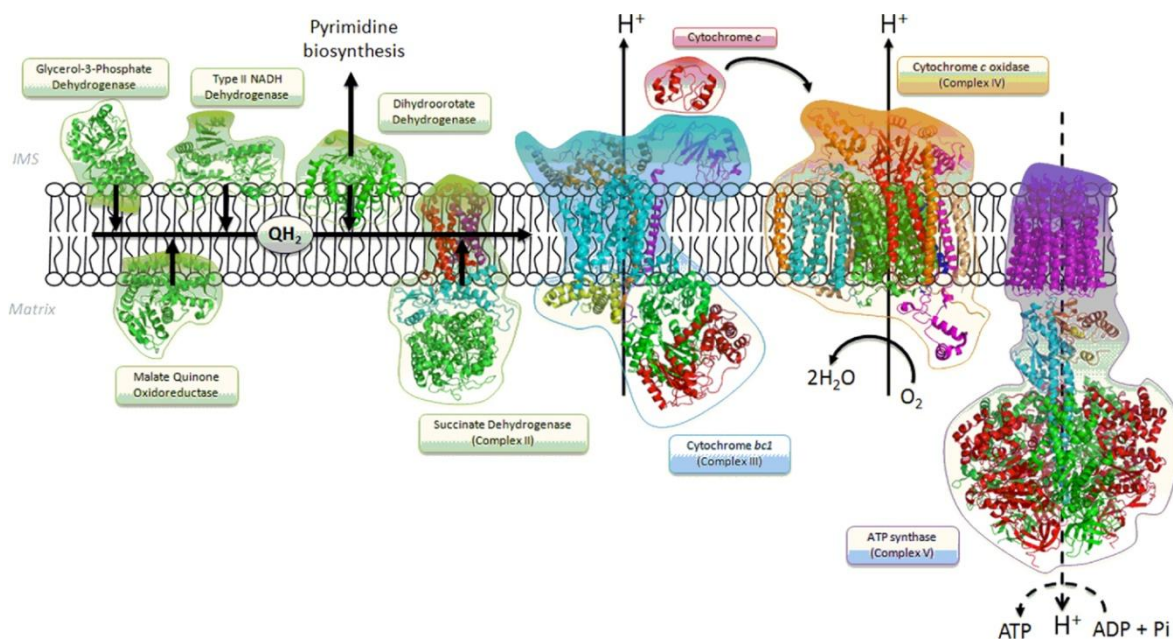


Figure 1.11. Parasite's mitochondrial electron transport chain. From Stocks *et al*⁶⁷.

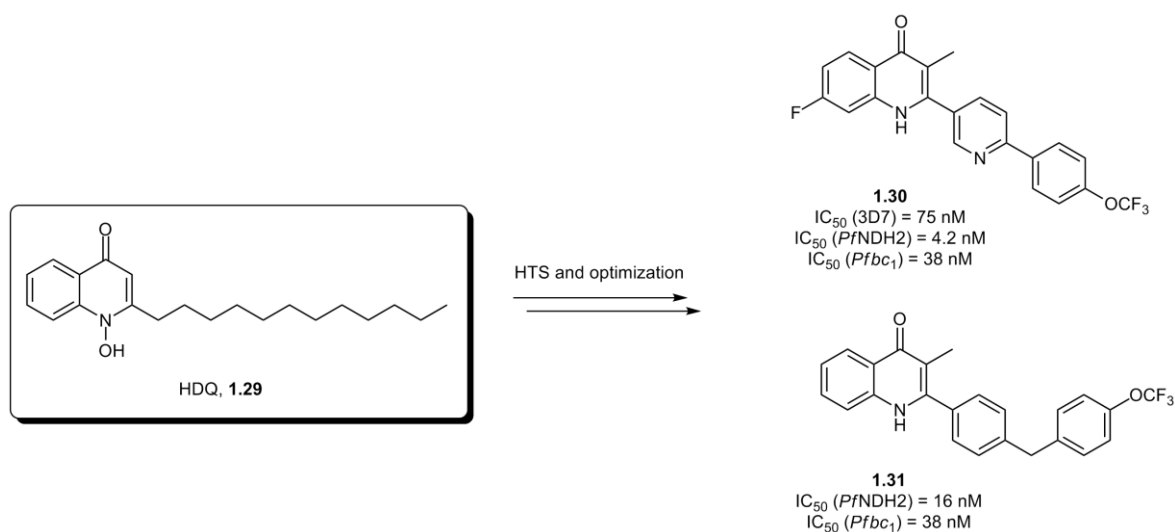
The last component of the mETC, unlike its mammalian homolog, is not recognized to generate ATP. Nevertheless, the ATP synthase (Complex V) is suggested to be an essential element, possibly acting as a proton leak for the mETC⁶⁸. In particular, regarding mETC, three drug targets are being currently exploited namely, two dehydrogenases (*Pf*NDH2 and *Pf*DHODH) and cytochrome *bc*₁⁶³.

i) *Pf*NDH2

*Pf*NDH2 is constituted by a single 52-kDa subunit and is responsible for catalyzing the electron transfer from NADH to ubiquinone and for maintaining a constant amount of NAD⁺ for reductive metabolic pathways⁶⁹. Moreover, unlike the homolog Complex I found in other organism, *Pf*NDH2 is not probably involved in the pumping of protons through the mitochondrial membrane. However, it is suggested that its activity may contribute to establish an electrochemical transmembrane potential⁶⁹⁻⁷⁰.

Studies performed in this dehydrogenase as a valuable antimalarial target are very recent and little information on potential inhibitors is still available. Nevertheless, hydroxy-2-dodecyl-4-(1*H*)-quinolone, HDQ (**1.29**, Scheme 1.3) showed to be a potent inhibitor of *Pf*NDH2 and proved also to be of extreme importance for developing a series of novel compounds acting against this target⁷¹⁻⁷³.

Compounds **1.30** and **1.31** are examples of strong inhibitors presenting also IC₅₀ values against *bc*₁ complex in the low nanomolar range. This class of compounds, diheteroaryl quinolones, was optimized based on the antimalarial potential of HDQ and using several techniques including chemoinformatics, virtual screening (VS) and high-throughput screening (HTS)⁷⁴. The optimization of these compounds permitted to obtain highly potent *Pf*NDH2 inhibitors that are also active against the parasitic *bc*₁ complex^{73, 75}. These studies suggest that the quinolone ring can be considered a privileged scaffold to design inhibitors for both drug targets in mETC.

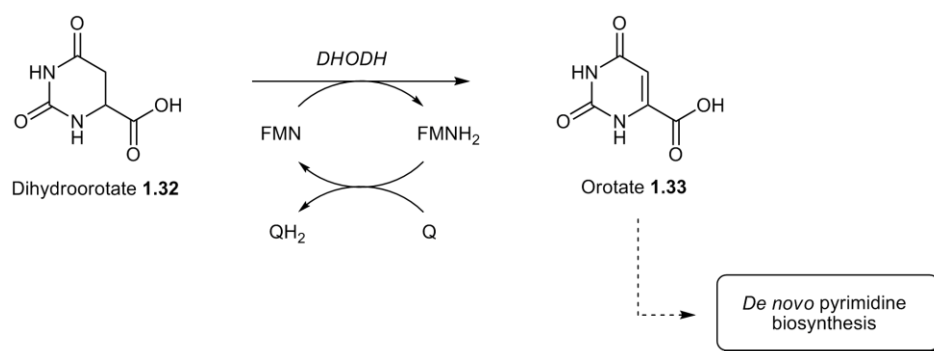


Scheme 1.3. Hydroxy-2-dodecyl-4-(1*H*)-quinolone (HDQ) and the rational design of novel quinolones as PfDHD2 inhibitors.

ii) DHODH

DHODH is the fourth and last enzyme involved in the *de novo* pyrimidine biosynthesis being also responsible for coupling this metabolic pathway with the mETC. This enzyme catalyses the oxidation of dihydroorotate (**1.32**) to orotate (**1.33**) allowing to supply the resulting pair of electrons into the mETC through flavin mononucleotide co-factor (Scheme 1.4)⁷⁶. The reoxidation of the flavin cofactor is achieved through reduction of ubiquinone to ubiquinol.

X-ray structures of both human and parasitic DHODH were already solved demonstrating the variations between the two structures and contributing to design new potential antimalarial drugs with improved selectivity⁷⁷⁻⁷⁹.



Scheme 1.4. Reaction catalysed by DHODH. Abbreviations: FMN – flavin mononucleotide; FMNH₂ – reduced flavin mononucleotide; Q – ubiquinone; QH₂ – ubiquinol. Adapted from Stocks *et al*⁶⁷.

Inhibitors of human DHODH were already recognized for their potential to be used not only in the treatment of rheumatoid arthritis but also to act as antitumor and immune suppressive agents (Figure 1.12)⁷⁶. Despite these compounds showed reduced inhibitory activity against *Pf*DHODH, both leflunomide (**1.34**) and brequinar (**1.36**) were considered good starting points to design novel potential antimalarial drugs acting in this target. Furthermore, studies performed with leflunomide and its active metabolite (**1.35**) permitted to obtain the x-ray crystal structure of this enzyme with **1.35** co-crystallized in its active site which represents a valuable tool to design new *Pf*DHODH inhibitors⁸⁰.

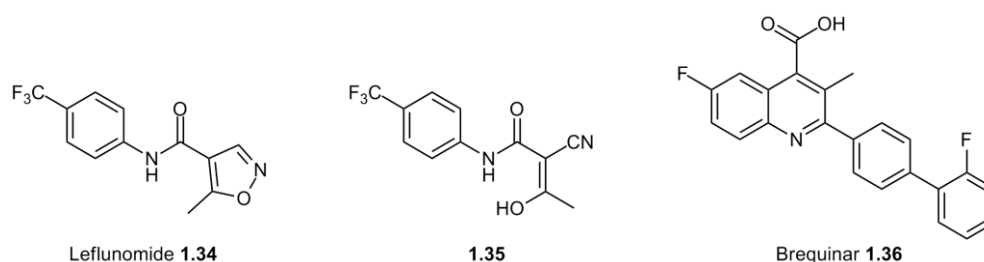


Figure 1.12. Examples of human dihydroorotate dehydrogenase inhibitors.

So far, several campaigns including HTS, computational methods and drug optimization allowed to obtain several classes of *Pf*DHODH inhibitors (Figure 1.13). The triazolopyrimidine-based derivatives were first recognized when compound **1.37** was

discovered during an HTS screening project⁸¹. This compound displayed an IC₅₀ value of 47 nM against the *Pf*DHODH and showed to be highly selective when compared with the human enzyme. However its activity against the mice model was reduced.

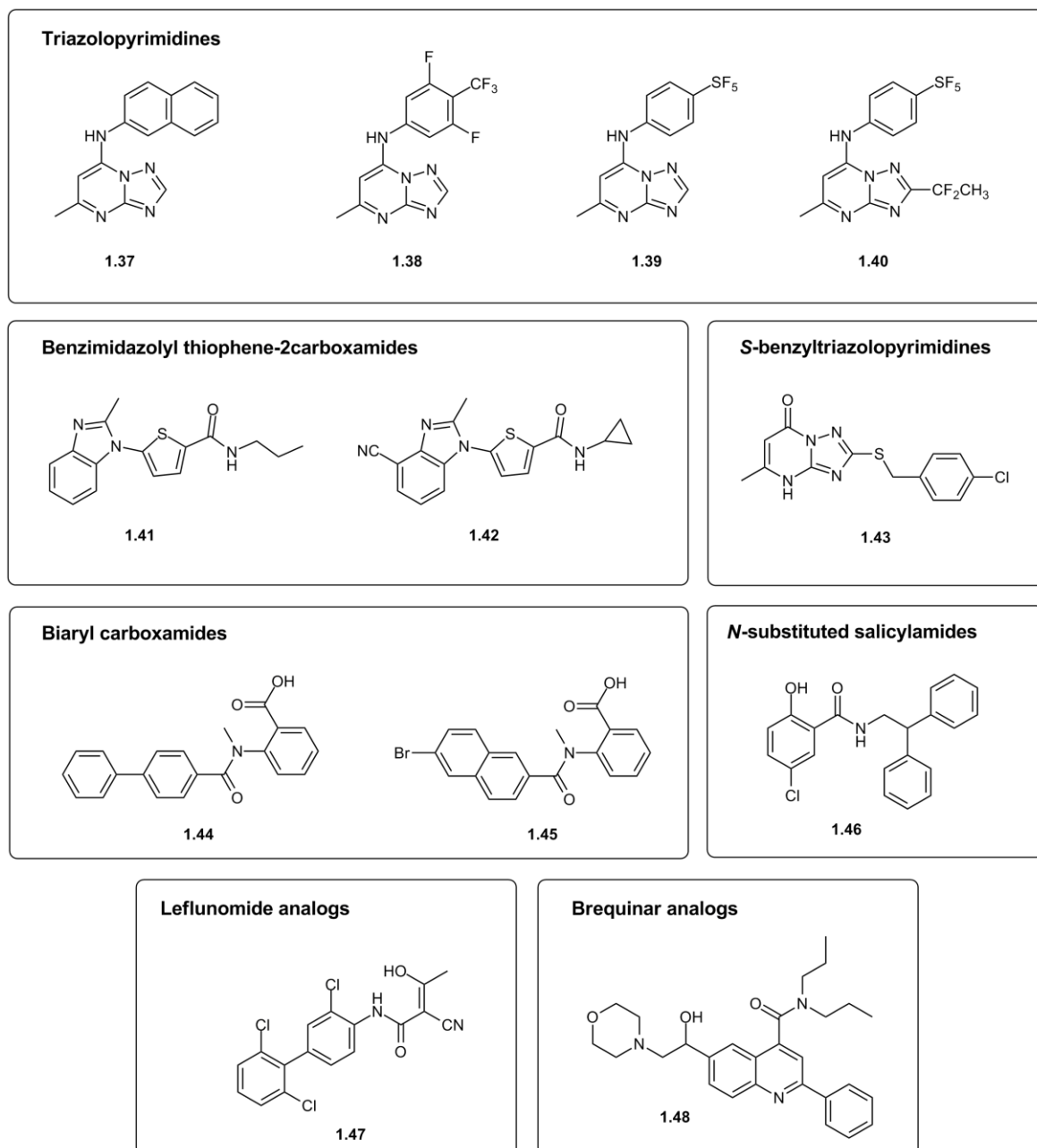


Figure 1.13. Examples of *P. falciparum* dihydroorotate dehydrogenase inhibitors.

This scaffold was further optimized permitting to obtain several compounds with improved antimalarial and pharmacological properties⁸²⁻⁸⁵. More specifically, compound **1.40** showed improved inhibitory activity against both *Pf* and *Pb*DHODH and good pharmacological profiles. Moreover, this compound was identified as a preclinical candidate⁸⁵.

Later, another HTS screening allowed to identify the benzimidazolyl thiophene-2-carboxamides as an important scaffold for *Pf*DHODH inhibitors⁸⁶. Further optimization of the lead compound **1.41** led to the identification of compounds showing double digit nanomolar potency against this target. Compound **1.42** was recognized as a potential drug development candidate due to its effective antimalarial activity and low toxicity⁸⁷⁻⁸⁸. Compound **1.37** was also used as input for the identification of novel chemical scaffolds through a VS study over a drug-like database. From this study, compound **1.43** emerged as the most active compound with an IC₅₀ value of 1 μM against this target⁷⁹

Also, the biaryl carboxamide scaffold was obtained after careful comparison of X-ray crystal structures of both *Pf* and human DHODH bound to compound **1.35** followed by the application of the molecular design program SPROUT⁸⁹. From this study twenty different templates resulted being the amides of the anthranilic acid the most attractive ones displaying binding affinities in the micromolar range. Compounds **1.44** and **1.45** are examples of compounds belonging to this class. More recently, some salicylamides derivatives with moderate inhibitory activity against *Pf*DHODH were also identified. Optimization of this class permitted to obtain compound **1.46** displaying moderate inhibitory activity against this target (IC₅₀ = 9.1 μM) and good selectivity⁹⁰. Some examples of leflunomide (**1.34**) and brequinar (**1.36**) analogs were also developed⁹¹⁻⁹². Compounds **1.47** and **1.48** are examples of *Pf*DHODH inhibitors successfully obtained after optimization of the parent compounds acting selectively in human DHODH.

iii) *bc*₁ complex

The mitochondrial *bc*₁ complex, a membrane-bound enzyme, is one of the essential components of the respiratory electron transfer chain being responsible for catalyzing the

electron transfer between ubiquinol and cytochrome *c*. Coupled to this process is the consequent translocation of two protons across the inner mitochondrial membrane with the resulting electrochemical gradient used for ATP production⁹³⁻⁹⁴. Being crucial for the survival of several species of the *Plasmodium* genus responsible for malaria, the cytochrome *bc*₁ complex is an attractive and already validated target for antimalarial drug development⁹³.

This enzymatic complex is a dimer with each monomer comprising 11 distinct polypeptides. Both monomers include four redox centers, specifically, two heme groups, *b*_H and *b*_L, in cytochrome *b*, one heme group in cytochrome *c*₁, and one iron-sulfur cluster in the Rieske protein (Figure 1.14).

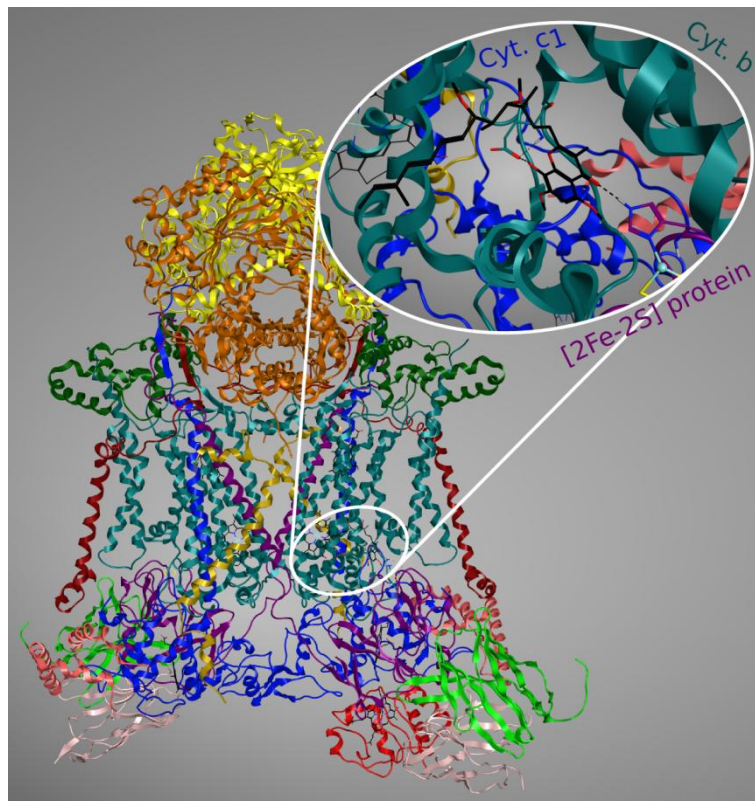


Figure 1.14. Structure of the dimeric *bc*₁ complex.

Moreover, the catalytic core of this complex is formed by three subunits, namely, cytochrome *b*, cytochrome *c*₁ and the Rieske iron-sulfur protein ([2Fe-2S], ISP). Together, these three subunits display a key role in the electron-transfer and proton translocation pathway. The biological function of the other subunits is still not completely understood but they are supposed to contribute for stabilizing the whole complex.

So far, the mechanism which better explains the proton translocation coupled to electron transport by this enzymatic complex is a version of the well known Q cycle of Mitchell (Figure 1.15)⁹⁵⁻⁹⁷. Briefly, Q cycle mechanism involves the two distinct quinone-binding sites, *i.e.*, the quinol oxidation site (Q_o) and the quinone reduction site (Q_i). These two binding sites are positioned in opposite sides of the membrane and are connected by a transmembrane electron-transfer pathway. As mentioned, ubiquinol (**1.49**, Scheme 1.5), produced by dehydrogenases, binds to Q_o and its oxidation permits the release of two protons and two electrons.

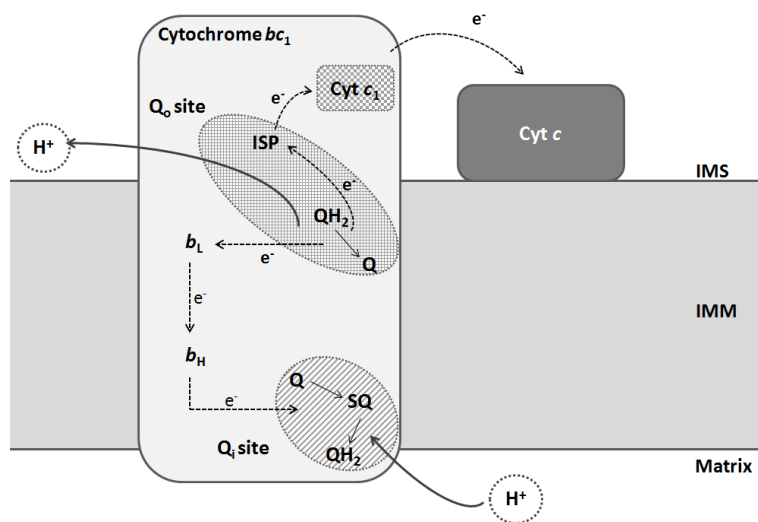
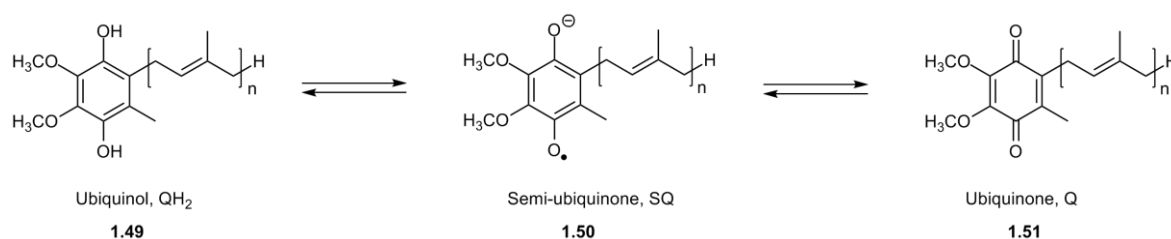


Figure 1.15. Q-cycle mechanism of the *bc*₁ complex catalytic core. The main components of cytochrome *bc*₁ are represented in the scheme: cytochrome *c*₁ – in checker board, Q_o binding site (including ISP) – in grid and, Q_i binding site – in diagonal lines. Abbreviations: Q – ubiquinone; QH₂ – ubiquinol; SQ – stable semi-ubiquinone intermediate; ISP – iron-sulfur protein; IMS – mitochondrial inter-membrane space; IMM – inner mitochondrial membrane.

The two electrons obtained from the ubiquinol's oxidation take different pathways. In a bifurcated reaction at the Q_o site, one of the electrons reduces the high potential [2Fe-2S] cluster while the second reduces the heme b_L of cytochrome b . The reduced heme b_L instantly transfers the electron to the heme b_H of cytochrome b at the Q_i site, where ubiquinone (**1.51**) is reduced to semi-ubiquinone (**1.50**).



Scheme 1.5. Two oxidation states of coenzyme Q: the fully reduced ubiquinol form (**1.49**) and the fully oxidized ubiquinone form (**1.51**), and the stable semi-ubiquinone intermediate (**1.50**).

The oxidation of a second molecule of ubiquinol leads to complete reduction of the ubiquinone at the Q_i site. This electron transfer to the [2Fe-2S] cluster is followed by a conformational shift of the head domain of this subunit allowing the approximation between the [2Fe-2S] cluster and the heme of cytochrome c_1 enabling its oxidation and subsequent reduction of cytochrome c ⁹⁸.

Solved structures of the mitochondrial bc_1 complex, using X-ray crystallography, have been reported for several species at different resolution^{96, 99-103} which can be considered a powerful starting point to design new and more effective drugs. However, until now, a solved crystallographic structure of *P. falciparum* bc_1 complex is still not available. Since cytochrome b , which provides the ubiquinol and ubiquinone binding pocket, of both *Saccharomyces cerevisiae* yeast and *P. falciparum* share a high sequence identity, this was the crystallographic structure adopted as a model to study the interactions involving this enzyme complex and possible inhibitors^{71, 104-109}. Although the overall structure of the bc_1 complex is highly conserved between several species, different

structural features have been observed that may confer selectivity between the parasite and the human host⁶⁹.

Cytochrome bc_1 has been considered the major drug target in the mETC and several inhibitors were already developed. This has been definitely the most studied target on mETC presenting the higher diversity and number of potential inhibitors. These inhibitors can be divided into four groups in agreement with their binding sites in the cytochrome. As a result, group I, II and IV include inhibitors binding Q_o site and, consequently, inhibiting electron transfer from the [2Fe-2S] cluster to cytochrome c_1 as well as electron transfer onto the b_L centre. Those three groups differ from each other by the chemical characteristics of their inhibitors. Group I inhibitors typically contain a β -metoxyacrilate group as a characteristic structural element while group II inhibitors include 2-hydroxyquinone analogues. Group IV inhibitors usually contain a chromone ring system and, in spite of blocking the Q_o site, these inhibitors display different properties from those of groups I and II. Group III includes the inhibitors that bind the Q_i site, being responsible for blocking electron transfer from b_H centre to ubiquinone⁶³.

- Hydroxynapthoquinones

Atovaquone (**1.52**, Figure 1.16) is, currently, the only drug targeting the bc_1 complex in use. As others drugs belonging to class II, atovaquone selectively inhibits electron transfer by binding to Q_o site. This drug induces collapse of the mitochondrial membrane potential at very low concentrations and, as a result, the mammalian system is not affected substantially. Initially, this drug was found to be a very effective antimalarial compound, but sooner was considered inappropriate for use as a single agent due to the relatively quick emergence of resistance. In an attempt to improve the efficiency and overcome the resistance issue, atovaquone is now used in combination with the synergistic agent proguanil (**1.53**)⁵.

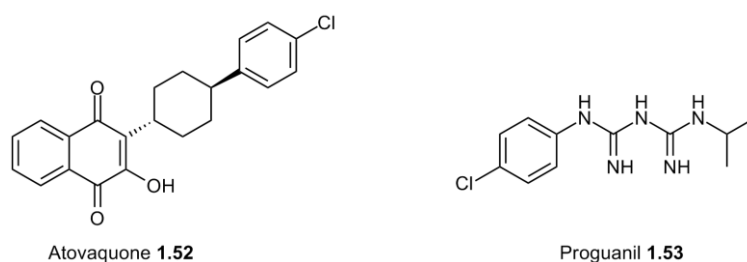


Figure 1.16. Chemical structures of atovaquone (**1.52**) and proguanil (**1.53**) that are the active molecules in Malarone.

Mutations associated with atovaquone's resistance are predominantly restricted to the conserved PEWY region being the most common mutation observed at position 268 in cytochrome *b*, where tyrosine is changed by a serine (Y268S) or, less frequently, by a cysteine (Y268C)¹¹⁰. Regarding atovaquone's binding mode, some computational studies were already performed and the interactions of this molecule with the *bc*₁ complex binding site are fully characterized using the X-ray coordinates of *S. cerevisiae* *bc*₁ complex (Figure 1.17)¹¹¹⁻¹¹².

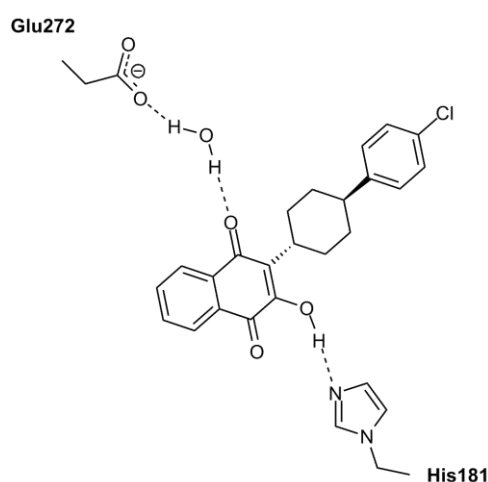


Figure 1.17. Binding mode of atovaquone into *bc*₁ complex Q_o site.

In the model obtained, the hydroxyl group of the hydroxynaphthoquinone binds to the imidazole nitrogen of His181 of the Rieske protein by a strong hydrogen bond. The

carbonyl group at 4-position on the quinone ring interacts with Glu272 of cytochrome *b* through a water molecule. The hydrophobic interactions of the hydrophobic *trans* substituted *p*-chlorophenyl ring with the side chains of several hydrophobic amino acids also contributes to stabilize the inhibitor inside the Q_o site.

Apart from acting as a competitive inhibitor of Q_o binding site, atovaquone also block the conformation change of the Rieske complex since it binds to His181. Consequently, this cluster will be immobilized, reducing or preventing electron transfer, which has also impact in other systems depending on the mETC, such as *Pf*DHODH¹¹³.

Although atovaquone display excellent antimalarial activity, this drug also displays poor pharmacological properties namely low bioavailability and high plasma protein binding¹¹⁴. In this way, in an attempt to improve the bioavailability of atovaquone, some new hydroxynaphthoquinones were designed by replacing the 3-hydroxyl function for more lipophilic ester and ether groups. Different series of atovaquone derivative were obtained with all compounds showing potent antimalarial activity, most of them exhibiting *in vitro* IC₅₀s below 5 nM. Ester derivatives (**1.54**, Figure 1.18) at the hydroxyl group of atovaquone presented the highest activity. Nevertheless, the modifications made in atovaquone's structure did not result in a major improvement in the oral bioavailability¹¹⁵.

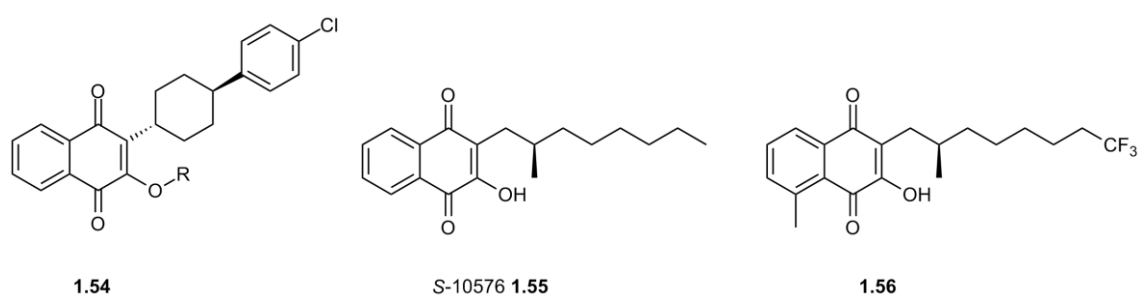


Figure 1.18. Examples of some atovaquone analogs.

A library of several hydroxynaphthoquinones including a wide variety of linear, branched, saturated, unsaturated and aromatic side-chain substitutions at 2-position on

the hydroxyquinone ring was also developed¹¹⁶. The linear alkyl side-chain derivatives exhibited significant inhibition of the yeast enzyme but they did not exhibit considerable species selectivity

The more active compound found was *S*-10576 (**1.55**), obtained when a methyl group was inserted in the beta position of a saturated 8-carbon linear side-chain. Nevertheless, studies designed to test the therapeutic potential of *S*-10576 *in vivo* showed that the two terminal carbons of the side chain are easily oxidized, resulting in a more water soluble compound. This rapid metabolic degradation, consequently, leads to a rapid excretion of the compound turning *S*-10576 ineffective as a potential drug¹¹⁷. In an attempt to overcome metabolic stability issues related with *S*-10576, a number of trifluoromethyl derivatives were synthesized with compound **1.56** showing enhanced metabolic stability¹¹⁸. In this way, fluorinated hydroxynaphthoquinones provide enhanced metabolic stability which can be considered a significant advantage over atovaquone¹¹⁹.

- Quinolones

Antimalarial activity of 4(1*H*)-quinolones was first recognized in the 1940's when endochin (**1.57**, Figure 1.19) was identified as a causal prophylactic, killing growing liver stage parasites, and potent erythrocytic stage agent in avian malaria models. However, this inhibitor was not efficacious against malaria parasites of mammals⁶⁷. Recently, several efforts have been made to develop new quinolones targeting the *P. falciparum* *bc*₁ complex allowing to obtain several compounds displaying exceptional antimalarial activity (Figure 1.19)^{71, 105, 107, 120-124}.

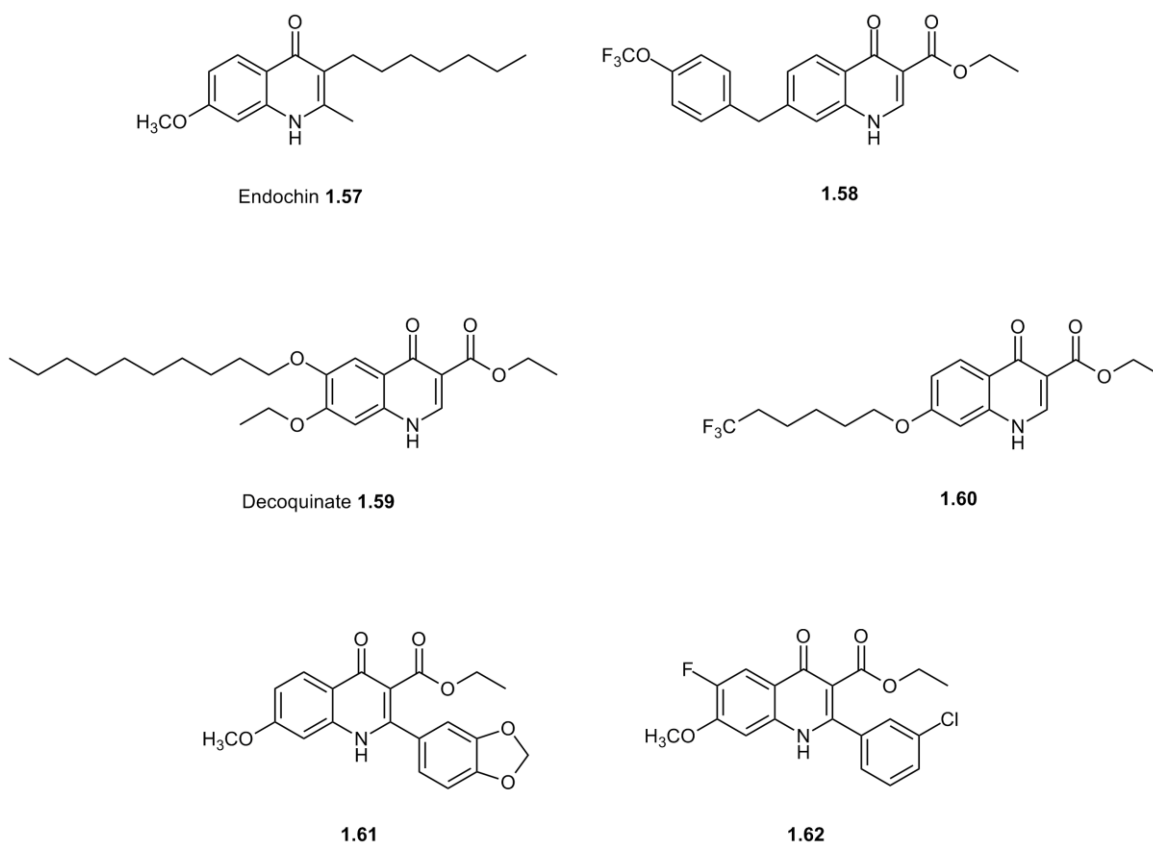
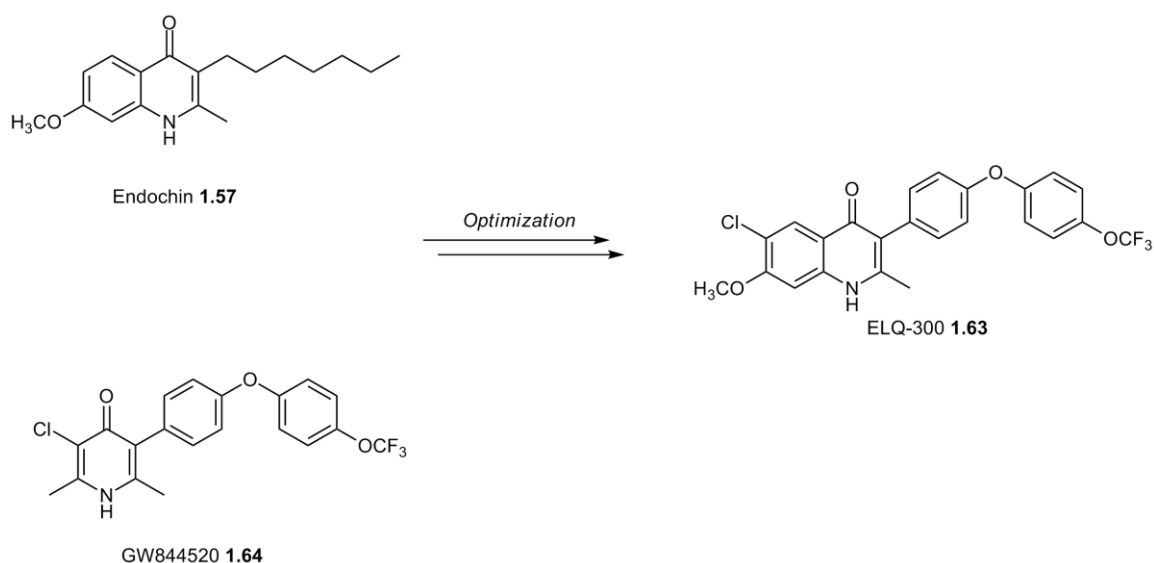


Figure 1.19. Examples of 4(1H)-quinolones with potent antimalarial activity.

From these efforts resulted also ELQ-300 (**1.63**, Scheme 1.6) that contains a diarylether moiety and acts selectively against *Plasmodium bc₁* complex¹²⁰. This compound was designed based on the chemical structure of endochin (**1.57**) through replacement of its metabolic unstable alkyl chain by the side chain from the well known *bc₁* complex inhibitor GW844520 (**1.64**). This compound demonstrated improved metabolic stability when compared with endochin and increased selectivity ratio for *P. falciparum bc₁* over the human homolog. Moreover, due its superior properties, this compound was selected for preclinical studies.

Despite the good antimalarial activity displayed by this class of compounds, they often lack aqueous solubility which affects the pharmacokinetics of the potential drug. Hence, some compounds were also synthesized to overcome this problem allowing to obtain compounds **1.61** and **1.62** (Figure 1.19) presenting good inhibitory potential against this target and also improved oral bioavailability¹²⁵.



Scheme 1.6. Design of ELQ-300 (**1.63**) based on the structure of endochin (**1.57**) and GW844520 (**1.64**).

- Pyridones

Pyridones are other important scaffold acting against the bc_1 complex. This antimalarial class is based on clopidol (**1.65**, Figure 1.20). This drug is known since the late 1960s for its antimalarial and anticocccidal activity by interfering with mitochondrial respiration¹²⁶. However, this inhibitor is rapidly excreted and present high insolubility in several solvents.

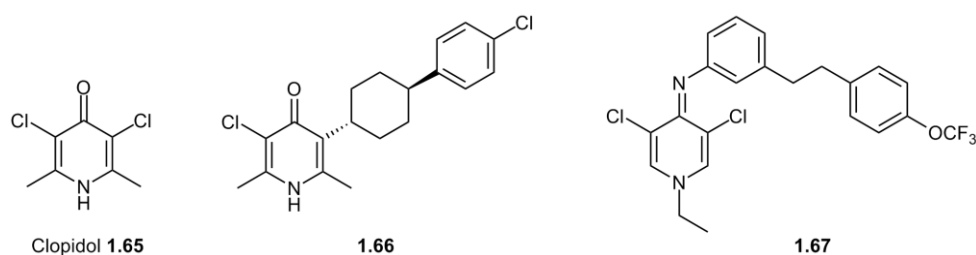


Figure 1.20. Examples of pyridones and analogs acting on $Pfbc_1$ complex.

During the last years, GlaxoSmithKline has developed a series of clopidol derivatives with more lipophilic side chains. The introduction of the atovaquone side

chain (as in compound **1.66**) and also the phenoxyaryl moiety (for example compound **1.64**, Scheme 1.6) permitted to highly increase the antimalarial activity of this class of compounds. The most promising antimalarial candidate was GW844520 (**1.64**). This compound displayed IC₅₀ values in the low nanomolar range for both T996 and 3D7A *P. falciparum* CQ-resistant and sensitive strains, respectively. Moreover, it also presented several drug-like properties reported in its preclinical evaluation. For instance, GW844520 has an appropriate half life for short term therapy and it is easy to synthesize¹²⁷. Nevertheless, the drug development of GW844520 terminated due to problems related to the unexpected cardiotoxicity¹²⁸. Recently, based on the evidence that the introduction of a lipophilic chain can improve antimalarial activity of 4(1*H*)-pyridones, a number of analogues of clopidol isosteres were synthesized¹⁰⁶. These analogues resulted from the incorporation of an aromatic moiety at the imine nitrogen atom of the (1*H*-pyridin-4-ylidene)amine scaffold. The antiplasmodial activity of these compounds was evaluated against *P. falciparum* W2 and FCR3, CQ and atovaquone-resistant strains, respectively, and IC₅₀ values were obtained in the range of 0.9 to 7 μM. The most active analogue incorporated a lipophilic phenyl ethyl side chain at the imine nitrogen and a *N*-ethyl group (**1.67**, Figure 1.20).

- Acridones and acridinediones

Acridine-based drugs are known in malaria chemotherapy since mepacrine (**1.68**, Figure 1.21) was introduced as the first synthetic antimalarial blood schizontocide used clinically¹²⁹⁻¹³¹. More recently, haloalkoxyacridones were identified as a new acridine-based scaffold. Compounds **1.69** and **1.70** (Figure 1.21) are examples of acridones derivatives displaying an IC₅₀ value in the subnanomolar range. The studies performed revealed structure activity patterns identical to the ones obtained for quinolones. Namely, the introduction of a longer alkoxy side chain in 3-position with terminal CF₃ groups contributed to enhance antimalarial activity. The nitrogen ring is also essential for activity since the activity strongly decreases when the nitrogen atom is replaced by oxygen. The antimalarial activity of these new compounds has been attributed to inhibition of mitochondrial *bc*₁. However, some of the recognized antimalarial activity of

this new class of compounds can be also a consequence of heme binding¹³². Specifically, like quinolines, acridines are believed to confer almost all of their antimalarial activity by preventing the crystallization of heme and, consequently, inhibiting hemozoin formation⁴⁷.

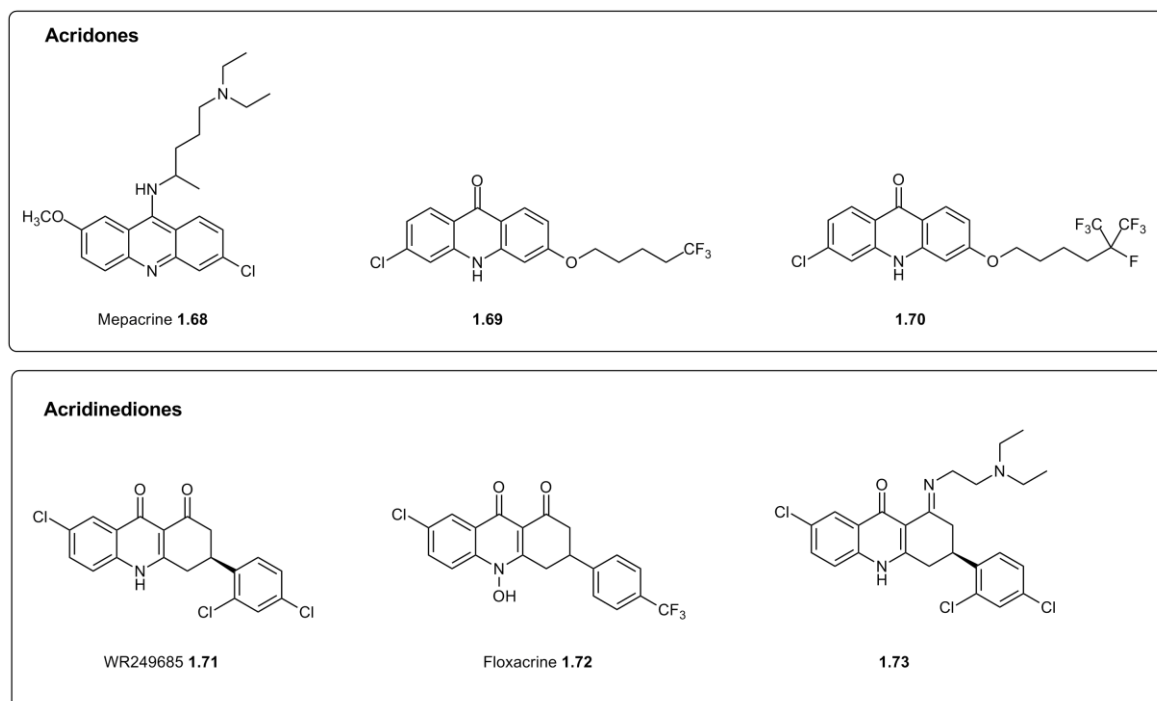


Figure 1.21. Examples of acridones and acridinediones derivatives.

Acridinediones are another acridine-based class of compounds known for their potent antimalarial activity. In accordance with acridones' mode of action, these drugs are thought to inhibit *in vitro* hemozoin formation in addition with their ability to block electron transfer in bc_1 complex¹³³⁻¹³⁴

The *S* enantiomer of WR249685 (**1.71**, Figure 1.21) and the racemic floxacrine (**1.72**) are two dihydroacridinediones that selectively bind bc_1 complex of *P. falciparum* with IC_{50} values, measured directly in the enzymatic complex, in the nanomolar range. However, floxacrine displays an IC_{50} value approximately 300 times higher than WR249685 indicating that the introduction of the hydroxyl group in the nitrogen atom of

the acridinedione ring probably reduces the antimalarial activity¹³³. Furthermore, the replacement of the ketone functionality at the 1-position by an imine group permitted to afford acridinedione derivatives like compound **1.73** with equivalent activities¹³⁵.

- Other inhibitors binding to Q_o site

Another class of compounds known to inhibit cytochrome *bc*₁ complex are the β -methoxyacrylates (for example compound **1.74**, Figure 1.22)¹³⁶. Despite binding to Q_o site, these inhibitors act in a different way than the others already mentioned being still possible for ubiquinol to bind to the Q_o site in the presence of this type of inhibitors. The presence of these inhibitors leads to a shift in the position of the natural ligand due to a conformational distortion in the binding pocket. As a result, ubiquinol electrons cannot be transferred to [2Fe-2S] cluster¹³⁷⁻¹³⁸.

Myxothiazol (**1.75**) and stigmatellin A (**1.76**) are two antibiotics with well known antimalarial activity. Myxothiazol is able to inhibit mitochondrial respiration in the *bc*₁ complex and has effects on the redox components of isolated succinate-cytochrome *c* reductase complex. This suggests that this drug is able to interact with both cytochrome *b* and the Rieske ISP of the *bc*₁ complex¹³⁹⁻¹⁴¹. By the other hand, stigmatellin A blocks the oxidation site preventing electron transfer. This inhibitor binds simultaneously to the *b*_L domain of cytochrome *b* and the Rieske ISP¹⁴⁰⁻¹⁴¹. The crystal structure of the cytochrome *bc*₁ complex, from yeast, with stigmatellin A bound to the Q_o site is currently available which contributes to elucidate the binding mode of these type of inhibitors¹⁰³.

More recently, several tetracyclic benzothiazepines were discovered as potent antimalarial drugs acting selectively in *P. falciparum* *bc*₁ complex. Examples of compounds belonging to this class are highlighted in Figure 1.22 (compounds **1.77**, **1.78** and **1.79**) with all displaying IC₅₀ values, both in the *Pf* *bc*₁ complex as well as in Dd2 strain, in the low nanomolar range¹⁴².

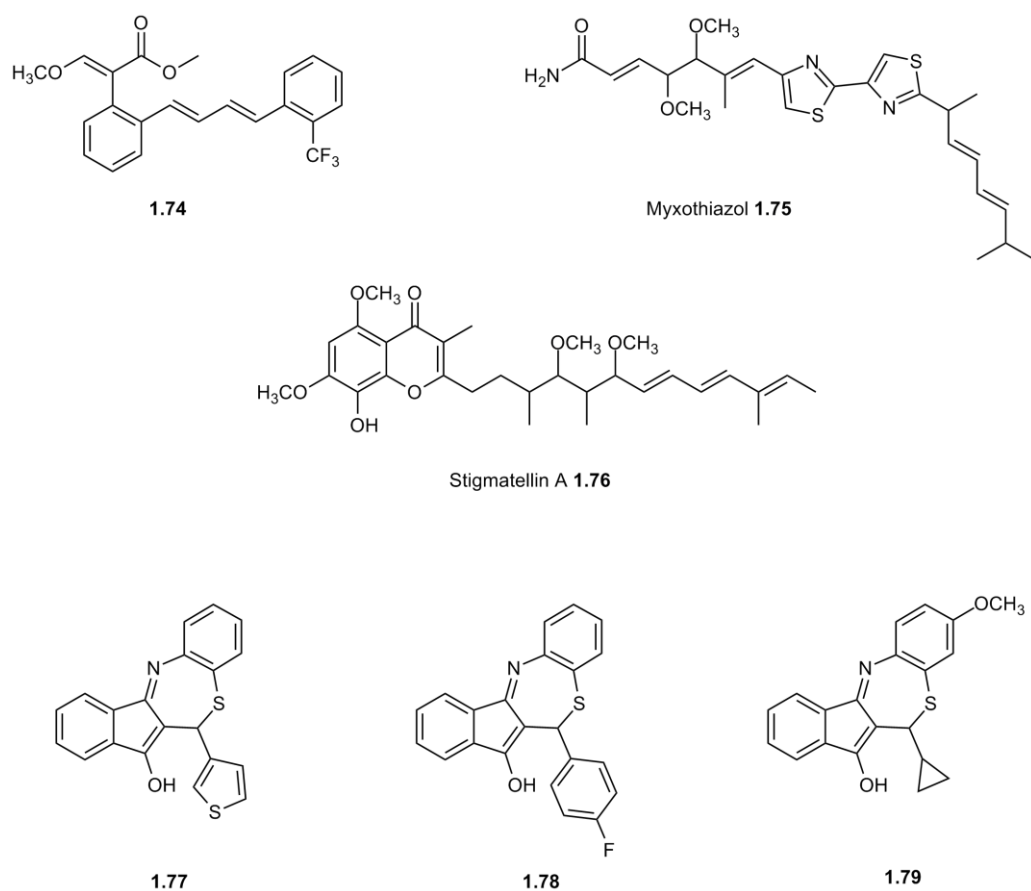


Figure 1.22. Examples of several compounds acting on *Pf* bc_1 complex.

- Inhibitors binding to Q_i site

While several compounds have been designed to act selectively against Q_o binding site of bc_1 complex, the Q_i site has been slightly neglected. Until now, only few inhibitors are known to act exclusively in this pocket. Antimycin A (**1.80**, Figure 1.23), a dilactone salicylamide, blocks the electron transfer in cytochrome bc_1 by inhibiting Q_i reduction site presenting an IC_{50} value against several *P. falciparum* strains around 10 nM^{141, 143}. SAR studies showed that the *N*-formylamino-salicyl-amide group is the main responsible for the binding specificity to Q_i site. Moreover, a low pK_a value for the phenolic hydroxyl group and an intramolecular H-bond between that OH and the carbonyl moiety of the salicylamide linkage are also important for activity¹⁴⁴. Like in the case of stigmatellin A, crystal structures of bovine cytochrome bc_1 complex, co-crystallized with this drug, are currently available¹⁴⁵⁻¹⁴⁶. Analogues of this drug were further obtained by replacement of

the dilactone moiety for simpler scaffolds (Figure 1.23). As a result, biphenyl ethers (for example **1.81**), benzotriazole (**1.82**) and indole (**1.83**) derivatives of antimycin were obtained with comparable *in vitro* inhibitory potency¹⁴⁷⁻¹⁴⁸. Funiculosin (**1.84**) is another antibiotic known for its ability to inhibit respiratory chain by binding both to Q_i and Q_o sites. It has been isolated from *Penicillium funiculosum* and has a broad antifungal spectrum showing also some antiviral activity¹⁴⁹.

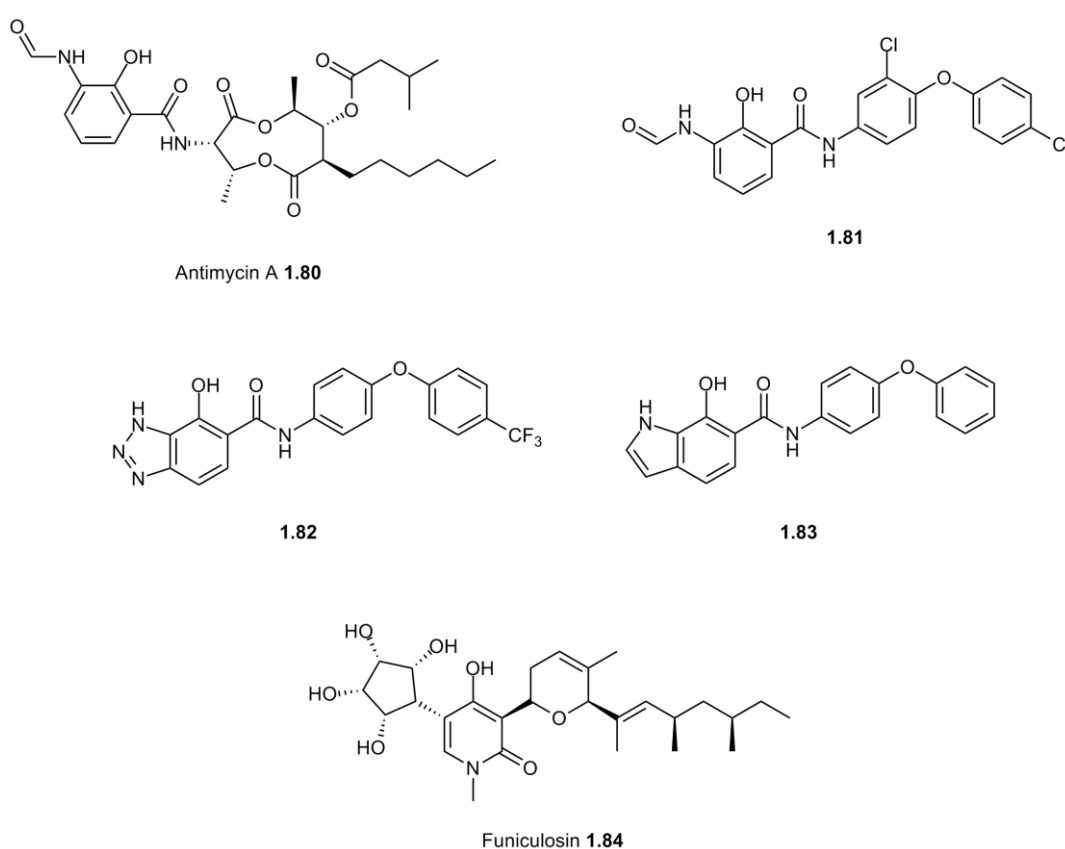


Figure 1.23. Examples of inhibitors of bc_1 complex Q_i binding site.

iv) Other elements of mTEC

Despite some inhibitors are already known for other elements of the mETC, these targets are relatively underinvestigated. Namely, SDH and ATP synthase can be viewed as two underexplored potential antimalarial targets. More specifically, SDH is mainly involved with the electron feeding to the mETC and, consequently, to bc_1 complex¹⁵⁰ while ATP

synthase displays minimal contribution to ATP synthesis being responsible for allowing protons to leave mETC⁶⁸. However, some inhibitors for both targets are already recognized. For instance, plumagin (**1.85**, Figure 1.24) and licochalcone A (**1.86**) have previously demonstrated their antimalarial mode of action by acting against SDH¹⁵¹ while almitrine (**1.87**) is able to interact with ATP synthase¹⁵².

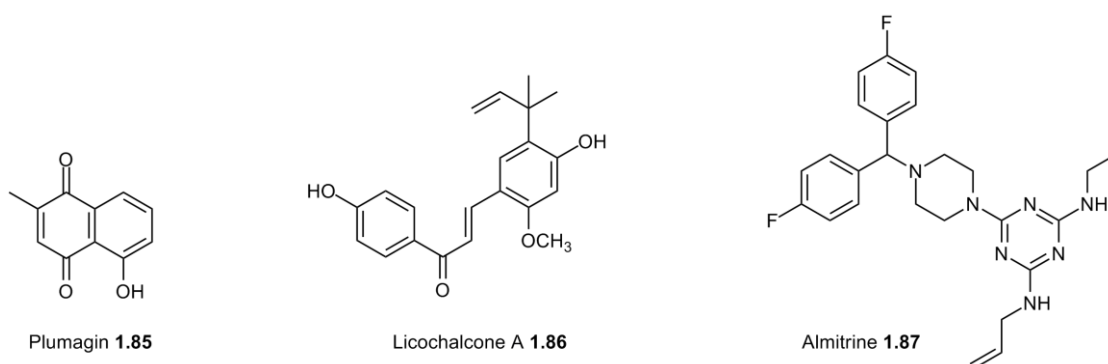


Figure 1.24. Examples of inhibitors of SDH and ATP synthase.

1.3.5. Targeting the apicoplast

The apicoplast of *Plasmodium* parasite apparently resulted from endosymbiosis, allowing to obtain an organelle that keeps unique metabolic pathways such as heme synthesis, fatty acid and isoprenoid metabolism that are not found in the human host¹⁵³. In this way, these parasitic specific pathways are an excellent source of drug targets¹⁵⁴.

Fatty acid biosynthesis is crucial to cell growth, differentiation and homeostasis and also for the synthesis of membranes which contributes to turn this pathway the major function of apicoplast. Fatty acids are produced through repeated cycles of elongation reactions that include condensation, dehydration, and reduction. The resultant acyl substrate is bound to the acyl carrier protein that delivers the substrate from one enzyme to the other¹⁵⁵. Several enzymes are important for this metabolic pathway being responsible for catalyzing different steps of this process⁹⁸. Some of these enzymes are β -ketoacyl-ACP-reductase (FabG), β -hydroxyacyl-ACP-dehydratase (FabZ)

and enoyl-ACP-reductase (FabI or ENR). The last enzyme is a key regulator of fatty acid biosynthesis and has already been validated for the development of antimalarial drugs¹⁵⁶. Contrasting with this process, fatty acid biosynthesis occurs in mammals by a multi-enzyme complex that control all the enzymatic steps needed. In this way, the two pathways are fundamentally distinct allowing the design of selective drugs against this target.

The natural antibiotic thiolactomycin (**1.88**, Figure 1.25) is able to inhibit several enzymes in this metabolic pathway displaying an IC_{50} value against the parasite growth of $50 \mu M$ ¹⁵⁷. Triclosan¹⁵⁸ (**1.89**) is a known inhibitor of FabI being also an important lead to design novel inhibitors against this specific target¹⁵⁹⁻¹⁶⁰ (for instance, compounds **1.90**, **1.91** and **1.92**). Triclosan is much more active against *P. falciparum* than thiolactomycin exhibiting an IC_{50} of $1 \mu M$.

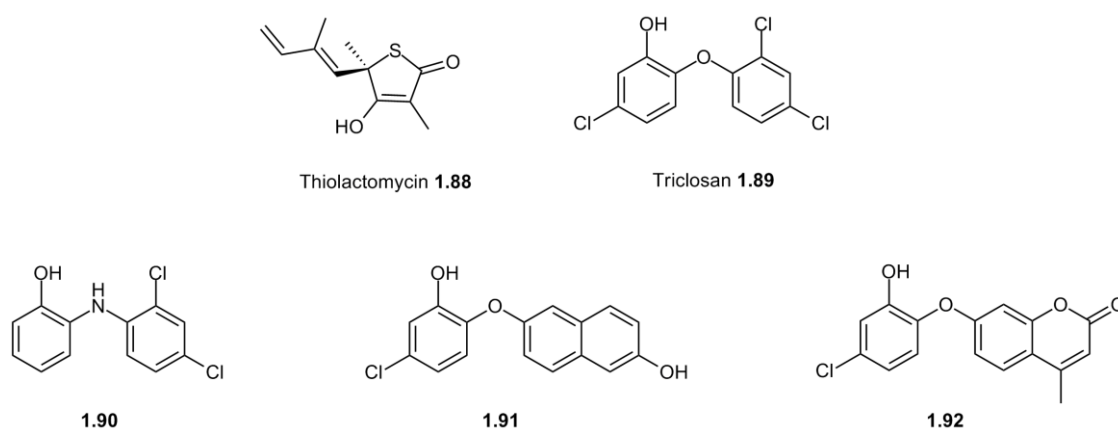


Figure 1.25. Examples of inhibitors of fatty acid biosynthesis.

Isoprenoids are an important class of lipid components forming prosthetic groups of some enzymes. These compounds are also often required for protein anchoring and for the synthesis of biologically important molecules such as ubiquinone. These molecules are constituted by repeated units of isopentenyl pyrophosphate (IPP) and dimethylallylpyrophosphate (DMAPP) being synthesized via a non-mevalonate pathway (1-deoxy-D-xylulose-5-phosphate pathway). Moreover, fosmidomycin (**1.93**, Figure 1.26)

is a phosphonic acid derivative with low toxicity that was found to inhibit this pathway leading to the parasite's death. This compound was also significant to suggest the importance of this pathway for the parasite's survival¹⁶¹.

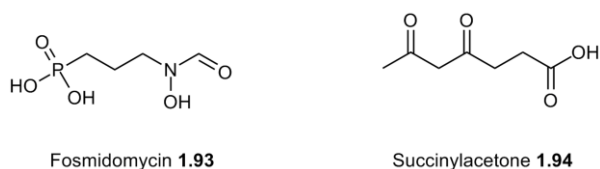


Figure 1.26. Examples of compounds inhibiting isoprenoids and heme biosynthesis.

Concerning heme biosynthesis, it has been shown that malaria parasite synthesizes heme *de novo* being both mitochondria and apicoplast involved in this metabolic procedure¹⁶². The parasite holds several cytochromes and the heme prosthetic group is essential for their correct function. In this way, malaria parasite synthesizes heme by *de novo* pathways, despite the accumulation of large quantities of polymeric heme derived from the hemoglobin of the host red cell¹⁶³. Furthermore, succinylacetone (**1.94**, Figure 1.26) was found to inhibit this pathway demonstrating not only the dependence of the parasite in the heme biosynthesis pathway but also the value of this target to develop new antimalarial drugs¹⁶⁴⁻¹⁶⁵.

Several antibiotics are already known to display an important antimalarial effect due to their action on bacterium-derived endosymbiotic organelles, the mitochondrion and/or the apicoplast. Both organelles have their own DNA and bacteria-like machinery for replication, transcription and translation^{98, 166}. Apart from tetracyclines, which are considered to act primarily against mitochondrion¹⁶⁷, all other antibiotics are thought to act on the apicoplast⁹⁸. Generally, the majority of antibiotics do not show any visible effect in the first intracellular cycle, nevertheless, during the second cycle, the parasites are killed after the invasion of the new host cell. It was proposed that the inhibition of the apicoplast due to the action of the antibiotic may cause liponic acid starvation, increasing the oxidative stress and mitochondrial injury during the subsequent asexual reproductive

cycle¹⁶⁸. A different theory states that apicoplasts inherited by parasites treated with antibiotics contain deficient levels of specific proteins required for the import and processing of nuclear gene-encoded proteins needed for normal function. Due to the delayed kill effect of these drugs, the symptoms of malaria remain for a longer time when antibiotics are used as single agents than when a classical antimalarial is used. As a result, antibiotics are only used in combination with a faster-acting drug in the case of acute malaria. In this kind of combination, classical antimalarials should quickly reduce the parasite burden while antibiotics will deal with the remaining parasites.

Until this moment, no significant resistance of malaria parasites against antibiotics was found¹⁶⁹. Included in the antibiotic group are a diversity of compounds like several quinolones, rifampicin (**1.96**, Figure 1.27), and some protein biosynthesis inhibitors like tetracycline (**1.97**) and macrolides.

One example of a quinoline used as antimalarial is ciprofloxacin (**1.95**). This drug has been shown to induce cleavage of the plastid DNA displaying the highest activity against *P. falciparum* parasites among the quinolines generally used in antibacterial therapy¹⁷⁰⁻¹⁷¹. Several antibiotics like tetracyclines, macrolides, and chloramphenicol, which are known for their translation inhibition in prokaryotic systems, are also proposed to inhibit protein synthesis inside the apicoplast¹⁷². Doxycyclin (**1.98**) is the most widely used antibiotic of the tetracycline class against malaria. This drug is used in combination with quinine or artesunate both for the treatment of uncomplicated and severe malaria¹⁷³. Concerning the macrolides class, azithromycin (**1.100**) was verified to be more active than erythromycin (**1.99**)¹⁷⁴. Moreover, an *in vitro* study demonstrated a synergistic effect when azithromycin was used with CQ on CQ-resistant strains¹⁷⁵ while clindamycin (**1.101**), a lincosamide, showed a synergistic or additive effect *in vitro* with dihydroartemisinin¹⁷⁶.

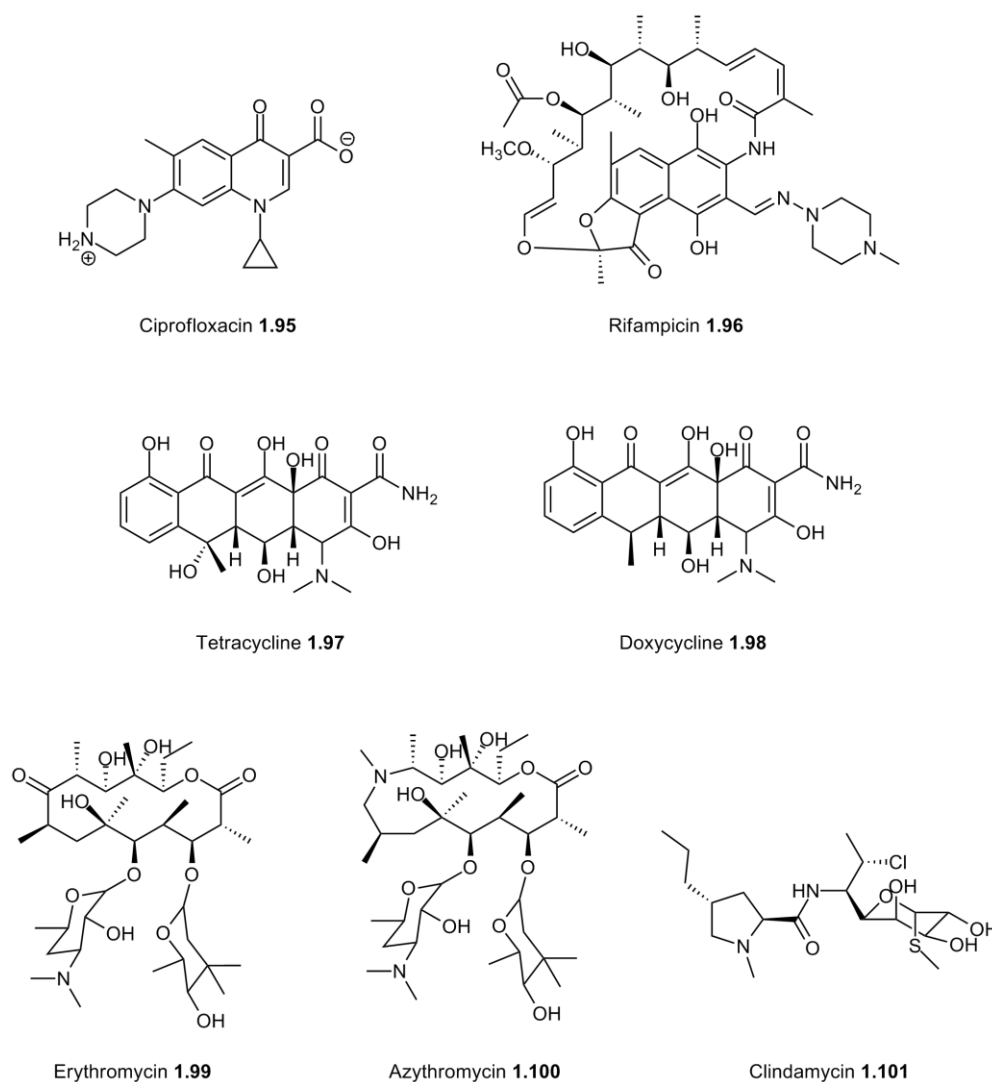
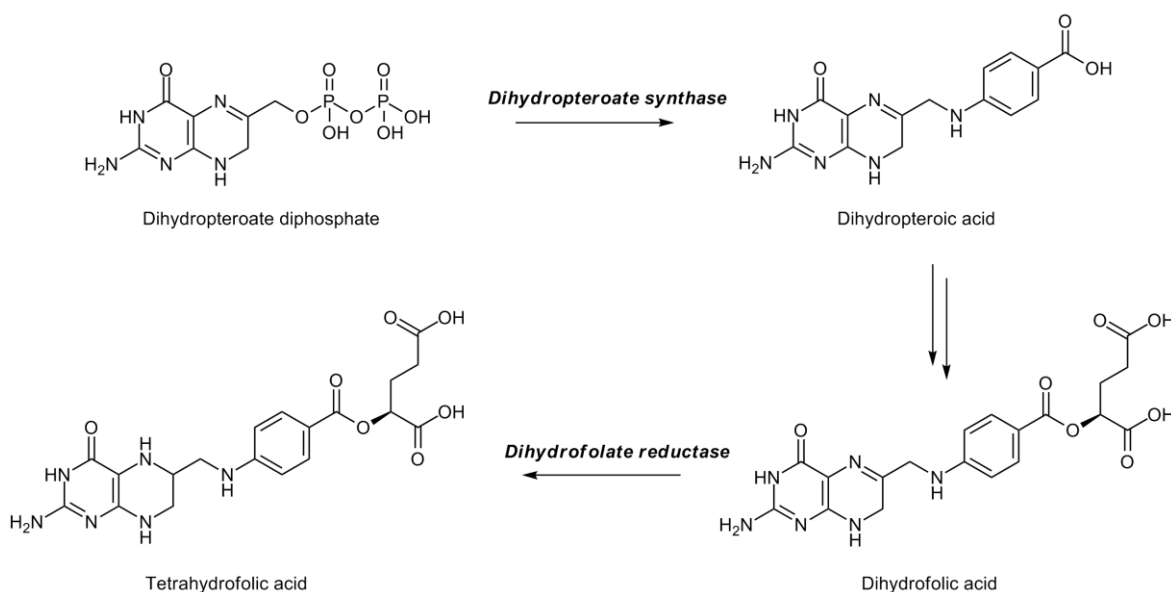


Figure 1.27. Examples of antibiotics acting against *P. falciparum*.

1.3.6. Targeting the cytosol

The cytosol is the location of several metabolic pathways, engaging in numerous enzymes that are essential for the survival of the parasite. Due to the vital importance of these enzymes, they could be considered potential drug targets. However, many of these metabolic pathways are well conserved between species leading to an increased difficulty on the identification of compounds that act selectively against the parasite. Nevertheless, folate metabolism has already been proved to be a valuable target for antimalarial drugs (Scheme 1.7)¹⁷⁷.



Scheme 1.7. Simplified folate pathway. Adapted from Schlitzer *et al*⁷.

Antifolate drugs target two related enzymes of the biosynthesis of tetrahydrofolic acid: the dihydropteroate synthase (DHPS) and dihydrofolate reductase (DHFR). In most species, DHFR has a key role in the folate biosynthesis pathway being responsible for the generation of the DNA base, deoxythymidinemonophosphate (dTMP). DHFR is also important for the biosynthesis of purine nucleotides and the amino acids histidine and methionine. While humans depend on dietary intake of pre-formed dihydrofolic acid as an essential nutrient to be further reduced to tetrahydrofolic acid, pathogenic microorganisms can synthesize this essential molecule from simple precursors using these two key enzymes of the folate biosynthetic pathway.

Consequently, inhibitors of these two key enzymes have been used in the treatment of bacterial and protozoal infections. Moreover, while DHPS is absolutely absent in humans, there are several differences between the DHFR in parasitic protozoa and in humans which allow the development of inhibitors that selectively target this enzyme¹⁷⁸. Inhibitors of DHPS include competitive inhibitors of 4-aminobenzoic acid (Figure 1.28), the endogenous substrate of this enzyme, like sulfonamides (sulfadoxine, **1.102**) and sulfones (dapson, **1.103**). Included in DHFR set of inhibitors are pyrimethamine (**1.104**) and cycloguanil (**1.105**). In therapy, not cycloguanil but its open

chain biguanid prodrug proguanil (**1.53**, Figure 1.16) is provided and the metabolic oxidative ring closure of proguanil results in cycloguanil¹⁷⁷. In contrast with other antimalarial drugs already considered, the mechanism of interaction of DHFR inhibitors with its target was already identified at a molecular level¹⁷⁹⁻¹⁸⁰. The X-ray structure of this enzyme is well known which contributes to clarify the interactions between the inhibitors and the active site of this target.

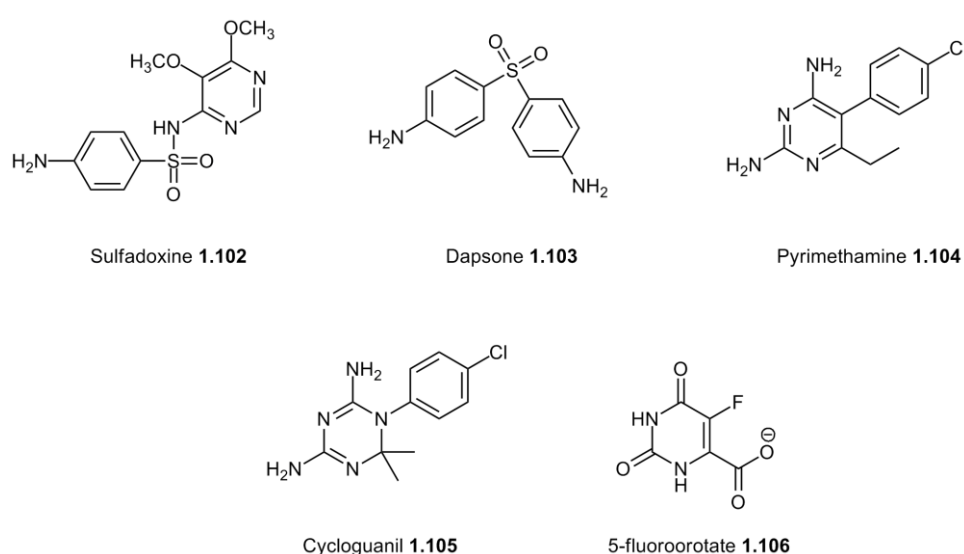


Figure 1.28. Examples of antifolates acting as antimalarial drugs.

Resistance against DHFR inhibitors developed due to the widespread use of these compounds. Therefore, several mutations were found in *dhfr* gene. The replacement of Ser108 by a residue of asparagine (S108N) is the key mutation for resistance and is responsible to decrease the sensitive of *PfDHFR* toward pyrimethamine and cycloguanil. The triple mutant S108N/N51I/C59S and the quadruple mutant S108N/N51I/C59R/I64L were also found making the parasite even less sensitive to pyrimethamine and cycloguanil inhibitors¹⁸⁰⁻¹⁸¹.

Some studies revealed that the combination of sulfonamides, inhibiting DHPS, with a DHFR inhibitor showed synergistic effects. Sulfadoxine (**1.102**) showed to potentiate pyrimethamine (**1.104**) effect on human *P. falciparum* infections,

demonstrating that the combination of these two drugs permitted to obtain better results than either drug alone. This synergism is thought to depend strongly on DHPS but its mechanism is not fully understood¹⁸².

Moreover, other folate pathway enzymes may also be effective as drug target for antimalarial drugs. For instance, 5-fluoroorotate (**1.106**) is a prodrug which metabolite is highly active against thymidylate synthase¹⁸³⁻¹⁸⁴.

Glycolysis is another cytosolic pathway of extreme interest for designing antimalarial drugs since malaria parasites rely on this pathway for energy production. More specifically, *Plasmodium* parasites are believed to lack a functional Krebs cycle during the intraerythrocytic growth phase depending mainly on glycolysis for its energy requirements¹⁸⁵. One of the enzymes present in this pathway is lactate dehydrogenase that is responsible for the reduction of pyruvate to lactate in order to generate NAD⁺. The disesquiterpene gossypol (**1.107**, Figure 1.29) demonstrated to be active against this target displaying moderate *in vitro* activity for both CQ-resistant and sensitive strains of *P. falciparum* with IC₅₀ values around 10 μM¹⁸⁶. Additionally, this enzyme was already structurally characterized which allowed to develop selective inhibitors¹⁸⁷⁻¹⁸⁸.

Nucleic acid metabolism can also be considered an important drug target within parasite cytosol. Nucleotides, being precursors of DNA and RNA biosynthesis, are essential for the survival of parasites. *Plasmodium* parasites are not able to synthesize purines relying on salvage of the human host. In contrast, the pyrimidines need to be synthesized *de novo* since they can not salvage these building blocks. In this way, both purine salvage and pyrimidine synthetic pathways can be considered potential drug targets. Both pathways involve several indispensable enzymes while pyrimidine synthesis also depends on mitochondrial electron transport¹⁸⁹. Moreover, it was also demonstrated that inhibition of the purine salvage pathway with transition state analogue inhibitors of *Plasmodium* purine nucleotides, such as Immucillin-H (**1.108**) can be lethal for *P. falciparum in vitro*.

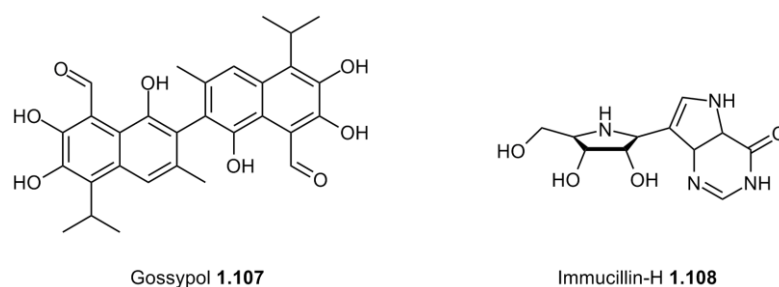


Figure 1.29. Inhibitors of glycolysis and purine salvage pathway.

1.4. Antimalarial chemotherapy during liver stage

The most currently used antimalarial drugs are mainly active against the blood stage acting quickly against the parasite forms that invade erythrocytes and cause the malaria symptoms. Nevertheless, before the entire clinical symptoms take place, pre-erythrocytic life cycle stages have already invaded and developed in the liver. In this way, since liver stage always comes first than blood stage, the complete inhibition of parasites in this stage would lead to causal prophylaxis blocking also the transmission. Accordingly, the liver stage of *Plasmodium* life cycle is of extreme importance for designing potent and effective antimalarial drugs¹⁹⁰⁻¹⁹¹. Moreover, it was also been suggested that this type of treatment might be preferred in order to minimize the risk of drug-resistance emergence. However, there is strong difficulty to develop drugs acting in this phase due to the intrinsic biology of *Plasmodium* species and the technical issues related with its study¹⁹⁰.

Several compounds with recognized antimalarial activity against blood stage are also considered to act against the liver stage. Included in this set are, for example, the bc_1 complex inhibitor atovaquone (**1.52**, Figure 1.16), the antibiotics clindamycin (**1.101**, Figure 1.27), tetracycline and oxycycline (**1.97** and **1.98**, respectively), the antifolate proguanil (**1.53**, Figure 1.16), and others^{190, 192}.

However, until now, only primaquine (**1.109**, Figure 1.30) is used against liver stage. Additionally, this drug is also able to kill the persistent hepatocytic forms (hypnozoites) that are responsible for causing relapsing malaria. Moreover, primaquine is still the only available drug against gametocytes, which are responsible for the

transmission of parasites between human host and mosquito¹⁹³. Unfortunately, this drug presents some inconveniences related mainly with its low bioavailability and its tendency to cause hemolytic anemia in patients with glucose-6-phosphate dehydrogenase deficiency, the most common human enzyme deficiency^{192, 194}.

Tafenoquine (**1.110**), a primaquine analog, is currently under Phase IIb/III clinical trials and was proven to be highly active against the latent hypnozoites. Although displaying the same secondary effects on patients with glucose-6-phosphate dehydrogenase deficiency, tafenoquine has the advantage of being a single-dose treatment¹⁹⁵.

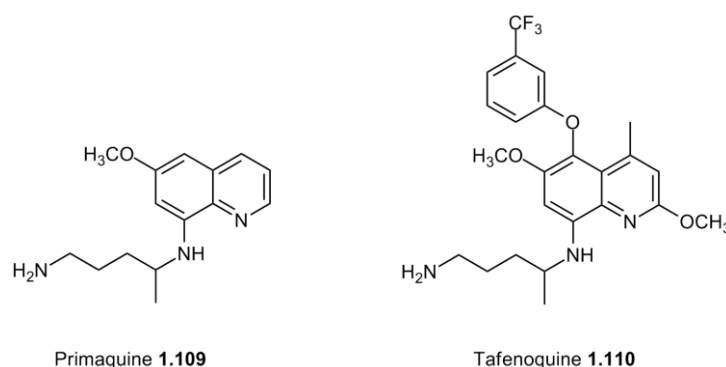


Figure 1.30. Compounds acting against *P. falciparum* liver stage.

Given that drugs able to act in this stage can provide efficient causal prophylaxis that would contribute to control the widespread of malaria, the development of antimalarial drugs acting specific in liver stage is highly desirable.

1.5. Antimalarial drug resistance and artemisinin-based combination therapies

In the 1940s, expectation on malaria eradication increased when CQ was discovered and introduced as potent antimalarial drug. Moreover, the use of this drug combined with the potent insecticide dichlorodiphenyltrichloroethane (DDT) promptly showed to be successful in reducing the malaria cases worldwide¹⁹⁶. However, resistance to CQ rapidly

emerged leading to a huge decline in its therapeutic efficacy and to a consequent impasse in all efforts to eradicate this disease.

After *P. falciparum* developed resistance against CQ, several other drugs including a combination of sulfadoxine-pyrimethamine, mefloquine, quinine, and others, were introduced but all these efforts were unproductive since multidrug-resistant parasites rapidly emerged¹⁹⁷. As consequence, there was an overall resurgence of morbidity and mortality due to this infection.

As a result of the emergence of resistance in the last decades, WHO started to recommend artemisinin-based combination therapy (ACT) as the key treatment of *P. falciparum* malaria¹⁹⁸. This type of treatment combines artemisinin or an artemisinin derivative (for example artesunate, artemether or dihydroartemisinin) and an additional drug presenting a longer half-life in the bloodstream. This second drug can be typically amodiaquine, mefloquine, piperaquine sulfadoxine-pyrimethamine, pyronaridine tetraphosphate or lumefantrine. The rationale behind this combination therapy is mainly related with the different properties of the two drugs used. More specifically, the combination of an artemisinin derivative, displaying poor pharmacokinetic properties, with a longer-lasting associated drug may guarantee the treatment efficacy due to a higher concentration of antimalarial drugs in the bloodstream during more time¹⁹⁹. In this way, the antimalarial treatment can benefit from the ability of the artemisinin derivative to reduce effectively the parasitemia which results in a smaller amount of parasites that are further eradicated by the combined drug^{198, 200}. Moreover, the combination of two drugs may also improve antimalarial efficacy providing additive or synergistic antiparasitic activity. Consequently, not only the overall treatment is more efficient but also drug resistance can be prevented since the drugs used in combination usually display different modes of action and, for that reason, different resistance mechanism¹⁹⁹.

Despite all efforts made to prevent artemisinin monotherapy and to introduce ACT as the first-line treatment, partial resistance has already emerged in some malarial endemic regions. Additionally, these resistant strains may reach other regions becoming a

further global risk for malaria control and treatment since currently there is no alternative drugs to substitute artemisinin derivatives for fighting malaria²⁰¹⁻²⁰².

1.6. Computational approaches in antimalarial drug discovery

The drug development of antimalarial drugs can be restrained by similar issues as any other drug development procedure. The new agents need to show efficacy, safety and, especially in the case of malaria, must be significantly widespread and easily afforded in developing countries. Moreover, in this specific case, drugs should be dosed orally and be effective in a single-dose regimen being curative in short time. However, new drugs against malaria are still greatly required and many approaches have been pursued in antimalarial drug discovery.

Throughout the first step of the drug development's process, the main goal is to identify new compounds with pharmacological interest. These compounds are usually small organic molecules that are able to interact with specific targets (for instance, receptors, enzymes, or nucleic acids) and that can cause a perturbation in their cellular functions²⁰³. During the last decades, several techniques were improved in order to revolutionize all the process of identifying new potential drugs. Therefore, experimental identification of small molecules with the desired activity can be achieved using high-throughput screening²⁰⁴ (HTS) allied with combinatorial chemistry²⁰⁵ techniques. As a result, the combination of both techniques enabled the synthesis of large libraries of chemical compounds and, in addition, the screening of these compounds against several targets in a fast and efficient way. However, all the procedure of obtaining and testing millions of compounds is very expensive which can be considered a huge limitation that reduces the usability of HTS²⁰³.

An alternative to experimental HTS is high-throughput virtual screening (VS), which has become a typical tool in medicinal chemistry²⁰⁶. This technique uses computational power to test large libraries of chemical compounds in few days at lower costs. Compounds are selected by predicting their binding affinity to a biomolecular

target using adequate computer programs. Using this approach, not only real compounds can be tested but also purely theoretical ones can be included in the virtual library and screened *in silico*. In addition, VS has been shown to be effective in several studies using a good set of filters (Lipinski's rule of five, ADME restrictions, substructure similarity searches or pharmacophores, for instance)^{203, 207}. As a result, VS is a very powerful tool that allows purchasing or synthesizing only a reduced set of selected compounds thus reducing significantly the cost and time of the entire study^{203, 206, 208}. However, some weaknesses have also to be considered. For instance, this technique also requires the knowledge of the tridimensional structure of the receptor, which sometimes is not available. In this way, the quality and the amount of information regarding the target under inspection is a critical factor to take into account when designing a computer-assisted drug design experiment like VS²⁰⁹.

In a virtual screening study, usually a funnel strategy is followed²¹⁰. More precisely, this is a multi-step structure-based filtering strategy that hierarchically combines several different docking methods in order to extract a small set of potential new hits from a vast library of drug-like compounds. Thereafter, this smaller set is analyzed in more detail. Structurally diverse libraries will lead to more varied results, permitting to obtain novel and innovative chemical structures. Moreover, the results of chemical database querying can be refined using docking programs with ligand-receptor algorithms that are able to rapidly process a large number of compounds. Afterward, structurally diverse scaffolds selected by this method need to be further analyzed using experimental validated enzymatic and/or cell-based assays and optimized in order to identify new interesting chemical structures.

Various docking programs can be used presently to assess the best conformations of each candidate in terms of the energy and positioning. These programs include Gold²¹¹⁻²¹², FlexX²¹³, Glide²¹⁴⁻²¹⁶, LigandFit²¹⁷, AutoDock (AD)²¹⁸, AutoDock Vina (AD Vina)²¹⁹, and others, presenting some differences mainly in their performance against specific targets. Moreover, these programs can optimise interactions in the active site allowing for the discovery of novel pharmacophoric groups. New drugs are further designed based on

previous leads and the stability of the ligands inside the binding pockets can be further refined using molecular dynamics simulations.

Several virtual screening studies were already successful in providing new classes of potential antimalarial drugs. Many of these studies include not only a structure-based virtual screening but also other computational techniques, for instance pharmacophore generation and homology modeling allowing to improve the efficacy of this procedure. In particular, several potential inhibitors were identified through this technique for enzymatic targets such as *Pf*DHFR²²⁰⁻²²², falcipains²²³⁻²²⁶, plasmepsins²²⁷⁻²²⁹, enoyl-acyl carrier protein reductase (*Pf*ENR) in fatty acid biosynthesis pathway²³⁰⁻²³¹, mETC^{74, 232-233}, and others. In Figure 1.31 are highlighted some examples of compounds active against different antimalarial targets that were discovered using this type of approaches.

Additionally, some computational studies were also made in order to discover new antimalarial compounds acting against non-specific targets. In this context, several approaches, including validated quantitative structure-activity relationship (QSAR) models and structural descriptors based on training sets that include known antimalarial compounds, can be employed²³⁴⁻²³⁷. This kind of procedure may increase the efficiency of the virtual screening method and, in spite of the specific antimalarial target being unknown, it may be successful in the early discovery of several compounds as starting points of novel antimalarial agents.

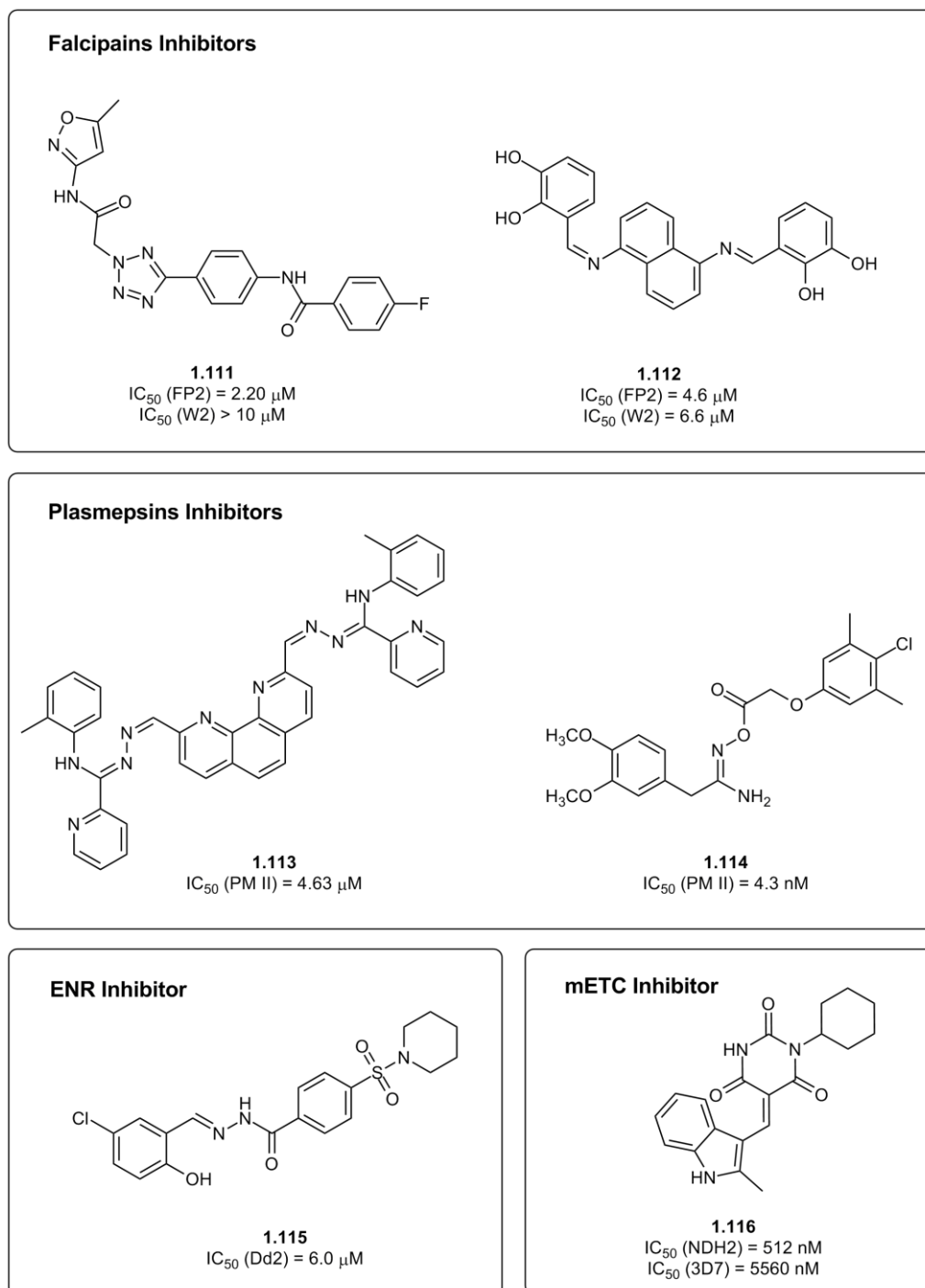


Figure 1.31. Examples of antimalarial compounds discovered by virtual screening.

1.7. Concluding remarks

Besides the importance of malaria as an emergent infection worldwide, the development of antimalarial chemotherapeutics has long been neglected by pharmaceutical industry in

industrialized countries. Unfortunately, current antimalarial therapeutics started to lose efficacy due to the increasing resistance developed in several endemic countries. As a result, discovery of new drug targets and potential new drugs are highly required. In the last years, considerable efforts have been made through public-private partnerships in order to expand the knowledge related with antimalarial chemotherapeutics. Further antimalarial drug development can follow several strategies, namely, it is possible to improve existing drugs by slight modifications or design new drugs that can act against new targets. Recent advances in genomics and proteomics in addition to the technical progress in structural biology and high-throughput screening methods were of extreme importance to develop new approaches in antimalarial chemotherapy.

The new drugs obtained in future studies, both acting in conventional and novel targets will definitely contribute to increase the therapeutic repertory in the fight against malaria.

CHAPTER TWO

List of contents

2.1. Background	57
2.2. Validation of <i>P. falciparum</i> bc_1 complex model and binding mode of stigmatellin	59
2.3. Binding mode of atovaquone	67
2.4. Binding mode of floxacrine and WR249685	69
2.5. Binding mode of GW844520	73
2.6. Concluding Remarks	76

2. *S. cerevisiae* bc_1 Complex as a Model for *P. falciparum* bc_1

Complex

2.1. Background

The bc_1 complex, one of the components of the mitochondrial electron transport chain, is crucial for the survival of *P. falciparum* and therefore is an attractive and already validated target for antimalarial drug development^{3, 238}. As a result, the structural information about this target is of extreme importance to successfully design new inhibitors for bc_1 complex. Unfortunately, until now, the crystallographic structure of this antimalarial target is still not available. Therefore, in the absence of a crystallographic structure for the bc_1 complex from *P. falciparum*, much of the key structural and mechanistic information has been obtained from analogous mammalian, bacterial and yeast bc_1 systems^{96, 99-103}. More specifically, the bc_1 complex of *S. cerevisiae* has already been chosen in previous studies to model the mechanism of action of antimalarial leads in the *P. falciparum* bc_1 complex^{105-109, 239}. This organism has been selected due to the (i) high sequence identity in the oxidation pocket (Q_o) between both species (in close contact with the pocket, there is only one non-conserved residue - Leu275Phe)^{104, 139}, (ii)

availability of an *S. cerevisiae* bc_1 crystal structure, with good resolution¹⁰¹⁻¹⁰³ and (iii) close relation between inhibitory activity in the two species¹³³.

Therefore, in a first attempt to design new bc_1 complex inhibitors that can interact with the oxidation pocket, a computational study was developed to better elucidate the binding mode and interaction mechanism between experimentally identified Q_o bc_1 inhibitors (Figure 2.1) and the bc_1 enzymatic complex of yeast.

In order to ensure comparable values for biological activity, only inhibitors experimentally screened in a single biological test and using the same protocol were chosen. Included in this set are stigmatellin, atovaquone, two dihydroacridinediones (floxacin and WR 249685) and a pyridone (GW844520). The IC_{50} values (Figure 2.1) were derived from inhibition of the *P. falciparum* bc_1 complex determined by reduction of cytochrome *c* with decylubiquinol as an electron donor¹³³.

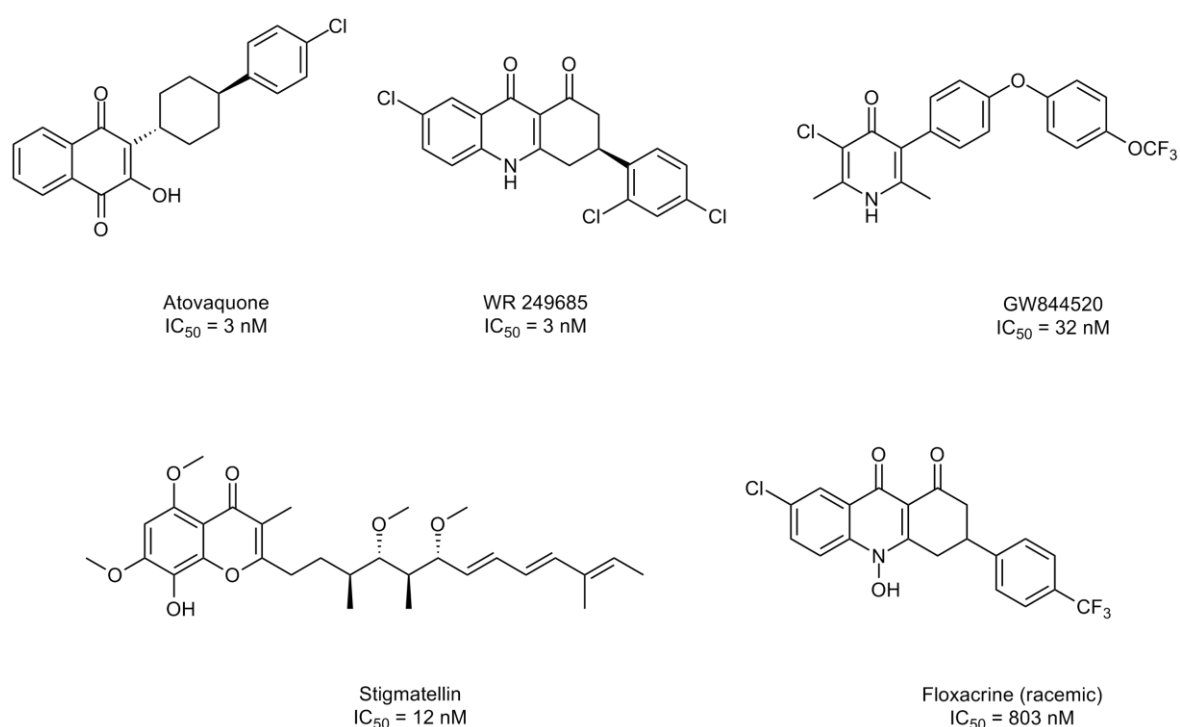


Figure 2.1. The Q_o bc_1 complex inhibitors studied.

Myxothiazol was excluded since it belongs to a different subgroup within the Q_o class inhibitors (binds in a very specific part of the pocket, proximal to the b_L heme, while the considered inhibitors bind in distally)²⁴⁰. In particular, this compound has a different binding mode since it causes the displacement of Glu272 rotamer inside the pocket, as seen in PDB 1SQP.

In order to obtain the best model for the Q_o binding site of bc_1 complex, several docking procedures were employed. As a result, not only the quality of the two more recently obtained PDB coordinates of *S. cerevisiae* bc_1 complex were tested but also the environment inside the Q_o binding site was taken into account. More specifically, two amino acid residues were more deeply studied – Glu272 from the highly conserved cytochrome *b* PEWY sequence²⁴¹ and His181, one of the [2Fe-2S] cluster ligands in the Rieske protein. These two residues were chosen since they were already shown to be essential in the catalytic process²⁴²⁻²⁴⁴ once they are direct ligands of the natural substrate and are the primary acceptors for the protons released upon substrate oxidation. Therefore, the interaction of both residues with potential bc_1 complex inhibitors is essential. In this study, the importance of the protonation state of His181 was investigated due to experimental evidence showing that when stigmatellin is bound in the Q_o pocket, this residue is protonated²⁴⁵. Additionally, computational studies indicate that the protonation state of this residue can change during the catalytic cycle depending on the oxidation state of the cytochrome bc_1 ²⁴². Furthermore, the influence of a catalytic water molecule in the vicinity of Glu272 was also tested in order to evaluate how the inhibitory ability of the selected compounds could be affected by its presence.

2.2. Validation of *P. falciparum* bc_1 complex model and binding mode of stigmatellin

In a first step, to assess the validity and reliability of the docking procedures used in this study, bound stigmatellin was redocked into the Q_o binding site of yeast bc_1 complex using AD as the docking software.

As mentioned before, two PDB structures, 1KYO¹⁰² and 3CX5¹⁰³, were chosen to perform this study. Yeast *bc*₁ complex coordinates with PDB code 3CX5 are more recent than 1KYO and display better resolution (1.90 Å). Furthermore, to test and optimize the docking procedure, the environment inside the pocket was also tested in the several docking experiments.

The results obtained were evaluated by comparing the best ranked pose of stigmatellin with the pose of this inhibitor crystallized in the PDB structure through a root mean square deviation (RMSD) calculation using VMD 1.8.7²⁴⁶ (Table 2.1). RMSD values were calculated both for the entire inhibitor structure and for the rigid aromatic moiety. An assessment of the predicted binding free energy (ΔG_{calc}) and the equivalent value obtained experimentally (ΔG_{exp}) was also made. For each PDB structure, the most favorable docking pose was identified by the scoring function/binding energy and its similarity with the crystallographic pose of stigmatellin in the active site.

Table 2.1. Root mean square deviation (RMSD) and binding free energy (ΔG) obtained for stigmatellin in different docking experiments with neutral His181 (His181), with His181 protonated (His181 H⁺) and with the crystallographic water near Glu272 (His181 + water).

X-ray structure	Experimental conditions	RMSD (Å)		ΔG (kcal.mol ⁻¹)	
		all atoms	aromatic moiety	Calculated	Experimental
1KY0	His181 H ⁺	1.119	0.759	-10.12	
	His181	1.798	0.839	-8.44	
3CX5	His181 H ⁺	1.570	0.585	-10.94	-12.12
	His181	2.138	0.743	-9.79	
	His181 + water	1.795	0.788	-9.36	

The total average RMSD value of 1.684 Å shows the ability of the docking procedure to predict the binding mode of stigmatellin. This is a satisfactory value taking

into account the size of the molecule and the number of rotatable bonds of this inhibitor (13). However, a consistent lower value was obtained when using protonated His181, which is in accordance with experimental evidence showing that His181 is protonated when stigmatellin is bound in the Q_o active site^{101, 245}. When considering only the benzopyranone ring of stigmatellin, which is responsible for specific interactions with the amino acid residues described as essential for inhibition (the rigid planar moiety of this molecule), a much better average RMSD is obtained (0.743 Å). Again, a lower RMSD value was obtained with protonated His181, showing that the docking procedures employed in this study are able to accurately predict the binding mode of stigmatellin in the Q_o binding site. The superposition of the best ranked pose of stigmatellin (considering His181 protonated) with the pose of this inhibitor crystallized in the X-ray structure is shown in Figure 2.2.

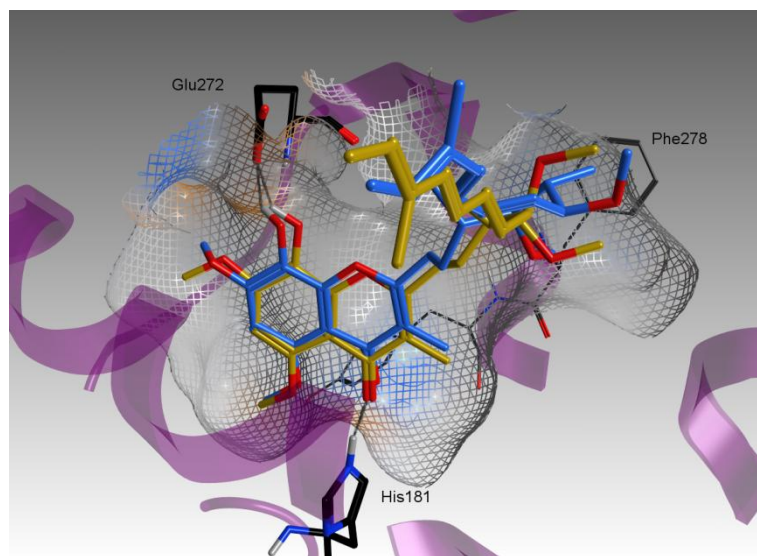


Figure 2.2. Comparison of the poses of crystallographic stigmatellin (carbon atoms in yellow) and the best ranked pose of this inhibitor (carbon atoms in blue). Hydrogen bonds are represented by grey lines.

Moreover, the differences between the binding free energy values obtained in these calculations and the experimental one for 1KY0 and 3CX5, $\Delta\Delta G_{(\text{exp-calc})}$, are within the residual standard error of AD (2.18 kcal/mol)²⁴⁷ only when His181 is protonated (2.00 and 1.18 kcal/mol, for 1KY0 and 3CX5, respectively).

It was previously recognized that the carbonyl oxygen atom of stigmatellin is positioned in a favorable geometry to establish a strong interaction between this moiety and His181^{101, 245}. Consequently, to enable hydrogen bond formation, the residue of His181 must be protonated or, if this residue is in its neutral state, the presence of a water molecule is required. However, there is no experimental evidence confirming the presence of a water molecule in the vicinity of His181 when stigmatellin is inside the Q_o pocket¹⁰¹⁻¹⁰³. As a result, His181 must be protonated, which is in line with the results achieved.

An important observation that also emphasizes the quality of the predictions can be drawn from the data of Table 2.1. The binding free energy is correlated with the RMSD obtained for the aromatic moiety (the benzopyranone ring), more specifically, the closer the pose to the crystallographic one, the lower is the free energy and the closer it is to the experimental free energy value.

Regarding the results obtained for the two different X-ray structures, some comparisons can be made. Interestingly, higher binding free energy values were found for 1KYO when compared with 3CX5. When both X-ray structures are aligned, in particular chains E and N (as described in RCSB Protein Data Bank²⁴⁸ and corresponding to the Rieske protein and cytochrome *b*, respectively) slight variations are found in the conformation of some residues. This can be related with the lower resolution of the structure 1KYO and can contribute to the differences of binding free energy values observed in the docking procedures. The energy values obtained for 3CX5 are lower than for 1KYO indicating that the interactions established between stigmatellin and the residues of the pocket site are more favorable when the former coordinates are used. Moreover, it is important to notice that residue 122 in Rieske protein (chain E) is not correctly assigned in 1KYO. According to the sequence of the mitochondrial *bc*₁ complex of *S. cerevisiae*²⁴⁹, this residue should be an isoleucine, as in 3CX5, rather than a threonine residue, as revealed by 1KYO. Although the interactions between this residue and the inhibitors in Q_o active site are not particularly strong, this amino acid is located in the access to the pocket and, therefore, its hydrophobic or hydrophilic characteristics are extremely important. In the case of stigmatellin, the presence of these two chemically

distinct amino acids also contribute to explain the poorer results obtained with structure 1KYO, since the hydrophobic chain of stigmatellin interacts directly with the active site entrance (within no more than 4 Å) where residue 122 is situated. This result strongly founded on the quality and resolution of both structures was the first indication that the 3CX5 could be a better model structure than 1KYO.

Currently, only the structure of stigmatellin co-crystallized in the Qo active site of the yeast bc1 complex is available. Therefore, the structural basis for binding to the active site by this inhibitor is an important tool to elucidate the binding mode of the bc1 inhibitors presented in Figure 2.1.

Considering that all inhibitors in this analysis bind the Qo active site and their structural similarities with stigmatellin, it is expected that these inhibitors interact with the ubiquinol oxidation pocket in a similar mode. Accordingly, the results obtained in this docking study for the different inhibitors were compared with the pose of stigmatellin inside the ubiquinol oxidation pocket and with the significant interactions formed between this inhibitor and the most important residues, namely His181 and Glu272.

The results obtained for all inhibitors (Figure 2.1) in the five docking experiments are presented in Table 2.2. As for stigmatellin, different docking conditions were applied i.e. the two PDB coordinates (1KYO and 3CX5), with different protonation states for His181 were tested.

In order to assess which docking procedure could better predict the inhibitory activity of the studied molecules, correlations between $\log IC_{50}$ and ΔG_{bind} were evaluated. Quite reasonably, the $\log IC_{50}$ for *P. falciparum* bc₁ inhibition correlated with the ΔG_{bind} values ($r^2=0.87$) determined using 3CX5 coordinates with neutral His181 (Figure 2.3).

Considering the relative strength of the correlations obtained based on the values in Table 2.2 for the different docking experiments, it was possible to conclude that for most of the inhibitors studied, the activity can be explained using as model the 3CX5 coordinates with the residue His181 in its neutral state. Although in the case of stigmatellin the protonation of the His181, as expected, stabilizes the complex ($\Delta\Delta G = -1.15$ kcal/mol), it has the opposite effect on the binding of myxothiazol ($\Delta\Delta G = 1.29$

kcal/mol) putting one of the best inhibitors at the bottom of this relative inhibition scale. For all others, the His181 protonation just shifts the values towards a higher stabilization by no more than 0.5 kcal/mol.

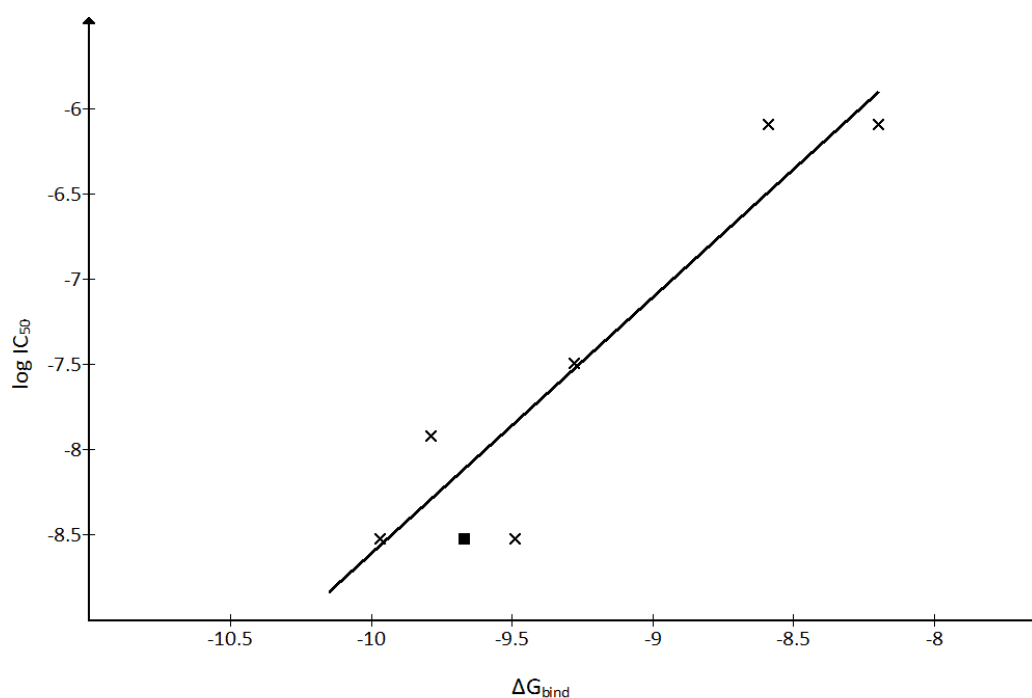


Figure 2.3. Correlation obtained between the experimental $\log IC_{50}$ and calculated ΔG_{bind} obtained using the 3CX5 coordinates with neutral His181 ($r^2=0.87$). The square represents the binding free energy obtained for atovaquone in the presence of the minimized water molecule in the vicinity of Glu272 ($r^2=0.92$; linear fit not presented).

When testing the effect of the presence of crystallographic water in the vicinity of Glu272 on the binding free energy, the best ranked pose had stigmatellin flipped (i.e. hydrophobic chain in the inner part of the pocket). Since this could be due to a sampling problem (sampling the three dimensional and conformational spaces) three more attempts were done using different random number generator seeds. The respective values, presented in Table 2.2, are the average values obtained for the docked poses of stigmatellin, with the aromatic moiety of the molecule located in the internal part of the pocket. However, the water can stabilize atovaquone, WR249685 and S-floxacin

suggesting that, for some of the inhibitors, a water molecule may be important to mediate a hydrogen bond between the inhibitor and Glu272. Therefore, and unless specifically stated otherwise, all discussion of the docking results will be drawn based on the docking of the ligands in the 3CX5 structure with neutral His181.

Table 2.2. Docking results of the available inhibitors at different experimental conditions: with neutral His181 (His), with His181 protonated (His H⁺) and with a crystallographic water near Glu272 (+ water). Free energies in kcal.mol⁻¹, K_i and IC₅₀ in nM. Experimental values obtained by Biagini *et al*¹³³

	1KY0		3CX5			Experimental	
	His H ⁺ $\Delta G_{\text{calc}} / K_{i\text{calc}}$	His H $\Delta G_{\text{calc}} / K_{i\text{calc}}$	His H ⁺ $\Delta G_{\text{calc}} / K_{i\text{calc}}$	His H $\Delta G_{\text{calc}} / K_{i\text{calc}}$	His + water $\Delta G_{\text{calc}} / K_{i\text{calc}}$	$\Delta G_{\text{exp}} / K_{i\text{exp}}$	IC ₅₀
Atovaquone	-9.29/153.86	-9.03/243.27	-9.96 / 50.35	-9.49 / 110.23	-9.67 / 81.75	-12.99 / 0.3	3 ± 2
WR 249685	-9.72 / 75.08	-9.76 / 70.20	-10.20 / 33.37	-9.97 / 49.27	-10.13 / 37.16	-12.99 / 0.3	3 ± 2
Stigmatellin	-10.12 / 38.35	-8.44 / 650.53	-10.94 / 9.56	-9.79 / 66.58	-9.78 / 67.12	-12.12 / 1.3	12 ± 1
GW844520	-8.89 / 232.88	-8.95 / 275.55	-9.44 / 120.10	-9.28 / 158.28	-9.25 / 164.28	-11.53 / 3.5	32 ± 13
S-Floxacrine	-8.53 / 527.52	-8.60 / 496.34	-8.49 / 598.37	-8.20 / 975.39	-8.57 / 518.01	-9.62 / 89	803 ± 183
R-Floxacrine	-8.97 / 265.24	-8.68 / 431.37	-9.00 / 252.23	-8.59 / 501.42	-8.54 / 544.93		

2.3. Binding mode of atovaquone

The binding mode of atovaquone inside the ubiquinol oxidation pocket is depicted in Figure 2.4. This antimalarial drug is able to inhibit selectively the parasite mitochondrial electron transport chain at the Q_o binding site⁵. It is possible to observe that the hydroxyl group at the position 3 of the hydroxynaphtoquinone, one of the principal features of this molecule that contribute to its activity²⁵⁰, interacts with the N_τ of His181 via a hydrogen bond (3.1 Å). Atovaquone may also establish an additional hydrogen bond between the carbonyl oxygen group at position 1 on the quinone ring and the carboxylate oxygen of Glu272 of cytochrome *b* (3.4 Å), mediated by a water molecule in the correct position, since the conformation of the docked structure is in a favorable geometry to allow the formation of this interaction. Considering that this amino acid residue is anionic, Glu272 acts as a proton acceptor. Consequently, in order to allow the formation of this hydrogen bond between the carbonyl group and the glutamate carboxylate, the presence of a water molecule is essential to mediate this interaction. Atovaquone was docked in the presence of the water molecule crystallized near Glu272 and showed almost no change in the binding energy (Table 2.2). It is important to notice that during the docking process, the coordinates of this molecule are rigid and are in accordance with the position of stigmatellin inside the oxidation pocket. Therefore, in the case of atovaquone, the position of this water molecule is not adequate to allow the formation of a strong hydrogen bond between the carbonyl oxygen group of the ligand and Glu272. In the absence of a water molecule, although the interactions found between atovaquone and the amino acid residues in the oxidation binding site can be considered favorable, the distance between the atoms that are involved in the hydrogen bonds are longer than what is expected for a strong hydrogen bond interaction (Figure 2.4). As a result, the weaker hydrogen bonds formed between this inhibitor and the amino acids in the binding pocket can contribute to the lower score and, consequently, to the higher binding free energy value (Table 2.2). These weak interactions can also be significant to explain the deviation obtained for atovaquone in the correlation achieved between the binding free energy of the docked ligands and the experimental IC_{50} value (Figure 2.3).

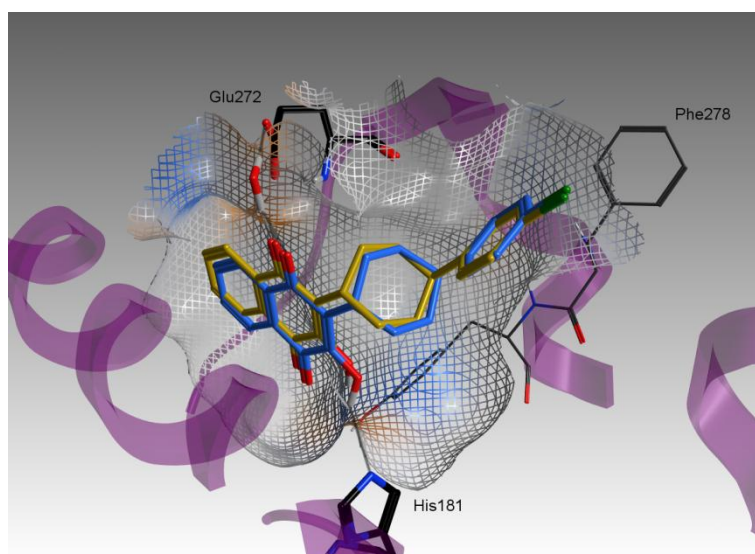


Figure 2.4. Predicted binding poses for atovaquone without the crystallographic water (carbon atoms in yellow) and in the presence of a minimized water molecule near Glu272 (carbon atoms in blue). Hydrogen bonds are represented by grey lines.

In a previous docking study of the binding mode of atovaquone, using PDB code 1EZV¹¹¹, it was possible to note that the presence of a water molecule is crucial to obtain a good interaction between this inhibitor and the binding pocket, especially with Glu272. Since the study of the flexible position of water molecules inside the binding pocket, to facilitate the arrangement of more favorable hydrogen bonds, is not possible to be performed directly with AD, the importance of the presence of this molecule in the inhibitory activity of atovaquone could only be deduced by optimizing the position of the water molecule inside the oxidation pocket. Therefore, to address this issue, the position of a water molecule crystallized in the vicinity of Glu272 was energy minimized, in the presence of docked atovaquone, using MOE. For this minimization, only water and atovaquone were considered flexible, keeping the bc_1 backbone and all the amino acid residues fixed as tethered atoms. Iterating between docking atovaquone with AD in the presence of rigid water and optimizing both molecules in MOE led to better docked poses and enhanced score values for this inhibitor (Figure 2.4).

The first binding free energy value obtained for atovaquone in the absence of the water molecule was -9.49 kcal/mol (Table 2.2) while, in the presence of the minimized

water molecule, the binding free energy was enhanced to -9.67 kcal/mol. This way, it was possible to get a more satisfactory correlation between the binding free energy and the IC_{50} values (Figure 2.3). It was observed that atovaquone in the presence of water that can mediate an H-bond with Glu272 moves closer to His181 making stronger hydrogen bonds that can explain this change in the binding free energy (Figure 2.4) i.e. the H-bond formed between the hydroxyl group of the hydroxynaphtoquinone and the N_{τ} of His181 was weaker in the absence of the water molecule than the one obtained with the water optimization (the distance decreased from 3.1 to 2.5 Å). In this case, an hydrogen bond is established between the carbonyl group of the inhibitor and water (1.7 Å) followed by a second H-bond between water and the carboxylate moiety of Glu272 (1.8 Å). It is important to notice that the aromatic and rigid moiety of atovaquone is maintained in the same plane in both poses (Figure 2.4) and that the position of atovaquone is only adjusted to allow the formation of two stronger hydrogen bonds. By moving towards His181 it promotes the formation of a stronger hydrogen bond with this residue and the interaction in a more favorable way with the water molecule near Glu272. This shows that although in the case of stigmatellin the crystallized water is relevant to stabilize the Glu272 charge, in the case of atovaquone, and possibly other molecules without a hydrogen donor group located near this residue (e.g. GW844520), water can both mediate a hydrogen bond and stabilize the complex.

Atovaquone's proximity to several aromatic residues that contribute to create an hydrophobic binding zone is also favorable. Since this inhibitor is mostly hydrophobic due to the cyclohexyl side-chain at position 2 and the chlorophenyl substituent that dock in the vicinity of this hydrophobic area, it allows π - π interactions with Phe278 and Tyr279 of the E-ef loop (conserved domain containing residues of cytochrome b^{101}), within a distance from the atovaquone aromatic moieties of about 3 and 4 Å, respectively.

2.4. Binding mode of floxacrine and WR249685

The binding modes of the two dihydroacridinediones considered in this study, floxacrine (a racemic mixture) and WR249685 (the *S* enantiomer of WR243246), in the most

energetically favorable conformation, are shown in Figure 2.5 and Figure 2.6. The mode of action of these inhibitors against *P. falciparum* has already been proposed based on experimental evidences^{133-134, 251}.

Surprisingly, when WR 249685 was docked in the Q_o site, no interaction with Glu272 or His181 was found. However, the hydrogen bond between the nitrogen atom of the dihydroacridinedione ring (2.56 Å) and the carbonyl backbone of Leu275 stabilizes the inhibitor inside the pocket. The other interactions are mostly hydrophobic, predominantly with the residues of the E-ef loop. It is also important to note that, in the most favorable pose, the dihydroacridinedione moiety is approximately parallel to Tyr279 at a distance of 3 Å and, in addition, it also interacts favorably with Phe278, which contributes to establish good π - π stacking interactions. Interestingly, the chlorine atom in the *para* position can also interact suitably with Tyr132 of cytochrome *b* through an edge-on Cl- π contact²⁵²⁻²⁵³. The halogen interactions have mostly an electrostatic nature and, although they are relatively weak, can help to explain binding affinity²⁵⁴⁻²⁵⁶. This specific halogen interaction may also contribute to the different fitting found for this inhibitor.

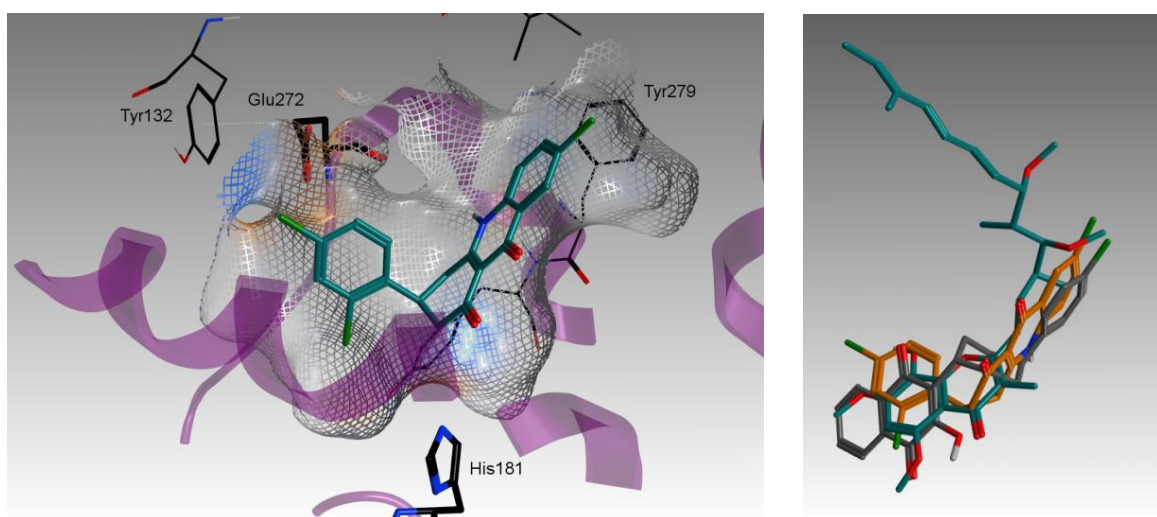


Figure 2.5. Predicted binding pose for WR249685 on the left, and a comparison of the poses of crystallographic stigmatellin (green), atovaquone (grey) and WR249685 (orange), on the right.

Figure 2.5 compares the pose obtained for WR249685 with the crystallographic pose of stigmatellin and the one obtained for atovaquone. Although the aromatic ring located deeper in the pocket is not perfectly parallel with the rings for the other molecules, this inhibitor adapts to the binding pocket in a very similar way as stigmatellin and, especially, atovaquone. The superimposition of these three inhibitors show that the poses obtained for atovaquone and WR249685 share similarity, being the aromatic moieties that interact closer to the pocket entrance coplanar and almost superposed in both structures.

Both enantiomers of floxacrine were docked in the Q_o binding pocket and the best ranked pose, for each, is shown in Figure 2.6. Both *S* and *R* enantiomers of floxacrine share similar interactions with His181 and Glu272. Interestingly, the two enantiomers are able to interact with these two residues using the same H-bond donor and acceptor groups. In both cases, the hydroxyl group of the dihydroacridinedione ring is in good position to interact with the Glu272, with a distance of 2.6 and 2.7 Å for *S* and *R*-floxacrine, respectively.

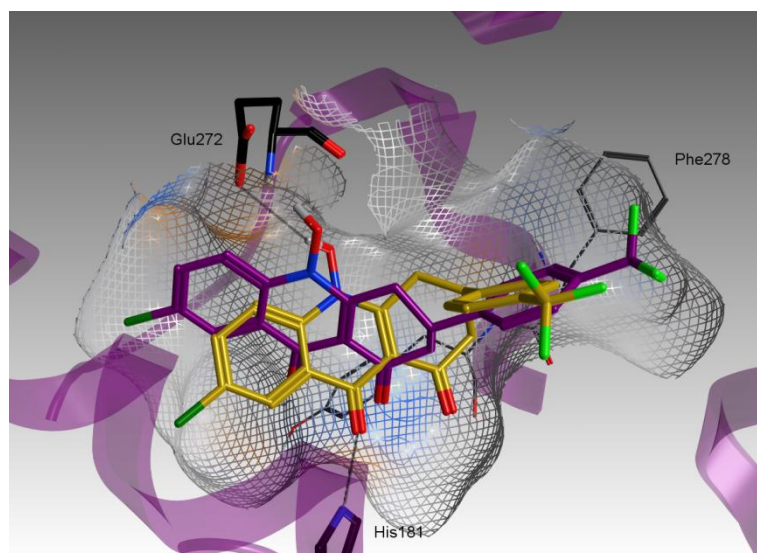


Figure 2.6. Predicted binding pose for enantiomers *R* (carbon atoms in yellow) and *S* (carbon atoms in purple) of floxacrine. Hydrogen bonds are represented by grey lines.

Like in the case of stigmatellin, the interaction between the H-acceptor of the dihydroacridinedione ring, the carbonyl oxygen atom, and His181, requires the intervention of a water molecule or a change of the protonation state.

For the *S* enantiomer, it is the carbonyl oxygen atom in position 1 that makes this interaction while in the case of *R* enantiomer it is the carbonyl in position 9. These small differences concerning the specific hydrogen interactions contribute to slightly different poses inside the pocket. A lower binding free energy value of -8.59 kcal/mol was obtained for *R*-floxacin when compared to -8.20 kcal/mol of *S*-floxacin. However, there are no experimental evidences that confirm the better activity of one of the enantiomers when compared to the other.

When considering *S*-floxacin and WR249685, the binding mode of these two inhibitors was thought to be similar due to the analogy existing in both structures. Since, WR249685 is a 10-desoxy derivative of floxacin, bearing a different C-3 phenyl pattern and an added chlorine atom in the benzene ring, the substitution of the chlorine by the trifluoromethyl group should have a small impact in the properties since these two substituents are bioisosters. In the case of WR249685, the aromatic moiety with the two chlorine substituents probably contributes to this different arrangement, not only due to the possibility of favorable halogen interactions, but also as a result of the added size due to the second chlorine atom. Although the size of a trifluoromethyl group is similar to chlorine, fluorine is a smaller halogen than chlorine having a different electrostatic nature and, therefore, the trifluoromethyl substituent in floxacin is not able to establish favorable halogen interactions with amino acid residues. Although both WR249685 and floxacin have donor groups at the same position, the added size of an OH group could also disallow floxacin to have a similar pose as WR249685.

Attempting to assure the reliability of the different poses obtained for these inhibitors and to get a clear picture of the relevant features conducting to the two completely different poses, an additional molecule based on the chemical structure of both WR249685 and floxacin, was also docked using the same experimental conditions. The chemical structure of this molecule includes the two main moieties of both inhibitors:

the hydroxyl substituent in the acridinedione ring, as floxacrine, and the aromatic side chain with the two chlorine substituents, as in the case of WR249685 (Figure 2.1). The comparison of the docked pose of this molecule and WR249685 (Figure 2.7) allows to conclude that it is the presence of the chlorine substituents in the aromatic ring that completely change the pose of the inhibitor inside the binding pocket, and, consequently, the interactions established between the inhibitor and the amino acids in the Q_o site. Moreover, it is also important to notice that the presence of this aromatic moiety decreased the binding free energy of floxacrine ($\Delta G = -8.20$ kcal/mol for *S*-floxacrine and $\Delta G = -10.25$ kcal/mol for the tested molecule) which indicates that the presence of the chlorine substituents contribute to increase the inhibitory ability of WR249685 when compared with the racemic mixture of floxacrine.

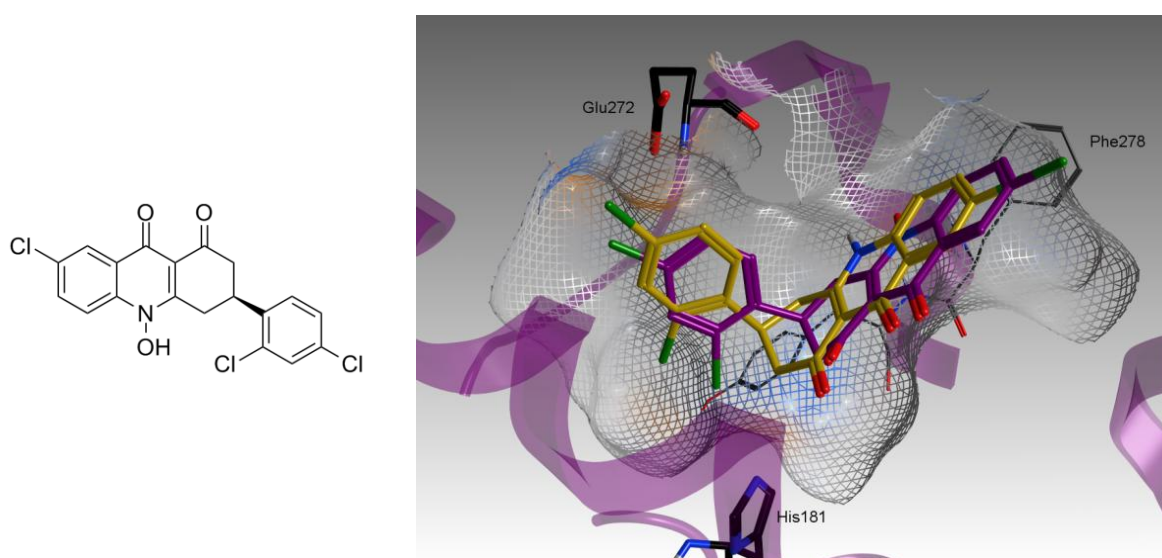


Figure 2.7. Chemical structure of the tested molecule on the left, and comparison between the predicted binding poses of WR249685 (carbon atoms in yellow) and of the new tested molecule (carbon atoms in purple) on the right.

2.5. Binding mode of GW844520

The analysis of the most favorable pose of GW844520 (Figure 2.8), a 4(1*H*)-pyridone that selectively inhibits the bc_1 complex^{63, 127}, shows that it interacts with the binding pocket

by several hydrophobic contacts between the aromatic substituent in position 3 and the E-ef loop (like in atovaquone, it is also stabilized by π - π stacking interactions with aromatic amino acids, specifically Phe278 and Tyr279). GW844520, comparable to other known pyridones, may establish two important H-bonds with Glu272 and His181 which are of extreme importance in keeping the ligand in the right position inside the pocket. The nitrogen atom of the pyridone ring is in an appropriate geometry to interact with N_{τ} of His181 (1.9 Å). Similar to atovaquone, the carbonyl oxygen of the pyridone ring, being a hydrogen bond acceptor, requires the presence of a water molecule to mediate an H-bond with Glu272.

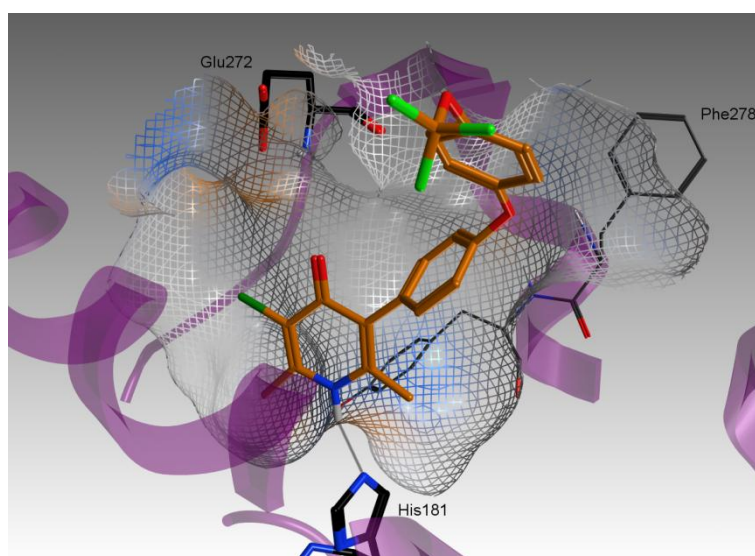


Figure 2.8. Predicted binding pose of GW844520. Hydrogen bonds are represented by grey lines.

Two docking experiments, in the absence and presence of a water molecule in the vicinity of Glu272, were performed to test this effect on the binding free energy of GW844520 (Table 2.2). Like in the case of atovaquone, the presence of the crystallized water molecule does not improve the value of binding free energy in spite of being needed to mediate a strong hydrogen bond between the carbonyl group of the pyridone and the Glu272 residue. The explanation for this weak interaction between GW844520 and the water molecule is identical to the one already stated for atovaquone: since the

coordinates of this molecule are rigid and are in accordance with the position of the co-crystallized ligand inside the pocket (stigmatellin), the position of this water molecule is not adequate for the formation of a strong H-bond between GW844520 and the Glu272 residue. As a result, the optimization of the position of this water molecule in the presence of the inhibitor was performed, decreasing the binding free energy in 0.46 kcal/mol. However, the presence of the optimized water molecule has no impact on the pose of GW844520 inside the pocket i.e. the presence of this additional H-bond between the carbonyl group of the pyridine ring and the water hydrogen (the same distance of 2.2 Å was found for the H-bond between the water hydrogen and Glu272), does not move GW844520 closer to Glu272 and keeps the distance between the nitrogen donor of the pyridone ring and N_τ of His181 constant (1.9 Å).

It is important to stress that some care should be taken when analyzing the results of the water optimizations. In the docking procedure the addition of extra hydrogen bonds will stabilize the complex and, therefore, will decrease the binding free energy. However, the contribution of breaking and making hydrogen bonds by changing water position is not accounted in the calculations. Comparing the docking processes, with and without water optimization, for GW844520 we are substituting two strong hydrogen bonds (between water and Glu272) with two weak hydrogen bonds (between GW844520 and water and between water and Glu272). This part of the physical process will not be spontaneous, the free energy will be positive and, therefore, the decrease in the total free energy of binding with water optimization is over-estimated. Moreover, the presence of the water shows basically no impact in the pose of GW844520 inside the pocket and, therefore, the binding free energy without the water optimization should give in this case a better estimation. It should also be noted that a different behaviour is found for atovaquone since, with the optimized water, the pose is closer to His181 (increasing the strength of the H-bond between atovaquone and His181) and two other strong hydrogen bonds are formed (1.8 and 1.7 Å).

2.6. Concluding remarks

Considering the results obtained with the two PDB structures used and the different docking procedures employed, it was possible to conclude that the most appropriate model is based on the 3CX5 coordinates, with a better resolution than 1KYO. Considering His181, only in the case of stigmatellin, and in agreement with experimental findings, the protonation of this residue was found to be very important. This result was expected having in mind the moiety of the inhibitor that interacts with this amino acid, specifically the carbonyl group. For the other molecules studied, it was possible to obtain a good prediction of the inhibitory activity considering the X-ray structure with His181 in its neutral state. Accordingly, this model was accepted as the preferred one to explain the molecular basis of inhibition in the Q_o active site. Moreover, when considering the presence of the water molecule in the vicinity of Glu272, the results obtained stress the importance of this molecule to mediate a strong H-bond between atovaquone and this residue through the consequent change of the molecule's pose and, therefore, on the positive impact upon the inhibitory activity. In the case of GW844520, and taking into account the good correlation found between the calculated binding free energy for all inhibitors and the logarithm of their IC_{50} , the high inhibition activity of this ligand could be explained in the absence of the water molecule. For that reason, the presence of a water molecule has no impact on the predicted docked pose of GW844520 inside the Q_o binding pocket.

By inspecting the predicted binding modes of the tested inhibitors it was possible to recognize that they are arranged in a very similar way inside the pocket and make similar interactions with Q_o active site residues. In general, part of the inhibitors' structure interacts favorably with both His181 of the Rieske protein and Glu272 of the conserved PEWY region and, consequently, the interactions with these two amino acid residues can be considered of extreme relevance for the inhibitory activity. The only exception found was for WR249685. However, despite presenting different interactions, this inhibitor displays a similar arrangement inside the active pocket to the one found for the crystallographic stigmatellin.

In conclusion, this study permitted to recognize the molecular basis of action of known bc_1 inhibitors inside the Q_o active site and establishes a good predictive method to determine the inhibitory potential of possible new inhibitors taking into consideration the binding free energy values obtained with the docking calculations.

CHAPTER THREE

List of contents

3.1. Background	81
3.2. Virtual screening of TCAMS	81
3.3. Virtual screening of MOE Database	87
3.4. Concluding Remarks	104

3. Virtual Screening Studies over *S. cerevisiae* bc₁ Complex

3.1. Background

Taken into account the advantages of performing a virtual screening study in order to identify hits with potential pharmacological interest, two different drug-like databases were screened over the *S. cerevisiae* bc₁ complex using the experimental conditions validated in the Chapter 2. The main goals of this study were to conclude about the reliability of *S. cerevisiae* bc₁ complex to be used to design new *P. falciparum* bc₁ complex inhibitors and, additionally, to obtain new hits that can be further optimized.

3.2. Virtual screening of TCAMS

The recently released Tres Cantos Antimalarial Set (TCAMS)²⁵⁷ was chosen to be used in the first screening with the yeast model. This database includes around 13500 compounds already confirmed to inhibit parasite growth *in vitro*, by at least 80% at 2 μM concentration, and was obtained after testing almost 2 million compounds present in GSK's screening collection using HTS. All molecules presented in this database were further separated in distinct classes concerning their mode of action. In the absence of specific target information, a similarity principle was used. More specifically, compounds in the same cluster, with analogous chemical structure, are supposed to share the same mode of action. Additionally, included in this set are 122 molecules which were

hypothesized to interfere with the mitochondrial electron transport chain (mETC). These molecules are mainly 4(1*H*)-pyridones and 4(1*H*)-quinolones, two classes of compounds already recognized to disrupt electron transfer by blocking cytochrome *bc*₁ complex¹³³.

This virtual screening study was first performed not only to test the validity of the yeast model but also to evaluate the performance of two available docking programs: AD 4.0^{247, 258} (using DAVIS 2.0 package²⁵⁹) and AD Vina 1.0.2²¹⁹.

3.2.1. Comparison between AutoDock and AutoDock Vina

Generally, docking programs may differ in two basic features: (i) the search method for exploring the conformational space available to the system and (ii) the scoring function used to predict the strength of the interaction between compounds and the potential target. To correctly evaluate the potential of a compound to interact with its target is also important to have in consideration the force field employed since it defines the energetic parameters of each conformation obtained during the docking calculation²⁶⁰⁻²⁶¹. Regarding AD and AD Vina, both programs operate in a very similar manner. The main differences rely in two features described above: the local search function and the scoring function. Concerning the search method that enables to explore the conformational space, AD uses a stochastic search based on genetic algorithms whilst AD Vina performs an iterative gradient-based local search^{219, 247, 258}. Genetic algorithms are based on genetics and biological evolution. More specifically, a compound can be defined by a selection of values that describe its translation, orientation, and conformation with respect to the protein target. These properties are the ligand's state variables and can be encoded into a gene. The evolutionary process starts from a population of randomly generated individual. In each generation, the interaction energy between each compound and the target is evaluated in order to obtain a fitness value. The more fit individuals are selected from the population and the genome of each individual suffers mutations in order to create a new generation. Then, the new generation of candidate solutions suffers the same process. Finally, the algorithm is finished when the maximum number of generations is produced or the desired fitness level is reached^{247, 258}.

For AD Vina, an iterated local search system is performed. With this algorithm, a sequence of steps consisting of a mutation and a local optimization are applied in order to find the best pose. The local optimization takes into account not only the position and orientation of the compound but also the values of the torsions for the compound's active rotatable bonds. One advantage that arises from using this type of algorithm is that the number of steps in a run is adjusted according to the complexity of the calculation²¹⁹.

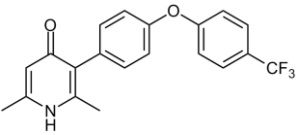
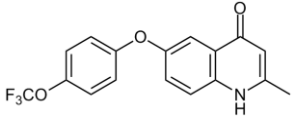
Regarding scoring functions, both programs consider similar energetic terms with parameters adjusted in different ways. More explicitly, the differences found in both scoring functions are not associated with the nature of the energetic contributions but are related with the importance of each term to design the scoring function equations. Therefore, both scoring functions are empirically weighted functions that contain terms that account for intermolecular and intramolecular contributions. Included in the scoring functions are dispersion/repulsion, hydrogen bonding, and electrostatics terms. Usually, the entropic contribution of changes in solvation and conformational mobility are also taken into account^{219, 258}. Moreover, AD Vina has the ability to allow a significant improvement in the virtual screening process since it achieves approximately two orders of magnitude speed-up when compared with the AD. Further speed-up can be achieved from parallelism, by using multithreading on multicore machines²¹⁹. However, the DAVIS package permits to run AD in parallel on hundreds of CPUs contributing to solve time related issues associated to large-scale high-throughput virtual screening²⁵⁹. Some differences can be found between the parallelization mode of both programs which results in the speed-up of AD Vina when compared with AD DAVIS. Namely, while AD Vina is able to perform the docking calculations simultaneously in several CPUs, AD DAVIS only performs the runs one molecule per CPU.

3.2.2. Structure-based virtual screening

The compounds included in TCAMS were independently screened against yeast model (PDB coordinates 3CX5) using the two docking programs mentioned before. Firstly, a special attention was given to the 122 compounds that are supposed to interact with the

mETC, namely, the 4(1*H*)-pyridones and 4(1*H*)-quinolones. This set of compounds were important not only to establish a comparison between the binding free energy values obtained with AD and AD Vina but also to verify if both are able to recognize the score values found for 4(1*H*)-pyridones during the validation process. The ranges of score and binding free energy values obtained for these two classes of molecules are summarized in Table 3.1.

Table 3.1. Summary of the results obtained for 4(1*H*)-pyridones and 4(1*H*)-quinolones during the screening of TCAMS.

Class of Compounds	Example	AD Score	AD Vina Energy (kcal/mol)
4(1 <i>H</i>)-pyridones		[4.60; 7.71]	[-5.9; -10.5]
4(1 <i>H</i>)-quinolones		[4.63; 7.39]	[-7.2; -10.4]

From the data available, it is possible to conclude that both 4(1*H*)-pyridones and 4(1*H*)-quinolones display score values in a wide range with non substituted compounds presenting lower binding affinity with the target. In addition, a more exhaustive analysis of all compounds' data showed that 93% of the 122 compounds hypothesized as mETC inhibitors exhibit score values between 6 and 8 in AD calculations. A comparison between the binding free energy values obtained in this screening and the same values obtained for GW844520 in the previous chapter permitted to conclude that AD was able to successfully predict the characteristic binding free energy values for 4(1*H*)-pyridones as *bc*₁ complex inhibitors. In addition, both programs are able to successfully reproduce the binding mode of this class of inhibitors inside the Q_o pocket. Figure 3.1 shows the predicted binding pose obtaining with AD for compound TCMDC-134570.

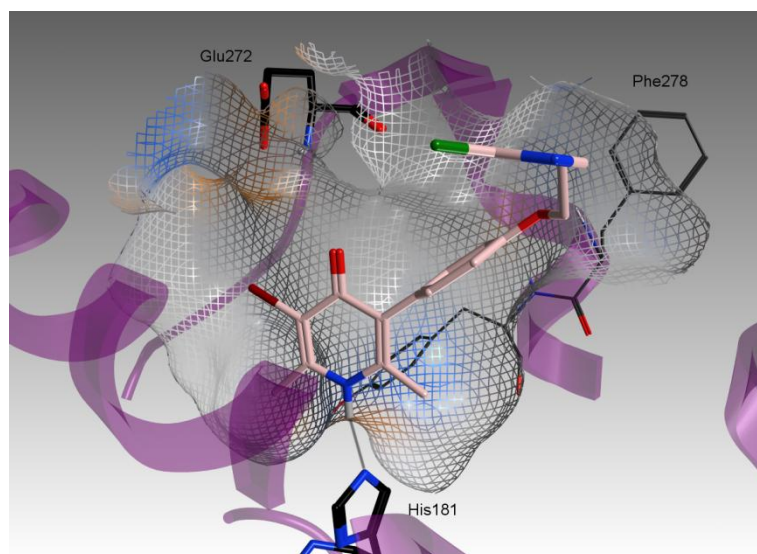


Figure 3.1. Predicted binding mode of TCMDC-134570 obtained with AD. Hydrogen bonds are represented by grey lines.

Furthermore, a correlation between the binding free energy values obtained for these two scaffolds in both docking procedures, was also calculated which permitted to obtain a Pearson correlation value of 0.67 (Figure 3.2).

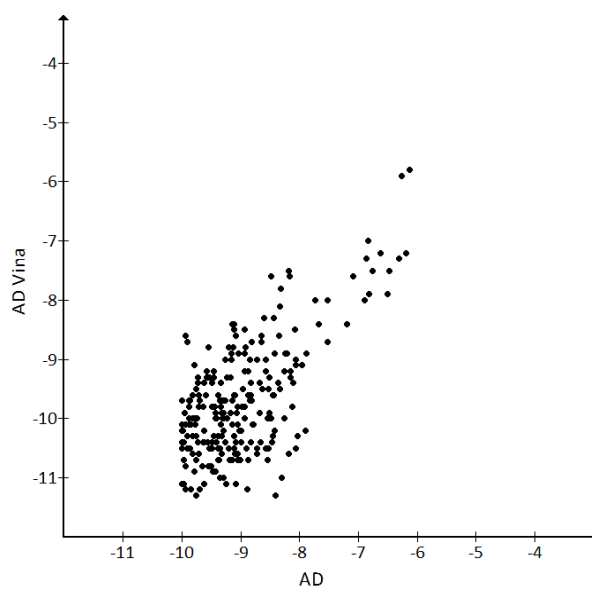


Figure 3.2. Binding free energy correlation between AD and AD Vina.

This value indicates that these two programs, in spite of sharing some differences, show some linear dependence and, consequently, they are both roughly able to recognize typical bc_1 complex inhibitors.

An examination of the results obtained was also done for all compounds presented in this library. More precisely, the score values found using AD were analyzed and collected in Figure 3.3. It is possible to observe that almost 20% of the tested compounds exhibited a score value higher than 8 indicating that several may establish potent interactions with Q_o binding site. In addition, this data suggests that some of the compounds showing *P. falciparum* growth arrest by inhibition of an unknown or different target may also demonstrate potential activity against cytochrome bc_1 and can be considered valuable scaffolds to design new antimalarial drugs targeting this specific enzyme.

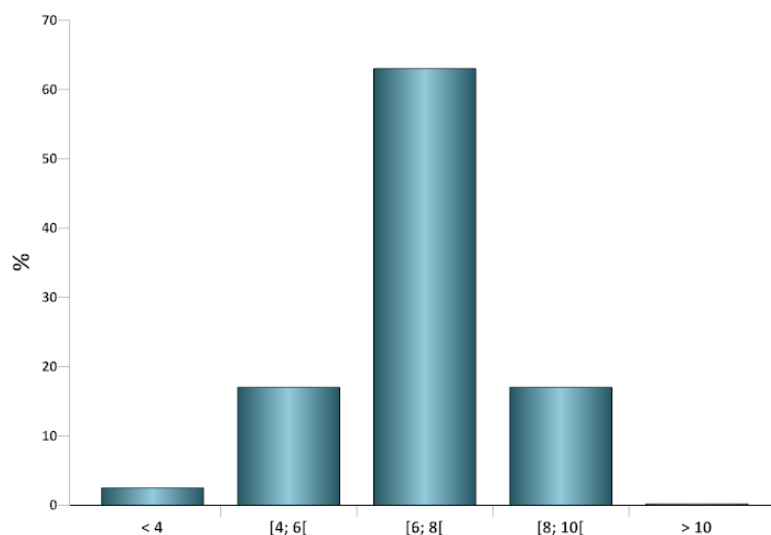


Figure 3.3. Overall score values obtained for TCAMS virtual screening using PDB 3CX5 and AD.

One example of the most interesting structure found (TCMDC-140353) is shown in Figure 3.4. This is an example of a compound having potential activity on the bc_1 complex: the hydrogen bond that can probably be established with the backbone carbonyl of Ile125

in the presence of a water molecule and the hydrophobic interactions with the Q_o site pocket assure the high score value for this molecule.

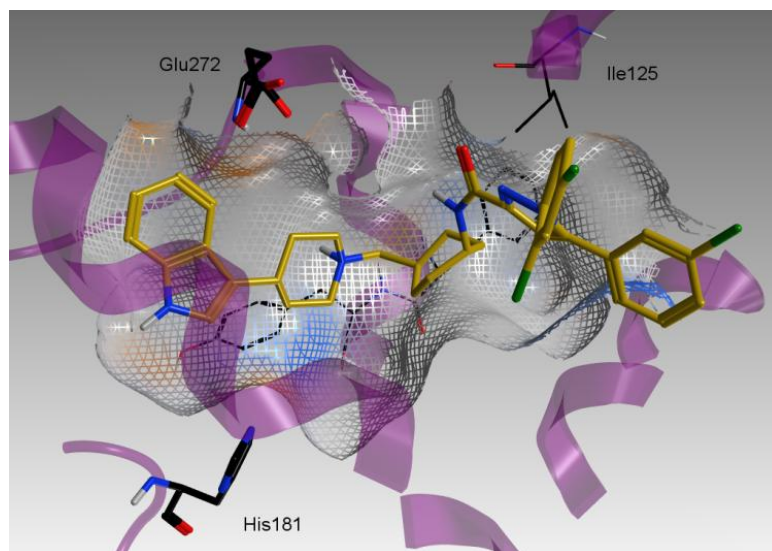
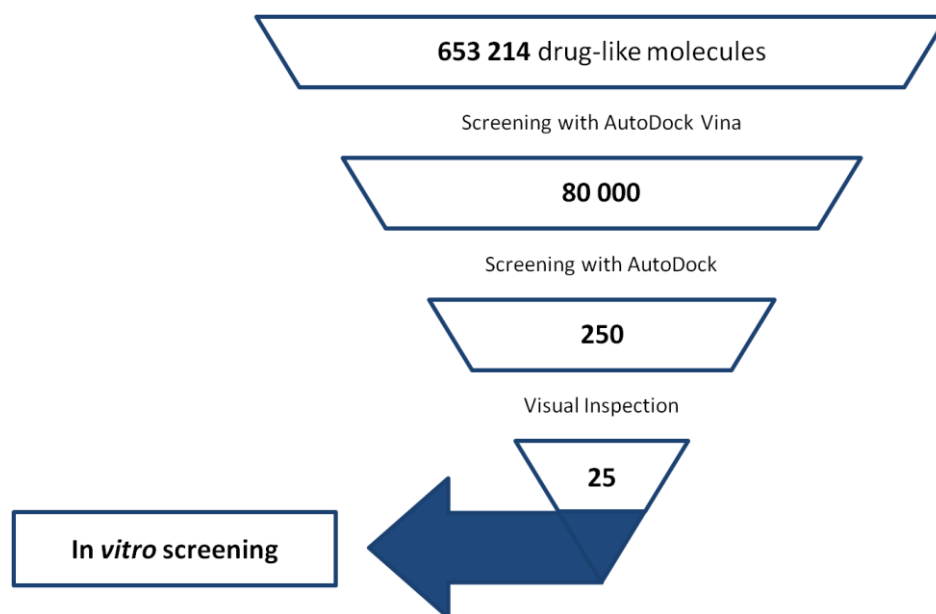


Figure 3.4. Predicted binding pose of TCMDC-140353 obtained with AD.

3.3. Virtual screening of MOE Database

A second receptor-based virtual screening against the druglike MOE database was also performed against the same target. The workflow followed is illustrated in Scheme 3.1.

A collection of 653214 drug-like compounds included in the MOE package²⁶² was screened against the yeast *bc*₁ complex Q_o binding site using AD Vina. This software was used to rank all database molecules, and the best 80000 molecules were further docked with AD. As previously shown, the binding free energy values obtained with both software have good enough correlation to exclude molecules screened with AD Vina having low predicted activity. Therefore, it was possible to use AD Vina to rapidly screen an extensive library of compounds before applying an exhaustive AD screen to the best putative compounds.



Scheme 3.1. Representation of the overall screening process.

The 250 top-ranked structures obtained after refinement with AD (score higher than 7) were visually inspected. Although some compounds possess high score values, some are located distant from the pocket zone where His181 and Glu272 are located. Since the model used for the docking experiments characterize competitive inhibitors that bind to the distal part of the pocket, like stigmatellin, the compounds that bind in a different part of the pocket were rejected. For the majority of the molecules it was possible to identify structural features that permit the formation of strong hydrophobic interactions with the hydrophobic part of the Q_o site. Furthermore, several molecules could establish π - π stacking interactions with Phe278 and Tyr279 as seen above for the inhibitors. Some of these compounds could also interact with Glu272 of the cytochrome *b* and/or His181 from the Rieske ISP.

After visual inspection, 25 potential inhibitors were selected to be purchased from commercial suppliers (Figure 3.5).

The compounds were chosen with the following criteria: (i) score obtained, (ii) interaction with the most important residues in the pocket, (iii) chemical diversity, and (iv) commercial availability.

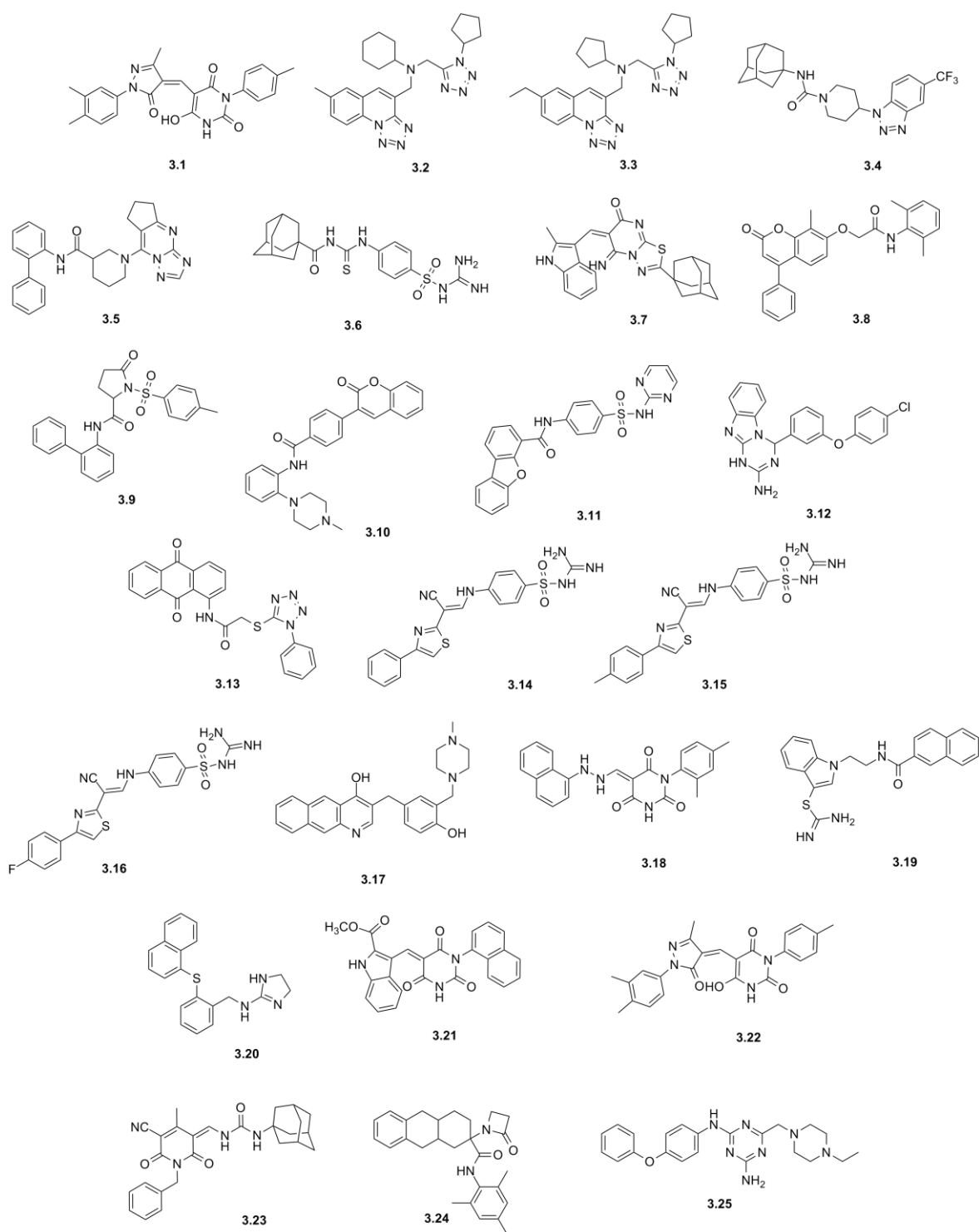


Figure 3.5. Chemical structures of the purchased compounds.

The compounds were obtained from different commercial sources and the respective commercial code is included in Table 3.2. Additional relevant pharmacological properties like $clogP$ were calculated using ALOGPS 2.1²⁶³.

Table 3.2. Some physical properties and antiplasmodial activity of the purchased compounds.

Compound	cLogP	MW / g.mol⁻¹	IC₅₀ (w2) / μM
3.1 Asinex ASN 03775157	3.18	440.54	> 10
3.2 Asinex ASN 06130215	3.26	445.56	> 10
3.3 Asinex ASN 06130599	3.26	445.56	9.16
3.4 Asinex ASN 06365235	4.13	447.50	> 2.5
3.5 Asinex ASN 07104188	4.25	438.52	> 2.5
3.6 Chembridge 5549172	2.72	435.56	> 10
3.7 Chembridge 7461561	4.74	443.56	> 10
3.8 Chembridge 7676526	4.95	413.47	> 10
3.9 Chembridge 7816742	3.35	434.51	> 10
3.10 Chembridge 7950798	4.56	439.51	> 5
3.11 Chemical Block A3959-0168692	3.42	444.46	> 10
3.12 Enamine T0507-8072	4.34	389.84	> 10
3.13 Enamine T0508-0678	3.20	441.46	> 2.5
3.14 InterBioScreen STOCK3S-45023	2.54	424.50	> 5
3.15 InterBioScreen STOCK3S-52483	2.80	438.53	> 10
3.16 InterBioScreen STOCK3S-52603	2.73	442.49	> 10
3.17 Labotest LT00135147	3.49	413.51	0.44
3.18 Labotest LT01121502	3.46	400.43	> 10
3.19 Life Chemicals F1386-0209	3.47	388.49	1.58
3.20 Specs AE-641 00605023	3.98	333.45	8.39
3.21 Specs AG-670 11859029	3.58	439.42	> 10
3.22 Specs AG-690 11632029	2.71	430.46	> 5
3.23 Specs AN-465 40809732	3.45	444.53	> 10
3.24 Toslab 802803	4.47	416.56	2.87
3.25 Toslab 865471	3.40	405.50	> 10

3.3.1. Biological activity

Antiplasmodial ability of the selected compounds was measured by *in vitro* tests against *P. falciparum* W2 (CQ-resistant) strain and the assay results are listed in Table 3.2. Among the purchased compounds, five showed antiplasmodial activity on the micromolar range with one compound having submicromolar activity. More specifically, compounds **3.3**, **3.19**, **3.20** and **3.24** presented an IC_{50} below 10 μ M while compound **3.17**, the most active compound, exhibited activity with an IC_{50} value of 440 nM. Unfortunately, several compounds (compounds **3.4**, **3.5**, **3.10**, **3.13**, **3.14**, and **3.22**) had solubility limitations that prevented measuring precise IC_{50} values. Additionally, some compounds did not present appreciable activity up to the tested concentrations.

Regarding the best two inhibitors obtained in this procedure, compounds **3.17** and **3.19**, additional *in vitro* assays were made in order to verify their mode of action. Therefore, the cytochrome bc_1 complex activity assay was used to investigate if the antimalarial mode of action of these compounds was due to the inhibition of this target. Since cytochrome bc_1 complex is a membranar enzymatic complex, several difficulties are related with its isolation and, for that reason, the biological assays were performed in the mitochondria and not in the isolated bc_1 complex. Specifically, cytochrome bc_1 complex activity was evaluated by reduction of cytochrome *c* using a synthetic ubiquinol (decylubiquinol) as the electron donor and atovaquone as positive control. Unfortunately, these two compounds did not show inhibition potential at the maximum concentration tested (Table 3.3). However, since compounds were not tested directly in the isolated bc_1 complex it is not possible to establish with no doubt that these compounds are not able to inhibit this target. Furthermore, inhibitors acting against bc_1 complex, or against other mETC component, have to pass through the mitochondrial inner membrane in order to reach their target. In this way, considering the biological studies performed, it is not possible to confirm their ability to achieve the target in order to further display their antimalarial activity by interacting with Q_o binding site.

Table 3.3. Sensitivity of cytochrome *bc*₁ complex activity on isolated mitochondria to compounds **3.17** and **3.19**.

Cytochrome <i>bc</i> ₁ complex	IC ₅₀ (μM)		
	Compound 3.17	Compound 3.19	Atovaquone
<i>P. falciparum</i>	>50	>50	0.0003 ± 0.0001

Furthermore, in order to study if compounds **3.17** and **3.19** could inhibit the enzyme DHODH which is a different target in mETC, the inhibitors were tested against a *P. falciparum* cell line transfected with cytoplasmic yeast DHODH (Dd2-γDHODH), a soluble DHODH that is independent of ubiquinone. In this way, the transgenic strain can bypass the *P. falciparum* DHODH counterpart by using yeast DHODH. This cell line is able to use fumarate instead of mitochondrial ubiquinone as the final acceptor and was previously demonstrated to turn the parasite resistant to both PfDHODH and *bc*₁ complex inhibitors¹¹³. Specifically, the wild type Dd2 strain shows sensitivity to both DHODH and *bc*₁ complex inhibitors while the transgenic strain should present no inhibition when testing compounds acting against these targets. Moreover, addition of proguanil has been shown to restore sensitivity of Dd2-γDHODH to *bc*₁ complex inhibitors (antimycin A, myxothiazol and atovaquone) but has no effect with specific PfDHODH inhibitors.

The biological results obtained demonstrated that two potential inhibitors **3.17** and **3.19** display similar activity in both wild type and transgenic strains indicating that these compounds do not lose their activity in the transgenic Dd2-γDHODH, with or without proguanil, when compared to the control Dd2 line. This suggests that inhibition of the *Plasmodium bc*₁ complex or DHODH is not the primary antimalarial mechanism of action for these compounds (Table 3.4).

Table 3.4. Growth inhibition of wild type (Dd2) and transgenic (Dd2- γ DHODH) *P. falciparum* strains in the absence and presence of 1 μ M proguanil with different compounds.

Parasite Strain	Proguanil (1 μ M)	IC ₅₀ (μ M)				
		3.17	3.19	DHODH inhibitor	Atovaquone	Artemisinin
Dd2	-	2.6	8.7	0.37	0.0013	0.036
Dd2	+	2.6	9.58	0.44	0.0005	0.037
Dd2_ γ DHODH	-	2.01	10.7	>5	>0.035	0.026
Dd2_ γ DHODH	+	1.57	10.1	>5	0.001	0.028

The most active compounds were also tested against the atovaquone-resistant *P. falciparum* FCR3 strain and against *S. cerevisiae* (Table 3.5). Significantly, three of these compounds also presented antiplasmodial activity against the FCR3 strain, with compound **3.20** displaying a 20-fold increase in potency when compared with W2 strain.

Table 3.5. Activity against CQ-resistant strain W2 and atovaquone-resistant strain FCR3 of *P. falciparum*, and *S. cerevisiae*.

Compound	IC ₅₀ / μ M		
	W2	FCR3	S.c.
3.3	9.16	> 10	N.D.
3.17	0.44	N.D.	N.D.
3.19	1.58	2.71	13.5
3.20	8.39	0.43	14.9
3.24	2.88	2.81	13.3

As an example, the docked pose of one of the most active compounds against the W2 strain (**3.19**) is illustrated in Figure 3.6. The thiuronium moiety of this compound is able to establish two H bonds with residues Val270 and Glu272 at a distance of 1.81 and 2.40 Å, respectively, which stabilizes this hit inside the active site. Although no specific

interaction is found between this inhibitor and His181, several hydrophobic interactions exist between the naphthalene ring and the hydrophobic pocket.

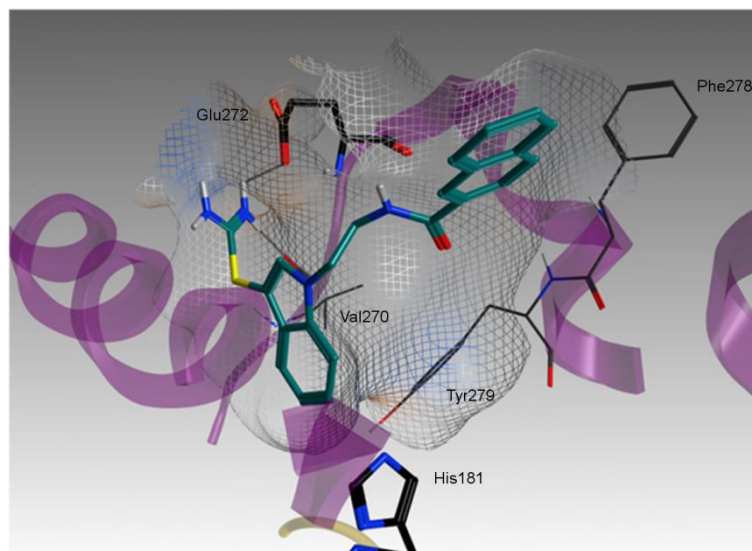
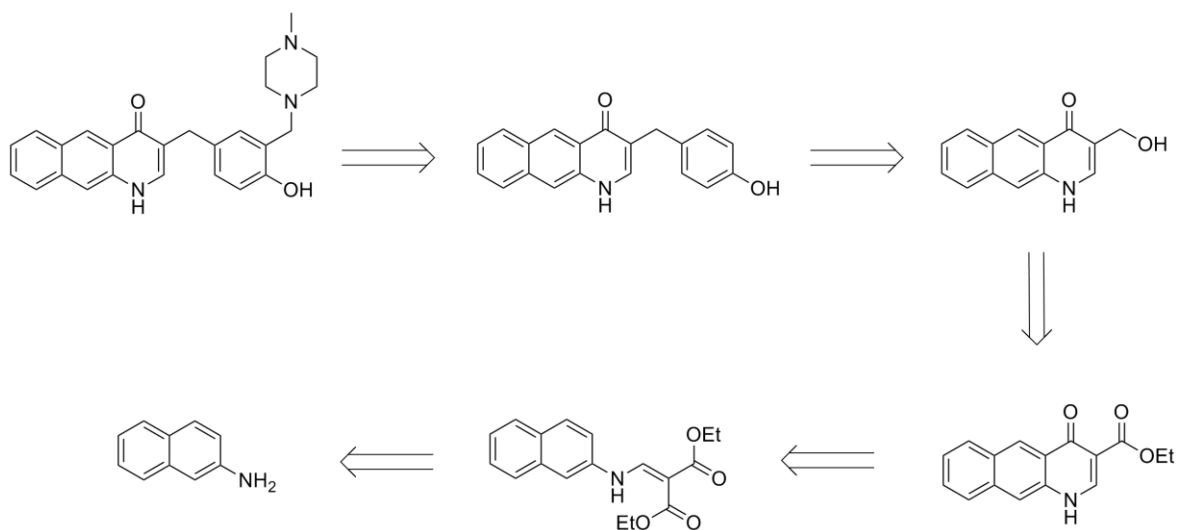


Figure 3.6. Predicted binding pose of compound **3.19**. Hydrogen bonds are represented by grey lines.

Unfortunately, compound **3.17** was excluded from the biological assays mentioned above (Table 3.5) since this purchased compound did not show a satisfactory degree of purity upon testing. Therefore, the results obtained for *P. falciparum* W2 and Dd2-yDHODH strains inhibition and for ubiquinol-cytochrome bc_1 oxidoreductase activity assay can not be considered conclusive.

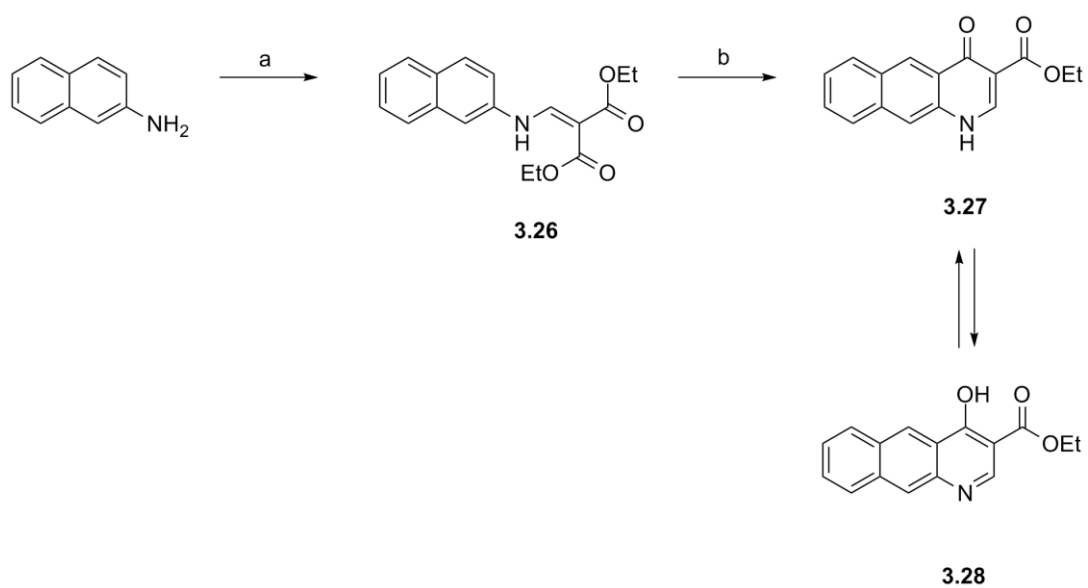
3.3.2. Synthetic approaches to obtain compound 3.17

In order to perform a second set of biological assays, some attempts were made to synthesize compound **3.17**. In Scheme 3.2 is described the retrosynthetic approach designed to obtain this compound.



Scheme 3.2. Retrosynthetic approach for the synthesis of compound **3.17**.

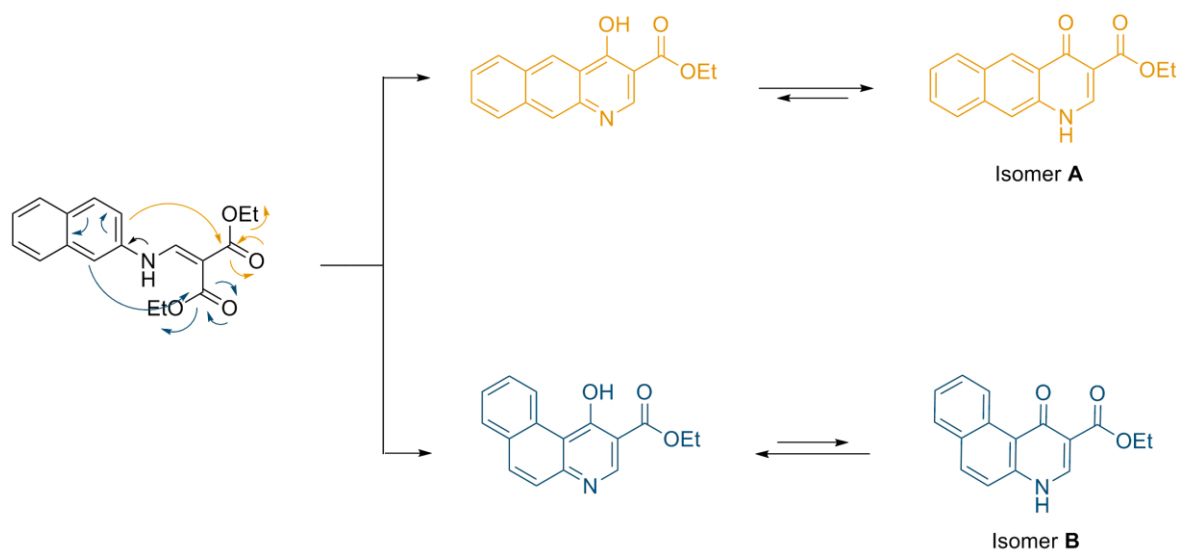
The Gould-Jacobs protocol was selected to prepare the benzoquinolone scaffold (compound **3.27**) starting from the appropriate aniline^{105, 264}, more specifically, 2-naphthylamine (Scheme 3.3). This is a very straightforward synthetic method that usually permits to obtain substituted quinoline in reasonable yields.



Scheme 3.3. Reaction conditions: (a) Diethyl ethoxymethylenemalonate, reflux; (b) Diphenyl ether, reflux.

The first step of the reaction consists in a nucleophilic attack of the amine to the double bond of diethyl ethoxymethylenemalonate with the consequent elimination of a molecule of ethanol. Compound **3.26** was easily obtained with a yield of 75%. The second step is a simple intramolecular cyclization facilitated by high temperatures. The final product can be obtained in one of the two tautomeric forms that are usually in equilibrium – 4-quinolinol (compound **3.27**) or 4(1*H*)-quinolone (compound **3.28**). However, the quinolone form is usually more abundant both in solid and solution state²⁶⁵⁻²⁶⁶.

In this case, due to the fact that the starting material used in this reaction is not symmetric, two products are expected to be formed during the reaction, isomer A, corresponding to the benzoquinolone of interest, and isomer B (Scheme 3.4).



Scheme 3.4. Mechanism of formation of both benzoquinolone isomers of compound **3.27**.

Unfortunately, the ¹H NMR spectra of the solid obtained in the cyclization step showed that only the isomer B was formed (Figure 3.7). For isomer A, it was expected a peak pattern that showed four singlets: two of them corresponding to the two protons of the center ring, one peak corresponding to the NH or OH moiety (depending on the tautomer obtained), and the last one belonging to the proton adjacent to the amine.

However, only the last two mentioned singlets were obtained. The duplet at 10.20 ppm (proton B - Figure 3.7) coupling with the multiplet at 7.65 ppm (proton H - Figure 3.7) indicates that both protons can interact with each other and this observation is in line with the peak pattern expected for isomer B. In this way, it is possible to conclude that only the isomer B was formed during the cyclization reaction. Moreover, the absence of a specific interaction between the more deshielded proton ($\delta = 12.54$ ppm) and the proton near the nitrogen atom ($\delta = 8.51$ ppm) indicates that isomer B is more stable as benzoquinolinol than as benzoquinoline. This fact is probable related to the formation of an intramolecular hydrogen bond that can confer more stability to this tautomer.

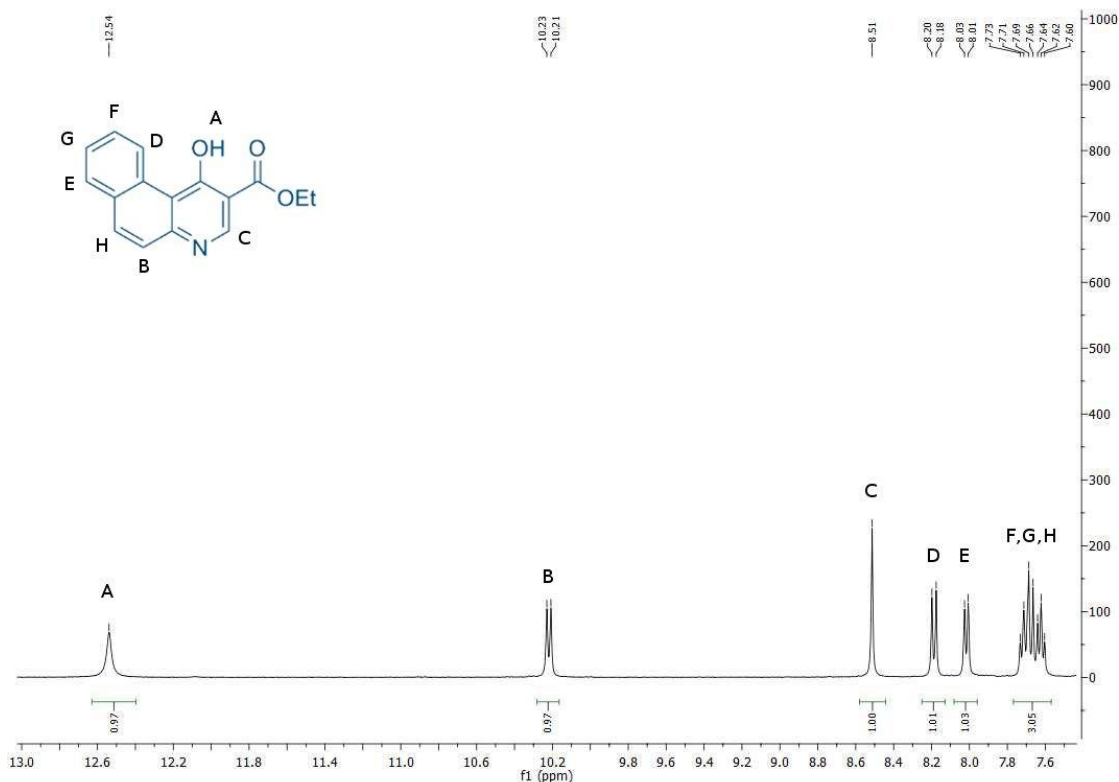
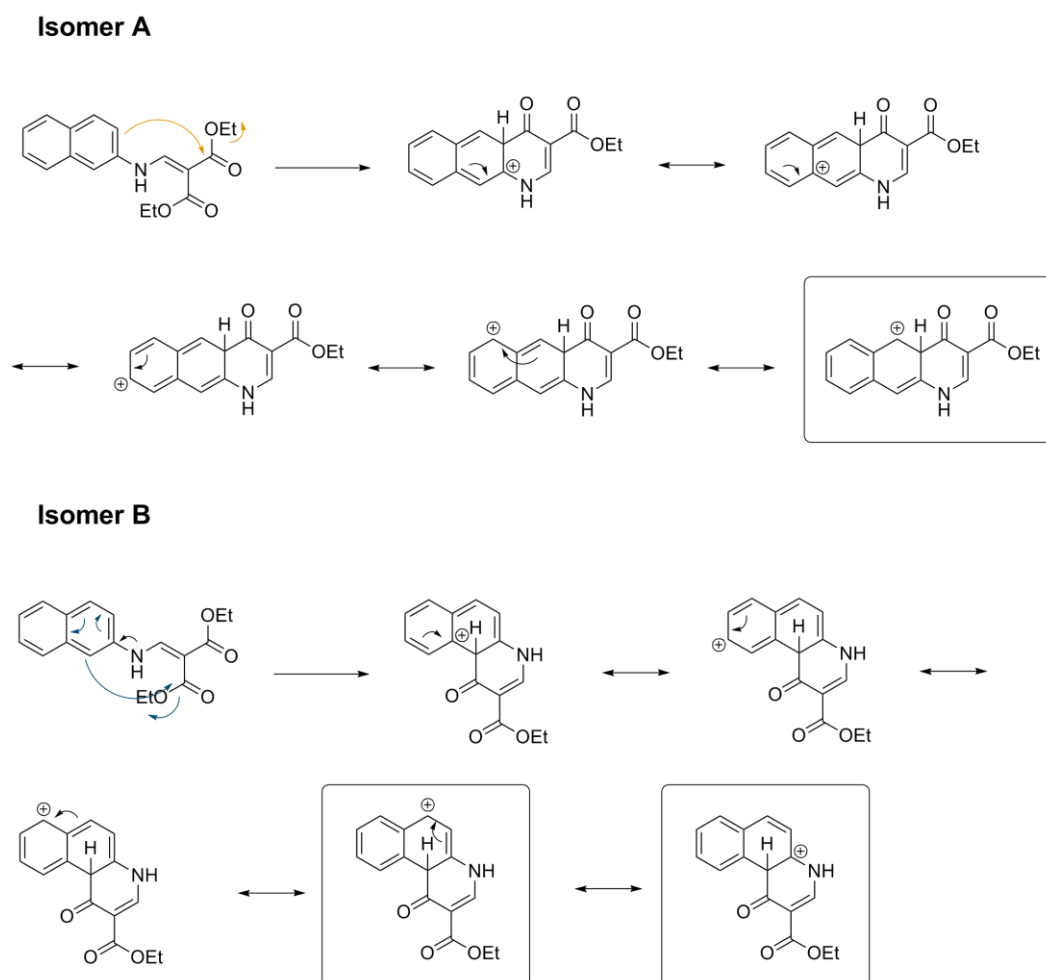


Figure 3.7. Expansion of the ¹H NMR spectra of isomer B of compound 3.27.

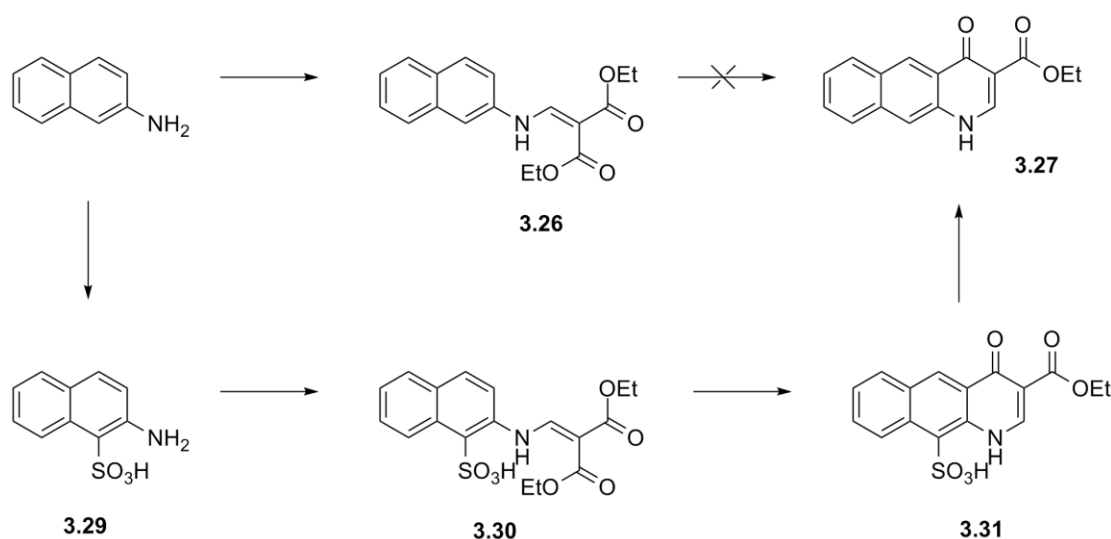
The regioselectivity in electrophilic aromatic substitutions depends on the stability of the cationic intermediate. In this way, comparing the two competing pathways, it is possible to notice that several resonance structures for each of the two cationic

intermediates can be written (Scheme 3.5). However, the cation resulting from cyclization in position 1, permitting to obtain the isomer B of compound **3.27**, has two contributing structures that retain the unbroken benzene-like structure whereas the cation from addition in position 3, which results in the formation of isomer A, only have one benzenoid contributing structures. Therefore, since the benzenoid bonding pattern is associated with aromatic stabilization, it is possible to conclude that the preferred pathway of cyclization will be the one that retains the greatest number of intact benzene-like rings among its resonance structures. Therefore, the formation of isomer B is preferred when compared with the formation of isomer A.



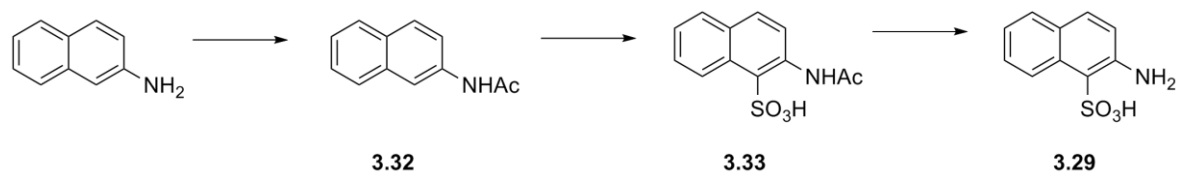
Scheme 3.5. Comparison between the resonance structures obtained for both isomers A and B of compound **3.27**.

As a result, efforts were made to block position 1 of 2-naphthylamine in order to try to successfully obtain the desired isomer. More specifically, this approach involved the sulfonation of 2-naphthylamine in position 1, followed by the reaction with diethyl ethoxymethylenemalonate. After the intramolecular cyclization, the sulfonic acid group should be easily removed (Scheme 3.6).



Scheme 3.6. Alternative approach to obtain intermediate **3.27**.

The sulfonation reaction performed in order to obtain the intermediate **3.29** was carried out in the presence of concentrated sulfuric acid, both at room temperature and in reflux, until the starting material was fully consumed. However, NMR spectroscopy and mass spectrometry did not confirm the formation of the desired product. Almost certainly, the protonation of the amine function in such extreme pH conditions led to a lesser activated specie that was not able to suffer electrophilic aromatic substitution. In this way, to succeed in the synthesis of the sulfonic acid derivative, the starting material 2-naphthylamine was first protected with an acetyl group (Scheme 3.7). Compound **3.32** was successfully obtained when reacted with a mixture of acetic anhydride and acetic acid with a yield of 39%.

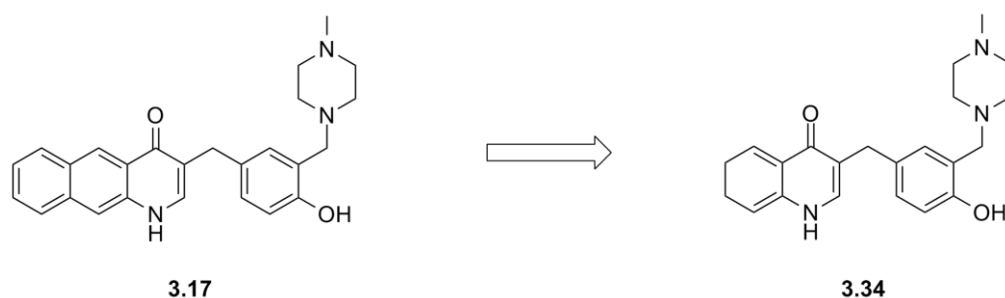


Scheme 3.7. Alternative approach to obtain intermediate **3.29**.

Unfortunately, once more, the formation of compound **3.33** was not confirmed using the available techniques and, since all efforts made to obtain this intermediate were not successful, the synthesis of compound **3.17** was abandoned.

3.3.3. Synthesis of quinoline **3.34** – A simpler model of compound **3.17**

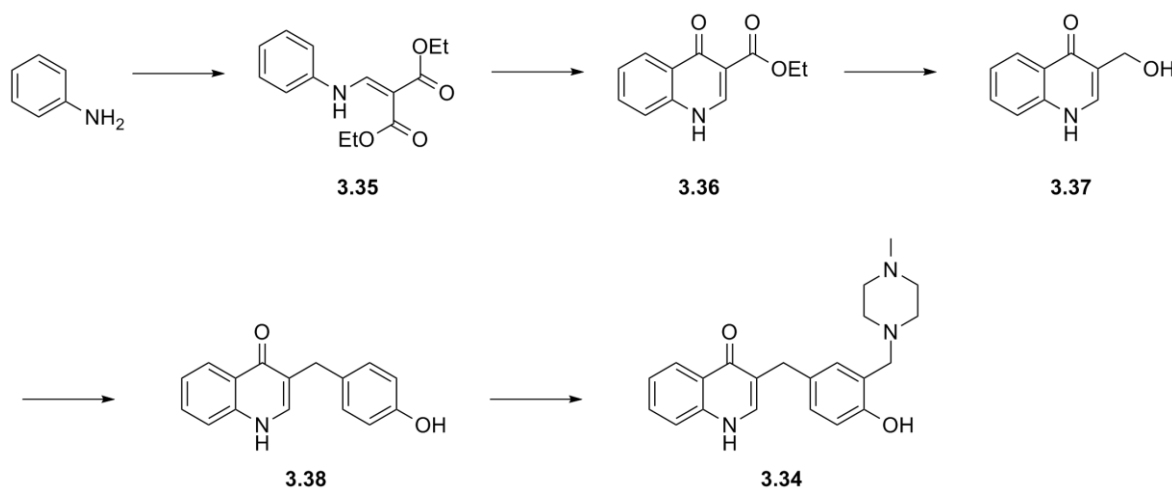
As an alternative to the synthesis of compound **3.17**, a similar quinolone derivative was synthesized (Scheme 3.8). The antimalarial activity of this class of compounds is well known and a large variety of compounds was already synthesized and biologically tested^{105, 121-123, 171, 239, 267}.



Scheme 3.8. Achievement of the model compound **3.34** from the tested compound **3.17**.

The retrosynthetic approach employed to obtain compound **3.34** was very similar to the one designed to achieve compound **3.17** (Scheme 3.2) involving also the application of the Gould-Jacobs protocol. Nevertheless, in this case, aniline was used as

the starting material to obtain the 4(1*H*)-quinolone ring **3.36** in 38% total yield (Scheme 3.9).



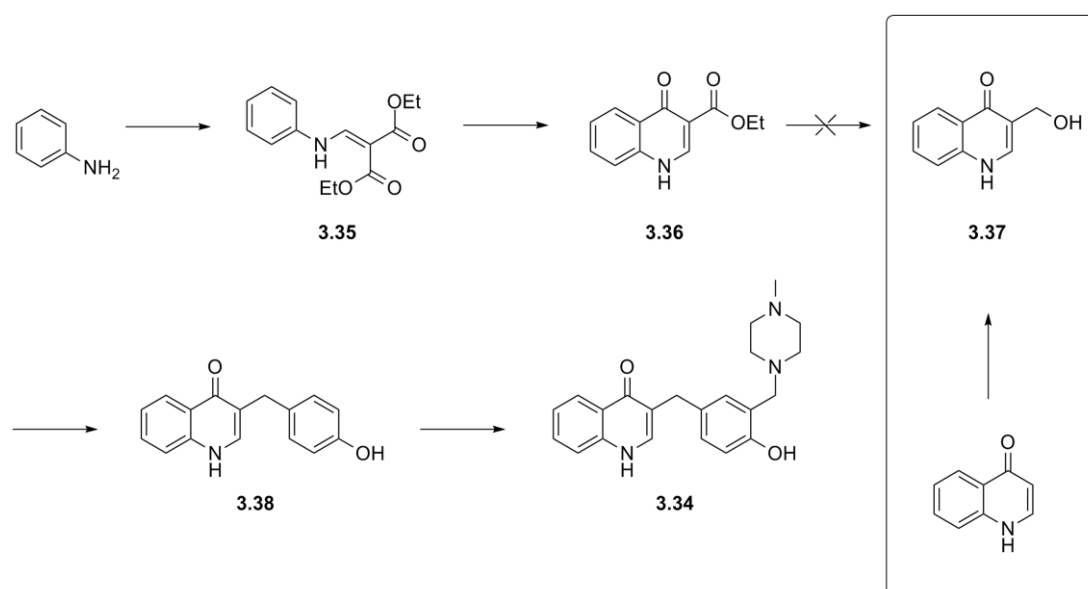
Scheme 3.9. Synthetic procedure to obtain compound **3.34**.

As in the case of compound **3.27**, the analysis of the ^1H NMR permitted to conclude that, in this synthetic procedure, compound **3.36** is obtained preferentially in its quinolinol form. In particular, the bidimensional data obtained showed no interaction between the NH proton and the vinylic CH in its vicinity, confirming the structure of this compound. In addition, the most deshielded proton, the OH proton, appears at $\delta = 12.54$ ppm which is consistent with the chemical shift value that can be obtained for an OH proton involved in an intramolecular H-bond²⁶⁸.

After, in order to proceed with the Friedel-Crafts alkylation to obtain compound **3.38**, the third step of this synthetic procedure included the reduction of the ester derivative **3.36** into the hydroxymethylquinoline **3.37**. In this way, compound **3.36** was reacted in several reaction conditions with different reducing agents but all efforts made to obtain this intermediate were ineffective and this compound was not achieved. More specifically, compound **3.36** was first reacted with LiAlH_4 in dry THF at room temperature but no reaction occurred and all the starting material was recovered. Then, in spite of being a weaker reducing agent, NaBH_4 was chosen in an attempt to perform this reaction

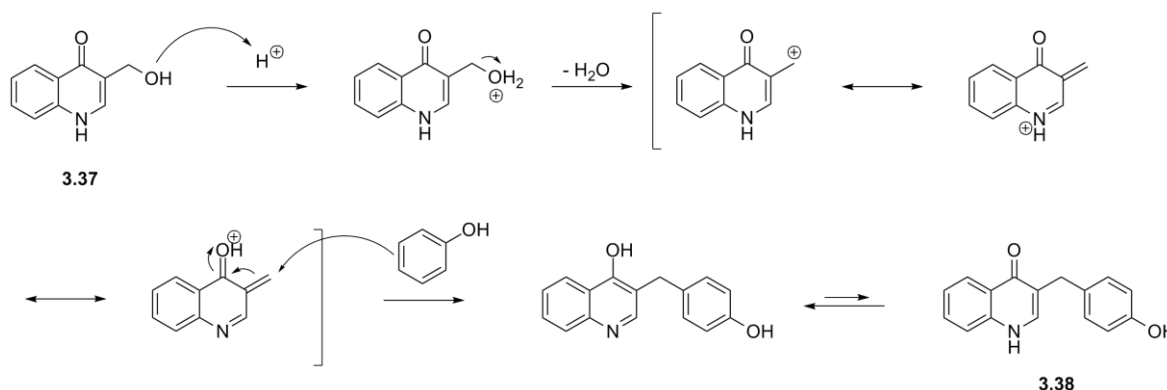
and obtain the desired product. It is already recognized that this reagent is not able to successfully reduce esters and other functional groups under mild conditions. However, several studies proved that its reactivity can be increased in the presence of certain additives²⁶⁹. Accordingly, the reaction was performed in the presence of NaBH₄ using MeOH²⁷⁰⁻²⁷¹, CaCl₂²⁷² and I₂²⁷³ as additives. In these cases, it was possible to verify the partial consumption of the starting material though, the desired product could not be identified in the ¹H NMR spectra. Once again, none of the synthetic procedures resulted in the synthesis of the hydroxymethylquinoline **3.37** and this approach was abandoned. Most probably, the presence of a very strong intramolecular H-bond between the hydroxyl group of the quinolinol ring and the ester substituent contributes to stabilize the ester function and to decrease its reactivity towards the reducing agents used in this step.

An alternative synthetic route was then designed using the commercially available unsubstituted quinolone as the starting material (Scheme 3.10). Therefore, this new starting material was reacted with aqueous formaldehyde in the presence of KOH²⁷⁴ permitting to obtain compound **3.37** in 96% yield.



Scheme 3.10. Alternative synthetic procedure to obtain compound **3.34** using an unsubstituted quinolone as starting material.

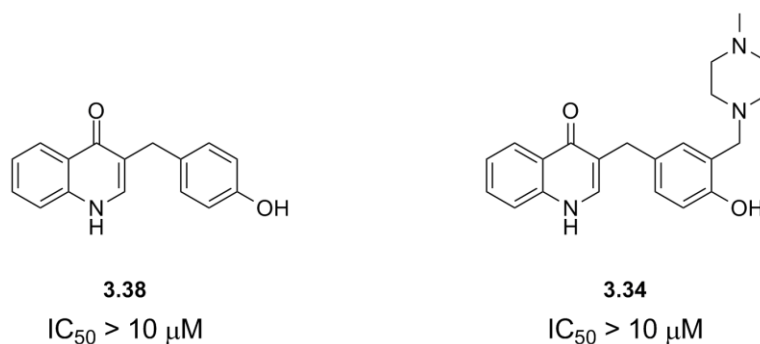
The subsequent step was the synthesis of intermediate **3.38** via a Friedel-Crafts alkylation. The main goal in this step was the formation of a stabilized carbocation that could suffer a nucleophilic attack of the phenol ring in order to obtain this compound as described in Scheme 3.11.



Scheme 3.11. Proposed mechanism for the synthesis of compound **3.38**.

To facilitate the loss of a water molecule in order to form the carbocation, compound **3.37** was reacted with different Lewis and Brønsted acids. More exactly, H_2SO_4 ²⁷⁵, and $\text{FeCl}_3 \cdot 6\text{H}_2\text{O}$ ²⁷⁶⁻²⁷⁷ were used in order to obtain the Friedel-Crafts product of the reaction between the hydroxymethylquinoline and phenol. However, compound **3.38** could only be synthesized in the presence of HClO_4 as catalyst²⁷⁷. This strategy permitted to obtain this compound in reasonable yields. In the last step, the Mannich-base derivative was achieved by reacting compound **3.38** with a small excess of *N*-methylpiperazine in the presence of aqueous formaldehyde in ethanol²⁷⁸ (Scheme 3.10). The final product **3.34** was isolated in low yield. Nevertheless, an increase in the amount of *N*-methylpiperazine and aqueous formaldehyde did not lead to an improvement of the yield but resulted in the formation of bis-Mannich side-product. Additionally, by inspection of the ¹H NMR data, it is possible to conclude that this compound is more stable in its quinoline form since the interaction between both the NH and the vinylic protons can be found in the bidimensional spectrum.

Finally, both compounds **3.34** and **3.38** were tested for their antimalarial activity against *P. falciparum* W2 strain but unfortunately none of the compounds showed to be active at the tested concentration (Scheme 3.12).



Scheme 3.12. Chemical structure of the two tested quinolone derivatives and their antimalarial activity against *P. falciparum* W2 strain.

3.4. Concluding remarks

The virtual screening approach showed to be a powerful tool in several important aspects within this study. First off all, the screening performed against TCAMS database permitted to evaluate the performance of two distinct docking programs (AD and AD Vina) and their ability to predict the inhibitory potential of a class of known mETC inhibitors. Significantly, a reasonable correlation between the binding free energy values found using both docking procedures was found, meaning that AD and AD Vina have both the ability to recognize typical bc_1 complex inhibitors. Since this second program has the advantage of being much faster than AD, AD Vina can be successfully used to screen large libraries of compounds. In this way, both programs were used to screen a large library of drug-like compounds using the yeast model developed in Chapter 2. The proof of concept was demonstrated since this procedure permitted the identification of five molecules with antimalarial activity. Unfortunately, the biological assays performed on the *Pf* cytochrome bc_1 complex and on the Dd2- γ DHODH transgenic cell line showed that the two best hits, compounds **3.17** and **3.19**, displayed no activity in the mETC. In consequence, it was

possible to conclude that the inhibition of this target is not the primary antimalarial mechanism of action of both compounds. Conversely, compounds **3.19**, **3.20** and **3.24** proved to be active against the atovaquone-resistant *Pf* FCR3 strain and *S. cerevisiae*. In this last set of biological tests, compound **3.17** could not be included due to purity issues. Several attempts were then made to synthesize this compound but all were found to be unproductive. Consequently, the mechanism of action of this compound could not be effectively studied and the biological assays performed can not be regarded as conclusive. In order to overcome the synthetic problems concerning compound **3.17**, a model of this compound (**3.34**) was obtained. Although several quinolones are already recognize to display high antimalarial activity, compound **3.34** showed no activity at 10 μ M concentration.

CHAPTER FOUR

List of contents

4.1. Background	109
4.2. Identity between species in <i>bc</i> ₁ complex Q _o binding site and definition of the pocket	111
4.3. Homology model building and docking studies	118
4.4. Virtual screening studies over the homology model of <i>P. falciparum bc</i> ₁ complex	128
4.5. Concluding Remarks	132

4. Homology model of *P. falciparum* Q_o site of *bc*₁ complex and

Virtual Screening Study

4.1. Background

The model presented in Chapter 2 was able to explain the binding mode of the selected inhibitors in order to clarify the interaction mechanism between experimentally known *bc*₁ inhibitors and the active pocket. A good correlation between the calculated binding free energy of each compound and its experimental inhibitory activity was also found and, therefore, this can be considered a good predictive method to determine the inhibitory potential of possible new inhibitors. However, this model was not able to explain the selectivity found for WR 249685 since this compound is highly active against *P. falciparum bc*₁ complex but loses completely its activity when tested against *S. cerevisiae*¹³³. In spite of sharing a high sequence identity, the Q_o pocket of both species must present different structural features that provide such selectivity and, therefore, a more accurate model is urgently needed to provide better predicted inhibitory potential for chemically diverse inhibitors.

To this point, some work has been developed addressing this issue and distinct homology models of *P. falciparum bc*₁ complex, specifically for the Q_o binding site^{133, 279},

were published. The first homology model¹³³ was built only considering the cytochrome *b* being, consequently, highly incomplete. As already mentioned, the Q_o binding site is established by the close contact between cytochrome *b*, of one monomer of *bc*₁ complex, and the Rieske ISP, of the second monomer and, therefore, the presence of both structures is essential to modulate this active site²⁸⁰⁻²⁸¹. As a result, this homology model cannot be recognized as a reliable model of Q_o binding site. More recently, Hughes *et al*²⁷⁹ published a more accurate homology model using as template the yeast cytochrome *b* and Rieske ISP. Nevertheless, this model was not validated with experimental results being only applied to obtain a very basic explanation for the molecular basis of atovaquone's resistance and its reliability cannot be deduced.

Presently, having in mind the crescent interest in *bc*₁ complex as a target to develop potential antimalarial drugs and considering the importance of having a reliable three-dimensional structure of this enzymatic complex to understand the mechanism of action of the inhibitors, a homology model of cytochrome *b* and Rieske ISP was generated based on yeast crystallographic structure.

In order to obtain the most reliable model of *bc*₁ complex Q_o binding site, the experimental procedure was pursued as follows:

- (i) Protein sequences alignment for *Plasmodium falciparum* and for four selected species;
- (ii) Definition of the amino acid residues that establish the Q_o active site;
- (iii) Evaluation of the best template for Q_o binding site of *Pf bc*₁ complex;
- (iv) Homology model built and optimization of the structure obtained;
- (v) Validation of the model by docking of known *Pf bc*₁ complex inhibitors.

4.2. Identity between species in bc_1 complex Q_o binding site and definition of the pocket

Since Q_o binding site is composed by both Rieske ISP and cytochrome b , the complete sequence of *P. falciparum* of the two subunits was searched and collected from UniProt database²⁴⁹ (Figure 4.1 and Figure 4.2).

In this way, as a first step to identify the most adequate template to construct the homology model of the target, both Rieske ISP and cytochrome b protein sequences for five homologous proteins (namely from *S. cerevisiae*, *B. Taurus*, *G. gallus*, *R. sphaeroides* and *P. falciparum*) were retrieved from UniProt and were aligned based on their conserved residues (Table 4.1.).

```

      10      20      30      40      50      60
MNNIKYVELF YKCKIFRKNG LNRIIRRNGG TFNHNIKENE RIPPASEDPS YKNLFDHAED
      70      80      90     100     110     120
IKLWEIEEKQ NVSHKKVEDL SELVEPSNHP HQYEGIFART RYAHYNQTAE PVFPRKPDLE
     130     140     150     160     170     180
KGELASGANV TRTDVWHNPK EPAIVSIGKF EPRNFRPAGY AENCNPESI NSDHHPDFRE
     190     200     210     220     230     240
YRLRSGNEDR RSFMYFISAS YFFIMSSIMR SAICKSVHFF WISKDLVAGG TTELDMRTVN
     250     260     270     280     290     300
PGEHVVIKWR GKPVFVKHRT PEDIQRAKED DKLIQTMRDP QLDSDRTIKP EWLVNIGICT
     310     320     330     340     350
HLGCVPAQGG NYSGYFCPCH GSHYDNSGRI RQGPAPSLE VPPYEFVDEN TIKIG

```

Figure 4.1. Sequence of *P. falciparum* Rieske Iron-Sulfur Protein (UniProt code Q8IL75).

```

10      20      30      40      50      60
MNFYSINLVK AHLINYPCL NINFLWNYGF LLGIIFFIQI ITGVFLASRY TPDVSYAYYS
70      80      90      100     110     120
IQHILRELWS GWCFRYMHAT GASLVFLLTY LHILRGLNYS YMYLPLSWIS GLILFMIFIV
130     140     150     160     170     180
TAFVGYVLPW GQMSYWGATV ITNLLSSIPV AVIWICGGYT VSDPTIKRFF VLHFILPFIG
190     200     210     220     230     240
LCIVFIHIFV LHLHGSTNPL GYDTALKIPF YPNLLSLDVK GFNNVIILFL IQSLFGIIPL
250     260     270     280     290     300
SHPDNAIVVN TYVTPSQIVP EWYFLPFYAM LKTVPSPKAG LVIVLLSLQL LFLLAEQRSL
310     320     330     340     350     360
TTIIQFKMIF GARDYSVPII WFMCAFYALL WIGCQLPQDI FILYGRFLFIV LFFCSGLFVL
370
VHYRRTHYDY SSQANI

```

Figure 4.2. Sequence of *P. falciparum* cytochrome *b* (UniProt code Q7HP03).

This four species were chosen to be initially tested as template for this procedure since their crystallographic structure is currently available. Additionally, all these structures present the same bound inhibitor — stigmatellin. The protein sequences of *Homo sapiens* were also included in order to verify the identity between species.

Table 4.1. Protein sequences of Rieske ISP and cytochrome *b* for the several species and summary of the crystal structures used as templates.

Source	UniProt code		PDB code	Reference	Resolution (Å)
	Rieske ISP	Cyt <i>b</i>			
<i>S. cerevisiae</i>	P08067	P00163	3CX5	103	1.90
<i>B. Taurus</i>	P13272	P00157	1PPJ	145	2.10
<i>G. gallus</i>	Q5ZLR5	P18946	3H1J	96	3.00
<i>R. sphaeroides</i>	Q02762	Q02761	2QJY	282	2.40
<i>P. falciparum</i>	Q8IL75	Q7HP03	-	-	-
<i>H. sapiens</i>	P47985	P00156	-	-	-

A visual inspection of the superposition of the four available X-ray structures allowed to verify that the secondary structure of these two subunits are well conserved between the considered species (Figure 4.3.). In this way, it is possible to conclude that, although these subunits may show some differences in their amino acid sequences, their secondary structure is very similar. Moreover, when considering the active site and the bound inhibitor stigmatellin, it is also important to notice an almost perfect superposition of the aromatic moiety of this compound.

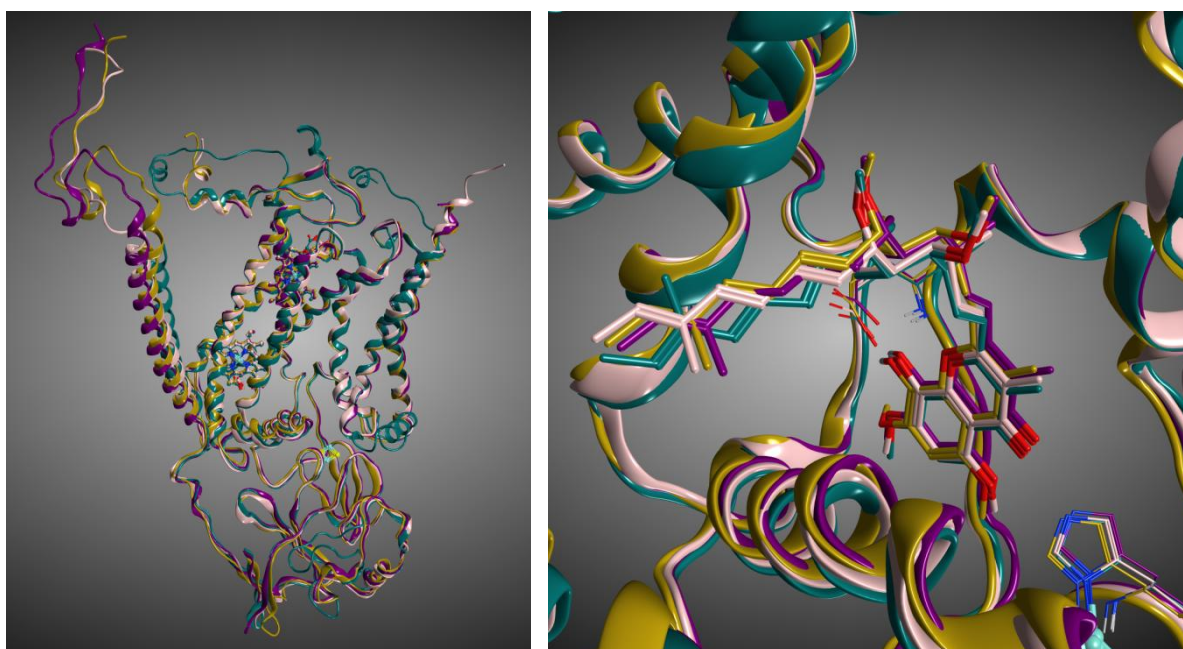


Figure 4.3. Superposition of Rieske ISP and cytochrome *b* of *S. cerevisiae* (in pink), *B. Taurus* (in purple), *G. gallus* (in yellow) and *R. shaeroides* (in green) on the left, and superposition of the bound stigmatellin in the active site of the respective species (the same color pattern was used for stigmatellin).

Furthermore, considering the protein sequences alignment obtained, the identity between the complete protein sequences was further calculated using UniProt and the values obtained are depicted in Table 4.2 and Table 4.3.

Table 4.2. Identity between species in Rieske ISP (complete protein sequence) for *Pf* (*P. falciparum*), *Sc* (*S. cerevisiae*), *Bt* (*B. Taurus*), *Gg* (*G. gallus*), *Rs* (*R. sphaeroides*) and *Hs* (*H. sapiens*). Values obtained from Uniprot²⁴⁹.

Species	<i>Pf</i>	<i>Sc</i>	<i>Bt</i>	<i>Gg</i>	<i>Rs</i>	<i>Hs</i>
<i>Pf</i>	100%	22.4%	24.1%	26.4%	18.4%	25.4%
<i>Sc</i>	22.4%	100%	37.2%	37.7%	32.0%	34.9%
<i>Bt</i>	24.1%	37.2%	100%	75.5%	24.9%	90.1%
<i>Gg</i>	26.4%	37.7%	75.5%	100%	25.8%	74.0%
<i>Rs</i>	18.4%	32.0%	24.9%	25.8%	100%	25.6%
<i>Hs</i>	25.4%	34.9%	90.1%	74.0%	25.6%	100%

Table 4.3. Identity between species in cytochrome *b* (complete protein sequence) for *Pf* (*P. falciparum*), *Sc* (*S. cerevisiae*), *Bt* (*B. Taurus*), *Gg* (*G. gallus*), *Rs* (*R. sphaeroides*) and *Hs* (*H. sapiens*). Values obtained from Uniprot²⁴⁹.

Species	<i>Pf</i>	<i>Sc</i>	<i>Bt</i>	<i>Gg</i>	<i>Rs</i>	<i>Hs</i>
<i>Pf</i>	100%	35.4%	39.8%	38.1%	30.5%	40.1%
<i>Sc</i>	35.4%	100%	50%	50.4%	41.1%	48.4%
<i>Bt</i>	39.8%	50%	100%	74.5%	42.6%	78.7%
<i>Gg</i>	38.1%	50.4%	74.5%	100%	41.3%	72.2%
<i>Rs</i>	30.5%	41.1%	42.6%	41.3%	100%	41.9%
<i>Hs</i>	40.1%	48.4%	78.7%	72.2%	41.9%	100%

Concerning the identity values obtained is important to highlight that the sequence of cytochrome *b* is more conserved between the considered species than the protein sequence of Rieske ISP. Moreover, when considering both the complete protein sequence of *P. falciparum* Rieske ISP and cytochrome *b*, the homologous proteins of *B. Taurus* and *G. gallus* present higher identity.

However, it is importance to notice that the Q_o binding site is specifically defined by the interaction between both Rieske ISP and cytochrome *b* and not for the entire proteins. More exactly, the Q_o binding site is located close to heme *b_L* and the [2Fe-2S]

cluster. As a result, in order to obtain a model with high quality, it is important to identify the amino acid residues that, being part of each protein sequence, contribute specifically to determine the active site and, subsequently, recognize the conserved amino acid residues.

The Q_0 active site was then defined based on the bc_1 complex crystal structure obtained from *S. cerevisiae* co-crystallized with a known inhibitor, stigmatellin. This X-ray structure was chosen to identify the amino acid residues in the pocket since previous studies were already performed based on *S. cerevisiae*. In addition, from all the considered structures, this one presented the higher resolution. Moreover, stigmatellin presents also a complex chemical structure being able to interact with a large amount of amino acid which allow to better identify the most significant residues in the pocket. In this way, the amino acid residues establishing important interactions with this inhibitor were considered to be essential to define the pocket (Figure 4.4).

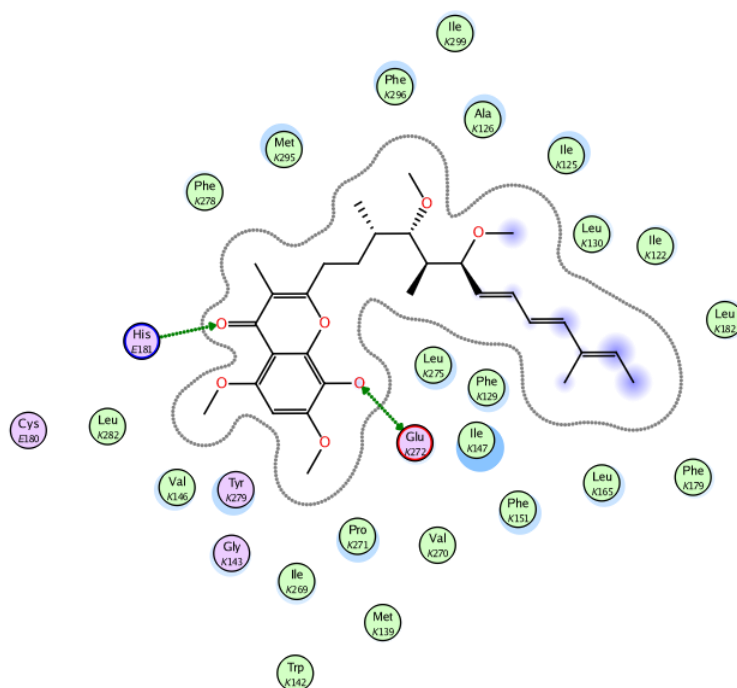


Figure 4.4. Interactions between stigmatellin and Q_0 binding site residues in *S. cerevisiae* X-ray structure (PDB code 3CX5).

In particular, Ile122, Ile125, Ala126, Phe129, Leu130, Met139, Trp142, Gly143, Val146, Ile147, Phe151, Leu165, Phe179, Leu182, Ile269, Val270, Pro271, Glu272, Leu275, Phe278, Tyr279, Leu282, Met295, Phe296, Ile299 (from cytochrome *b*) and Cys180 and His181 (from Rieske ISP) were considered to be located in proximity to stigmatellin and strongly interacting with this inhibitor. For simplicity purposes, amino acid residues numbering is according with *S. cerevisiae* protein sequence and all discussion will be done considering the yeast numbering.

Although only two amino acid residues from the Rieske ISP were considered to be important to define the binding pocket, these residues can be considered essential for the correct function of this catalytic site. Specifically, both Cys180 and His181 are coordinated with the [2Fe-2S] cluster contributing for its stability. Moreover, His181 is responsible for anchoring the natural substrate and the inhibitors to the binding site and, therefore, its presence is crucial for obtaining reliable docking results.

As a result, the identity in Q_o binding site between the considered species can be determined more accurately (Table 4.4). It is possible to conclude that *P. falciparum* Q_o binding site displays higher identity with the homologous sequence of *S. cerevisiae* and *B. taurus* since in both cases 18 in 27 amino acid residues are conserved.

Table 4.4. Identity between species in Q_o binding site.

Species	<i>Pf</i>	<i>Sc</i>	<i>Bt</i>	<i>Gg</i>	<i>Rs</i>	<i>Hs</i>
<i>Pf</i>	27/27	18/27	18/27	17/27	17/27	18/27
<i>Sc</i>	18/27	27/27	17/27	17/27	24/27	16/27
<i>Bt</i>	18/27	17/27	27/27	21/27	20/27	25/27
<i>Gg</i>	17/27	17/27	21/27	27/27	19/27	21/27
<i>Rs</i>	17/27	24/27	20/27	19/27	27/27	19/27
<i>Hs</i>	18/27	16/27	25/27	21/27	19/27	27/27

However, the crystal structure of *Scbc*₁ complex presents better resolution (1.90 Å) and, therefore, this was the structure chosen as template to obtain the homology model of *bc*₁ complex Q_o binding site of *P. falciparum*. In Figure 4.5 are highlighted the amino acid residues of Q_o binding site that differ in both *S. cerevisiae* and *P. falciparum* species.

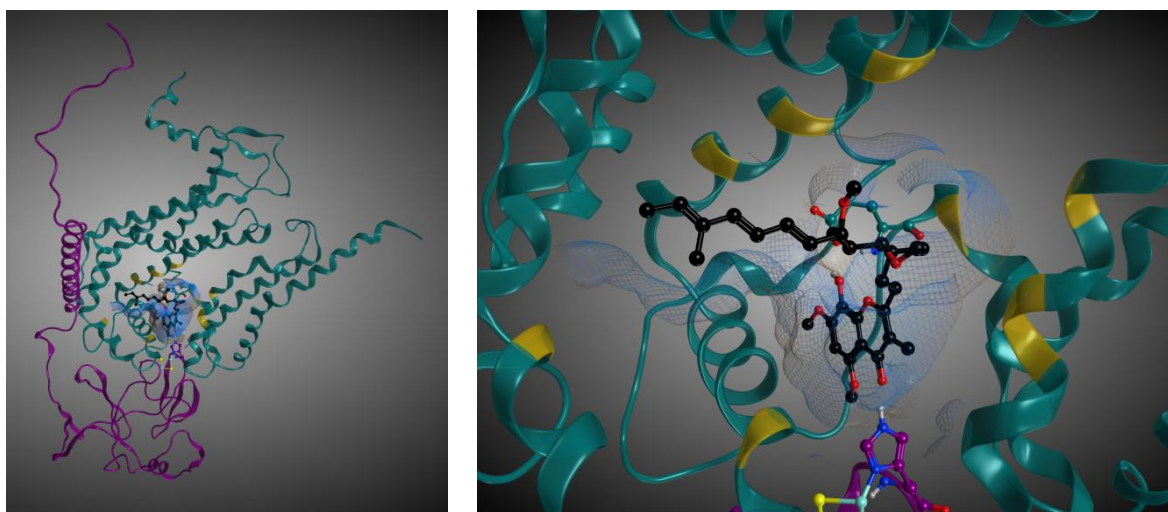


Figure 4.5. Cytochrome *b* and Rieske ISP on the left and Q_o binding site of yeast *bc*₁ complex on the right with bound stigmatellin highlighting in yellow the amino acid residues that are mutated in *P. falciparum*.

Moreover, bovine and human Rieske ISP and cytochrome *b* must share high identity since both are mammalian species. Indeed, a simple alignment of the protein sequences of the two species using UniProt showed that Rieske ISP and cytochrome *b* share 90% and 79% identity, respectively. In this specific case, the main goal is to obtain a reliable model of the *P. falciparum* *bc*₁ complex that explains not only the inhibitory potential of several compounds but that can be also applied to further design selective inhibitors concerning the human host. For all these reasons pointed, the structure of *S. cerevisiae* *bc*₁ complex was chosen instead of the structure of *B. taurus*.

In summary, *S. cerevisiae* crystallographic structure was chosen as template since:

- (i) This structure displays higher resolution;
- (ii) Both *S. cerevisiae* and *B. taurus* display similar identity in the Q_o binding pocket;
- (iii) *B. taurus* presents higher identity with *H. sapiens* than *S. cerevisiae* which contributes to lower selectivity.

4.3. Homology model building and docking studies

In a first step to obtain a homology model of *Pf bc*₁ complex Q_o site, the program Modeller 9v7²⁸³ provided by Chimera²⁸⁴ was used. This approach permitted to obtain independently the models for both cytochrome *b* and Rieske ISP from the yeast template (PDB entry 3CX5). These two protein subunits were then coupled in the end of calculation allowing to obtain the model of cytochrome *b* and Rieske ISP. Moreover, the [2Fe-2S] cluster was added manually to this model having in consideration the position of these 4 atoms in the yeast structure. However, this effort showed to be unproductive since the newly created subunits display several superposed segments. Moreover, a simple minimization of the whole structure did not allow to solve this issue and, as a result, this methodology was abandoned.

In a second approach to obtain an homology model of *Pfbc*₁ complex Q_o binding site, the calculations were performed using MOE. In this case, it was possible to model both subunits at the same time using the Homology Model tool available. Moreover, the model was built including also the known inhibitor stigmatellin and the [2Fe-2S] cluster in the active site in order to create an induced fit whilst calculating the final structure. Finally, the higher scored model was chosen to pursue the study and went through a energy minimization of the active site in the presence of the same bound inhibitor.

The crystal structures of *bc*₁ complex, namely Rieske ISP and cytochrome *b* sequences, from *S. cerevisiae*, *B. Taurus*, *G. gallus* and *R. sphaeroides* were aligned with the model obtained and a careful visual inspection of all amino acid residues of the Q_o

binding site was performed. The main goal of this examination was to compare the rotamers and the relative position of the residues, essentially the conserved ones, and confirm the validation of the rotamers obtained in the modulating process. Taking into consideration the difference observed in the relative position of residue Pro260 when comparing the structures and that this residue is highly conserved in all species, an energy minimization of the position of this residue was performed. The new arrangement of this residue permitted to slightly increase the pocket size in order to better accommodate inhibitors inside the pocket (Figure 4.6).

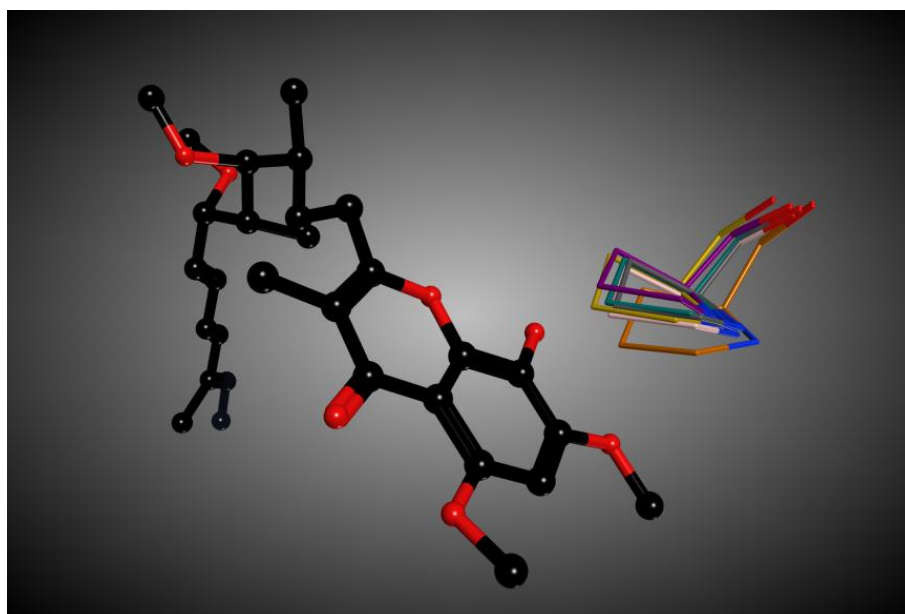


Figure 4.6. Comparison between the position of Pro260 in the several species: *S. cerevisiae* (in pink), *B. Taurus* (in purple), *G. gallus* (in yellow) and *R. shaeroides* (in green), and the one obtained by homology modeling before and after energy minimization (in orange and grey, respectively).

Special attention was also given to residue Phe264. This residue is conserved between several species, namely *P. falciparum*, *B. Taurus* and *G. gallus* but, in the case of *S. cerevisiae* is replaced by a Leu residue. Experimental evidences¹³³ already shown that some compounds, more specifically, WR 249685, are highly active against *Pfbc*₁ complex but show no activity against *Scbc*₁ complex. Therefore, the presence of this residue is probably one of the most important features that provide the selectivity observed

between these two species. In the homology model obtained, the aromatic ring of Phe264 was pointing towards the pocket center (Figure 4.7) contributing to decrease the pocket size. After energy minimization of Phe264 side chain, with stigmatellin in the active site, it was possible to obtain more favorable interactions between this residue and the inhibitor. However, the relative position obtained for this aromatic ring was still not in accordance with the position found in other species. As a result, the rotamer was manually adjusted and the aromatic ring was turned 46° in order to stay parallel to the phenyl rings of the same residue in both bovine and avian structures. Once more, the position of the aromatic ring was energy minimized in order to obtain a more stable structure.

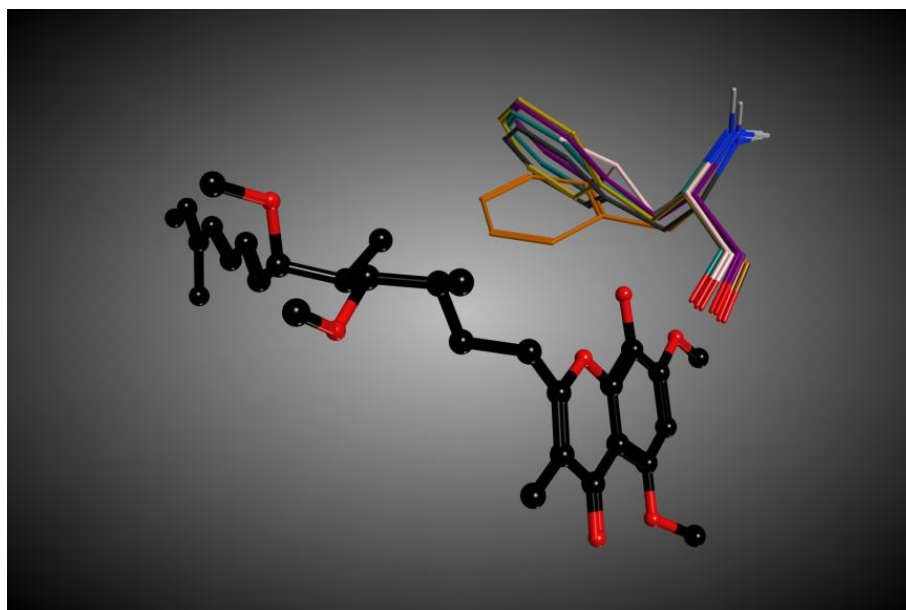


Figure 4.7. Comparison between the position of Phe264 in the several species: *S. cerevisiae* (in pink), *B. Taurus* (in purple), *G. gallus* (in yellow) and *R. shaeroides* (in green), and the one obtained by homology modeling before and after energy minimization (in orange and grey, respectively).

The quality of the built model was first evaluated using the available validation tools in MOE. These tools are considered of extreme importance to assess the 3D structure obtained concerning both energy and structural parameters. The model was also evaluated with other tools. According to PROCHECK²⁸⁵ and to the Ramachandran plot

obtained (Figure 4.8), only 81% of the amino acid is in the most favored regions being 16.5% of the residues in additional allowed regions. In comparison, the template structure displays 92% of the amino acid in the most favored regions and only 7% of the residues in additional allowed regions. The number of residues in the most favored regions is quite lower than it was expected since a good quality model must present at least 90% of its residues in this region²⁸⁵.

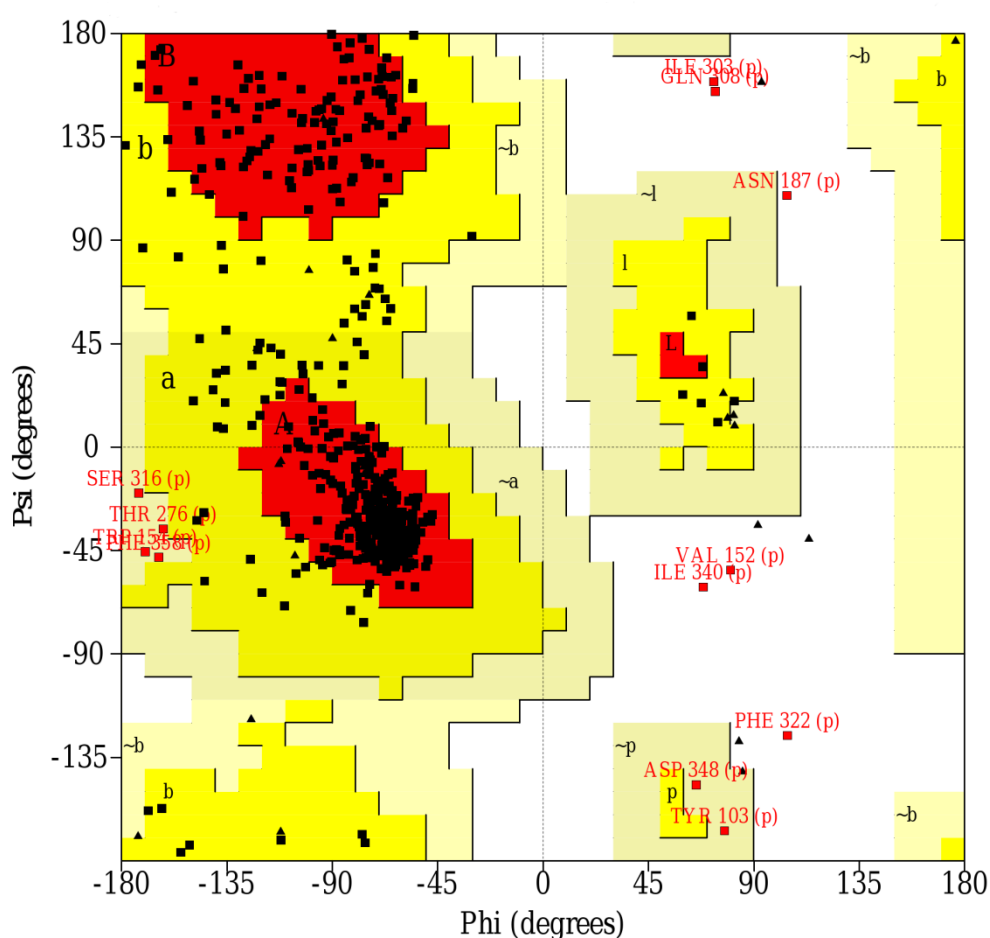


Figure 4.8. Ramachandran plot of the modeled 3D structure of *P. falciparum* bc_1 complex Q_o binding site obtained with PROCHECK²⁸⁵. The different colorated areas specify: most favored regions (in red), additional allowed regions (in yellow), generously allowed regions (in beige), and disallowed regions (in white).

This can probably be related to the fact that the two protein sequences were built in the absence of the overall cytochrome structure. More specifically, since bc_1 complex is

comprised by several subunits, each contributing to keep stable the secondary structure of the entire cytochrome, the lack of the adjacent subunits could lead to an increase of the flexibility of some parts of both cytochrome *b* and Rieske ISP. In this way, the high flexibility of the amino acid chains could be responsible for decreasing the number of residues in the most favored regions of Ramachandran plot. In addition, only six residues are found in the disallowed region. However, the analysis of the structure demonstrated that all these amino acids are very distant from the Q_o binding site which suggests that the conformation of these specific residues should have no repercussion on further calculations. Additionally, both Pro260 and Phe264, the two amino acid residues which conformation were optimized during the model built, show to be in the most favored allowed regions in Ramachandran plot.

The reliability of the model was further verified through a docking study of a small database of experimentally known *P. falciparum* bc₁ complex inhibitors. To guarantee comparable values for biological activity, only compounds experimentally screened using the same protocol were included in the set. This is the set of compounds including the same bc₁ complex inhibitors already employed in Chapter 2 for validating the *S. cerevisiae* bc₁ complex. Nevertheless, a recently obtained quinolone derivative (Quinolone 1) was also integrated in this set in order to increase chemical diversity (Figure 4.9)¹⁰⁵. In spite of not being tested in the same biological assay, this new compound was evaluated using the same protocol and in similar conditions.

All compounds were docked separately into the modeled Q_o binding site using AD and ranked according to AD scoring function. The binding free energy values obtained in this docking calculation can be found in Table 4.5. AD was chosen again to perform the docking procedure since it showed previously to be successful in calculations over this target. Namely, this program was able to reproduce the experimentally observed binding mode of stigmatellin as described in Chapter 2.

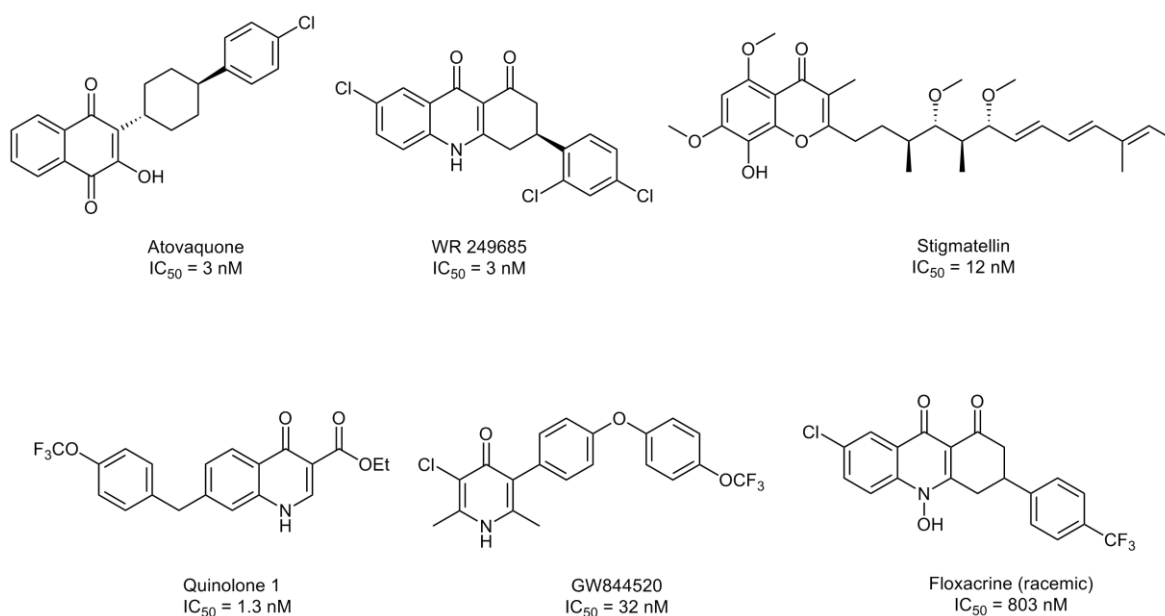


Figure 4.9. The Q_o bc₁ complex inhibitors used to validate the homology model.

Overall, the binding mode of the inhibitors tested is very similar to the one found when using the yeast model. However, the analysis of Table 4.5 allows to conclude that all inhibitors present an higher score after docking calculations over the homology model of *P. falciparum* Q_o binding site when compared with the yeast model. As a result, it is possible to verify that this new model allows to improve the inhibitors' predicted binding free energy meaning that the interactions between all inhibitors and the newly build Q_o active site are much more favorable. For Quinolone 1 and GW844520, better results were obtained when a water molecule was introduced in the active site near Glu272. These results were quite expected since, in the presence of this molecule, these inhibitors may establish a second hydrogen bond with Glu272. The docking results obtained in Chapter 2 already indicated that this molecule could be of extreme importance to explain the strong interactions between some inhibitors and the Q_o binding site.

Table 4.5. Docking results for the tested inhibitors. Free energies in kcal/mol, K_i and IC_{50} in units of nM. Experimental values obtained from Cowley *et al*¹⁰⁵ (for Quinolone 1) and Biagini *et al*¹³³ (for the other compounds). Docking calculations performed with His181 in its neutral state.

Inhibitor	Yeast model			Homology model			K_i (<i>Pfbc</i> ₁)	IC_{50} (<i>Pfbc</i> ₁)
	Score	ΔG_{calc}	K_{icalc}	Score	ΔG_{calc}	K_{icalc}		
Quinolone 1 ^a	6.22	-8.47	611.48	7.02	-9.56	97.09	-	1.3
Atovaquone	7.09	-9.67	81.75	8.38	-11.42	4.26	0.3	3
WR 249685	7.32	-9.97	49.27	7.62	-10.38	24.44	0.3	3
Stigmatellin	7.18	-9.79	66.58	7.88	-10.74	13.39	1.3	12
GW844520 ^a	6.78	-9.25	164.28	7.48	-10.03	44.47	3.5	32
S-Floxacrine	6.02	-8.20	975.39	6.78	-9.24	168.13	89	803
R-Floxacrine	6.30	-8.59	501.42	7.11	-9.69	78.61	89	

a) Docking calculations performed with H₂O molecule in the active site.

Due to the comprehensive description of the binding mode of all *bc*₁ complex inhibitors already presented in Chapter 2, only some comments will be made about specific inhibitors. In this way, the binding mode of stigmatellin is depicted in Figure 4.10. Stigmatellin fits into the active site quite nicely, strongly interacting with His181 and Glu272. This inhibitor adopts a conformation that is very close to the one found in the several crystallographic structures used for this study. Moreover, the analysis of the superposition of all structures shows that the benzopyranone ring stays almost in the same plane. However, when considering the side chain of stigmatellin, some conformational differences can be found since the predicted pose for this inhibitor shows its aliphatic chain pointing toward a different part of the pocket. Most likely, the size of the Q_o binding pocket obtained by homology modeling is slightly enlarged in the pocket entrance when compared with the same pocket in the other species contributing to increase the pocket space.

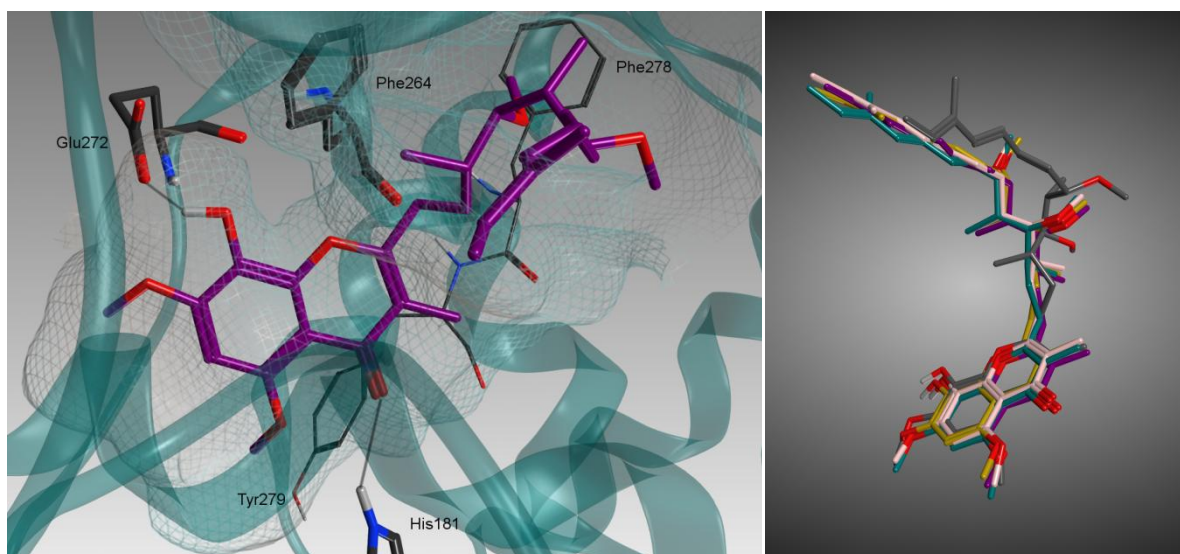


Figure 4.10. Predicted binding pose for stigmatellin on the left. Hydrogen bonds are represented by grey lines. Superposition of the bound stigmatellin in the crystallographic structures of several species: *S. cerevisiae* (in pink), *B. Taurus* (in purple), *G. gallus* (in yellow) and *R. shaeroides* (in green), and the one predicted by docking calculations (in grey) on the right.

Concerning WR 249685 some observations can also be made. This inhibitor, as already mentioned, was of extreme importance for building this homology model since this dihydroacridinedione is the only *P. falciparum* bc_1 complex inhibitor that is completely selective for yeast. In this way, it was expected that the predicted binding free energy value for this inhibitor should decrease when compared with the same value obtained for yeast model. However, this value only slightly decreased not reaching the binding free energy value obtained for atovaquone. More specifically, although these two compounds present the same IC_{50} value (3 nM), the binding free energy obtained are -11.42 and -10.38 kcal/mol for atovaquone and WR 249685, respectively. The predicted binding mode of WR 249685 in the *Pf* model is illustrated in Figure 4.11 and allows to verify that a potential interaction between the aromatic moiety of this inhibitor with Phe264 is essential to explain the inhibitory activity of this compound. Additionally, a more favorable interaction can be probably found if the flexible loop to which this residue belongs suffers an adjustment in order to increase the strength of the π - π contacts. Almost certainly, the predicted binding free energy value obtained for this inhibitor is not

in the same range than the one obtained for atovaquone as a result of the diminished effectiveness of this type of interactions due to the use of a rigid interaction model.

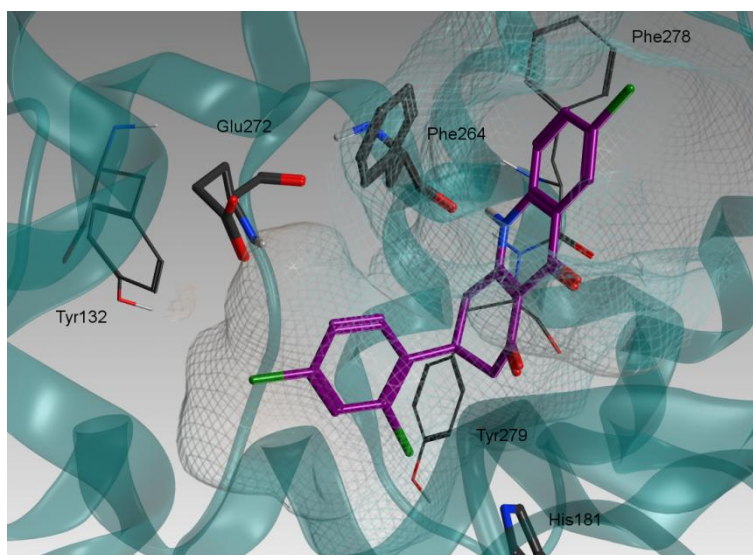


Figure 4.11. Predicted binding poses for WR 249685.

Further studies can still be done in order to verify this hypothesis. Namely, a molecular dynamics study could be performed to check if Phe264 side chain may adjust to the position of WR 249685, highly increasing the interactions between the two aromatic moieties. Unfortunately, it was not possible to perform this study due to time and computer power limitations.

Moreover, when considering Quinolone 1, this inhibitor also did not display the expected binding free energy value. Although this compound was not considered in the first study over the yeast model, some calculations were further made using the yeast structure in order to verify the ability of the homology model to improve its predicted inhibitory potential. Indeed, in spite of the low score value obtained when compared with the remain inhibitors, the score value of Quinolone 1 is improved when the docking calculations are performed in the homology model. As already mentioned, although this molecule was not tested with the remain inhibitors in the same biological assay, this compound was chosen to be included in this set since it was tested in the same

experimental conditions. Nonetheless, no positive control was used when testing Quinolone 1 and, as a result, a comparison between IC_{50} values measured in these two biological assays is quite difficult to formulate since IC_{50} values may differ considerably between the same assays at different times. In this way, it is not possible to assure a reliable comparison between all IC_{50} values and, consequently, between the predicted binding free energy values.

The analysis of Figure 4.12 allows to conclude that this inhibitor fits quite well in the pocket, interacting with both His181 and Glu272 through a water mediated hydrogen bond. Moreover, this compound presents a similar conformation to the one obtained for pyridone GW844520.

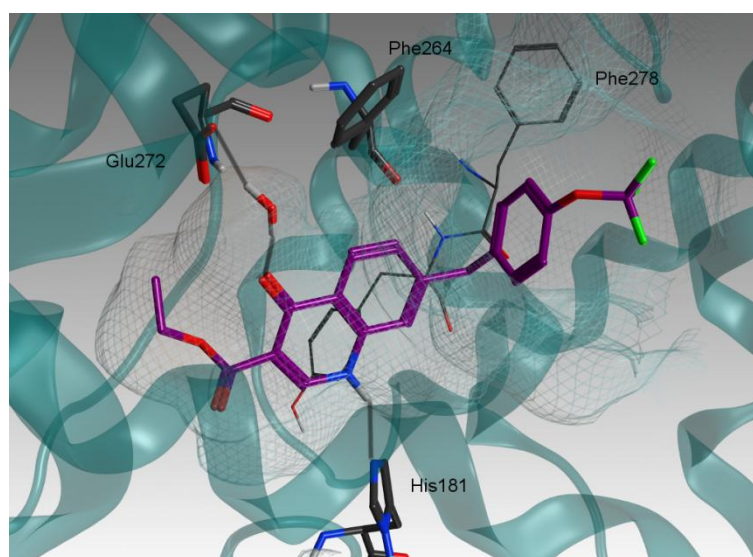


Figure 4.12. Predicted binding pose for Quinolone 1. Hydrogen bonds are represented by grey lines.

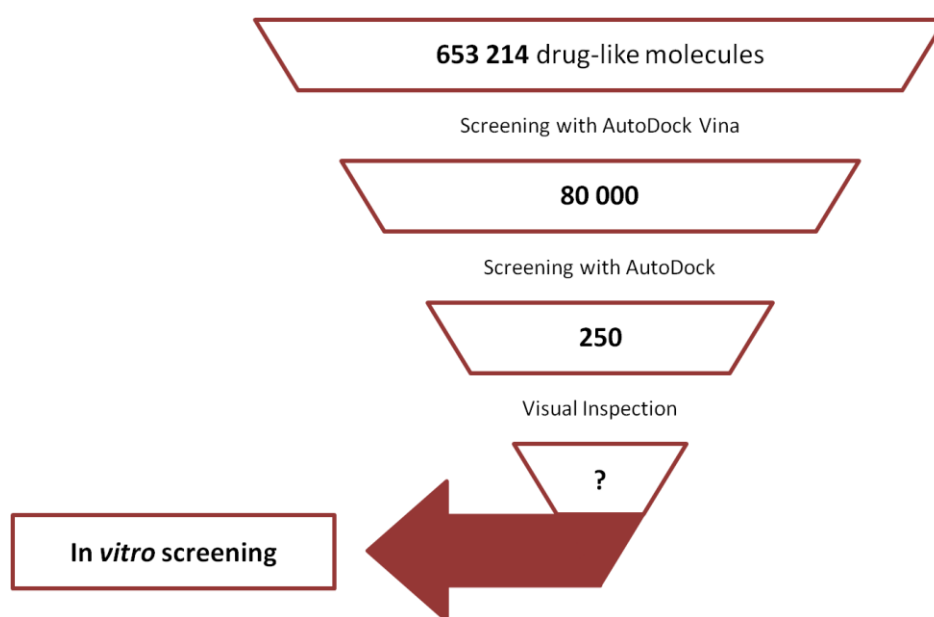
Some docking calculations were already made by Cowley *et al*¹⁰⁵ regarding this class of compounds. In this study, the authors performed the docking calculations using the yeast bc_1 complex as a model for *P. falciparum* which permitted to obtain the quinolone ring interacting also with both His181 and Glu272 residues. However, in this case, the NH moiety establishes a hydrogen bond with Glu272 while the carbonyl group

interacts with His181 which is not in line with the results obtained with the homology model here in presented.

However, the pose obtained for this compound during the docking calculations performed on the homology model of *P. falciparum* Q_o binding site appears to be more favorable given that the H-bond donor group (NH) interacts with the neutral His181 while the H-bond acceptor group (carbonyl) is able to establish a strong hydrogen bond with Glu272 mediated by a water molecule.

4.4. Virtual screening studies over the homology model of *P. falciparum* bc₁ complex

Considering the recently obtained homology model structure, a virtual screening study against the same druglike MOE database already used in Chapter 3 was performed. In order to establish a reliable comparison between the results obtained in both procedures, the experimental methodology followed was identical (Scheme 4.1).



Scheme 4.1. Representation of the overall screening process.

Shortly, the 653214 drug-like compounds included in the MOE package²⁶² was screened against the *P. falciparum* bc_1 complex Q_o binding site obtained by homology modeling using AD Vina. As before, this software was also used to rank all database molecules, and the best 80000 molecules were further docked with AD.

The 250 top-ranked structures obtained after refinement with AD (score higher than 8) were visually inspected. As previously, only compounds presenting structural features that allow not only the formation of strong hydrophobic interactions with the hydrophobic part of the Q_o site but also than can interact with Glu272 of the cytochrome *b* and/or His181 from the Rieske ISP were selected for purchase from commercial suppliers. Other than the score obtained and the docking pose, the chemical diversity, and the commercial availability of the compounds are other important aspects to have in mind. Examples of the most interesting potential bc_1 complex inhibitors are highlighted in Figure 4.13 and their score values are included in Table 4.6.

Table 4.6. Some physical properties and score of the selected compounds. cLogP values obtained from ALOGPS 2.1²⁶³.

Compound	cLogP	MW / g.mol ⁻¹	Score
4.1	4.90	441.48	9.56
4.2	5.27	446.55	9.40
4.3	4.36	417.46	9.24
4.4	4.54	447.55	9.18
4.5	4.83	435.93	9.05
4.6	3.36	432.45	9.03
4.7	4.81	447.11	8.99
4.8	3.47	444.42	8.94
4.9	5.36	441.50	8.93
4.10	4.22	437.13	8.92
4.11	3.41	423.16	8.76
4.12	3.74	407.13	8.66

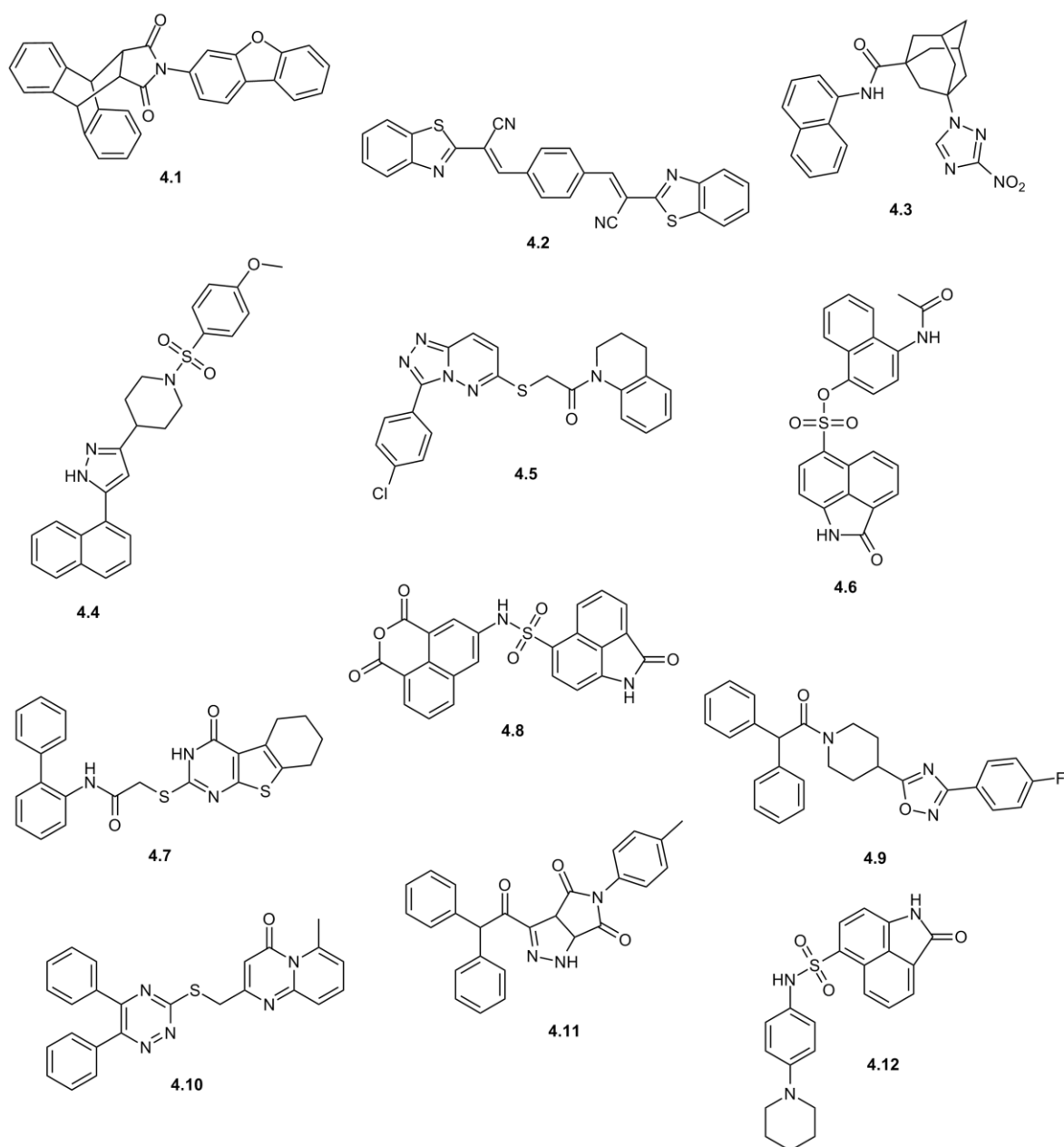


Figure 4.13. Chemical structures of the selected potential bc_1 complex inhibitors.

A comparison between the chemical structures of the compounds obtained after the virtual screening, with both yeast Q_0 binding site model and *P. falciparum* homology model, allows to conclude that the potential bc_1 complex inhibitors obtained in this second study present higher molecular volume than the ones obtained in the first study. As a result, it is possible to observe that the recently obtained Q_0 binding site exhibits a larger pocket than the yeast pocket which is in line with the results already obtained for

stigmatellin. The predicted binding poses of some of these potential inhibitors are illustrated in Figure 4.14.

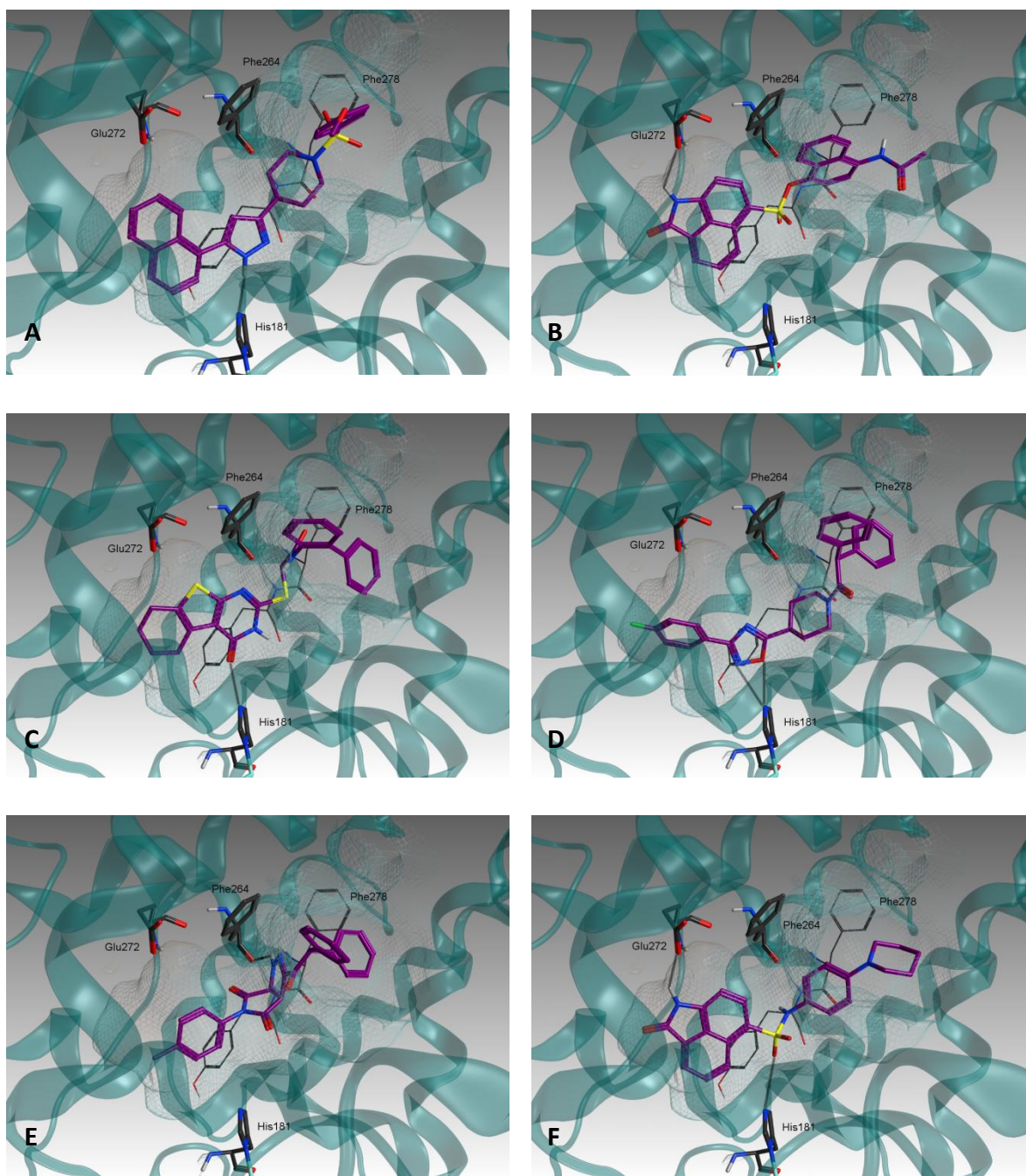


Figure 4.14. Predicted binding poses of compounds **4.4** (A), **4.6** (B), **4.7** (C), **4.9** (D), **4.11** (E) and **4.12** (F). Hydrogen bonds are represented by grey lines.

The selected inhibitors are able to establish strong interactions with different amino acid residues in the pocket, more specifically with His181, Phe264 and Glu272. Additional hydrophobic interactions can also be found between Phe264 and all these compounds.

Although, as of the writing of this thesis, no biological results are until now available for these compounds, the docking results indicate that the new ligands can be tested as potential antimalarial drugs acting on *bc*₁ complex and also be used to further develop novel and effective classes of inhibitors following a hit to lead drug discovery optimization techniques.

4.5. Concluding remarks

With this study it was possible to solve the structure of the Q_o binding site of *P. falciparum* *bc*₁ complex by homology modeling using the yeast crystallographic structure as template. The best output model was further refined and subjected to comparison with other available structures before being validated by PROCHECK.

An additional validation procedure was conducted by docking known *P. falciparum* *bc*₁ complex inhibitors in this newly build Q_o binding pocket. The predict binding free energy values for all inhibitors were quite satisfactory and showed that this model allowed to enhance the interactions between the compounds and the binding site. Furthermore, special attention was given to WR 249685 since this compound is key to explain the selectivity found between both *P. falciparum* and *S. cerevisiae* *bc*₁ complex. Although the predict binding free energy value for this compound was not as lower as expected, the results indicate that the interaction between the aromatic moiety of WR 249685 and Phe264, only existing in *P. falciparum*, is crucial to explain its inhibitory activity. Only a molecular dynamics study, which was not possible to be performed in due time, can confirm this hypothesis.

A second virtual screening study was performed against this new model and the same drug-like database used in Chapter 3 by following identical procedure. After visual

inspection of the top-ranked compounds, some of them were selected to be purchased and to be further biologically assayed.

Although no biological results are so far available that permits to validate this model as a reliable tridimensional structure of *P. falciparum* bc_1 complex Q_o binding site, some additional steps were made in order to better understand the structure of this target. Moreover, this model can be considered an important tool to recognize substrate specificity and, more relevant, it may be used for the development of new specific *Pf* bc_1 complex inhibitors.

CHAPTER FIVE

List of contents

5.1. Background	137
5.2. Synthetic approaches	140
5.3. Biological evaluation	147
5.4. Concluding remarks	157

5. Synthesis of Aurone Derivatives as Potential Antimalarials

5.1. Background

Aurones, 2-benzylidenebenzofuran-3-(2*H*)-ones (Figure 5.1), are structural isomers of flavones that contain an exocyclic carbon-carbon double bond bridging the benzofuranone and phenyl rings²⁸⁶⁻²⁸⁷. The therapeutic potential of aurones has been highlighted with recent studies that revealed their anti-cancer²⁸⁸⁻²⁹³, antimicrobial²⁹⁴, antiparasitic²⁹⁵⁻²⁹⁸, anti-viral²⁹⁹, and anti-inflammatory²⁹⁴⁻³⁰⁰ activities. In addition, aurones can also act as modulators of ABC drug transporters³⁰¹⁻³⁰⁵ and present inhibitory activity against acetylcholinesterase³⁰⁶ and MAO-B³⁰⁷.

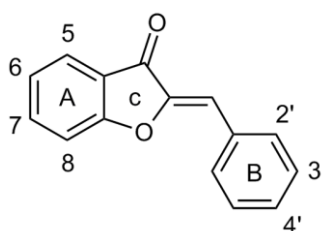
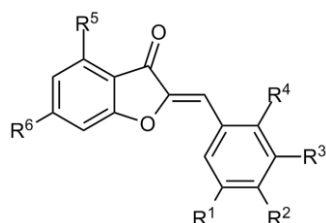


Figure 5.1. General structure of aurones.

The antimalarial potential of aurones was first reported by Kayser *et al.*²⁹⁶. In this study, several naturally occurring aurones were synthesized and tested for their ability to

inhibit erythrocytic stages of *P. falciparum* K1 and NF54 strains *in vitro*. Some of these compounds exhibit antiplasmodial activity in the micromolar range and are more potent against the multiple drug-resistant strain K1 (Table 5.1). Additionally, these aurone derivatives showed no cytotoxicity in mammalian tumor cell lines. The analysis of the biological data permitted to conclude that the presence of hydroxyl and methoxy substituents display a strong effect in the IC₅₀ values for either *P. falciparum* strain. More specifically, the introduction of a higher number of oxygenated substituents led to better antiplasmodial compounds (for example, compound **5.8**). On the other hand, compounds displaying more lipophilic character, with less oxygen substituents, showed only moderate or no activity. Moreover, the SAR analysis permitted also to conclude that the introduction of an oxygenated substituent in positions 6 of ring A and positions 3' and/or 4' of ring B allowed increasing antimalarial activity of this class of compounds.

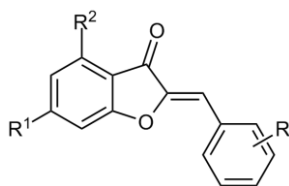
Table 5.1. Structure and *in vitro* antimalarial activity of selected naturally occurring aurones²⁹⁶.



Comp	R ¹	R ²	R ³	R ⁴	R ⁵	R ⁶	IC ₅₀ (μM)	
							K1	NF54
5.1	H	H	H	H	H	OH	> 0.400	> 0.400
5.2	H	OH	OH	H	H	OH	0.300	0.300
5.3	H	H	OH	H	H	OH	0.500	> 0.390
5.4	H	OH	H	OH	H	OH	0.030	0.170
5.5	H	OH	H	H	H	OH	> 0.390	> 0.390
5.6	H	OMe	OMe	H	H	OH	0.120	0.190
5.7	H	OH	OMe	H	OH	OH	0.030	0.200
5.8	OMe	OAc	OMe	H	OMe	OAc	0.007	0.180
5.9	OMe	OAc	OMe	H	GlcAc	OAc	> 0.100	> 0.130

In 2010, Souard *et al.*²⁹⁸ obtained a series of synthetic aurones with potential antimalarial activity. All the compounds were found to be non-cytotoxic in human cell lines and six exhibit an IC₅₀ below 50 μM in the antiplasmodial assay (Table 5.2).

Table 5.2. Structure and *in vitro* antimalarial activity of synthetic aurone derivatives²⁹⁸.



Compound	R	R ¹	R ²	IC ₅₀ (μM)
5.10	H	OH	OH	94.5
5.11	H	OMe	OMe	60.3
5.12	4'-Me	OH	OH	63.4
5.13	2'-Et	OMe	OMe	21
5.14	2'-Et	OH	OH	113.5
5.15	4'-Et	OH	H	28
5.16	4'-tBu	OMe	OMe	13.3
5.17	4'-Bu	OMe	OMe	11.8
5.18	4'-Br	OMe	OMe	49.8
5.19	4'-F	OMe	OMe	86.7
5.20	4'-OH	OH	H	130
5.21	4'-OMe	OMe	OMe	11
5.22	4'-Ph	OMe	OMe	234
5.23	4'-Py	OMe	OMe	85
CQ	-	-	-	0.19

The SAR elucidation confirmed, once again, that the presence of methoxy groups was highly favorable for the antimalarial activity. Additionally, the presence of a hydrophobic group in ring B was also highly favorable. The chain elongation also resulted

in a significant increase in activity. However, introduction of an additional aromatic ring led to less active derivatives.

Furthermore, *in vivo* assays showed that the most active compound was not toxic to the mouse itself although the antiplasmodial effect appeared to be less efficient when compared with the *in vitro* studies.

More recently, Adhikari *et al.*³⁰⁸ developed a computational study involving DFT-based QSAR, and CoMFA-CoMSIA techniques to explore the structural requirements of aurone derivatives as antimalarial drugs. This study was supported by the results obtained by Souard²⁹⁸ highlighted that not only the methoxy fragments in ring A are important for biological activity but also that the introduction of positively charged and/or bulky hydrophobic groups in ring B are essential for antimalarial potential in this class of compounds.

Most of aurone-based libraries already screened against *P. falciparum* were inspired by naturally occurring aurones, typically containing hydroxy, methoxy, acetoxy or other small groups at different positions of this scaffold, leading to a limited diversity of compounds tested in this parasite. Therefore, in order to increase the antimalarial ability of this class of natural compounds, a diverse range of substituents should be introduced in this scaffold. Therefore, the main goal is to incorporate different moieties in a known scaffold in order to identify the most relevant modifications responsible for biological activity.

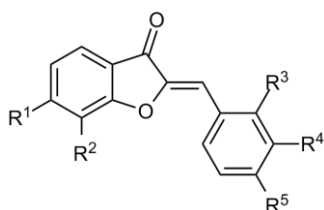
5.2. Synthetic approaches

A library of novel aurone derivatives were designed and synthesized in order to probe the chemical space around this scaffold. Palladium-catalyzed reactions can provide an excellent platform for increasing the chemical diversity of known scaffolds due to the wide range of transformations mediated by this catalyst³⁰⁹. Therefore, considering the advantageous of the palladium-catalyzed reactions, many of the target compounds were obtained through Suzuki-Miyaura and Buchwald-Hartwig cross-coupling reactions.

Furthermore, taking in account recent evidences suggesting antimalarial activity of aurone-Mannich base derivatives³¹⁰, some compounds were also obtained via the introduction of different aliphatic amines in the benzofuranone ring.

A total of 35 aurones derivatives were synthesized by varying substituents both in ring A and B (Figure 5.1) to explore the potential of this scaffold as a platform to design new antimalarial agents (Table 5.3).

Table 5.3. Structure, $\log P$ values, Lipinski rule of 5 violations, and yields for the synthesis (final step) of aurones 5.24-5.58.



	R ₁	R ₂	R ₃	R ₄	R ₅	LogP ²⁶³	Rule of 5 violations	Yield/%	
Series A	5.24	H	H	H	H	H	3.39	0	41
	5.25	H	H	Br	H	H	4.12	0	55
	5.26	H	H	H	Br	H	4.13	0	54
	5.27	H	H	H	H	Br	4.12	0	54
	5.28	H	H	H	H	NMe ₂	3.51	0	49
	5.29	H	OMe	H	H	H	3.09	0	62

Table 5.3. Structure, *clogP* values, rule of 5 violations, and yields for the synthesis (final step) of aurones 5.24-5.58 (cont.).

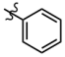
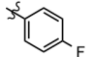
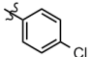
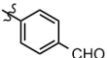
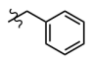
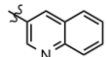
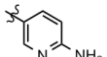
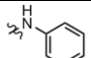
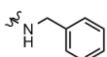
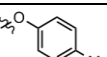
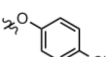
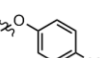
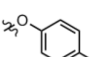
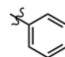
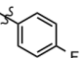
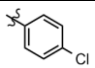
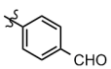
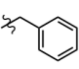
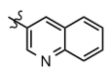
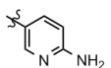
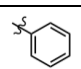
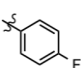
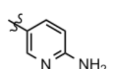
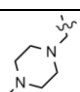
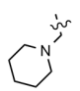
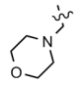
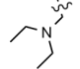
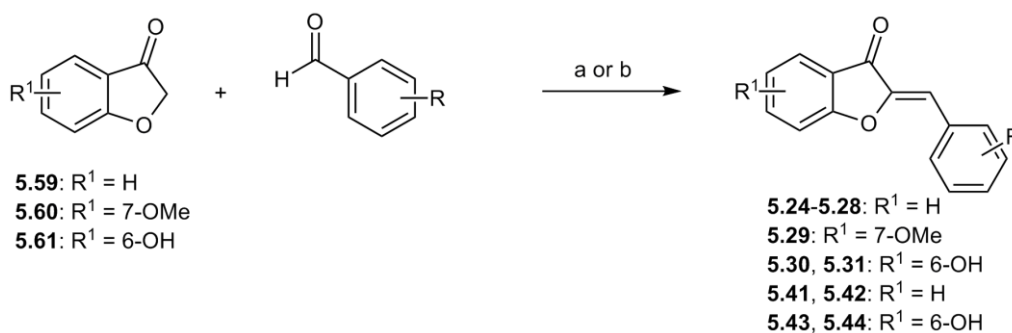
		R ₁	R ₂	R ₃	R ₄	R ₅	Log <i>P</i> ²⁶³	Rule of 5 violations	Yield/%
Series B	5.30	OH	H	H	H	H	3.02	0	99
	5.31	OH	H	H	H	NMe ₂	3.17	0	71
Series C	5.32	H	H	H	H		5.06	1	77
	5.33	H	H	H	H		5.21	1	66
	5.34	H	H	H	H		5.65	1	64
	5.35	H	H	H	H		4.70	0	83
	5.36	H	H	H	H		5.24	1	70
	5.37	H	H	H	H		5.16	1	87
	5.38	H	H	H	H		3.69	0	98
Series D	5.39	H	H	H	H		4.83	0	71
	5.40	H	H	H	H		4.62	0	49
Series E	5.41	H	H	H	H		5.40	1	33
	5.42	H	H	H	H		5.51	1	51
	5.43	OH	H	H	H		5.27	1	51
	5.44	OH	H	H	H		5.13	1	84
Series F	5.45	H	H	H		H	5.05	1	71
	5.46	H	H	H		H	5.21	1	65

Table 5.3. Structure, $\log P$ values, rule of 5 violations, and yields for the synthesis (final step) of aurones 5.24-5.58 (cont.).

	R_1	R_2	R_3	R_4	R_5	$\text{Log}P^{263}$	Rule of 5 violations	Yield/%	
Series F	5.47	H	H	H		H	5.65	1	51
	5.48	H	H	H		H	4.70	0	63
	5.49	H	H	H		H	5.24	1	49
	5.50	H	H	H		H	5.16	1	68
	5.51	H	H	H		H	3.69	0	76
Series G	5.52		H	H	H	H	5.24	1	78
	5.53		H	H	H	H	5.05	1	66
	5.54		H	H	H	H	5.20	1	99
Series H	5.55	OH		H	H	H	2.55	0	61
	5.56	OH		H	H	H	3.73	0	63
	5.57	OH		H	H	H	2.47	0	54
	5.58	OH		H	H	H	3.55	0	29

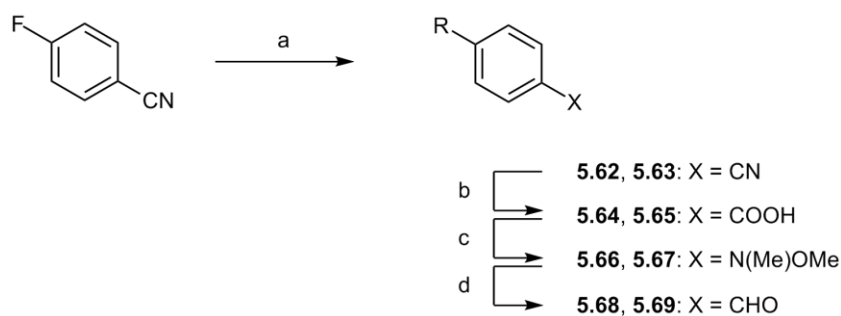
Compounds in series A and compounds **5.41-5.42** were synthesized from commercially available benzofuran-3(2*H*)-one, **5.59**, or 7-methoxy-3(2*H*)-benzofuranone, **5.60**, which were reacted with appropriately substituted benzaldehydes in the presence of neutral alumina³¹¹ (Scheme 5.1), in order to give the desired aurones with moderate yields. Only commercially available benzofuranone derivatives were used in this study which limited the chemical diversity in ring A of the compounds synthesized.



Scheme 5.1. Reagents and conditions: (a) **5.59** or **5.60**, Al₂O₃, MeOH, reflux under N₂, 24 hours. (b) **5.61**, glacial AcOH, HCl (cat), RT, 4 hours. R substituents are according to Table 5.3.

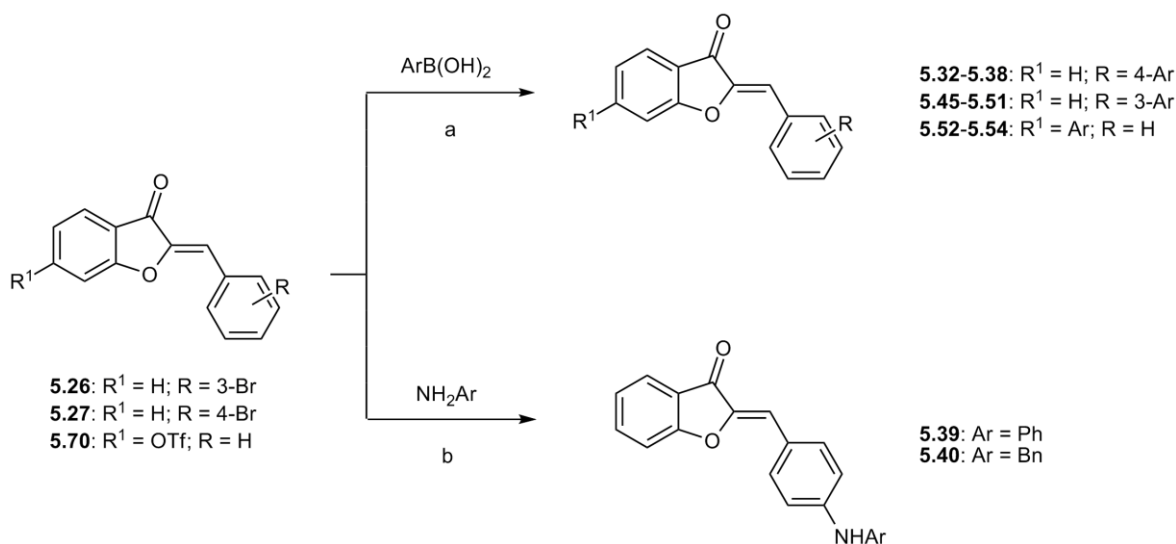
However, this method failed to provide the 6-hydroxy aurones in reasonable yields. Possibly, the favorable interaction of alumina with the free hydroxyl group in the benzofuranone ring contributed to decrease its catalytic efficiency and, consequently, to decrease the formation of the product. In contrast, for these compounds, the acidic catalysis in the presence of glacial acetic acid and hydrochloric acid was preferred³¹². Accordingly, the acid-catalyzed aldol condensation of 6-hydroxy-3(2*H*)-benzofuranone, **5.61**, with benzaldehydes afforded aurones in series B (compounds **5.30** and **5.31**) and compounds **5.43** and **5.44** in moderate to good yields (Scheme 5.1).

The aldehydes required for aurones **5.41-5.44** were synthesized from 4-fluorobenzonitrile and the appropriate phenol, and via the Weinreb amides **5.66** and **5.67**, as described in Scheme 5.2. In the first step, the appropriate phenol was reacted with 4-fluorobenzonitrile in the presence of Na₂CO₃ in order to obtain the phenoxybenzonitrile derivatives (**5.62** and **5.63**) via an aromatic nucleophilic substitution. These intermediates suffered subsequent hydrolysis in the presence of H₂O₂ and KOH to provide the benzoic acids **5.64** and **5.65**. Compounds **5.66** and **5.67** were obtained in very good yields using TBTU as a coupling agent. In the last step, the phenoxybenzaldehydes **5.68** and **5.69** were synthesized in quantitative yields from simple LiAlH₄ reduction in anhydrous conditions.



Scheme 5.2. Reactions and conditions: (a) substituted phenol, Na_2CO_3 , dry DMF, reflux, 24 hours; (b) H_2O_2 (30%), KOH, MeOH, EtOH, reflux, 5 hours; (c) *N,O*-dimethylhydroxylamine, TEA, TBTU, dry DMF, RT, overnight; (d) LiAlH_4 , dry THF, -5°C .

Compounds in series C, F and G were obtained through a standard Suzuki-Miyaura cross-coupling reaction in the presence of $\text{Pd}(\text{PPh}_3)_2\text{Cl}_2$ as catalyst, as described by Liu *et al*³¹³ (Scheme 5.3).

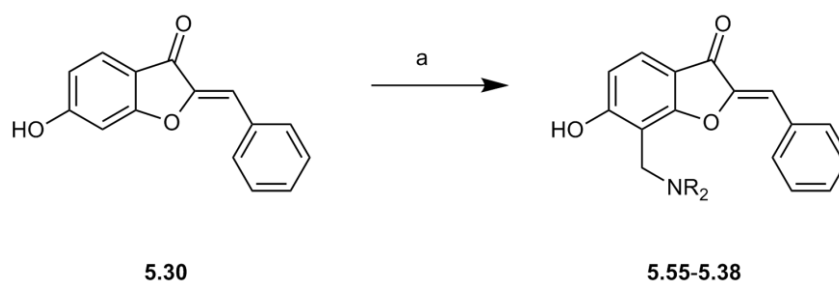


Scheme 5.3. Reactions and conditions: (a) $\text{Pd}(\text{PPh}_3)_2\text{Cl}_2$, Na_2CO_3 (1M), 1,4-dioxane, 100°C , 3 hours; (b) $\text{Pd}_2(\text{dba})_3$, (*R*)-BINAP, NaO^tBu , dry toluene, 110°C , 15 min, MW.

Performing the cross-coupling reactions on starting materials **5.27** and **5.26** afforded auronones **5.32-5.38** (series C) and **5.45-5.51** (series F), respectively, in moderate

to very good yields. The synthesis of compounds **5.52-5.54** (series G) was accomplished through the Suzuki-Miyaura cross-coupling reaction of triflate **5.70**, obtained from the starting material **5.30**. Aurones in series D (compounds **5.39** and **5.40**) were prepared via the Buchwald-Hartwig cross-coupling reaction following the Fitzmaurice *et al.* procedure³⁰⁹. Starting material **5.27** was reacted with the appropriate amine in the presence of Pd₂(dba)₃, (*R*)-BINAP, and NaO^tBu in microwave conditions to afford **5.39** and **5.40** in moderate yields (Scheme 5.3). This reaction was also performed in the presence of Pd(OAc)₂ and ^tBu-Xantphos in both termic and MW conditions but the desired product was not obtained.

Finally, the Mannich-base derivatives **5.55-5.58** (series H) were synthesized in moderate yields by reacting the starting material **5.30** with the appropriate aliphatic secondary amine in aqueous formaldehyde (Scheme 5.4).



Scheme 5.4. Reactions and conditions: (a) aliphatic amine, formaldehyde solution, EtOH, reflux, 5 hours.

Due to the presence of an exocyclic double bond in the synthesized aurones is important to formulate some considerations about their stereochemistry. Therefore, it is possible to obtain these compounds in two configurational isomers, *E* (trans) or *Z* (cis), being the *Z* isomer generally regarded as the thermodynamically more stable form³¹⁴. These two isomers present very specific ¹H and ¹³C chemical shifts in the NMR spectra. Experimental evidences show that typical chemical shift value in ¹H NMR for vinylic proton in *E* isomer is around 7.01 ppm while for *Z* isomer is *ca.* 6.70 ppm³¹⁵⁻³¹⁶. For ¹³C NMR, the chemical shift reported for *Z* isomer is 111 ppm while the *E* isomer is usually

observed at a higher frequency (*ca.* 120–130 ppm)³⁰¹. Moreover, the x-ray structures of some aurone derivatives also support the assignment of the double bond configuration.

In this case, the ¹³C NMR data obtained for these compounds shows that the chemical shift for the exocyclic carbon in all compounds appears in the range of 108–112 ppm indicating that this double bond must be in *Z* configuration. However, the ¹H chemical shifts for the same compounds present values around 7 ppm which are consistent with reported values for *E* configuration. This ambiguity in ¹H and ¹³C chemical shifts values may be related to the electronic properties of the substituents in ring B. Nevertheless, due to experimental evidences that indicate the thermodynamical stability of the *Z* isomer, it is reasonable to hypothesize that the majority of the compounds are at the *Z* configuration. The same ambiguity was already found for some aurone derivatives that are correctly assigned by X-ray structure²⁹⁸. For instance, some aurone derivatives with substituents in position 2' of ring B presented chemical shift values ranging from 7.00 to 7.38 ppm suggesting the presence of an *E* configuration. In contrast, aurones substituted in position 4' of ring B showed the ¹H chemical shift of the β hydrogen of 6.87 ppm. In both cases, the X-ray structures of the compounds showed that these aurone derivatives are in *Z* configuration.

5.3. Biological evaluation

5.3.1. Activity against *P. falciparum* W2 strain

All compounds were assayed for their antiplasmodial activity against the chloroquine-resistant *P. falciparum* W2 strain and for their toxicity against Human Embryonic Kidney 293T cells. The data presented in Table 5.4 reveals that 20 aurones displayed relevant antiplasmodial activity, with IC₅₀ values ranging from 1.2 to 9.9 μM. In addition, aurones derivatives presented negligible cytotoxicity, with EC₅₀ values against cultured human cells ranging from 68 to ≥100 μM. In general, most of the compounds presented selectivity indices (SI = EC₅₀(HEK293T)/IC₅₀(W2)) higher than 10, indicating that aurones are selective and nontoxic antiplasmodial agents. Concerning the bioavailability, Lipinski

rule³¹⁷ was applied to the synthesized compounds and showed that the majority of aurone derivatives passed the Lipinski filter with some compounds presenting only one violation (Table 5.3).

Table 5.4. Antiplasmodial activity (IC₅₀) against the CQ-resistant *Plasmodium falciparum* W2 strain, cytotoxicity (EC₅₀) against Human Embryonic Kidney 293T cells and selectivity index (SI = EC₅₀/IC₅₀) for aurones **5.24-5.58**.

Compound	IC ₅₀ / μM	EC ₅₀ / μM	SI	Compound	IC ₅₀ / μM	EC ₅₀ / μM	SI	Compound	IC ₅₀ / μM	EC ₅₀ / μM	SI
5.24	> 10	> 100	> 10	5.36	7.34	87	> 12	5.48	> 10	> 100	> 10
5.25	> 10	> 100	> 10	5.37	6.59	> 100	> 10	5.49	2.31	71	> 31
5.26	4.70	> 100	> 10	5.38	3.70	> 100	> 10	5.50	4.78	> 100	> 10
5.27	3.21	> 100	> 10	5.39	8.59	> 100	> 10	5.51	2.56	79	> 31
5.28	7.99	> 100	> 10	5.40	5.00	> 100	> 10	5.52	> 10	> 100	> 10
5.29	> 10	> 100	> 10	5.41	> 10	> 100	> 10	5.53	> 10	> 100	> 10
5.30	> 10	> 100	> 10	5.42	> 10	> 100	> 10	5.54	3.03	> 100	> 10
5.31	>10	> 100	> 10	5.43	5.84	95	> 16	5.55	4.01	> 100	> 10
5.32	> 10	> 100	> 10	5.44	9.88	12	> 1	5.56	1.18	> 100	> 10
5.33	> 10	> 100	> 10	5.45	5.21	> 100	> 10	5.57	3.34	> 100	> 10
5.34	> 10	> 100	> 10	5.46	4.41	> 100	> 10	5.58	3.47	> 100	> 10
5.35	> 10	> 100	> 10	5.47	> 10	> 100	> 10	CQ	0.14	ND	ND

ND: not determined

Inspection of the data in Table 5.4 allowed to conclude that, overall, the introduction of a second aromatic or aliphatic moiety in the aurone scaffold allowed enhancing the antimalarial potential of this class of compounds. More precisely, compounds containing only the aurone skeleton showed no significant activity with only three compounds (**5.26**, **5.27**, and **5.28**) presenting an IC_{50} value lower than 10 μM . Concerning the simpler aurone derivatives in series A and B (compounds **5.24** to **5.31**), results showed that the introduction of a bromine or amine substituent increase the antimalarial activity when comparing to the parent compound **5.24**. However, the bromine substituent is preferred in ring B of aurone scaffold when compared with the amine substituent (compound **5.27** vs compound **5.28**). Moreover, the evaluation of the biological results obtained for compounds **5.25**, **5.26** and **5.27** permitted to conclude that the *para* and *meta* positions are favored when compared to the *orto* position.

In most cases, for compounds in series C, D and E, the inhibitory potential of these compounds could only be increased when a more flexible substituent is added (benzyl group in compound **5.36**) or when the additional aromatic moiety includes a heteroatom as in aurones **5.37** to **5.40**. Additionally, the activity data for ether derivatives (series E) show that only the hydroxylated derivatives presented relevant inhibitory activity against *P. falciparum* W2 strain. Specifically, compounds **5.43** and **5.44** present IC_{50} values of 5.84 and 9.88 μM , respectively, while compounds **5.41** and **5.42**, lacking the hydroxyl group, show no appreciable inhibitory activity at the tested concentration (10 μM). Accordingly, a comparison between the IC_{50} values obtained for these compounds and for compounds **5.30** and **5.31** allowed to conclude that an additional aromatic ring is essential to increase the inhibitory potential of 6-hydroxyaurones. These results are in line with the computational results obtained by Adhikari³⁰⁸ showing that the introducing of an additional bulky substituent in ring B contributes to increase the antimalarial activity of these compounds.

Regarding aurone derivatives with an additional aromatic moiety in position 3' of ring B (Serie F), inspection of Table 5.4 allowed to conclude that the inhibitory activity of these compounds is superior to the one found for their analogous substituted in position 4' (series C). Accordingly, the introduction of an additional aromatic moiety in aurone

scaffold is preferred in *meta* position. As observed in series C (compounds **5.32** to **2.38**), the most potent inhibitor includes a flexible side chain or a heteroatom in the additional aromatic moiety (compounds **2.49** and **2.51**, respectively). Concerning aurone derivatives substituted in position 6 of ring A (compounds **2.52** to **2.54**), these compounds present comparable activity to their analogous substituted in position 4' of ring B (compounds **2.32**, **2.33**, and **2.38**) with only compound **2.54** showing appreciable inhibitory activity.

Finally, the IC_{50} values obtained for Mannich-base aurone derivatives (series H) permitted to conclude that the introduction of a protonable aliphatic amine in position 7 of ring A increased the inhibitory activity of these compounds when compared with the parent compound **5.30**. These results were already expected since the antimalarial activity of Mannich-base derivatives was previously established with well known antimalarials drugs such as amodiaquine and pyronaridine⁵⁷.

Overall, these results suggest that aurones containing basic moieties, *i.e.*, 3-(2'-amino)pyridine, **5.38**, **5.51**, **5.54**, 3-quinoline, **5.37**, **5.50**, and Mannich-bases, **5.55** to **5.58**, generally present improved antiplasmodial activity when compared to their non-basic counterparts. Moreover, it is also important to notice that the basic moiety can exert its beneficial effect on activity independently of its localization in the aurone scaffold. For example, compound **5.54**, containing a 2-aminopyridine moiety in ring A, is equipotent to its counterparts **5.38** and **5.51**, which contain the basic moiety at positions 4' and 3' of ring B, respectively. A similar effect was already reported for chalcones, where substitution with a quinoline moiety at ring A or ring B provided compounds with antiplasmodial activity in the low micromolar range³¹⁸. It is also worth noting that replacement of the benzyl group at ring B by its anilino or phenoxy isosters had a detrimental effect on antiplasmodial activity (**5.36** versus **5.39**, **5.41** and **5.42**). The same trend in activity was observed when the benzylamine moiety at position 4' of ring B was replaced by its aniline counterpart (**5.39** versus **5.40**).

In conclusion, the results obtained indicate that the introduction of an additional aromatic or aliphatic moiety to the aurone scaffold can improve the inhibitory ability of this class of compounds. Better inhibitors are achieved when a basic moiety is introduced

in the aurone scaffold. In this way, aurone **5.56** emerged as the most promising compound, with an IC_{50} value of 1.2 μ M and an excellent selectivity index $SI > 85$.

5.3.2. Heme polymerization inhibition assay

Plasmodium parasites dispose the free, toxic heme that results from digestion of host erythrocyte hemoglobin by crystallizing it into hemozoin. Heme detoxification takes place in the acidic DV of the parasite (pH 5.2), and is believed to be the target of several antimalarial drugs³¹⁹. It has been recently reported that Mannich-base aurone derivatives might interfere with heme polymerization inside the DV of erythrocytic parasites during the hemoglobin digestion³¹⁰. There is strong evidence that pH trapping in the DV (pH 5.2) plays a role in the activity of basic antimalarials such as CQ³¹⁹. In this way, the possibility of the quinoline (**5.37** and **5.50**), 2-aminopyridine (**5.38**, **5.51** and **5.54**) and Mannich-base aurone derivatives (**5.55** to **5.58**) being trapped in the acidic DV was assessed, by calculating the vacuolar accumulation ratio (VAR) based on the pH-dependent distribution of these compounds between water and lipid (log D) (Table 5.5). The lipid accumulation ratio (LAR), which measures the expected ratio of compound that would concentrate within the lipid component within the DV was also determined³¹⁹.

Log D, VAR and LAR values were obtained by application of Equations 1-4 using the calculated values of log P and pK_a ³¹⁹. Additionally, Equation 1 and 2 allowed to obtain the log D values for both 7.4 and 5.2 pH values for the monoprotic and diprotic compounds, respectively.

$$\log D = \log P - \log (1 + 10^{(pK_a - pH)})$$

Equation 1

$$\log D = \log P - \log (1 + 10^{(pK_{a1} - pH)} + 10^{(pK_{a1} + pK_{a2} - 2pH)})$$

Equation 2

$$VAR = 10^{(\log D_{pH\ 7.4} - \log D_{pH\ 5.2})}$$

Equation 3

$$LAR = VAR \times 10^{\log D_{pH\ 5.2}}$$

Equation 4

Table 5.5. Physicochemical parameters for chosen compounds. *cLogP* values were calculated using AlogPS 2.1 software from Virtual Computational Chemistry Laboratory²⁶³. *pKa* values were obtained from SPARC software³²⁰, except when indicated. Values of *logD*, *VAR* and *LAR* were calculated using the equations available in ref 319.

Comp	<i>clogP</i>	<i>pKa</i> ¹	<i>pKa</i> ²	<i>logD</i> _{7.4}	<i>logD</i> _{5.2}	<i>VAR</i>	<i>LAR</i>	<i>MIC</i> /μM	<i>IC</i> ₅₀ /μM
5.37	5.16	4.49 ^a	-	5.16	5.08	1.19	144366	ND	6.59
5.38	3.69	6.14 ^b	-	3.67	2.70	9.20	4643	NI	3.70
5.50	5.16	4.49 ^a	-	5.16	5.08	1.19	144366	ND	4.78
5.51	3.69	6.14 ^b	-	3.67	2.70	9.20	4643	NI	2.56
5.54	5.20	6.14 ^b	-	5.18	4.21	9.20	150233	NI	3.03
5.55	2.55	8.50	7.78	1.02	-3.33	22589	10.6	NI	4.01
5.56	3.73	9.08	-	2.04	-0.15	155	110	NI	1.18
5.57	2.47	6.46	-	2.42	1.19	17.2	265	NI	3.34
5.58	3.55	9.15	-	1.79	-0.40	156	62.0	NI	3.47
CQ	7.72	10.18	8.38	0.92	-3.44	22749	8.25	125	0.14

NI: no inhibition of hemozoin-like crystal formation; ND: not determined; a) Calculated from reference 321; b) Calculated from reference 322.

As shown by the *VAR* values presented in Table 5.5, basic aurones have the potential to accumulate within the DV, with compound **5.55** exhibiting a *VAR* value comparable to that of CQ, reflecting the predominance of its double positively charged

form at pH 5.2. With exception of the piperazine Mannich-base **5.55**, most of the basic aurones exhibit high LAR values, suggesting the preference of these compounds for a lipophilic environment. Consequently, upon entrance into the digestive food vacuole, the compounds could accumulate within the neutral lipid particles at the sight of hemozoin formation³²³⁻³²⁴. However, no clear correlation emerged between the pIC₅₀ values for antiplasmodial activity of compounds **5.37**, **5.38**, **5.50**, **5.51**, **5.54**, and **5.55-5.58**, and their LAR or VAR values. Furthermore, in order to effectively verify the ability of these derivatives to inhibit the heme polymerization, these compounds were submitted to a hemozoin-like crystal inhibition assay³²⁵. All compounds were tested in concentrations ranging 0 to 1000 μ M. Interestingly, none of the compounds showed heme polymerization inhibition at the concentrations tested, which strongly indicates that this is not the main mechanism of acting of these aurone derivatives during the erythrocytic stage of infection. However, the VAR value obtained for these compounds show their ability to accumulate in the DV, and, as a result, this class of compounds may probably interact with other targets within this compartment. Examples of possible targets contained in the DV of *P. falciparum* are the proteases which are of particular interest as therapeutic target due to its role in parasite development^{44, 326-327}. Within the falcipain family, falcipain-2 is one of the most promising targets for antimalarial therapy. This cysteine protease is localized in the parasite's DV and plays a key role in the hydrolysis of host hemoglobin into amino acids essential to parasite growth^{48, 328}. Moreover, plasmepsins are other family of aspartic proteases which are involved in early hemoglobin degradation and are essential for growth and maturation of *Plasmodium* species³²⁹⁻³³⁰. Concerning the falcipain family, it was already reported that some potent inhibitors contain a Michael acceptor warhead³³¹. In this way, since this family of compounds is well known for containing a Michael acceptor²⁸⁶, they may exert its antimalarial activity by interacting with this family of enzymes. However, to evaluate the potential of these compounds to inhibit one of these proteases, additional biochemical studies are necessary.

5.3.3. *In vitro* drug combination assay

Previous studies showed that aurone derivatives also display the ability to inhibit ABC proteins, a family of proteins recognized to be involved in the mechanism of multidrug resistance (MDR)³⁰¹⁻³⁰⁵. Moreover, the importance of this family of transporters, in particular the multidrug resistance transporter (*PfMDR1*), was also highlighted for the resistance of *P. falciparum* to specific antimalarial drugs, more specifically, to CQ³³²⁻³³³. Some observations also confirmed that CQ resistant *P. falciparum* accumulate less drug than more sensitive parasites³³⁴ but also that CQ resistance could be modulated *in vitro* by the MDR modulator verapamil³³⁵. However, the decrease of accumulation of CQ in DV can result not only from drug efflux mechanism but also a reduced uptake of the drug³³⁶.

In order to perform the synergism studies, five distinct compounds were chosen to be tested against the mefloquine and CQ resistant *P. falciparum* strain Dd2. The IC₅₀ values obtained in this study are included in Table 5.6.

Table 5.6. Antiplasmodial activity (IC₅₀) against the CQ-resistant (W2) and mefloquine and CQ resistant (Dd2) *P. falciparum* strains.

Compound	IC ₅₀ / μ M (W2 strain)	IC ₅₀ / μ M (Dd2 strain)
5.40	5.00	4.31
5.43	5.84	7.56
5.51	2.56	7.15
5.54	3.03	6.55
5.57	3.34	3.87

Compound **5.57** was selected to evaluate the potential of these new aurone derivatives to exhibit a mechanism of synergism in the presence of CQ. This compound was chosen from all the set of compounds since it displays similar antiplasmodial in both W2 and Dd2 strains. The analysis of the combination effects of compound **5.57** with CQ was determined by a modified fixed ratio isobologram method³³⁷⁻³⁴⁰. Isobologram analysis, based on calculation of the sum of FICs (FICs = IC₅₀ of drug in the combination /

IC₅₀ of drug when tested alone) or combination index (CI)³⁴⁰ is able to give an indication of whether the interaction is antagonistic, additive or synergistic. A recent study defined synergism between two drugs as $CI < 0.9$, additive effect as $0.90 \leq CI < 1.10$ and antagonism as $CI \geq 1.10$ ³⁴¹. In the present case, the CI value of 1.06 obtained for compound **5.57**, allowed to conclude that there is an additive interaction between this compound and CQ (Figure 5.2).

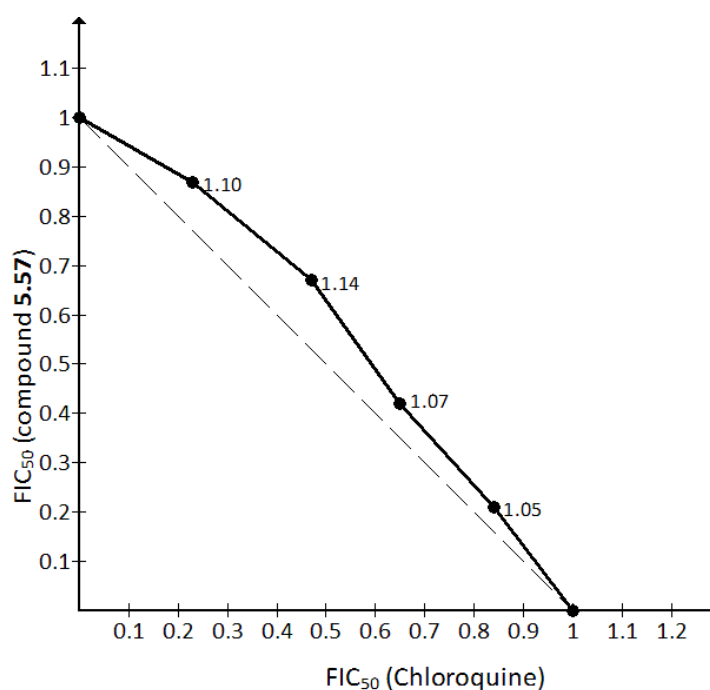


Figure 5.2. Isobologram showing the relationship between the FIC₅₀s of CQ and compound **5.57** against *Plasmodium falciparum* Dd2 strain. Numbers on each plotted point correspond to the calculated CI value for the utilized combination ratio.

Unfortunately, the synergistic potential of this class of compounds could not be demonstrated. Therefore, this study indicates that aurone derivatives do not interfere with the uptake of CQ into the DV.

5.4. Concluding remarks

Novel aurone derivatives with additional structural complexity and diversity were synthesized and screened against a CQ-resistant *P. falciparum* strain. This study demonstrated that aurones can provide a useful platform to develop diverse synthetic strategies to generate novel bioactive compounds. Furthermore, appropriate functionalization of the aurone scaffold yielded compounds with antiplasmodial activity in the low micromolar range and with low cytotoxicity. In particular, aurones containing basic moieties with capacity to protonate under weakly acidic conditions (for example 2-aminopyridine and Mannich-bases) emerged as the most active in this series. These results also indicated that the primary mechanism of action of these basic aurones does not involve inhibition of hemozoin formation. However, the high VAR values obtained for the basic aurones indicate their ability to accumulate in the DV which may be related with their mode of action. Further studies are essential to unravel the antimalarial mechanism of this class of compounds. Finally, these results highlight the potential of the aurone scaffold for future antiplasmodial lead optimization.

CHAPTER SIX

List of contents

6.1. Background	161
6.2. Synthetic approaches	163
6.3. Biological evaluation	179
6.4. Docking studies over bc_1 complex	187
6.5. Concluding remarks	189

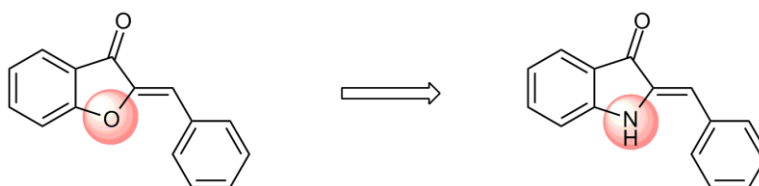
6. Synthesis of Azaaurone Derivatives as Potential bc_1 Complex Inhibitors

Inhibitors

6.1. Background

The results previously obtained with aurone derivatives were very significant since they suggested the potential of this class of compounds to be further optimized in order to develop new antimalarial compounds. However, to be effective, these compounds must show a higher potency against the parasites.

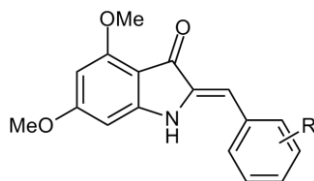
Azaaurone derivatives (Scheme 6.1) are obtained from aurones by bioisosteric replacement of the intracyclic oxygen by NH. Some compounds of this class were also developed by Suard *et al*²⁹⁸ which allow to demonstrate the ability of azaaurones to inhibit parasite growth at concentrations lower than aurone derivatives.



Scheme 6.1. General structure of aurones (left) and azaaurones.

When compared with similar aurone derivatives, Souard *et al*²⁹⁸ could decrease the IC₅₀ of these compounds to one-digit micromolar concentrations (Table 6.1).

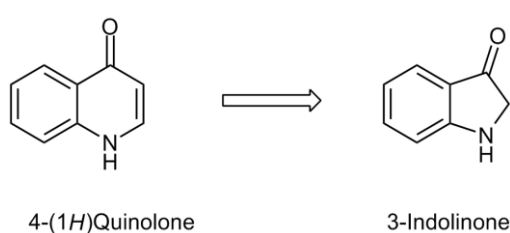
Table 6.1. Structure and *in vitro* antimalarial activity of published azaaurone derivatives²⁹⁸.



Compound	R	IC ₅₀ (μM)
6.1	4'-Br	49.8
6.2	4'-Cl	17
6.3	2'-Cl	9.9
6.4	2',5'-Cl	8.4
6.5	2'-Cl, 6'-F	9
6.6	4'-Et	1
6.7	2'-Et	12.8
6.8	2',6'-Me	9.1
6.9	2',4'-Me	3.6
6.10	2',4',5'-Me	5.6
6.11	2',3',5',6'-Me	8.9
6.12	4'-iPr	4.4
6.13	4'-tBu	7.2
6.14	4'-Bu	4.1
6.15	4'-CCH	13.4
6.16	2',4'-OMe	5
6.17	2',4',6'-OMe	1.9
6.18	3',4',5'-OMe	1.9
6.19	4'-SMe	6.7
6.20	4'-Morpholino	8.9
6.21	4'-N(Me) ₂	3.7
CQ	-	0.19

Although these compounds show no diversity in ring A, it is possible to notice that the ethyl group at position 4' could increase their antimalarial potential (compound **6.6**). However, the introduction of the ethyl group in position 2' led to a huge decrease in the antimalarial activity of compound **6.7**. The methoxylation of ring B was also favorable as shown by the IC_{50} values obtained for compounds **6.16** to **6.18**. The overall results demonstrate that both the size and the lipophilic properties of the compounds affect the inhibitory ability of this class of compounds.

Nevertheless, the results obtained previously with aurone scaffold showed that the introduction of additional aliphatic and aromatic moieties in both ring A and B could in fact increase the antimalarial potential of these compounds. In this way, similar approach was followed in order to expand the chemical diversity with this new scaffold. Moreover, the structural similarity between azaaurones and 4-(1*H*)quinolones also suggests that these compounds may interact with bc_1 complex. This new scaffold can be considered to be obtained after contraction of the quinolone ring (Scheme 6.2). In this way, it is expected that these molecules interact favorably with Glu272 and His181 through carbonyl and amine groups, respectively. Molecules included in this new set will contain a hydrophobic side chain that will interact with the pocket.



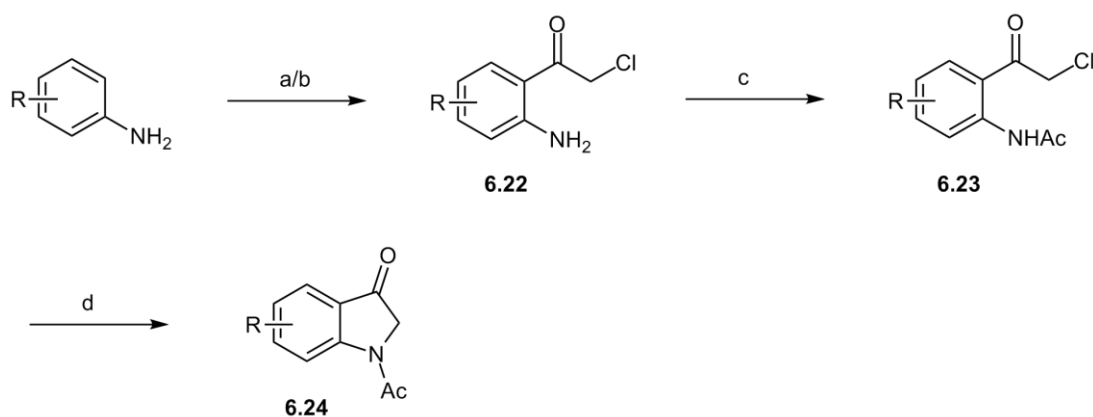
Scheme 6.2. Schematic contraction of the quinolone ring to obtain 3-indolinone.

6.2. Synthetic approaches

In order to obtain a library of chemically distinct azaaurones, the same approach used to synthesize the aurone derivatives was applied. Accordingly, this scaffold was also tested

as a platform for potential synthesis exploration by using, once again, palladium-catalyzed reactions.

Unlike the aurone derivatives that were simply obtained by reacting the commercially available benzofuranone rings with the substituted benzaldehyde, in this case, all 3-indolinone starting materials were synthesized from the appropriate aniline since these compounds were not available in the usual suppliers. As a result, 3-indolinone derivatives were obtained as described by Wager *et al*³⁴² (Scheme 6.3).

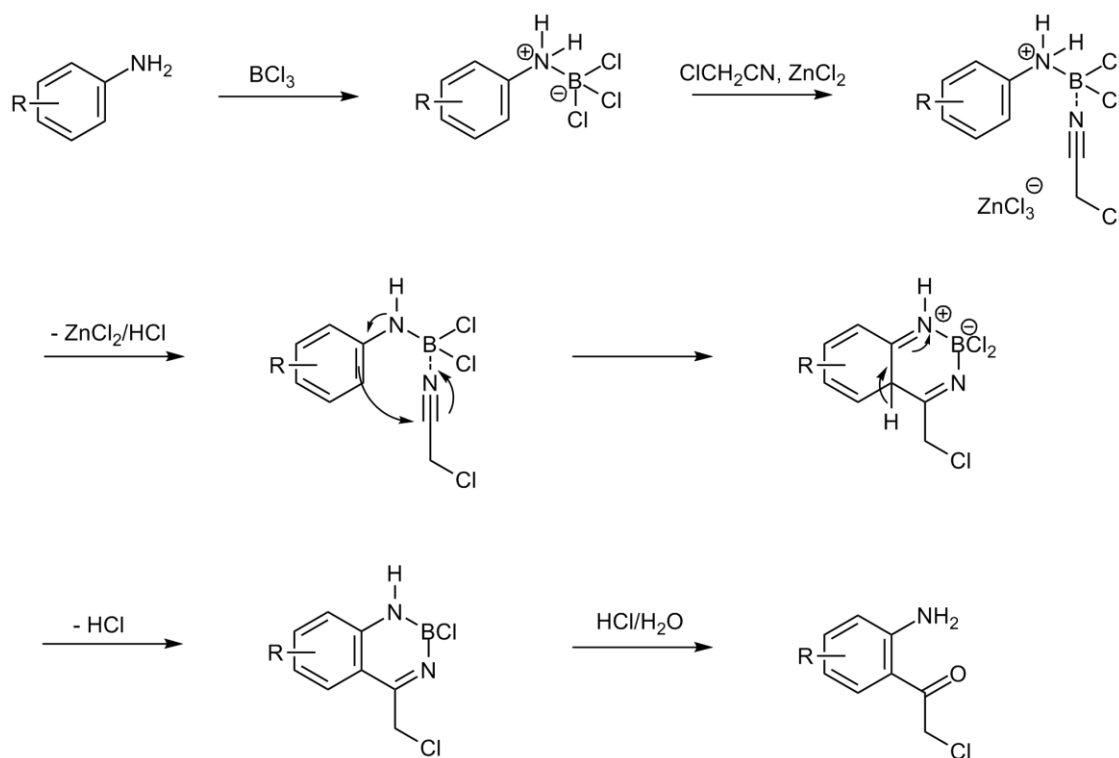


Scheme 6.3. Reagents and conditions: (a) BCl_3 1M in DCM, chloroacetonitrile, ZnCl_2 , dry 1,2-DCE, reflux. (b) HCl 1M, reflux. (c) AcOH , Ac_2O . (c) NaH , dry DMF.

Specifically, the appropriate aniline is reacted with chloroacetonitrile in the presence of BCl_3 and ZnCl_2 . This first reaction is a simple Friedel-Crafts acylation nevertheless, the addition of BCl_3 allows to obtain an exclusive ortho substitution of anilines. This specific reaction is known by Sugawara reaction³⁴³⁻³⁴⁴ and the mechanism is depicted in Scheme 6.4. The first step implies the interaction between the aniline and BCl_3 which is essential for the selective ortho acylation since BCl_3 allows the formation of the intermediate anilinochloroborane species. In this way, after addition of chloroacetonitrile, the nitrogen of the nitrile group will interact with the boron forming a stable complex. The following step consists of the nucleophilic attack to the electrodeficient carbon (in nitrile group) and subsequent electronic rearrangement. The

hydrolysis in acidic media of the anilinochloroborane intermediate allowed to obtain the desired compound (**6.22**). This first step of the reaction allows to obtain the final compound in moderate yields ranging from 40 to 70%, depending on the type of substitution in aniline ring.

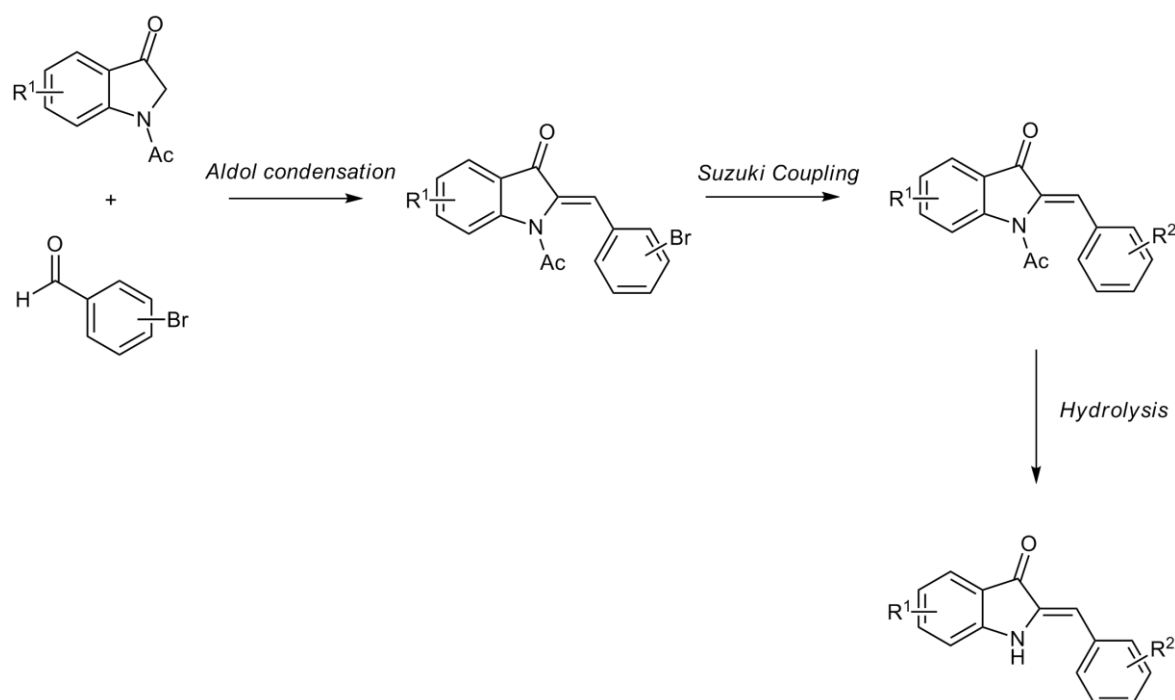
In the second step of the reaction compound **6.22** is acylated in order to form the corresponding acetanilide **6.23** in good yields. The main goal with this procedure is to obtain a more acidic proton that can be more easily removed. The last step consists in a straightforward intramolecular nucleophilic substitution assisted by NaH as a base allowing to obtain the cyclic starting material **6.24** in low yields. The cyclization step was first tried with Na_2CO_3 in dry acetone but the yields obtained were even lower.



Scheme 6.4. Sugasawa reaction mechanism.

In order to obtain the library of azaaurone derivatives, the initial approach involved the aldol condensation between the 3-indolinone starting material and the

bromobenzaldehyde in the presence of a base as catalyst (Scheme 6.5). The product of this reaction could then be used in the subsequent Suzuki coupling in order to expand the chemical diversity of this scaffold. In the last step, the hydrolysis of the acetyl group in basic media would generate the final compound.



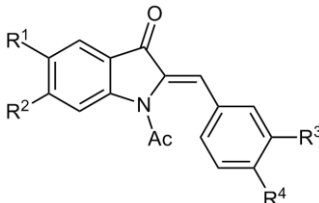
Scheme 6.5. Proposed reaction procedure for the synthesis of the azaaurone derivatives.

A library including 62 azaaurone derivatives were synthesized by varying the substituents in ring A and B (Table 6.2 and Table 6.4). The acetylated derivatives were also considered in this study in order to evaluate the influence of the free amine moiety in the antimalarial activity.

Compounds in series A (**6.25-6.27**), series B (**6.28-6.31**) and series E (**6.52-6.55**) were obtained by reaction of the synthesized 3-indolinone ring with the appropriate aldehyde. Only aldehydes required for obtaining compounds **6.28** to **6.30** were previously synthesized from the substituted phenol and fluorobenzonitrile as described in Chapter 5. All other aldehydes were obtained from commercial suppliers. Furthermore, compounds

6.52 to **6.55** were obtained by reacting the substituted 3-indolinone ring with benzaldehyde. The substituted 3-indolinone starting materials were also previously synthesized, as described in Scheme 6.3, from the appropriate and commercially available aniline.

Table 6.2. Structure, cLogP values, Lipinski rule of 5 violations, and yields for the synthesis (final step) of acetylated azaaurones **6.25**–**6.55**.



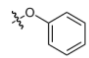
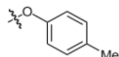
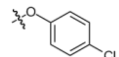
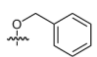
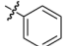
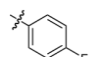
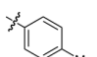
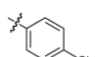
		R₁	R₂	R₃	R₄	cLogP²⁶³	Rule of 5 violations	Yield/%
Series A	6.25	H	H	H	H	2.98	0	72
	6.26	H	H	H	Br	3.67	0	64
	6.27	H	H	H	N(Me) ₂	3.10	0	70
Series B	6.28	H	H	H		4.42	0	57
	6.29	H	H	H		4.78	0	53
	6.30	H	H	H		4.99	0	61
	6.31	H	H	H		4.38	0	57
Series C	6.32	H	H	H		4.57	0	94
	6.33	H	H	H		4.74	0	80
	6.34	H	H	H		4.94	0	65
	6.35	H	H	H		5.16	1	75

Table 6.2. Structure, clogP values, Lipinski rule of 5 violations, and yields for the synthesis (final step) of acetylated azaaurones **6.25-6.55** (cont).

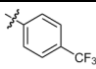
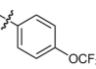
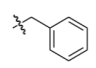
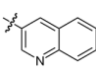
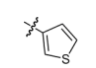
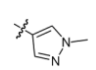
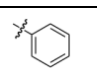
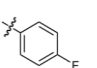
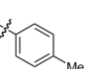
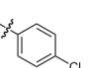
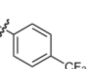
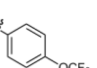
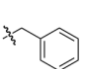
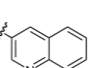
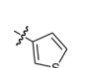
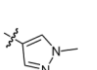
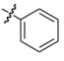
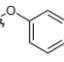
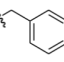
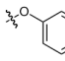
	R ₁	R ₂	R ₃	R ₄	cLogP ²⁶³	Rule of 5 violations	Yield/%	
Series C	6.36	H	H	H		5.34	1	78
	6.37	H	H	H		5.50	1	71
	6.38	H	H	H		4.78	0	73
	6.39	H	H	H		4.67	0	69
	6.40	H	H	H		4.28	0	72
	6.41	H	H	H		3.04	0	77
Series D	6.42	H	H		H	4.56	0	65
	6.43	H	H		H	4.74	0	69
	6.44	H	H		H	4.93	0	62
	6.45	H	H		H	5.16	1	66
	6.46	H	H		H	5.33	1	75
	6.47	H	H		H	5.50	1	72
	6.48	H	H		H	4.77	0	73
	6.49	H	H		H	4.67	0	62
	6.50	H	H		H	4.28	0	69
	6.51	H	H		H	3.04	0	68

Table 6.2. Structure, $cLogP$ values, Lipinski rule of 5 violations, and yields for the synthesis (final step) of acetylated azaaurones **6.25-6.55** (cont).

	R₁	R₂	R₃	R₄	cLogP²⁶³	Rule of 5 violations	Yield/%	
Series E	6.52		H	H	H	4.58	0	67
	6.53		H	H	H	4.45	0	62
	6.54		H	H	H	4.80	0	65
	6.55	H		H	H	4.45	0	61

In order to successfully obtain the azaaurone derivatives via aldol condensation, several attempts were made since this reaction did not pursue easily as in the case of aurone derivatives (Table 6.3).

Table 6.3. Reactions conditions for aldol condensation to obtain azaaurone derivatives.

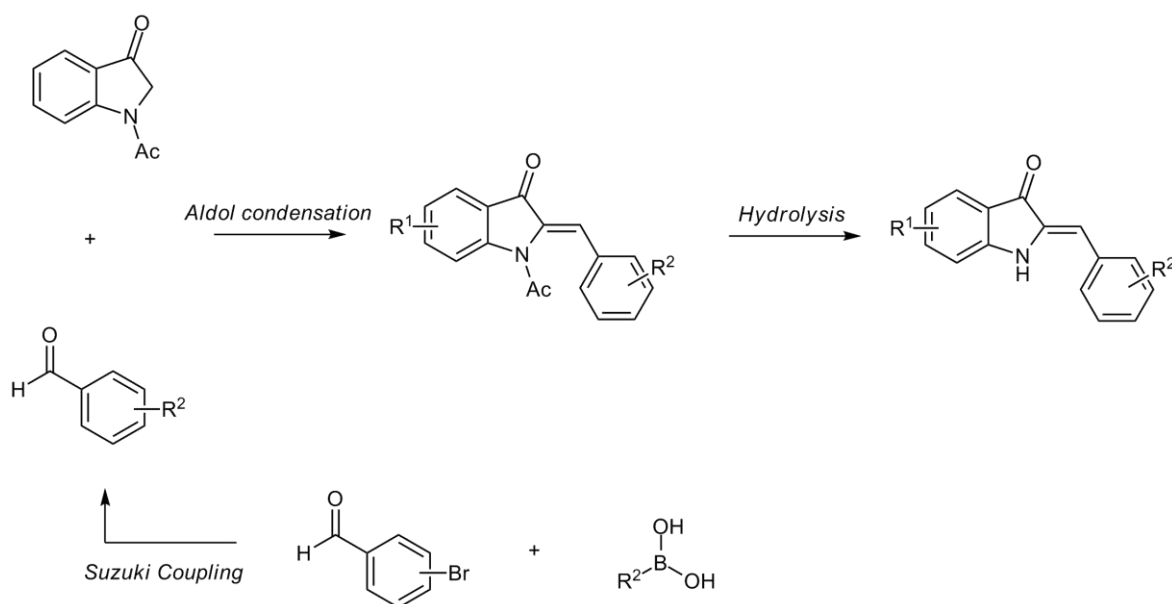
	Reaction Conditions	Observations
A	Al ₂ O ₃ , dry MeOH, reflux	No product formed.
B	KOH (50% in H ₂ O), MeOH, reflux	No product formed
C	NaH, dry DMF, RT	Product formed in low yields.
D	piperidine (cat), toluene, reflux under Dean-Stark conditions	Product formed in low yields.
E	piperidine (cat), toluene, reflux	Product formed in moderate yields.

In the first attempt (conditions **A**), the same reaction procedure used to obtain aurone derivatives were applied, although, in this case, no product was obtain. Afterward, the conditions followed by Souard *et al*²⁹⁸ (conditions **B**) using KOH as base also did not allow to obtain the desired product. The first azaaurone derivative was only obtained when NaH, a very strong base, was used (conditions **C**). This reaction conditions

permitted to synthesize the product only in low yields probably due to the complexity of the reaction mixture and to the consequent issues related with its purification. The reaction conditions described by Buzas *et al*³⁴⁵ (conditions **D**) allowed also to obtain the azaaurone but, as in the previous case, the yields were low and the reaction was not complete. All efforts made to enhance the reaction yield led to the increase of side products and also to the degradation of the final compound. More recently, Leung *et al*⁷⁵ performed this reaction using the conditions described by Buzas but in the absence of the Dean-Stark apparatus (conditions **E**). This last reaction condition allowed to obtain the desired compounds in moderate yields and, as a result, this was the one chosen to pursue with the synthesis of azaaurone derivatives.

In this way, compound **6.26**, containing a bromine substituent in position 4' was chosen as a platform for increasing the structural complexity of these compounds via the Suzuki coupling reaction (Scheme 6.5). The procedure applied for the synthesis of these compounds was the one already employed for obtaining aurones derivatives. Accordingly, compound **6.26** was reacted with a boronic acid in the presence of Pd(PPh₃)₂Cl₂ as catalyst and Na₂CO₃ 1M in dioxane, as described by Liu *et al*³¹³. Although the reaction was complete, the complexity of the reaction mixture prevented the isolation of the final product in acceptable yields. Moreover, the presence of a basic aqueous solution in the reaction mixture also contributed to increase the number of side products due to its ability to remove the acetyl group of the amine moiety.

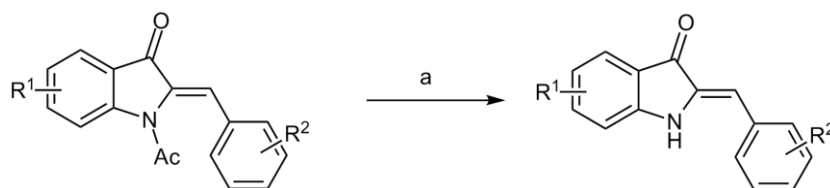
Since in the majority of the reactions performed, namely, the cyclization step, the aldol condensation and the Suzuki coupling, displayed low yields, the approach employed to obtain the final compounds was inevitably modified. As a consequence, a convergent approach (Scheme 6.6) was chosen in detriment of the linear synthesis described in Scheme 6.5.



Scheme 6.6. Alternative reaction procedure for the synthesis of the azaaurone derivatives.

Accordingly, all aldehydes were first synthesized starting from both 3- and 4-bromobenzaldehyde and the appropriate boronic acids in the presence of Pd(PPh₃)₂Cl₂ as catalyst. These compounds were obtained in very high to quantitative yields. Subsequently, compounds in series C and D (**6.32-6.51**) were obtained after reaction of the 3-indolinone with the resulting aldehydes, as depicted in Scheme 6.6, in moderate yields.

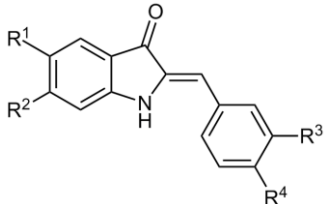
In order to obtain the deacetylated azaaurone derivatives, compounds in series A to E were treated with an aqueous solution of KOH in order to remove the acetyl group of the amine moiety (Scheme 6.7).



Scheme 6.7. Reagents and conditions: KOH (50% in H₂O), MeOH, RT.

Although this deprotection step was expected to occur smoothly, again, some purification related issues were responsible for decreasing the predictable yields of this reaction (Table 6.4).

Table 6.4. Structure, $c\log P$ values, Lipinski rule of 5 violations, and yields for the synthesis (final step) of azaaurones **6.56-6.86**.



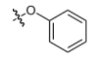
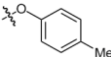
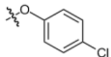
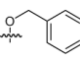
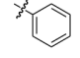
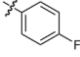
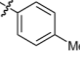
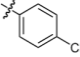
		R ₁	R ₂	R ₃	R ₄	$c\log P^{263}$	Rule of 5 violations	Yield/%
Series F	6.56	H	H	H	H	3.41	0	90
	6.57	H	H	H	Br	4.14	0	91
	6.58	H	H	H	N(Me) ₂	3.48	0	87
Series G	6.59	H	H	H		4.87	0	93
	6.60	H	H	H		5.24	1	92
	6.61	H	H	H		5.47	1	89
	6.62	H	H	H		4.82	0	89
Series H	6.63	H	H	H		4.98	0	94
	6.64	H	H	H		5.14	1	91
	6.65	H	H	H		5.35	1	92
	6.66	H	H	H		5.60	1	87

Table 6.4. Structure, *clogP* values, Lipinski rule of 5 violations, and yields for the synthesis (final step) of azaaurones **6.56-6.86** (cont.).

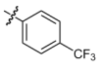
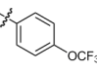
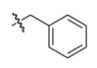
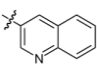
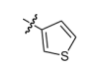
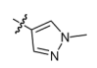
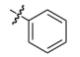
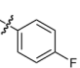
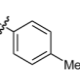
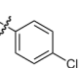
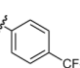
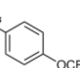
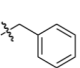
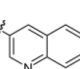
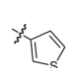
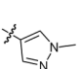
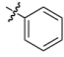
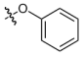
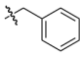
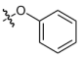
	R₁	R₂	R₃	R₄	cLogP²⁶³	Rule of 5 violations	Yield/%	
Series H	6.67	H	H	H		5.84	1	90
	6.68	H	H	H		5.98	1	92
	6.69	H	H	H		5.18	1	91
	6.70	H	H	H		5.14	1	97
	6.71	H	H	H		4.71	0	93
	6.72	H	H	H		3.43	0	92
Series I	6.73	H	H		H	4.98	0	93
	6.74	H	H		H	5.14	1	95
	6.75	H	H		H	5.34	1	94
	6.76	H	H		H	5.60	1	90
	6.77	H	H		H	5.83	1	91
	6.78	H	H		H	5.97	1	92
	6.79	H	H		H	5.18	1	96
	6.80	H	H		H	5.13	1	94
	6.81	H	H		H	4.71	0	93
	6.82	H	H		H	3.42	0	94

Table 6.4. Structure, clogP values, Lipinski rule of 5 violations, and yields for the synthesis (final step) of azaaurones **6.56-6.86** (cont.).

	R ₁	R ₂	R ₃	R ₄	cLogP ²⁶³	Rule of 5 violations	Yield/%	
Series J	6.83		H	H	H	4.97	0	91
	6.84		H	H	H	4.87	0	91
	6.85		H	H	H	5.18	1	92
	6.86	H		H	H	4.87	0	89

As in the case of aurone derivatives, some observations can be done concerning the stereochemistry of the exocyclic double bond. In this case, contrasting with the aurone derivatives synthesized, the ¹H and ¹³C NMR confirmed that all acetylated azaaurones (series A to E) were obtained as a mixture of both isomers *E* and *Z*. Interestingly, it was also possible to conclude that the ratio between the two isomers could vary in solution which suggests that the two isomers can suffer interconversion.

Buzas et al previously described the mixture of two isomers for acetylated azaaurones³⁴⁵. Moreover, the possibility of obtaining pure isomers depending on the electronic nature of the substituents and their position in the ring B was also demonstrated.

Examples of the ¹H NMR of both compounds **6.27** and **6.58** are illustrated in Figure 6.1 and Figure 6.2, respectively.

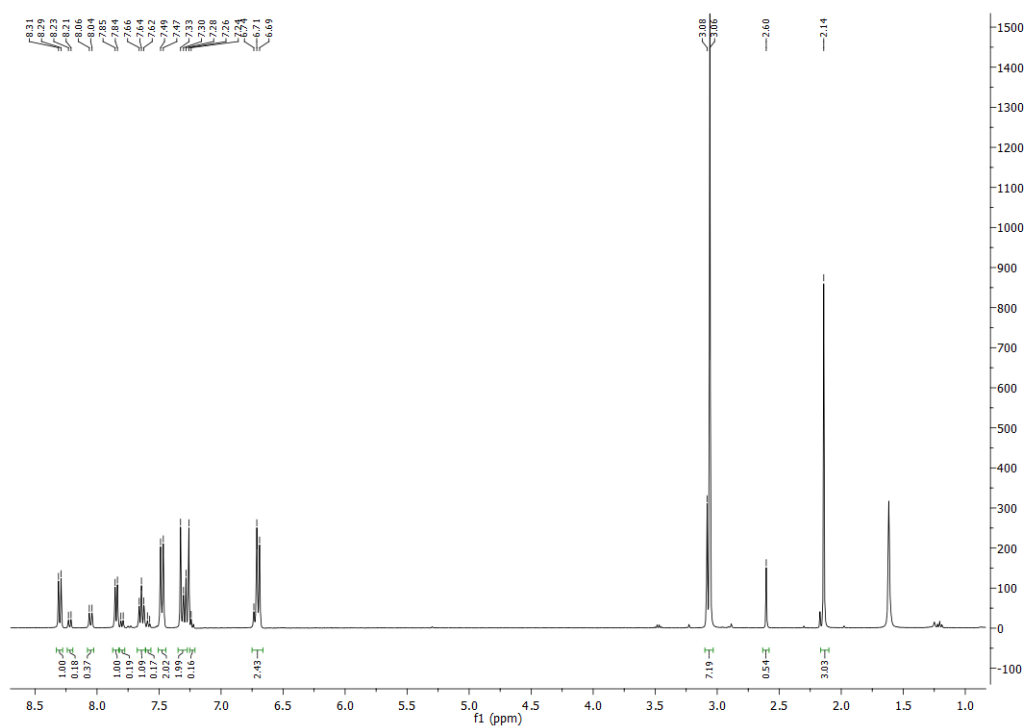


Figure 6.1. ^1H NMR of compound 6.27.

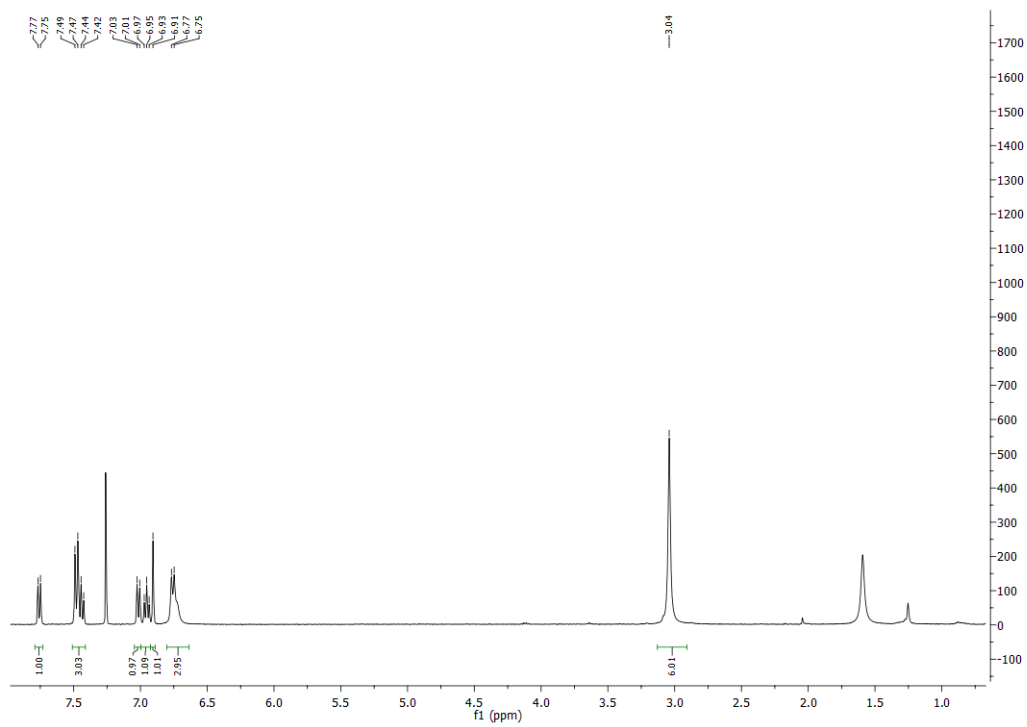


Figure 6.2. ^1H NMR of compound 6.58.

The observation of Figure 6.1 allowed to conclude that all peaks are present in duplicate which is in accordance with some experimental evidences showing that azaaurones can be obtained as a mixture of two isomers³⁴⁵. Moreover, it is important to notice that, for this specific compound, the more abundant specie presents the vinylic proton with a chemical shift of 7.33 ppm while the less abundant appears at lower frequency ($\delta \sim 6.7$ ppm). Considering the low number of examples available in literature, it is difficult to confirm undoubtedly which isomer is more abundant. Nevertheless, taking into consideration the studies performed with aurones, it is expected that *Z* isomer is predominant since this is usually regarded as the thermodynamically more stable form³¹⁴.

However, after deacetylation, all final compounds (series F to J) were obtained as a single isomer. In the specific case of compound **6.58**, the vinylic proton appears at $\delta = 6.91$ ppm which is consistent with the chemical shift values obtained by Souard *et al*²⁹⁸ for *Z*-azaaurones (Figure 6.2). Nevertheless, this NMR data indicating that a mixture of two isomers could result in only one isomer raised the question if the two species formed during the aldol condensation could probably be different rotamers, due to the rotation of the acetyl group, and not isomers *E* and *Z*. In this way, in order to confirm this possibility, some experiences were made with ¹H NMR at different temperatures. The main goal was to verify if the increase of the solution temperature would contribute to merge the two sets of peaks. In this way, if the two peaks fused by increasing the temperature, it was possible to assure that the two species in solution were rotamers and not isomers. In Figure 6.3 is depicted the superposition of ¹H NMR spectra of compound **6.30** at different temperatures. It is possible to observe that when temperature increases, some aromatic peaks change slightly their positions but this alteration is not significative. Furthermore, the two peaks corresponding to the CH₃ of the acetyl group (of the more and less abundant species) almost no suffer alterations keeping their chemical shifts constant while the temperature increases. In this way, it is possible to conclude that the two species are isomers and not rotamers.

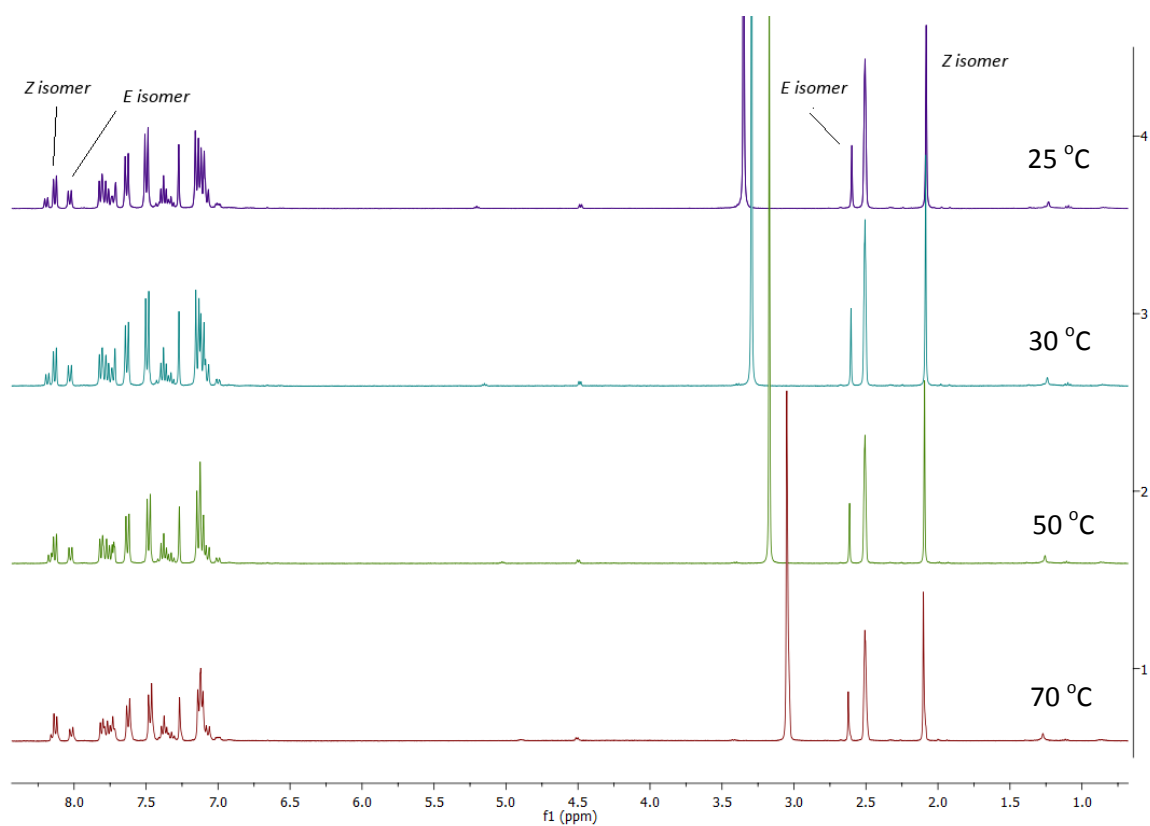


Figure 6.3. Superposition of the ¹H NMR spectra of compound **6.30** at 25 °C (in purple), 30 °C (in blue), 50 °C (in green) and 70 °C (in red).

Concerning the stereochemistry of the exocyclic double bond of azaaurones in series F to J, the crystallographic structure of compound **6.64** allowed to undoubtedly confirm that these compounds are obtained as *Z* isomers as anticipated (Figure 6.4).

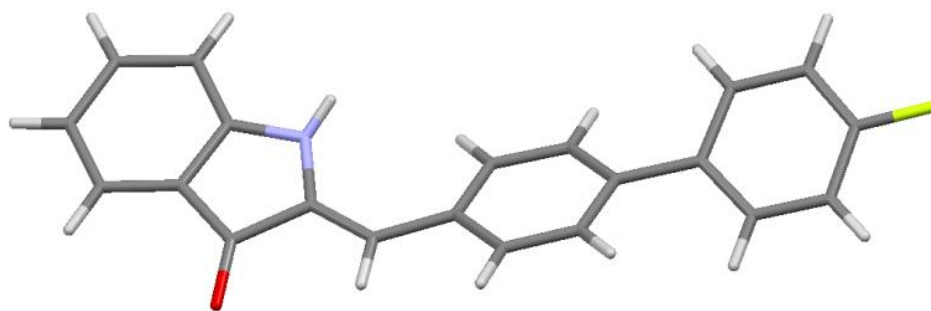


Figure 6.4. X-ray crystallographic structure of compound **6.64**.

In order to introduce additional chemical diversity to this class of compounds and also to evaluate the importance of the double bond for the antimalarial activity, several attempts were made to reduce the double bond of the azaaurone scaffold (Scheme 6.8). The main goal of this procedure was to obtain the reduced product before the deprotection of the amine moiety.



Scheme 6.8. Proposed reaction procedure for the reduction of azaaurone derivatives.

The reaction conditions applied to obtain the reduced azaaurone derivatives are indicated in Table 6.5. In a first attempt, the azaaurone derivative was reacted with TES as the hydrogen source in the presence of Pd/C in EtOH (conditions **A**). Although some starting material was consumed during this reaction, the desired product was not identified. Further attempts were made using TES and TFA, both as reagent (conditions **B**) and as solvent (conditions **C**)³⁴⁶⁻³⁴⁷. Only when conditions **C** were used the starting material was completely consumed, nevertheless the product formed was not identified.

Table 6.5. Reactions conditions for the reduction of azaaurone derivatives.

	Reaction Conditions	Observations
A	TES, Pd/C, EtOH, RT	No product formed.
B	TFA, TES, DCM, reflux	No product formed
C	TES, TFA (solvent), RT	Starting material consumed but no product formed.
D	H ₂ , Pd/C, MeOH, RT	No product formed.

Concerning conditions **D**³⁴⁵, the amount of H₂ was increased from atmospheric pressure to 4 atm in order to improve the efficiency of this reaction but, once again, the desired product was not obtained. In this way, and considering all the unsuccessful attempts, the synthesis of the reduced azaaurone derivatives was abandoned.

6.3. Biological Evaluation

6.3.1. Activity against *P. falciparum* W2 strain

All compounds were assayed for their antiplasmodial activity against the CQ-resistant *P. falciparum* W2 strain. The biological results obtained for all series of azaaurones derivatives are presented in Table 6.6 and Table 6.7. Further, the most promising azaaurones derivatives were also tested against Human Embryonic Kidney 293T cells presenting small cytotoxicity, with EC₅₀ values against cultured human cells ranging from 7 to ≥ 100 μM. In most cases, the compounds presented selectivity indices (SI = EC₅₀(HEK293T)/IC₅₀(W2)) higher than 10, showing that these compounds can be considered selective and nontoxic antiplasmodial agents. However, the selected acetylated azaaurone derivatives (compounds **6.33**, **6.34**, **6.37**, **6.39**, **6.44**, **6.49**, and **6.52**) showed significant cytotoxicity. Concerning the bioavailability, Lipinski rule³¹⁷ was applied to the synthesized compounds and showed that the majority of azaaurone derivatives passed the Lipinski filter with some compounds presenting only one violation, more exactly, the lipophilicity (Table 6.2 and Table 6.4).

The first analysis of Table 6.6 and Table 6.7 shows that all azaaurone derivatives lacking the acetyl group (compounds **6.56** to **6.86**) display extremely increased antimalarial activity when compared to the same acetylated derivatives. Moreover, it is also possible to verify that the antimalarial potential of acetylated azaaurones (compounds **6.25** to **6.55**) is in the same range of the aurone derivatives presented in Chapter 5. Generally, acetylated azaaurone derivatives displayed IC_{50} values ranging between 2.0 and 9.8 μ M while azaaurone derivatives with free amine exhibited antimalarial activity in nanomolar range. Moreover, some compounds present an increase of 50 fold in antimalarial activity when the acetyl group of the azaaurone is removed (for instance compounds **6.46** and **6.77**). In this way, these results indicate that NH group in the azaaurone scaffold is essential for the antimalarial activity, being probably essential to establish a strong interaction with a H-bond acceptor in the target.

Table 6.6. Antiplasmodial activity (IC₅₀) against the CQ-resistant *Plasmodium falciparum* W2 strain, cytotoxicity (EC₅₀) against Human Embryonic Kidney 293T cells and selectivity index (SI = EC₅₀/IC₅₀) for azaaurones **6.25-6.55** (Series A-E).

Compound	IC ₅₀ / μM	EC ₅₀ / μM	SI	Compound	IC ₅₀ / μM	EC ₅₀ / μM	SI	Compound	IC ₅₀ / μM	EC ₅₀ / μM	SI
6.25	A.R.	N.D.	N.D.	6.36	5.06	N.D.	N.D.	6.47	5.08	N.D.	N.D.
6.26	5.99	N.D.	N.D.	6.37	3.21	8	2	6.48	> 10	N.D.	N.D.
6.27	> 10	N.D.	N.D.	6.38	> 10	N.D.	N.D.	6.49	3.92	14	4
6.28	5.02	N.D.	N.D.	6.39	2.03	19	9	6.50	8.74	N.D.	N.D.
6.29	5.13	N.D.	N.D.	6.40	9.83	N.D.	N.D.	6.51	> 10	N.D.	N.D.
6.30	A.R.	N.D.	N.D.	6.41	9.43	N.D.	N.D.	6.52	3.75	12	3
6.31	A.R.	N.D.	N.D.	6.42	9.78	N.D.	N.D.	6.53	> 10	N.D.	N.D.
6.32	8.42	N.D.	N.D.	6.43	9.38	N.D.	N.D.	6.54	6.77	N.D.	N.D.
6.33	4.59	7	2	6.44	3.65	16	4	6.55	A.R.	N.D.	N.D.
6.34	3.78	9	2	6.45	> 10	N.D.	N.D.	CQ	0.14	N.D.	N.D.
6.35	5.64	N.D.	N.D.	6.46	6.12	N.D.	N.D.				

A.R. – awaiting results; N.D. – not determined

Table 6.7. Antiplasmodial activity (IC₅₀) against the CQ-resistant *Plasmodium falciparum* W2 strain, cytotoxicity (EC₅₀) against Human Embryonic Kidney 293T cells and selectivity index (SI = EC₅₀/IC₅₀) for azaaurones **6.56-6.86** (Series F-J).

Compound	IC ₅₀ / μM	EC ₅₀ / μM	SI	Compound	IC ₅₀ / μM	EC ₅₀ / μM	SI	Compound	IC ₅₀ / μM	EC ₅₀ / μM	SI
6.56	A.R.	> 100	A.R.	6.67	A.R.	> 100	A.R.	6.78	A.R.	> 100	A.R.
6.57	0.56	> 100	> 10	6.68	0.86	> 100	> 10	6.79	A.R.	> 100	A.R.
6.58	2.90	> 100	> 10	6.69	0.52	> 100	> 10	6.80	0.26	> 100	> 10
6.59	0.36	> 100	> 10	6.70	0.44	22	> 10	6.81	0.47	> 100	> 10
6.60	0.32	> 100	> 10	6.71	0.48	> 100	> 10	6.82	A.R.	> 100	A.R.
6.61	A.R.	> 100	A.R.	6.72	1.35	> 100	> 10	6.83	A.R.	> 100	A.R.
6.62	A.R.	> 100	A.R.	6.73	0.45	> 100	> 10	6.84	A.R.	> 100	A.R.
6.63	0.31	> 100	> 10	6.74	0.26	> 100	> 10	6.85	A.R.	> 100	A.R.
6.64	0.27	> 100	> 10	6.75	0.20	> 100	> 10	6.86	A.R.	> 100	A.R.
6.65	0.83	> 100	> 10	6.76	0.20	20	> 10	CQ	0.14	> 100	N.D.
6.66	0.53	> 100	> 10	6.77	0.11	> 100	> 10				

A.R. – awaiting results; N.D. – not determined

The examination of Table 6.7 allows to conclude that, in general, the introduction of an additional aromatic moiety to azaaurone scaffold permitted to increase the antimalarial activity when compared to compound **6.57** possessing only a bromine substituent in *para* position. Moreover, compound **6.58** display antimalarial activity in the micromolar range which suggests that the dimethylamino substituent is not favorable for this class of compounds.

Concerning compounds in series G (compounds **6.59-6.62**) only compounds **6.59** and **6.60** were so far tested for their antimalarial activity with both compounds presenting similar biological activity.

In series H (compounds **6.63-6.72**), the azaaurone derivatives present a large range of IC₅₀ values with compounds **6.64** and **6.72** presenting antimalarial activity at 0.27 and 1.35 μ M, respectively. When considering the introduction of a second aromatic moiety in the position 4' of azaaurone scaffold, the fluorine substituent allowed to increase the antimalarial activity while the chlorine, the methyl and the trifluoromethoxy lead to a drop of the potency of these compounds. This effect in the antimalarial activity is more evident for compound **6.65** and **6.68** showing an increase of the IC₅₀ values around 3 fold when comparing with the non substituted derivative **6.63**. In addition, compound **6.69**, containing a benzyl substituent, shows to be less active than its analogous **6.59** having an oxygen atom connecting the two aromatic moieties rather than the isoster group CH₂. Moreover, the introduction of a heterocyclic substituent in the position 4' of the azaaurone scaffold also allowed to obtain potent inhibitors with IC₅₀ values around 400 nM. However, when introducing the pyrazole substituent (compound **6.72**), the antimalarial activity drops to values in the micromolar range.

When considering compounds in series I (compounds **6.73-6.82**), with exception of compound **6.73**, all compounds presented comparable or higher inhibitory activity than their analogous in series H. More precisely, the comparison between the results obtained for compounds **6.65** and **6.75**, both containing a methylphenyl substituent, and for compounds **6.66** and **6.76**, bearing a chlorophenyl substituent, allow to conclude that the introduction of these aromatic substituents in position 3' of azaaurone scaffold increase the inhibitory activity by 4 and 2.5 fold, respectively. Moreover, the azaaurone derivative

containing the quinoliny substituent in position 3' (compound **6.80**) also increased the inhibitory potential when comparing with compound **6.70** while the two compounds having the tiophenyl substituents (compounds **6.71** and **6.81**) showed identical biological activity. Furthermore, it is also worth notice that the introduction of substituents containing fluorine atoms is desirable for the antimalarial activity of this class of compounds as highlighted by the contrasting IC_{50} values obtained for compounds **6.63** and **6.64** and also for compounds **6.73**, **6.74**, **6.75** and **6.77**. Additionally, compound **6.77** demonstrated to be the most potent compound with an IC_{50} value of 110 nM.

Unfortunately, the biological results for compounds in series J are still not available and therefore, the relevance of the substituents in ring A of azaaurone scaffold can not be discussed.

Overall, putting together all the biological data of both acetylated and non acetylated azaaurone derivatives, it is not possible to establish a correlation between the IC_{50} values obtained for these two set of compounds. More specifically, the IC_{50} values do not vary in the same way taking into account the substituent introduced. For instance, compound **6.34** shows an IC_{50} value of 3.78 μ M while its non acetylated counterpart (compound **6.70**) presents inhibitory activity at 0.83 μ M. In the other hand, the acetylated derivative **6.46** displays an IC_{50} of 6.12 μ M while its analogous **6.77** exhibit much more inhibitory potential with an IC_{50} value of 0.11 μ M.

6.3.2. Activity against falcipain-2

As in the case of aurone derivatives described in Chapter 5, this family of compounds also encloses a Michael acceptor and, therefore, these compounds may exert their antimalarial activity by inhibiting the falcipain family of enzymes.

In this way, azaaurones in series A-J were then screened for inhibition of cysteine protease from *P. falciparum*, falcipain-2, which is of particular interest as therapeutic target due to its role in parasite development⁴⁴. Falcipain-2 is localized in the parasite's DV and plays a key role in the hydrolysis of host hemoglobin into amino acids essential to

parasite growth³²⁸. Falcipain inhibitors that contain a Michael acceptor warhead³³¹ have been reported to block the development of cultured erythrocytic parasites and to cure mice having lethal malaria infections³⁴⁸. Although azaaurones are Michael acceptors, these compounds showed no inhibition of falcipain-2 in concentrations up to 50 μM . Only three azaaurone derivatives (compounds **6.27**, **6.57** and **6.58**) showed to be weak falcipain-2 inhibitors with IC_{50} values ranging from 10.6 to 19 μM . The observation that falcipain-2 is inhibited only in the high μM range, suggests that azaaurone scaffold is not suitable for enzyme binding.

6.3.3. *In vitro* drug combination assay

Having in mind the studies already performed showing the potential of aurone derivatives to inhibit transporters involved in the mechanism of MDR³⁰¹⁻³⁰⁵ and, therefore, to modulate CQ resistance, one of the most potent azaaurone derivatives (compound **6.60**) was selected to test the potential of this class of antimalarial drugs to exhibit a mechanism of synergism in the presence of CQ.

In order to perform the synergism studies, compound **6.60** was first tested against the mefloquine and CQ resistant and sensitive *P. falciparum* strain Dd2 and 3D7, respectively. The IC_{50} values obtained in this study are included in Table 6.8.

Table 6.8. Antiplasmodial activity (IC_{50}) against the CQ-resistant (W2), mefloquine (MEF) and CQ resistant (Dd2) and sensitive (3D7) *P. falciparum* strains.

Compound	IC_{50} / μM (W2)	IC_{50} / μM (Dd2)	IC_{50} / μM (3D7)
6.60	0.32	2.20	1.20
CQ	0.14	0.34	0.02
MEF	-	0.09	0.03

In this case, the synergistic potential of compound **6.60** was evaluated not only in the presence of CQ but also of mefloquine. Once again, the analysis of the combination

effects of compound **6.60** with both CQ and mefloquine was determined by a modified fixed ratio isobologram method³³⁷⁻³⁴⁰. Moreover, the isobologram analysis was based on the calculation of the sum of FICs (FICs = IC₅₀ of drug in the combination / IC₅₀ of drug when tested alone) or the combination index (CI)³⁴⁰. In this way, this value is able to give an indication of whether the interaction is antagonistic (CI ≥ 1.10), additive (0.90 ≤ CI < 1.10) or synergistic (CI < 0.9)³⁴¹.

The inspection of the isobologram in Figure 6.5 allow to conclude that a synergistic effect can be found between the selected compound and mefloquine both in 3D7 and Dd2 strains, with CI values of 0.77 and 0.88 respectively. On the other hand, only an additive effect can be established between compound **6.60** and CQ for both strains (CI values of 1.19 and 1.22 for 3D7 and Dd2 strains, respectively).

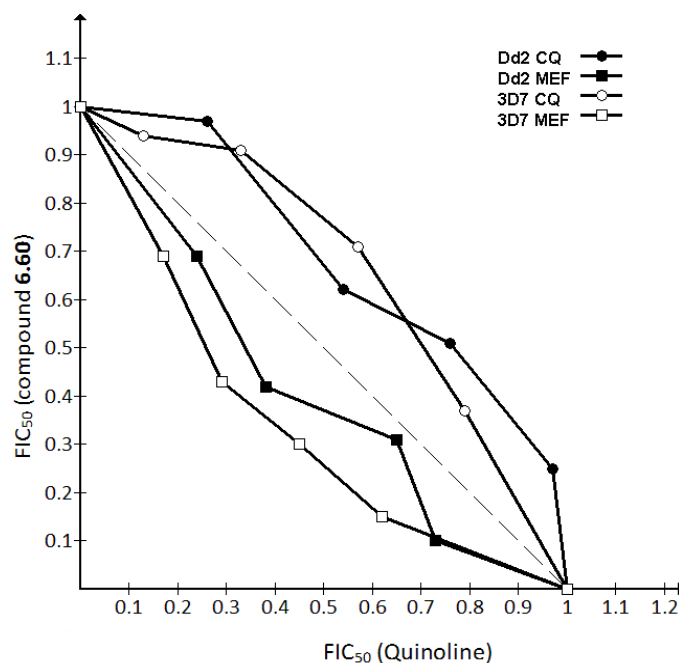


Figure 6.5. Isobologram showing the relationship between the FIC₅₀s of the quinolines CQ and mefloquine and compound **6.60** against *Plasmodium falciparum* Dd2 and 3D7 strains. Numbers on each plotted point correspond to the calculated CI value for the utilized combination ratio.

Although this compound shows to induce a synergistic effect in the presence of mefloquine for both tested strains, interestingly, the most promising result was obtained with the 3D7 sensitive strain which lacks the mutations related with drug resistance. In this way, it is possible to deduce that compound **6.60** may interact with *PfMDR1* transporter responsible for mefloquine resistance in the resistant strain³⁴⁹. In addition, the results obtained for 3D7 strain allow to presume that the azaaurone derivative may possible induce moderate synergistic effect in the presence of mefloquine by a different mechanism.

Considering the studies performed in the presence of CQ, the results demonstrated no synergistic effect.

6.4. Docking studies over *P. falciparum* bc₁ complex

Considering the potential of the azaaurone derivatives to act in the bc₁ complex, some docking studies were performed in the newly built *P. falciparum* Q_o binding pocket. In this way, all synthesized compounds were docked into the active site obtained by homology modeling using AD as docking tool and the same experimental parameters already employed in Chapters 2 and 4.

IFigure 6.6 depicts the predicted binding mode of selected azaaurone derivatives. The inspection of the binding pose of these compounds allows to conclude that these compounds, with exception of compound **6.66**, can strongly interact with His181 through the carbonyl group of azaaurone scaffold. Moreover, an additional hydrogen bond may be established between the Glu272 and the NH moiety in the presence of a water molecule. Also, as displayed in Figure 6-B, C and D, strong π - π interactions can also be found between the aromatic side chain of the azaaurone derivatives and Phe264.

Interestingly, the predicted binding pose of compound **6.66** (Figure 6-A), displaying lower inhibitory activity, shows that its arrangement inside the pocket does not allow the interaction between the carbonyl moiety and His181 as in compounds **6.60**, **6.75** and **6.77**.

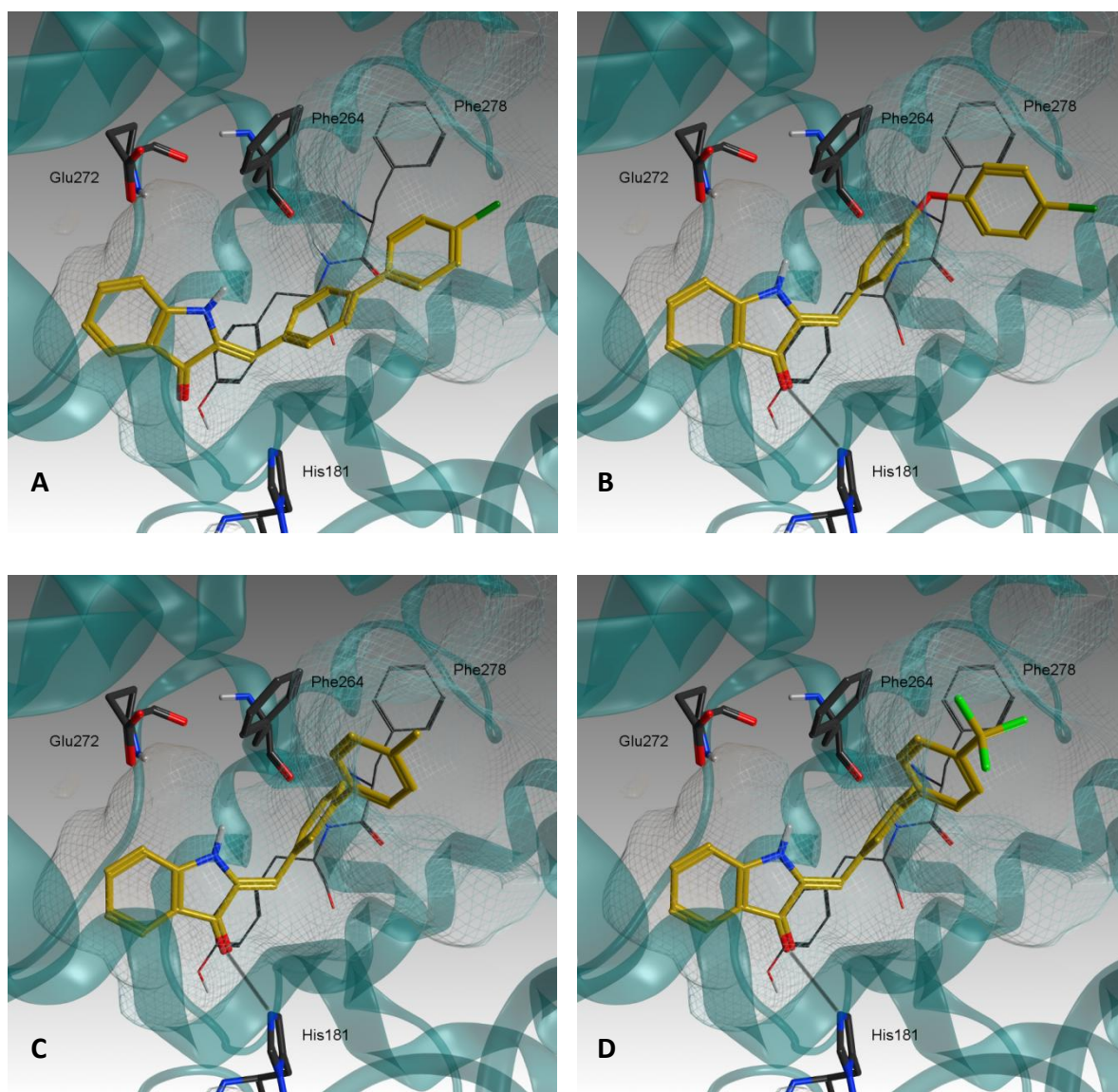
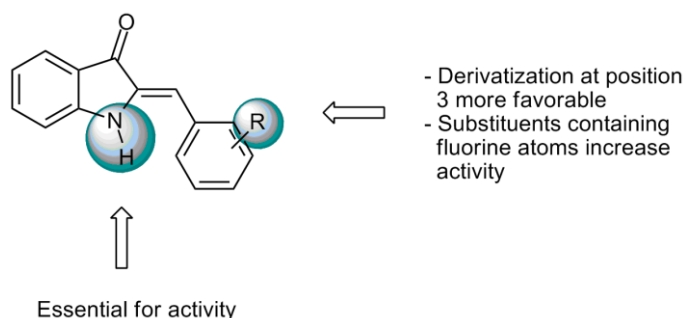


Figure 6.6. Predicted binding poses of compounds **6.66** (A), **6.60** (B), **6.75** (C), and **6.77** (D). Hydrogen bonds are represented by grey lines.

Additionally, the distance between the NH group of azaaurone scaffold is also longer for this compound when compared to the other selected azaaurone derivatives. In this way, the reduced favorable interactions between compound **6.66** and the Q_o binding pocket of bc_1 complex may be responsible for the decreased antimalarial activity of this compound. However, this docking study is merely suggestive of a potential antimalarial mode of action of this class of compounds and, therefore, additional biological studies are indispensable to undoubtedly identify the target of azaaurone derivatives.

6.5. Concluding remarks

A library of novel azaaurones containing a large structural diversity was synthesized and tested against the CQ-resistant *P. falciparum* W2 strain. Unlike aurones, this scaffold did not provide a platform to generate new antimalarial compounds using simple synthetic strategies due to several issues related with the synthetic strategies. However, azaaurones can be considered a valuable scaffold for developing new potential antimalarial drugs. In this way, the derivatization of this scaffold allowed to highly increase their antimalarial potential when compared with aurone derivatives. Moreover, compound **6.77** emerged as the more active compound with an IC_{50} value of 110 nM. Although not all synthesized compounds were already tested, some SAR elucidation can be made (Scheme 6.9).



Scheme 6.9. Structure-activity relationships for azaaurone derivatives.

In this way, it was possible to conclude that the free NH is essential for antimalarial activity and that the protection of this group with the acetyl group highly decreased the potency of this class of compounds. Moreover, better inhibitory activity was obtained when azaaurone scaffold were derivatized at position 3' of ring B. Furthermore, substituents containing fluorine also contributed to increase the antimalarial potential of these compounds.

Additional biological studies were performed to identify the mechanism of action of azaaurone derivatives. More specifically, all compounds were screened against

falcipain-2 due to the structural characteristics of this class but only low inhibitory activity was found for three inhibitors suggesting that this is not the primary mechanism of action of this class of compounds. Although the docking studies suggest that these compounds may establish strong interactions with Q_o binding site of bc₁ complex fitting quite well in the pocket, added biological studies need to be done to test for the inhibition of this target and, consequently, the mode of action of this class of compounds.

Lastly, synergistic studies revealed that this class of compounds may establish a synergistic effect with mefloquine when tested against both mefloquine and CQ resistant and sensitive *P. falciparum* strain Dd2 and 3D7.

CHAPTER SEVEN

7. Conclusions

The first part of this project focused essentially in understanding the mechanism of inhibition of bc_1 complex inhibitors acting on Q_o binding site. For that, an exhaustive study was pursued in order to evaluate the potential of the crystallographic structure of *S. cerevisiae* bc_1 complex to be used as a model for the *P. falciparum* homologous. Furthermore, a good prediction of the inhibitory activity of the inhibitors selected was obtained using the yeast coordinates and, accordingly, this model was accepted to explain the molecular basis of inhibition in the Q_o active site. Additionally, this model was considered a good predictive method to determine the inhibitory potential of promising new inhibitors acting in this target by considering the binding free energy values obtained through docking calculations.

Using the validated model, a virtual screening study over a drug-like database was performed allowing to identify five new compounds with moderate antimalarial activity. Further studies performed on the *Pf* cytochrome bc_1 complex and on the Dd2- γ DHODH transgenic cell line showed that the two best hits, compounds **5.17** and **5.19**, displayed no activity in the mETC. As a result, it was not possible to conclude that the inhibition of this target is the primary antimalarial mechanism of action of both compounds. On the other hand, compounds **5.19**, **5.20** and **5.24** proved to be reasonably active against the atovaquone-resistant *Pf* FCR3 strain and *S. cerevisiae*.

Considering the importance related with the reliability of the target's tridimensional structure, the structure of the Q_o binding site of *P. falciparum* bc_1 complex was further solved using homology modeling techniques based on the yeast crystallographic structure as template. Although this model allowed to improve the interactions between the compounds and the binding site, the potential of WR 249685 to selectively inhibit this target was not fully explained. In this way, a molecular dynamics study can be considered of extreme importance to obtain a more accurate and satisfactory tridimensional structure of this target. A second virtual screening study was also performed in order to provide a proof-of-concept on an experimental basis. In spite

of several interesting potential new inhibitors have been identified, all biological studies related with this new set of compounds have still to be performed in order to verify their inhibitory potential.

In the second part of this project, two libraries of compounds were also synthesized. The library comprising aurone derivatives was synthesized with the main goal of increasing the chemical space around this known scaffold and also to evaluate its potential to be considered a useful platform to apply simple synthetic strategies to generate novel bioactive compounds. In this way, the appropriate functionalization of this scaffold allowed to obtain diverse compounds with moderate antimalarial activity displaying IC_{50} values in the micromolar range. Unfortunately, although these compounds appear to accumulate in the DV of the parasite, their mechanism of action is still unclear and additional biological assays need to be done. Moreover, the presence of a Michael acceptor in this scaffold and the accumulation in the DV suggest that this class of compounds may interact with proteases present in this organelle.

The introduction of the amine moiety in the aurone scaffold allowed to increase extremely the antimalarial activity of these compounds. Moreover, it was possible to obtain compounds displaying IC_{50} values in the nanomolar range. Considering the structural similarity between 4(1*H*)-quinolones and azaaurones and the docking results obtained using the bc_1 complex structure obtained by homology modeling, this set of compounds may probably interact with this target. Nevertheless, the docking studies are only an indication of a possible mechanism of action and additional biological studies are essential. As performed for the compounds obtained by virtual screening, the best azaaurone derivatives should be tested against the mitochondrial bc_1 complex and also against the Dd2- γ DHODH transgenic cell line in order to assure their inhibitory mechanism.

Finally, the work developed during this project was fundamental not only to understand the mechanism of action of bc_1 complex inhibitors regarding the structural features of *P. falciparum* Q_0 binding site but also to identify potential new antimalarial scaffolds that can be effectively further optimized.

CHAPTER EIGHT

List of contents

8.1. Molecular docking over <i>S. cerevisiae</i> bc_1 complex	197
8.2. Virtual screening studies over <i>S. cerevisiae</i> bc_1 complex	198
8.3. Homology model of <i>P. falciparum</i> bc_1 complex Q_o binding site	199
8.4. Chemistry	200
8.5. Synthesis of quinolone derivatives	201
8.6. Synthesis of aurone derivatives	204
8.7. Synthesis of azaaurone derivatives	224
8.8. Biological Assays	266

8. Experimental Part

8.1. Molecular docking over *S. cerevisiae* bc_1 complex

8.1.1. Structure preparation

The yeast bc_1 crystallographic structures were obtained from the RCSB Protein Data Bank²⁴⁸ (PDB codes 1KYO and 3CX5). Bound inhibitors and other coordinated molecules were removed from the PDB file. All crystallized water molecules were also removed, except when a catalytic water molecule was used in the docking calculations. The protonation states of the residues were assigned using the Protonate 3D algorithm within the Molecular Operating Environment (MOE) program²⁶². Only the polar hydrogens were kept, and the correct protonation state of His181 was assigned for each docking experiment. The 3D molecular structures of the docked molecules were built and parameterized, and energy was minimized within MOE using the MMFF94x force field. In the case of floxacrine, which was experimentally assayed as a racemic mixture, separate files for each enantiomer were prepared.

8.1.2. Docking of the inhibitors

AD 4.0 was chosen for the docking calculations within the DOVIS 2.0 package²⁵⁹. The grid box was set with 40 points in the x and y and 44 in the z direction. The default value of 0.375 Å for spacing between grid points was used, leading to a box size of 15 Å in x and y and 16.5 Å in z, allowing the crystallographic pose of stigmatellin to be in the middle of the box. The Lamarckian genetic algorithm conformational search with a population size of 150, 250000 energy evaluations and a maximum of 27000 generations per run, was used. 200 docking runs were applied in all calculations. The docking results were ranked using the AD 4.0 scoring function, and Pymol³⁵⁰ was used for visual inspection of the docking results.

8.2. Virtual screening studies over *S. cerevisiae* bc₁ complex

8.2.1. Structure preparation and docking

The PDB structure 3CX5 was prepared as described in section 8.5.1. keeping His181 neutral. A druglike database included in the MOE 2009.10²⁶² package was used for this virtual screening study. The PDBQT input files for receptor and ligands were prepared using the available tools included in the AD package. All structures were docked and scored using AD Vina 1.0.2²¹⁹. This software was used as the initial screening tool, with the center of the docking box defined as above (box dimensions: x=y=15 Å, z=16.5 Å) and keeping the other parameters as default.

The top-ranked ligands given by AD Vina were redocked with AD 4.0 (using DOVIS 2.0 parallel implementation) and scored with the AD4.0 scoring function. All parameters were the same as described in section 8.5.2., leading to the same box size as described for AD Vina. The interactions of the ligands with the Q_o binding pocket were evaluated using the results of this AD screening.

8.2.2. Tested compounds

Compounds were purchased from commercial vendors such as Asinex³⁵¹, ChemBrigde³⁵², Chemical Block³⁵³, Enamine³⁵⁴, InterBioScreen³⁵⁵, LaboTest³⁵⁶, Life Chemicals³⁵⁷, Specs³⁵⁸, and TOSLab³⁵⁹.

8.3. Homology model of *P. falciparum* bc_1 complex Q_o binding site

8.3.1. Template structures

Protein sequences of Rieske ISP and cytochrome *b*, essential elements of bc_1 complex Q_o binding site, from the species *Saccharomyces cerevisiae*, *Bos Taurus*, *Gallus gallus*, *Rhodobacter sphaeroides* and *Plasmodium falciparum* were obtained from UniProt²⁴⁹. Crystal structures of bc_1 complex available from the stated sources with stigmatellin co-crystallized were retrieved as potential templates based on their sequence similarity with *P. falciparum* bc_1 complex Q_o site.

8.3.2. Definition of Q_o binding site.

The *S. cerevisiae* crystal structure and the co-crystallized inhibitor, stigmatellin, were used in order to define the Q_o binding site. MOE software²⁶² was applied to establish the interactions between this inhibitor and the binding pocket using the Ligand Interactions tool. The amino acid residues interacting with the stigmatellin were considered to be essential to define the pocket.

8.3.3. Sequence alignment

Protein sequences of Rieske ISP and cytochrome *b* from the templates and *P. falciparum* were aligned on the basis of conserved residues using Uniprot tools.

8.3.4. Model building.

S. cerevisiae high-resolution crystal structure (PDB code 3CX5) of the homologous *bc*₁ complex was used as template. For structure preparation, bound inhibitors and other coordinated molecules were removed from the PDB file. The protonation state of the residues was assigned using the Protonate 3D algorithm within the MOE software²⁶² The key residue His181 was kept neutral. Only chains E and N, corresponding to Rieske ISP and cytochrome *b*, respectively, were maintained for model generation purposes.

To obtain the model, the Homology Model tool available in MOE package was applied. For that, the two sequences of both Rieske ISP and cytochrome *b* of *P. falciparum* were aligned with the template (chains E and N) taking into account positions of highly conserved residues. Both the [2Fe-2S] cluster and stigmatellin were included in this calculation in order to permit induced fit. A total of 25 independent models were generated at 300K and the highest scoring intermediate model was chosen as the final model. The model was then minimized with stigmatellin in the active site and, after visual comparison with all crystal structures considered in this study, the rotamers of Phe254 and Pro260 were set as adequate. Amino acid residues numbering is according with *P. falciparum* protein sequence.

8.4. Chemistry

All reagents and solvents were obtained from commercial suppliers and were used without further purification. Melting points were determined using a Kofler camera Bock monoscope M and are uncorrected. Merck Silica Gel 60 F254 plates were used as analytical TLC and flash column chromatography was performed on Merck Silica Gel (200–400 mesh). ¹H and ¹³C NMR spectra were recorded on a Bruker 400 Ultra-Shield (400 MHz). ¹H and ¹³C chemical shifts are expressed in parts per million (ppm, δ) referenced to the solvent used and the proton coupling constants (*J*) in hertz. Proton coupling patterns were described as singlet (s), doublet (d), triplet (t), quartet (q), multiplet (m), doublet of doublets (dd), and broad (br). Low-resolution mass spectra were recorded using a VG

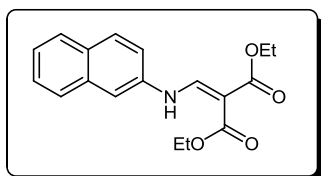
Quattro LCMS instruments. HR-ESI-MS were recorded on an ESI-TOF spectrometer (Biotof II Model, Bruker). Elemental analyses were performed using an EA 1110 CE Instruments automatic analyser. The microwave-assisted synthesis was performed in a CEM Corporation Discover[®] Labmate[™].

8.5. Synthesis of quinolone derivatives

8.5.1. Synthesis of compounds 3.26 and 3.35

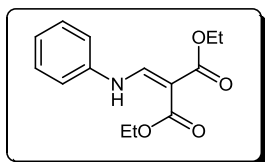
The appropriate aniline (1 mmol) was dissolved in diethyl ethoxymethylenemalonate (222 μL , 1.1 mmol) and the mixture was refluxed for 1 hour. After cooling, the reaction mixture was poured in hexane. The solid formed was further filtrated and washed with hexane to provide the pure product.

Diethyl 2-((naphthalen-2-ylamino)methylene)malonate (3.26)



Obtained as white solid, yield 75%, mp 88-90 °C. ¹H NMR (400 MHz, DMSO-d₆) δ = 10.89 (d, J = 13.8 Hz, 1H, NH), 8.57 (d, J = 13.9 Hz, 1H, H_{vin}), 7.96-7.87 (m, 4H, H₁+H₂+H₃+H₈), 7.60 (d, J = 8.8 Hz, 1H, H₆), 7.52 (t, J = 8.8 Hz, 1H, H₅), 7.44 (t, J = 8.8 Hz, 1H, H₇), 4.26-4.13 (m, 4H, 2CH₂)+ 1.27 (q, J = 6.9 Hz, 6H, 2CH₃).

Diethyl 2-((phenylamino)methylene)malonate (3.35)

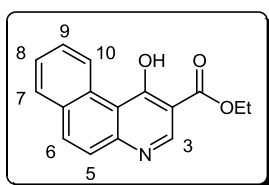


Obtained as white solid, yield 75%, mp 49-51 °C. ¹H NMR (400 MHz, CDCl₃) δ = 11.01 (d, J = 13.5 Hz, 1H, NH), 8.54 (d, J = 13.5 Hz, 1H, H_{vin}), 7.37 (t, J = 7.9 Hz, 2H, 2H₃), 7.17-7.13 (m, 3H, 2H₂+H₄), 4.34-4.22 (m, 4H, 2CH₂), 1.40-1.31 (m, 6H, 2CH₃).

8.5.2. Synthesis of compounds 3.27 and 3.36

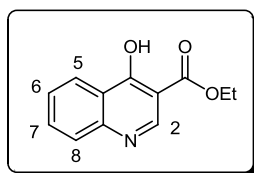
The appropriate malonate derivative (1 mmol) was dissolved in biphenyl ether (7 mL) was the mixture was refluxed for 1 hour. After cooling, the reaction mixture was poured in hexane. The solid formed was further filtrated and washed with hexane to provide the pure product.

Ethyl 1-hydroxybenzo[*f*]quinoline-2-carboxylate (3.27)



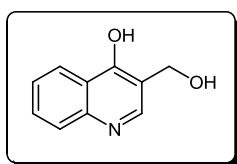
Obtained as white solid, yield 32%, mp 170-172 °C. ¹H NMR (400 MHz, DMSO-*d*₆) δ = 12.54 (br, 1H, OH), 10.22 (d, *J* = 8.6 Hz, 1H, H₆), 8.51 (s, 1H, H₃), 8.19 (d, *J* = 8.7 Hz, 1H, H₁₀), 8.02 (d, *J* = 8.7 Hz, 1H, H₇), 7.73-7.60 (m, 3H, H₆+H₈+H₉), 4.26 (q, *J* = 7.1 Hz, 2H, CH₂), 1.31 (t, *J* = 7.1 Hz, 3H, CH₃).

Ethyl 4-hydroxyquinoline-3-carboxylate (3.36)



Obtained as white solid, yield 50%, mp 255-256 °C. ¹H NMR (400 MHz, DMSO-*d*₆) δ = 12.35 (br, 1H, OH), 8.55 (s, 1H, H₂), 8.15 (d, *J* = 8.1 Hz, H₈), 7.71 (t, *J* = 8.1 Hz, 1H, H₆), 7.62 (d, *J* = 8.1 Hz, 1H, H₅), 7.41 (t, *J* = 8.1 Hz, 1H, H₇), 4.21 (q, *J* = 7.1 Hz, 2H, CH₂), 1.28 (t, *J* = 7.1 Hz, 3H, CH₃).

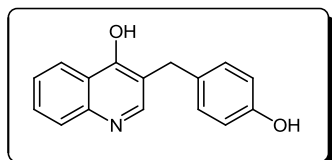
8.5.3. Synthesis of 3-(hydroxymethyl)-6,7-dihydroquinolin-4-ol (3.37)



To a solution of 6,7-dihydroquinolin-4-ol (500 mg, 3.4 mmol) in KOH 1M (4.2 mL) was added formaldehyde solution (600 μL). The reaction mixture was stirred at 45 °C during 15 hours. After cooling, a solution of HCl 2 N (2.1 mL) was added and the aqueous solution was washed with ethyl acetate. The solvent was removed under vacuum to provide the pure product. Obtained as a white solid, yield 96%, mp 133-135 °C. ¹H NMR (400 MHz, MeOH) δ = 8.28 (d, *J* = 8.3 Hz, 1H, H₈),

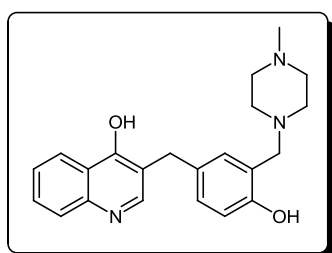
8.05 (s, 1H, H₂), 7.68 (t, $J = 8.3$ Hz, 1H, H₆), 7.58 (d, $J = 8.3$ Hz, 1H, H₅), 7.39 (t, $J = 8.3$ Hz, 1H, H₇), 4.64 (s, 2H, CH₂).

8.5.4. Synthesis of 3-(4-hydroxybenzyl)quinolin-4(1H)-one (3.38)



To a solution of 3-(hydroxymethyl)-6,7-dihydroquinolin-4-ol (200 mg, 1.04 mmol) in CH₂Cl₂ (960 μL) was added phenol (100 mg, 1.04 mmol) and HClO₄ 60% (628 μL). The reaction mixture was stirred at room temperature during 48 hours. The mixture was after neutralized with a solution of NaOH 1M. The aqueous phase was removed and the organic solvent was removed and vacuum. Obtained as a beige oil, yield 72%. ¹H NMR (400 MHz, MeOH) δ = 8.43 (d, $J = 8.2$ Hz, 1H, H₈), 8.18 (s, 1H, H₂), 7.90 (t, $J = 8.2$ Hz, 1H, H₆), 7.82 (d, $J = 8.2$ Hz, 1H, H₅), 7.66 (t, $J = 8.2$ Hz, 1H, H₇), 7.13 (d, $J = 7.9$ Hz, 2H, 2H_{2'}), 6.76 (d, $J = 7.9$ Hz, 2H, 2H_{3'}), 4.03 (s, 2H, CH₂). ¹³C NMR (400 MHz, MeOH) δ = 166.80 (C_q), 156.29 (C_q), 150.89 (C_{ar}), 142.29 (C_q), 131.24 (C_q), 129.52 (C_{ar}), 129.06 (C_{ar}), 128.55 (C_{ar}), 125.31 (C_{ar}), 124.23 (C_{ar}), 123.02 (C_q), 121.39 (C_q), 115.19 (C_{ar}), 28.33 (CH₂).

8.5.5. Synthesis of 3-(4-hydroxy-3-((4-methylpiperazin-1-yl)methyl)benzyl)-6,7-dihydroquinolin-4-ol (3.34)



To a solution of 3-(4-hydroxybenzyl)-6,7-dihydroquinolin-4-ol (84 mg, 0.32 mmol) in absolute ethanol (1 mL) was added *N*-methylpiperazine (39 μL, 0.35 mmol) followed by formaldehyde solution (28 μL, 0.35 mmol). The reaction mixture was refluxed during 5 hours. The solvent was removed under vacuum and the crude was dissolved in CH₂Cl₂ (3 mL). The organic phase was extracted with a solution of HCl 1N. The aqueous phase was neutralized with a solution of NaHCO₃ and washed with CH₂Cl₂. The solvent was removed under vacuum to provide the crude product. Purified by TLC (CH₂Cl₂/MeOH/TEA = 90:9:1). Obtained as a beige oil, yield 32%. ¹H NMR (400 MHz, MeOH) δ = 8.26 (d, $J = 8.0$ Hz, 1H, H₈), 7.69 (s, 1H,

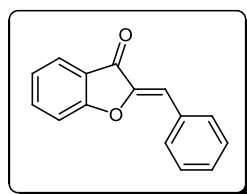
H₂), 7.62 (t, $J = 8.0$ Hz, 1H, H₆), 7.51 (d, $J = 8.0$ Hz, 1H, H₅), 7.35 (t, $J = 8.0$ Hz, 1H, H₇), 7.06 (d, $J = 8.3$ Hz, 1H, H_{6'}), 6.99 (s, 1H, H_{2'}), 6.68 (d, $J = 8.3$ Hz, 1H, H_{5'}), 3.79 (s, 2H, CH₂), 3.65 (s, 2H, CH₂-piperazine), 2.56 (br, 8H, piperazine), 2.31 (s, 3H, CH₃). ¹³C NMR (101 MHz, MeOH) $\delta = 166.72$ (C_q), 156.00 (C_q), 150.78 (C_{ar}), 142.22 (C_q), 132.34 (C_q), 129.56 (C_{ar}), 128.78 (C_{ar}), 127.55 (C_{ar}), 126.89 (C_{ar}), 125.93 (C_{ar}), 125.33 (C_q), 124.62 (C_{ar}), 123.34 (C_q), 121.78 (C_q), 116.39 (C_{ar}), 59.23 (CH₂-piperazine), 54.67 (piperazine), 53.02 (piperazine), 46.01 (CH₃), 28.87 (CH₂).

8.6. Synthesis of aurone derivatives

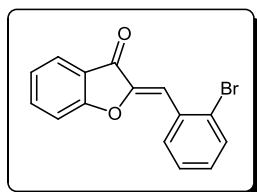
8.6.1. General procedure for the synthesis of aurones 5.24 to 5.29

To a solution of benzofuran-3(2*H*)-one (134 mg, 1 mmol) in dry methanol (20 mL) at room temperature was added the appropriate aldehyde (1.2 mmol) and Al₂O₃ (1 mmol). The mixture was refluxed, under N₂, for 48 hours. After, the solvent was removed and the solid residue was dissolved in CH₂Cl₂. The organic layer was washed with water, dried with anhydrous Na₂SO₄ and concentrated under reduced pressure to give the crude product.

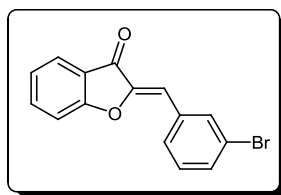
(*Z*)-2-benzylidenebenzofuran-3(2*H*)-one (5.24)



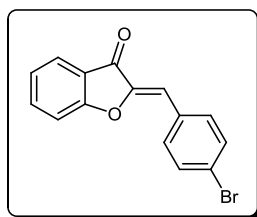
Purified by flash chromatography (Hexane/EtOAc = 90:10). Obtained as yellow solid, yield 41%, mp 113-114 °C. ¹H NMR (400 MHz, CDCl₃) $\delta = 7.93$ (d, $J = 7.1$ Hz, 2H, 2H_{2'}), 7.80 (d, $J = 7.6$ Hz, 1H, H₄), 7.66 (d, $J = 7.8$ Hz, 1H, H₆), 7.49-7.39 (m, 3H, 2H_{3'+H_{4'}}), 7.34 (d, $J = 7.8$ Hz, 1H, H₇), 7.23 (t, $J = 7.6$ Hz, 1H), 6.91 (s, 1H, H_{vin}). ¹³C NMR (101 MHz, CDCl₃) $\delta = 186.22$ (C=O), 167.63 (C_q), 138.77 (C_{ar}), 132.71 (C_{ar}), 132.09 (C_{ar}), 131.23 (C_q), 130.04 (C_{ar}), 129.42 (C_q), 125.38 (C_{ar}), 124.98 (C_{ar}), 122.52 (C_q), 114.24 (C_{ar}), 114.15 (C_{vin}). Anal. Calcd. (C₁₅H₁₀O₂•0.15H₂O): C, 80.09; H, 4.62%. Found: C, 80.35; H, 4.97%.

(Z)-2-(2-bromobenzylidene)benzofuran-3(2H)-one (5.25)

Purified by flash chromatography (Hexane/EtOAc = 95:5). Obtained as yellow solid, yield 55%, mp 169-171 °C. ^1H NMR (400 MHz, DMSO- d_6): δ = 8.32 (dd, J_1 = 7.9 Hz, J_2 = 1.5 Hz, 1H, H_4), 7.85-7.79 (m, 3H, $H_6+H_3'+H_5'$), 7.59-7.56 (m, 2H, H_7+H_6'), 7.40-7.33 (m, 2H, H_5+H_4'), 7.07 (s, 1H, H_{vin}). ^{13}C NMR (101 MHz, DMSO- d_6): δ = 184.15 (C=O), 166.14 (C_q), 147.66 (C_q), 138.55 (C_{ar}), 133.87 (C_{ar}), 132.47 (C_{ar}), 132.09 (C_{ar}), 131.51 (C_q), 128.88 (C_{ar}), 126.06 (C_q), 125.03 (C_{ar}), 124.78 (C_{ar}), 121.02 (C_q), 113.78 (C_{ar}), 109.23 (C_{vin}). ESI-MS m/z (abund.): 625 [$M+M+Na$] $^+$ (100). Anal. Calcd. ($C_{15}H_9BrO_2$): C, 59.82; H, 3.02%. Found: C, 59.67; H, 3.13%.

(Z)-2-(3-bromobenzylidene)benzofuran-3(2H)-one (5.26)

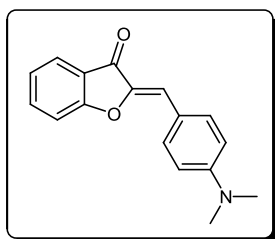
Purified by flash chromatography (Hexane/EtOAc = 95:5). Obtained as yellow solid, yield 54%, mp 123-124 °C. ^1H NMR (400 MHz, DMSO- d_6): δ = 8.18 (s, 1H, $H_{2'}$), 8.03 (d, J = 7.9 Hz, 1H, H_4), 7.83-7.81 (m, 2H, H_6+H_4'), 7.66 (d, J = 7.9 Hz, 1H, H_7), 7.61 (d, J = 8.2 Hz, 1H, $H_{6'}$), 7.48 (t, J = 7.9 Hz, 1H, H_5), 7.34 (t, J = 8.2 Hz, 1H, $H_{5'}$), 6.96 (s, 1H, H_{vin}). ^{13}C NMR (101 MHz, DMSO- d_6): δ = 184.15 (C=O), 166.02 (C_q), 147.31 (C_q), 138.42 (C_{ar}), 134.81 (C_q), 133.88 (C_{ar}), 133.03 (C_{ar}), 131.56 (C_{ar}), 130.59 (C_{ar}), 124.90 (C_{ar}), 124.67 (C_{ar}), 122.68 (C_q), 121.14 (C_q), 113.82 (C_{ar}), 110.80 (C_{vin}). ESI-MS m/z (abund.): 625 [$M+M+Na$] $^+$ (100). Anal. Calcd. ($C_{15}H_9BrO_2$): C, 59.82; H, 3.02%. Found: C, 59.81; H, 3.05%.

(Z)-2-(4-bromobenzylidene)benzofuran-3(2H)-one (5.27)

Purified by flash chromatography (Hexane/EtOAc = 95:5). Obtained as yellow solid, yield 56%, mp 180-182 °C. ^1H NMR (400 MHz, DMSO- d_6): δ = 7.91 (d, J = 8.3 Hz, 2H, $H_{2'}$), 7.84-7.80 (m, 2H, H_4+H_6), 7.72 (d, J = 8.3 Hz, 2H, $H_{3'}$), 7.56 (d, J = 8.5 Hz, 1H, H_7), 7.33 (t, J = 7.5 Hz, 1H, H_5), 6.95 (s, 1H, H_{vin}). ^{13}C NMR (101 MHz, DMSO- d_6): δ = 183.66 (C=O), 165.47 (C_q),

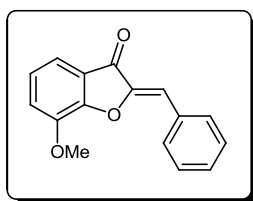
146.59 (C_q), 137.88 (C_{ar}), 133.14 (C_{ar}), 132.10 (C_{ar}), 131.21 (C_q), 124.42 (C_{ar}), 124.16 (C_{ar}), 123.65 (C_q), 120.78 (C_q), 113.28 (C_{ar}), 110.92 (C_{vin}). ESI-MS *m/z* (abund.): 625 [M+M+Na]⁺ (100). Anal. Calcd. (C₁₅H₉BrO₂): C, 59.82; H, 3.02%. Found: C, 59.88; H, 3.04%.

(Z)-2-(4-(dimethylamino)benzylidene)benzofuran-3(2H)-one (5.28)



Purified by flash chromatography (Hexane/CH₂Cl₂ = 50:50). Obtained as orange solid, 49% yield, mp 150-152 °C. ¹H NMR (400 MHz, CDCl₃): δ = 7.85 (d, *J* = 8.8 Hz, 2H, 2H_{2'}), 7.81 (d, *J* = 7.5 Hz, 1H, H₄), 7.61 (t, *J* = 8.3 Hz, 1H, H₆), 7.32 (d, *J* = 8.3 Hz, 1H, H₇), 7.19 (t, *J* = 7.5 Hz, 1H, H₅), 6.93 (s, 1H, H_{vin}), 6.75 (d, *J* = 8.8 Hz, 2H, 2H_{3'}), 3.07 (s, 6H, 2CH₃). ¹³C NMR (101 MHz, CDCl₃): δ = 184.14 (C=O), 165.42 (C_q), 151.47 (C_q), 145.16 (C_q), 135.96 (C_{ar}), 133.78 (C_{ar}), 124.46 (C_{ar}), 123.02 (C_{ar}), 122.59 (C_q), 120.15 (C_q), 115.45 (C_{vin}), 112.90 (C_{ar}), 112.08 (C_{ar}), 40.23 (CH₃). Anal. Calcd. (C₁₇H₁₅NO₂•0.15H₂O): C, 76.18; H, 5.77, N, 5.28%. Found: C, 76.20; H, 5.60, N, 5.33%.

(Z)-2-benzylidene-7-methoxybenzofuran-3(2H)-one (5.29)

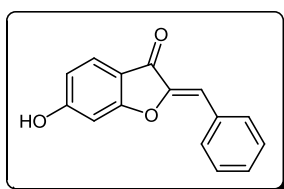


Purified by flash chromatography (Hexane/EtOAc = 90:10). Obtained as yellow solid, 62% yield, mp 168-169 °C. ¹H NMR (400 MHz, CDCl₃): δ = 8.00 (d, *J* = 7.3 Hz, 2H, 2H_{2'}), 7.56-7.47 (m, 4H, 2H_{3'}+H₄+H_{4'}), 7.35 (d, *J* = 7.8 Hz, 1H, H₆), 7.26 (t, *J* = 7.8 Hz, 1H, H₅), 6.99 (s, 1H), 4.01 (s, 3H). ¹³C NMR (101 MHz, DMSO-d₆): δ = 183.88 (C=O), 154.91 (C_q), 146.32 (C_q), 145.62 (C_q), 131.89 (C_q), 131.44 (C_{ar}), 130.29 (C_{ar}), 129.17 (C_{ar}), 129.71 (C_{ar}), 122.16 (C_q), 119.64 (C_{ar}), 115.17 (C_{ar}), 112.75 (C_{vin}), 56.35 (CH₃). Anal. Calcd. (C₁₆H₁₂O₃): C, 76.18; H, 4.80%. Found: C, 76.32; H, 5.03%.

8.6.2. General procedure for the synthesis of aurones 5.30 and 5.31

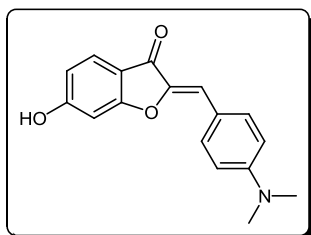
To a solution of 6-hydroxybenzofuran-3(2*H*)-one (0.57 mmol) in glacial acetic acid (5.7 mL) at room temperature was added the appropriate benzaldehyde (0.68 mmol) and HCl (3 drops). The reaction mixture was stirred for 4 hours at room temperature. After, the mixture was dropped in cold water and the precipitate formed was filtered and washed with water.

(*Z*)-2-benzylidene-6-hydroxybenzofuran-3(2*H*)-one (5.30)



Obtained as yellow solid, 99% yield, mp 228-230 °C. ¹H NMR (400 MHz, DMSO) δ = 11.26 (s, 1H), 7.95 (d, *J* = 7.4 Hz, 1H, 2H_{2'}), 7.64 (d, *J* = 8.4 Hz, 1H, H₄), 7.52-7.42 (m, 3H, 2H_{3'+H4'}), 6.81-6.80 (m, 2H, H_{7+H_{vin}}), 6.73 (d, *J* = 8.4 Hz, 1H, H₅). ¹³C NMR (101 MHz, DMSO) δ = 181.51 (C=O), 168.02 (C_q), 166.67 (C_q), 147.41 (C_q), 132.11 (C_q), 131.10 (C_{ar}), 129.71 (C_{ar}), 129.03 (C_{ar}), 126.07 (C_{ar}), 113.15 (C_{ar}), 112.75 (C_q), 110.38 (C_{vin}), 98.69 (C_{ar}). Anal. Calcd. (C₁₅H₁₀O₃•0.15H₂O): C, 74.77; H, 4.32%. Found: C, 74.50; H, 4.19%.

(*Z*)-2-(4-(dimethylamino)benzylidene)-6-hydroxybenzofuran-3(2*H*)-one (5.31)

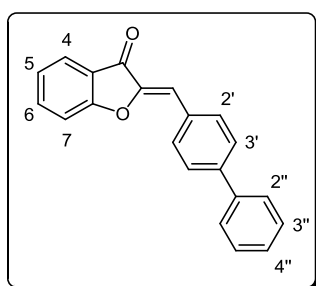


Obtained as orange solid, 71% yield, mp 235-237 °C. ¹H NMR (400 MHz, CDCl₃): δ = 10.00 (s, 1H, OH), 7.73 (d, *J* = 8.8 Hz, 2H, 2H_{2'}), 7.55 (d, *J* = 8.3 Hz, 1H, H₄), 6.70-6.61 (m, 5H, H_{5+H7+2H3'+H_{vin}}), 2.99 (s, 6H, 2CH₃). ¹³C NMR (101 MHz, CDCl₃): δ = 182.10 (C=O), 167.38 (C_q), 165.43 (C_q), 150.17 (C_q), 145.56 (C_q), 132.77 (C_{ar}), 125.15 (C_{ar}), 119.69 (C_q), 114.04 (C_q), 112.79 (C_{ar}), 112.27 (C_{ar}), 111.59 (C_{vin}), 98.40 (2CH₃). Anal. Calcd. (C₁₇H₁₅NO₃): C, 72.58; H, 5.39, N, 4.98%. Found: C, 72.19; H, 5.31, N, 5.09%.

8.6.3. General procedure for the synthesis of aurones derivatives 5.32-5.38 and 5.45-5.54 via Suzuki Coupling

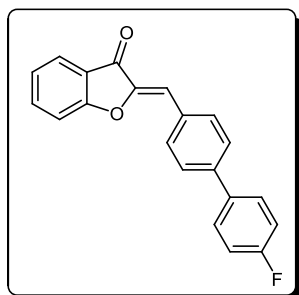
To a solution of the appropriate aurone derivative (0.23 mmol) in dioxane (2.3 mL) was added Pd(PPh₃)₂Cl₂ (0.023 mmol) and Na₂CO₃ 1M (690 μL) followed by the proper boronic acid (0.28 mmol). The resulting mixture was degassed and stirred at 100 °C for 3 hours under N₂. After cooling to room temperature, the reaction mixture was diluted with CH₂Cl₂, filtered under celite and concentrated under pressure to give the crude product.

(Z)-2-(biphenyl-4-ylmethylene)benzofuran-3(2H)-one (5.32)



Purified by flash chromatography (Hexane/EtOAc = 90:10). Obtained as yellow solid, 77% yield, mp 133-135 °C. ¹H NMR (400 MHz, DMSO-d₆): δ = 8.10 (d, *J* = 8.0 Hz, 2H, 2H_{2'}), 7.85-7.75 (m, 6H, H₄+H₆+2H_{3'}+2H_{2''}), 7.61 (d, *J* = 8.4 Hz, 1H, H₇), 7.52-7.49 (m, 2H, 2H_{3''}), 7.41 (m, 1H, H_{4''}), 7.34 (t, *J* = 7.3 Hz, 1H, H₅), 7.03 (s, 1H, H_{vin}). ¹³C NMR (101 MHz, DMSO-d₆): δ = 183.60 (C=O), 165.45 (C_q), 146.42 (C_q), 141.50 (C_q), 139.11 (C_q), 137.73 (C_{ar}), 132.08 (C_{ar}), 131.08 (C_{ar}), 129.10 (C_{ar}), 128.15 (C_{ar}), 127.23 (C_{ar}), 126.82 (C_{ar}), 124.38 (C_{ar}), 124.07 (C_{ar}), 120.94 (C_q), 113.30 (C_{ar}), 111.97 (C_{vin}). Anal. Calcd. (C₂₁H₁₄O₂•0.15H₂O): C, 83.78; H, 4.80%. Found: C, 83.67; H, 4.89%.

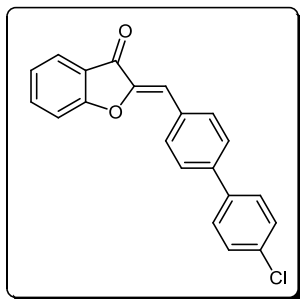
(Z)-2-((4'-fluorobiphenyl-4-yl)methylene)benzofuran-3(2H)-one (5.33)



Purified by flash chromatography (Hexane/EtOAc = 92:8). Obtained as yellow solid, 66% yield, mp 174-175 °C. ¹H NMR (400 MHz, DMSO-d₆): δ = 8.10 (d, *J* = 8.2 Hz, 2H, 2H_{2'}), 7.84-7.80 (m, 6H, H₄+H₆+2H_{3'}+2H_{2''}), 7.61 (d, *J* = 8.5 Hz, 1H, H₇), 7.36-7.31 (m, 3H, H₅+2H_{3''}), 7.03 (s, 1H, H_{vin}). ¹³C NMR (101 MHz, DMSO-d₆): δ = 183.61 (C=O), 165.45 (C_q), 162.27 (CF), 146.43 (C_q), 140.41 (C_q), 137.75 (C_{ar}), 135.60 (C_q), 132.08 (C_{ar}), 131.05 (C_q), 128.90 (C_{ar}), 127.18 (C_{ar}),

124.39 (C_{ar}), 124.09 (C_{ar}), 120.94 (C_q), 115.94 (C_{ar}), 113.31 (C_{ar}), 111.90 (C_{vin}). Anal. Calcd. (C₂₁H₁₃FO₂•0.1H₂O): C, 79.28; H, 4.19%. Found: C, 79.07; H, 4.33%.

(Z)-2-((4'-chlorobiphenyl-4-yl)methylene)benzofuran-3(2H)-one (5.34)

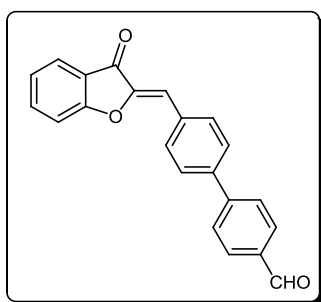


Purified by flash chromatography (Hexane/EtOAc = 90:10).

Obtained as yellow solid, 64% yield, mp 171-173 °C. ¹H NMR (400 MHz, DMSO-d₆): δ = 8.10 (d, *J* = 8.3 Hz, 2H, 2H_{2'}), 7.86-7.79 (m, 6H, H₄+H₆+2H_{3'}+2H_{2''}), 7.61 (d, *J* = 8.7 Hz, 1H, H₇), 7.56 (d, *J* = 8.5 Hz, 2H, 2H_{3''}), 7.35 (t, *J* = 7.4 Hz, 1H, H₅), 7.03 (s, 1H, H_{vin}). ¹³C NMR (101 MHz, DMSO-d₆): δ = 184.05 (C=O), 165.91 (C_q), 146.95

(C_q), 140.52 (C_q), 138.35 (C_q), 138.20 (C_{ar}), 133.47 (C_q), 132.53 (C_{ar}), 131.86 (C_q), 129.49 (C_{ar}), 129.01 (C_{ar}), 127.63 (C_{ar}), 124.82 (C_{ar}), 124.54 (C_{ar}), 121.36 (C_q), 113.74 (C_{ar}), 112.22 (C_{vin}). Anal. Calcd. (C₂₁H₁₃ClO₂•0.15H₂O): C, 75.18; H, 4.00%. Found: C, 75.16; H, 3.97%.

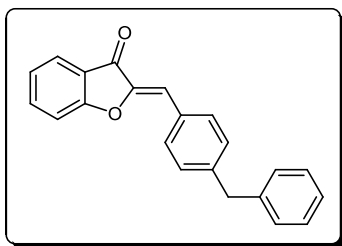
(Z)-4'-((3-oxobenzofuran-2(3H)-ylidene)methyl)biphenyl-4-carbaldehyde (5.35)



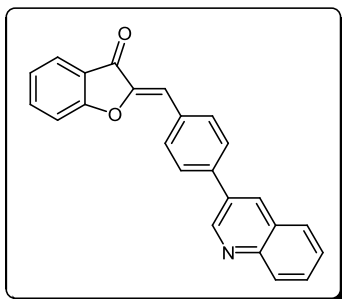
Purified by flash chromatography (Hexane/EtOAc = 90:20).

Obtained as yellow solid, 83% yield, mp 189-190 °C. ¹H NMR (400 MHz, DMSO-d₆): δ = 10.07 (s, 1H, H_{ald}), 8.14 (d, *J* = 8.3 Hz, 2H, 2H_{2'}), 8.04-7.99 (m, 4H, 2H_{2''}+2H_{3''}), 7.94 (d, *J* = 8.3 Hz, 2H, 2H_{3'}), 7.83-7.81 (m, 2H, H₄+H₆), 7.61 (d, *J* = 8.4 Hz, 1H, H₇), 7.35 (t, *J* = 7.4 Hz, 1H, H₅), 7.04 (s, 1H, H_{vin}). ¹³C NMR (101 MHz,

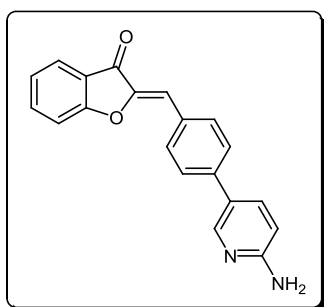
DMSO-d₆): δ = 192.81 (C_{ald}), 183.69 (C=O), 165.52 (C_q), 146.70 (C_q), 144.76 (C_q), 139.95 (C_q), 137.85 (C_{ar}), 135.49 (C_q), 132.22 (C_q), 132.13 (C_{ar}), 130.26 (C_{ar}), 127.75 (C_{ar}), 127.53 (C_{ar}), 124.45 (C_{ar}), 124.17 (C_{ar}), 120.89 (C_q), 113.34 (C_{ar}), 111.61 (C_{vin}). Anal. Calcd. (C₂₁H₁₄O₃•0.75H₂O): C, 77.74; H, 4.61%. Found: C, 77.43; H, 4.47%.

(Z)-2-(4-benzylbenzylidene)benzofuran-3(2H)-one (5.36)

Purified by flash chromatography (Hexane/EtOAc = 92:8). Obtained as yellow solid, 70% yield, 154-156 °C. ^1H NMR (400 MHz, DMSO- d_6): δ = 7.93 (d, J = 7.9 Hz, 2H, $2\text{H}_2'$), 7.81-7.79 (m, 2H, H_4+H_6), 7.56 (d, J = 8.6 Hz, 1H, H_7), 7.39 (d, J = 7.9 Hz, 2H, $2\text{H}_3'$), 7.34-7.25 (m, 5H, $2\text{H}_2''+2\text{H}_3''+\text{H}_4''$), 7.20 (t, J = 7.2 Hz, 1H, H_5), 6.93 (s, 1H, H_{vin}), 4.01 (s, 2H, CH_2). ^{13}C NMR (101 MHz, DMSO- d_6): δ = 183.60 (C=O), 165.43 (C_q), 146.11 (C_q), 143.86 (C_q), 140.71 (C_q), 137.69 (C_{ar}), 131.67 (C_{ar}), 129.75 (C_q), 129.48 (C_{ar}), 128.77 (C_{ar}), 128.54 (C_{ar}), 126.16 (C_{ar}), 124.33 (C_{ar}), 124.01 (C_{ar}), 120.95 (C_q), 113.26 (C_{ar}), 112.33 (C_{vin}), 41.01 (CH_2). Anal. Calcd. ($\text{C}_{22}\text{H}_{16}\text{O}_2 \cdot 0.15\text{H}_2\text{O}$): C, 83.86; H, 5.23%. Found: C, 83.87; H, 5.12%.

(Z)-2-(4-(quinolin-3-yl)benzylidene)benzofuran-3(2H)-one (5.37)

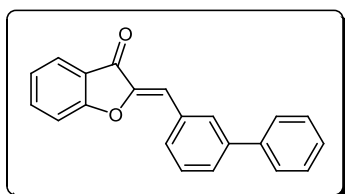
Purified by flash chromatography (Hexane/EtOAc = 70:30). Obtained as yellow solid, 87% yield, mp 205-207 °C. ^1H NMR (400 MHz, DMSO- d_6): δ = 9.35 (s, 1H, $\text{H}_{2''}$), 8.77 (s, 1H, $\text{H}_{4''}$), 8.19 (d, J = 8.3 Hz, 2H, $2\text{H}_2'$), 8.09-8.07 (m, 4H, $\text{H}_4+2\text{H}_3'+\text{H}_8''$), 7.86-7.78 (m, 3H, $\text{H}_6+\text{H}_6''+\text{H}_7''$), 7.69-7.62 (m, 2H, $\text{H}_7+\text{H}_5''$), 7.35 (t, J = 7.4 Hz, 1H, H_5), 7.07 (s, 1H, H_{vin}). ^{13}C NMR (101 MHz, DMSO- d_6): δ = 184.08 (C=O), 165.93 (C_q), 149.78 (C_{ar}), 147.47 (C_q), 147.07 (C_q), 138.80 (C_q), 138.24 (C_{ar}), 133.68 (C_{ar}), 132.65 (C_{ar}), 132.24 (C_q), 130.38 (C_{ar}), 129.15 (C_{ar}), 129.02 (C_{ar}), 128.12 (C_{ar}), 128.05 (C_q), 127.65 (C_{ar}), 127.62 (C_{ar}), 124.86 (C_{ar}), 124.58 (C_{ar}), 121.35 (C_q), 113.78 (C_{ar}), 112.15 (C_{vin}). Anal. Calcd. ($\text{C}_{24}\text{H}_{15}\text{NO}_2 \cdot 0.4\text{H}_2\text{O}$): C, 80.87; H, 4.48; N, 3.93%. Found: C, 80.67; H, 4.27; N, 4.06%.

(Z)-2-(4-(6-aminopyridin-3-yl)benzylidene)benzofuran-3(2H)-one (5.38)

Purified by flash chromatography (EtOAc/MeOH = 97:3).

Obtained as orange solid, 99% yield, mp 195-197 °C. ¹H NMR (400 MHz, DMSO-d₆): δ = 8.38 (s, 1H, H_{2''}), 8.04 (d, *J* = 8.3 Hz, 2H, 2H_{2'}), 7.84-7.80 (m, 3H, H₄+H₆+H_{6''}), 7.76 (d, *J* = 8.3 Hz, 2H, 2H_{3'}), 7.61 (d, *J* = 8.5 Hz, 1H, H₇), 7.34 (t, *J* = 7.4 Hz, 1H, H₅), 7.00 (s, 1H, H_{vin}), 6.55 (d, *J* = 8.6 Hz, 1H, H_{5''}), 6.24 (s, 2H, NH₂).

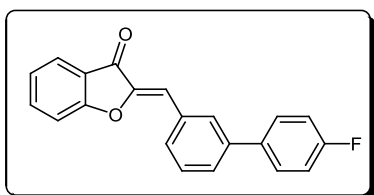
¹³C NMR (101 MHz, DMSO-d₆): δ = 183.91 (C=O), 165.75 (C_q), 160.10 (C_q), 146.75 (C_{ar}), 146.52 (C_{ar}), 140.16 (C_q), 138.03 (C_{ar}), 135.74 (C_{ar}), 132.62 (C_{ar}), 130.16 (C_q), 125.95 (C_{ar}), 124.75 (C_{ar}), 124.44 (C_{ar}), 123.02 (C_q), 121.46 (C_q), 113.72 (C_{ar}), 112.83 (C_{vin}), 108.48 (C_{ar}). Anal. Calcd. (C₂₀H₁₄N₂O₂•0.4H₂O): C, 74.70; H, 4.65; N, 8.71%. Found: C, 74.57; H, 4.43; N, 8.79%.

(Z)-2-(biphenyl-3-ylmethylene)benzofuran-3(2H)-one (5.45)

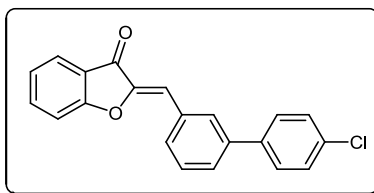
Purified by flash chromatography (Hexane/EtOAc = 92:8).

Obtained as yellow solid, 71% yield, mp 123-125 °C. ¹H NMR (400 MHz, DMSO-d₆): δ = 8.24 (s, 1H, H_{2'}), 8.08 (d, *J* = 7.7 Hz, 1H, H₄), 7.84-7.80 (m, 2H, H₆+H_{4'}), 7.77-7.73 (m, 3H, H_{6'}+H_{2''}),

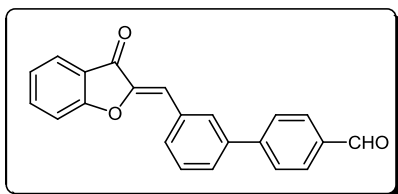
7.64-7.60 (m, 2H, H₅+H_{5'}), 7.54-7.50 (m, 2H, H₄+H_{3''}), 7.42 (t, *J* = 7.3 Hz, 1H, H_{4''}), 7.34 (t, *J* = 7.4 Hz, 1H, H₇), 7.07 (s, 1H, H_{vin}). ¹³C NMR (101 MHz, DMSO-d₆): δ = 183.79 (C=O), 165.59 (C_q), 146.57 (C_q), 140.96 (C_q), 139.51 (C_q), 137.84 (C_{ar}), 132.62 (C_q), 130.06 (C_{ar}), 129.99 (C_{ar}), 129.76 (C_{ar}), 129.13 (C_{ar}), 128.47 (C_{ar}), 127.90 (C_{ar}), 126.87 (C_{ar}), 124.43 (C_{ar}), 124.13 (C_{ar}), 120.89 (C_q), 113.41 (C_{ar}), 112.27 (C_{vin}). Anal. Calcd. (C₂₁H₁₄O₂•0.1H₂O): C, 84.03; H, 4.78%. Found: C, 83.94; H, 4.80%.

(Z)-2-((4'-fluorobiphenyl-3-yl)methylene)benzofuran-3(2H)-one (5.46)

Purified by flash chromatography (Hexane/EtOAc = 92:8). Obtained as yellow solid, 65% yield, mp 103-105 °C. ^1H NMR (400 MHz, DMSO- d_6): δ = 8.22 (s, 1H, $\text{H}_{2'}$), 8.08 (d, J = 7.7 Hz, 1H, H_4), 7.81-7.78 (m, 5H, $\text{H}_6+\text{H}_{4'}+\text{H}_{6'}+2\text{H}_{2''}$), 7.64-7.60 (m, 2H, $\text{H}_5+\text{H}_{5'}$), 7.37-7.32 (m, 3H, $\text{H}_7+2\text{H}_{3''}$), 7.06 (s, 1H, H_{vin}). ^{13}C NMR (101 MHz, DMSO- d_6): δ = 183.78 (C=O), 165.59 (C_q), 162.15 (CF), 146.58 (C_q), 139.89 (C_q), 137.85 (C_{ar}), 135.95 (C_q), 132.63 (C_q), 129.96 (C_{ar}), 129.78 (C_{ar}), 128.93 (C_{ar}), 128.85 (C_{ar}), 128.38 (C_{ar}), 124.43 (C_{ar}), 124.14 (C_{ar}), 120.88 (C_q), 116.03-115.82 (C_{ar}), 113.41 (C_{ar}), 112.18 (C_{vin}). Anal. Calcd. ($\text{C}_{21}\text{H}_{13}\text{FO}_2 \cdot 0.1\text{H}_2\text{O}$): C, 79.28; H, 4.19%. Found: C, 79.23; H, 4.15%.

(Z)-2-((4'-chlorobiphenyl-3-yl)methylene)benzofuran-3(2H)-one (5.47)

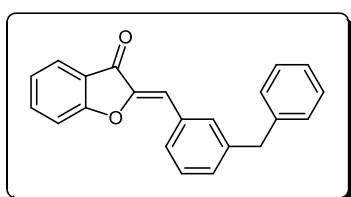
Purified by flash chromatography (Hexane/EtOAc = 85:15). Obtained as yellow solid, 51% yield, mp 187-189 °C. ^1H NMR (400 MHz, DMSO- d_6): δ = 8.24 (s, 1H, $\text{H}_{2'}$), 8.09 (d, J = 7.7 Hz, 1H, H_4), 7.85-7.76 (m, 5H, $\text{H}_6+\text{H}_{4'}+\text{H}_{6'}+2\text{H}_{2''}$), 7.65-7.56 (m, 4H, $\text{H}_5+\text{H}_7+2\text{H}_{3''}$), 7.34 (t, J = 7.4 Hz, 1H, $\text{H}_{5'}$), 7.06 (s, 1H, H_{vin}). ^{13}C NMR (101 MHz, DMSO- d_6): δ = 183.82 (C=O), 165.62 (C_q), 146.64 (C_q), 139.63 (C_q), 138.33 (C_q), 137.91 (C_{ar}), 132.83 (C_q), 132.73 (C_q), 130.35 (C_{ar}), 129.94 (C_{ar}), 129.89 (C_{ar}), 129.11 (C_{ar}), 128.67 (C_{ar}), 128.38 (C_{ar}), 124.47 (C_{ar}), 124.19 (C_{ar}), 120.88 (C_q), 113.44 (C_{ar}), 112.11 (C_{vin}). Anal. Calcd. ($\text{C}_{21}\text{H}_{13}\text{ClO}_2 \cdot 0.15\text{H}_2\text{O}$): C, 75.18; H, 4.00%. Found: C, 74.79; H, 4.20%.

(Z)-3'-((3-oxobenzofuran-2(3H)-ylidene)methyl)biphenyl-4-carbaldehyde (5.48)

Purified by flash chromatography (Hexane/EtOAc = 75:25). Obtained as yellow solid, 63% yield, mp 193-195 °C. ^1H NMR (400 MHz, DMSO- d_6): δ = 10.09 (s, 1H, ald), 8.35 (s, 1H, $\text{H}_{2'}$), 8.15 (d, J = 7.8 Hz, 1H, H_4), 8.06-7.98 (m, 4H, $2\text{H}_{2''}+2\text{H}_{3''}$), 7.88-7.82 (m, 3H, $\text{H}_6+\text{H}_{4'}+\text{H}_{6'}$), 7.68 (t, J = 7.8 Hz, 1H, H_5), 7.62 (d, J = 8.4

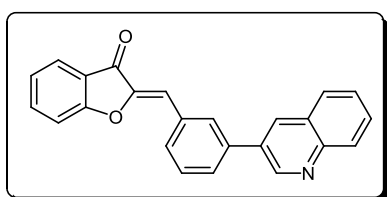
Hz, 1H, H₇), 7.35 (t, *J* = 7.4 Hz, 1H, H_{5'}), 7.09 (s, 1H, H_{vin}). ¹³C NMR (101 MHz, DMSO-d₆): δ = 192.83 (C_{ald}), 183.76 (C=O), 165.59 (C_q), 146.66 (C_q), 145.13 (C_q), 139.54 (C_q), 137.86 (C_{ar}), 135.38 (C_q), 132.81 (C_q), 130.97 (C_{ar}), 130.29 (C_{ar}), 128.73 (C_{ar}), 127.95 (C_{ar}), 127.55 (C_{ar}), 124.43 (C_{ar}), 124.15 (C_{ar}), 120.84 (C_q), 113.42 (C_{ar}), 111.89 (C_{vin}). Anal. Calcd. (C₂₂H₁₄O₃•0.25H₂O): C, 79.86; H, 4.43%. Found: C, 79.48; H, 4.57%.

(Z)-2-(3-benzylbenzylidene)benzofuran-3(2H)-one (5.49)



Purified by flash chromatography (Hexane/EtOAc = 92:8). Obtained as yellow oil, 60%. ¹H NMR (400 MHz, DMSO-d₆): δ = 7.86-7.79 (m, 4H, H₄+H₆+H₂'+H₆'), 7.52 (t, *J* = 8.1 Hz, 1H, H₇), 7.44 (t, *J* = 7.6 Hz, 1H, H₅), 7.34-7.27 (m, 6H, H₄'+2H₂''+2H₃''+H₄''), 7.23-7.22 (m, 1H, H_{5'}), 6.90 (s, 1H, H_{vin}), 4.02 (s, 2H, CH₂). ¹³C NMR (101 MHz, DMSO-d₆): δ = 183.80 (C=O), 165.54 (C_q), 146.41 (C_q), 142.41 (C_q), 140.94 (C_q), 137.90 (C_{ar}), 132.11 (C_q), 131.77 (C_{ar}), 130.72 (C_{ar}), 129.32 (C_{ar}), 129.26 (C_{ar}), 128.93 (C_{ar}), 128.67 (C_{ar}), 126.26 (C_{ar}), 124.48 (C_{ar}), 124.17 (C_{ar}), 120.94 (C_q), 113.33 (C_{ar}), 112.39 (C_{vin}), 41.00 (CH₂). HRMS calc. (C₂₂H₁₇O₂): 313.1223. Found: 313.1226.

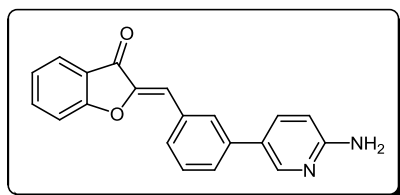
(Z)-2-(3-(quinolin-3-yl)benzylidene)benzofuran-3(2H)-one (5.50)



Purified by flash chromatography (Hexane/EtOAc = 80:20). Obtained as yellow solid, 68% yield, mp 195-196 °C. ¹H NMR (400 MHz, pyridine-d₆): δ = 9.53 (s, 1H, H₂''), 8.53 (s, 1H, H₄''), 8.42 (d, *J* = 8.0 Hz, 1H, H₄), 8.37 (s, 1H, H₂'), 8.19 (d, *J* = 7.9 Hz, 1H, H₄'), 8.05 (d, *J* = 7.9 Hz, 1H, H₅''), 7.90 (d, *J* = 7.7 Hz, 1H, H₈''), 7.85 (d, *J* = 7.7 Hz, 1H, H₇''), 7.78 (t, *J* = 8.0 Hz, 1H, H₅), 7.67-7.61 (m, 3H, H₅'+H₆'+H₆''), 7.40 (d, *J* = 8.1 Hz, 1H, H₇), 7.26-7.18 (m, 2H, H₆+H_{vin}). ¹³C NMR (101 MHz, pyridine-d₆): δ = 184.80 (C=O), 166.74 (C_q), 148.56 (C_q), 147.97 (C_q), 139.23 (C_q), 137.84 (C_{ar}), 134.13 (C_q), 133.94 (C_{ar}), 133.66 (C_q), 131.43 (C_{ar}), 131.21 (C_{ar}), 130.56 (C_{ar}), 130.29 (C_{ar}), 130.13 (C_{ar}), 129.46 (C_{ar}), 129.11 (C_{ar}), 128.83 (C_q), 127.83 (C_{ar}), 125.05 (C_{ar}), 124.45 (C_{ar}), 124.17 (C_{ar}),

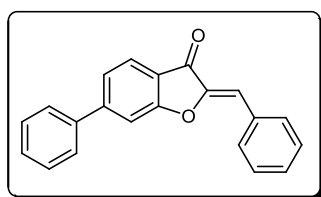
122.24 (C_q), 113.85 (C_{ar}), 112.55 (C_{vin}). Anal. Calcd. (C₂₄H₁₅NO₂•0.3H₂O): C, 81.24; H, 4.44; N, 3.95%. Found: C, 81.59; H, 4.83; N, 3.92%.

(Z)-2-(3-(6-aminopyridin-3-yl)benzylidene)benzofuran-3(2H)-one (5.51)

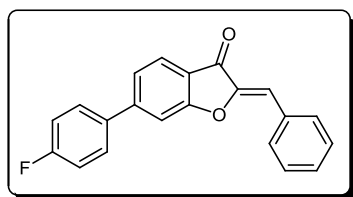


Purified by flash chromatography (CH₂Cl₂/MeOH = 97:3). Obtained as yellow solid, 76% yield, mp 187-189 °C. ¹H NMR (400 MHz, DMSO-d₆): δ = 8.32 (s, 1H, H_{2''}), 8.14 (s, 1H, H_{2'}), 7.98 (d, *J* = 7.7 Hz, 1H, H₄), 7.83-7.80 (m, 2H, H_{4'}+H_{6'}), 7.77 (dd, *J*₁ = 8.6 Hz, *J*₂ = 2.5 Hz, 1H, H_{6''}), 7.67 (d, *J* = 7.8 Hz, 1H, H₇), 7.63-7.61 (m, 1H, H₆), 7.55 (t, *J* = 7.7 Hz, 1H, H₅), 7.34 (t, *J* = 7.3 Hz, 1H, H_{5'}), 7.03 (s, 1H, H_{vin}), 6.56 (d, *J* = 8.6 Hz, 1H, H_{5''}), 6.15 (s, 2H, NH₂). ¹³C NMR (101 MHz, DMSO-d₆): δ = 184.17 (C=O), 165.97 (C_q), 159.89 (C_q), 145.87 (C_q), 146.35 (C_{ar}), 138.19 (C_{ar}), 135.87 (C_{ar}), 132.93 (C_q), 131.99 (C_{ar}), 130.09 (C_{ar}), 129.28 (C_{ar}), 127.50 (C_{ar}), 124.80 (C_{ar}), 123.52 (C_q), 121.31 (C_q), 113.82 (C_{ar}), 112.89 (C_{vin}), 108.49 (C_{ar}). Anal. Calcd. (C₂₀H₁₄N₂O₂•0.5H₂O): C, 74.28; H, 4.69; N, 8.67%. Found: C, 74.43; H, 4.55; N, 8.97%.

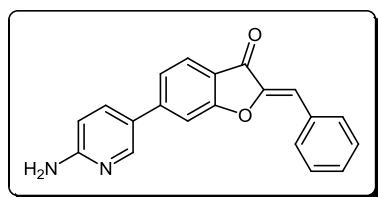
(Z)-2-benzylidene-6-phenylbenzofuran-3(2H)-one (5.52)



Purified by flash chromatography (Hexane/CH₂Cl₂ = 70:30). Obtained as yellow solid, 78% yield, mp 141-143 °C. ¹H NMR (400 MHz, CDCl₃): δ = 7.95 (d, *J* = 7.2 Hz, 2H, 2H_{2'}), 7.87 (d, *J* = 7.9 Hz, 1H, H₄), 7.57 (d, *J* = 7.0 Hz, 2H, 2H_{2''}), 7.56 (s, 1H, H₇), 7.53-7.40 (m, 7H, H₅+2H_{3'}+H_{4'}+2H_{2''}+H_{4''}), 6.92 (s, 1H, H_{vin}). ¹³C NMR (101 MHz, DMSO-d₆): δ = 183.14 (C=O), 166.24 (C_q), 149.52 (C_q), 146.92 (C_q), 138.58 (C_q), 131.99 (C_{ar}), 131.44 (C_{ar}), 130.16 (C_{ar}), 129.23 (C_{ar}), 129.20 (C_{ar}), 129.10 (C_{ar}), 127.44 (C_{ar}), 124.79 (C_{ar}), 122.86 (C_{ar}), 124.48 (C_{ar}), 119.81 (C_q), 112.18 (C_{ar}), 111.06 (C_{vin}). Anal. Calcd. (C₂₁H₁₄O₂•0.6H₂O): C, 81.58; H, 4.97%. Found: C, 81.41; H, 5.28%.

(Z)-2-benzylidene-6-(4-fluorophenyl)benzofuran-3(2H)-one (5.53)

Purified by flash chromatography (Hexane/EtOAc = 90:10). Obtained as yellow solid, 66% yield, mp 172-174 °C. ^1H NMR (400 MHz, DMSO- d_6): δ = 8.04 (d, J = 7.1 Hz, 2H, $2\text{H}_2'$), 7.94-7.90 (m, 3H, $\text{H}_7+2\text{H}_2''$), 7.87 (d, J = 8.0 Hz, 1H, H_4), 7.64 (dd, J_1 = 8.0 Hz, J_2 = 1.3 Hz, 1H, H_5), 7.55-7.48 (m, 3H, $2\text{H}_3'+\text{H}_4'$), 7.38 (t, J = 8.84 Hz, 2H, $2\text{H}_3''$), 6.98 (s, 1H, H_{vin}). ^{13}C NMR (101 MHz, DMSO- d_6): δ = 183.10 (C=O), 166.22 (C_q), 164.08-161.63 (C_q), 148.35 (C_q), 146.91 (C_q), 135.03 (C_q), 131.98 (C_q), 131.43 (C_{ar}), 130.17 (C_{ar}), 129.73-129.64 (C_{ar}), 129.10 (C_{ar}), 124.81 (C_{ar}), 122.78 (C_{ar}), 119.76 (C_q), 116.21-115.99 (C_{ar}), 112.21 (C_{ar}), 111.04 (C_{vin}). Anal. Calcd. ($\text{C}_{21}\text{H}_{13}\text{FO}_2 \cdot 0.3\text{H}_2\text{O}$): C, 78.39; H, 4.27%. Found: C, 78.14; H, 4.22%.

(Z)-6-(6-aminopyridin-3-yl)-2-benzylidenebenzofuran-3(2H)-one (5.54)

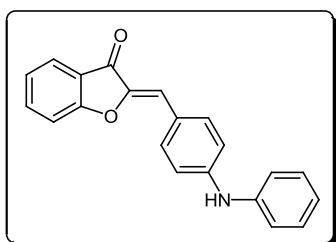
Purified by flash chromatography ($\text{CH}_2\text{Cl}_2/\text{MeOH}$ = 98:2). Obtained as orange solid, 98% yield, mp 191-192 °C. ^1H NMR (400 MHz, DMSO- d_6): δ = 8.50 (s, 1H, H_2'), 8.02 (d, J = 7.2 Hz, 2H, $2\text{H}_2'$), 7.92 (dd, J_1 = 8.7 Hz, J_2 = 2.5 Hz, 1H, H_6''), 7.82-7.78 (m, 1H, H_4+H_7), 7.58 (d, J = 8.1 Hz, 1H, H_5), 7.53 (t, J = 7.2 Hz, 2H, $2\text{H}_3'$), 7.48-7.45 (m, 1H, H_4'), 6.92 (s, 1H, H_{vin}), 6.56 (d, J = 8.7 Hz, 1H, H_5''), 6.44 (s, 2H, NH_2). ^{13}C NMR (101 MHz, DMSO- d_6): δ = 182.75 (C=O), 166.53 (C_q), 160.35 (C_q), 147.83 (C_q), 147.36 (C_{ar}), 147.12 (C_q), 135.82 (C_{ar}), 132.09 (C_q), 131.32 (C_{ar}), 130.01 (C_{ar}), 129.08 (C_{ar}), 124.76 (C_{ar}), 121.94 (C_q), 121.00 (C_{ar}), 118.51 (C_q), 111.52 (C_{vin}), 108.53 (C_{ar}), 108.02 (C_{ar}). Anal. Calcd. ($\text{C}_{20}\text{H}_{14}\text{N}_2\text{O}_2 \cdot 0.3\text{H}_2\text{O}$): C, 75.12; H, 4.61; N, 8.76%. Found: C, 74.91; H, 4.55; N, 8.64%.

8.6.4. General procedure for the synthesis of aurones derivatives 5.39 and 5.40 via Buchwald Coupling

(Z)-2-(4-bromobenzylidene)benzofuran-3(2H)-one (**5.27**) (0.23 mmol), $\text{Pd}_2(\text{dba})_3$ (0.0115 mmol), (*R*)-BINAP (0.075 mmol) and NaO^tBu (0.322 mmol) were dissolved in dry toluene

(2.3 mL). The resulting mixture was degassed and the appropriate amine (0.276 mmol) was added. The mixture was stirred at 100 °C for 15 minutes under MW conditions. After cooling to room temperature, the reaction mixture was diluted with Et₂O, filtered under celite and concentrated under pressure to give the crude product.

(Z)-2-(4-(phenylamino)benzylidene)benzofuran-3(2H)-one (5.39)

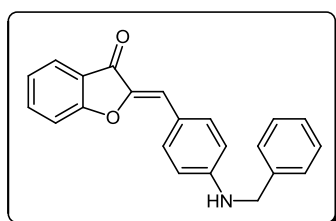


Purified by flash chromatography (Hexane/EtOAc = 80:20).

Obtained as orange solid, 71% yield, mp 191-192 °C. ¹H NMR (400 MHz, DMSO-d₆): δ = 8.87 (s, 1H, NH), 7.90 (d, *J* = 8.7 Hz, 2H, 2H_{2'}), 7.79-7.76 (m, 2H, H₄+H₆), 7.55 (d, *J* = 7.4 Hz, 1H, H₇), 7.34-7.29 (m, 3H, 2H_{2''}+H_{4''}), 7.20 (d, *J* = 7.5 Hz, 2H, 2H_{3''}), 7.15

(d, *J* = 8.7 Hz, 2H, 2H_{3'}), 6.98 (t, *J* = 7.2 Hz, 1H, H₅), 6.91 (s, 1H, H_{vin}). ¹³C NMR (100 MHz, DMSO-d₆): δ = 183.21 (C=O), 165.18 (C_q), 146.57 (C_q), 144.95 (C_q), 141.80 (C_q), 137.36 (C_{ar}), 134.02 (C_{ar}), 129.80 (C_{ar}), 124.46 (C_{ar}), 124.08 (C_{ar}), 122.61 (C_q), 122.13 (C_{ar}), 121.92 (C_q), 119.41 (C_{ar}), 115.66 (C_{ar}), 114.30 (C_{vin}), 113.58 (C_{ar}). Anal. Calcd. (C₂₁H₁₅NO₂•0.15H₂O): C, 79.80; H, 4.89; N, 4.43%. Found: C, 79.56; H, 5.12; N, 4.68%.

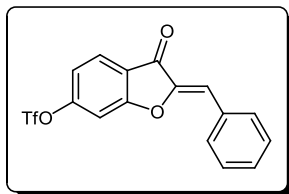
(Z)-2-(4-(benzylamino)benzylidene)benzofuran-3(2H)-one (5.40)



Purified by flash chromatography (Hexane/EtOAc = 80:20) followed by TLC (Hexane/EtOAc = 70:30). Obtained as orange oil, 49% yield. ¹H NMR (400 MHz, CDCl₃): δ = 7.82-7.80 (m, 3H, H₄+2H_{2'}), 7.62 (t, *J* = 7.6 Hz, 1H, H₆), 7.39-7.28 (m, 6H,

H₇+2H_{2''}+2H_{3''}+H_{4''}), 7.20 (m, 1H, H₅), 6.91 (s, 1H, H_{vin}), 6.70 (d, *J* = 8.5 Hz, 2H, 2H_{3'}), 4.66 (br, H, NH), 4.43 (s, 2H, CH₂). ¹³C NMR (100 MHz, CDCl₃): δ = 184.22 (C=O), 165.41 (C_q), 149.82 (C_q), 145.12 (C_q), 138.47 (C_q), 136.08 (C_{ar}), 133.93 (C_{ar}), 128.86 (C_{ar}), 127.59 (C_{ar}), 127.44 (C_{ar}), 124.40 (C_{ar}), 123.03 (C_{ar}), 122.37 (C_q), 121.48 (C_q), 115.21 (C_{vin}), 112.90 (C_{ar}), 112.86 (C_{ar}), 47.71 (CH₂). HRMS calc. (C₂₂H₁₇NO₂): 328.1332. Found: 328.1334.

8.6.5. Synthesis of (Z)-2-benzylidene-3-oxo-2,3-dihydrobenzofuran-6-yl trifluoromethanesulfonate (5.70)

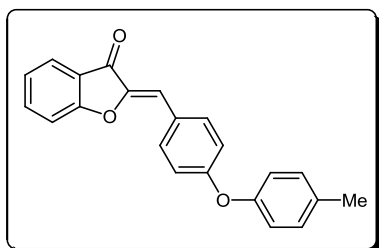


Compound **5.30** (0.25 mmol) was dissolved in dry CH_2Cl_2 (1 mL) and dry TEA (0.275 mmol) was added to the solution followed by Tf_2O (0.275 mmol). The mixture was stirred for 45 minutes at room temperature under N_2 . After completion, water was added to the reaction mixture and the product was extracted with CH_2Cl_2 . The organic layer was washed with water, dried with anhydrous Na_2SO_4 and concentrated under reduced pressure permitting to obtain the pure product. Obtained as yellow solid, 98% yield. ^1H NMR (400 MHz, DMSO-d_6): δ = 8.04-7.97 (m, 4H), 7.53-7.44 (m, 4H), 7.05 (s, 1H, H_{vin}). ^{13}C NMR (101 MHz, DMSO-d_6): δ = 182.17 (C=O), 165.67 (C_q), 154.11 (C_q), 146.55 (C_q), 131.69 (C_{ar}), 131.59 (C_q), 130.56 (C_{ar}), 129.13 (C_{ar}), 126.56 (C_{ar}), 121.37 (C_q), 118.23 (CF_3), 117.57 (C_{ar}), 113.51 (C_{ar}), 107.89 (C_{vin}).

8.6.6. General procedure for the synthesis of ethers derivatives 5.41 and 5.42

To a solution of benzofuran-3(2H)-one (0.57 mmol) in dry methanol (10 mL) at room temperature was added the appropriate aldehyde (0.68 mmol) and Al_2O_3 (0.57 mmol). The mixture was refluxed, under N_2 , for 48 hours. After, the solvent was removed and the solid residue was dissolved in CH_2Cl_2 . The organic layer was washed with water, dried with anhydrous Na_2SO_4 and concentrated under reduced pressure to give the crude product.

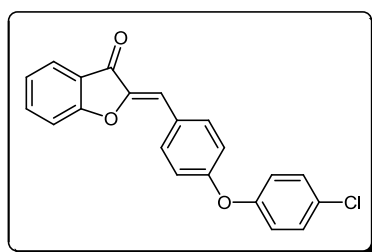
(Z)-2-(4-(p-tolyloxy)benzylidene)benzofuran-3(2H)-one (5.41)



Purified by flash chromatography (Hexane/EtOAc = 80:20). Obtained as yellow solid, 33% yield, mp 116-118 °C. ^1H NMR (400 MHz, DMSO-d_6): δ = 8.02 (d, J = 8.7 Hz, 2H, $2\text{H}_2'$), 7.82-7.79 (m, 2H, H_4+H_6), 7.55 (d, J = 8.5 Hz, 1H, H_7),

7.32 (t, $J = 7.4$ Hz, 1H, H_5), 7.25 (d, $J = 8.3$ Hz, 2H, $2H_{3''}$), 7.07 (d, $J = 8.7$ Hz, 2H, $2H_{3'}$), 7.02 (d, $J = 8.3$ Hz, 2H, $2H_{2''}$), 6.97 (s, 1H, H_{vin}), 2.32 (s, 3H, CH_3). ^{13}C NMR (101 MHz, DMSO-d_6): $\delta = 183.39$ (C=O), 165.72 (C_q), 159.49 (C_q), 153.41 (C_q), 146.06 (C_q), 138.00 (C_{ar}), 134.10 (C_q), 133.99 (C_{ar}), 131.07 (C_{ar}), 126.92 (C_q), 124.72 (C_{ar}), 124.39 (C_{ar}), 121.47 (C_q), 120.11 (C_{ar}), 118.32 (C_{ar}), 113.66 (C_{ar}), 112.51 (C_{vin}), 20.80 (CH_3). Anal. Calcd. ($\text{C}_{22}\text{H}_{16}\text{O}_3 \cdot 0.15\text{H}_2\text{O}$): C, 79.81; H, 5.28%. Found: C, 79.59; H, 5.01%.

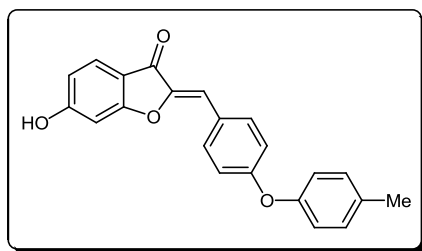
(Z)-2-(4-(4-chlorophenoxy)benzylidene)benzofuran-3(2H)-one (5.42)



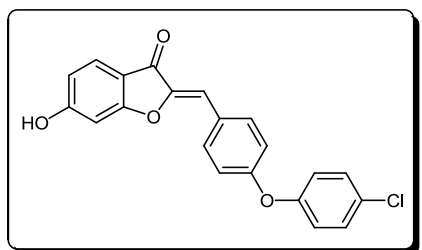
Purified by flash chromatography (Hexane/ $\text{CH}_2\text{Cl}_2 = 50:50$). Obtained as yellow solid, 51% yield, 112-113 °C. ^1H NMR (400 MHz, DMSO-d_6): $\delta = 8.05$ (d, $J = 8.6$ Hz, 2H, $2H_{2'}$), 7.83-7.80 (m, 2H, H_4+H_6), 7.55 (d, $J = 8.5$ Hz, 1H, H_7), 7.48 (d, $J = 8.8$ Hz, 2H, $2H_{2''}$), 7.33 (t, $J = 7.4$ Hz, 1H, H_5), 7.16-7.13 (m, 4H, $2H_{3'}+2H_{3''}$), 6.98 (s, 1H, H_{vin}). ^{13}C NMR (100 MHz, DMSO-d_6): $\delta = 183.95$ (C=O), 165.80 (C_q), 158.44 (C_q), 155.01 (C_q), 146.26 (C_q), 138.08 (C_{ar}), 134.06 (C_{ar}), 130.55 (C_{ar}), 128.54 (C_q), 127.76 (C_q), 124.76 (C_{ar}), 124.44 (C_{ar}), 121.57 (C_{ar}), 121.44 (C_q), 119.14 (C_{ar}), 113.68 (C_{ar}), 112.26 (C_{vin}). Anal. Calcd. ($\text{C}_{21}\text{H}_{13}\text{ClO}_3 \cdot 0.15\text{H}_2\text{O}$): C, 71.76; H, 3.82%. Found: C, 71.37; H, 3.84%.

8.6.7. General procedure for the synthesis of ethers derivatives 5.43 and 5.44

To a solution of 6-hydroxybenzofuran-3(2H)-one (0.57 mmol) in glacial acetic acid (5.7 mL) at room temperature was added the appropriate aldehyde (0.68 mmol) and HCl (cat, 3 drops). The reaction mixture was stirred for 4 hours at room temperature. After, the mixture was dropped in cold water and the precipitate formed was filtered and washed with water.

(Z)-6-hydroxy-2-(4-(*p*-tolylloxy)benzylidene)benzofuran-3(2H)-one (5.43)

Obtained as yellow solid, 51% yield, mp 248-250 °C. ^1H NMR (400 MHz, CDCl_3): δ = 11.22 (br, 1H, OH), 7.96 (d, J = 8.7 Hz, 2H, $2\text{H}_2'$), 7.62 (d, J = 8.4 Hz, 1H, H_4), 7.24 (d, J = 8.1 Hz, 1H, H_3''), 7.06-6.99 (m, 4H, $2\text{H}_3'+2\text{H}_2''$), 6.79-6.77 (m, 2H, $\text{H}_7+\text{H}_{\text{vin}}$), 6.71 (dd, J_1 = 8.4 Hz, J_2 = 1.8 Hz, 1H, H_5). ^{13}C NMR (101 MHz, CDCl_3): δ = 181.38 (C=O), 167.82 (C_q), 166.53 (C_q), 158.67 (C_q), 153.14 (C_q), 146.71 (C_q), 133.59 (C_q), 133.17 (C_{ar}), 130.64 (C_{ar}), 126.73 (C_q), 125.99 (C_{ar}), 119.64 (C_{ar}), 117.92 (C_{ar}), 113.11 (C_{ar}), 112.92 (C_q), 110.14 (C_{ar}), 98.61 (C_{vin}), 20.38 (CH_3). Anal. Calcd. ($\text{C}_{22}\text{H}_{14}\text{O}_4 \cdot 0.2\text{H}_2\text{O}$): C, 75.93; H, 5.05%. Found: C, 75.66; H, 5.03%.

(Z)-2-(4-(4-chlorophenoxy)benzylidene)-6-hydroxybenzofuran-3(2H)-one (5.44)

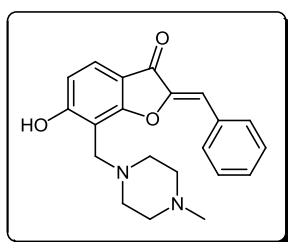
Obtained as yellow solid, 84% yield, mp 243-244 °C. ^1H NMR (400 MHz, CDCl_3): δ = 10.21 (br, 1H, OH), 7.80 (d, J = 8.7 Hz, 2H, $2\text{H}_2'$), 7.56 (d, J = 9.0 Hz, 1H, H_4), 7.27-7.25 (m, 2H, $2\text{H}_2''$), 6.97-6.93 (m, 4H, $2\text{H}_3'+2\text{H}_3''$), 6.67-6.63 (m, 3H, $\text{H}_5+\text{H}_7+\text{H}_{\text{vin}}$). ^{13}C NMR (101 MHz, CDCl_3): δ = 181.39 (C=O), 167.86 (C_q), 166.56 (C_q), 157.59 (C_q), 154.71 (C_q), 146.88 (C_q), 133.24 (C_{ar}), 130.11 (C_{ar}), 128.00 (C_q), 127.56 (C_q), 126.02 (C_{ar}), 121.06 (C_{ar}), 118.72 (C_{ar}), 113.12 (C_{ar}), 112.87 (C_q), 109.91 (C_{vin}), 98.62 (C_{ar}). Anal. Calcd. ($\text{C}_{21}\text{H}_{13}\text{ClO}_4 \cdot 0.15\text{H}_2\text{O}$): C, 68.63; H, 3.66%. Found: C, 68.57; H, 3.64%.

8.6.8. General procedure for the synthesis of Mannich Bases derivatives 5.55 to 5.58

To a solution of (Z)-2-benzylidene-6-hydroxybenzofuran-3(2H)-one (0.29 mmol) in absolute ethanol (1 mL) was added the appropriate amine (0.32 mmol) followed by formaldehyde solution (0.32 mmol). The mixture was refluxed for 3h30. After, the solvent was removed and the solid residue was dissolved in CH_2Cl_2 and extracted with HCl 1M. The aqueous layer was neutralized with NaHCO_3 saturated solution and extracted with

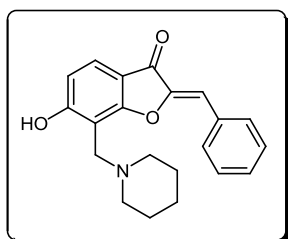
CH₂Cl₂. The organic layer was dried with anhydrous Na₂SO₄ and concentrated under reduced pressure to give the crude product.

(Z)-2-benzylidene-6-hydroxy-7-((4-methylpiperazin-1-yl)methyl)benzofuran-3(2H)-one (5.55)

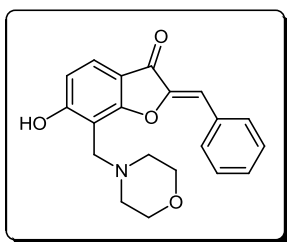


Purified by flash chromatography (CH₂Cl₂/MeOH = 98:2). Obtained as yellow solid, 61% yield, mp 178-179 °C. ¹H NMR (400 MHz, DMSO-d₆): δ = 7.97 (d, *J* = 7.3 Hz, 2H, 2H_{2'}), 7.54-7.49 (m, 3H, H₄+2H_{3'}), 7.45-7.41 (m, 1H, H_{4'}), 6.77 (s, 1H, H_{vin}), 6.65 (d, *J* = 7.3 Hz, 1H, H₅), 3.90 (s, 2H, CH₂), 2.50 (br, 8H, piperazine), 2.18 (s, 3H, CH₃). ¹³C NMR (101 MHz, DMSO-d₆): δ = 181.24 (C=O), 167.75 (C_q), 166.19 (C_q), 147.67 (C_q), 132.32 (C_q), 131.07 (C_{ar}), 129.57 (C_{ar}), 129.05 (C_{ar}), 124.62 (C_{ar}), 113.64 (C_{ar}), 111.48 (C_q), 109.91 (C_{vin}), 105.77 (C_q), 54.30 (CH₂-piperazine), 52.00 (CH₂-piperazine), 50.83 (CH₂), 45.47 (CH₃). Anal. Calcd. (C₂₁H₂₂N₂O₃•0.3H₂O): C, 70.88; H, 6.42; N, 7.87%. Found: C, 70.75; H, 6.48; N, 7.66%.

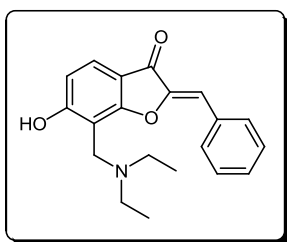
(Z)-2-benzylidene-6-hydroxy-7-(piperidin-1-ylmethyl)benzofuran-3(2H)-one (5.56)



Purified by flash chromatography (CH₂Cl₂/MeOH = 98:2). Obtained as yellow solid, 63% yield, mp 198-200 °C. ¹H NMR (400 MHz, DMSO-d₆): δ = 7.94 (d, *J* = 7.4 Hz, 2H, 2H_{2'}), 7.51-7.41 (m, 4H, H₄+H_{4'}+2H_{3'}), 6.70 (s, 1H, H_{vin}), 6.50-6.45 (m, 1H, H₅), 4.06 (s, 2H, CH₂), 2.82-2.76 (m, 4H, 4H-piperidine), 1.63-1.48 (m, 6H, 6H-piperidine). ¹³C NMR (101 MHz, DMSO-d₆): δ = 180.26 (C=O), 171.55 (C_q), 166.39 (C_q), 148.16 (C_q), 132.50 (C_q), 130.91 (C_{ar}), 129.05 (C_{ar}), 128.28 (C_{ar}), 124.90 (C_{ar}), 115.03 (C_{ar}), 109.47 (C_q), 109.07 (C_{vin}), 103.14 (C_q), 52.69 (CH₂-piperidine), 51.91 (CH₂), 24.49 (CH₂-piperidine), 22.69 (CH₂-piperidine). HRMS calc. (C₂₁H₂₂NO₃): 336.1594. Found: 336.1594.

(Z)-2-benzylidene-6-hydroxy-7-(morpholinomethyl)benzofuran-3(2H)-one (5.57)

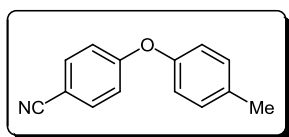
Purified by flash chromatography (CH₂Cl₂/MeOH = 99:1). Obtained as yellow solid, 54% yield, 179-181 °C. ¹H NMR (400 MHz, acetone-d₆): δ = 7.99 (d, *J* = 7.3 Hz, 2H, 2H_{2'}), 7.58-7.44 (m, 4H, H₄+H_{4'}+2H_{3'}), 6.74 (s, 1H, H_{vin}), 6.67 (d, *J* = 8.3 Hz, 1H, H₅), 4.11 (s, 2H, CH₂), 3.96-3.75 (m, 8H, morpholine). ¹³C NMR (101 MHz, acetone-d₆): δ = 167.85 (C_q), 133.51 (C_q), 132.06 (C_{ar}), 129.83 (C_{ar}), 125.38 (C_{ar}), 114.11 (C_{ar}), 111.03 (C_{vin}), 67.21 (CH₂-morpholine), 53.71 (CH₂). Anal. Calcd. (C₂₀H₁₉NO₄•0.25H₂O): C, 70.26; H, 5.76; N, 4.10%. Found: C, 70.17; H, 5.72; N, 4.24%.

(Z)-2-benzylidene-7-((diethylamino)methyl)-6-hydroxybenzofuran-3(2H)-one (5.58)

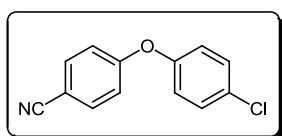
Purified by flash chromatography (CH₂Cl₂/MeOH = 97:3) followed by TLC (CH₂Cl₂/MeOH = 95:5). Obtained as yellow solid, 29% yield, mp 165-167 °C. ¹H NMR (400 MHz, CDCl₃): δ = 7.83 (d, *J* = 7.3 Hz, 2H, 2H_{2'}), 7.60 (d, *J* = 8.4 Hz, 1H, H₄), 7.46 (t, *J* = 7.4 Hz, 2H, 2H_{3'}), 7.40-7.38 (m, 1H, H_{4'}), 6.78 (s, 1H, H_{vin}), 6.62 (d, *J* = 8.4 Hz, 1H, H₅), 4.06 (s, 2H, CH₂), 2.78 (q, *J* = 7.1 Hz, 4H, 2CH₂), 1.21 (t, *J* = 7.1 Hz, 6H, 2CH₃). ¹³C NMR (101 MHz, CDCl₃): δ = 168.93 (C_q), 148.28 (C_q), 132.88 (C_q), 131.23 (C_{ar}), 129.48 (C_{ar}), 129.01 (C_{ar}), 125.22 (C_{ar}), 114.05 (C_{ar}), 112.94 (C_q), 111.17 (C_{vin}), 104.51 (C_q), 49.54 (CH₂), 47.10 (CH₂CH₃), 11.34 (CH₂CH₃).

8.6.9. General procedure for the synthesis of benzonitrile derivatives 5.62 and 5.63

To a solution of the appropriate phenol (1.25 mmol) and 4-fluorobenzonitrile (1.25 mmol) in dry DMF (6 mL) was added Na₂CO₃ (2.5 mmol). The reaction mixture was refluxed for 24 hours. After cooling to room temperature, water was added to the crude and the product was extracted with EtOAc. The organic layer was dried with anhydrous Na₂SO₄ and concentrated under reduced pressure to give the product.

4-(*p*-tolylloxy)benzonitrile (5.62)

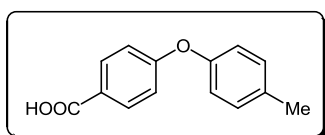
Obtained as transparent oil, 85% yield. ^1H NMR (400 MHz, CDCl_3): $\delta = 7.67$ (d, $J = 9.0$ Hz, 2H, 2H_2), 7.25 (d, $J = 8.9$ Hz, 2H, $2\text{H}_3'$), 7.02 (d, $J = 9.0$ Hz, 2H, 2H_3), 6.98 (d, $J = 8.9$ Hz, 2H, $2\text{H}_2'$), 2.36 (s, 3H, CH_3).

4-(4-chlorophenoxy)benzonitrile (5.63)

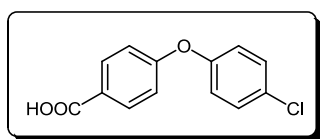
Obtained as white solid, 95%, 67-68 °C. ^1H NMR (400 MHz, CDCl_3): $\delta = 7.71$ (d, $J = 8.5$ Hz, 2H, 2H_2), 7.44 (d, $J = 9.4$ Hz, 2H, $2\text{H}_3'$), 7.10 - 7.07 (m, 4H, $2\text{H}_3+2\text{H}_2'$).

8.6.10. General procedure for the synthesis of carboxylic acid derivatives 5.64 and 5.65

To a solution of the 4-phenoxybenzonitrile derivative (1 mmol) and KOH (20 mmol) in MeOH (0.6 mL) and EtOH (2.6 mmol), H_2O_2 30% (1 mL) was added dropwise. The reaction mixture was refluxed for 4h30. After cooling to room temperature, the mixture was acidized with HCl 3M to pH 1 and the product was extracted with CH_2Cl_2 . The organic layer was dried with anhydrous Na_2SO_4 and concentrated under reduced pressure to give the product.

4-(*p*-tolylloxy)benzoic acid (5.64)

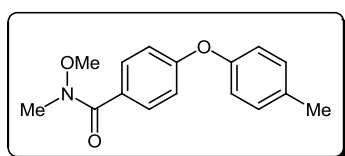
Obtained as white solid, 100% yield, mp 145-147 °C. ^1H NMR (400 MHz, CDCl_3): $\delta = 7.96$ (d, $J = 8.9$ Hz, 2H, 2H_2), 7.21 (d, $J = 8.1$ Hz, 2H, $2\text{H}_3'$), 6.95 - 6.92 (m, 4H, $2\text{H}_3+2\text{H}_2'$), 2.34 (s, 3H, CH_3).

4-(4-chlorophenoxy)benzoic acid (5.65)

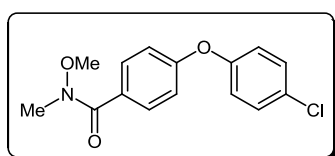
Obtained as white solid, 98% yield, mp 150-152 °C. ^1H NMR (400 MHz, CDCl_3): $\delta = 8.01$ (d, $J = 8.7$ Hz, 2H, 2H_2), 7.39 (d, $J = 8.2$ Hz, 2H, $2\text{H}_3'$), 7.07-7.04 (m, 4H, $2\text{H}_3+2\text{H}_2'$).

8.6.11. General procedure for the synthesis of hydroxamate derivatives 5.66 and 5.67

To a solution of the 4-phenoxybenzoic acid derivative (1 mmol) in dry DMF (8 ml) was added TEA (1 mmol) and TBTU (1.1 mmol) and the mixture was stirred for 30 minutes at room temperature. After, *N,O*-dimethylhydroxylamine (1.2 mmol) and TEA (1.2 mmol) were added, and the final mixture was kept stirring at room temperature for 24 hours. The solvent was removed and the solid residue was dissolved in EtOAc and washed with HCl 3M, saturated solution of Na_2CO_3 and brine. The organic layer was dried with anhydrous Na_2SO_4 and concentrated under reduced pressure to give the crude product.

***N*-methoxy-*N*-methyl-4-(*p*-tolylloxy)benzamide (5.66)**

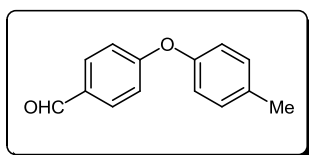
Obtained as transparent oil, 99% yield. ^1H NMR (400 MHz, CDCl_3): $\delta = 7.70$ (d, $J = 8.8$ Hz, 2H, 2H_2), 7.17 (d, $J = 8.3$ Hz, 2H, $2\text{H}_3'$), 6.97-6.94 (m, 4H, $2\text{H}_3+2\text{H}_2'$), 3.57 (s, 3H, OCH_3), 3.36 (s, 3H, NCH_3), 2.35 (s, 3H, CH_3).

4-(4-chlorophenoxy)-*N*-methoxy-*N*-methylbenzamide (5.67)

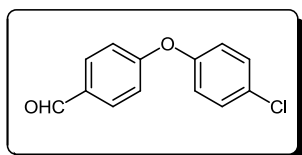
Obtained as yellow oil, 98% yield. ^1H NMR (400 MHz, CDCl_3): $\delta = 7.73$ (d, $J = 8.8$ Hz, 2H, 2H_2), 7.33 (d, $J = 8.9$ Hz, 2H, $2\text{H}_3'$), 7.00-6.96 (m, 4H, $2\text{H}_3+2\text{H}_2'$), 3.57 (s, 3H, OCH_3), 3.36 (s, 3H, NCH_3).

8.6.12. General procedure for the synthesis of benzaldehyde derivatives 5.68 and 5.69

To a solution of the *N*-methoxy-*N*-methyl-4-phenoxybenzoic acid derivative (1 mmol) in dry THF (10 mL) was added LiAlH₄ (1.3 eq). The mixture was stirred for 1 hour at 0 °C. After, a solution of KHSO₄ 5% was added to stop the reaction and the product was extracted with Et₂O. The organic layer was then washed with HCl 3M, saturated solution of Na₂CO₃, H₂O and brine. The organic layer was dried with anhydrous Na₂SO₄ and concentrated under reduced pressure to give the crude product.

4-(*p*-toloxy)benzaldehyde (5.68)

Obtained as white solid, 100% yield, mp 49-51 °C. ¹H NMR (400 MHz, CDCl₃): δ = 9.91 (s, 1H, H_{ald}), 7.83 (d, *J* = 8.7 Hz, 2H, 2H₂), 7.21 (d, *J* = 8.3 Hz, 2H, 2H_{3'}), 7.03 (d, *J* = 8.7 Hz, 2H, 2H₃), 6.98 (d, *J* = 8.3 Hz, 2H, 2H_{2'}), 2.37 (s, 3H, CH₃).

4-(4-chlorophenoxy)benzaldehyde (5.69)

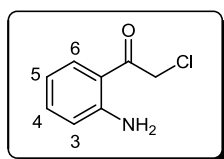
Obtained as white solid, 89%, mp 57-58 °C. ¹H NMR (400 MHz, CDCl₃): δ = 9.93 (s, 1H, H_{ald}), 7.86 (d, *J* = 8.7 Hz, 2H, 2H₂), 7.38 (d, *J* = 8.9 Hz, 2H, 2H_{3'}), 7.07-7.02 (m, 4H, 2H₃+2H_{2'}).

8.7. Synthesis of azaaurone derivatives**8.7.1. General procedure for the synthesis of compounds 6.87 to 6.91**

To a solution of the appropriate aniline (1.6 mmol) in dry dichloroethane (10 mL) at room temperature, a solution of BCl₃ 1M in CH₂Cl₂ (5.2 mL, 5.2 mmol) was added dropwise. After that, chloroacetonitrile (350 μL, 5.5 mmol) and ZnCl₂ (870 mg, 6.4 mmol) was added to the reaction mixture. The mixture was refluxed, under N₂, for 24 hours. Afterward, a

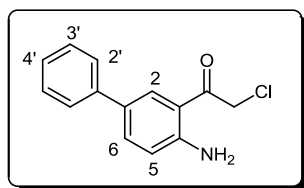
solution of HCl 1M (10 mL) was added and the mixture was refluxed once more during 1 hour. After cooling, the reaction mixture was extracted with CH_2Cl_2 , dried with anhydrous Na_2SO_4 and concentrated under reduced pressure to give the product.

1-(2-aminophenyl)-2-chloroethanone (6.87)



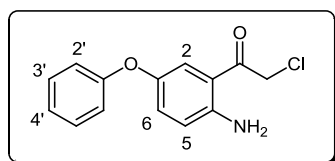
Obtained as yellow solid, yield 72%, mp 107-109 °C. ^1H NMR (400 MHz, CDCl_3) δ = 7.62 (dd, J_1 = 8.2 Hz, J_2 = 1.4 Hz, 1H, H_6), 7.23 (dt, J_1 = 8.2 Hz, J_2 = 1.4 Hz, 1H, H_5), 6.65 (dd, J_1 = 8.5 Hz, J_2 = 1.4 Hz, 1H, H_3), 6.60 (dt, J_1 = 8.5 Hz, J_2 = 1.4 Hz, 1H, H_4), 4.61 (s, 2H, CH_2).

1-(4-aminobiphenyl-3-yl)-2-chloroethanone (6.88)

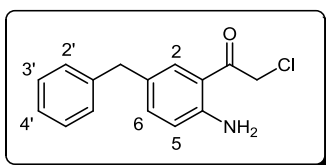


Obtained as brown oil, yield 47%. ^1H NMR (400 MHz, CDCl_3) δ = 7.83 (s, 1H, H_2), 7.58 (d, 1H, J = 8.5 Hz, H_6), 7.51 (d, 2H, J = 7.7 Hz, $2\text{H}_{2'}$), 7.43 (t, 2H, J = 7.6 Hz, $2\text{H}_{3'}$), 7.32 (t, 1H, J = 7.6 Hz, $\text{H}_{4'}$), 6.82 (d, 1H, J = 8.5 Hz, H_5), 4.75 (s, 2H, CH_2Cl).

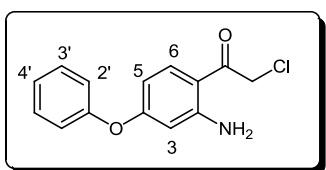
1-(2-amino-5-phenoxyphenyl)-2-chloroethanone (6.89)



Obtained as brown oil, yield 70%. ^1H NMR (400 MHz, CDCl_3) δ = 7.33-7.29 (m, 3H, $\text{H}_2+2\text{H}_{3'}$), 7.12-7.04 (m, 2H, $\text{H}_6+\text{H}_{4'}$), 6.93 (d, 2H, J = 8.5 Hz, $2\text{H}_{2'}$), 6.63 (d, 1H, J = 9.0 Hz, H_5), 4.60 (s, 2H, CH_2Cl).

1-(2-amino-5-benzylphenyl)-2-chloroethanone (6.90)

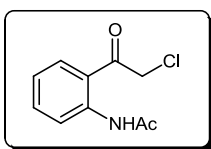
Obtained as brown oil, yield 43%. $^1\text{H NMR}$ (400 MHz, CDCl_3) δ = 7.63 (s, 1H, H_2), 7.27-7.19 (m, 6H, $\text{H}_6+2\text{H}_{2'}+2\text{H}_{3'}+\text{H}_{4'}$), 6.71 (d, $J = 8.7$ Hz, 1H, H_5), 4.61 (s, 2H, CH_2Cl), 3.71 (s, 2H, CH_2).

1-(2-amino-4-phenoxyphenyl)-2-chloroethanone (6.91)

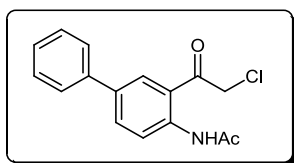
Obtained as brown oil, yield 43%. $^1\text{H NMR}$ (400 MHz, CDCl_3) δ = 7.61 (d, $J = 8.56$ Hz, 1H, H_6), 7.23 (t, $J = 8.3$ Hz, 2H, $2\text{H}_{3'}$), 7.01-6.97 (m, 3H, $2\text{H}_{2'}+\text{H}_{4'}$), 6.57 (d, $J = 8.5$ Hz, 1H, H_5), 6.42 (s, 1H, H_3), 4.69 (s, 2H, CH_2Cl).

8.7.2. General procedure for the synthesis of compounds 6.92 to 6.96

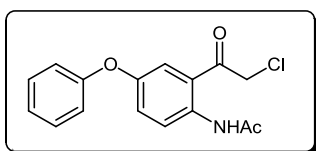
The appropriate starting material (5 mmol) was dissolved in acetic anhydride (5 mL) and the solution was heated at 90 °C for 1 hour. After completion, the solvent was evaporated under vacuum. The residue was dissolved in CH_2Cl_2 and passed through a silica gel layer to remove the polar fraction. The eluate was concentrated under reduced pressure to give the product.

***N*-(2-(2-chloroacetyl)phenyl)acetamide (6.92)**

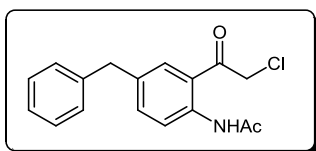
Obtained as beige solid, yield 92%, mp 120-121 °C. $^1\text{H NMR}$ (400 MHz, CDCl_3) δ = 11.36 (s, 1H, NH), 8.78 (d, $J = 8.0$ Hz, 1H, H_3), 7.82 (d, $J = 8.1$ Hz, 1H, H_6), 7.61 (t, $J = 8.0$ Hz, 1H, H_4), 7.14 (t, $J = 8.1$ Hz, 1H, H_5), 4.80 (s, 2H, CH_2), 2.25 (s, 3H, CH_3).

***N*-(3-(2-chloroacetyl)biphenyl-4-yl)acetamide (6.93)**

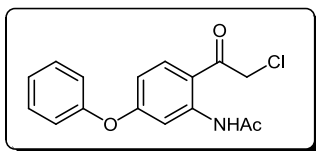
Obtained as yellow oil, yield 70%. ^1H NMR (400 MHz, CDCl_3) δ = 11.34 (s, 1H, NH), 8.86 (d, J = 8.8 Hz, 1H, H_5), 7.99 (s, 1H, H_2), 7.83 (d, J = 8.8 Hz, 1H, H_4), 7.57-7.38 (m, 5H, $2\text{H}_2'+2\text{H}_3'+\text{H}_4'$), 4.85 (s, 2H, CH_2Cl), 2.27 (s, 3H, CH_3).

***N*-(2-(2-chloroacetyl)-4-phenoxyphenyl)acetamide (6.94)**

Obtained as yellow oil, yield 91%. ^1H NMR (400 MHz, CDCl_3) δ = 11.05 (s, 1H, NH), 8.75 (d, J = 9.2 Hz, 1H, H_5), 7.45-7.05 (m, 5H, $\text{H}_2+\text{H}_5+2\text{H}_3'+\text{H}_4'$), 6.99 (d, J = 8.4 Hz, 2H, H_2'), 4.69 (s, 2H, CH_2Cl), 2.24 (s, 3H, CH_3).

***N*-(4-benzyl-2-(2-chloroacetyl)phenyl)acetamide (6.95)**

Obtained as yellow oil, yield 87%. ^1H NMR (400 MHz, CDCl_3) δ = 11.24 (s, 1H, NH), 8.69 (d, J = 8.7 Hz, 1H, H_5), 7.57 (s, 1H, H_2), 7.45 (d, J = 8.7 Hz, 1H, H_4), 7.33-7.22 (m, 5H, H), 7.16 (d, J = 7.4 Hz, 2H, H_2'), 4.71 (s, 2H, CH_2Cl), 3.99 (s, 2H, CH_2), 2.23 (s, 3H, CH_3).

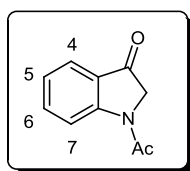
***N*-(2-(2-chloroacetyl)-5-phenoxyphenyl)acetamide (6.96)**

Obtained as yellow oil, yield 83%. ^1H NMR (400 MHz, CDCl_3) δ = 11.63 (s, 1H, NH), 8.45 (s, 1H, H_3), 7.79 (d, J = 9.0 Hz, 1H, H_6), 7.47-7.42 (m, 2H, $2\text{H}_3'$), 7.27 (t, J = 7.5 Hz, 1H, H_4'), 7.12 (d, J = 7.5 Hz, 2H, $2\text{H}_2'$), 4.72 (s, 2H, CH_2Cl), 2.22 (s, 3H, CH_3).

8.7.3. General procedure for the synthesis of compounds 6.97 to 6.101

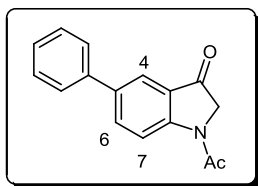
The appropriate starting material (4 mmol) was dissolved in dry DMF (10 mL) and NaH (6 mmol) was added slowly to the reaction mixture, under N₂, at 0 °C. The mixture was stirred for 1 hour at room temperature and the reaction was quenched with the addition of a solution of KHSO₄ (5%). The reaction mixture was extracted with ethyl acetate and the organic layers were combined, dried with anhydrous Na₂SO₄ and concentrated under reduced pressure to give the crude product.

1-acetylimidolin-3-one (6.97)



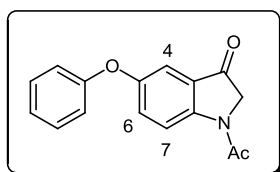
Purified by flash chromatography (CH₂Cl₂). Obtained as white solid, yield 45%, mp 131-133 °C. ¹H NMR (400 MHz, CDCl₃) δ = 8.56 (d, *J* = 8.0 Hz, 1H, H₄), 7.75 (d, *J* = 7.8 Hz, 1H, H₇), 7.67 (t, *J* = 8.0 Hz, 1H, H₅), 7.22 (t, *J* = 7.8 Hz, 1H, H₆), 4.30 (s, 2H, CH₂), 2.32 (s, 3H, CH₃).

1-acetyl-5-phenylimidolin-3-one (6.98)



Purified by flash chromatography (CH₂Cl₂). Obtained as yellow oil, yield 38%. ¹H NMR (400 MHz, CDCl₃) δ = 8.63 (d, *J* = 8.3 Hz, 1H, H₇), 7.97 (s, 1H, H₄), 7.93 (d, *J* = 8.3 Hz, 1H, H₆), 7.60 (d, *J* = 7.4 Hz, 2H, 2H_{2'}), 7.46 (t, *J* = 7.4 Hz, 2H, 2H_{3'}), 7.39 (t, *J* = 7.4, 1H, H_{4'}), 4.36 (s, 2H, CH₂), 2.35 (s, 3H, CH₃).

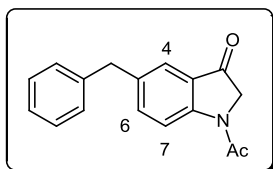
1-acetyl-5-phenoxyimidolin-3-one (6.99)



Purified by flash chromatography (CH₂Cl₂). Obtained as yellow oil, yield 31%. ¹H NMR (400 MHz, CDCl₃) δ = 8.75 (d, *J* = 9.3 Hz, 1H, H₇), 7.44 (s, 1H, H₄), 7.37 (t, *J* = 7.4 Hz, 2H, 2H_{3''}), 7.31 (d, *J* = 9.3,

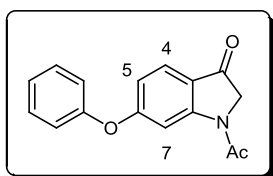
1H, H₆), 7.15 (t, *J* = 7.4 Hz, 1H, H_{4'}), 6.99 (d, *J* = 7.4 Hz, 2H, 2H_{2'}), 4.32 (s, 2H, CH₂), 2.37 (s, 3H, CH₃).

1-acetyl-5-benzylindolin-3-one (6.100)



Purified by flash chromatography (CH₂Cl₂). Obtained as yellow oil, yield 35%. ¹H NMR (400 MHz, CDCl₃) δ = 8.46 (d, *J* = 8.4 Hz, 1H, H₇), 7.54 (s, 1H, H₄), 7.51 (d, *J* = 8.4 Hz, 1H, H₆), 7.32-7.12 (m, 5H, 2H_{2'}+2H_{3'}+H_{4'}), 4.27 (s, 2H, CH₂), 3.98 (s, 2H, ArCH₂Ar), 2.29 (s, 3H, CH₃).

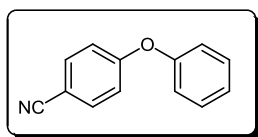
1-acetyl-6-phenoxyindolin-3-one (6.101)



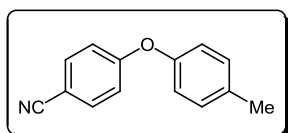
Purified by flash chromatography (CH₂Cl₂). Obtained as yellow oil, yield 29%. ¹H NMR (400 MHz, CDCl₃) δ = 8.22 (d, *J* = 8.7 Hz, 1H, H₄), 7.74 (t, *J* = 7.5 Hz, 2H, 2H_{3'}), 7.55 (d, *J* = 8.7 Hz, 1H, H₅), 7.01-6.98 (m, 4H, H₇+2H_{2'}+H_{4'}), 4.34 (s, 2H, CH₂), 2.26 (s, 3H, CH₃).

8.7.4. General procedure for the synthesis of benzonitrile derivatives 6.102 and 6.104

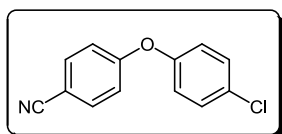
To a solution of the appropriate phenol (1.25 mmol) and 4-fluorobenzonitrile (1.25 mmol) in dry DMF (6 mL) was added Na₂CO₃ (2.5 mmol). The reaction mixture was refluxed for 24 hours. After cooling to room temperature, water was added to the crude and the product was extracted with EtOAc. The organic layer was dried with anhydrous Na₂SO₄ and concentrated under reduced pressure to give the product.

4-phenoxybenzonitrile (6.102)

Obtained as yellow oil, 94%, yield. ^1H NMR (400 MHz, CDCl_3): $\delta = 7.59$ (d, $J = 9.21$ Hz, 2H, 2H_2), 7.41 (t, $J = 8.6$ Hz, 2H, $2\text{H}_3'$), 7.22 (t, $J = 8.6$ Hz, 1H, H_4'), 7.06 (d, $J = 8.6$ Hz, 2H, $2\text{H}_2'$), 7.00 (d, $J = 9.2$ Hz, 2H, 2H_3).

4-(*p*-toloxy)benzonitrile (6.103)

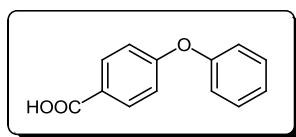
Obtained as white oil, 85%, yield. ^1H NMR (400 MHz, CDCl_3): $\delta = 7.67$ (d, $J = 9.0$ Hz, 2H, 2H_2), 7.25 (d, $J = 8.9$ Hz, 2H, $2\text{H}_3'$), 7.02 (d, $J = 9.0$ Hz, 2H, 2H_3), 6.98 (d, $J = 8.9$ Hz, 2H, $2\text{H}_2'$), 2.36 (s, 3H, CH_3).

4-(4-chlorophenoxy)benzonitrile (6.104)

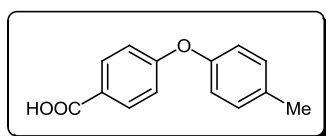
Obtained as white solid, 95%, 67-68 °C. ^1H NMR (400 MHz, CDCl_3): $\delta = 7.71$ (d, $J = 8.5$ Hz, 2H, 2H_2), 7.44 (d, $J = 9.4$ Hz, 2H, $2\text{H}_3'$), 7.10 - 7.07 (m, 4H, $2\text{H}_3+2\text{H}_2'$).

8.7.5. General procedure for the synthesis of carboxylic acid derivatives 6.105 and 6.107

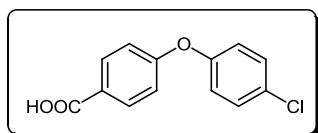
To a solution of the 4-phenoxybenzonitrile derivative (1 mmol) and KOH (20 mmol) in MeOH (0.6 mL) and EtOH (2.6 mmol), H_2O_2 30% (1 mL) was added dropwise. The reaction mixture was refluxed for 4h30. After cooling to room temperature, the mixture was acidized with HCl 3M to pH 1 and the product was extracted with CH_2Cl_2 . The organic layer was dried with anhydrous Na_2SO_4 and concentrated under reduced pressure to give the product.

4-phenoxybenzoic acid (6.105)

Obtained as white solid, 96% yield, mp 161-163 °C. ^1H NMR (400 MHz, CDCl_3): δ = 8.08 (d, J = 8.7 Hz, 2H, 2H_2), 7.41 (t, J = 7.4 Hz, 2H, $2\text{H}_3'$), 7.21 (t, J = 7.4 Hz, 1H, H_4'), 7.09 (d, J = 7.4 Hz, 2H, $2\text{H}_2'$), 7.01 (d, J = 8.7 Hz, 2H, $2\text{H}_3'$).

4-(*p*-tolylloxy)benzoic acid (6.106)

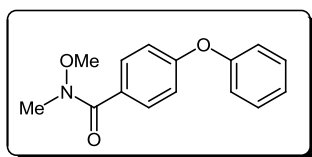
Obtained as white solid, 100% yield, mp 145-147 °C. ^1H NMR (400 MHz, CDCl_3): δ = 7.96 (d, J = 8.9 Hz, 2H, 2H_2), 7.21 (d, J = 8.1 Hz, 2H, $2\text{H}_3'$), 6.95-6.92 (m, 4H, $2\text{H}_3+2\text{H}_2'$), 2.34 (s, 3H, CH_3).

4-(4-chlorophenoxy)benzoic acid (6.107)

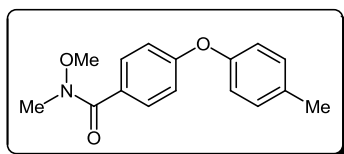
Obtained as transparent solid, 98% yield, mp 150-152 °C. ^1H NMR (400 MHz, CDCl_3): δ = 8.01 (d, J = 8.7 Hz, 2H, 2H_2), 7.39 (d, J = 8.2 Hz, 2H, $2\text{H}_3'$), 7.07-7.04 (m, 4H, $2\text{H}_3+2\text{H}_2'$).

8.7.6. General procedure for the synthesis of hydroxamate derivatives 6.108 and 6.110

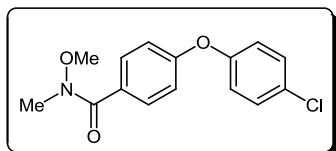
To a solution of the 4-phenoxybenzoic acid derivative (1 mmol) in dry DMF (8 ml) was added TEA (1 mmol) and TBTU (1.1 mmol) and the mixture was stirred for 30 minutes at room temperature. After, *N,O*-dimethylhydroxylamine (1.2 mmol) and TEA (1.2 mmol) were added, and the final mixture was kept stirring at room temperature for 24 hours. The solvent was removed and the solid residue was dissolved in EtOAc and washed with HCl 3M, saturated solution of Na_2CO_3 and brine. The organic layer was dried with anhydrous Na_2SO_4 and concentrated under reduced pressure to give the crude product.

***N*-methoxy-*N*-methyl-4-phenoxybenzamide (6.108)**

Obtained as yellow oil, 90% yield. ^1H NMR (400 MHz, CDCl_3): δ = 7.64 (d, J = 8.7 Hz, 2H, 2H_2), 7.36 (t, J = 8.2 Hz, 2H, $2\text{H}_3'$), 7.15 (t, J = 8.2 Hz, 1H, H_4'), 7.01 (d, J = 8.2 Hz, 2H, $2\text{H}_2'$), 6.95 (d, J = 8.7 Hz, 2H, 2H_3), 3.55 (s, 3H, OCH_3), 3.31 (s, 3H, NCH_3).

***N*-methoxy-*N*-methyl-4-(*p*-tolxyloxy)benzamide (6.109)**

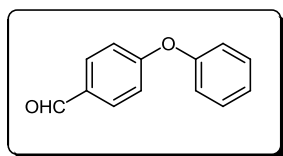
Obtained as transparent oil, 99% yield. ^1H NMR (400 MHz, CDCl_3): δ = 7.70 (d, J = 8.8 Hz, 2H, 2H_2), 7.17 (d, J = 8.3 Hz, 2H, $2\text{H}_3'$), 6.97-6.94 (m, 4H, $2\text{H}_3+2\text{H}_2'$), 3.57 (s, 3H, OCH_3), 3.36 (s, 3H, NCH_3), 2.35 (s, 3H, CH_3).

4-(4-chlorophenoxy)-*N*-methoxy-*N*-methylbenzamide (6.110)

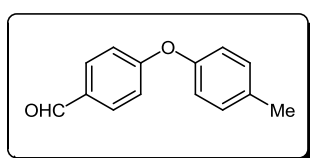
Obtained as yellow oil, 98% yield. ^1H NMR (400 MHz, CDCl_3): δ = 7.73 (d, J = 8.8 Hz, 2H, 2H_2), 7.33 (d, J = 8.9 Hz, 2H, $2\text{H}_3'$), 7.00-6.96 (m, 4H, $2\text{H}_3+2\text{H}_2'$), 3.57 (s, 3H, OCH_3), 3.36 (s, 3H, NCH_3).

8.7.7. General procedure for the synthesis of benzaldehyde derivatives 6.111 and 6.113

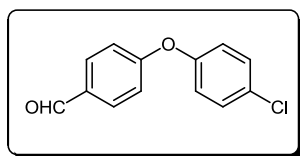
To a solution of the *N*-methoxy-*N*-methyl-4-phenoxybenzoic acid derivative (1 mmol) in dry THF (10 mL) was added LiAlH_4 (1.3 eq). The mixture was stirred for 1 hour at 0 °C. After, a solution of KHSO_4 5% was added to stop the reaction and the product was extracted with Et_2O . The organic layer was then washed with HCl 3M, saturated solution of Na_2CO_3 , H_2O and brine. The organic layer was dried with anhydrous Na_2SO_4 and concentrated under reduced pressure to give the product.

4-phenoxybenzaldehyde (6.111)

Obtained as yellow oil, 96% yield. ^1H NMR (400 MHz, CDCl_3): δ = 9.87 (s, 1H, H_{ald}), 7.88 (d, J = 8.6 Hz, 2H, 2H_2), 7.44 (t, J = 8.3 Hz, 2H, $2\text{H}_{3'}$), 7.24 (t, J = 8.3 Hz, 1H, $\text{H}_{4'}$), 7.10-7.05 (m, 4H, $2\text{H}_3+2\text{H}_2'$).

4-(*p*-tolxyloxy)benzaldehyde (6.112)

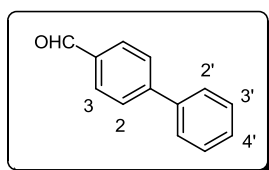
Obtained as transparent solid, 100% yield, mp 49-51 °C. ^1H NMR (400 MHz, CDCl_3): δ = 9.91 (s, 1H, H_{ald}), 7.83 (d, J = 8.7 Hz, 2H, 2H_2), 7.21 (d, J = 8.3 Hz, 2H, $2\text{H}_{3'}$), 7.03 (d, J = 8.7 Hz, 2H, 2H_3), 6.98 (d, J = 8.3 Hz, 2H, $2\text{H}_2'$), 2.37 (s, 3H, CH_3).

4-(4-chlorophenoxy)benzaldehyde (6.113)

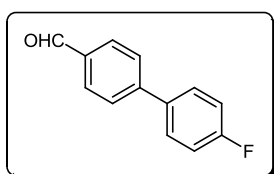
Obtained as white solid, 89%, mp 57-58 °C. ^1H NMR (400 MHz, CDCl_3): δ = 9.93 (s, 1H, H_{ald}), 7.86 (d, J = 8.7 Hz, 2H, 2H_2), 7.38 (d, J = 8.9 Hz, 2H, $2\text{H}_{3'}$), 7.07-7.02 (m, 4H, $2\text{H}_3+2\text{H}_2'$).

8.7.8. General procedure for the synthesis of benzaldehydes derivatives 6.114 to 6.133 via Suzuki Coupling

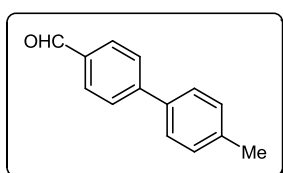
To a solution of the appropriate benzaldehyde (1 mmol) in dioxane (10 mL) was added $\text{Pd}(\text{PPh}_3)_2\text{Cl}_2$ (0.1 mmol) and Na_2CO_3 1M (3 mL) followed by the proper boronic acid (1.2 mmol). The resulting mixture was degassed and stirred at 100 °C for 3 hours under N_2 . After cooling to room temperature, the reaction mixture was diluted with CH_2Cl_2 , filtered under celite and concentrated under pressure to give the crude product.

Biphenyl-4-carbaldehyde (6.114)

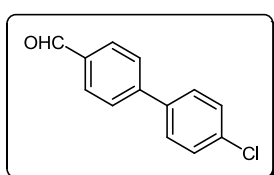
Purified by flash chromatography (Hexane/EtOAc = 90:10). Obtained as white solid, yied 99%, mp 58-59 °C. ^1H NMR (400 MHz, CDCl_3) δ = 10.05 (s, 1H, H_{ald}), 7.95 (d, J = 8.1 Hz, 2H, 2H_3), 7.74 (d, J = 8.1 Hz, 2H, 2H_2), 7.64 (d, J = 7.4 Hz, 2H, $2\text{H}_{2'}$), 7.49 (t, J = 7.4 Hz, 2H, $2\text{H}_{3'}$), 7.42 (t, J = 7.4 Hz, 1H, $\text{H}_{4'}$).

4'-fluorobiphenyl-4-carbaldehyde (6.115)

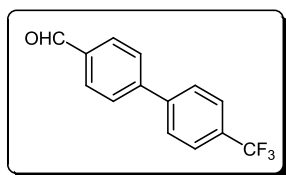
Purified by flash chromatography (Hexane/EtOAc = 90:10). Obtained as transparent oil, yied 96%. ^1H NMR (400 MHz, CDCl_3) δ = 10.06 (s, 1H, H_{ald}), 7.95 (d, J = 8.2 Hz, 2H, 2H_3), 7.71 (d, J = 8.2 Hz, 2H, 2H_2), 7.65-7.56 (m, 2H, $\text{H}_{2'}$), 7.17 (t, J = 8.7 Hz, 2H, $\text{H}_{3'}$).

4'-methylbiphenyl-4-carbaldehyde (6.116)

Purified by flash chromatography (Hexane/EtOAc = 90:10). Obtained as white solid, yied 94%, mp 104-106 °C. ^1H NMR (400 MHz, CDCl_3) δ = 10.05 (s, 1H, H_{ald}), 7.94 (d, J = 8.0 Hz, 2H, 2H_3), 7.74 (d, J = 8.0 Hz, 2H, 2H_2), 7.55 (d, J = 7.9 Hz, 2H, $2\text{H}_{2'}$), 7.28 (d, J = 7.9 Hz, 2H, $2\text{H}_{3'}$), 2.42 (s, 3H, CH_3).

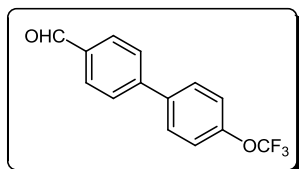
4'-chlorobiphenyl-4-carbaldehyde (6.117)

Purified by flash chromatography (Hexane/EtOAc = 90:10). Obtained as white solid, yied 99%, mp 115-117 °C. ^1H NMR (400 MHz, CDCl_3) δ = 10.05 (s, 1H, H_{ald}), 7.95 (d, J = 8.3 Hz, 2H, $2\text{H}_{3'}$), 7.71 (d, J = 8.3 Hz, 2H, $2\text{H}_{2'}$), 7.56 (d, J = 8.6 Hz, 2H, 2H_2), 7.44 (d, J = 8.6 Hz, 2H, 2H_3).

4'-(trifluoromethyl)biphenyl-4-carbaldehyde (6.118)

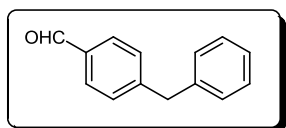
7.78-7.74 (m, 6H, 2H₂+2H_{2'}+2H_{3'}).

Purified by flash chromatography (Hexane/EtOAc = 92:8).
Obtained as white solid, yied 89%, mp 71-73 °C. ¹H NMR (400 MHz, CDCl₃) δ = 10.09 (s, 1H, H_{ald}), 7.99 (d, *J* = 8.1 Hz, 2H, 2H₃),

4'-(trifluoromethoxy)biphenyl-4-carbaldehyde (6.119)

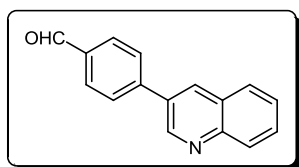
Hz, 2H, 2H₂), 7.63 (d, *J* = 7.8 Hz, 2H, H_{2'}), 7.11 (d, *J* = 7.8 Hz, 2H, 2H_{3'}).

Purified by flash chromatography (Hexane/EtOAc = 90:10).
Obtained as transparent oil, yied 91%. ¹H NMR (400 MHz, CDCl₃)
δ = 10.03 (s, 1H, H_{ald}), 7.98 (d, *J* = 8.2 Hz, 2H, 2H₃), 7.82 (d, *J* = 8.2

4-benzylbenzaldehyde (6.120)

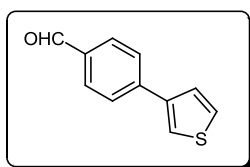
2H₂+2H_{2'}+2H_{3'}), 4.09 (s, 2H, CH₂).

Purified by flash chromatography (Hexane/EtOAc = 95:5).
Obtained as transparent oil, yied 78%. ¹H NMR (400 MHz, CDCl₃) δ
= 10.00 (s, 1H, H_{ald}), 7.84 (d, *J* = 7.9 Hz, 2H, 2H₃), 7.39-7.21 (m, 6H,

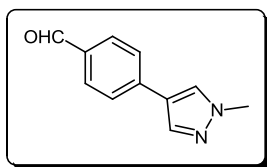
4-(quinolin-3-yl)benzaldehyde (6.121)

Hz, 1H, H_{6'}), 7.62 (t, *J* = 8.1, 1H, H_{7'}).

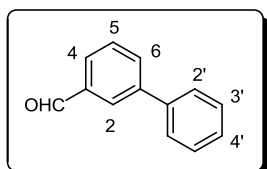
Purified by flash chromatography (Hexane/EtOAc = 85:15).
Obtained as light yellow oil, yied 98%. ¹H NMR (400 MHz, CDCl₃)
δ = 10.10 (s, 1H, H_{ald}), 9.21 (s, 1H, H_{2'}), 8.39 (s, 1H, H_{4'}), 8.17 (d, *J*
= 8.2 Hz, 1H, H_{5'}), 8.04 (d, *J* = 8.2 Hz, 2H, 2H₃), 7.93-7.88 (m, 3H, 2H₂+H_{8'}), 7.78 (t, *J* = 8.2

4-(thiophen-3-yl)benzaldehyde (6.122)

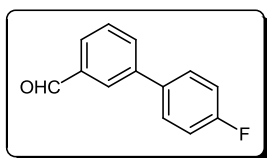
Purified by flash chromatography (Hexane/EtOAc = 92:8). Obtained as light yellow oil, yield 89%. ^1H NMR (400 MHz, CDCl_3) δ = 10.02 (s, 1H, H_{ald}), 7.92 (d, J = 8.1 Hz, 2H, 2H_3), 7.76 (d, J = 8.1 Hz, 2H, 2H_2), 7.62 (s, 1H, $\text{H}_{2'}$), 7.45 (s, 2H, $\text{H}_{4'}+\text{H}_{5'}$).

4-(1-methyl-1H-pyrazol-4-yl)benzaldehyde (6.123)

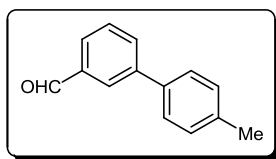
Purified by flash chromatography (Hexane/EtOAc = 60:40). Obtained as light yellow oil, yield 91%. ^1H NMR (400 MHz, CDCl_3) δ = 9.94 (s, 1H, H_{ald}), 7.84-7.82 (m, 3H, $2\text{H}_3+\text{H}_{3'}$), 7.70 (s, 1H, $\text{H}_{5'}$), 7.59 (d, J = 8.0 Hz, 2H, 2H_2), 3.94 (s, 3H, CH_3).

Biphenyl-3-carbaldehyde (6.124)

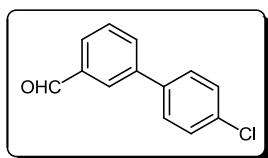
Purified by flash chromatography (Hexane/EtOAc = 90:10). Obtained as transparent oil, yield 99%. ^1H NMR (400 MHz, CDCl_3) δ = 10.07 (s, 1H, H_{ald}), 8.10 (s, 1H, H_2), 7.88-7.83 (m, 2H, H_4+H_6), 7.72-7.54 (m, 3H, $\text{H}_5+2\text{H}_{2'}$), 7.48 (t, J = 7.5 Hz, 2H, $2\text{H}_{3'}$), 7.40 (t, J = 7.5 Hz, 1H, $\text{H}_{4'}$).

4'-fluorobiphenyl-3-carbaldehyde (6.125)

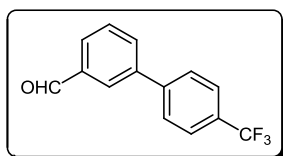
Purified by flash chromatography (Hexane/EtOAc = 90:10). Obtained as transparent oil, yield 95%. ^1H NMR (400 MHz, CDCl_3) δ = 10.06 (s, 1H, H_{ald}), 8.03 (s, 1H, H_2), 7.84 (d, J = 7.5 Hz, 1H, H_4), 7.79 (d, J = 7.5 Hz, 1H, H_6), 7.60-7.55 (m, 3H, $\text{H}_5+2\text{H}_{2'}$), 7.14 (t, J = 8.7 Hz, 2H, $2\text{H}_{3'}$).

4'-methylbiphenyl-3-carbaldehyde (6.126)

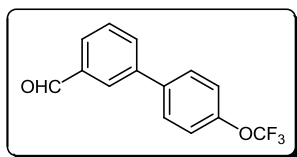
Purified by flash chromatography (Hexane/EtOAc = 90:10).
 Obtained as transparent oil, yield 96%. $^1\text{H NMR}$ (400 MHz, CDCl_3) δ = 10.08 (s, 1H, H_{ald}), 8.09 (s, 1H, H_2), 7.90-7.76 (m, 2H, H_4+H_6), 7.60 (t, $J = 7.7$ Hz, 1H, H_5), 7.53 (d, $J = 8.0$ Hz, 2H, $2\text{H}_2'$), 7.29 (d, $J = 8.0$ Hz, 2H, $2\text{H}_3'$), 2.42 (s, 3H, CH_3).

4'-chlorobiphenyl-3-carbaldehyde (6.127)

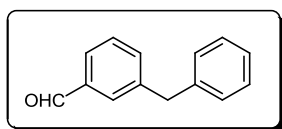
Purified by flash chromatography (Hexane/EtOAc = 90:10).
 Obtained as white solid, yield 97%, mp 58-60 °C. $^1\text{H NMR}$ (400 MHz, CDCl_3) δ = 10.07 (s, 1H, H_{ald}), 8.05 (s, 1H, H_2), 7.86 (d, $J = 7.6$ Hz, 1H, H_4), 7.80 (d, $J = 7.6$ Hz, 1H, H_6), 7.60 (t, $J = 7.6$ Hz, 1H, H_5), 7.54 (d, $J = 8.5$ Hz, 2H, $2\text{H}_2'$), 7.43 (d, $J = 8.5$ Hz, 2H, $2\text{H}_3'$).

4'-(trifluoromethyl)biphenyl-3-carbaldehyde (6.128)

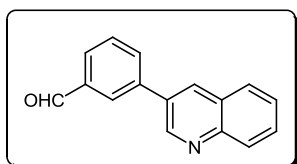
Purified by flash chromatography (Hexane/EtOAc = 92:8).
 Obtained as transparent oil, yield 82%. $^1\text{H NMR}$ (400 MHz, CDCl_3) δ = 10.11 (s, 1H, H_{ald}), 8.12 (s, 1H, H_2), 7.92 (d, $J = 7.6$ Hz, 1H, H_4), 7.87 (d, $J = 7.6$ Hz, 1H, H_6), 7.74 (s, 4H, $2\text{H}_2'+2\text{H}_3'$), 7.66 (t, $J = 7.6$ Hz, 1H, H_5).

4'-(trifluoromethoxy)biphenyl-3-carbaldehyde (6.129)

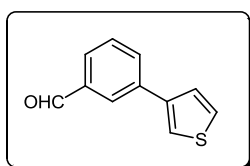
Purified by flash chromatography (Hexane/EtOAc = 90:10).
 Obtained as transparent oil, yield 89%. $^1\text{H NMR}$ (400 MHz, CDCl_3) δ = 10.09 (s, 1H, H_{ald}), 8.25 (s, 1H, H_2), 7.90 (d, $J = 7.6$ Hz, 1H, H_4), 7.87 (d, $J = 7.6$ Hz, 1H, H_6), 7.65-7.62 (m, 3H, $\text{H}_5+2\text{H}_2'$), 7.10 (d, $J = 8.5$ Hz, 2H, $2\text{H}_3'$).

3-benzylbenzaldehyde (6.130)

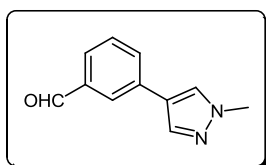
Purified by flash chromatography (Hexane/EtOAc = 95:5).
 Obtained as transparent oil, yield 69%. $^1\text{H NMR}$ (400 MHz, CDCl_3) δ = 10.01 (s, 1H, H_{ald}), 7.77-7.75 (m, 2H, H_2+H_4), 7.51-7.48 (m, 2H, H_5+H_6), 7.50-7.48 (m, 2H, $2\text{H}_{2'}$), 7.29-7.24 (m, 3H, $2\text{H}_{3'}+\text{H}_{4'}$).

3-(quinolin-3-yl)benzaldehyde (6.131)

Purified by flash chromatography (Hexane/EtOAc = 85:15).
 Obtained as light yellow oil, yield 92%. $^1\text{H NMR}$ (400 MHz, CDCl_3) δ = 10.14 (s, 1H, H_{ald}), 9.20 (s, 1H, $\text{H}_{2'}$), 8.38 (s, 1H, $\text{H}_{4'}$), 8.24 (s, 1H, H_2), 8.16 (d, $J = 8.1$ Hz, 1H, $\text{H}_{5'}$), 8.05-7.84 (m, 3H, $\text{H}_4+\text{H}_6+\text{H}_8$), 7.79-7.69 (m, 2H, H_5+H_6), 7.61 (t, $J = 8.0$ Hz, 1H, $\text{H}_{7'}$).

3-(thiophen-3-yl)benzaldehyde (6.132)

Purified by flash chromatography (Hexane/EtOAc = 92:8). Obtained as light yellow oil, yield 82%. $^1\text{H NMR}$ (400 MHz, CDCl_3) δ = 10.07 (s, 1H, H_{ald}), 8.10 (s, 1H, H_2), 7.87 (d, $J = 7.7$ Hz, 1H, H_4), 7.80 (d, $J = 7.7$ Hz, 1H, H_6), 7.59-7.56 (m, 2H, $\text{H}_5+\text{H}_{2'}$), 7.44 (s, 2H, $\text{H}_{4'}+\text{H}_{5'}$).

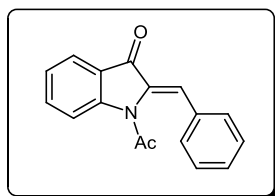
3-(1-methyl-1H-pyrazol-4-yl)benzaldehyde (6.133)

Purified by flash chromatography (Hexane/EtOAc = 60:40).
 Obtained as light yellow oil, yield 86%. $^1\text{H NMR}$ (400 MHz, CDCl_3) δ = 9.99 (s, 1H, H_{ald}), 7.92 (s, 1H, H_2), 7.79 (s, 1H, $\text{H}_{3'}$), 7.68-7.67 (m, 3H, $\text{H}_4+\text{H}_6+\text{H}_{5'}$), 7.48 (t, $J = 7.6$ Hz, 1H, H_5).

8.7.9. General procedure for the synthesis of azaaurone derivatives 6.25 to 6.55

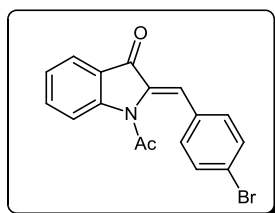
To a solution of the appropriate 1-acetylindolin-3-one derivative (0.5 mmol) in toluene (5 mL) at room temperature was added the proper aldehyde (1.2 mmol) and piperidine (1 drop). The mixture was refluxed for 24 hours. After reaction completion, the solvent was removed to provide the crude product.

(Z)-1-acetyl-2-benzylideneindolin-3-one

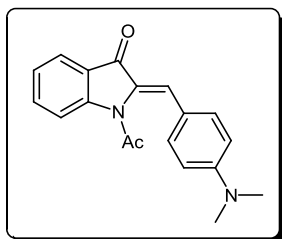


Purified by flash chromatography (Hexane/EtOAc = 95:5). Obtained as light yellow oil, yield 72%. Mixture of isomers *Z/E* = 1:0.60. ^1H NMR (400 MHz, CDCl_3 , more abundant isomer) δ = 8.30 (d, J = 8.3 Hz, 1H, H_4), 7.86 (d, J = 7.6 Hz, 2H, $2\text{H}_{2'}$), 7.70-7.61 (m, 1H, H_5), 7.55 (d, J = 7.6 Hz, 2H, $2\text{H}_{3'}$), 7.45-7.38 (m, 2H, H_6+H_7), 7.35 (s, 1H, H_{vin}), 7.31 (t, J = 7.6 Hz, 1H, $\text{H}_{4'}$), 1.96 (s, 3H, CH_3). ^{13}C NMR (101 MHz, CDCl_3) δ = 186.01 (C=O), 170.53 (C=O), 150.27 (C_q), 136.45 (C_{ar}), 135.02 (C_q), 133.90 (C_q), 130.21 (C_{ar}), 129.94 (C_{ar}), 129.25 (C_{ar}), 124.99 (C_{ar}), 124.20 (C_{ar}), 123.89 (C_q), 122.44 (C_{ar}), 117.88 (C_{vin}), 25.12 (Ac- CH_3).

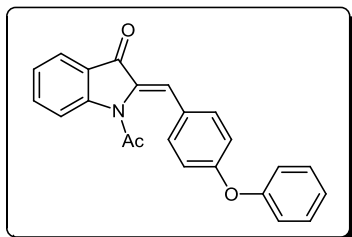
1-acetyl-2-(4-bromobenzylidene)indolin-3-one (6.26)



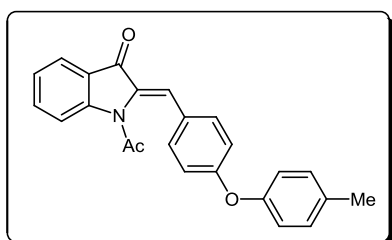
Purified by flash chromatography (Hexane/EtOAc = 80:20). Obtained as yellow solid, yield 64%, mp 138-141 °C. Mixture of isomers *Z/E* = 1:0.70. ^1H NMR (400 MHz, CDCl_3 , more abundant isomer) δ = 8.25 (d, J = 8.2 Hz, 1H, H_4), 7.87 (d, J = 8.1 Hz, 1H, H_7), 7.69-7.64 (m, 1H, H_6), 7.60-7.54 (m, 2H, $2\text{H}_{2'}$), 7.41 (d, J = 8.3 Hz, 2H, $2\text{H}_{3'}$), 7.34-7.29 (m, 1H, H_5), 7.27 (s, 1H, H_{vin}), 2.03 (s, 3H, CH_3). ^{13}C NMR (101 MHz, CDCl_3 , more abundant isomer) δ = 185.84 (C=O), 170.20 (C=O), 150.47 (C_q), 136.65 (C_{ar}), 135.34 (C_q), 133.08 (C_q), 132.62 (C_{ar}), 131.74 (C_{ar}), 125.27 (C_{ar}), 124.45 (C_{ar}), 124.35 (C_q), 124.07 (C_q), 121.05 (C_{ar}), 117.98 (C_{vin}), 26.71 (Ac- CH_3).

1-acetyl-2-(4-(dimethylamino)benzylidene)indolin-3-one (6.27)

Purified by flash chromatography ($\text{CH}_2\text{Cl}_2/\text{MeOH} = 99:1$). Obtained as yellow solid, yied 70%, mp 147-150 °C. Mixture of isomers $Z/E = 1:0.20$. ^1H NMR (400 MHz, CDCl_3 , more abundant isomer) $\delta = 8.30$ (d, $J = 8.3$ Hz, 1H, H_4), 7.84 (d, $J = 8.2$ Hz, 1H, H_7), 7.64 (t, $J = 8.3$ Hz, 1H, H_5), 7.48 (d, $J = 8.8$ Hz, 2H, $2\text{H}_{2'}$), 7.33-7.28 (m, 2H, $\text{H}_6+\text{H}_{\text{vin}}$), 6.70 (d, $J = 8.8$ Hz, 2H, $2\text{H}_{3'}$), 3.06 (s, 6H, $\text{N}(\text{CH}_3)_2$), 2.14 (s, 3H, CH_3). ^{13}C NMR (101 MHz, CDCl_3 , more abundant isomer) $\delta = 185.92$ (C=O), 171.53 (C=O), 151.39 (C_q), 149.74 (C_q), 135.66 (C_{ar}), 133.06 (C_{ar}), 131.82 (C_q), 125.09 (C_{ar}), 124.93 (C_q), 124.75 (C_{ar}), 123.88 (C_{ar}), 120.50 (C_q), 117.95 (C_{vin}), 111.97 (C_{ar}), 40.16 ($\text{N}(\text{CH}_3)_2$), 25.47 (Ac- CH_3).

1-acetyl-2-(4-phenoxybenzylidene)indolin-3-one (6.28)

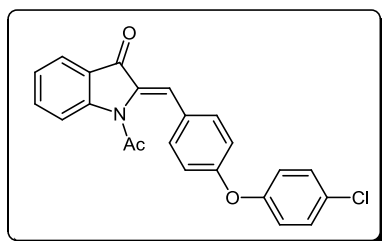
Purified by flash chromatography (Hexane/ $\text{CH}_2\text{Cl}_2 = 50:50$). Obtained as yellow oil, yied 57%. Mixture of isomers $Z/E = 1:0.30$. ^1H NMR (400 MHz, CDCl_3 , more abundant isomer) $\delta = 8.33$ (d, $J = 8.1$ Hz, 1H, H_4), 8.01 (d, $J = 8.0$ Hz, 1H, H_7), 7.71 (t, $J = 8.1$ Hz, 1H, H_5), 7.56 (d, $J = 8.7$ Hz, 2H, $2\text{H}_{2'}$), 7.39-7.35 (m, 3H, $\text{H}_6+2\text{H}_{3''}$), 7.29-7.24 (m, 2H, $\text{H}_{\text{vin}}+\text{H}_{4'}$), 7.10-7.07 (m, 4H, $2\text{H}_{3'}+2\text{H}_{2''}$). ^{13}C NMR (101 MHz, CDCl_3 , more abundant isomer) $\delta = 184.08$ (C=O), 168.94 (C=O), 159.12 (C_q), 154.12 (C_q), 149.98 (C_q), 135.76 (C_{ar}), 134.21 (C_{ar}), 133.78 (C_q), 131.46 (C_{ar}), 129.31 (C_{ar}), 128.98 (C_q), 128.12 (C_{ar}), 126.75 (C_q), 124.12 (C_{ar}), 122.28 (C_{ar}), 121.23 (C_{ar}), 119.21 (C_{ar}), 117.56 (C_{vin}), 26.63 (Ac- CH_3).

1-acetyl-2-(4-(*p*-tolylloxy)benzylidene)indolin-3-one (6.29)

Purified by flash chromatography (Hexane/ $\text{CH}_2\text{Cl}_2 = 50:50$). Obtained as yellow oil, yied 53%. Mixture of isomers $Z/E = 1:0.25$. ^1H NMR (400 MHz, CDCl_3 , more

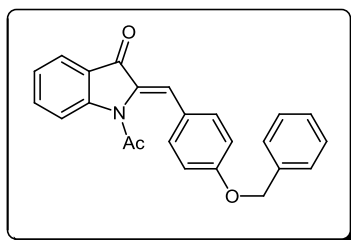
abundant isomer) $\delta = 8.27$ (d, $J = 8.2$ Hz, 1H, H_4), 7.89 (d, $J = 8.1$ Hz, 1H, H_7), 7.71-7.66 (m, 3H, H_5+2H_2'), 7.29-7.34 (m, 4H, $H_6+2H_3''+H_{vin}$), 7.01-6.98 (m, 4H, $2H_3'+2H_2''$). ^{13}C NMR (101 MHz, CDCl_3 , more abundant isomer) $\delta = 183.87$ (C=O), 166.98 (C=O), 158.72 (C_q), 153.82 (C_q), 148.67 (C_q), 134.55 (C_q), 134.27 (C_{ar}), 132.28 (C_q), 131.62 (C_{ar}), 129.93 (C_{ar}), 128.92 (C_q), 127.62 (C_{ar}), 126.15 (C_q), 123.89 (C_{ar}), 122.56 (C_{ar}), 121.65 (C_{ar}), 120.02 (C_{ar}), 118.33 (C_{vin}), 25.93 (Ac- CH_3), 21.24 (CH_3).

1-acetyl-2-(4-(4-chlorophenoxy)benzylidene)indolin-3-one (6.30)



Purified by flash chromatography (Hexane/ $\text{CH}_2\text{Cl}_2 = 50:50$). Obtained as yellow solid, yied 61%, mp 108-111 °C. Mixture of isomers $Z/E = 1:0.70$. ^1H NMR (400 MHz, CDCl_3 , more abundant isomer) $\delta = 8.26$ (d, $J = 8.1$ Hz, 1H, H_4), 7.86 (d, $J = 8.0$ Hz, 1H, H_7), 7.69-7.62 (m, 1H, H_5), 7.55-7.52 (m, 2H, $2H_2'$), 7.36-7.31 (m, 3H, $H_{vin}+2H_2''$), 7.03-7.00 (m, 5H, $H_6+2H_3'+2H_3''$). ^{13}C NMR (101 MHz, CDCl_3 , more abundant isomer) $\delta = 186.05$ (C=O), 170.53 (C=O), 158.87 (C_q), 154.43 (C_q), 150.30 (C_q), 136.44 (C_{ar}), 134.48 (C_q), 133.55 (C_{ar}), 132.46 (C_{ar}), 130.22 (C_{ar}), 128.72 (C_q), 127.32 (C_q), 125.15 (C_{ar}), 124.32 (C_{ar}), 124.28 (C_q), 121.34 (C_{ar}), 118.58 (C_{ar}), 117.60 (C_{vin}), 25.34 (Ac- CH_3).

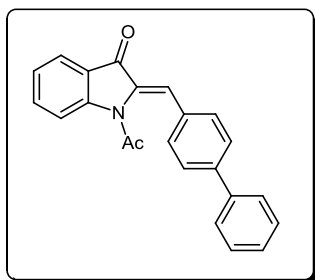
1-acetyl-2-(4-(benzyloxy)benzylidene)indolin-3-one (6.31)



Purified by flash chromatography (Hexane/ $\text{EtOAc} = 95:5$). Obtained as yellow solid, yied 57%, mp 151-154 °C. Mixture of isomers $Z/E = 1:0.10$. ^1H NMR (400 MHz, CDCl_3 , more abundant isomer) $\delta = 8.29$ (d, $J = 8.3$ Hz, 1H, H_4), 7.85 (d, $J = 8.2$ Hz, 1H, H_7), 7.67 (t, $J = 8.2$ Hz, 1H, H_5), 7.52 (d, $J = 8.5$ Hz, 2H, $2H_2'$), 7.45-7.28 (m, 7H, $H_6+H_{vin}+2H_2''+2H_3''+H_4''$), 7.04 (d, $J = 8.5$ Hz, 2H, $2H_3'$), 5.11 (s, 2H, CH_2), 2.06 (s, 3H, CH_3). ^{13}C NMR (101 MHz, CDCl_3 , more abundant isomer) $\delta = 186.10$ (C=O), 170.87 (C=O), 160.23 (C_q), 150.17 (C_q), 136.26 (C_{ar}), 133.80 (C_q), 132.50 (C_{ar}),

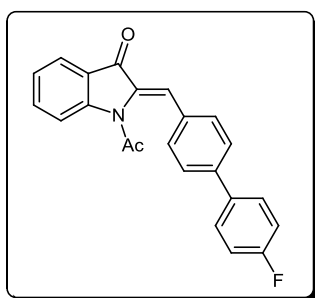
128.84 (C_{ar}), 128.42 (C_{ar}), 127.68 (C_{ar}), 126.37 (C_q), 125.02 (C_{ar}), 124.37 (C_q), 124.17 (C_{ar}), 123.00 (C_{ar}), 118.02 (C_{vin}), 115.69 (C_{ar}), 70.31 (CH₂), 25.33 (Ac-CH₃).

1-acetyl-2-(biphenyl-4-ylmethylene)indolin-3-one (6.32)

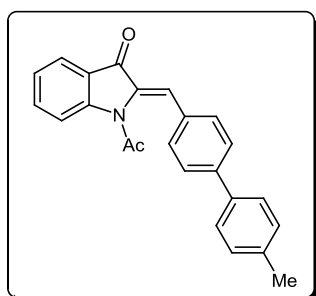


Purified by flash chromatography (Hexane/EtOAc = 80:20). Obtained as yellow solid, yied 94%, mp 172-175 °C. Mixture of isomers *Z/E* = 1:0.10. ¹H NMR (400 MHz, CDCl₃, more abundant isomer) δ = 8.31 (d, *J* = 8.3 Hz, 1H, H₄), 7.88 (d, *J* = 8.2 Hz, 1H, H₇), 7.71-7.60 (m, 6H, H₅+2H_{2'}+2H_{3'}+H_{4''}), 7.48 (t, *J* = 6.9 Hz, 2H, 2H_{3''}), 7.41-7.39 (m, 2H, 2H_{2''}), 7.32 (t, *J* = 8.2 Hz, 1H, H₆), 7.27 (s, 1H, H_{vin}), 2.06 (s, 3H, CH₃). ¹³C NMR (101 MHz, CDCl₃, more abundant isomer) δ = 186.10 (C=O), 170.71 (C=O), 150.36 (C_q), 142.72 (C_q), 139.82 (C_q), 136.53 (C_{ar}), 135.05 (C_q), 132.84 (C_q), 131.02 (C_{ar}), 129.13 (C_{ar}), 128.25 (C_{ar}), 127.86 (C_{ar}), 127.17 (C_{ar}), 125.14 (C_{ar}), 124.33 (C_{ar}), 124.12 (C_q), 122.29 (C_{ar}), 118.01 (C_{ar}), 25.39 (Ac-CH₃).

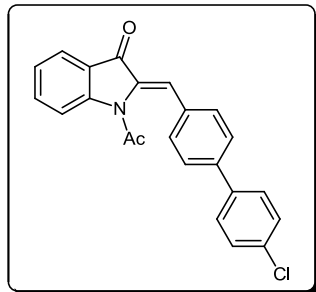
1-acetyl-2-((4'-fluorobiphenyl-4-yl)methylene)indolin-3-one (6.33)



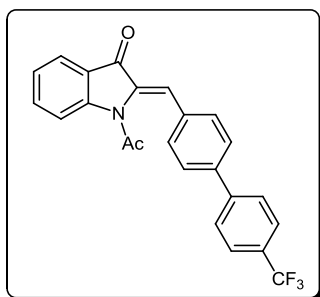
Purified by flash chromatography (Hexane/EtOAc = 80:20). Obtained as yellow solid, yied 80%, mp 70-73 °C. Mixture of isomers *Z/E* = 1:0.40. ¹H NMR (400 MHz, CDCl₃, more abundant isomer) δ = 8.30 (d, *J* = 8.3 Hz, 1H, H₄), 7.87 (d, *J* = 8.0 Hz, 1H, H₇), 7.69 (t, *J* = 8.3 Hz, 1H, H₅), 7.65-7.58 (m, 6H, 2H_{2'}+2H_{3'}+2H_{2''}), 7.37 (s, 1H, H_{vin}), 7.32 (*J* = 8.0 Hz, 1H, H₆), 7.18-7.14 (m, 2H, 2H_{3''}), 2.06 (s, 1H, CH₃). ¹³C NMR (101 MHz, CDCl₃, more abundant isomer) δ = 186.07 (C=O), 170.64 (C=O), 163.01 (CF), 150.34 (C_q), 141.66 (C_q), 136.55 (C_{ar}), 135.96 (C_q), 135.08 (C_q), 132.87 (C_q), 131.05 (C_{ar}), 128.82 (C_{ar}), 127.69 (C_{ar}), 125.17 (C_{ar}), 124.35 (C_{ar}), 124.10 (C_q), 122.13 (C_{ar}), 117.98 (C_{vin}), 116.08 (C_{ar}), 25.38 (Ac-CH₃).

1-acetyl-2-((4'-methylbiphenyl-4-yl)methylene)indolin-3-one (6.34)

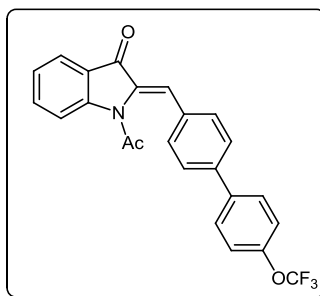
Purified by flash chromatography (Hexane/EtOAc = 90:10). Obtained as yellow solid, yied 65%, mp 135-138 °C. Mixture of isomers $Z/E = 1:0.50$. ^1H NMR (400 MHz, CDCl_3 , more abundant isomer) $\delta = 8.15$ (d, $J = 8.2$ Hz, 1H, H_4), 7.98 (d, $J = 8.2$ Hz, 2H, $2\text{H}_2'$), 7.80 (d, $J = 8.1$ Hz, 1H, H_7), 7.69-7.60 (m, 3H, $\text{H}_5+2\text{H}_3'$), 7.57-7.52 (m, 3H, $\text{H}_{\text{vin}}+2\text{H}_2''$), 7.34-7.27 (m, 3H, $\text{H}_6+2\text{H}_3''$), 2.41 (s, 3H, CH_3), 2.06 (s, 3H, Ac- CH_3). ^{13}C NMR (101 MHz, CDCl_3 , more abundant isomer) $\delta = 186.04$ (C=O), 169.35 (C=O), 148.26 (C_q), 143.04 (C_q), 138.25 (C_q), 137.89 (C_q), 137.59 (C_q), 136.05 (C_{ar}), 134.96 (C_q), 131.98 (C_{ar}), 130.92 (C_q), 130.23 (C_{ar}), 129.75 (C_{ar}), 127.10 (C_{ar}), 126.52 (C_{ar}), 124.79 (C_{ar}), 124.33 (C_{ar}), 117.49 (C_{vin}), 26.56 (CH_3), 25.38 (Ac- CH_3).

1-acetyl-2-((4'-chlorobiphenyl-4-yl)methylene)indolin-3-one (6.35)

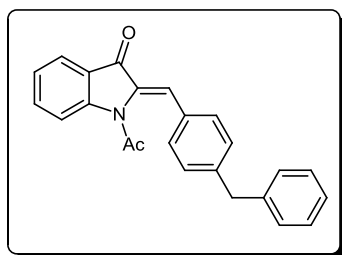
Purified by flash chromatography (Hexane/EtOAc = 80:20). Obtained as yellow solid, yied 75%, mp 107-110 °C. Mixture of isomers $Z/E = 1:0.35$. ^1H NMR (400 MHz, CDCl_3 , more abundant isomer) $\delta = 8.29$ (d, $J = 8.2$ Hz, 1H, H_4), 7.87 (d, $J = 8.0$ Hz, 1H, H_7), 7.71-7.55 (m, 7H, $\text{H}_5+2\text{H}_2'+2\text{H}_3'+2\text{H}_2''$), 7.45-7.42 (m, 2H, $2\text{H}_3''$), 7.37 (s, 1H, H_{vin}), 7.32 (t, $J = 8.0$ Hz, 1H, H_6), 2.06 (s, 3H, CH_3). ^{13}C NMR (101 MHz, CDCl_3 , more abundant isomer) $\delta = 186.06$ (C=O), 170.59 (C=O), 150.35 (C_q), 141.37 (C_q), 138.28 (C_q), 136.57 (C_{ar}), 135.15 (C_q), 134.39 (C_q), 133.23 (C_q), 131.08 (C_{ar}), 129.30 (C_{ar}), 128.40 (C_{ar}), 127.67 (C_{ar}), 125.18 (C_{ar}), 124.37 (C_{ar}), 124.09 (C_q), 122.00 (C_{ar}), 117.98 (C_{vin}), 25.39 (Ac- CH_3).

1-acetyl-2-((4'-(trifluoromethyl)biphenyl-4-yl)methylene)indolin-3-one (6.36)

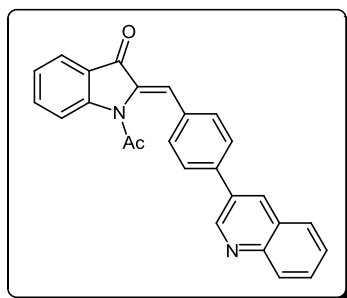
Purified by flash chromatography (Hexane/EtOAc = 95:5). Obtained as yellow solid, yied 78%, mp 124-127 °C. Mixture of isomers $Z/E = 1:0.80$. ^1H NMR (400 MHz, CDCl_3 , more abundant isomer) $\delta = 8.09$ (d, $J = 8.2$ Hz, 1H, H_4), 7.98 (d, $J = 8.2$ Hz, 2H, $2\text{H}_2'$), 7.80 (d, $J = 8.1$ Hz, 1H, H_7), 7.76-7.64 (m, 8H, $\text{H}_5 + \text{H}_{\text{vin}} + 2\text{H}_3' + 2\text{H}_2'' + 2\text{H}_3''$), 7.34-7.27 (m, 1H, H_6), 2.06 (s, 3H, CH_3). ^{13}C NMR (101 MHz, CDCl_3 , more abundant isomer) $\delta = 186.11$ (C=O), 170.48 (C=O), 162.71 (C_q), 148.38 (C_q), 141.19 (C_q), 136.22 (C_{ar}), 135.37 (C_q), 133.98 (C_q), 132.31 (C_q), 131.93 (C_{ar}), 129.50 (C_{ar}), 127.54 (C_{ar}), 126.89 (C_{ar}), 125.99 (C_{ar}), 124.86 (C_{ar}), 124.68 (C_q), 124.10 (CF_3), 121.68 (C_{ar}), 117.40 (C_{vin}), 25.37 (Ac- CH_3).

1-acetyl-2-((4'-(trifluoromethoxy)biphenyl-4-yl)methylene)indolin-3-one (6.37)

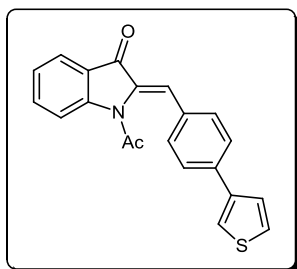
Purified by flash chromatography (Hexane/EtOAc = 90:5). Obtained as yellow solid, yied 71%, mp 121-124 °C. Mixture of isomers $Z/E = 1:0.60$. ^1H NMR (400 MHz, CDCl_3 , more abundant isomer) $\delta = 8.29$ (d, $J = 8.2$ Hz, 1H, H_4), 7.88 (d, $J = 8.0$ Hz, 1H, H_7), 7.72-7.62 (m, 7H, $\text{H}_5 + 2\text{H}_2' + 2\text{H}_3' + 2\text{H}_2''$), 7.38 (s, 1H, H_{vin}), 7.34-7.31 (m, 3H, $\text{H}_6 + 2\text{H}_3''$), 2.06 (s, 3H, CH_3). ^{13}C NMR (101 MHz, CDCl_3 , more abundant isomer) $\delta = 186.07$ (C=O), 170.41 (C=O), 166.54 (C_q), 150.13 (C_q), 141.19 (C_q), 138.61 (C_q), 136.58 (C_{ar}), 133.15 (C_q), 131.65 (C_q), 131.08 (C_{ar}), 129.72 (CF_3), 128.59 (C_{ar}), 127.84 (C_{ar}), 126.70 (C_{ar}), 124.40 (C_{ar}), 123.90 (C_q), 121.90 (C_{ar}), 121.55 (C_{ar}), 118.00 (C_{vin}), 25.59 (Ac- CH_3).

1-acetyl-2-(4-benzylbenzylidene)indolin-3-one (6.38)

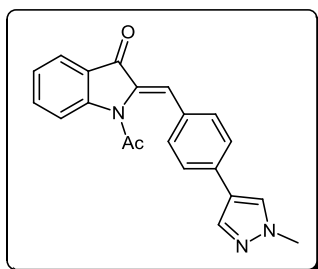
Purified by flash chromatography (Hexane/EtOAc = 92:8). Obtained as yellow oil, yied 73%. Mixture of isomers *Z/E* = 1:0.40. ^1H NMR (400 MHz, CDCl_3 , more abundant isomer) δ = 8.30 (d, J = 8.2 Hz, 1H, H_4), 7.87-7.84 (m, 1H, H_7), 7.69-7.64 (m, 1H, H_5), 7.50-7.47 (m, 2H, $2\text{H}_2'$), 7.33-7.18 (m, 9H, $\text{H}_6+\text{H}_{\text{vin}}+2\text{H}_3'+2\text{H}_2''+2\text{H}_3''+\text{H}_4''$), 4.02 (s, 2H, CH_2), 2.00 (s, 3H, CH_3). ^{13}C NMR (101 MHz, CDCl_3 , more abundant isomer) δ = 186.10 (C=O), 170.68 (C=O), 150.37 (C_q), 143.67 (C_q), 140.11 (C_q), 136.43 (C_{ar}), 134.83 (C_q), 131.80 (C_q), 130.63 (C_{ar}), 129.89 (C_{ar}), 129.07 (C_{ar}), 128.78 (C_{ar}), 126.55 (C_{ar}), 125.04 (C_{ar}), 124.25 (C_{ar}), 124.07 (C_q), 122.59 (C_{ar}), 117.98 (C_{vin}), 41.95 (CH_2), 25.25 (Ac- CH_3).

1-acetyl-2-(4-(quinolin-3-yl)benzylidene)indolin-3-one (6.39)

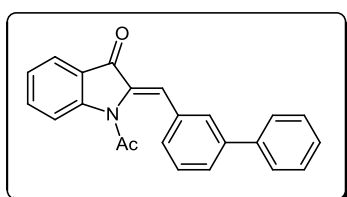
Purified by flash chromatography (Hexane/EtOAc = 70:30). Obtained as yellow solid, yied 69%, mp 168-171 °C. Mixture of isomers *Z/E* = 1:0.70. ^1H NMR (400 MHz, CDCl_3 , more abundant isomer) δ = 9.25 (s, 1H, H_2''), 8.39 (s, 1H, H_4''), 8.29 (d, J = 8.3 Hz, 1H, H_4), 8.17 (d, J = 8.0 Hz, 1H, H_7), 7.93-7.88 (m, 2H, $2\text{H}_2'$), 7.84-7.60 (m, 7H, $\text{H}_5+\text{H}_6+2\text{H}_3'+\text{H}_5''+\text{H}_7''+\text{H}_8''$), 7.40 (s, 1H, H_{vin}), 7.33 (t, J = 7.5 Hz, 1H, H_6''), 2.07 (s, 3H, CH_3). ^{13}C NMR (101 MHz, CDCl_3 , more abundant isomer) δ = 186.18 (C=O), 170.47 (C=O), 150.45 (C_q), 149.46 (C_{ar}), 147.67 (C_q), 139.29 (C_q), 137.82 (C_q), 136.62 (C_{ar}), 136.22 (C_{ar}), 135.41 (C_q), 133.92 (C_q), 133.70 (C_{ar}), 131.31 (C_{ar}), 129.45 (C_{ar}), 128.12 (C_{ar}), 128.05 (C_{ar}), 126.96 (C_{ar}), 125.24 (C_{ar}), 124.79 (C_q), 124.44 (C_{ar}), 123.64 (C_q), 122.70 (C_{ar}), 118.00 (C_{vin}), 25.41 (Ac- CH_3).

1-acetyl-2-(4-(thiophen-3-yl)benzylidene)indolin-3-one (6.40)

Purified by flash chromatography (Hexane/EtOAc = 70:30). Obtained as yellow solid, yied 72%, mp 126-129 °C. Mixture of isomers *Z/E* = 1:0.25. ¹H NMR (400 MHz, CDCl₃, more abundant isomer) δ = 8.30 (d, *J* = 8.2 Hz, 1H, H₄), 7.87 (d, *J* = 8.1 Hz, 1H, H₇), 7.70-7.56 (m, 6H, H₅+2H_{2'}+2H_{3'}+H_{2''}), 7.45 (s, 2H, H_{4''}+H_{5''}), 7.36 (s, 1H, H_{vin}), 7.31 (t, *J* = 8.1 Hz, H₆), 2.05 (s, 3H, CH₃). ¹³C NMR (101 MHz, CDCl₃, more abundant isomer) δ = 186.22 (C=O), 170.77 (C=O), 150.40 (C_q), 137.33 (C_q), 136.50 (C_{ar}), 134.96 (C_q), 134.45 (C_q), 132.62 (C_q), 131.12 (C_{ar}), 127.11 (C_{ar}), 126.94 (C_{ar}), 126.12 (C_{ar}), 125.13 (C_{ar}), 124.32 (C_{ar}), 124.17 (C_q), 122.27 (C_{ar}), 118.00 (C_{vin}), 25.35 (Ac-CH₃).

1-acetyl-2-(4-(1-methyl-1H-pyrazol-4-yl)benzylidene)indolin-3-one (6.41)

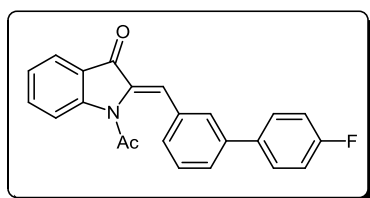
Purified by flash chromatography (CH₂Cl₂/MeOH = 99:1). Obtained as yellow solid, yied 77%, mp 161-164 °C. Mixture of isomers *Z/E* = 1:0.20. ¹H NMR (400 MHz, CDCl₃, more abundant isomer) δ = 8.29 (d, *J* = 8.2 Hz, 1H, H₄), 7.86 (d, *J* = 8.1 Hz, 1H, H₇), 7.81 (s, 1H, H_{5''}), 7.69-7.65 (m, 2H, H₅+H_{3''}), 7.54-7.52 (m, 4H, 2H_{2'}+2H_{3'}), 7.33-7.29 (m, 2H, H₆+H_{vin}), 3.96 (s, 3H, NCH₃), 2.05 (s, 3H, Ac-CH₃). ¹³C NMR (101 MHz, CDCl₃, more abundant isomer) δ = 186.06 (C=O), 170.77 (C=O), 150.30 (C_q), 137.08 (C_{ar}), 136.42 (C_{ar}), 134.70 (C_q), 134.55 (C_q), 131.72 (C_q), 131.24 (C_{ar}), 127.52 (C_{ar}), 126.01 (C_{ar}), 125.09 (C_{ar}), 124.28 (C_{ar}), 124.21 (C_q), 122.51 (C_{ar}), 122.35 (C_q), 117.98 (C_{vin}), 39.37 (NCH₃), 25.35 (Ac-CH₃).

1-acetyl-2-(biphenyl-3-ylmethylene)indolin-3-one (6.42)

Purified by flash chromatography (Hexane/EtOAc = 80:20). Obtained as yellow solid, yied 65%, mp 100-103 °C. Mixture of isomers *Z/E* = 1:0.30. ¹H NMR (400 MHz, CDCl₃, more abundant isomer) δ = 8.31 (d, *J* = 8.3 Hz, 1H, H₄), 7.87 (d, *J* =

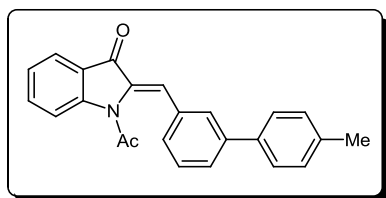
8.2 Hz, 1H, H₇), 7.76 (s, 1H, H_{2'}), 7.71-7.67 (m, 1H, H₅), 7.63-7.52 (m, 5H, H_{4'}+H_{5'}+H_{6'}+2H_{2''}), 7.48 (t, *J* = 7.6 Hz, 2H, 2H_{3''}), 7.41-7.37 (m, 2H, H_{vin}+H_{4''}), 7.32 (t, *J* = 8.2 Hz, 1H, H₆), 2.03 (s, 3H, CH₃). ¹³C NMR (101 MHz, CDCl₃, more abundant isomer) δ = 186.10 (C=O), 170.62 (C=O), 150.41 (C_q), 142.40 (C_q), 140.04 (C_q), 136.61 (C_{ar}), 135.31 (C_q), 134.55 (C_q), 129.81 (C_{ar}), 129.14 (C_{ar}), 129.00 (C_{ar}), 128.93 (C_{ar}), 128.82 (C_{ar}), 128.05 (C_{ar}), 127.24 (C_{ar}), 125.12 (C_{ar}), 124.36 (C_{ar}), 123.97 (C_q), 122.33 (C_{ar}), 117.94 (C_{vin}), 25.39 (Ac-CH₃).

1-acetyl-2-((4'-fluorobiphenyl-3-yl)methylene)indolin-3-one (6.43)



Purified by flash chromatography (Hexane/EtOAc = 80:20). Obtained as yellow solid, yied 69%, mp 165-168 °C. Mixture of isomers *Z/E* = 1:0.15. ¹H NMR (400 MHz, CDCl₃, more abundant isomer) δ = 8.30 (d, *J* = 8.0 Hz, 1H, H₄), 7.87 (d, *J* = 7.9 Hz, 1H, H₇), 7.71-7.49 (m, 7H, H₅+H_{2'}+H_{4'}+H_{5'}+H_{6'}+2H_{2''}), 7.39 (s, 1H, H_{vin}), 7.32 (t, *J* = 7.9 Hz, 1H, H₆), 7.16 (t, *J* = 8.4 Hz, 2H, 2H_{3''}), 2.02 (s, 3H, CH₃). ¹³C NMR (101 MHz, CDCl₃, more abundant isomer) δ = 186.06 (C=O), 170.60 (C=O), 164.14 (C_q), 161.68 (CF), 150.39 (C_q), 141.41 (C_q), 136.64 (C_{ar}), 135.36 (C_q), 134.66 (C_q), 129.88 (C_{ar}), 128.93 (C_{ar}), 128.80 (C_{ar}), 128.62 (C_{ar}), 125.15 (C_{ar}), 124.39 (C_{ar}), 123.94 (C_q), 122.12 (C_{ar}), 117.88 (C_{vin}), 116.18 (C_{ar}), 115.97 (C_{ar}), 25.40 (Ac-CH₃).

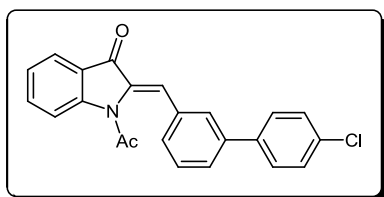
1-acetyl-2-((4'-methylbiphenyl-3-yl)methylene)indolin-3-one (6.44)



Purified by flash chromatography (Hexane/EtOAc = 90:10). Obtained as yellow oil, yied 62%. Mixture of isomers *Z/E* = 1:0.40. ¹H NMR (400 MHz, CDCl₃, more abundant isomer) δ = 8.16-8.12 (m, 2H, H₄+H_{2'}), 7.81-7.79 (m, 2H, H_{4'}+H_{5'}), 7.69-7.57 (m, 4H, H₅+H₇+2H_{2''}), 7.51-7.47 (m, 2H, H₆+H_{6'}), 7.29-7.26 (m, 3H, H_{vin}+2H_{3''}), 2.41 (CH₃), 2.02 (Ac-CH₃). ¹³C NMR (101 MHz, CDCl₃, more abundant isomer) δ = 186.13 (C=O), 169.30 (C=O), 148.33 (C_q), 140.98 (C_q), 137.92 (C_q), 137.40 (C_q), 136.08 (C_{ar}), 135.24 (C_q), 132.50 (C_q), 139.24 (C_{ar}), 129.84 (C_{ar}), 129.69 (C_{ar}), 128.80 (C_{ar}),

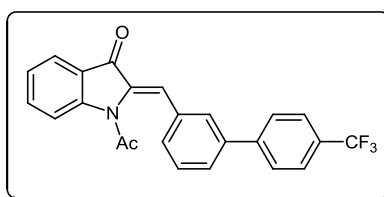
128.47 (C_{ar}), 127.19 (C_{ar}), 124.78 (C_{ar}), 124.71 (C_q), 124.32 (C_{ar}), 122.41 (C_{ar}), 117.49 (C_{vin}), 26.53 (CH₃), 25.36 (Ac-CH₃).

1-acetyl-2-((4'-chlorobiphenyl-3-yl)methylene)indolin-3-one (6.45)

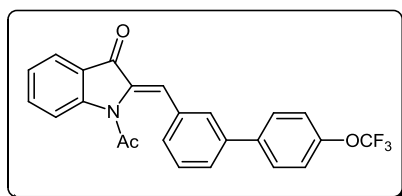


Purified by flash chromatography (Hexane/EtOAc = 80:20). Obtained as yellow solid, yied 66%, mp 180-183 °C. Mixture of isomers *Z/E* = 1:0.20. ¹H NMR (400 MHz, CDCl₃, more abundant isomer) δ = 8.29 (d, *J* = 8.3 Hz, 1H, H₄), 7.87 (d, *J* = 8.0 Hz, 1H, H₇), 7.70-7.50 (m, 7H, H₅+H₂+H₄+H₅+H₆+2H₂''), 7.44 (d, *J* = 8.4 Hz, 2H, 2H₃''), 7.39 (s, 1H, H_{vin}), 7.32 (t, *J* = 8.0 Hz, 1H, H₆), 2.02 (s, 3H, CH₃). ¹³C NMR (101 MHz, CDCl₃, more abundant isomer) δ = 186.04 (C=O), 170.55 (C=O), 150.39 (C_q), 141.18 (C_q), 138.51 (C_q), 136.66 (C_{ar}), 135.40 (C_q), 134.75 (C_q), 134.23 (C_q), 129.93 (C_{ar}), 129.33 (C_{ar}), 129.22 (C_{ar}), 128.78 (C_{ar}), 128.56 (C_{ar}), 128.50 (C_{ar}), 125.17 (C_{ar}), 124.41 (C_{ar}), 123.94 (C_q), 122.00 (C_{ar}), 117.88 (C_{vin}), 25.39 (Ac-CH₃).

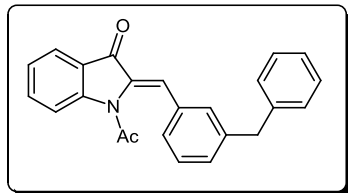
1-acetyl-2-((4'-(trifluoromethyl)biphenyl-3-yl)methylene)indolin-3-one (6.46)



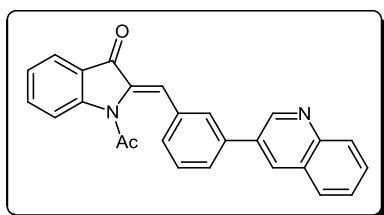
Purified by flash chromatography (Hexane/EtOAc = 95:5). Obtained as yellow solid, yied 75%, mp 144-145 °C. Mixture of isomers *Z/E* = 1:0.80. ¹H NMR (400 MHz, CDCl₃, more abundant isomer) δ = 8.28 (d, *J* = 8.2 Hz, 1H, H₄), 8.21 (s, 1H, H₂''), 7.88 (d, *J* = 8.1 Hz, 1H, H₇), 7.81-7.51 (m, 8H, H₅+H₄+H₅+H₆+2H₂''+2H₃''), 7.40 (s, 1H, H_{vin}), 7.32 (t, *J* = 8.1 Hz, 1H, H₆), 2.04 (s, 3H, CH₃). ¹³C NMR (101 MHz, CDCl₃, more abundant isomer) δ = 186.04 (C=O), 170.52 (C=O), 150.37 (C_q), 148.35 (C_q), 140.95 (C_q), 139.52 (C_q), 136.27 (C_{ar}), 135.43 (C_q), 134.93 (C_q), 132.88 (C_q), 130.82 (C_{ar}), 130.10 (C_{ar}), 129.70 (C_{ar}), 128.75 (C_{ar}), 127.69 (C_{ar}), 125.92 (C_{ar}), 124.89 (C_{ar}), 124.49 (C_{ar}), 123.94 (CF₃), 121.75 (C_{ar}), 117.41 (C_{vin}), 26.56 (Ac-CH₃).

1-acetyl-2-((4'-(trifluoromethoxy)biphenyl-3-yl)methylene)indolin-3-one (6.47)

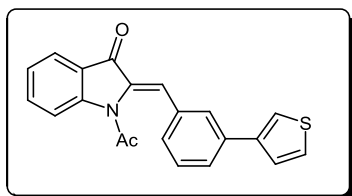
Purified by flash chromatography (Hexane/EtOAc = 90:10). Obtained as yellow solid, yied 72%, mp 115-117 °C. Mixture of isomers *Z/E* = 1:0.45. ¹H NMR (400 MHz, CDCl₃, more abundant isomer) δ = 8.18 (s, 1H, H_{2'}), 8.10 (d, *J* = 8.3 Hz, 1H, H₄), 7.82-7.49 (m, 7H, H₅+H₆+H_{4'}+H_{5'}+H_{6'}+2H_{2''}), 7.32-7.27 (m, 4H, H₇+H_{vin}+2H_{3''}), 2.06 (s, 3H, CH₃). ¹³C NMR (101 MHz, CDCl₃, more abundant isomer) δ = 186.12 (C=O), 169.31 (C=O), 151.42 (C_q), 150.42 (C_q), 148.37 (C_q), 138.63 (C_q), 138.82 (C_q), 136.23 (C_{ar}), 132.79 (C_q), 130.37 (C_{ar}), 129.98 (C_{ar}), 129.85 (C_{ar}), 129.65 (CF₃), 128.76 (C_{ar}), 128.67 (C_{ar}), 124.87 (C_{ar}), 124.67 (C_q), 124.46 (C_{ar}), 121.60 (C_{ar}), 121.45 (C_{ar}), 117.44 (C_{vin}), 26.87 (Ac-CH₃).

1-acetyl-2-(3-benzylbenzylidene)indolin-3-one (6.48)

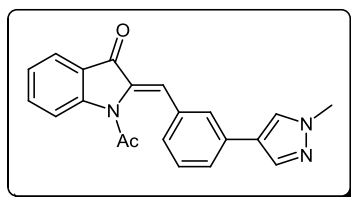
Purified by flash chromatography (Hexane/EtOAc = 92:8). Obtained as yellow oil, yied 72%. Mixture of isomers *Z/E* = 1:0.40. ¹H NMR (400 MHz, CDCl₃, more abundant isomer) δ = 8.29 (d, *J* = 8.2 Hz, 1H, H₄), 7.86 (d, *J* = 8.0 Hz, 1H, H₇), 7.70-7.62 (m, 2H, H₅+H_{2'}), 7.41-7.19 (m, 10H, H₆+H_{vin}+H_{4'}+H_{5'}+H_{6'}+2H_{2''}+2H_{3''}+H_{4''}), 4.01 (s, 2H, CH₂), 1.94 (s, 3H, CH₃). ¹³C NMR (101 MHz, CDCl₃, more abundant isomer) δ = 186.14 (C=O), 170.48 (C=O), 150.41 (C_q), 142.53 (C_q), 140.34 (C_q), 136.48 (C_{ar}), 135.10 (C_q), 134.22 (C_q), 130.78 (C_{ar}), 130.67 (C_{ar}), 129.47 (C_{ar}), 129.01 (C_{ar}), 128.82 (C_{ar}), 129.13 (C_{ar}), 126.53 (C_{ar}), 125.03 (C_{ar}), 124.28 (C_{ar}), 124.04 (C_q), 122.54 (C_{ar}), 117.98 (C_{vin}), 41.90 (CH₂), 25.22 (Ac-CH₃).

1-acetyl-2-(3-(quinolin-3-yl)benzylidene)indolin-3-one (6.49)

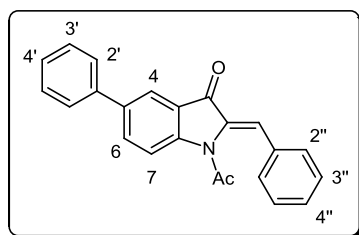
Purified by flash chromatography (Hexane/EtOAc = 70:30). Obtained as yellow solid, yied 62%, mp 145-148 °C. Mixture of isomers *Z/E* = 1:0.70. ¹H NMR (400 MHz, CDCl₃, more abundant isomer) δ = 9.27 (s, 1H, H_{2''}), 8.43 (s, 1H, H_{4''}), 8.28 (d, *J* = 8.2 Hz, 1H, H₄), 8.80 (d, *J* = 8.0 Hz, 1H, H₇), 7.94-7.57 (m, 10H, H₅+H₆+H_{vin}+H_{2'}+H_{4'}+H_{5'}+H_{6'}+H_{5''}+H_{7''}+H_{8''}), 7.32 (t, *J* = 7.5 Hz, 1H, H_{6''}), 2.07 (s, 1H, CH₃). ¹³C NMR (101 MHz, CDCl₃, more abundant isomer) δ = 185.99 (C=O), 169.39 (C=O), 150.47 (C_q), 149.87 (C_{ar}), 148.33 (C_q), 139.12 (C_q), 137.62 (C_q), 136.25 (C_{ar}), 135.23 (C_q), 133.83 (C_{ar}), 133.16 (C_q), 130.71 (C_{ar}), 130.16 (C_{ar}), 129.73 (C_{ar}), 129.49 (C_{ar}), 129.24 (C_{ar}), 128.94 (C_{ar}), 128.28 (C_{ar}), 127.24 (C_{ar}), 124.88 (C_{ar}), 124.68 (C_q), 124.52 (C_{ar}), 123.97 (C_q), 121.69 (C_{ar}), 117.40 (C_{vin}), 25.43 (Ac-CH₃).

1-acetyl-2-(3-(thiophen-3-yl)benzylidene)indolin-3-one (6.50)

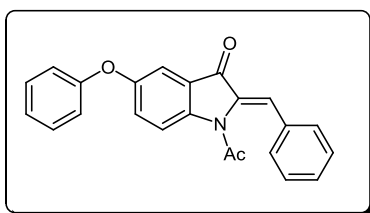
Purified by flash chromatography (Hexane/EtOAc = 70:30). Obtained as yellow solid, yied 69%, mp 150-153 °C. Mixture of isomers *Z/E* = 1:0.75. ¹H NMR (400 MHz, CDCl₃, more abundant isomer) δ = 8.31 (d, *J* = 8.2 Hz, 1H, H₄), 7.87 (d, *J* = 8.1 Hz, 1H, H₇), 7.80-7.60 (m, 4H, H₅+H_{2'}+H_{4'}+H_{6'}), 7.50-7.38 (m, 5H, H_{vin}+H_{5'}+H_{2''}+H_{4''}+H_{5''}), 7.31 (t, *J* = 8.1 Hz, 1H, H₆), 2.01 (s, 3H, CH₃). ¹³C NMR (101 MHz, CDCl₃, more abundant isomer) δ = 186.06 (C=O), 170.73 (C=O), 150.40 (C_q), 141.21 (C_q), 136.98 (C_q), 136.62 (C_{ar}), 135.38 (C_q), 134.62 (C_q), 129.88 (C_{ar}), 128.82 (C_{ar}), 128.15 (C_{ar}), 126.95 (C_{ar}), 126.21 (C_{ar}), 125.11 (C_{ar}), 124.38 (C_{ar}), 123.96 (C_q), 122.15 (C_{ar}), 121.37 (C_{ar}), 117.85 (C_{vin}), 25.37 (Ac-CH₃).

1-acetyl-2-(3-(1-methyl-1H-pyrazol-4-yl)benzylidene)indolin-3-one (6.51)

Purified by flash chromatography (CH₂Cl₂/MeOH = 99:1). Obtained as yellow solid, yield 68%, mp 198-201 °C. Mixture of isomers *Z/E* = 1:0.60. ¹H NMR (400 MHz, CDCl₃, more abundant isomer) δ = 8.30 (d, *J* = 8.2 Hz, 1H, H₄), 7.86 (d, *J* = 8.0 Hz, 1H, H₇), 7.77 (s, 1H, H_{5''}), 7.70-7.63 (m, 3H, H₅+H₂+H_{3''}), 7.53-7.38 (m, 3H, H₄+H₅+H₆'), 7.35 (s, 1H, H_{vin}), 7.33 (t, *J* = 8.0 Hz, 1H, H₆), 3.96 (s, 3H, NCH₃), 2.00 (s, 3H, Ac-CH₃). ¹³C NMR (101 MHz, CDCl₃, more abundant isomer) δ = 186.06 (C=O), 170.76 (C=O), 150.40 (C_q), 136.90 (C_{ar}), 136.58 (C_{ar}), 135.29 (C_q), 134.62 (C_q), 133.91 (C_q), 129.89 (C_{ar}), 128.05 (C_{ar}), 127.29 (C_{ar}), 127.11 (C_{ar}), 127.03 (C_{ar}), 125.08 (C_{ar}), 124.36 (C_{ar}), 123.94 (C_q), 122.30 (C_q), 122.17 (C_{ar}), 117.80 (C_{vin}), 39.35 (NCH₃), 25.35 (Ac-CH₃).

1-acetyl-2-benzylidene-5-phenylindolin-3-one (6.52)

Purified by flash chromatography (Hexane/EtOAc = 90:10). Obtained as yellow solid, yield 67%, mp 131-134 °C. Mixture of isomers *Z/E* = 1:0.25. ¹H NMR (400 MHz, CDCl₃, more abundant isomer) δ = 8.36 (d, *J* = 8.1 Hz, 1H, H₇), 8.08 (s, 1H, H₄), 7.93 (d, *J* = 8.1 Hz, 1H, H₆), 7.64-7.56 (m, 4H, 2H₂' + 2H₂''), 7.49-7.38 (m, 7H, H_{vin} + 2H₃' + H₄' + 2H₃'' + H₄''), 1.99 (s, 1H, CH₃). ¹³C NMR (101 MHz, CDCl₃, more abundant isomer) δ = 186.12 (C=O), 170.58 (C=O), 149.40 (C_q), 140.22 (C_q), 135.15 (C_q), 134.12 (C_q), 133.78 (C_q), 131.76 (C_{ar}), 129.44 (C_{ar}), 128.95 (C_{ar}), 128.62 (C_{ar}), 128.43 (C_{ar}), 128.02 (C_{ar}), 127.66 (C_{ar}), 127.12 (C_q), 127.02 (C_{ar}), 121.15 (C_{ar}), 117.70 (C_{vin}), 26.05 (Ac-CH₃).

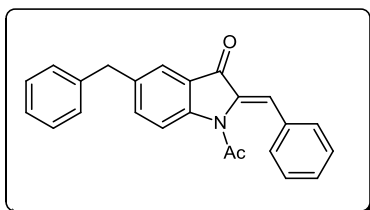
(Z)-1-acetyl-2-benzylidene-5-phenoxyindolin-3-one (6.53)

Purified by flash chromatography (Hexane/EtOAc = 90:10).

Obtained as yellow oil, yied 62%. Mixture of isomers *Z/E* = 1:0.20. ¹H NMR (400 MHz, CDCl₃, more abundant isomer)

δ = 8.30 (d, *J* = 8.1 Hz, 1H, H₇), 7.56 (d, *J* = 7.5 Hz, 2H, 2H_{2''}),

7.47-7.33 (m, 8H, H₄+H₆+H_{vin}+2H_{2'}+2H_{3''}+H_{4''}), 7.16 (t, *J* = 7.4 Hz, 1H, H_{4'}), 7.04-6.99 (m, 2H, 2H_{3'}), 1.98 (s, 3H, CH₃). ¹³C NMR (101 MHz, CDCl₃, more abundant isomer) δ = 186.01 (C=O), 170.49 (C=O), 155.11 (C_q), 146.16 (C_q), 135.51 (C_q), 133.98 (C_q), 131.25 (C_{ar}), 130.42 (C_{ar}), 130.18 (C_{ar}), 129.40 (C_{ar}), 127.45 (C_{ar}), 125.25 (C_q), 124.15 (C_{ar}), 122.99 (C_{ar}), 120.28 (C_q), 119.63 (C_{ar}), 119.26 (C_{vin}), 112.74 (C_{ar}), 25.13 (Ac-CH₃).

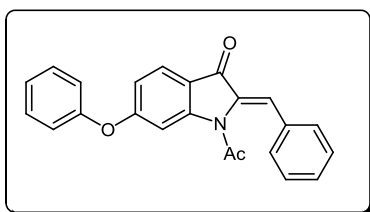
1-acetyl-5-benzyl-2-benzylideneindolin-3-one (6.54)

Purified by flash chromatography (Hexane/EtOAc = 90:10).

Obtained as yellow oil, yied 65%. Mixture of isomers *Z/E* = 1:0.45. ¹H NMR (400 MHz, CDCl₃, more abundant isomer)

δ = 8.20 (d, *J* = 8.1 Hz, 1H, H₇), 7.67 (s, 1H, H₄), 7.54-7.51

(m, 2H, 2H_{2''}), 7.47-7.36 (m, 3H, H₆+2H_{3''}), 7.32-7.15 (m, 7H, H_{vin}+2H_{2'}+2H_{3'}+H_{4'}+H_{4''}), 4.04 (s, 2H, CH₂), 1.98 (s, 3H, CH₃). ¹³C NMR (101 MHz, CDCl₃, more abundant isomer) δ = 186.14 (C=O), 170.49 (C=O), 148.99 (C_q), 140.40 (C_q), 138.60 (C_q), 137.35 (C_{ar}), 135.41 (C_q), 134.03 (C_q), 131.17 (C_{ar}), 130.34 (C_{ar}), 129.35 (C_{ar}), 128.98 (C_{ar}), 128.07 (C_{ar}), 126.60 (C_{ar}), 124.30 (C_q), 124.13 (C_{ar}), 122.50 (C_{ar}), 118.11 (C_{vin}), 41.42 (CH₂), 25.17 (Ac-CH₃).

1-acetyl-2-benzylidene-6-phenoxyindolin-3-one (6.55)

Purified by flash chromatography (Hexane/EtOAc = 90:10).

Obtained as yellow oil, yied 61%. Mixture of isomers *Z/E* = 1:0.30. ¹H NMR (400 MHz, CDCl₃, more abundant isomer)

δ = 8.22 (d, *J* = 8.3 Hz, 1H, H₄), 7.67-7.61 (m, 5H,

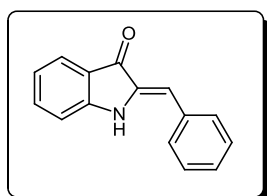
H₇+2H_{2'}+2H_{2''}), 7.53 (t, *J* = 7.6 Hz, 2H, 2H_{3'}), 7.31-7.12 (m, 6H, H₅+H_{vin}+H_{4'}+2H_{3''}+H_{4''}), 2.01

(s, 3H, CH₃). ¹³C NMR (101 MHz, CDCl₃, more abundant isomer) δ = 185.94 (C=O), 170.09 (C=O), 149.15 (C_q), 145.56 (C_q), 136.71 (C_q), 134.03 (C_q), 130.95 (C_{ar}), 129.82 (C_{ar}), 129.68 (C_{ar}), 128.70 (C_{ar}), 127.75 (C_{ar}), 125.55 (C_q), 123.95 (C_{ar}), 123.06 (C_{ar}), 121.18 (C_q), 119.23 (C_{ar}), 118.26 (C_{vin}), 115.74 (C_{ar}), 26.03 (Ac-CH₃).

8.7.10. General procedure for the synthesis of azaaurone derivatives 6.56 to 6.86

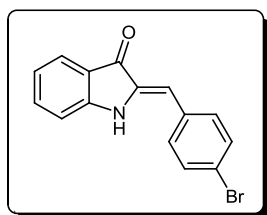
To a solution of the proper acetylated azaaurone derivative (0.25 mmol) in MeOH (2.5 mL) at room temperature was added a solution of KOH 50% in water (375 μ L). The mixture was stirred for 45 minutes. After reaction completion, the reaction mixture was neutralized with extracted with EtOAc. The organic layer was dried with anhydrous Na₂SO₄ and concentrated under reduced pressure to give the crude product.

(Z)-2-benzylideneindolin-3-one (6.56)



Purified by TLC (Toluene/EtOH = 80:20). Obtained as orange solid, yield 90%, mp 189-191 °C. ¹H NMR (400 MHz, CDCl₃) δ = 7.75 (d, *J* = 7.7 Hz, 1H, H₄), 7.56 (d, *J* = 7.5 Hz, 2H, 2H_{2'}), 7.50-7.43 (m, 3H, H₇+2H_{3''}), 7.34 (t, *J* = 7.4 Hz, 1H, H₆), 7.01-6.98 (m, 2H, H₅+H_{4'}), 6.87 (br, 2H, H_{vin}+NH). ¹³C NMR (101 MHz, CDCl₃) δ = 186.68 (C=O), 153.27 (C_q), 136.30 (C_{ar}), 135.50 (C_q), 134.90 (C_q), 129.63 (C_{ar}), 129.37 (C_{ar}), 128.67 (C_{ar}), 125.21 (C_{ar}), 121.91 (C_q), 120.84 (C_{ar}), 112.09 (C_{ar}), 111.69 (C_{vin}).

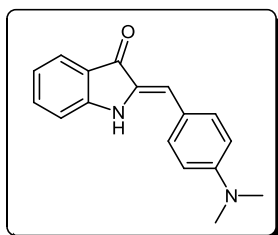
(Z)-2-(4-bromobenzylidene)indolin-3-one (6.57)



Purified by TLC (Toluene/EtOH = 80:20). Obtained as orange solid, yield 91%, mp 241-243 °C. ¹H NMR (400 MHz, DMSO-d₆) δ = 9.84 (s, 1H, NH), 7.69-7.64 (m, 4H, 2H₂+2H_{3'}), 7.69 (d, *J* = 7.7 Hz, 1H, H₄), 7.53 (t, *J* = 7.7 Hz, 1H, H₆), 7.13 (d, *J* = 7.7 Hz, H₇), 6.93 (t, *J* = 7.7 Hz, 1H, H₅), 6.59 (s, 1H, H_{vin}). ¹³C NMR (101 MHz, DMSO-d₆) δ = 186.34 (C=O), 154.24 (C_q),

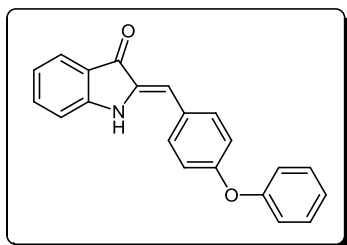
136.51 (C_{ar}), 134.78 (C_q), 133.34 (C_q), 131.79 (C_{ar}), 131.57 (C_{ar}), 124.23 (C_q), 121.40 (C_q), 119.85 (C_{ar}), 112.62 (C_{vin}), 108.34 (C_{ar}).

(Z)-2-(4-(dimethylamino)benzylidene)indolin-3-one (6.58)

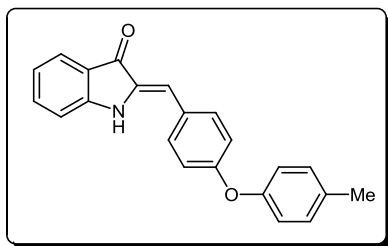


Purified by TLC (Toluene/EtOH = 80:20). Obtained as red solid, yied 87%, mp 250-252 °C. ¹H NMR (400 MHz, CDCl₃) δ = 7.76 (d, *J* = 7.7 Hz, 1H, H₄), 7.49-7.43 (m, 3H, H₆+2H_{2'}), 7.02 (d, *J* = 7.7 Hz, 1H, H₇), 6.95 (t, *J* = 7.7 Hz, 1H, H₅), 6.90 (s, 1H, H_{vin}), 6.77-6.75 (m, 3H, 2H₃+NH). ¹³C NMR (101 MHz, CDCl₃) δ = 186.18 (C=O), 152.98 (C_q), 135.40 (C_{ar}), 133.15 (C_q), 131.59 (C_{ar}), 124.87 (C_{ar}), 122.54 (C_q), 120.40 (C_{ar}), 118.44 (C_q), 117.10 (C_q), 114.30 (C_{ar}), 122.30 (C_{ar}), 112.23 (C_{vin}), 40.35 (CH₃).

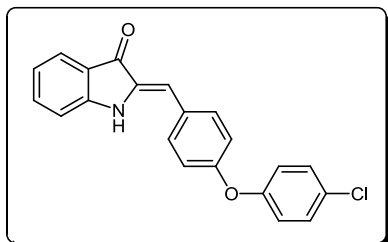
(Z)-2-(4-phenoxybenzylidene)indolin-3-one (6.59)



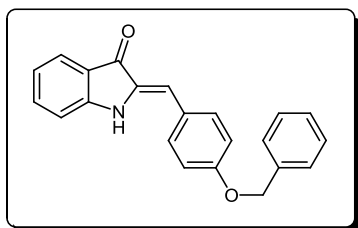
Purified by TLC (Toluene/EtOH = 80:20). Obtained as orange solid, yied 93%, mp 209-211 °C. ¹H NMR (400 MHz, CDCl₃) δ = 7.78 (d, *J* = 7.6 Hz, 1H, H₄), 7.55 (d, *J* = 8.7 Hz, 2H, 2H_{2'}), 7.50 (t, *J* = 7.5 Hz, 1H, H₆), 7.43-7.39 (m, 2H, 2H_{3''}), 7.20 (t, *J* = 7.6 Hz, 1H, H₅), 7.10-7.08 (m, 4H, 2H_{3'}+2H_{2''}), 7.03-7.01 (m, 2H, H₇+H_{4''}), 6.89 (s, 1H, H_{vin}), 6.78 (br, 1H, NH). ¹³C NMR (101 MHz, CDCl₃) δ = 186.09 (C=O), 153.20 (C_q), 136.16 (C_{ar}), 131.31 (C_{ar}), 130.11 (C_{ar}), 125.17 (C_{ar}), 124.24 (C_{ar}), 120.87 (C_{ar}), 119.72 (C_{ar}), 119.11 (C_{ar}), 112.18 (C_{ar}), 111.55 (C_{vin}).

(Z)-2-(4-(p-tolyloxy)benzylidene)indolin-3-one (6.60)

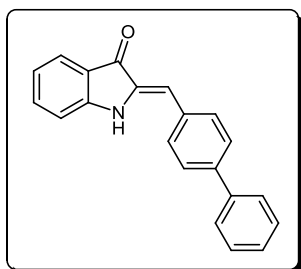
Purified by TLC (Toluene/EtOH = 80:20). Obtained as orange solid, yied 92%, mp 175-176 °C. ^1H NMR (400 MHz, DMSO- d_6) δ = 9.74 (s, 1H, NH), 7.75 (d, J = 8.4 Hz, 2H, $2\text{H}_{2'}$), 7.58 (d, J = 7.5 Hz, 1H, H_4), 7.52 (t, J = 7.5 Hz, 1H, H_6), 7.24 (d, J = 8.0 Hz, 2H, $2\text{H}_{2''}$), 7.13 (d, J = 7.5 Hz, 1H, H_7), 7.05-6.99 (m, 4H, $2\text{H}_{3'}+2\text{H}_{3''}$), 6.92 (t, J = 7.5 Hz, 1H, H_5), 6.65 (s, 1H, H_{vin}), 2.32 (s, 3H, CH_3). ^{13}C NMR (101 MHz, DMSO- d_6) δ = 186.15 (C=O), 157.50 (C_q), 154.10 (C_q), 153.53 (C_q), 136.22 (C_{ar}), 133.80 (C_q), 133.33 (C_q), 131.78 (C_{ar}), 130.53 (C_{ar}), 128.88 (C_q), 124.08 (C_{ar}), 120.18 (C_q), 119.62 (C_{ar}), 119.31 (C_{ar}), 118.12 (C_{ar}), 112.57 (C_{ar}), 109.70 (C_{vin}), 20.34 (CH_3).

(Z)-2-(4-(4-chlorophenoxy)benzylidene)indolin-3-one (6.61)

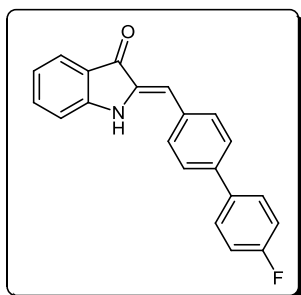
Purified by TLC (Toluene/EtOH = 80:20). Obtained as orange solid, yied 89%, mp 192-194 °C. ^1H NMR (400 MHz, CDCl_3) δ = 7.83 (d, J = 8.2 Hz, 2H, $2\text{H}_{2'}$), 7.62 (d, J = 7.5 Hz, 1H, H_4), 7.58 (t, J = 7.5 Hz, 1H, H_6), 7.26 (d, J = 8.1 Hz, 2H, $2\text{H}_{2''}$), 7.17 (d, J = 7.5 Hz, 1H, H_7), 7.15-7.00 (m, 5H, $\text{H}_5+2\text{H}_{3'}+2\text{H}_{3''}$), 6.71 (br, 2H, $\text{H}_{\text{vin}}+\text{NH}$). ^{13}C NMR (101 MHz, CDCl_3) δ = 186.05 (C=O), 156.95 (C_q), 153.98 (C_q), 152.83 (C_q), 136.07 (C_{ar}), 133.55 (C_q), 133.17 (C_q), 131.07 (C_{ar}), 130.65 (C_{ar}), 128.98 (C_q), 123.98 (C_{ar}), 120.35 (C_q), 119.32 (C_{ar}), 119.11 (C_{ar}), 117.92 (C_{ar}), 111.95 (C_{ar}), 110.62 (C_{vin}).

(Z)-2-(4-(benzyloxy)benzylidene)indolin-3-one (6.62)

Purified by TLC (Toluene/EtOH = 80:20). Obtained as orange solid, yield 89%, mp 231-233 °C. ^1H NMR (400 MHz, CDCl_3) δ = 7.76 (d, J = 7.42 Hz, 1H, H_4), 7.52-7.35 (m, 8H, $\text{H}_6+\text{H}_7+2\text{H}_2'+2\text{H}_2''+2\text{H}_3''$), 7.05 (d, J = 8.72 Hz, 2H, $2\text{H}_3'$), 7.01-6.95 (m, 2H, $\text{H}_5+\text{H}_4''$), 6.87 (s, 1H, H_{vin}), 6.74 (br, 1H, NH), 5.12 (CH_2). ^{13}C NMR (101 MHz, CDCl_3) δ = 185.99 (C=O), 159.18 (C_q), 153.15 (C_q), 136.53 (C_q), 136.01 (C_{ar}), 134.41 (C_q), 131.35 (C_{ar}), 128.84 (C_{ar}), 128.34 (C_{ar}), 127.67 (C_q), 127.62 (C_{ar}), 125.10 (C_{ar}), 122.19 (C_q), 120.74 (C_{ar}), 115.84 (C_{ar}), 112.28 (C_{ar}), 112.18 (C_{vin}), 70.26 (CH_2).

(Z)-2-(biphenyl-4-ylmethylene)indolin-3-one (6.63)

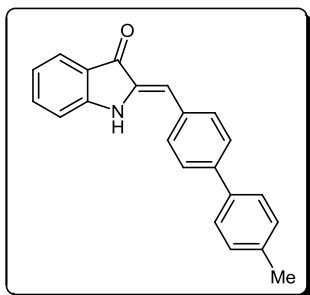
Purified by TLC (Toluene/EtOH = 80:20). Obtained as orange solid, yield 94%, mp 233-235 °C. ^1H NMR (400 MHz, CDCl_3) δ = 7.77 (d, J = 7.6 Hz, 1H, H_4), 7.70-7.62 (m, 6H, $2\text{H}_2'+2\text{H}_3'+2\text{H}_2''$), 7.51-7.45 (m, 3H, $\text{H}_7+2\text{H}_3''$), 7.38 (t, J = 7.3 Hz, 1H, H_4''), 7.04-6.97 (m, 2H, H_5+H_6), 6.91 (br, 2H, $\text{H}_{\text{vin}}+\text{NH}$). ^{13}C NMR (101 MHz, CDCl_3) δ = 186.65 (C=O), 153.21 (C_q), 141.35 (C_q), 140.25 (C_q), 136.28 (C_{ar}), 135.51 (C_q), 133.86 (C_q), 130.15 (C_{ar}), 129.09 (C_{ar}), 127.96 (C_{ar}), 127.52 (C_{ar}), 127.13 (C_{ar}), 125.21 (C_{ar}), 121.95 (C_q), 120.91 (C_{ar}), 112.16 (C_{ar}), 111.41 (C_{vin}).

(Z)-2-((4'-fluorobiphenyl-4-yl)methylene)indolin-3-one (6.64)

Purified by TLC (Toluene/EtOH = 80:20). Obtained as orange solid, yield 91%, mp 265-267 °C. ^1H NMR (400 MHz, DMSO-d_6) δ = 9.90 (s, 1H, NH), 7.80 (d, J = 7.6 Hz, 1H, H_4), 7.66-7.60 (m, 6H, $\text{H}_6+\text{H}_7+2\text{H}_2'+2\text{H}_3''$), 7.52 (t, J = 7.6 Hz, 1H, H_6), 7.19 (d, J = 7.8 Hz, 2H, $2\text{H}_2''$), 7.06-7.02 (m, 2H, $2\text{H}_3''$), 6.93 (s, 1H, H_{vin}). ^{13}C NMR (101 MHz, DMSO-d_6) δ = 186.38 (C=O), 162.63 (CF), 154.14 (C_q),

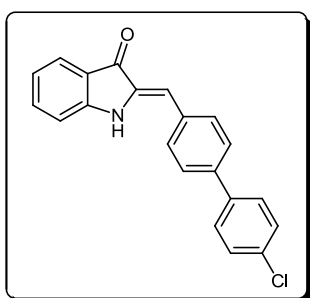
138.77 (C_q), 136.43 (C_{ar}), 135.81 (C_q), 134.48 (C_q), 133.33 (C_q), 130.59 (C_{ar}), 128.73 (C_{ar}), 127.06 (C_{ar}), 124.17 (C_{ar}), 120.03 (C_q), 118.88 (C_{ar}), 115.92 (C_{ar}), 112.67 (C_{ar}), 109.35 (C_{vin}).

(Z)-2-((4'-methylbiphenyl-4-yl)methylene)indolin-3-one (6.65)

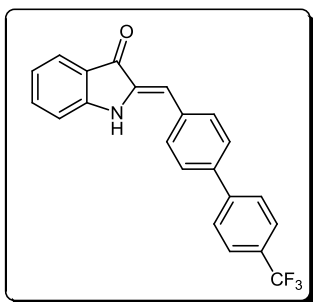


Purified by TLC (Toluene/EtOH = 80:20). Obtained as orange solid, yied 92%, mp 169-171 °C. ¹H NMR (400 MHz, CDCl₃) δ = 7.77 (d, 1H, *J* = 7.7 Hz, 1H, H₄), 7.68 (d, *J* = 8.1 Hz, 2H, 2H_{2'}), 7.62 (d, *J* = 8.1 Hz, 2H, 2H_{3'}), 7.56-7.47 (m, 3H, H₇+2H_{3''}), 7.28 (d, *J* = 8.0 Hz, 2H, 2H_{3''}), 7.03-6.97 (m, 2H, H₅+H₆), 6.91 (s, 1H, H_{vin}), 6.88 (br, 1H, NH), 2.41 (s, 3H, CH₃). ¹³C NMR (101 MHz, CDCl₃) δ = 186.12 (C=O), 153.16 (C_q), 147.86 (C_q), 137.95 (C_q), 137.34 (C_q), 136.25 (C_{ar}), 135.41 (C_q), 133.57 (C_q), 130.14 (C_{ar}), 129.82 (C_{ar}), 127.75 (C_{ar}), 126.97 (C_{ar}), 125.21 (C_{ar}), 120.89 (C_{ar}), 112.14 (C_{ar}), 11.57 (C_{vin}), 21.12 (CH₃).

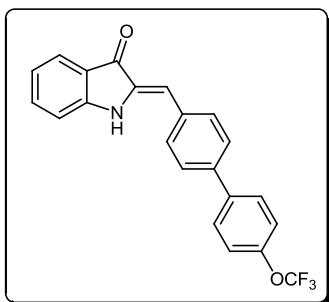
(Z)-2-((4'-chlorobiphenyl-4-yl)methylene)indolin-3-one (6.66)



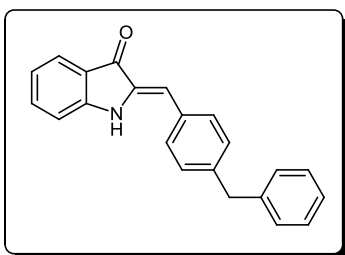
Purified by TLC (Toluene/EtOH = 80:20). Obtained as orange solid, yied 87%, mp 259-261 °C. ¹H NMR (400 MHz, DMSO-d₆) δ = 9.92 (s, 1H, NH), 7.85-7.78 (m, 5H, H₄+2H_{2'}+2H_{3'}), 7.71-7.52 (m, 5H, H₆+2H_{2''}+2H_{3''}), 7.16 (d, *J* = 8.1 Hz, 1H, H₇), 6.94 (t, *J* = 8.1 Hz, 1H, H₅), 6.68 (s, 1H, H_{vin}). ¹³C NMR (101 MHz, DMSO-d₆) δ = 186.34 (C=O), 154.13 (C_q), 138.38 (C_q), 138.09 (C_q), 136.43 (C_{ar}), 134.54 (C_q), 133.72 (C_q), 132.71 (C_q), 130.60 (C_{ar}), 129.03 (C_{ar}), 128.43 (C_{ar}), 127.05 (C_{ar}), 124.17 (C_{ar}), 120.00 (C_q), 119.89 (C_{ar}), 112.66 (C_{ar}), 109.20 (C_{vin}).

(Z)-2-((4'-(trifluoromethyl)biphenyl-4-yl)methylene)indolin-3-one (6.67)

Purified by TLC (Toluene/EtOH = 80:20). Obtained as orange solid, yied 90%, mp 289-291 °C. ^1H NMR (400 MHz, DMSO- d_6) δ = 9.95 (s, 1H, NH), 7.99 (d, J = 8.1 Hz, 2H, $2\text{H}_2'$), 7.87-7.84 (m, 6H, $2\text{H}_3'+2\text{H}_2''+2\text{H}_3''$), 7.60 (d, J = 7.6 Hz, 1H, H_4), 7.55 (d, J = 7.6 Hz, 1H, H_6), 7.17 (d, J = 7.6 Hz, 1H, H_7), 6.94 (t, J = 7.6 Hz, 1H, H_5), 6.70 (s, 1H, H_{vin}). ^{13}C NMR (101 MHz, DMSO- d_6) δ = 186.37 (C=O), 154.16 (C_q), 143.31 (C_q), 138.02 (C_q), 136.49 (C_{ar}), 134.72 (C_q), 134.40 (C_q), 130.62 (C_{ar}), 127.51 (C_{ar}), 127.47 (C_{ar}), 125.92 (C_{ar}), 124.20 (C_{ar}), 119.99 (C_q), 119.90 (C_{ar}), 112.66 (C_{ar}), 108.94 (C_{vin}).

(Z)-2-((4'-(trifluoromethoxy)biphenyl-4-yl)methylene)indolin-3-one (6.68)

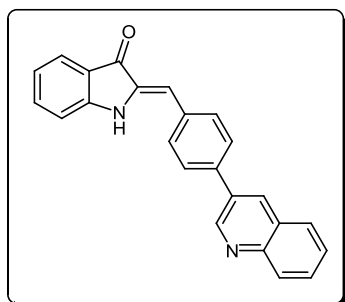
Purified by TLC (Toluene/EtOH = 80:20). Obtained as orange solid, yied 92%, mp 280-282 °C. ^1H NMR (400 MHz, DMSO- d_6) δ = 9.92 (s, 1H, NH), 7.89-7.79 (m, 7H, $\text{H}_4+2\text{H}_2'+2\text{H}_3'+2\text{H}_2''$), 7.61-7.46 (m, 3H, $\text{H}_6+2\text{H}_3''$), 7.16 (d, J = 7.8 Hz, 1H, H_7), 6.94 (t, J = 7.8 Hz, 1H, H_5), 6.69 (s, 1H, H_{vin}). ^{13}C NMR (101 MHz, DMSO- d_6) δ = 186.33 (C=O), 154.14 (C_q), 152.16 (C_q), 149.11 (C_q), 148.06 (C_q), 138.65 (C_q), 136.44 (C_{ar}), 134.57 (C_q), 133.80 (C_q), 130.58 (C_{ar}), 128.61 (C_{ar}), 127.26 (C_{ar}), 126.47 (C_{ar}), 124.17 (C_{ar}), 121.61 (C_{ar}), 119.98 (C_q), 112.65 (C_{ar}), 109.13 (C_{vin}).

(Z)-2-(4-benzylbenzylidene)indolin-3-one (6.69)

Purified by TLC (Toluene/EtOH = 80:20). Obtained as orange solid, yied 91%, , mp 194-196 °C. ^1H NMR (400 MHz, CDCl_3) δ = 7.75 (d, J = 7.6 Hz, 1H, H_4), 7.47-7.45 (m, 3H, $\text{H}_6+2\text{H}_2'$), 7.13-7.19 (m, 7H, $2\text{H}_3'+2\text{H}_2''+2\text{H}_3''+\text{H}_4''$), 6.99-6.95 (m, 2H,

H₅+H₇), 6.86 (s, 1H, H_{vin}), 6.82 (br, 1H, NH), 4.01 (s, 2H, CH₂). ¹³C NMR (101 MHz, CDCl₃) δ = 186.63 (C=O), 153.19 (C_q), 142.12 (C_q), 140.59 (C_q), 136.20 (C_{ar}), 135.26 (C_q), 132.75 (C_q), 129.94 (C_{ar}), 129.85 (C_{ar}), 129.06 (C_{ar}), 128.75 (C_{ar}), 126.47 (C_{ar}), 125.16 (C_{ar}), 121.96 (C_q), 120.78 (C_{ar}), 112.09 (C_{ar}), 111.80 (C_{vin}), 41.93 (CH₂).

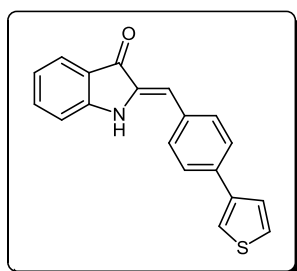
(Z)-2-(4-(quinolin-3-yl)benzylidene)indolin-3-one (6.70)



Purified by TLC (Toluene/EtOH = 80:20). Obtained as orange solid, yied 97%, mp 271-273 °C. ¹H NMR (400 MHz, CDCl₃) δ = 9.22 (s, 1H, H_{2''}), 8.37 (s, 1H, H_{4''}), 8.17 (d, *J* = 7.9 Hz, 1H, H₄), 7.92 (d, *J* = 7.6 Hz, 1H, H_{5''}), 7.83-7.71 (m, 6H, H₆+2H_{2'}+2H_{3'}+H_{8''}), 7.62 (t, *J* = 7.6 Hz, 1H, H_{7''}), 7.51 (t, *J* = 7.6 Hz, 1H, H_{6''}), 7.05-6.98 (m, 3H, H₅+H₇+NH), 6.92 (s, 1H, H_{vin}).

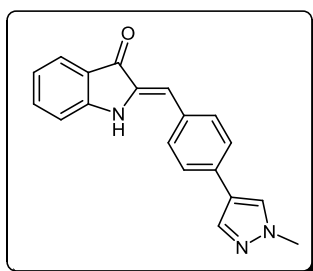
¹³C NMR (101 MHz, CDCl₃) δ = 186.32 (C=O), 153.26 (C_q), 149.47 (C_{ar}), 138.76 (C_{ar}), 136.41 (C_{ar}), 134.84 (C_q), 133.58 (C_{ar}), 130.44 (C_{ar}), 130.01 (C_{ar}), 129.22 (C_{ar}), 128.21 (C_{ar}), 127.48 (C_{ar}), 125.28 (C_{ar}), 121.87 (C_q), 121.07 (C_{ar}), 112.19 (C_{ar}), 110.71 (C_{vin}).

(Z)-2-(4-(thiophen-3-yl)benzylidene)indolin-3-one (6.71)

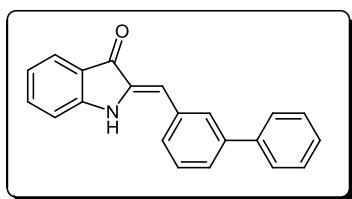


Purified by TLC (Toluene/EtOH = 80:20). Obtained as orange solid, yied 93%, mp 255-257 °C. ¹H NMR (400 MHz, DMSO-d₆) δ = 9.88 (s, 1H, NH), 8.03 (s, 1H, H_{2''}), 7.84 (d, *J* = 8.3 Hz, 2H, 2H_{2'}), 7.78 (d, *J* = 8.3 Hz, 2H, 2H_{3'}), 7.67 (s, 2H, H_{4''}+H_{5''}), 7.59 (d, *J* = 7.6 Hz, 1H, H₄), 7.53 (t, *J* = 7.6 Hz, 1H, H₆), 7.16 (d, *J* = 7.6 Hz, 1H, H₇),

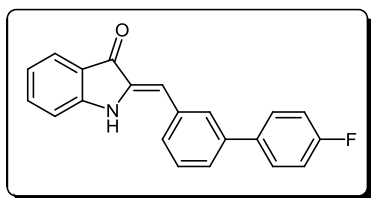
6.93 (t, *J* = 7.6 Hz, 1H, H₅), 6.67 (s, 1H, H_{vin}). ¹³C NMR (101 MHz, DMSO-d₆) δ = 186.25 (C=O), 154.05 (C_q), 140.77 (C_q), 136.33 (C_{ar}), 134.89 (C_q), 134.23 (C_q), 132.89 (C_{ar}), 130.58 (C_q), 127.36 (C_{ar}), 126.49 (C_{ar}), 126.18 (C_{ar}), 124.12 (C_{ar}), 121.86 (C_{ar}), 120.04 (C_q), 119.81 (C_{ar}), 112.64 (C_{ar}), 109.62 (C_{vin}).

(Z)-2-(4-(1-methyl-1H-pyrazol-4-yl)benzylidene)indolin-3-one (6.72)

Purified by TLC (Toluene/EtOH = 80:20). Obtained as orange solid, yied 92%, mp 247-249 °C. ^1H NMR (400 MHz, DMSO- d_6) δ = 9.82 (s, 1H, NH), 8.26 (s, 1H, $\text{H}_{3''}$), 7.98 (s, 1H, $\text{H}_{5''}$), 7.73 (d, J = 8.1 Hz, 2H, $2\text{H}_{2'}$), 7.67 (d, J = 8.1 Hz, 2H, $2\text{H}_{3'}$), 7.59 (d, J = 7.5 Hz, 1H, H_4), 7.52 (t, J = 7.5 Hz, 1H, H_6), 7.15 (d, J = 7.5 Hz, 1H, H_7), 6.92 (t, J = 7.4 Hz, 1H, H_5), 6.65 (s, 1H, H_{vin}), 3.88 (s, 3H, CH_3). ^{13}C NMR (101 MHz, DMSO- d_6) δ = 136.14 (C_{ar}), 135.96 (C_{ar}), 130.38 (C_{ar}), 128.05 (C_{ar}), 125.00 (C_{ar}), 123.81 (C_{ar}), 119.45 (C_{ar}), 112.36 (C_{ar}), 109.83 (C_{vin}), 38.51 (CH_3).

(Z)-2-(biphenyl-3-ylmethylene)indolin-3-one (6.73)

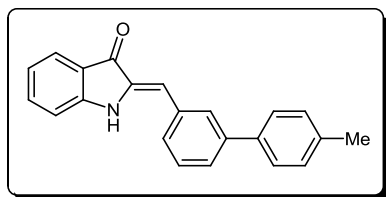
Purified by TLC (Toluene/EtOH = 80:20). Obtained as orange solid, yied 93%, mp 173-175 °C. ^1H NMR (400 MHz, DMSO- d_6) δ = 9.90 (s, 1H, NH), 8.00 (s, 1H, $\text{H}_{2'}$), 7.77-7.74 (m, 3H, $\text{H}_4+\text{H}_{4'}+\text{H}_6'$), 7.76-7.49 (m, 6H, $\text{H}_5'+2\text{H}_{2''}+2\text{H}_{3''}+\text{H}_{4''}$), 7.40 (t, J = 7.5 Hz, 1H, H_6), 7.16 (d, J = 7.6 Hz, 1H, H_7), 6.93 (t, J = 7.6 Hz, 1H, H_5), 6.74 (s, 1H, H_{vin}). ^{13}C NMR (101 MHz, DMSO- d_6) δ = 136.19 (C_{ar}), 129.29 (C_{ar}), 128.71 (C_{ar}), 128.48 (C_{ar}), 128.07 (C_{ar}), 126.80 (C_{ar}), 126.65 (C_{ar}), 123.91 (C_{ar}), 119.60 (C_{ar}), 112.45 (C_{ar}), 109.58 (C_{vin}).

(Z)-2-((4'-fluorobiphenyl-3-yl)methylene)indolin-3-one (6.74)

Purified by TLC (Toluene/EtOH = 80:20). Obtained as orange solid, yied 95%, mp 297-299 °C. ^1H NMR (400 MHz, DMSO- d_6) δ = 8.98 (s, 1H, NH), 7.95 (s, 1H, $\text{H}_{2'}$), 7.84-7.80 (m, 2H, $2\text{H}_{2''}$), 7.74 (d, J = 7.6 Hz, 1H, H_4), 7.64-7.52 (m, 4H, $\text{H}_6+\text{H}_{4'}+\text{H}_5'+\text{H}_6'$), 7.36-7.32 (m, 2H, $2\text{H}_{3''}$), 7.16 (d, J = 7.6 Hz, 1H, H_7), 6.95 (t, 1H, J = 7.6 Hz, H_5), 6.73 (s, 1H, H_{vin}). ^{13}C NMR (101 MHz, DMSO- d_6) δ = 186.44 ($\text{C}=\text{O}$), 162.08 (CF), 154.31 (C_q), 139.93 (C_q), 136.47 (C_{ar}), 136.23 (C_q), 123.84 (C_q), 134.71 (C_q), 129.57 (C_{ar}), 129.10

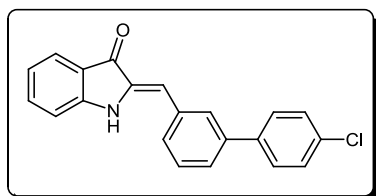
(C_{ar}), 128.70 (C_{ar}), 128.25 (C_{ar}), 126.81 (C_{ar}), 124.18 (C_{ar}), 120.07 (C_q), 119.87 (C_{ar}), 115.64 (C_{ar}), 112.69 (C_{ar}), 109.74 (C_{vin}).

(Z)-2-((4'-methylbiphenyl-3-yl)methylene)indolin-3-one (6.75)

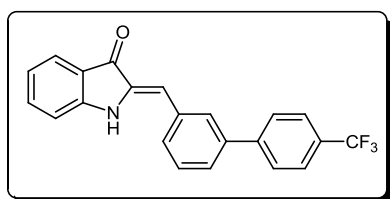


Purified by TLC (Toluene/EtOH = 80:20). Obtained as orange solid, yied 94%, mp 201-202 °C. ¹H NMR (400 MHz, DMSO-d₆) δ = 9.88 (s, 1H, NH), 7.91 (s, 1H, H_{2'}), 7.71 (d, *J* = 7.6 Hz, 1H, H₄), 7.65-7.52 (m, 6H, H₆+H_{4'}+H_{5'}+H_{6'}+2H_{2''}), 7.30 (d, *J* = 7.8 Hz, 2H, 2H_{3''}), 7.12 (d, *J* = 7.6 Hz, 1H, H₇), 6.94 (t, *J* = 7.6 Hz, 1H, H₅), 6.72 (s, 1H, H_{vin}), 2.35 (s, 3H, CH₃). ¹³C NMR (101 MHz, DMSO-d₆) δ = 186.62 (C=O), 154.43 (C_q), 141.02 (C_q), 137.22 (C_q), 136.96 (C_q), 136.61 (C_{ar}), 134.85 (C_{ar}), 134.78 (C_{ar}), 129.69 (C_{ar}), 128.49 (C_{ar}), 128.24 (C_{ar}), 126.96 (C_{ar}), 126.79 (C_{ar}), 124.30 (C_{ar}), 120.17 (C_q), 120.01 (C_{ar}), 112.84 (C_{ar}), 110.15 (C_{vin}), 20.84 (CH₃).

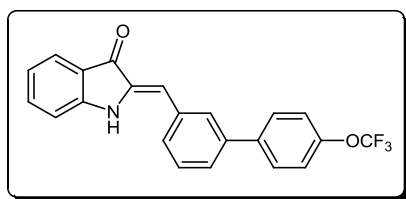
(Z)-2-((4'-chlorobiphenyl-3-yl)methylene)indolin-3-one (6.76)



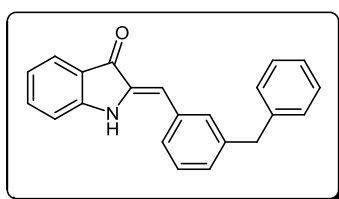
Purified by TLC (Toluene/EtOH = 80:20). Obtained as orange solid, yied 90%, mp 189-191 °C. ¹H NMR (400 MHz, DMSO-d₆) δ = 9.89 (s, 1H, NH), 7.97 (s, 1H, H_{2'}), 7.82-7.73 (m, 4H, H_{4'}+H_{6'}+2H_{2''}), 7.67-7.52 (m, 5H, H₄+H₆+H_{5'}+2H_{3''}), 7.16 (d, *J* = 7.6 Hz, 1H, H₇), 6.94 (t, *J* = 7.6 Hz, 1H, H₅), 6.73 (s, 1H, H_{vin}). ¹³C NMR (101 MHz, DMSO-d₆) δ = 186.13 (C=O), 154.30 (C_q), 139.62 (C_q), 138.59 (C_q), 136.49 (C_{ar}), 134.91 (C_q), 134.74 (C_q), 132.64 (C_q), 129.64 (C_{ar}), 129.04 (C_{ar}), 128.91 (C_{ar}), 128.83 (C_{ar}), 128.27 (C_{ar}), 126.77 (C_{ar}), 124.19 (C_{ar}), 119.88 (C_{ar}), 112.68 (C_{ar}), 109.63 (C_{vin}).

(Z)-2-((4'-(trifluoromethyl)biphenyl-3-yl)methylene)indolin-3-one (6.77)

Purified by TLC (Toluene/EtOH = 80:20). Obtained as orange solid, yied 91%, mp 228-230 °C. ^1H NMR (400 MHz, CDCl_3) δ = 7.76 (d, J = 7.7 Hz, 1H, H_4), 7.69 (s, 1H, $\text{H}_{2'}$), 7.62 (d, J = 8.5 Hz, 2H, $2\text{H}_{2''}$), 7.55-7.47 (m, 4H, $\text{H}_6+\text{H}_{4'}+\text{H}_5'+\text{H}_{6'}$), 7.33 (d, J = 8.5 Hz, 2H, $2\text{H}_{3''}$), 7.02-6.97 (m, 2H, H_5+H_7), 6.91 (s, 1H, H_{vin}), 6.88 (br, 1H, NH). ^{13}C NMR (101 MHz, CDCl_3) δ = 186.51 (C=O), 164.86 (C_q), 153.15 (C_q), 148.98 (C_q), 140.95 (C_q), 139.25 (C_q), 136.27 (C_{ar}), 135.68 (C_q), 135.46 (C_q), 129.77 (C_{ar}), 128.58 (C_{ar}), 128.39 (C_{ar}), 128.28 (C_{ar}), 127.28 (C_{ar}), 125.12 (C_{ar}), 121.70 (C_q), 121.41 (C_{ar}), 120.86 (C_{ar}), 112.04 (C_{ar}), 111.03 (C_{vin}).

(Z)-2-((4'-(trifluoromethoxy)biphenyl-3-yl)methylene)indolin-3-one (6.78)

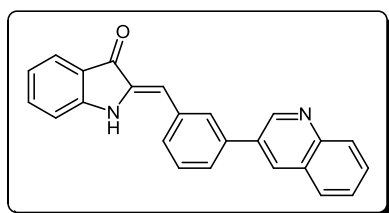
Purified by TLC (Toluene/EtOH = 80:20). Obtained as orange solid, yied 92%, mp 223-225 °C. ^1H NMR (400 MHz, DMSO-d_6) δ = 9.92 (s, 1H, NH), 7.93 (s, 1H, $\text{H}_{2'}$), 7.84-7.70 (m, 5H, $\text{H}_4+\text{H}_{4'}+\text{H}_{6'}+2\text{H}_{2''}$), 7.65-7.43 (m, 5H, $\text{H}_4+\text{H}_6+\text{H}_7+\text{H}_5'+2\text{H}_{3''}$), 6.98 (t, J = 7.6 Hz, 1H, H_5), 6.78 (s, 1H, H_{vin}). ^{13}C NMR (101 MHz, DMSO-d_6) δ = 186.45 (C=O), 152.98 (C_q), 144.80 (C_q), 141.82 (C_{ar}), 141.46 (C_q), 139.33 (C_q), 135.27 (C_q), 129.57 (C_{ar}), 128.17 (C_{ar}), 127.28 (C_{ar}), 126.87 (C_{ar}), 126.12 (C_{ar}), 125.13 (C_q), 123.13 (C_{ar}), 121.78 (C_q), 121.16 (C_{ar}), 121.01 (C_{ar}), 120.22 (C_q), 114.23 (C_{ar}), 109.56 (C_{vin}).

(Z)-2-(3-benzylbenzylidene)indolin-3-one (6.79)

Purified by TLC (Toluene/EtOH = 80:20). Obtained as orange oil, yied 96%. ^1H NMR (400 MHz, CDCl_3) δ = 7.73 (d, J = 7.7 Hz, 1H, H_4), 7.47 (t, J = 7.7 Hz, 1H, H_6), 7.38-7.31 (m, 4H, $\text{H}_2'+\text{H}_4'+\text{H}_5'+\text{H}_6'$), 7.27-7.17 (m, 5H, $2\text{H}_{2''}+2\text{H}_{3''}+\text{H}_{4''}$), 6.98-6.93 (m, 2H, H_5+H_7), 6.82 (s, 1H, H_{vin}), 6.71 (br, 1H, NH), 4.04 (s, 2H, CH_2). ^{13}C NMR (101 MHz, CDCl_3) δ = 186.61 (C=O), 153.19 (C_q), 142.43 (C_q), 140.69 (C_q), 136.24 (C_{ar}), 135.46 (C_q),

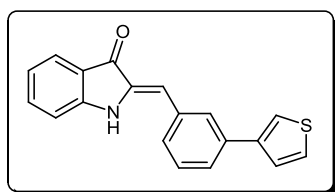
135.06 (C_q), 130.19 (C_{ar}), 129.46 (C_{ar}), 129.33 (C_{ar}), 129.17 (C_{ar}), 128.79 (C_{ar}), 127.32 (C_{ar}), 126.51 (C_{ar}), 125.17 (C_{ar}), 121.86 (C_q), 120.79 (C_{ar}), 112.04 (C_{ar}), 111.71 (C_{vin}), 41.85 (CH₂).

(Z)-2-(3-(quinolin-3-yl)benzylidene)indolin-3-one (6.80)

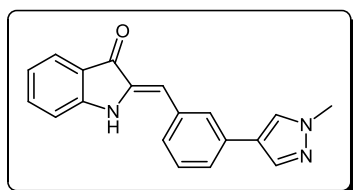


Purified by TLC (Toluene/EtOH = 80:20). Obtained as orange solid, yied 94%, mp 266-268 °C. ¹H NMR (400 MHz, DMSO-d₆) δ = 9.95 (s, 1H, NH), 9.37 (s, 1H, H_{2''}), 8.76 (s, 1H, H_{4''}), 8.20 (s, 1H, H_{2'}), 8.09 (d, *J* = 8.1 Hz, 2H, H_{4'}+H_{6'}), 7.89-7.79 (m, 3H, H₄+H_{5''}+H_{8''}), 7.70-7.61 (m, 3H, H_{5'}+H_{6''}+H_{7''}), 7.55 (t, *J* = 7.7 Hz, 1H, H₆), 7.17 (d, *J* = 7.7 Hz, 1H, H₇), 6.95 (d, *J* = 7.7 Hz, 1H, H₅), 6.78 (s, 1H, H_{vin}). ¹³C NMR (101 MHz, DMSO-d₆) δ = 186.43 (C=O), 154.29 (C_q), 149.70 (C_{ar}), 146.90 (C_q), 137.86 (C_q), 136.52 (C_{ar}), 135.12 (C_q), 134.78 (C_q), 133.33 (C_{ar}), 132.39 (C_q), 129.84 (C_{ar}), 129.74 (C_{ar}), 129.39 (C_{ar}), 128.71 (C_{ar}), 128.50 (C_{ar}), 127.62 (C_q), 127.22 (C_{ar}), 127.13 (C_{ar}), 124.22 (C_{ar}), 120.03 (C_q), 119.92 (C_{ar}), 112.67 (C_{ar}), 109.47 (C_{vin}).

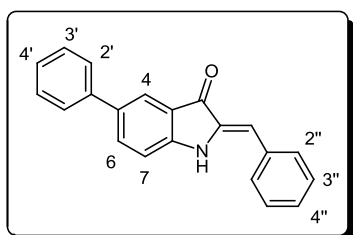
(Z)-2-(3-(thiophen-3-yl)benzylidene)indolin-3-one (6.81)



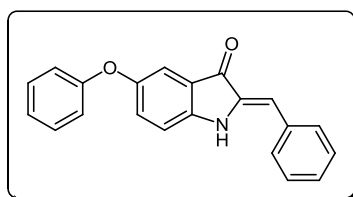
Purified by TLC (Toluene/EtOH = 80:20). Obtained as orange solid, yied 93%, mp 202-204 °C. ¹H NMR (400 MHz, DMSO-d₆) δ = 9.88 (s, 1H, NH), 8.02-8.01 (m, 2H, H_{2'}+H_{2''}), 7.72-7.68 (m, 4H, H_{4'}+H_{6'}+H_{4''}+H_{5''}), 7.60 (d, *J* = 7.8 Hz, 1H, H₄), 7.56-7.50 (m, 2H, H₆+H_{5'}), 7.16 (d, *J* = 7.8 Hz, 1H, H₇), 6.94 (t, *J* = 7.8 Hz, 1H, H₅), 6.71 (s, 1H, H_{vin}). ¹³C NMR (101 MHz, DMSO-d₆) δ = 136.27 (C_{ar}), 129.32 (C_{ar}), 128.09 (C_{ar}), 127.58 (C_{ar}), 126.96 (C_{ar}), 126.32 (C_{ar}), 126.01 (C_{ar}), 123.98 (C_{ar}), 121.52 (C_{ar}), 119.67 (C_{ar}), 112.51 (C_{ar}), 109.64 (C_{vin}).

(Z)-2-(3-(1-methyl-1H-pyrazol-4-yl)benzylidene)indolin-3-one (6.82)

Purified by TLC (Toluene/EtOH = 80:20). Obtained as orange solid, yied 94%, mp 212-213 °C. ^1H NMR (400 MHz, CDCl_3) δ = 7.80 (s, 1H, $\text{H}_{2'}$), 7.75 (d, J = 7.8 Hz, 1H, H_4), 7.66 (s, 1H, $\text{H}_{3''}$), 7.62 (s, 1H, H_5), 7.47 (t, J = 7.8 Hz, 1H, H_6), 7.43-7.39 (m, 3H, $\text{H}_{4'}+\text{H}_{5'}+\text{H}_{6'}$), 7.02 (d, J = 7.8 Hz, 1H, H_7), 6.97 (t, J = 7.8 Hz, 1H, H_5), 6.86 (br, 2H, $\text{H}_{\text{vin}}+\text{NH}$), 3.94 (s, 3H, CH_3). ^{13}C NMR (101 MHz, CDCl_3) δ = 186.76 (C=O), 153.42 (C_q), 136.63 (C_{ar}), 136.35 (C_{ar}), 135.73 (C_q), 135.51 (C_q), 133.54 (C_q), 129.82 (C_{ar}), 127.55 (C_{ar}), 127.39 (C_{ar}), 126.85 (C_{ar}), 125.77 (C_{ar}), 125.18 (C_{ar}), 122.72 (C_q), 121.82 (C_q), 120.82 (C_{ar}), 112.21 (C_{ar}), 111.40 (C_{vin}), 39.26 (CH_3).

(Z)-2-benzylidene-5-phenylindolin-3-one (6.83)

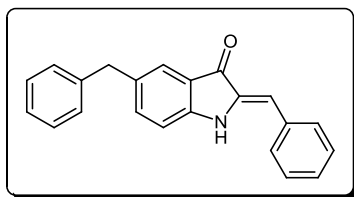
Purified by TLC (Toluene/EtOH = 80:20). Obtained as orange solid, yied 91%, mp 234-236 °C. ^1H NMR (400 MHz, CDCl_3) δ = 8.00 (s, 1H, H_4), 7.75 (d, J = 8.1 Hz, 1H, H_6), 7.59-7.57 (m, 4H, $2\text{H}_{2'}+2\text{H}_{2''}$), 7.49-7.42 (m, 4H, $2\text{H}_{3'}+2\text{H}_{3''}$), 7.38-7.32 (m, 2H, $\text{H}_{4'}+\text{H}_{4''}$), 7.08 (d, J = 8.1 Hz, H_7), 6.91 (br, 2H, $\text{H}_{\text{vin}}+\text{NH}$). ^{13}C NMR (101 MHz, CDCl_3) δ = 186.68 (C=O), 152.49 (C_q), 140.20 (C_q), 135.82 (C_q), 135.41 (C_{ar}), 134.82 (C_q), 134.27 (C_q), 129.67 (C_{ar}), 129.41 (C_{ar}), 129.04 (C_{ar}), 128.78 (C_{ar}), 127.28 (C_{ar}), 126.79 (C_{ar}), 123.34 (C_{ar}), 122.32 (C_q), 112.38 (C_{ar}), 112.08 (C_{vin}).

(Z)-2-benzylidene-5-phenoxyindolin-3-one (6.84)

Purified by TLC (Toluene/EtOH = 80:20). Obtained as orange solid, yied 91%, mp 212-214 °C. ^1H NMR (400 MHz, CDCl_3) δ = 7.82 (s, 1H, H_4), 7.77-7.68 (m, 4H, $2\text{H}_{2'}+2\text{H}_{2''}$), 7.48-7.27 (m, 7H, $\text{H}_6+2\text{H}_{3'}+2\text{H}_{3''}+\text{H}_{4'}+\text{H}_{4''}$), 7.03 (d, J = 7.6 Hz, 1H, H_7), 6.85 (br, 2H, $\text{H}_{\text{vin}}+\text{NH}$). ^{13}C NMR (101 MHz, CDCl_3) δ = 186.55 (C=O), 151.98 (C_q), 141.02 (C_q), 136.05 (C_{ar}), 135.34 (C_q), 134.09 (C_q), 133.02 (C_q), 129.02 (C_{ar}), 128.95 (C_{ar}), 128.87

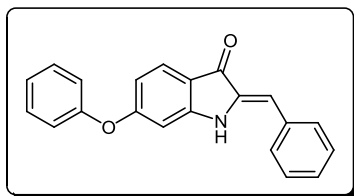
(C_{ar}), 128.34 (C_{ar}), 128.03 (C_{ar}), 126.22 (C_{ar}), 124.08 (C_{ar}), 122.44 (C_q), 112.01 (C_{ar}), 110.98 (C_{vin}).

(Z)-5-benzyl-2-benzylideneindolin-3-one (6.85)



Purified by TLC (Toluene/EtOH = 80:20). Obtained as orange solid, yield 92%, mp 203-205 °C. ¹H NMR (400 MHz, CDCl₃) δ = 7.61 (s, 1H, H₄), 7.57 (d, *J* = 7.9 Hz, 2H, 2H_{2''}), 7.47 (t, *J* = 7.9 Hz, 2H, 2H_{3''}), 7.38-7.20 (m, 7H, H₆+2H_{2'}+2H_{3'}+H_{4'}+H_{4''}), 6.94 (d, *J* = 7.6 Hz, 1H, H₇), 6.87 (s, 1H, H_{vin}), 6.79 (br, 1H, NH), 3.98 (s, 2H, CH₂). ¹³C NMR (101 MHz, CDCl₃) δ = 186.70 (C=O), 152.00 (C_q), 140.96 (C_q), 137.30 (C_{ar}), 135.94 (C_q), 134.93 (C_q), 134.02 (C_q), 129.64 (C_{ar}), 129.35 (C_{ar}), 128.97 (C_{ar}), 128.74 (C_{ar}), 128.63 (C_{ar}), 126.41 (C_{ar}), 124.99 (C_{ar}), 122.08 (C_q), 112.21 (C_{ar}), 111.67 (C_{vin}), 41.35 (CH₂).

(Z)-2-benzylidene-6-phenoxyindolin-3-one (6.86)



Purified by TLC (Toluene/EtOH = 80:20). Obtained as orange oil, yield 89%. ¹H NMR (400 MHz, CDCl₃) δ = 8.02 (d, *J* = 8.3 Hz, 1H, H₄), 7.57-7.43 (m, 5H, H₇+2H_{2'}+2H_{2''}), 7.53 (t, *J* = 7.6 Hz, 2H, 2H_{3'}), 7.36-7.24 (m, 5H, H₅+ H_{4'}+2H_{3''}+H_{4''}), 6.91 (s, 1H, H_{vin}), 6.85 (br, 1H, NH). ¹³C NMR (101 MHz, CDCl₃) δ = 186.54 (C=O), 150.41 (C_q), 144.26 (C_q), 137.02 (C_q), 134.87 (C_q), 131.05 (C_{ar}), 130.02 (C_{ar}), 129.18 (C_{ar}), 128.23 (C_{ar}), 127.34 (C_{ar}), 125.08 (C_q), 124.01 (C_{ar}), 122.89 (C_{ar}), 121.01 (C_q), 118.83 (C_{ar}), 112.03 (C_{ar}), 110.84 (C_{ar}).

8.8. Biological assays

8.8.1. Biological activity against *P. falciparum* W2 and FCR3 strains

Compounds were assayed against human red blood cells infected with 1% ring stage W2 -strain *P. falciparum* synchronized with 5% sorbitol. These cells were incubated with tested compounds in 96-well plates at 37 °C for 48 hours in RPMI-1640 medium supplemented with 25 mM HEPES pH 7.4, 10% heat inactivated human serum (or 0.5% Albumax/2% human serum), and 100 µM hypoxanthine under an atmosphere of 3% O₂, 5% CO₂, 91% N₂. After 48 hours, the cells were fixed in 2% formaldehyde in PBS, transferred into PBS with 100 mM NH₄Cl, 0.1% Triton X-100, 1 nM YOYO-1, and then analyzed in a flow cytometer (FACSort, Beckton Dickinson; EX 488 nm, EM 520 nm). Values of IC₅₀ were calculated using GraphPad PRISM software.

8.8.2. Biological activity against *P. falciparum* Dd2 and 3D7 strain

Laboratory-adapted *P. falciparum* Dd2 and 3D7 strains were continuously cultured as previously described³⁶⁰, with minor modifications. Parasites were cultivated on human erythrocytes suspended in RPMI 1640 medium supplemented with 25 mM HEPES, 6.8 mM hypoxanthine and 10% AlbuMAX II, at pH 7.2. Cultures were maintained at 37 °C under an atmosphere of 5% O₂, 3–5% CO₂, and N₂ and synchronized by double sorbitol treatment prior to the assays³⁶¹. Staging and parasitaemia were determined by light microscopy of Giemsa-stained thin blood smears. The antimalarial activity of the inhibitors and CQ were determined using the SYBR Green I assay as previously described. Stock solutions of the drugs (10 mM) were prepared in DMSO and serially diluted in complete media. Parasitized erythrocytes at the early ring stage were added to a final 1% parasitaemia and 3% hematocrit to each triplicate well of a 96-well plate, and incubated for 48h at 37 °C prior to growth assessment with SYBR Green I nucleic acid. Each compound was analyzed at a final concentration range of 0-50 µM (0.2% DMSO), whereas CQ was assayed at a concentration range of 0-10 µM. SYBR Green I fluorescence was

quantified using a multi-mode microplate reader (Dynex Triad) and analyzed by nonlinear regression using GraphPad Prism 5 demo version.

8.8.3. Biological activity against *S. cerevisiae*

Activity against *S. cerevisiae* was performed using the microdilution method³⁶². The culture compounds were obtained from Oxoid (Hampshire, UK) and Biokar Diagnostics (Beauvais, France). *S. cerevisiae* was incubated with the tested compounds, based on serial dilutions, in YPG medium (glucose 1.0% w/v, yeast extract 0.5 % w/v, peptone 0.5% w/v) in 96-well plates for 48 hours at 30 °C. After 48 hours, the absorbance was measured at 600 nm in a spectrofluorimeter (Zenith Anthos 3100). All assays were performed in triplicate and in three independent experiments. Values of IC₅₀ were calculated using GraphPad PRISM Software.

8.8.4. Hemozoin-like crystals growth inhibition

Inhibition of hemozoin-like crystals formation by tested compounds was assessed using the previously described *in vitro* method³²⁵. In short, a hemozoin-like crystals stock suspension was sonicated for 3 minutes and diluted in fresh broth medium to the final concentration of 2 µM (heme equivalents) in the wells of a 96-wells plate. Stock solutions of tested compounds were prepared at 25 mM in DMSO while stock solutions of CQ (positive control) and gentamicin (negative control) were prepared at 100 mM in distilled water. All solutions were 0.22 µm-filtered previous to being diluted to 0-1000 µM final concentrations in the wells. Plates were incubated at 37 °C in a 5% CO₂ atmosphere for 5 days to observe the presence or absence of crystal growth. All tests were performed in triplicate.

8.8.5. *In vitro* drug combination assay

Analysis of the combination effects of inhibitors with CQ were determined by a modified fixed ratio isobologram method^{337-339, 363}. Initially, the 50% inhibitory concentration (IC₅₀) values of the individual test compounds were determined. Subsequently, dose-response experiments at 2-fold dilutions were run for different drug combinations (IC₅₀ ratios equals 5:0, 4:1, 3:2, 2:3, 1:4 or 0:5) and their IC₅₀s in the combination determined. The fractional inhibitory concentration (FIC; FIC₅₀ = IC₅₀ of drug in the combination/IC₅₀ of drug when tested alone) of each drug was calculated and plotted as an isobologram.

8.8.6. Cytochrome *bc*₁ complex activity

Mitochondria from *P. falciparum* 3D7A strain were isolated by a method that employed nitrogen cavitation, differential centrifugation and a sucrose density gradient. Cytochrome *bc*₁ complex activity was measured as the reduction of cytochrome *c*. The reduction of cytochrome *c* was monitored by the increase in absorbance at 550 nm. An appropriate amount of purified mitochondria was diluted in an assay mixture containing 50 mM KH₂PO₄ pH 7.4, 0.2 mM EDTA, 1 mM NaN₃, 2.5 mM KCN, 250 mM Sucrose and 50 μM cytochrome *c*. The reaction was started by the addition of 25 μM decylubiquinol. To measure the non enzymatic reduction of cytochrome *c* by decylubiquinol, 800 nM myxothiazol and 100 nM antimycin A were added. SoftMax Pro software provided data acquisition. Non-linear regression analysis was used to fit the normalized results of the dose response curves and IC₅₀s were determined using the Grafit5 software package³⁶⁴.

8.8.7. Growth inhibition assays

ScURA1 gene from *S. cerevisiae* was amplified from genomic DNA and cloned into vector pLN-14. *P. falciparum* Dd2attB strain was transfected by electroporation and stable transfectants were selected with blasticidin. Dd2attB_yeastDHODH and its parental strain Dd2attB were used in these assays. The sensitivity of *P. falciparum*-infected erythrocytes

to various drugs was determined using the [³H]hypoxanthine incorporation method with an inoculum size of 0.5% parasitemia and 2% hematocrit. Plates are incubated at 37 °C, 5% CO₂, 5% O₂, 95% N₂. After 24h of incubation, [³H]hypoxanthine was added and plates were incubated for another 24 h. After that period, plates were harvested on a glass fiber filter using a TOMTEC Cell harvester 96. Filters were dried and melt on scintillator sheets and the incorporated radioactivity was quantified by use of a Wallac Microbeta Trilux (Model 1450 LS- Perkin Elmer). The Dd2 cell line containing yeast DHODH and its parental strain were cultured in the absence and in the presence of proguanil (1 μM). Non-linear regression analysis is used to fit the normalized results of the dose response curves and IC₅₀s determined using the Grafit5 software package³⁶⁴.

8.8.8. *In vitro* cytotoxicity

The cytotoxicity was assessed using general cell viability endpoint MTT (3-(4,5-dimethyl-2-thiazolyl)-2,5-diphenyl-2H-tetrazolium bromide)³⁶⁵⁻³⁶⁶. Briefly, the day before experiment cells NIH 3T3 (mouse embryonic fibroblast cell line, ATCC CRL-1658) or HEK 293T (human embryonic kidney epithelial cell line, ATCC CRL-11268) are seeded in 96 well tissue culture plates, in RPMI 1640 culture medium supplemented with 10% fetal serum bovine, 100 units of penicillin G (sodium salt) and 100 μg of streptomycin sulfate and 2mM L-glutamine, at a concentration that allow cells to grow exponentially during the time of the assay. Compounds to be tested are diluted in dimethylsulfoxide (DMSO) and then serially diluted in the culture medium. Compounds at different concentrations and DMSO are then added to the cells. Cells are incubated at 37 °C in humidified 5% CO₂ atmosphere. After 48 hours, cell media containing DMSO (for control cells) or tested compound solution (for test cells) was removed and replaced with fresh medium containing MTT dye. After 3h of incubation the complete media was removed and the intracellular formazan crystals were solubilised and extracted with DMSO. After 15 min at room temperature the absorbance was measured at 570 nm in microplate reader.

The percentage of cell viability was determined for each concentration of tested compound as described previously³⁶⁵⁻³⁶⁶. The concentration of a compound reflecting a

50% inhibition of cell viability (i.e. IC_{50}) was determined from the concentration-response curve. This was done by applying non-linear regression procedure to the concentration response data using GraphPad PRISM software.

APPENDICES

Appendix A – Protein sequences

1	MNNIKYVELFYKCKIFRKNGLNRIIRRNNGGTFNHNIKENERIPPAEDPSYKNLFDHAED	60	Q8IL75	Q8IL75_PLAF7
1	-----	0	P08067	UCRI_YEAST
1	-----	0	P13272	UCRI_BOVIN
1	-----	0	Q5ZLR5	UCRI_CHICK
1	-----	0	Q02762	UCRI_RHOSH
61	IKLWEIEEKQNVSHKKVEDLSELVEPSNHPHQYEGIFARTRYAHYNQTAEPVF-----	113	Q8IL75	Q8IL75_PLAF7
1	-----	0	P08067	UCRI_YEAST
1	-----MLSVAA----RSGPFAPVLSATSRGVAGALRPLVQAAV	34	P13272	UCRI_BOVIN
1	-----MLSVAA----RSGPFAPYLSAAAHAVPGPLKALAPAL	34	Q5ZLR5	UCRI_CHICK
1	-----	0	Q02762	UCRI_RHOSH
114	PRKPDLEKELASGANVTRIDVWH-NPKPAIVSIGKFEPRNFRPAGYAENCNP--PESI	170	Q8IL75	Q8IL75_PLAF7
1	-----MLGIRSSVKTCFKPM-----SLTS---KRL-I	23	P08067	UCRI_YEAST
35	PATSESPVLDLKRVS-LCRESLRQQAAGRPLV-----ASVSLNVPASVRYSH	80	P13272	UCRI_BOVIN
35	--RAEKVVLDLKRPL-LCRESMSGRSARRDLV-----AGISLNPASVRYVH	78	Q5ZLR5	UCRI_CHICK
1	-----	0	Q02762	UCRI_RHOSH
171	NSDHHPDFREYRL-----RSGNEDRRSFMFYFISASYFFIMSSIMRSAICKSVHFF	220	Q8IL75	Q8IL75_PLAF7
24	SQSLASKSTYRTPNFDDVLKEN-NDADKGRSYAYFMVGAMGLSSAGAKSTVETFISSM	82	P08067	UCRI_YEAST
81	TDIKVPDFSDYRREPEVLDSTKSSKESSEARKGFSYLVTATTVGVAIAAKNVVSQFVSSM	140	P13272	UCRI_BOVIN
79	NDVTVPDFSAYRREDVMDATISSQTSSEDRKGFSLVTATACVATAYAAKNVVTQFISSL	138	Q5ZLR5	UCRI_CHICK
1	-----MSNAEDHAGTRRDFLYYATAGAGAV---ATGAAVWPLINQM	38	Q02762	UCRI_RHOSH
	: : * . : : : :			
221	WISKDLVAGGTTELDMRTVNPGEHVVIKWRGKPVFVKHRTPEDIQRAKEDDKLIQTMRDP	280	Q8IL75	Q8IL75_PLAF7
83	TATADVLAMAKVEVNLAAIPLGKNVVVKWQKPVFIRHRTPEIQEANSVD--MSALKDP	140	P08067	UCRI_YEAST
141	SASADVLAMSKIEIKLSDIPEGKNMAFKWRGKPLFVRHRTKKEIDQEAAVE--VSQLRDP	198	P13272	UCRI_BOVIN
139	SASADVLALSKIEIKLSDIPEGKNVAFKWRGKPLFVRHRTQAEINQEAQEV--VSKLRDP	196	Q5ZLR5	UCRI_CHICK
39	NPSADVQALASIFVDVSSVEPGVQLTVKFLGKPIFIRRRTEADIELGRSVQ--LGQLVDT	96	Q02762	UCRI_RHOSH
	: * : * . . : : : * . . . * : * : * : * : * : * : * : *			
281	QLDS-----DRIKPEWLVNIGICTHLGCVPAQG--GNYSYGFPCPCHGSHY	324	Q8IL75	Q8IL75_PLAF7
141	QTDA-----DRVKDPQWLIMLGICTHLGCVPIGE--AGDFGGWFPCPCHGSHY	185	P08067	UCRI_YEAST
199	QHDL-----ERVKKPEWVILIGVCTHLGCVPIAN--AGDFGGYYCPCPCHGSHY	243	P13272	UCRI_BOVIN
197	QHDL-----DRVKKPEWVILVGVCTHLGCVPIAN--SGDFGGYYCPCPCHGSHY	241	Q5ZLR5	UCRI_CHICK
97	NARNANIDAGAEATDQNRTLDEAGEWLVWGVCTHLGCVPIGGVSGDFGGWFPCPCHGSHY	156	Q02762	UCRI_RHOSH
	: : : * : * : * : * : * : * : * : * : * : * : * : * : * : *			
325	DNSGRIRQGPAPSNLEVPPEYFVDENTIKIG	355	Q8IL75	Q8IL75_PLAF7
186	DISGRIRKGPAPLNLEIPAYEFDGDKVIVG-	215	P08067	UCRI_YEAST
244	DASGRIRKGPAPLNLEVPSEYFTSDDMVIVG	274	P13272	UCRI_BOVIN
242	DASGRIRKGPAPYNLEVPYQFVGGDDLVVVG	272	Q5ZLR5	UCRI_CHICK
157	DSAGRIRKGPAPENLPIPLAKFIDETTIQLG	187	Q02762	UCRI_RHOSH
	* : * * * : * * * : * : * : * : * : *			

Figure 2. Sequence alignment between Rieske ISP of *P. falciparum* and the four potential templates.

1	-----MNFYSINLVKAHLINYPCLNINFLWNYGFLLGIIFFIQII	41	Q7HP03	Q7HP03_PLAF7
1	-----MAFRKSNVYLSLVNSYIIDSPPQSSINYWNNMGSLGLCLVIQIV	45	P00163	CYB_YEAST
1	-----MTNIRKSHPLMKIVNNAFIDLPAASNISSWNFGSLLGICLILQIL	46	P00157	CYB_BOVIN
1	-----MAPNIRKSHPLKMINNSLIDLPAASNISAWNFGSLLAVCLMTQIL	47	P18946	CYB_CHICK
1	MSGIPHDHYEPRTGIEKWLHSRLPIVALAYDTIMIPTRNLNMMWIWGVVLAFCVLVLIQIV	60	Q02761	CYB_RHOSH
	: : : * * * . . . * * : : : . . . * : *			
42	TGVFLASRYTPDVSYAYYSIQHILRELWSGCFRYMHAATGASLVFLTYLHLIRGLNYSY	101	Q7HP03	Q7HP03_PLAF7
46	TGIFMAMHYSSNIELAFSSVEHIMRDVHNGYILRYLHANGASFFFMMVMFMHMAKGLYYS	105	P00163	CYB_YEAST
47	TGLFLAMHYTSDTTTAFSSVTHICRDVNYGWIIRYMHANGASMMFFICLYMHVGRGLYYS	106	P00157	CYB_BOVIN
48	TGLLLAMHYTADTSLAFSSVAHTCRNVQYQWLIIRNLHANGASFFFCIFLHIGRGLYYS	107	P18946	CYB_CHICK
61	TGIVLAMHYTPHVDLAFASVEHIMRNNGGFMLRYLHANGASLFFIAYVLHIFRGLYYS	120	Q02761	CYB_RHOSH
	** : : * * : . . * : * * * * : : * : * : * : * : * : * : * : *			
102	MYL--PLWSIGLILFIMFIVTAFVGYVLPWQMSYWGATVITNLLSSIPV---AVIWI	155	Q7HP03	Q7HP03_PLAF7
106	YRSPRVTLWNVGVIIIFILTIATAFLGYCCVYQMSHWGATVITNLFSAIPFVGNDIVSWL	165	P00163	CYB_YEAST
107	YTF--LETWNIGVILLTLMATAFMGYVLPWQMSFWGATVITNLLSAIPYIGTNLVEWI	164	P00157	CYB_BOVIN
108	YLY--KETWNGVILLTLMATAFMGYVLPWQMSFWGATVITNLFSAIPYIGTNLVEWA	165	P18946	CYB_CHICK
121	YKAPREVTVIVGMILYLAMMATAFMGYVLPWQMSFWGATVITGLFGAIPGIGHSIQITWL	180	Q02761	CYB_RHOSH
	* * : : : . : * * : * * * * : * * * * * * * * : : * : *			
156	CGGYTVSDPTIKRFFVLHFIPLPFIGLCIVFIHIFLHLHGSTNPLGYD-----TAL	206	Q7HP03	Q7HP03_PLAF7
166	WGGFSVSNPTIQRFALHYLVFPFIIAAMVIMHMLALHIGSSNPLGIT-----GNLD	217	P00163	CYB_YEAST
165	WGGFSVDKATLIRFFAFHFIPLPFIIAAMVHLLFLHETGSNNPTGIS-----SDVD	216	P00157	CYB_BOVIN
166	WGGFSVDNPTLIRFFALHFLLPFAIAGITIIHLLTFLHESGSGNPLGIS-----SDSD	217	P18946	CYB_CHICK
181	LGGPVDNATLNRFFSLHYLLPFVIALVAIHIAFWAFHSTGNNPTGVEVRRTSKAEAQKD	240	Q02761	CYB_RHOSH
	** : : * . . * * * : * * * : : . . * : * : * * * * * * * * * * *			
207	KIPFYPNLLSLDVKGFNNVILFLIQSLFGIIPLSHPDNAIVVNTYVTPSQIVPEWYFLP	266	Q7HP03	Q7HP03_PLAF7
218	RIPMHSYFIKDLVTVFLFMLLALFVYSPNTLGHDPDNIIPGNPLVTPASIVPEWYLLP	277	P00163	CYB_YEAST
217	KIPFHPYITIKDILGALLLILALMLLVLFAPDLLGDPDNYTPANPLNTPPHIKPEWYFLF	276	P00157	CYB_BOVIN
218	KIPFHPYYSFKDILGLTMLTPTFLTLALFSPNLLGDPDNFTPANPLVTPPHIKPEWYFLF	277	P18946	CYB_CHICK
241	TVPFWPYFIIKDVFAFVLLVFFFAIVGFMFNYLGHDPDNYIEANPLSTPAHIVPEWYFLP	300	Q02761	CYB_RHOSH
	: * : . . . : : : : * . . * * * * * * * * * * * * * * * * * *			
267	FYAMLKTV-----PSKPAGLVIVLLSLQLLFLLAEE-QRSLTTIIQFK	307	Q7HP03	Q7HP03_PLAF7
278	FYAILRSI-----PDKLLGVITMFAAILVLLVLPFTDRSVVRGNTFK	319	P00163	CYB_YEAST
277	AYAILRSI-----PNKLGGLALAFSILILALIPLLHTSKQRSMMFR	318	P00157	CYB_BOVIN
278	AYAILRSI-----PNKLGGLALAAASVLLIFLIPFLHKSQRMTMFR	319	P18946	CYB_CHICK
301	FYAILRAFTADVWVQIANFISFGIIDAQFFGVLAMFGAILVMALVFWLDTSPVRSGRYR	360	Q02761	CYB_RHOSH
	** : * : * * * : : : : : : : : * * * * * * * * * * *			
308	MIFGARDYSVPIIWF-MCAFYALLWIGCQLPQDIFILYGRFLFVLFCCSGLFVLVH----	362	Q7HP03	Q7HP03_PLAF7
320	-----VLSKFFFFIFVFNFVLLGQIGACHVEVPYVLMGQIATFIYFAYFLIIVPVISTI	373	P00163	CYB_YEAST
319	-----PLSQCLFWALVADLLTLTWIGGQPVHEHPYITIGQASVLYVLLILVLMPTAGTI	372	P00157	CYB_BOVIN
320	-----PLSQTLFWLVANLLTLTWIGSQQVHEHPYITIGQMASLSYFTILLILFPTIGTL	373	P18946	CYB_CHICK
361	-----PMFKIYFWLLAADFVILTWVGAQQTFFPYDWSLIASAYWFAYFLVILPILGAI	414	Q02761	CYB_RHOSH
	: : : * * : * : . . . : : : : * * * * * * * * * * * * * * * *			
363	-----YRTHYDYSSQANI-----	376	Q7HP03	Q7HP03_PLAF7
374	ENVLFYIGRVNK-----	385	P00163	CYB_YEAST
373	ENKLLK-----	379	P00157	CYB_BOVIN
374	ENKMLNY-----	380	P18946	CYB_CHICK
415	EKPVAPPATIEEDFNAHYSPATGGTKTVVAE	445	Q02761	CYB_RHOSH

Figure 3. Sequence alignment between cytochrome *b* of *P. falciparum* and the four potential templates.

Appendix B – Identity in Q_o binding site

Table 1. Comparison between the amino acid residues in Q_o binding pocket for *S. cerevisiae* (*Sc*), *P. falciparum* (*Pf*), *B. Taurus* (*Bt*), *G. gallus* (*Gg*), *R. sphaeroides* (*Rs*) and *H. sapiens* (*Hs*). Highlighted in green and are the amino acid residues that are conserved in all species.

	Cytochrome <i>b</i>								
<i>Sc</i>	I122	I125	A126	F129	L130	M139	W142	G143	V146
<i>Pf</i>	M116	I119	V120	F123	V124	M133	W136	G137	V140
<i>Bt</i>	L121	M124	A125	F128	M129	M138	W141	G142	V145
<i>Gg</i>	L122	M125	A126	F129	V130	M139	W142	G143	V146
<i>Rs</i>	L137	M140	A141	F144	M145	M154	W157	G158	V161
<i>Hs</i>	L121	M124	A125	F128	M129	M138	W141	G142	V145

	Cytochrome <i>b</i>								
<i>Sc</i>	I147	F151	L165	F179	L182	I269	V270	P271	E272
<i>Pf</i>	I141	L145	I155	F169	L172	I258	V259	P260	E261
<i>Bt</i>	I146	L150	I164	F178	F181	I268	V269	P270	E271
<i>Gg</i>	I147	F151	A165	F179	L182	I269	K270	P271	E272
<i>Rs</i>	I162	F166	L180	F194	L197	I292	V293	P294	E295
<i>Hs</i>	I146	L150	I164	F178	F181	I268	K269	P270	E271

	Cytochrome <i>b</i>							Rieske ISP	
<i>Sc</i>	L275	F278	Y279	L282	M295	F296	I299	C180	H181
<i>Pf</i>	F264	F267	Y268	L271	V284	L285	L288	C319	H320
<i>Bt</i>	F272	A277	Y278	L281	L294	A295	I298	C138	H139
<i>Gg</i>	F275	A278	Y279	L282	L295	A296	V299	C236	H237
<i>Rs</i>	L298	F301	Y302	L305	M336	F337	I340	C150	H151
<i>Hs</i>	F274	A277	Y278	L281	L294	L295	I298	C238	H239

REFERENCES

1. World Health Organization.
www.who.int/malaria/publications/world_malaria_report_2012/report/en/ (accessed 02.01.2014).
2. Wu, T.; Nagle, A. S.; Chatterjee, A. K., Road Towards New Antimalarials - Overview of the Strategies and their Chemical Progress. *Curr Med Chem* **2011**, *18* (6), 853-871.
3. Rodrigues, T.; Moreira, R.; Lopes, F., New hope in the fight against malaria? *Future Med Chem* **2011**, *3* (1), 1-3.
4. Shetty, P., The numbers game. *Nature* **2012**, *484* (7395), S14-S14.
5. Fry, M.; Pudney, M., Site of Action of the Antimalarial Hydroxynaphthoquinone, 2-[Trans-4-(4'-Chlorophenyl) Cyclohexyl]-3-Hydroxy-1,4-Naphthoquinone (566c80). *Biochem Pharmacol* **1992**, *43* (7), 1545-1553.
6. Sachs, J.; Malaney, P., The economic and social burden of malaria. *Nature* **2002**, *415* (6872), 680-685.
7. Schlitzer, M., Malaria chemotherapeutics part 1: History of antimalarial drug development, currently used therapeutics, and drugs in clinical development. *ChemMedChem* **2007**, *2* (7), 944-986.
8. White, N. J., Plasmodium knowlesi: The fifth human malaria parasite. *Clin Infect Dis* **2008**, *46* (2), 172-173.
9. Tuteja, R., Malaria - an overview. *Febs J* **2007**, *274* (18), 4670-4679.
10. Ashley, E.; McGready, R.; Proux, S.; Nosten, F., Malaria. *Travel Med Infect Dis* **2006**, *4* (3), 159-173.
11. Mehlotra, R. K.; Henry-Halldin, C. N.; Zimmerman, P. A., Application of pharmacogenomics to malaria: a holistic approach for successful chemotherapy. *Pharmacogenomics* **2009**, *10* (3), 435-449.
12. Price, R. N.; Douglas, N. M.; Anstey, N. M., New developments in Plasmodium vivax malaria: severe disease and the rise of chloroquine resistance. *Curr Opin Infect Dis* **2009**, *22* (5), 430-435.
13. Mueller, I.; Galinski, M. R.; Baird, J. K.; Carlton, J. M.; Kochar, D. K.; Alonso, P. L.; del Portillo, H. A., Key gaps in the knowledge of Plasmodium vivax, a neglected human malaria parasite. *Lancet Infect Dis* **2009**, *9* (9), 555-566.

14. Fidock, D. A.; Eastman, R. T.; Ward, S. A.; Meshnick, S. R., Recent highlights in antimalarial drug resistance and chemotherapy research. *Trends Parasitol* **2008**, *24* (12), 537-544.
15. Hemingway, J.; Ranson, H., Insecticide resistance in insect vectors of human disease. *Annu Rev Entomol* **2000**, *45*, 371-391.
16. Girard, M. P.; Reed, Z. H.; Friede, M.; Kieny, M. P., A review of human vaccine research and development: Malaria. *Vaccine* **2007**, *25* (9), 1567-1580.
17. Flannery, E. L.; Chatterjee, A. K.; Winzeler, E. A., Antimalarial drug discovery - approaches and progress towards new medicines. *Nat Rev Microbiol* **2013**, *11* (12), 849-862.
18. Arav-Boger, R.; Shapiro, T. A., Molecular mechanisms of resistance in antimalarial chemotherapy: The unmet challenge. *Annu Rev Pharmacol* **2005**, *45*, 565-585.
19. Frederich, M.; Dogne, J. M.; Angenot, L.; De Mol, P., New trends in anti-malarial agents. *Curr Med Chem* **2002**, *9* (15), 1435-56.
20. Mantel, P. Y.; Hoang, A. N.; Goldowitz, I.; Potashnikova, D.; Hamza, B.; Vorobjev, I.; Ghiran, I.; Toner, M.; Irimia, D.; Ivanov, A. R.; Barteneva, N.; Marti, M., Malaria-infected erythrocyte-derived microvesicles mediate cellular communication within the parasite population and with the host immune system. *Cell Host Microbe* **2013**, *13* (5), 521-34.
21. Regev-Rudzki, N.; Wilson, D. W.; Carvalho, T. G.; Sisquella, X.; Coleman, B. M.; Rug, M.; Bursac, D.; Angrisano, F.; Gee, M.; Hill, A. F.; Baum, J.; Cowman, A. F., Cell-Cell Communication between Malaria-Infected Red Blood Cells via Exosome-like Vesicles. *Cell* **2013**, *153* (5), 1120-1133.
22. Aly, A. S. I.; Vaughan, A. M.; Kappe, S. H. I., Malaria Parasite Development in the Mosquito and Infection of the Mammalian Host. *Annu Rev Microbiol* **2009**, *63*, 195-221.
23. Kumar, A.; Katiyar, S. B.; Agarwal, A.; Chauhan, P. M. S., Perspective in antimalarial chemotherapy. *Curr Med Chem* **2003**, *10* (13), 1137-1150.
24. Burrows, J. N.; Chibale, K.; Wells, T. N. C., The State of the Art in Anti-Malarial Drug Discovery and Development. *Curr Top Med Chem* **2011**, *11* (10), 1226-1254.
25. Gardner, M. J.; Hall, N.; Fung, E.; White, O.; Berriman, M.; Hyman, R. W.; Carlton, J. M.; Pain, A.; Nelson, K. E.; Bowman, S.; Paulsen, I. T.; James, K.; Eisen, J. A.; Rutherford, K.; Salzberg, S. L.; Craig, A.; Kyes, S.; Chan, M. S.; Nene, V.; Shallom, S. J.; Suh, B.; Peterson, J.;

- Angiuoli, S.; Pertea, M.; Allen, J.; Selengut, J.; Haft, D.; Mather, M. W.; Vaidya, A. B.; Martin, D. M. A.; Fairlamb, A. H.; Fraunholz, M. J.; Roos, D. S.; Ralph, S. A.; McFadden, G. I.; Cummings, L. M.; Subramanian, G. M.; Mungall, C.; Venter, J. C.; Carucci, D. J.; Hoffman, S. L.; Newbold, C.; Davis, R. W.; Fraser, C. M.; Barrell, B., Genome sequence of the human malaria parasite *Plasmodium falciparum*. *Nature* **2002**, *419* (6906), 498-511.
26. Kappe, S. H. I.; Vaughan, A. M.; Boddey, J. A.; Cowman, A. F., That Was Then But This Is Now: Malaria Research in the Time of an Eradication Agenda. *Science* **2010**, *328* (5980), 862-866.
27. Calas, M.; Ancelin, M. L.; Cordina, G.; Portefaix, P.; Piquet, G.; Vidal-Sailhan, V.; Vial, H., Antimalarial activity of compounds interfering with *Plasmodium falciparum* phospholipid metabolism: Comparison between mono- and bisquaternary ammonium salts. *J Med Chem* **2000**, *43* (3), 505-516.
28. Ancelin, M. L.; Calas, M.; Vidal-Sailhan, V.; Herbute, S.; Ringwald, P.; Vial, H. J., Potent inhibitors of *Plasmodium* phospholipid metabolism with a broad spectrum of in vitro antimalarial activities. *Antimicrob Agents Ch* **2003**, *47* (8), 2590-2597.
29. Le Roch, K. G.; Johnson, J. R.; Ahiboh, H.; Chung, D. W. D.; Prudhomme, J.; Plouffe, D.; Henson, K.; Zhou, Y. Y.; Witola, W.; Yates, J. R.; Ben Mamoun, C.; Winzeler, E. A.; Vial, H., A systematic approach to understand the mechanism of action of the bithiazolium compound T4 on the human malaria parasite, *Plasmodium falciparum*. *BMC Genomics* **2008**, *9*.
30. Roggero, R.; Zufferey, R.; Minca, M.; Richier, E.; Calas, M.; Vial, H.; Ben Mamoun, C., Unraveling the mode of action of the antimalarial choline analog G25 in *Plasmodium falciparum* and *Saccharomyces cerevisiae*. *Antimicrob Agents Ch* **2004**, *48* (8), 2816-2824.
31. Wengelnik, K.; Vidal, V.; Ancelin, M. L.; Cathiard, A. M.; Morgat, J. L.; Kocken, C. H.; Calas, M.; Herrera, S.; Thomas, A. W.; Vial, H. J., A class of potent antimalarials and their specific accumulation in infected erythrocytes. *Science* **2002**, *295* (5558), 1311-1314.
32. Nicolas, O.; Margout, D.; Taudon, N.; Wein, S.; Calas, M.; Vial, H. J.; Bressolle, F. M. M., Pharmacological properties of a new antimalarial bithiazolium salt, T3, and a corresponding prodrug, TE3. *Antimicrob Agents Ch* **2005**, *49* (9), 3631-3639.

33. Vial, H. J.; Wein, S.; Farenc, C.; Kocken, C.; Nicolas, O.; Ancelin, M. L.; Bressolle, F.; Thomas, A.; Calas, M., Prodrugs of bisthiazolium salts are orally potent antimalarials. *P Natl Acad Sci USA* **2004**, *101* (43), 15458-15463.
34. Caldarelli, S. A.; Boisbrun, M.; Alarcon, K.; Hamze, A.; Ouattara, M.; Salom-Roig, X.; Maynadier, M.; Wein, S.; Peyrottes, S.; Pellet, A.; Calas, M.; Vial, H., Exploration of potential prodrug approach of the bis-thiazolium salts T3 and T4 for orally delivered antimalarials. *Bioorg Med Chem Lett* **2010**, *20* (13), 3953-3956.
35. Caldarelli, S. A.; El Fangour, S.; Wein, S.; Tran van Ba, C.; Perigaud, C.; Pellet, A.; Vial, H. J.; Peyrottes, S., New bis-thiazolium analogues as potential antimalarial agents: design, synthesis, and biological evaluation. *J Med Chem* **2013**, *56* (2), 496-509.
36. Ortial, S.; Denoyelle, S.; Wein, S.; Berger, O.; Durand, T.; Escale, R.; Pellet, A.; Vial, H.; Vo-Hoang, Y., Synthesis and evaluation of hybrid bis-cationic salts as antimalarial drugs. *ChemMedChem* **2010**, *5* (1), 52-5.
37. Degardin, M.; Wein, S.; Gouni, S.; Tran Van Ba, C.; Duckert, J. F.; Durand, T.; Escale, R.; Vial, H.; Vo-Hoang, Y., Evaluation of bis-alkylamidoxime O-alkylsulfonates as orally available antimalarials. *ChemMedChem* **2012**, *7* (6), 991-1001.
38. Staines, H. M.; Derbyshire, E. T.; Slavic, K.; Tattersall, A.; Vial, H.; Krishna, S., Exploiting the therapeutic potential of Plasmodium falciparum solute transporters. *Trends Parasitol* **2010**, *26* (6), 284-296.
39. Staines, H. M.; Ellory, J. C.; Chibale, K., The new permeability pathways: Targets and selective routes for the development of new antimalarial agents. *Comb Chem High T Scr* **2005**, *8* (1), 81-88.
40. Chinappi, M.; Via, A.; Marcatili, P.; Tramontano, A., On the Mechanism of Chloroquine Resistance in Plasmodium falciparum. *Plos One* **2010**, *5* (11).
41. Sanchez, C. P.; Dave, A.; Stein, W. D.; Lanzer, M., Transporters as mediators of drug resistance in Plasmodium falciparum. *Int J Parasitol* **2010**, *40* (10), 1109-1118.
42. Olliaro, P. L.; Goldberg, D. E., The Plasmodium Digestive Vacuole - Metabolic Headquarters and Choice Drug Target. *Parasitol Today* **1995**, *11* (8), 294-297.
43. Liu, J.; Istvan, E. S.; Gluzman, I. Y.; Gross, J.; Goldberg, D. E., Plasmodium falciparum ensures its amino acid supply with multiple acquisition pathways and redundant proteolytic enzyme systems. *P Natl Acad Sci USA* **2006**, *103* (23), 8840-8845.

44. Rosenthal, P. J., Falcipains and Other Cysteine Proteases of Malaria Parasites. *Adv Exp Med Biol* **2011**, *712*, 30-48.
45. Rosenthal, P. J.; Meshnick, S. R., Hemoglobin catabolism and iron utilization by malaria parasites. *Mol Biochem Parasit* **1996**, *83* (2), 131-139.
46. Weissbuch, I.; Leiserowitz, L., Interplay Between Malaria, Crystalline Hemozoin Formation, and Antimalarial Drug Action and Design. *Chem Rev* **2008**, *108* (11), 4899-4914.
47. Kumar, S.; Guha, M.; Choubey, V.; Maity, P.; Bandyopadhyay, U., Antimalarial drugs inhibiting hemozoin (beta-hematin) formation: A mechanistic update. *Life Sci* **2007**, *80* (9), 813-828.
48. Ettari, R.; Bova, F.; Zappala, M.; Grasso, S.; Micale, N., Falcipain-2 Inhibitors. *Med Res Rev* **2010**, *30* (1), 136-167.
49. Goldberg, D. E., Hemoglobin degradation. *Curr Top Microbiol* **2005**, *295*, 275-291.
50. Noteberg, D.; Hamelink, E.; Hulten, J.; Wahlgren, M.; Vrang, L.; Samuelsson, B.; Hallberg, A., Design and synthesis of plasmepsin I and plasmepsin II inhibitors with activity in *Plasmodium falciparum*-infected cultured human erythrocytes. *J Med Chem* **2003**, *46* (5), 734-746.
51. Corminboeuf, O.; Dunet, G.; Hafsi, M.; Grimont, J.; Grisostomi, C.; Meyer, S.; Binkert, C.; Bur, D.; Jones, A.; Prade, L.; Brun, R.; Boss, C., Inhibitors of Plasmepsin II - potential antimalarial agents. *Bioorg Med Chem Lett* **2006**, *16* (24), 6194-6199.
52. Schulz, F.; Gelhaus, C.; Degel, B.; Vicik, R.; Heppner, S.; Breuning, E.; Leippe, M.; Gut, J.; Rosenthal, P. J.; Schirmeister, T., Screening of protease inhibitors as antiplasmodial agents. part 1: Aziridines and Epoxides. *ChemMedChem* **2007**, *2* (8), 1214-1224.
53. Coteron, J. M.; Catterick, D.; Castro, J.; Chaparro, M. J.; Diaz, B.; Fernandez, E.; Ferrer, S.; Gamo, F. J.; Gordo, M.; Gut, J.; de las Heras, L.; Legac, J.; Marco, M.; Miguel, J.; Munoz, V.; Porras, E.; de la Rosa, J. C.; Ruiz, J. R.; Sandoval, E.; Ventosa, P.; Rosenthal, P. J.; Fiandor, J. M., Falcipain Inhibitors: Optimization Studies of the 2-Pyrimidinecarbonitrile Lead Series. *J Med Chem* **2010**, *53* (16), 6129-6152.

54. Eggleston, K. K.; Duffin, K. L.; Goldberg, D. E., Identification and characterization of falcilysin, a metallopeptidase involved in hemoglobin catabolism within the malaria parasite *Plasmodium falciparum*. *J Biol Chem* **1999**, *274* (45), 32411-32417.
55. Deu, E.; Leyva, M. J.; Albrow, V. E.; Rice, M. J.; Ellman, J. A.; Bogoy, M., Functional Studies of *Plasmodium falciparum* Dipeptidyl Aminopeptidase I Using Small Molecule Inhibitors and Active Site Probes. *Chem Biol* **2010**, *17* (8), 808-819.
56. Gardiner, D. L.; Trenholme, K. R.; Adams, T. S. S.; Stack, C. M.; Dalton, J. P., Overexpression of leucyl aminopeptidase in *Plasmodium falciparum* parasites - Target for the antimalarial activity of bestatin. *J Biol Chem* **2006**, *281* (3), 1741-1745.
57. O'Neill, P. M.; Ward, S. A.; Berry, N. G.; Jeyadevan, J. P.; Biagini, G. A.; Asadollaly, E.; Park, B. K.; Bray, P. G., A medicinal chemistry perspective on 4-aminoquinoline antimalarial drugs. *Curr Top Med Chem* **2006**, *6* (5), 479-507.
58. Egan, T. J.; Hunter, R.; Kaschula, C. H.; Marques, H. M.; Miplon, A.; Walden, J., Structure-function relationships in aminoquinolines: Effect of amino and chloro groups on quinoline-hematin complex formation, inhibition of beta-hematin formation, and antiplasmodial activity. *J Med Chem* **2000**, *43* (2), 283-291.
59. Dondorp, A. M.; Nosten, F.; Yi, P.; Das, D.; Phyto, A. P.; Tarning, J.; Lwin, K. M.; Ariey, F.; Hanpithakpong, W.; Lee, S. J.; Ringwald, P.; Silamut, K.; Imwong, M.; Chotivanich, K.; Lim, P.; Herdman, T.; An, S. S.; Yeung, S.; Singhasivanon, P.; Day, N. P. J.; Lindegardh, N.; Socheat, D.; White, N. J., Artemisinin Resistance in *Plasmodium falciparum* Malaria. *New Engl J Med* **2009**, *361* (5), 455-467.
60. Olliaro, P. L.; Haynes, R. K.; Meunier, B.; Yuthavong, Y., Possible modes of action of the artemisinin-type compounds. *Trends Parasitol* **2001**, *17* (3), 122-126.
61. Posner, G. H.; O'Neill, P. M., Knowledge of the proposed chemical mechanism of action and cytochrome P450 metabolism of antimalarial trioxanes like artemisinin allows rational design of new antimalarial peroxides. *Accounts Chem Res* **2004**, *37* (6), 397-404.
62. Charman, S. A.; Arbe-Barnes, S.; Bathurst, I. C.; Brun, R.; Campbell, M.; Charman, W. N.; Chiu, F. C. K.; Chollet, J.; Craft, J. C.; Creek, D. J.; Dong, Y. X.; Matile, H.; Maurer, M.; Morizzi, J.; Nguyen, T.; Papastogiannidis, P.; Scheurer, C.; Shackleford, D. M.; Sriraghavan, K.; Stingelin, L.; Tang, Y. Q.; Urwyler, H.; Wang, X. F.; White, K. L.; Wittlin, S.; Zhou, L.;

- Vennerstrom, J. L., Synthetic ozonide drug candidate OZ439 offers new hope for a single-dose cure of uncomplicated malaria. *P Natl Acad Sci USA* **2011**, *108* (11), 4400-4405.
63. Rodrigues, T.; Lopes, F.; Moreira, R., Inhibitors of the Mitochondrial Electron Transport Chain and de novo Pyrimidine Biosynthesis as Antimalarials: The Present Status. *Curr Med Chem* **2010**, *17* (10), 929-956.
64. Ke, H. J.; Morrisey, J. M.; Ganesan, S. M.; Painter, H. J.; Mather, M. W.; Vaidya, A. B., Variation among Plasmodium falciparum Strains in Their Reliance on Mitochondrial Electron Transport Chain Function. *Eukaryotic Cell* **2011**, *10* (8), 1053-1061.
65. Mather, M. W.; Henry, K. W.; Vaidya, A. B., Mitochondrial drug targets in apicomplexan parasites. *Curr Drug Targets* **2007**, *8* (1), 49-60.
66. Vaidya, A. B.; Mather, M. W., Mitochondrial Evolution and Functions in Malaria Parasites. *Annu Rev Microbiol* **2009**, *63*, 249-267.
67. Stocks, P. A.; Barton, V.; Antoine, T.; Biagini, G. A.; Ward, S. A.; O'Neill, P. M., Novel inhibitors of the Plasmodium falciparum electron transport chain. *Parasitology* **2014**, *141* (1), 50-65.
68. Nina, P. B.; Morrisey, J. M.; Ganesan, S. M.; Ke, H. J.; Pershing, A. M.; Mather, M. W.; Vaidya, A. B., ATP Synthase Complex of Plasmodium falciparum dimeric assembly in mitochondrial membranes and resistance to genetic disruption. *J Biol Chem* **2011**, *286* (48), 41312-41322.
69. Fisher, N.; Bray, P. G.; Ward, S. A.; Biagini, G. A., The malaria parasite type II NADH:quinone oxidoreductase: an alternative enzyme for an alternative lifestyle. *Trends Parasitol* **2007**, *23* (7), 305-10.
70. Biagini, G. A.; Viriyavejakul, P.; O'Neill P, M.; Bray, P. G.; Ward, S. A., Functional characterization and target validation of alternative complex I of Plasmodium falciparum mitochondria. *Antimicrob Agents Ch* **2006**, *50* (5), 1841-51.
71. Biagini, G. A.; Fisher, N.; Shone, A. E.; Mubaraki, M. A.; Srivastava, A.; Hill, A.; Antoine, T.; Warman, A. J.; Davies, J.; Pidathala, C.; Amewu, R. K.; Leung, S. C.; Sharma, R.; Gibbons, P.; Hong, D. W.; Pacorel, B.; Lawrenson, A. S.; Charoensutthivarakul, S.; Taylor, L.; Berger, O.; Mbekeani, A.; Stocks, P. A.; Nixon, G. L.; Chadwick, J.; Hemingway, J.; Delves, M. J.; Sinden, R. E.; Zeeman, A. M.; Kocken, C. H.; Berry, N. G.; O'Neill, P. M.; Ward, S. A., Generation of quinolone antimalarials targeting the Plasmodium falciparum

mitochondrial respiratory chain for the treatment and prophylaxis of malaria. *Proc Natl Acad Sci USA* **2012**, *109* (21), 8298-303.

72. Sharma, R.; Lawrenson, A. S.; Fisher, N. E.; Warman, A. J.; Shone, A. E.; Hill, A.; Mbekeani, A.; Pidathala, C.; Amewu, R. K.; Leung, S.; Gibbons, P.; Hong, D. W.; Stocks, P.; Nixon, G. L.; Chadwick, J.; Shearer, J.; Gowers, I.; Cronk, D.; Parel, S. P.; O'Neill, P. M.; Ward, S. A.; Biagini, G. A.; Berry, N. G., Identification of novel antimalarial chemotypes via chemoinformatic compound selection methods for a high-throughput screening program against the novel malarial target, PfNDH2: increasing hit rate via virtual screening methods. *J Med Chem* **2012**, *55* (7), 3144-54.

73. Pidathala, C.; Amewu, R.; Pacorel, B.; Nixon, G. L.; Gibbons, P.; Hong, W. D.; Leung, S. C.; Berry, N. G.; Sharma, R.; Stocks, P. A.; Srivastava, A.; Shone, A. E.; Charoensutthivarakul, S.; Taylor, L.; Berger, O.; Mbekeani, A.; Hill, A.; Fisher, N. E.; Warman, A. J.; Biagini, G. A.; Ward, S. A.; O'Neill, P. M., Identification, design and biological evaluation of bisaryl quinolones targeting Plasmodium falciparum type II NADH:quinone oxidoreductase (PfNDH2). *J Med Chem* **2012**, *55* (5), 1831-43.

74. Sharma, R.; Lawrenson, A. S.; Fisher, N. E.; Warman, A. J.; Shone, A. E.; Hill, A.; Mbekeani, A.; Pidathala, C.; Amewu, R. K.; Leung, S.; Gibbons, P.; Hong, D. W.; Stocks, P.; Nixon, G. L.; Chadwick, J.; Shearer, J.; Gowers, I.; Cronk, D.; Parel, S. P.; O'Neill, P. M.; Ward, S. A.; Biagini, G. A.; Berry, N. G., Identification of Novel Antimalarial Chemotypes via Chemoinformatic Compound Selection Methods for a High-Throughput Screening Program against the Novel Malarial Target, PfNDH2: Increasing Hit Rate via Virtual Screening Methods. *J Med Chem* **2012**, *55* (7), 3144-3154.

75. Leung, S. C.; Gibbons, P.; Amewu, R.; Nixon, G. L.; Pidathala, C.; Hong, W. D.; Pacorel, B.; Berry, N. G.; Sharma, R.; Stocks, P. A.; Srivastava, A.; Shone, A. E.; Charoensutthivarakul, S.; Taylor, L.; Berger, O.; Mbekeani, A.; Hill, A.; Fisher, N. E.; Warman, A. J.; Biagini, G. A.; Ward, S. A.; O'Neill, P. M., Identification, Design and Biological Evaluation of Heterocyclic Quinolones Targeting Plasmodium falciparum Type II NADH:Quinone Oxidoreductase (PfNDH2). *J Med Chem* **2012**, *55* (5), 1844-1857.

76. Baldwin, J.; Farajallah, A. M.; Malmquist, N. A.; Rathod, P. K.; Phillips, M. A., Malarial dihydroorotate dehydrogenase. *J Biol Chem* **2002**, *277* (44), 41827-41834.

77. Baumgartner, R.; Walloschek, M.; Kralik, M.; Gotschlich, A.; Tasler, S.; Mies, J.; Leban, J., Dual binding mode of a novel series of DHODH inhibitors. *J Med Chem* **2006**, *49* (4), 1239-1247.
78. Deng, X. Y.; Gujjar, R.; El Mazouni, F.; Kaminsky, W.; Malmquist, N. A.; Goldsmith, E. J.; Rathod, P. K.; Phillips, M. A., Structural Plasticity of Malaria Dihydroorotate Dehydrogenase Allows Selective Binding of Diverse Chemical Scaffolds. *J Biol Chem* **2009**, *284* (39), 26999-27009.
79. Bedingfield, P. T. P.; Cowen, D.; Acklam, P.; Cunningham, F.; Parsons, M. R.; McConkey, G. A.; Fishwick, C. W. G.; Johnson, A. P., Factors Influencing the Specificity of Inhibitor Binding to the Human and Malaria Parasite Dihydroorotate Dehydrogenases. *J Med Chem* **2012**, *55* (12), 5841-5850.
80. Hurt, D. E.; Widom, J.; Clardy, J., Structure of Plasmodium falciparum dihydroorotate dehydrogenase with a bound inhibitor. *Acta Crystallogr D* **2006**, *62*, 312-323.
81. Baldwin, J.; Michnoff, C. H.; Malmquist, N. A.; White, J.; Roth, M. G.; Rathod, P. K.; Phillips, M. A., High-throughput screening for potent and selective inhibitors of Plasmodium falciparum dihydroorotate dehydrogenase. *J Biol Chem* **2005**, *280* (23), 21847-21853.
82. Phillips, M. A.; Gujjar, R.; Malmquist, N. A.; White, J.; El Mazouni, F.; Baldwin, J.; Rathod, P. K., Triazolopyrimidine-based dihydroorotate dehydrogenase inhibitors with potent and selective activity against the malaria parasite Plasmodium falciparum. *J Med Chem* **2008**, *51* (12), 3649-3653.
83. Gujjar, R.; Marwaha, A.; El Mazouni, F.; White, J.; White, K. L.; Creason, S.; Shackleford, D. M.; Baldwin, J.; Charman, W. N.; Buckner, F. S.; Charman, S.; Rathod, P. K.; Phillips, M. A., Identification of a Metabolically Stable Triazolopyrimidine-Based Dihydroorotate Dehydrogenase Inhibitor with Antimalarial Activity in Mice. *J Med Chem* **2009**, *52* (7), 1864-1872.
84. Gujjar, R.; El Mazouni, F.; White, K. L.; White, J.; Creason, S.; Shackleford, D. M.; Deng, X. Y.; Charman, W. N.; Bathurst, I.; Burrows, J.; Floyd, D. M.; Matthews, D.; Buckner, F. S.; Charman, S. A.; Phillips, M. A.; Rathod, P. K., Lead Optimization of Aryl and Aralkyl

- Amine-Based Triazolopyrimidine Inhibitors of Plasmodium falciparum Dihydroorotate Dehydrogenase with Antimalarial Activity in Mice. *J Med Chem* **2011**, *54* (11), 3935-3949.
85. Coteron, J. M.; Marco, M.; Esquivias, J.; Deng, X. Y.; White, K. L.; White, J.; Koltun, M.; El Mazouni, F.; Kokkonda, S.; Katneni, K.; Bhamidipati, R.; Shackelford, D. M.; Angulo-Barturen, I.; Ferrer, S. B.; Jimenez-Diaz, M. B.; Gamo, F. J.; Goldsmith, E. J.; Charman, W. N.; Bathurst, I.; Floyd, D.; Matthews, D.; Burrows, J. N.; Rathod, P. K.; Charman, S. A.; Phillips, M. A., Structure-Guided Lead Optimization of Triazolopyrimidine-Ring Substituents Identifies Potent Plasmodium falciparum Dihydroorotate Dehydrogenase Inhibitors with Clinical Candidate Potential. *J Med Chem* **2011**, *54* (15), 5540-5561.
86. Patel, V.; Booker, M.; Kramer, M.; Ross, L.; Celatka, C. A.; Kennedy, L. M.; Dvorin, J. D.; Duraisingh, M. T.; Sliz, P.; Wirth, D. F.; Clardy, J., Identification and Characterization of Small Molecule Inhibitors of Plasmodium falciparum Dihydroorotate Dehydrogenase. *J Biol Chem* **2008**, *283* (50), 35078-35085.
87. Booker, M. L.; Bastos, C. M.; Kramer, M. L.; Barker, R. H.; Skerlj, R.; Sidhu, A. B.; Deng, X. Y.; Celatka, C.; Cortese, J. F.; Bravo, J. E. G.; Llado, K. N. C.; Serrano, A. E.; Angulo-Barturen, I.; Jimenez-Diaz, M. B.; Viera, S.; Garuti, H.; Wittlin, S.; Papastogiannidis, P.; Lin, J. W.; Janse, C. J.; Khan, S. M.; Duraisingh, M.; Coleman, B.; Goldsmith, E. J.; Phillips, M. A.; Munoz, B.; Wirth, D. F.; Klinger, J. D.; Wiegand, R.; Sybertz, E., Novel Inhibitors of Plasmodium falciparum Dihydroorotate Dehydrogenase with Anti-malarial Activity in the Mouse Model. *J Biol Chem* **2010**, *285* (43), 33054-33064.
88. Skerlj, R. T.; Bastos, C. M.; Booker, M. L.; Kramer, M. L.; Barker, R. H.; Celatka, C. A.; O'Shea, T. J.; Munoz, B.; Sidhu, A. B.; Cortese, J. F.; Wittlin, S.; Papastogiannidis, P.; Angulo-Barturen, I.; Jimenez-Diaz, M. B.; Sybertz, E., Optimization of Potent Inhibitors of P. falciparum Dihydroorotate Dehydrogenase for the Treatment of Malaria. *ACS Med Chem Lett* **2011**, *2* (9), 708-713.
89. Heikkila, T.; Thirumalairajan, S.; Davies, M.; Parsons, M. R.; McConkey, A. G.; Fishwick, C. W.; Johnson, A. P., The first de novo designed inhibitors of Plasmodium falciparum dihydroorotate dehydrogenase. *Bioorg Med Chem Lett* **2006**, *16* (1), 88-92.
90. Fritzon, I.; Bedingfield, P. T. P.; Sundin, A. P.; McConkey, G.; Nilsson, U. J., N-Substituted salicylamides as selective malaria parasite dihydroorotate dehydrogenase inhibitors. *MedChemComm* **2011**, *2* (9), 895-898.

91. Boa, A. N.; Canavan, S. P.; Hirst, P. R.; Ramsey, C.; Stead, A. M. W.; McConkey, G. A., Synthesis of brequinar analogue inhibitors of malaria parasite dihydroorotate dehydrogenase. *Bioorgan Med Chem* **2005**, *13* (6), 1945-1967.
92. Davies, M.; Heikkila, T.; McConkey, G. A.; Fishwick, C. W. G.; Parsons, M. R.; Johnson, A. P., Structure-Based Design, Synthesis, and Characterization of Inhibitors of Human and Plasmodium falciparum Dihydroorotate Dehydrogenases. *J Med Chem* **2009**, *52* (9), 2683-2693.
93. Brandt, U.; Trumpower, B., The Protonmotive Q-Cycle in Mitochondria and Bacteria. *Crit Rev Biochem Mol* **1994**, *29* (3), 165-197.
94. Trumpower, B. L.; Gennis, R. B., Energy Transduction by Cytochrome Complexes in Mitochondrial and Bacterial Respiration - the Enzymology of Coupling Electron-Transfer Reactions to Transmembrane Proton Translocation. *Annu Rev Biochem* **1994**, *63*, 675-716.
95. Mitchell, P., Protonmotive Q-Cycle - General Formulation. *Febs Lett* **1975**, *59* (2), 137-139.
96. Zhang, Z. L.; Huang, L. S.; Shulmeister, V. M.; Chi, Y. I.; Kim, K. K.; Hung, L. W.; Crofts, A. R.; Berry, E. A.; Kim, S. H., Electron transfer by domain movement in cytochrome bc(1). *Nature* **1998**, *392* (6677), 677-684.
97. Hunte, C.; Palsdottir, H.; Trumpower, B. L., Protonmotive pathways and mechanisms in the cytochrome bc(1) complex. *Febs Lett* **2003**, *545* (1), 39-46.
98. Vaidya, A. B., Mitochondrial and plastid functions as antimalarial drug targets. *Curr Drug Targ Infect Dis* **2004**, *4* (1), 11-23.
99. Xia, D.; Yu, C. A.; Kim, H.; Xian, J. Z.; Kachurin, A. M.; Zhang, L.; Yu, L.; Deisenhofer, J., Crystal structure of the cytochrome bc(1) complex from bovine heart mitochondria (vol 277, pg 60, 1997). *Science* **1997**, *277* (5322), 60-66.
100. Iwata, S.; Lee, J. W.; Okada, K.; Lee, J. K.; Iwata, M.; Rasmussen, B.; Link, T. A.; Ramaswamy, S.; Jap, B. K., Complete structure of the 11-subunit bovine mitochondrial cytochrome bc(1) complex. *Science* **1998**, *281* (5373), 64-71.
101. Hunte, C.; Koepke, J.; Lange, C.; Rossmann, T.; Michel, H., Structure at 2.3 angstrom resolution of the cytochrome bc(1) complex from the yeast *Saccharomyces cerevisiae* co-crystallized with an antibody Fv fragment. *Structure* **2000**, *8* (6), 669-684.

102. Lange, C.; Hunte, C., Crystal structure of the yeast cytochrome bc(1) complex with its bound substrate cytochrome c. *P Natl Acad Sci USA* **2002**, *99* (5), 2800-2805.
103. Solmaz, S. R. N.; Hunte, C., Structure of complex III with bound cytochrome c in reduced state and definition of a minimal core interface for electron transfer. *J Biol Chem* **2008**, *283* (25), 17542-17549.
104. Hill, P.; Kessl, J.; Fisher, N.; Meshnick, S.; Trumppower, B. L.; Meunier, B., Recapitulation in *Saccharomyces cerevisiae* of cytochrome b mutations conferring resistance to atovaquone in *Pneumocystis jirovecii*. *Antimicrob Agents Ch* **2003**, *47* (9), 2725-2731.
105. Cowley, R.; Leung, S.; Fisher, N.; Al-Helal, M.; Berry, N. G.; Lawrenson, A. S.; Sharma, R.; Shone, A. E.; Ward, S. A.; Biagini, G. A.; O'Neill, P. M., The development of quinolone esters as novel antimalarial agents targeting the *Plasmodium falciparum* bc(1) protein complex. *MedChemComm* **2012**, *3* (1), 39-44.
106. Rodrigues, T.; Guedes, R. C.; dos Santos, D. J. V. A.; Carrasco, M.; Gut, J.; Rosenthal, P. J.; Moreira, R.; Lopes, F., Design, synthesis and structure-activity relationships of (1H-pyridin-4-ylidene)amines as potential antimalarials. *Bioorg Med Chem Lett* **2009**, *19* (13), 3476-3480.
107. da Cruz, F. P.; Martin, C.; Buchholz, K.; Lafuente-Monasterio, M. J.; Rodrigues, T.; Sonnichsen, B.; Moreira, R.; Gamo, F. J.; Marti, M.; Mota, M. M.; Hannus, M.; Prudencio, M., Drug Screen Targeted at *Plasmodium* Liver Stages Identifies a Potent Multistage Antimalarial Drug. *J Infect Dis* **2012**, *205* (8), 1278-1286.
108. Fisher, N.; Majid, R. A.; Antoine, T.; Al-Helal, M.; Warman, A. J.; Johnson, D. J.; Lawrenson, A. S.; Ranson, H.; O'Neill, P. M.; Ward, S. A.; Biagini, G. A., Cytochrome b Mutation Y268S Conferring Atovaquone Resistance Phenotype in Malaria Parasite Results in Reduced Parasite bc(1) Catalytic Turnover and Protein Expression. *J Biol Chem* **2012**, *287* (13), 9731-9741.
109. Dong, C. K.; Uргаonkar, S.; Cortese, J. F.; Gamo, F. J.; Garcia-Bustos, J. F.; Lafuente, M. J.; Patel, V.; Ross, L.; Coleman, B. I.; Derbyshire, E. R.; Clish, C. B.; Serrano, A. E.; Cromwell, M.; Barker, R. H.; Dvorin, J. D.; Duraisingh, M. T.; Wirth, D. F.; Clardy, J.; Mazitschek, R., Identification and Validation of Tetracyclic Benzothiazepines as *Plasmodium falciparum* Cytochrome bc(1) Inhibitors. *Chem Biol* **2011**, *18* (12), 1602-1610.

110. Korsinczky, M.; Chen, N. H.; Kotecka, B.; Saul, A.; Rieckmann, K.; Cheng, Q., Mutations in Plasmodium falciparum cytochrome b that are associated with atovaquone resistance are located at a putative drug-binding site. *Antimicrob Agents Ch* **2000**, *44* (8), 2100-2108.
111. Kessl, J. J.; Lange, B. B.; Merbitz-Zahradnik, T.; Zwicker, K.; Hill, P.; Meunier, B.; Palsdottir, H.; Hunte, C.; Meshnick, S.; Trumpower, B. L., Molecular basis for atovaquone binding to the cytochrome bc(1) complex. *J Biol Chem* **2003**, *278* (33), 31312-31318.
112. Carrasco, M. P.; Gut, J.; Rodrigues, T.; Ribeiro, M. H. L.; Lopes, F.; Rosenthal, P. J.; Moreira, R.; dos Santos, D. J. V. A., Exploring the Molecular Basis of Q(o) bc(1) Complex Inhibitors Activity to Find Novel Antimalarials Hits. *Mol Inform* **2013**, *32* (7), 659-670.
113. Painter, H. J.; Morrisey, J. M.; Mather, M. W.; Vaidya, A. B., Specific role of mitochondrial electron transport in blood-stage Plasmodium falciparum. *Nature* **2007**, *446* (7131), 88-91.
114. Srivastava, I. K.; Rottenberg, H.; Vaidya, A. B., Atovaquone, a broad spectrum antiparasitic drug, collapses mitochondrial membrane potential in a malarial parasite. *J Biol Chem* **1997**, *272* (7), 3961-3966.
115. El Hage, S.; Ane, M.; Stigliani, J. L.; Marjorie, M.; Vial, H.; Baziard-Mouysset, G.; Payard, M., Synthesis and antimalarial activity of new atovaquone derivatives. *Eur J Med Chem* **2009**, *44* (11), 4778-4782.
116. Kessl, J. J.; Moskalev, N. V.; Gribble, G. W.; Nasr, M.; Meshnick, S. R.; Trumpower, B. L., Parameters determining the relative efficacy of hydroxy-naphthoquinone inhibitors of the cytochrome bc(1) complex. *BBA-Bioenergetics* **2007**, *1767* (4), 319-326.
117. Fieser, L. F.; Chang, F. C.; Dauben, W. G.; Heidelberger, C.; Heymann, H.; Seligman, A. M., Naphthoquinone Antimalarials .18. Metabolic Oxidation Products. *J Pharmacol Exp Ther* **1948**, *94* (2), 85-96.
118. Hughes, L. M.; Covian, R.; Gribble, G. W.; Trumpower, B. L., Probing binding determinants in center P of the cytochrome bc(1) complex using novel hydroxy-naphthoquinones. *BBA-Bioenergetics* **2010**, *1797* (1), 38-43.
119. Barton, V.; Fisher, N.; Biagini, G. A.; Ward, S. A.; O'Neill, P. M., Inhibiting Plasmodium cytochrome bc(1): a complex issue. *Curr Opin Chem Biol* **2010**, *14* (4), 440-446.

120. Nilsen, A.; LaCrue, A. N.; White, K. L.; Forquer, I. P.; Cross, R. M.; Marfurt, J.; Mather, M. W.; Delves, M. J.; Shackelford, D. M.; Saenz, F. E.; Morrissey, J. M.; Steuten, J.; Mutka, T.; Li, Y. X.; Wirjanata, G.; Ryan, E.; Duffy, S.; Kelly, J. X.; Sebayang, B. F.; Zeeman, A. M.; Noviyanti, R.; Sinden, R. E.; Kocken, C. H. M.; Price, R. N.; Avery, V. M.; Angulo-Barturen, I.; Jimenez-Diaz, M. B.; Ferrer, S.; Herreros, E.; Sanz, L. M.; Gamo, F. J.; Bathurst, I.; Burrows, J. N.; Siegl, P.; Guy, R. K.; Winter, R. W.; Vaidya, A. B.; Charman, S. A.; Kyle, D. E.; Manetsch, R.; Riscoe, M. K., Quinolone-3-Diarylethers: A New Class of Antimalarial Drug. *Sci Transl Med* **2013**, *5* (177).
121. Winter, R.; Kelly, J. X.; Smilkstein, M. J.; Hinrichs, D.; Koop, D. R.; Riscoe, M. K., Optimization of endochin-like quinolones for antimalarial activity. *Exp Parasitol* **2011**, *127* (2), 545-551.
122. Winter, R. W.; Kelly, J. X.; Smilkstein, M. J.; Dodean, R.; Hinrichs, D.; Riscoe, M. K., Antimalarial quinolones: Synthesis, potency, and mechanistic studies. *Exp Parasitol* **2008**, *118* (4), 487-497.
123. Cross, R. M.; Monastyrskiy, A.; Mukta, T. S.; Burrows, J. N.; Kyle, D. E.; Manetsch, R., Endochin Optimization: Structure-Activity and Structure-Property Relationship Studies of 3-Substituted 2-Methyl-4(1H)-quinolones with Antimalarial Activity. *J Med Chem* **2010**, *53* (19), 7076-7094.
124. Cross, R. M.; Namelikonda, N. K.; Mutka, T. S.; Luong, L.; Kyle, D. E.; Manetsch, R., Synthesis, Antimalarial Activity, and Structure-Activity Relationship of 7-(2-Phenoxyethoxy)-4(1H)-quinolones. *J Med Chem* **2011**, *54* (24), 8321-8327.
125. Zhang, Y. Q.; Clark, J. A.; Connelly, M. C.; Zhu, F. Y.; Min, J. K.; Guiguemde, W. A.; Pradhan, A.; Iyer, L.; Furimsky, A.; Gow, J.; Parman, T.; El Mazouni, F.; Phillips, M. A.; Kyle, D. E.; Mirsalis, J.; Guy, R. K., Lead Optimization of 3-Carboxyl-4(1H)-Quinolones to Deliver Orally Bioavailable Antimalarials. *J Med Chem* **2012**, *55* (9), 4205-4219.
126. Fry, M.; Williams, R. B., Effects of Decoquinatone and Clopidol on Electron-Transport in Mitochondria of *Eimeria-Tenella* (Apicomplexa, Coccidia). *Biochem Pharmacol* **1984**, *33* (2), 229-240.
127. Xiang, H.; McSurdy-Freed, J.; Moorthy, G. S.; Hugger, E.; Bambal, R.; Han, C.; Ferrer, S.; Gargallo, D.; Davis, C. B., Preclinical drug metabolism and pharmacokinetic

evaluation of GW844520, a novel anti-malarial mitochondrial electron transport inhibitor. *J Pharm Sci-U.S.* **2006**, *95* (12), 2657-2672.

128. Bathurst, I.; Hentschel, C., Medicines for Malaria Venture: sustaining antimalarial drug development. *Trends Parasitol* **2006**, *22* (7), 301-307.

129. Mepacrine for malaria - Statement by MRC Committee on malaria. *Lancet* **1944**, *2*, 667-668.

130. Turner, R. W. D., Quinine and mepacrine in malaria. *Lancet* **1944**, *2*, 737-737.

131. Ederer, P., Advantages of mepacrine. *Lancet* **1944**, *2*, 769-769.

132. Winter, R. W.; Kelly, J. X.; Smilkstein, M. J.; Dodean, R.; Bagby, G. C.; Rathbun, R. K.; Levin, J. I.; Hinrichs, D.; Riscoe, M. K., Evaluation and lead optimization of anti-malarial acridones. *Exp Parasitol* **2006**, *114* (1), 47-56.

133. Biagini, G. A.; Fisher, N.; Berry, N.; Stocks, P. A.; Meunier, B.; Williams, D. P.; Bonar-Law, R.; Bray, P. G.; Owen, A.; O'Neill, P. M.; Ward, S. A., Acridinediones: Selective and potent inhibitors of the malaria parasite mitochondrial bc(1) complex. *Mol Pharmacol* **2008**, *73* (5), 1347-1355.

134. Dorn, A.; Scovill, J. P.; Ellis, W. Y.; Matile, H.; Ridley, R. G.; Vennerstrom, J. L., Floxacrine analog WR 243251 inhibits hemozoin polymerization. *Am J Trop Med Hyg* **2001**, *65* (1), 19-20.

135. Kesten, S. J.; Degnan, M. J.; Hung, J.; McNamara, D. J.; Ortwine, D. F.; Uhlendorf, S. E.; Werbel, L. M., Synthesis and antimalarial properties of 1-imino derivatives of 7-chloro-3-substituted-3,4-dihydro-1,9(2H,10H)-acridinediones and related structures. *J Med Chem* **1992**, *35* (19), 3429-47.

136. Alzeer, J.; Chollet, J.; Heinze-Krauss, I.; Hubschwerlen, C.; Matile, H.; Ridley, R. G., Phenyl beta-methoxyacrylates: A new antimalarial pharmacophore. *J Med Chem* **2000**, *43* (4), 560-568.

137. Brandt, U.; Schagger, H.; Vonjagow, G., Characterization of Binding of the Methoxyacrylate Inhibitors to Mitochondrial Cytochrome-C Reductase. *Eur J Biochem* **1988**, *173* (3), 499-506.

138. Pember, S. O.; Fleck, L. C.; Moberg, W. K.; Walker, M. P., Mechanistic differences in inhibition of ubiquinol cytochrome c reductase by the proximal Qo-site inhibitors famoxadone and methoxyacrylate stilbene. *Arch Biochem Biophys* **2005**, *435* (2), 280-290.

139. Thierbach, G.; Reichenbach, H., Myxothiazol, a New Inhibitor of the Cytochrome B-C1 Segment of the Respiratory-Chain. *Biochim Biophys Acta* **1981**, *638* (2), 282-289.
140. Vonjagow, G.; Ljungdahl, P. O.; Graf, P.; Ohnishi, T.; Trumpower, B. L., An Inhibitor of Mitochondrial Respiration Which Binds to Cytochrome-B and Displaces Quinone from the Iron-Sulfur Protein of the Cytochrome-Bc1 Complex. *J Biol Chem* **1984**, *259* (10), 6318-6326.
141. Smilkstein, M. J.; Forquer, I.; Kanazawa, A.; Kelly, J. X.; Winter, R. W.; Hinrichs, D. J.; Kramer, D. A.; Riscoe, M. K., A drug-selected Plasmodium falciparum lacking the need for conventional electron transport. *Mol Biochem Parasit* **2008**, *159* (1), 64-68.
142. Dong, C.; Uргаonkar, S.; Cortese, J.; Francisco, J.; Garcia-Bustos, J. F.; Gomez-de-las-Heras, F. M.; Patel, V.; Ross, L.; Dvorin, J. D.; Duraisingh, M. T.; Wirth, D.; Mazitschek, R.; Clardy, J., Tetracyclic Benzothiazepines: A Novel Class of Plasmodium Falciparum Cytochrome Bc1 Inhibitors. *Am J Trop Med Hyg* **2009**, *81* (5), 252-253.
143. Kim, H.; Esser, L.; Hossain, M. B.; Xia, D.; Yu, C. A.; Riso, J.; van der Helm, D.; Deisenhofer, J., Structure of antimycin A1, a specific electron transfer inhibitor of ubiquinol-cytochrome c oxidoreductase. *J Am Chem Soc* **1999**, *121* (20), 4902-4903.
144. Rieske, J. S., Inhibitors of Respiration at Energy-Coupling Site 2 of the Respiratory-Chain. *Pharmacol Therapeut* **1980**, *11* (2), 415-450.
145. Huang, L. S.; Cobessi, D.; Tung, E. Y.; Berry, E. A., Binding of the respiratory chain inhibitor antimycin to the mitochondrial bc1 complex: a new crystal structure reveals an altered intramolecular hydrogen-bonding pattern. *J Mol Biol* **2005**, *351* (3), 573-97.
146. Gao, X. G.; Wen, X. L.; Esser, L.; Quinn, B.; Yu, L.; Yu, C. A.; Xia, D., Structural basis for the quinone reduction in the bc(1) complex: A comparative analysis of crystal structures of mitochondrial cytochrome bc(1) with bound substrate and inhibitors at the Qi site. *Biochemistry-Us* **2003**, *42* (30), 9067-9080.
147. Tokutake, N.; Miyoshi, H.; Nakazato, H.; Iwamura, H., Inhibition of Electron-Transport of Rat-Liver Mitochondria by Synthesized Antimycin-a Analogs. *Biochim Biophys Acta* **1993**, *1142* (3), 262-268.
148. Bolgunas, S.; Clark, D. A.; Hanna, W. S.; Mauvais, P. A.; Pember, S. O., Potent inhibitors of the Qi site of the mitochondrial respiration complex III. *J Med Chem* **2006**, *49* (15), 4762-4766.

149. Moser, U. K.; Walter, P., Funiculosin - New Specific Inhibitor of Respiratory-Chain in Rat-Liver Mitochondria. *Febs Lett* **1975**, *50* (2), 279-282.
150. Suraveratum, N.; Krungkrai, S. R.; Leangaramgul, P.; Prapunwattana, P.; Krungkrai, J., Purification and characterization of Plasmodium falciparum succinate dehydrogenase. *Mol Biochem Parasitol* **2000**, *105* (2), 215-22.
151. Kita, K.; Hirawake, H.; Miyadera, H.; Amino, H.; Takeo, S., Role of complex II in anaerobic respiration of the parasite mitochondria from Ascaris suum and Plasmodium falciparum. *BBA-Bioenergetics* **2002**, *1553* (1-2), 123-139.
152. Basco, L. K.; Lebras, J., In-Vitro Activity of Mitochondrial Atp-Synthetase Inhibitors against Plasmodium-Falciparum. *J Eukaryot Microbiol* **1994**, *41* (3), 179-183.
153. McFadden, G. I.; Roos, D. S., Apicomplexan plastids as drug targets. *Trends Microbiol* **1999**, *7* (8), 328-333.
154. Ralph, S. A.; D'Ombrain, M. C.; McFadden, G. I., The apicoplast as an antimalarial drug target. *Drug Resist Update* **2001**, *4* (3), 145-151.
155. Colizzi, F.; Recanatini, M.; Cavalli, A., Mechanical Features of Plasmodium falciparum Acyl Carrier Protein in the Delivery of Substrates. *J Chem Inf Model* **2008**, *48* (12), 2289-2293.
156. Waller, R. F.; Ralph, S. A.; Reed, M. B.; Su, V.; Douglas, J. D.; Minnikin, D. E.; Cowman, A. F.; Besra, G. S.; McFadden, G. I., A type II pathway for fatty acid biosynthesis presents drug targets in Plasmodium falciparum. *Antimicrob Agents Ch* **2003**, *47* (1), 297-301.
157. Waller, R. F.; Keeling, P. J.; Donald, R. G. K.; Striepen, B.; Handman, E.; Lang-Unnasch, N.; Cowman, A. F.; Besra, G. S.; Roos, D. S.; McFadden, G. I., Nuclear-encoded proteins target to the plastid in Toxoplasma gondii and Plasmodium falciparum. *P Natl Acad Sci USA* **1998**, *95* (21), 12352-12357.
158. Surolia, N.; Surolia, A., Triclosan offers protection against blood stages of malaria by inhibiting enoyl-ACP reductase of Plasmodium falciparum. *Nat Med* **2001**, *7* (2), 167-173.
159. Perozzo, R.; Kuo, M.; Sidhu, A. B. S.; Valiyaveetil, J. T.; Bittman, R.; Jacobs, W. R.; Fidock, D. A.; Sacchettini, J. C., Structural elucidation of the specificity of the antibacterial

agent triclosan for malarial enoyl acyl carrier protein reductase. *J Biol Chem* **2002**, *277* (15), 13106-13114.

160. Belluti, F.; Perozzo, R.; Lauciello, L.; Colizzi, F.; Kostrewa, D.; Bisi, A.; Gobbi, S.; Rampa, A.; Bolognesi, M. L.; Recanatini, M.; Brun, R.; Scapozza, L.; Cavalli, A., Design, Synthesis, and Biological and Crystallographic Evaluation of Novel Inhibitors of Plasmodium falciparum Enoyl-ACP-reductase (PfFabI). *J Med Chem* **2013**, *56* (19), 7516-7526.

161. Botte, C. Y.; Dubar, F.; McFadden, G. I.; Marechal, E.; Biot, C., Plasmodium falciparum Apicoplast Drugs: Targets or Off-Targets? *Chem Rev* **2012**, *112* (3), 1269-1283.

162. Sato, S.; Clough, B.; Coates, L.; Wilson, R. J. M., Enzymes for heme biosynthesis are found in both the mitochondrion and plastid of the malaria parasite Plasmodium falciparum. *Protist* **2004**, *155* (1), 117-125.

163. Padmanaban, G.; Rangarajan, P. N., Heme metabolism of plasmodium is a major antimalarial target. *Biochem Bioph Res Co* **2000**, *268* (3), 665-668.

164. Bonday, Z. Q.; Taketani, S.; Gupta, P. D.; Padmanaban, G., Heme biosynthesis by the malarial parasite - Import of delta-aminolevulinic acid dehydratase from the host red cell. *J Biol Chem* **1997**, *272* (35), 21839-21846.

165. Padmanaban, G.; Nagaraj, V. A.; Rangarajan, P. N., An alternative model for heme biosynthesis in the malarial parasite. *Trends Biochem Sci* **2007**, *32* (10), 443-449.

166. Goodman, C. D.; Su, V.; McFadden, G. I., The effects of anti-bacterials on the malaria parasite Plasmodium falciparum. *Mol Biochem Parasit* **2007**, *152* (2), 181-191.

167. Kiatfuengfoo, R.; Suthiphongchai, T.; Prapunwattana, P.; Yuthavong, Y., Mitochondria as the Site of Action of Tetracycline on Plasmodium-Falciparum. *Mol Biochem Parasit* **1989**, *34* (2), 109-115.

168. Toler, S., The plasmodial apicoplast was retained under evolutionary selective pressure to assuage blood stage oxidative stress. *Med Hypotheses* **2005**, *65* (4), 683-690.

169. Schlitzer, M., Antimalarial drugs - What is in use and what is in the pipeline. *Arch Pharm* **2008**, *341* (3), 149-163.

170. Weissig, V.; Vetro-Widenhouse, T. S.; Rowe, T. C., Topoisomerase II inhibitors induce cleavage of nuclear and 35-kb plastid DNAs in the malarial parasite Plasmodium falciparum. *DNA Cell Biol* **1997**, *16* (12), 1483-1492.

171. Mahmoudi, N.; Ciceron, L.; Franetich, J. F.; Farhati, K.; Silvie, O.; Eling, W.; Sauerwein, R.; Danis, M.; Mazier, D.; Derouin, F., In vitro activities of 25 quinolones and fluoroquinolones against liver and blood stage Plasmodium spp. *Antimicrob Agents Ch* **2003**, *47* (8), 2636-2639.
172. Pradel, G.; Schlitzer, M., Antibiotics in Malaria Therapy and their Effect on the Parasite Apicoplast. *Curr Mol Med* **2010**, *10* (3), 335-349.
173. Ashley, E. A.; White, N. J., Artemisinin-based combinations. *Curr Opin Infect Dis* **2005**, *18* (6), 531-536.
174. Gingras, B. A.; Jensen, J. B., Activity of Azithromycin (Cp-62,993) and Erythromycin against Chloroquine-Sensitive and Chloroquine-Resistant Strains of Plasmodium-falciparum In vitro. *Am J Trop Med Hyg* **1992**, *47* (3), 378-382.
175. Ohrt, C.; Willingmyre, G. D.; Lee, P.; Knirsch, C.; Milhous, W., Assessment of azithromycin in combination with other antimalarial drugs against Plasmodium falciparum in vitro. *Antimicrob Agents Ch* **2002**, *46* (8), 2518-2524.
176. Ramharter, M.; Noedl, H.; Winkler, H.; Graninger, W.; Wernsdorfer, W. H.; Kremsner, P. G.; Winkler, S., In vitro activity and interaction of clindamycin combined with dihydroartemisinin against Plasmodium falciparum. *Antimicrob Agents Ch* **2003**, *47* (11), 3494-3499.
177. Nzila, A., The past, present and future of antifolates in the treatment of Plasmodium falciparum infection. *J Antimicrob Chemoth* **2006**, *57* (6), 1043-1054.
178. Anderson, A. C., Targeting DHFR in parasitic protozoa. *Drug Discov Today* **2005**, *10* (2), 121-128.
179. Rathod, P. K.; Phillips, M. A., Prized malaria drug target nailed. *Nat Struct Biol* **2003**, *10* (5), 316-318.
180. Yuvaniyama, J.; Chitnumsub, P.; Kamchonwongpaisan, S.; Vanichtanankul, J.; Sirawaraporn, W.; Taylor, P.; Walkinshaw, M. D.; Yuthavong, Y., Insights into antifolate resistance from malarial DHFR-TS structures. *Nat Struct Biol* **2003**, *10* (5), 357-365.
181. Gregson, A.; Plowe, C. V., Mechanisms of resistance of malaria parasites to antifolates. *Pharmacol Rev* **2005**, *57* (1), 117-145.
182. Hurly, M. G., Potentiation of pyrimethamine by sulphadiazine in human malaria. *T Roy Soc Trop Med H* **1959**, *53*, 412-3.

183. Rathod, P. K.; Leffers, N. P.; Young, R. D., Molecular targets of 5-fluoroorotate in the human malaria parasite, *Plasmodium falciparum*. *Antimicrob Agents Ch* **1992**, *36* (4), 704-11.
184. Hekmat-Nejad, M.; Rathod, P. K., Kinetics of *Plasmodium falciparum* thymidylate synthase: interactions with high-affinity metabolites of 5-fluoroorotate and D1694. *Antimicrob Agents Ch* **1996**, *40* (7), 1628-32.
185. Lang-Unnasch, N.; Murphy, A. D., Metabolic changes of the malaria parasite during the transition from the human to the mosquito host. *Annu Rev Microbiol* **1998**, *52*, 561-90.
186. Deck, L. M.; Royer, R. E.; Chamblee, B. B.; Hernandez, V. M.; Malone, R. R.; Torres, J. E.; Hunsaker, L. A.; Piper, R. C.; Makler, M. T.; Vander Jagt, D. L., Selective inhibitors of human lactate dehydrogenases and lactate dehydrogenase from the malarial parasite *Plasmodium falciparum*. *J Med Chem* **1998**, *41* (20), 3879-3887.
187. Dunn, C. R.; Banfield, M. J.; Barker, J. J.; Higham, C. W.; Moreton, K. M.; Turgut-Balik, D.; Brady, R. L.; Holbrook, J. J., The structure of lactate dehydrogenase from *Plasmodium falciparum* reveals a new target for anti-malarial design. *Nat Struct Biol* **1996**, *3* (11), 912-5.
188. Penna-Coutinho, J.; Cortopassi, W. A.; Oliveira, A. A.; Franca, T. C.; Krettli, A. U., Antimalarial activity of potential inhibitors of *Plasmodium falciparum* lactate dehydrogenase enzyme selected by docking studies. *Plos One* **2011**, *6* (7), e21237.
189. Cassera, M. B.; Zhang, Y.; Hazleton, K. Z.; Schramm, V. L., Purine and Pyrimidine Pathways as Targets in *Plasmodium falciparum*. *Curr Top Med Chem* **2011**, *11* (16), 2103-2115.
190. Mazier, D.; Renia, L.; Snounou, G., A pre-emptive strike against malaria's stealthy hepatic forms. *Nat Rev Drug Discov* **2009**, *8* (11), 854-64.
191. Derbyshire, E. R.; Mota, M. M.; Clardy, J., The next opportunity in anti-malaria drug discovery: the liver stage. *PLoS Pathogens* **2011**, *7* (9), e1002178.
192. Rodrigues, T.; Prudencio, M.; Moreira, R.; Mota, M. M.; Lopes, F., Targeting the Liver Stage of Malaria Parasites: A Yet Unmet Goal. *J Med Chem* **2012**, *55* (3), 995-1012.
193. Baird, J. K.; Hoffman, S. L., Primaquine therapy for malaria. *Clin Infect Dis* **2004**, *39* (9), 1336-1345.

194. Cappellini, M. D.; Fiorelli, G., Glucose-6-phosphate dehydrogenase deficiency. *Lancet* **2008**, *371* (9606), 64-74.
195. Biamonte, M. A.; Wanner, J.; Le Roch, K. G., Recent advances in malaria drug discovery. *Bioorg Med Chem Lett* **2013**, *23* (10), 2829-2843.
196. Eastman, R. T.; Fidock, D. A., Artemisinin-based combination therapies: a vital tool in efforts to eliminate malaria. *Nat Rev Microbiol* **2009**, *7* (12), 864-874.
197. Hyde, J. E., Mechanisms of resistance of Plasmodium falciparum to antimalarial drugs. *Microbes Infect* **2002**, *4* (2), 165-174.
198. Fairhurst, R. M.; Nayyar, G. M.; Breman, J. G.; Hallett, R.; Vennerstrom, J. L.; Duong, S.; Ringwald, P.; Wellems, T. E.; Plowe, C. V.; Dondorp, A. M., Artemisinin-resistant malaria: research challenges, opportunities, and public health implications. *Am J Trop Med Hyg* **2012**, *87* (2), 231-41.
199. Nosten, F.; White, N. J., Artemisinin-based combination treatment of falciparum malaria. *Am J Trop Med Hyg* **2007**, *77* (6), 181-192.
200. Klein, E. Y., Antimalarial drug resistance: a review of the biology and strategies to delay emergence and spread. *Int J Antimicrob Ag* **2013**, *41* (4), 311-317.
201. Dondorp, A. M.; Yeung, S.; White, L.; Nguon, C.; Day, N. P.; Socheat, D.; von Seidlein, L., Artemisinin resistance: current status and scenarios for containment. *Nat Rev Microbiol* **2010**, *8* (4), 272-80.
202. Ariey, F.; Witkowski, B.; Amaratunga, C.; Beghain, J.; Langlois, A. C.; Khim, N.; Kim, S.; Duru, V.; Bouchier, C.; Ma, L.; Lim, P.; Leang, R.; Duong, S.; Sreng, S.; Suon, S.; Chhor, C. M.; Bout, D. M.; Menard, S.; Rogers, W. O.; Genton, B.; Fandeur, T.; Miotto, O.; Ringwald, P.; Le Bras, J.; Berry, A.; Barale, J. C.; Fairhurst, R. M.; Benoit-Vical, F.; Mercereau-Puijalon, O.; Menard, D., A molecular marker of artemisinin-resistant Plasmodium falciparum malaria. *Nature* **2014**, *505* (7481), 50-5.
203. Ma, D. L.; Chan, D. S. H.; Leung, C. H., Drug repositioning by structure-based virtual screening. *Chem Soc Rev* **2013**, *42* (5), 2130-2141.
204. Bleicher, K. H.; Bohm, H. J.; Muller, K.; Alanine, A. I., Hit and lead generation: Beyond high-throughput screening. *Nat Rev Drug Discov* **2003**, *2* (5), 369-378.

205. Geysen, H. M.; Schoenen, F.; Wagner, D.; Wagner, R., Combinatorial compound libraries for drug discovery: An ongoing challenge. *Nat Rev Drug Discov* **2003**, *2* (3), 222-230.
206. Tanrikulu, Y.; Kruger, B.; Proschak, E., The holistic integration of virtual screening in drug discovery. *Drug Discov Today* **2013**, *18* (7-8), 358-364.
207. Ekins, S.; Williams, A. J.; Krasowski, M. D.; Freundlich, J. S., In silico repositioning of approved drugs for rare and neglected diseases. *Drug Discov Today* **2011**, *16* (7-8), 298-310.
208. Heikamp, K.; Bajorath, J., The Future of Virtual Compound Screening. *Chem Biol Drug Des* **2013**, *81* (1), 33-40.
209. Klebe, G., Virtual ligand screening: strategies, perspectives and limitations. *Drug Discov Today* **2006**, *11* (13-14), 580-594.
210. Beautrait, A.; Leroux, V.; Chavent, M.; Ghemtio, L.; Devignes, M. D.; Smaiel-Tabbone, M.; Cai, W.; Shao, X.; Moreau, G.; Bladon, P.; Yao, J.; Maigret, B., Multiple-step virtual screening using VSM-G: overview and validation of fast geometrical matching enrichment. *J Mol Model* **2008**, *14* (2), 135-148.
211. Jones, G.; Willett, P.; Glen, R. C.; Leach, A. R.; Taylor, R., Development and validation of a genetic algorithm for flexible docking. *J Mol Biol* **1997**, *267* (3), 727-748.
212. Verdonk, M. L.; Cole, J. C.; Hartshorn, M. J.; Murray, C. W.; Taylor, R. D., Improved protein-ligand docking using GOLD. *Proteins* **2003**, *52* (4), 609-623.
213. Rarey, M.; Kramer, B.; Lengauer, T.; Klebe, G., A fast flexible docking method using an incremental construction algorithm. *J Mol Biol* **1996**, *261* (3), 470-489.
214. Schrödinger, L.; dinger, L., New York, *Glide*, 5.7; New York, 2011.
215. Friesner, R. A.; Banks, J. L.; Murphy, R. B.; Halgren, T. A.; Klicic, J. J.; Mainz, D. T.; Repasky, M. P.; Knoll, E. H.; Shelley, M.; Perry, J. K.; Shaw, D. E.; Francis, P.; Shenkin, P. S., Glide: A new approach for rapid, accurate docking and scoring. 1. Method and assessment of docking accuracy. *J Med Chem* **2004**, *47* (7), 1739-1749.
216. Halgren, T. A.; Murphy, R. B.; Friesner, R. A.; Beard, H. S.; Frye, L. L.; Pollard, W. T.; Banks, J. L., Glide: A new approach for rapid, accurate docking and scoring. 2. Enrichment factors in database screening. *J Med Chem* **2004**, *47* (7), 1750-1759.

217. Venkatachalam, C. M.; Jiang, X.; Oldfield, T.; Waldman, M., LigandFit: a novel method for the shape-directed rapid docking of ligands to protein active sites. *J Mol Graph Model* **2003**, *21* (4), 289-307.
218. Morris, G. M.; Huey, R.; Lindstrom, W.; Sanner, M. F.; Belew, R. K.; Goodsell, D. S.; Olson, A. J., AutoDock4 and AutoDockTools4: Automated Docking with Selective Receptor Flexibility. *J Comput Chem* **2009**, *30* (16), 2785-2791.
219. Trott, O.; Olson, A. J., Software News and Update AutoDock Vina: Improving the Speed and Accuracy of Docking with a New Scoring Function, Efficient Optimization, and Multithreading. *J Comput Chem* **2010**, *31* (2), 455-461.
220. Adane, L.; Bharatam, P. V.; Sharma, V., A common feature-based 3D-pharmacophore model generation and virtual screening: identification of potential PfDHFR inhibitors. *J Enzym Inhib Med Ch* **2010**, *25* (5), 635-645.
221. Adane, L.; Patel, D. S.; Bharatam, P. V., Shape- and Chemical Feature-Based 3D-Pharmacophore Model Generation and Virtual Screening: Identification of Potential Leads for P-falciparum DHFR Enzyme Inhibition. *Chem Biol Drug Des* **2010**, *75* (1), 115-126.
222. Wadood, A.; Zaheer-ulhaq, In silico identification of novel inhibitors against Plasmodium falciparum dihydroorotate dehydrogenase. *J Mol Graph Model* **2013**, *40*, 40-47.
223. Desai, P. V.; Patny, A.; Gut, J.; Rosenthal, P. J.; Tekwani, B.; Srivastava, A.; Avery, M., Identification of novel parasitic cysteine protease inhibitors by use of virtual screening. 2. The available chemical directory. *J Med Chem* **2006**, *49* (5), 1576-1584.
224. Desai, P. V.; Patny, A.; Sabnis, Y.; Tekwani, B.; Gut, J.; Rosenthal, P.; Srivastava, A.; Avery, M., Identification of novel parasitic cysteine protease inhibitors using virtual screening. 1. The ChemBridge database. *J Med Chem* **2004**, *47* (26), 6609-6615.
225. Li, H. L.; Huang, J.; Chen, L. L.; Liu, X. F.; Chen, T.; Zhu, J.; Lu, W. Q.; Shen, X.; Li, J.; Hilgenfeld, R.; Jiang, H. L., Identification of Novel Falcipain-2 Inhibitors as Potential Antimalarial Agents through Structure-Based Virtual Screening. *J Med Chem* **2009**, *52* (15), 4936-4940.
226. Shah, F.; Gut, J.; Legac, J.; Shivakumar, D.; Sherman, W.; Rosenthal, P. J.; Avery, M. A., Computer-Aided Drug Design of Falcipain Inhibitors: Virtual Screening, Structure-

Activity Relationships, Hydration Site Thermodynamics, and Reactivity Analysis. *J Chem Inf Model* **2012**, *52* (3), 696-710.

227. Degliesposti, G.; Kasam, V.; Da Costa, A.; Kang, H. K.; Kim, N.; Kim, D. W.; Breton, V.; Kim, D.; Rastelli, G., Design and Discovery of Plasmepsin II Inhibitors Using an Automated Workflow on Large-Scale Grids. *ChemMedChem* **2009**, *4* (7), 1164-1173.

228. McKay, P. B.; Peters, M. B.; Carta, G.; Flood, C. T.; Dempsey, E.; Bell, A.; Berry, C.; Lloyd, D. G.; Fayne, D., Identification of plasmepsin inhibitors as selective anti-malarial agents using ligand based drug design. *Bioorg Med Chem Lett* **2011**, *21* (11), 3335-3341.

229. Song, Y. W.; Jin, H. T.; Liu, X. F.; Zhu, L. L.; Huang, J.; Li, H. L., Discovery of non-peptide inhibitors of Plasmepsin II by structure-based virtual screening. *Bioorg Med Chem Lett* **2013**, *23* (7), 2078-2082.

230. Frecer, V.; Megnassan, E.; Miertus, S., Design and in silico screening of combinatorial library of antimalarial analogs of triclosan inhibiting Plasmodium falciparum enoyl-acyl carrier protein reductase. *Eur J Med Chem* **2009**, *44* (7), 3009-3019.

231. Nicola, G.; Smith, C. A.; Lucumi, E.; Kuo, M. R.; Karagyozev, L.; Fidock, D. A.; Sacchettin, J. C.; Abagyan, R., Discovery of novel inhibitors targeting enoyl-acyl carrier protein reductase in Plasmodium falciparum by structure-based virtual screening. *Biochem Bioph Res Co* **2007**, *358* (3), 686-691.

232. Ojha, P. K.; Mitra, I.; Kar, S.; Das, R. N.; Roy, K., Lead Hopping for PfDHODH Inhibitors as Antimalarials Based on Pharmacophore Mapping, Molecular Docking and Comparative Binding Energy Analysis (COMBINE): A Three-Layered Virtual Screening Approach. *Mol Inform* **2012**, *31* (10), 711-718.

233. Rodrigues, T.; Moreira, R.; Gut, J.; Rosenthal, P. J.; O'Neill, P. M.; Biagini, G. A.; Lopes, F.; dos Santos, D. J. V. A.; Guedes, R. C., Identification of new antimalarial leads by use of virtual screening against cytochrome bc(1). *Bioorgan Med Chem* **2011**, *19* (21), 6302-6308.

234. Marrero-Ponce, Y.; Iyarreta-Veitia, M.; Montero-Torres, A.; Romero-Zaldivar, C.; Brandt, C. A.; Avila, P. E.; Kirchgatter, K.; Machado, Y., Ligand-based virtual screening and in silico design of new antimalarial compounds using nonstochastic and stochastic total and atom-type quadratic maps. *J Chem Inf Model* **2005**, *45* (4), 1082-1100.

235. Mahmoudi, N.; de Julian-Ortiz, J. V.; Ciceron, L.; Galvez, J.; Mazier, D.; Danis, M.; Derouin, F.; Garcia-Domenech, R., Identification of new antimalarial drugs by linear discriminant analysis and topological virtual screening. *J Antimicrob Chemoth* **2006**, *57* (3), 489-497.
236. Sullivan, D. J.; Kaludov, N.; Martinov, M. N., Discovery of potent, novel, non-toxic anti-malarial compounds via quantum modelling, virtual screening and in vitro experimental validation. *Malaria J* **2011**, *10*.
237. Zhang, L. Y.; Fourches, D.; Sedykh, A.; Zhu, H.; Golbraikh, A.; Ekins, S.; Clark, J.; Connelly, M. C.; Sigal, M.; Hodges, D.; Guiguemde, A.; Guy, R. K.; Tropsha, A., Discovery of Novel Antimalarial Compounds Enabled by QSAR-Based Virtual Screening. *J Chem Inf Model* **2013**, *53* (2), 475-492.
238. Mather, M. W.; Vaidya, A. B., Mitochondria in malaria and related parasites: ancient, diverse and streamlined. *J Bioenerg Biomembr* **2008**, *40* (5), 425-433.
239. Biagini, G. A.; Fisher, N.; Shone, A. E.; Mubarak, M. A.; Srivastava, A.; Hill, A.; Antoine, T.; Warman, A. J.; Davies, J.; Pidathala, C.; Amewu, R. K.; Leung, S. C.; Sharma, R.; Gibbons, P.; Hong, D. W.; Pacorel, B.; Lawrenson, A. S.; Charoensutthivarakul, S.; Taylor, L.; Berger, O.; Mbekeani, A.; Stocks, P. A.; Nixon, G. L.; Chadwick, J.; Hemingway, J.; Delves, M. J.; Sinden, R. E.; Zeeman, A. M.; Kocken, C. H. M.; Berry, N. G.; O'Neill, P. M.; Ward, S. A., Generation of quinolone antimalarials targeting the Plasmodium falciparum mitochondrial respiratory chain for the treatment and prophylaxis of malaria. *P Natl Acad Sci USA* **2012**, *109* (21), 8298-8303.
240. Esser, L.; Quinn, B.; Li, Y. F.; Zhang, M. Q.; Elberry, M.; Yu, L.; Yu, C. A.; Xia, D., Crystallographic studies of quinol oxidation site inhibitors: A modified classification of inhibitors for the cytochrome bc(1) complex. *J Mol Biol* **2004**, *341* (1), 281-302.
241. Degliesposti, M.; Devries, S.; Crimi, M.; Ghelli, A.; Patarnello, T.; Meyer, A., Mitochondrial Cytochrome-B - Evolution and Structure of the Protein. *Biochim Biophys Acta* **1993**, *1143* (3), 243-271.
242. Klingen, A. R.; Palsdottir, H.; Hunte, C.; Ullmann, G. M., Redox-linked protonation state changes in cytochrome bc(1) identified by Poisson-Boltzmann electrostatics calculations. *BBA-Bioenergetics* **2007**, *1767* (3), 204-221.

243. Crofts, A. R.; Holland, J. T.; Victoria, D.; Kolling, D. R. J.; Dikanov, S. A.; Gilbreth, R.; Lhee, S.; Kuras, R.; Kuras, M. G., The Q-cycle reviewed: How well does a monomeric mechanism of the bc(1) complex account for the function of a dimeric complex? *BBA-Bioenergetics* **2008**, *1777* (7-8), 1001-1019.
244. Schafer, G.; Penefsky, H. S., Bioenergetics: energy conservation and conversion . Introduction. *Results Probl Cell Differ* **2008**, *45*, IV-VIII.
245. Ritter, M.; Palsdottir, H.; Abe, M.; Mantele, W.; Hunte, C.; Miyoshi, H.; Hellwig, P., Direct evidence for the interaction of stigmatellin with a protonated acidic group in the bc(1) complex from *Saccharomyces cerevisiae* as monitored by FTIR difference spectroscopy and C-13 specific labeling. *Biochemistry-Us* **2004**, *43* (26), 8439-8446.
246. Humphrey, W.; Dalke, A.; Schulten, K., VMD: Visual molecular dynamics. *J Mol Graphics* **1996**, *14* (1), 33-&.
247. Morris, G. M.; Goodsell, D. S.; Halliday, R. S.; Huey, R.; Hart, W. E.; Belew, R. K.; Olson, A. J., Automated docking using a Lamarckian genetic algorithm and an empirical binding free energy function. *J Comput Chem* **1998**, *19* (14), 1639-1662.
248. The RCSB Protein Data Bank. www.rcsb.org (accessed 10.10.2011).
249. UniProt. <http://www.uniprot.org/> (accessed 05.06.2012).
250. Hudson, A. T.; Dickins, M.; Ginger, C. D.; Gutteridge, W. E.; Holdich, T.; Hutchinson, D. B. A.; Pudney, M.; Randall, A. W.; Latter, V. S., 566c80 - a Potent Broad-Spectrum Antiinfective Agent with Activity against Malaria and Opportunistic Infections in Aids Patients. *Drug Exp Clin Res* **1991**, *17* (9), 427-435.
251. Kesten, S. J.; Degnan, M. J.; Hung, J. L.; Mcnamara, D. J.; Ortwine, D. F.; Uhlendorf, S. E.; Werbel, L. M., Antimalarial-Drugs .64. Synthesis and Antimalarial Properties of 1-Imino Derivatives of 7-Chloro-3-Substituted-3,4-Dihydro-1,9(2h,10h)-Acridinediones and Related Structures. *J Med Chem* **1992**, *35* (19), 3429-3447.
252. Zhu, W. L.; Lu, Y. X.; Wang, Y., Nonbonding interactions of organic halogens in biological systems: implications for drug discovery and biomolecular design. *Phys Chem Chem Phys* **2010**, *12* (18), 4543-4551.
253. Imai, Y. N.; Inoue, Y.; Nakanishi, I.; Kitaura, K., Cl-pi interactions in protein-ligand complexes. *Protein Sci* **2008**, *17* (7), 1129-1137.

254. Glaser, R.; Chen, N. J.; Wu, H.; Knotts, N.; Kaupp, M., C-13 NMR study of halogen bonding of haloarenes: Measurements of solvent effects and theoretical analysis. *J Am Chem Soc* **2004**, *126* (13), 4412-4419.
255. Sarwar, M. G.; Dragisic, B.; Salsberg, L. J.; Gouliaras, C.; Taylor, M. S., Thermodynamics of Halogen Bonding in Solution: Substituent, Structural, and Solvent Effects. *J Am Chem Soc* **2010**, *132* (5), 1646-1653.
256. Bissantz, C.; Kuhn, B.; Stahl, M., A Medicinal Chemist's Guide to Molecular Interactions. *J Med Chem* **2010**, *53* (14), 5061-5084.
257. Gamo, F. J.; Sanz, L. M.; Vidal, J.; de Cozar, C.; Alvarez, E.; Lavandera, J. L.; Vanderwall, D. E.; Green, D. V. S.; Kumar, V.; Hasan, S.; Brown, J. R.; Peishoff, C. E.; Cardon, L. R.; Garcia-Bustos, J. F., Thousands of chemical starting points for antimalarial lead identification. *Nature* **2010**, *465* (7296), 305-U56.
258. Huey, R.; Morris, G. M.; Olson, A. J.; Goodsell, D. S., A semiempirical free energy force field with charge-based desolvation. *J Comput Chem* **2007**, *28* (6), 1145-52.
259. Jiang, X. H.; Kumar, K.; Hu, X.; Wallqvist, A.; Reifman, J., DOVIS 2.0: an efficient and easy to use parallel virtual screening tool based on AutoDock 4.0. *Chem Cent J* **2008**, *2*, -.
260. Kitchen, D. B.; Decornez, H.; Furr, J. R.; Bajorath, J., Docking and scoring in virtual screening for drug discovery: methods and applications. *Nat Rev Drug Discov* **2004**, *3* (11), 935-49.
261. Cosconati, S.; Forli, S.; Perryman, A. L.; Harris, R.; Goodsell, D. S.; Olson, A. J., Virtual Screening with AutoDock: Theory and Practice. *Expert Opin Drug Discov* **2010**, *5* (6), 597-607.
262. MOE, Chemical Computing Group Inc, Montreal.
263. Tetko, I. V.; Gasteiger, J.; Todeschini, R.; Mauri, A.; Livingstone, D.; Ertl, P.; Palyulin, V.; Radchenko, E.; Zefirov, N. S.; Makarenko, A. S.; Tanchuk, V. Y.; Prokopenko, V. V., Virtual computational chemistry laboratory - design and description. *J Comput Aid Mol Des* **2005**, *19* (6), 453-463.
264. Gould, R. G.; Jacobs, W. A., The Synthesis of Certain Substituted Quinolines and 5,6-Benzoquinolines. *J Am Chem Soc* **1939**, *61* (10), 2890-2895.
265. Pollock, B. J.; Sikes, C. A.; Ter Louw, R. P.; Hawken, S. R.; Speelman, A. L.; Lynch, E. J.; Stanford, D. J.; Wheeler, K. A.; Gillmore, J. G., Synthesis and Structural Investigation of

an "Oxazinoquinolinespirohexadienone" That Only Exists as Its Long-Wavelength Ring-Opened Quinonimine Isomer. *J Org Chem* **2012**, *77* (19), 8689-8695.

266. Mphahlele, M. J.; El-Nahas, A. M., Tautomeric 2-arylquinolin-4(1H)-one derivatives-spectroscopic, X-ray and quantum chemical structural studies. *J Mol Struct* **2004**, *688* (1-3), 129-136.

267. Casey, A. C., 4(1h)-Quinolones .2. Antimalarial Effect of Some 2-Methyl-3-(1'-Alkenyl)-or-3-Alkyl-4(1h)-Quinolones. *J Med Chem* **1974**, *17* (2), 255-256.

268. Li, G. X.; Liu, Z. Q.; Luo, X. Y., Dichloro-4-quinolinol-3-carboxylic acid: Synthesis and antioxidant abilities to scavenge radicals and to protect methyl linoleate and DNA. *Eur J Med Chem* **2010**, *45* (5), 1821-1827.

269. Periasamy, M.; Thirumalaikumar, P., Methods of enhancement of reactivity and selectivity of sodium borohydride for applications in organic synthesis. *J Organomet Chem* **2000**, *609* (1-2), 137-151.

270. Boechat, N.; da Costa, J. C. S.; Mendonca, J. D.; de Oliveira, P. S. M.; de Souza, M. V. N., A simple reduction of methyl aromatic esters to alcohols using sodium borohydride-methanol system. *Tetrahedron Lett* **2004**, *45* (31), 6021-6022.

271. Boechat, N.; da Costa, J. C. S.; Mendonca, J. D.; Paes, K. C.; Fernandes, E. L.; de Oliveira, P. S. M.; Vasconcelos, T. R. A.; de Souza, M. V. N., Simple reduction of heteroaromatic esters to alcohols using a sodium borohydride-methanol system. *Synthetic Commun* **2005**, *35* (24), 3187-3190.

272. Brown, H. C.; Narasimhan, S.; Choi, Y. M., Selective Reductions .30. Effect of Cation and Solvent on the Reactivity of Saline Borohydrides for Reduction of Carboxylic Esters - Improved Procedures for the Conversion of Esters to Alcohols by Metal Borohydrides. *J Org Chem* **1982**, *47* (24), 4702-4708.

273. Prasad, A. S. B.; Kanth, J. V. B.; Periasamy, M., Convenient Methods for the Reduction of Amides, Nitriles, Carboxylic Esters, Acids and Hydroboration of Alkenes Using NaBH_4/I_2 System. *Tetrahedron* **1992**, *48* (22), 4623-4628.

274. Proudfoot, J. R.; Regan, J. R.; Thomson, D. S.; Kuzmich, D.; Lee, T. W.; Hammach, A.; Ralph, M. S.; Zindell, R.; Bekkali, Y.; Kirrane Jr., T. M., 1-propanol and 1-propylamine derivatives and their use as glucocorticoid ligands. 2004.

275. Shen, Y. S.; Liu, H. X.; Wu, M.; Du, W. Q.; Chen, Y. Q.; Li, N. P., Friedel-Crafts Alkylation of Benzenes Substituted with Meta-Directing Groups. *J Org Chem* **1991**, *56* (25), 7160-7162.
276. Iovel, I.; Mertins, K.; Kischel, J.; Zapf, A.; Beller, M., An efficient and general iron-catalyzed arylation of benzyl alcohols and benzyl carboxylates. *Angew Chem Int Edit* **2005**, *44* (25), 3913-3917.
277. De Castro, K. A.; Rhee, H., Selective nosylation of 1-phenylpropane-1,3-diol and perchloric acid mediated Friedel-Crafts alkylation: Key steps for the new and straightforward synthesis of tolterodine. *Synthesis-Stuttgart* **2008**, (12), 1841-1844.
278. Raynes, K. J.; Stocks, P. A.; O'Neill, P. M.; Park, B. K.; Ward, S. A., New 4-aminoquinoline mannich base antimalarials. 1. Effect of an alkyl substituent in the 5'-position of the 4'-hydroxyanilino side chain. *J Med Chem* **1999**, *42* (15), 2747-2751.
279. Hughes, L. M.; Lanteri, C. A.; O'Neil, M. T.; Johnson, J. D.; Gribble, G. W.; Trumpower, B. L., Design of anti-parasitic and anti-fungal hydroxy-naphthoquinones that are less susceptible to drug resistance. *Mol Biochem Parasit* **2011**, *177* (1), 12-19.
280. Covian, R.; Trumpower, B. L., Regulatory interactions in the dimeric cytochrome bc(1) complex: The advantages of being a twin. *BBA-Bioenergetics* **2008**, *1777* (9), 1079-1091.
281. Crofts, A. R., The cytochrome bc(1) complex: Function in the context of structure. *Annu Rev Physiol* **2004**, *66*, 689-733.
282. Xia, D.; Esser, L.; Yu, C. A., Inhibitor Complexed Structures of the Cytochrome bc1 from the Photosynthetic Bacterium *Rhodobacter sphaeroides*. *Faseb J* **2008**, *22*.
283. Sali, A.; Blundell, T. L., Comparative Protein Modeling by Satisfaction of Spatial Restraints. *J Mol Biol* **1993**, *234* (3), 779-815.
284. Pettersen, E. F.; Goddard, T. D.; Huang, C. C.; Couch, G. S.; Greenblatt, D. M.; Meng, E. C.; Ferrin, T. E., UCSF chimera - A visualization system for exploratory research and analysis. *J Comput Chem* **2004**, *25* (13), 1605-1612.
285. Laskowski, R. A.; Macarthur, M. W.; Moss, D. S.; Thornton, J. M., Procheck - a Program to Check the Stereochemical Quality of Protein Structures. *J Appl Crystallogr* **1993**, *26*, 283-291.

286. Haudecoeur, R.; Boumendjel, A., Recent Advances in the Medicinal Chemistry of Aurones. *Curr Med Chem* **2012**, *19* (18), 2861-2875.
287. Boumendjel, A., Aurones: A subclass of flavones with promising biological potential. *Curr Med Chem* **2003**, *10* (23), 2621-2630.
288. Lee, C. Y.; Chew, E. H.; Go, M. L., Functionalized aurones as inducers of NAD(P)H:quinone oxidoreductase 1 that activate AhR/XRE and Nrf2/ARE signaling pathways: Synthesis, evaluation and SAR. *Eur J Med Chem* **2010**, *45* (7), 2957-2971.
289. Gerby, B.; Boumendjel, A.; Blanc, M.; Bringuier, P. P.; Champelovier, P.; Fortune, A.; Ronot, X.; Boutonnat, J., 2-Arylidenedihydroindole-3-ones: Design, synthesis, and biological activity on bladder carcinoma cell lines. *Bioorg Med Chem Lett* **2007**, *17* (1), 208-213.
290. Huang, W.; Liu, M. Z.; Li, Y.; Tan, Y.; Yang, G. F., Design, syntheses, and antitumor activity of novel chromone and aurone derivatives. *Bioorgan Med Chem* **2007**, *15* (15), 5191-5197.
291. Dubois, C.; Haudecoeur, R.; Orio, M.; Belle, C.; Bochot, C.; Boumendjel, A.; Hardre, R.; Jamet, H.; Reglier, M., Versatile Effects of Aurone Structure on Mushroom Tyrosinase Activity. *Chembiochem* **2012**, *13* (4), 559-565.
292. Manjulatha, K.; Srinivas, S.; Mulakayala, N.; Rambabu, D.; Prabhakar, M.; Arunasree, K. M.; Alvala, M.; Rao, M. V. B.; Pal, M., Ethylenediamine diacetate (EDDA) mediated synthesis of aurones under ultrasound: Their evaluation as inhibitors of SIRT1. *Bioorg Med Chem Lett* **2012**, *22* (19), 6160-6165.
293. Okombi, S.; Rival, D.; Bonnet, S.; Mariotte, A. M.; Perrier, E.; Boumendjel, A., Discovery of benzylidenebenzofuran-3(2H)-one (aurones) as inhibitors of tyrosinase derived from human melanocytes. *J Med Chem* **2006**, *49* (1), 329-333.
294. Bandgar, B. R.; Patil, S. A.; Korbadi, B. L.; Biradar, S. C.; Nile, S. N.; Khobragade, C. N., Synthesis and biological evaluation of a novel series of 2,2-bisaminomethylated aurone analogues as anti-inflammatory and antimicrobial agents. *Eur J Med Chem* **2010**, *45* (7), 3223-3227.
295. Kayser, O.; Kiderlen, A. F.; Folkens, U.; Kokodziej, H., In vitro leishmanicidal activity of aurones. *Planta Med* **1999**, *65* (4), 316-319.

296. Kayser, O.; Kiderlen, A. F.; Brun, R., In vitro activity of aurones against *Plasmodium falciparum* strains K1 and NF54. *Planta Med* **2001**, *67* (8), 718-721.
297. Kayser, O.; Chen, M.; Kharazmi, A.; Kiderlen, A. F., Aurones interfere with *Leishmania major* mitochondrial fumarate reductase. *Z Naturforsch C* **2002**, *57* (7-8), 717-720.
298. Souard, F.; Okombi, S.; Beney, C.; Chevalley, S.; Valentin, A.; Boumendjel, A., 1-Azaaurones derived from the naturally occurring aurones as potential antimalarial drugs. *Bioorgan Med Chem* **2010**, *18* (15), 5724-5731.
299. Haudecoeur, R.; Ahmed-Belkacem, A.; Yi, W.; Fortune, A.; Brilllet, R.; Belle, C.; Nicolle, E.; Pallier, C.; Pawlotsky, J. M.; Boumendjel, A., Discovery of Naturally Occurring Aurones That Are Potent Allosteric Inhibitors of Hepatitis C Virus RNA-Dependent RNA Polymerase. *J Med Chem* **2011**, *54* (15), 5395-5402.
300. Shin, S. Y.; Shin, M. C.; Shin, J. S.; Lee, K. T.; Lee, Y. S., Synthesis of aurones and their inhibitory effects on nitric oxide and PGE(2) productions in LPS-induced RAW 264.7 cells. *Bioorg Med Chem Lett* **2011**, *21* (15), 4520-4523.
301. Sim, H. M.; Lee, C. Y.; Ee, P. L. R.; Go, M. L., Dimethoxyaurones: Potent inhibitors of ABCG2 (breast cancer resistance protein). *Eur J Pharm Sci* **2008**, *35* (4), 293-306.
302. Sim, H. M.; Loh, K. Y.; Yeo, W. K.; Lee, C. Y.; Go, M. L., Aurones as Modulators of ABCG2 and ABCB1: Synthesis and Structure-Activity Relationships. *ChemMedChem* **2011**, *6* (4), 713-724.
303. Sim, H. M.; Wu, C. P.; Ambudkar, S. V.; Go, M. L., In vitro and in vivo modulation of ABCG2 by functionalized aurones and structurally related analogs. *Biochem Pharmacol* **2011**, *82* (11), 1562-1571.
304. Hadjeri, M.; Barbier, M.; Ronot, X.; Mariotte, A. M.; Boumendjel, A.; Boutonnat, J., Modulation of P-glycoprotein-mediated multidrug resistance by flavonoid derivatives and analogues. *J Med Chem* **2003**, *46* (11), 2125-2131.
305. Boumendjel, A.; Beney, C.; Deka, N.; Mariotte, A. M.; Lawson, M. A.; Trompier, D.; Baubichon-Cortay, H.; Di Pietro, A., 4-hydroxy-6-methoxyaurones with high-affinity binding to cytosolic domain of P-glycoprotein. *Chem Pharm Bull* **2002**, *50* (6), 854-856.

306. Sheng, R.; Xu, Y.; Hu, C. Q.; Zhang, J.; Lin, X.; Li, J. Y.; Yang, B.; He, Q. J.; Hu, Y. Z., Design, synthesis and AChE inhibitory activity of indanone and aurone derivatives. *Eur J Med Chem* **2009**, *44* (1), 7-17.
307. Geldenhuys, W. J.; Funk, M. O.; Van der Schyf, C. J.; Carroll, R. T., A scaffold hopping approach to identify novel monoamine oxidase B inhibitors. *Bioorg Med Chem Lett* **2012**, *22* (3), 1380-3.
308. Adhikari, N.; Halder, A. K.; Mondal, C.; Jha, T., Exploring structural requirements of aurone derivatives as antimalarials by validated DFT-based QSAR, HQSAR, and COMFA-COMSIA approach. *Med Chem Res* **2013**, *22* (12), 6029-6045.
309. Fitzmaurice, R. J.; Etheridge, Z. C.; Jumel, E.; Woolfson, D. N.; Caddick, S., Microwave enhanced palladium catalysed coupling reactions: A diversity-oriented synthesis approach to functionalised flavones. *Chem Commun* **2006**, (46), 4814-4816.
310. Guiguemde, W. A.; Shelat, A. A.; Bouck, D.; Duffy, S.; Crowther, G. J.; Davis, P. H.; Smithson, D. C.; Connelly, M.; Clark, J.; Zhu, F. Y.; Jimenez-Diaz, M. B.; Martinez, M. S.; Wilson, E. B.; Tripathi, A. K.; Gut, J.; Sharlow, E. R.; Bathurst, I.; El Mazouni, F.; Fowble, J. W.; Forquer, I.; McGinley, P. L.; Castro, S.; Angulo-Barturen, I.; Ferrer, S.; Rosenthal, P. J.; DeRisi, J. L.; Sullivan, D. J.; Lazo, J. S.; Roos, D. S.; Riscoe, M. K.; Phillips, M. A.; Rathod, P. K.; Van Voorhis, W. C.; Avery, V. M.; Guy, R. K., Chemical genetics of *Plasmodium falciparum*. *Nature* **2010**, *465* (7296), 311-315.
311. Varma, R. S.; Varma, M., Alumina-Mediated Condensation - a Simple Synthesis of Aurones. *Tetrahedron Lett* **1992**, *33* (40), 5937-5940.
312. Geissman, T. A.; Harborne, J. B., Anthochlor Pigments .10. Aureusin and Cernuoside. *J Am Chem Soc* **1955**, *77* (17), 4622-4624.
313. Liu, Q. S.; Chang, J. W.; Wang, J. H.; Kang, S. A.; Thoreen, C. C.; Markhard, A.; Hur, W.; Zhang, J. M.; Sim, T.; Sabatini, D. M.; Gray, N. S., Discovery of 1-(4-(4-Propionylpiperazin-1-yl)-3-(trifluoromethyl)phenyl)-9-(quinolin-3-yl)benzo[h][1,6]naphthyridin-2(1H)-one as a Highly Potent, Selective Mammalian Target of Rapamycin (mTOR) Inhibitor for the Treatment of Cancer. *J Med Chem* **2010**, *53* (19), 7146-7155.

314. Atta-Ur-Rahman; Choudhary, M. I.; Hayat, S.; Khan, A. M.; Ahmed, A., Two new aurones from marine brown alga *Spatoglossum variabile*. *Chem Pharm Bull* **2001**, *49* (1), 105-107.
315. Thakkar, K.; Cushman, M., A Novel Oxidative Cyclization of 2'-Hydroxychalcones to 4,5-Dialkoxyaurone by Thallium(III) Nitrate. *J Org Chem* **1995**, *60* (20), 6499-6510.
316. Beney, C.; Mariotte, A. M.; Boumendjel, A., An efficient synthesis of 4,6 dimethoxyaurones. *Heterocycles* **2001**, *55* (5), 967-972.
317. Lipinski, C. A.; Lombardo, F.; Dominy, B. W.; Feeney, P. J., Experimental and computational approaches to estimate solubility and permeability in drug discovery and development settings. *Adv Drug Deliver Rev* **1997**, *23* (1-3), 3-25.
318. Liu, M.; Wilairat, P.; Go, M. L., Antimalarial alkoxyated and hydroxylated chalcones: Structure-activity relationship analysis. *J Med Chem* **2001**, *44* (25), 4443-4452.
319. Warhurst, D. C.; Craig, J. C.; Adagu, P. S.; Guy, R. K.; Madrid, P. B.; Fivelman, Q. L., Activity of piperazine and other 4-aminoquinoline antiplasmodial drugs against chloroquine -sensitive and resistant blood-stages of *Plasmodium falciparum* - Role of beta-haematin inhibition and drug concentration in vacuolar water- and lipid-phases. *Biochem Pharmacol* **2007**, *73* (12), 1910-1926.
320. Hilal, S. H.; Karickhoff, S. W.; Carreira, L. A., A rigorous test for SPARC's chemical reactivity models: Estimation of more than 4300 ionization pK(a)s. *Quant Struct-Act Rel* **1995**, *14* (4), 348-355.
321. Clark, J.; Perrin, D. D., Prediction of the Strengths of Organic Bases. *Q Rev Chem Soc* **1964**, *18* (3), 295-320.
322. Charton, M., Electrical Effects of Ortho-Substituents in Pyridines + Quinolines. *J Am Chem Soc* **1964**, *86* (10), 2033-&.
323. Sandlin, R. D.; Carter, M. D.; Lee, P. J.; Auschwitz, J. M.; Leed, S. E.; Johnson, J. D.; Wright, D. W., Use of the NP-40 Detergent-Mediated Assay in Discovery of Inhibitors of beta-Hematin Crystallization. *Antimicrob Agents Ch* **2011**, *55* (7), 3363-3369.
324. Omodeo-Sale, F.; Cortelezzi, L.; Basilico, N.; Casagrande, M.; Sparatore, A.; Taramelli, D., Novel Antimalarial Aminoquinolines: Heme Binding and Effects on Normal or *Plasmodium falciparum*-Parasitized Human Erythrocytes. *Antimicrob Agents Ch* **2009**, *53* (10), 4339-4344.

325. Thomas, V.; Gois, A.; Ritts, B.; Burke, P.; Hanscheid, T.; McDonnell, G., A Novel Way to Grow Hemozoin-Like Crystals In Vitro and Its Use to Screen for Hemozoin Inhibiting Antimalarial Compounds. *Plos One* **2012**, *7* (7).
326. Moura, P. A.; Dame, J. B.; Fidock, D. A., Role of Plasmodium falciparum Digestive Vacuole Plasmepsins in the Specificity and Antimalarial Mode of Action of Cysteine and Aspartic Protease Inhibitors. *Antimicrob Agents Ch* **2009**, *53* (12), 4968-4978.
327. Blackman, M. J., Malarial proteases and host cell egress: an 'emerging' cascade. *Cell Microbiol* **2008**, *10* (10), 1925-1934.
328. Dahl, E. L.; Rosenthal, P. J., Biosynthesis, localization, and processing of falcipain cysteine proteases of Plasmodium falciparum. *Mol Biochem Parasit* **2005**, *139* (2), 205-212.
329. Banerjee, R.; Liu, J.; Beatty, W.; Pelosof, L.; Klemba, M.; Goldberg, D. E., Four plasmepsins are active in the Plasmodium falciparum food vacuole, including a protease with an active-site histidine. *P Natl Acad Sci USA* **2002**, *99* (2), 990-995.
330. Coombs, G. H.; Goldberg, D. E.; Klemba, M.; Berry, C.; Kay, J.; Mottram, J. C., Aspartic proteases of Plasmodium falciparum and other parasitic protozoa as drug targets. *Trends Parasitol* **2001**, *17* (11), 532-537.
331. Santos, M. M. M.; Moreira, R., Michael acceptors as cysteine protease inhibitors. *Mini-Rev Med Chem* **2007**, *7* (10), 1040-1050.
332. Sauvage, V.; Aubert, D.; Bonhomme, A.; Pinon, J. M.; Millot, J. M., P-glycoprotein inhibitors modulate accumulation and efflux of xenobiotics in extra and intracellular Toxoplasma gondii. *Mol Biochem Parasit* **2004**, *134* (1), 89-95.
333. Bray, P. G.; Martin, R. E.; Tilley, L.; Ward, S. A.; Kirk, K.; Fidock, D. A., Defining the role of PfCRT in Plasmodium falciparum chloroquine resistance. *Mol Microbiol* **2005**, *56* (2), 323-333.
334. Krogstad, D. J.; Gluzman, I. Y.; Kyle, D. E.; Oduola, A. M. J.; Martin, S. K.; Milhous, W. K.; Schlesinger, P. H., Efflux of Chloroquine from Plasmodium-Falciparum - Mechanism of Chloroquine Resistance. *Science* **1987**, *238* (4831), 1283-1285.
335. Martin, S. K.; Oduola, A. M. J.; Milhous, W. K., Reversal of Chloroquine Resistance in Plasmodium-Falciparum by Verapamil. *Science* **1987**, *235* (4791), 899-901.

336. Bray, P. G.; Ward, S. A., A comparison of the phenomenology and genetics of multidrug resistance in cancer cells and quinoline resistance in *Plasmodium falciparum*. *Pharmacol Therapeut* **1998**, *77* (1), 1-28.
337. Semenov, A.; Olson, J. E.; Rosenthal, P. J., Antimalarial synergy of cysteine and aspartic protease inhibitors. *Antimicrob Agents Ch* **1998**, *42* (9), 2254-2258.
338. Wiesner, J.; Henschker, D.; Hutchinson, D. B.; Beck, E.; Jomaa, H., In vitro and in vivo synergy of fosmidomycin, a novel antimalarial drug, with clindamycin. *Antimicrob Agents Ch* **2002**, *46* (9), 2889-2894.
339. Farnert, A.; Lindberg, J.; Gil, P.; Swedberg, G.; Berqvist, Y.; Thapar, M. M.; Lindegardh, N.; Berezcky, S.; Bjorkman, A., Evidence of *Plasmodium falciparum* malaria resistant to atovaquone and proguanil hydrochloride: case reports. *Brit Med J* **2003**, *326* (7390), 628-629.
340. Wijayanti, M. A.; Sholikhah, E. N.; Hadanu, R.; Jumina, J.; Supargiyono, S.; Mustofa, M., Additive in vitro antiplasmodial effect of N-alkyl and N-benzyl-1,10-phenanthroline derivatives and cysteine protease inhibitor e64. *Malar Res Treat* **2010**, *2010*, 540786.
341. Alcantara, L. M.; Kim, J.; Moraes, C. B.; Franco, C. H.; Franzoi, K. D.; Lee, S.; Freitas-Junior, L. H.; Ayong, L. S., Chemosensitization potential of P-glycoprotein inhibitors in malaria parasites. *Exp Parasitol* **2013**, *134* (2), 235-243.
342. Wager, C. A. B.; Miller, S. A., Two robust, efficient syntheses of [phenyl ring-U-14 C]indole through use of [phenyl ring-U-C-14]aniline. *J Labelled Compd Rad* **2006**, *49* (7), 615-622.
343. Sugawara, T.; Toyoda, T.; Adachi, M.; Sasakura, K., Aminohaloborane in Organic-Synthesis .1. Specific Ortho Substitution-Reaction of Anilines. *J Am Chem Soc* **1978**, *100* (15), 4842-4852.
344. Adachi, M.; Sugawara, T., Exclusive Ortho Cyanation and Alkylthiocarbonylation of Anilines and Phenols Using Boron-Trichloride. *Synthetic Commun* **1990**, *20* (1), 71-84.
345. Buzas, A.; Merour, J. Y., Synthesis and Reactions of 1-Acetyl-2-Benzylidene-3-Oxo-2,3-Dihydroindoles. *Synthesis-Stuttgart* **1989**, (6), 458-461.
346. Zhou, Y. G.; Yang, P. Y.; Han, X. W., Synthesis and highly enantioselective hydrogenation of exocyclic enamides: (Z)-3-arylidene-4-acetyl-3,4-dihydro-2H-1,4-benzoxazines. *J Org Chem* **2005**, *70* (5), 1679-1683.

347. Lucarini, S.; Alessi, M.; Bedini, A.; Giorgini, G.; Piersanti, G.; Spadoni, G., Diastereo- and Enantioselective Hydrogenation of a Challenging Enamide Derived from 4-Phenyl-2-tetralone: An Appealing Shortcut Towards Enantiopure cis-2-Aminotetraline Derivatives. *Chem-Asian J* **2010**, *5* (3), 550-554.
348. Olson, J. E.; Lee, G. K.; Semenov, A.; Rosenthal, P. J., Antimalarial effects in mice of orally administered peptidyl cysteine protease inhibitors. *Bioorgan Med Chem* **1999**, *7* (4), 633-638.
349. Price, R. N.; Uhlemann, A. C.; Brockman, A.; McGready, R.; Ashley, E.; Phaipun, L.; Patel, R.; Laing, K.; Looareesuwan, S.; White, N. J.; Nosten, F.; Krishna, S., Mefloquine resistance in Plasmodium falciparum and increased pfmdr1 gene copy number. *Lancet* **2004**, *364* (9432), 438-447.
350. *The PyMOL Molecular Graphics System*, DeLano Scientific, Palo Alto, CA, USA: 2002.
351. Asinex. <http://www.asinex.com/> (accessed 05.09.2010).
352. ChemBridge. <http://www.chembridge.com/> (accessed 05.09.2010).
353. Chemical Block. <http://www.chemblock.com/> (accessed 05.09.2010).
354. Enamine. <http://www.enamine.net/> (accessed 05.09.2010).
355. InterBioScreen. <http://www.ibscreen.com/> (accessed 05.09.2010).
356. LaboTest. <http://www.labotest.com/> (accessed 05.09.2010).
357. Life Chemicals. <http://www.lifechemicals.com/> (accessed 05.09.2010).
358. Specs. <http://www.specs.net> (accessed 05.09.2010).
359. TOSLab. <http://www.toslab.com/> (accessed 05.09.2010).
360. Trager, W.; Jensen, J. B., Human Malaria Parasites in Continuous Culture. *Science* **1976**, *193* (4254), 673-675.
361. Lambros, C.; Vanderberg, J. P., Synchronization of Plasmodium-Falciparum Erythrocytic Stages in Culture. *J Parasitol* **1979**, *65* (3), 418-420.
362. Lorian, V., Macroscopic Patterns of Bacteria after Development in Drops of Liquid Medium. *J Bacteriol* **1963**, *86* (3), 582.
363. Wijayanti, M. A.; Sholikhah, E. N.; Hadanu, R.; Jumina, J.; Supargiyono, S.; Mustofa, M., Additive in vitro antiplasmodial effect of N-alkyl and N-benzyl-1,10-phenanthroline

derivatives and cysteine protease inhibitor e64. *Malar Res Treat* **2010**, 2010, Article ID 540786.

364. Software, E. *Grafit program*.

365. Kumar, S. P.; Gloria, P. M. C.; Goncalves, L. M.; Gut, J.; Rosenthal, P. J.; Moreira, R.; Santos, M. M. M., Squaric acid: a valuable scaffold for developing antimalarials? *MedChemComm* **2012**, 3 (4), 489-493.

366. Lucas, S. D.; Goncalves, L. M.; Cardote, T. A. F.; Correia, H. F.; Moreira, R.; Guedes, R. C., Structure based virtual screening for discovery of novel human neutrophil elastase inhibitors. *MedChemComm* **2012**, 3 (10), 1299-1304.